Deformation Prediction of Geosynthetic Reinforced Soil Retaining Walls

by

Stanley R. Boyle

A dissertation submitted in partial fulfillment
of the requirements for the degree of

Doctor of Philosophy

University of Washington

1995

Approved by _____
Chairperson of Supervisory Committee

_____

_____

_____

_____

Program Authorized
to Offer Degree CIVIL ENGINEERING

Date JUNE 1, 1995

In presenting this dissertation in partial fulfillment of the requirements for the Doctoral degree at the University of Washington, I agree that the Library shall make its copies freely available for inspection. I further agree that extensive copying of this dissertation is allowable only for scholarly purposes, consistent with "fair use" as prescribed in the U.S. Copyright Law. Requests for copying or reproduction of this dissertation may be referred to University Microfilms, 1490 Eisenhower Place, P.O. Box 975, Ann Arbor, MI 48106, to whom the author has granted "the right to reproduce and sell (a) copies of the manuscript in microform and or (b) printed copies of the manuscript made from microform."

Signature 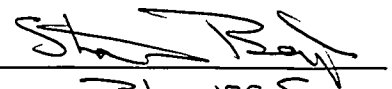

Date May 31, 1995

University of Washington

Abstract

Deformation Prediction of Geosynthetic Reinforced Soil Retaining Walls

by Stanley R. Boyle

Chairperson of the Supervisory Committee: Professor Robert D. Holtz
Department of Civil Engineering

A program to investigate the behavior of geosynthetic reinforced soil and the deformation of geosynthetic reinforced soil retaining walls is presented. This investigation included laboratory testing of geosynthetic reinforcements and geosynthetic reinforced cohesionless soils, and finite element analysis of reinforced soil retaining walls.

Two sands, two polypropylene nonwoven needle-punched geotextiles, three polypropylene woven slit-film geotextiles, and a multi-filament polyester woven geotextile were the focus of the testing program. In-soil testing of the geotextiles was performed using a plane strain unit cell device. Tension induced in the reinforcement during loading of reinforced soil specimens increased the confining pressure acting on the soil, which permitted the soil to support a greater load than it could when unreinforced. Soil dilation played an important role in defining the stress-strain behavior of the reinforced soil composite. Higher modulus reinforcements were able to restrict soil dilation.

The woven geotextiles experienced creep and stress relaxation at low strains and over short time periods in tests conducted in the unit cell device. To further study these mechanisms, a series of in-isolation wide width tests, conducted at various strain rates, as well as short term creep tests on the woven geotextiles were performed. In-isolation wide width tests on the nonwoven geotextiles were conducted because the changing normal pressure conditions which occurred in unit cell device tests complicated determination of the in-soil modulus for these reinforcements. The in-isolation tests determined that the strength and modulus of the woven geotextiles decreased with decreasing strain rate and that the modulus of the nonwoven geotextiles increased with decreasing specimen gage length.

The deformation of geosynthetic reinforced soil retaining walls was investigated using the finite element method. Assuming linear elastic material properties, the influence of wall geometry, applied loads, and boundary conditions were investigated. It was determined that these factors played a major role in defining the pattern of deformation and reinforcing strains observed in reinforced soil retaining walls.

The findings of the laboratory tests and finite element analysis were applied to the Rainier Avenue wall. Conclusions reached from earlier investigations of this wall were evaluated. Recommendations for determining soil and geosynthetic properties and using them for predicting reinforced soil retaining wall deformations were also made. The finite element method was determined to be the best means for accurately predicting deformations of individual reinforced soil walls.

TABLE OF CONTENTS

Page

Page

Page

Page

LIST OF FIGURES

Number *Page*

Number *Page*

Number *Page*

Number *Page*

Number *Page*

Number *Page*

LIST OF TABLES

ACKNOWLEDGMENTS

The work presented in this dissertation was funded by the Washington State Department of Transportation and the U.S. Federal Highway Administration. Their financial support is greatly appreciated.

The author wishes to express sincere appreciation to Professor Robert D. Holtz for his guidance provided throughout the research phase of this work and for his assistance in the preparation of this manuscript. Additional thanks to Professors Sunirmal Banerjee, Steven Kramer, Gregory Miller, and Teresa Taylor, for their many helpful discussions and for reviewing the manuscript. The laboratory testing program could not have been completed without the assistance of the civil engineering shop staff. Special recognition is due to Mr. Ken Knowlan who's input to the design and manufacture of the Unit Cell Device was invaluable. Thanks also to Mr. Matthew Gallagher for his contributions and for performing the in-isolation tests which form a part of this work.

The author is grateful for the assistance of the many people who offered ideas and solutions and freely provided assistance when requested, including: Mr. Tony Allen, Mr. Steve Anderson, Mr. Robert Metcalfe, Mr. Sujan Punyamurthula, Mr. N. Sivaneswaran, and Mr. Shaun Stauffer. The guidance and friendship provided by Mr. James Strout during the author's first year of adjustment to graduate school was greatly appreciated and made the experience more enjoyable. Special thanks to Mr. Wen-Sen Tsai for making himself available as a sounding board when things were not going quite the way they should, and for offering critical review of the author's ideas and work.

To my wife, Lynda, who's love and support made this possible.

CHAPTER 1
INTRODUCTION

1.1 The Need to Predict Reinforced Soil Wall Deformations

In the mid 1960's Henri Vidal introduced Reinforced Earth as a commercial, economically feasible means of reinforcing soil (Vidal, 1969, Schlosser and Vidal, 1969). Steel straps were placed in the backfill soil during placement while flexible or stiff facing elements were used to confine the soil at the face of the reinforced structure. Reinforced Earth, and variations that use steel bars or wire mats, have since been used on thousands of projects worldwide.

In the 1970's geosynthetics were first introduced as alternate tensile resisting materials for use in reinforced soil structures (Bell and Steward, 1977). The increased flexibility, resistance to corrosive soils, and reduced costs were primary motivators for using these materials. A wide variety of geosynthetic materials, e.g. geotextiles and geogrids, have since been introduced for this purpose. Numerous geosynthetic reinforced walls and slopes have been constructed. However, most of these geosynthetic reinforced soil (GRS) structures have been used in temporary applications or in locations where the deformation of the structure would not affect its performance. The reduced cost realized by using geosynthetic reinforcing, instead of steel strap, bar or mat reinforcing, could be taken advantage of more often if geosynthetic reinforced soil structures could be used in permanent applications. For this to occur, an understanding of the deformation characteristics of geosynthetic reinforced soil walls and the long term durability of geosynthetics is necessary.

In connection with the reconstruction of Interstate 90 in Seattle, Washington, the Washington State Department of Transportation (WSDOT) designed and supervised the construction of a series of geotextile reinforced soil retaining walls at the interchange with Rainier Avenue. One wall had a maximum height of 12.6 meters and supported a 5.3 meter high surcharge fill above the top of the wall. Since this wall was higher than any geotextile reinforced wall previously built and was located next to a busy interchange, it was extensively instrumented and monitored during construction and for sometime afterwards to evaluate its performance. Preliminary analysis of the reinforcement strains and overall deformation was reported by Christopher, et al. (1991), Holtz, et al. (1991) and Allen, et al. (1992). The wall behaved very well. Strains

measured in the reinforcing and overall deformation were much less than expected. Consequently, a research project, of which the work presented in this dissertation is a part, was initiated to analyze the strain and deformation measurements collected from the Rainier Avenue wall. This project included interpretation of these measurements in view of the in-soil geosynthetics properties to expand our understanding of wall deformations and reinforcing strains that should be expected in GRS walls.

Current geosynthetic reinforced soil wall design procedures are based on ultimate or failure stress analysis, an approach that has been found to be very conservative (Allen, 1991; Koerner, 1990). The inherent conservativeness of these procedures was verified through the Rainier Avenue wall monitoring program (Allen, et al., 1992). Predicting wall deformations with these limit state methods has not been possible. Performance evaluation and performance based designs have been feasible only through the use of finite element analysis programs. A working stress or deformation type design approach should be more realistic than the limit state procedures, easier to use than finite element analysis, and potentially result in more economical designs. However, no such procedure is widely available or accepted. Development of such an approach would permit prediction of wall deflections, improved external stability calculations, and improved seismic stability design, especially of facings and connections. This was the ultimate goal of the research presented in this dissertation.

1.2 Thesis Overview

To develop a working stress or deformation type design procedure it is necessary to determine the appropriate geosynthetic material properties, both short- and long-term. Because the behavior of geosynthetics when confined in soil may be significantly different than when they are conventionally tested in isolation, obtaining correct and meaningful geosynthetic properties for design is not easy (McGown, et al., 1982). Numerous test methods and apparatus have been developed for obtaining these properties. A few procedures, such as pull-out tests, direct shear tests and creep tests, have gained acceptance for measuring certain geosynthetic properties and have been standardized by ASTM or the Geosynthetics Research Institute. However, obtaining the in-soil stress-strain properties of reinforcing geosynthetics with these procedures has not proven to be practicable. Consequently, a number of confined load-elongation apparatus have been developed specifically for this purpose (McGown, et al., 1982; Wu and

Arabian, 1990; Ling, et al., 1991, 1992). None of these devices has yet gained wide acceptance; however, some laboratory procedures (such as one of the available methods or a new method), are required for determining in-soil load-elongation properties of reinforcement geosynthetics.

A review of the literature determined that no existing laboratory tests satisfactorily characterized the in-soil strength properties of geosynthetics. This review identified confinement in soil, simulation of field loading conditions, and polymer creep as factors which may influence measured geosynthetic strength properties. The importance of measuring soil properties at simulated field density and confinement, and under plane strain conditions, was also emphasized in the literature. Since no single existing in-soil geosynthetic test device met all these conditions, a new plane strain unit cell test was specially constructed for this project.

Two sands, four woven geotextiles, and two nonwoven geotextiles were the focus of the unit cell testing program. Since furthering the understanding of the Rainier Avenue wall behavior was one objective of this research, one of the sands and all four geotextiles were the same as were used in the wall. Evaluation of initial tests in the unit cell device determined that the woven geotextile modulus decreased with decreasing strain rate. Creep and stress relaxation of these geotextiles was also observed, even at small stress and strain levels. To further study these mechanisms a series of in-isolation wide width tests, conducted at various strain rates, and short term creep tests on the woven geotextiles were added to this research program. In-isolation wide width tests on nonwoven geotextile specimens of various gage lengths were also added because the changing normal pressure conditions which occurred in the unit cell tests complicated determination of the in-soil modulus for these reinforcements.

A number of detailed parametric studies of reinforced soil wall behavior have been previously performed and reported in the literature. Numerous factors which influence reinforced soil retaining wall deformations and strains had been identified through these studies and their results had even been used to aid in constructing design charts for predicting wall behavior. While the influence of various parameters was quantified, none of the studies looked at the general behavior which should be expected for these walls due to geometry, loading, and boundary conditions. That is, the expected structure response had not been separated from the influences of the soil and reinforcing. Utilizing linear elastic material properties and the finite element method, a study was undertaken to identify which of the factors influencing wall deformations were functions

of the problem being evaluated (i.e., a rectangular mass subjected to loads) and not functions of the specific soil and reinforcing properties assumed.

To bring the pieces of this project together the findings of the laboratory tests and the FEM analysis were applied to the observed behavior of the Rainier Avenue wall. The research results were also used to make recommendations for determining soil and geosynthetic properties and for predicting GRS wall deformations.

1.3 Thesis Organization

The remainder of this dissertation is divided into eight chapters.

Chapter 2: The findings of a literature review of existing geosynthetic test devices and procedures are presented. Existing in-soil geosynthetic test devices are evaluated and creep characteristics of geosynthetics are discussed.

Chapter 3: The behavior of geosynthetic reinforced soil and geosynthetic reinforced soil retaining wall deformations are discussed. Methods for predicting wall deformations are reviewed.

Chapter 4: The specific objectives of this research and the scope of work are stated.

Chapter 5: The results of in-isolation tests on the geotextile reinforcements included in this program are presented.

Chapter 6: The results of in-soil load-elongation tests using the unit cell device are presented. The response of the soils, geotextiles, and reinforced soil composites are evaluated and discussed.

Chapter 7: The results of a finite element analysis of reinforced soil retaining wall behavior are presented.

Chapter 8: An evaluation of the measured behavior of the Rainier Avenue wall using the research findings discussed in Chapters 5 - 7 is presented. Recommendations are made for measuring soil and geotextile reinforcement properties for use in predicting reinforced soil retaining wall deformations. An approach for predicting deformations is recommended.

Chapter 9: Conclusions are presented and recommendations for further research are made.

Appendices: Miscellaneous items related to the dissertation have been collected in the appendices. Appendix A contains information on the Unit Cell Device, including design rationale, manufacturing drawings, instrumentation and data acquisition system, sample preparation and test procedures, and a list of suppliers of materials and instruments used for construction of the UCD or during testing. Soil property test data are included in Appendix B. Unit Cell Test results for individual tests are presented in Appendix C. Finally, Appendix D contains derivations of equations used in Chapter 7.

CHAPTER 2
LITERATURE REVIEW - GEOSYNTHETIC PROPERTIES

2.1 Stress-Strain Characterization of Geosynthetics

2.1.1 Introduction

Predicting geosynthetic reinforced soil retaining wall deformation requires an understanding of the stress-strain properties of the soil, the geosynthetic, and the composite soil-geosynthetic system. Characterization of these materials requires that some sort of test be performed in which the pertinent properties may be measured. Since geosynthetics were first used for reinforcement of soils, various methods have been developed for measuring in-isolation geosynthetic properties. However, the strength and deformation characteristics of some geosynthetics have been found to be significantly altered when they are confined in soil (McGown, et al., 1982; El-Fermaoui and Nowatzki, 1982). In-soil load-elongation (stress-strain) properties of geosynthetics are influenced by the properties of the particular soils and geosynthetics in the system as well as the confining pressures. Tests have also been conducted to define the composite reinforced soil behavior. Devices which have been utilized in attempts to determine the in-soil geosynthetic properties or the composite response are described in this section. Each apparatus is evaluated with respect to its potential applicability for determining load-elongation properties of confined geosynthetics and, when appropriate, composite behavior. These devices were typically developed to model one or more of the assumed modes of interaction between the soils and geosynthetics, Figure 2.1.

2.1.2 Full Scale and Model Walls

Full scale wall tests may be the most appropriate means of determining the true behavior of geosynthetic reinforced soil (GRS) walls since the actual conditions can be accurately reproduced. Instrumented full scale walls and steep slopes have been constructed both in the field and in laboratories (Bell and Steward, 1977; Bell, et al.,

1983; Bathurst, et al., 1988; Bathurst and Koerner, 1988; Jarrett, 1988; Fannin and Hermann, 1990; Christopher, et al. 1990; Wu, 1992d; Allen, et al., 1992). However, because of the expense of instrumenting and monitoring GRS walls very few full scale field instrumentation programs have been undertaken (Yako and Christopher, 1988).

Much of the same data collected from instrumented full scale walls may be obtained more economically from instrumented model GRS walls constructed in laboratories. Model walls are small scale GRS walls which may be loaded and monitored for response to conditions of interest, Figure 2.2. Failure mode, reinforcement strain and earth pressure data are most often reported from these tests (Bell and Steward, 1977; Fabian, 1990; Resl, 1990), although deformations may also be measured (Andrawes, et al., 1991; Chandrasekaran, 1992; Palmeira and Lanz, 1993). Because the weight of soil in the wall has been found to be responsible for much of the initial loads imparted on the reinforcings during construction of actual walls, the soil weight and reinforcing strength must be properly scaled and differences accounted for when comparing model wall test results with full scale wall behavior.

While full scale and model wall tests provide information which can be used directly in understanding expected GRS wall behavior, they are time consuming and more expensive to perform than the smaller laboratory tests presented below. Extensive instrumentation, with proper calibration, is required for measuring geosynthetic load-extension properties and soil stress and strain states. Accordingly, these tests are not ideal for routine broad based soil-geosynthetic characterization programs for selecting acceptable geosynthetics and soils during the design stages of GRS walls. It must not be forgotten, however, that any prediction of GRS wall behavior made using the results of laboratory tests must be verified by comparison with full scale GRS walls before the results are used for designing new walls.

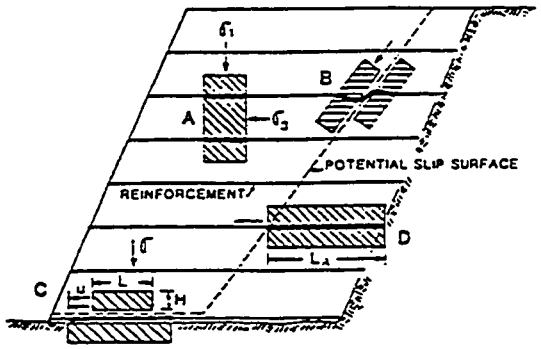

Figure 2.1: Reinforced soil failure modes (after Gourc and Beech, 1989).

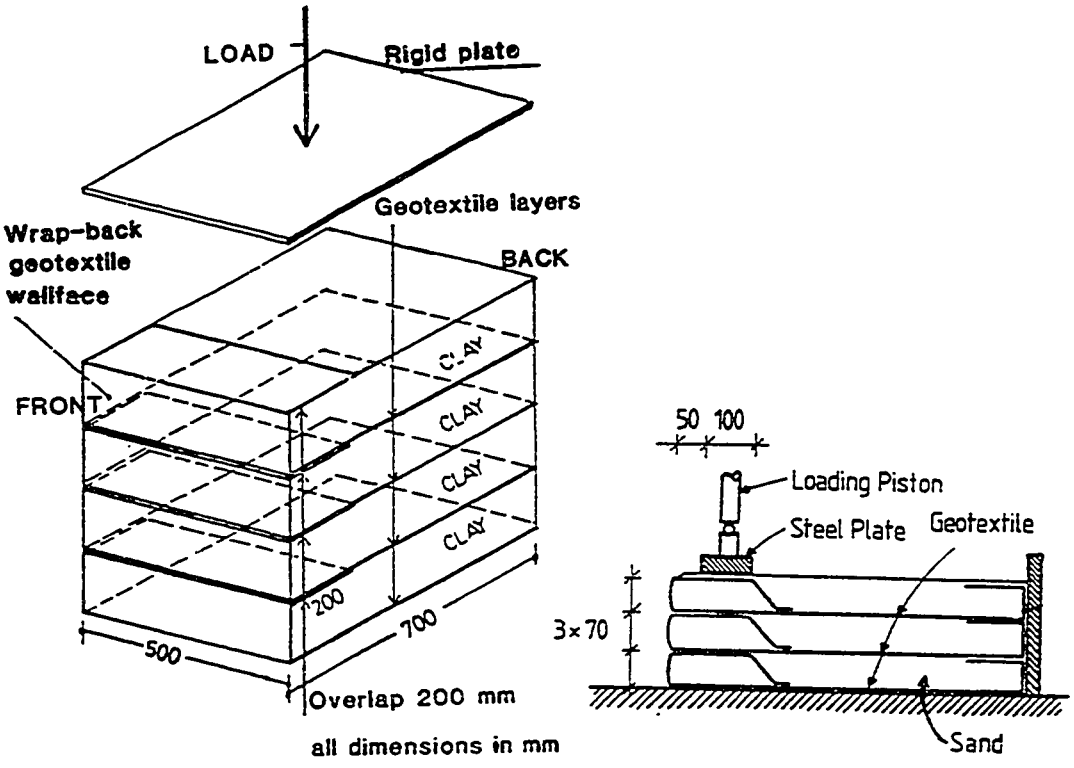

Figure 2.2: Schematic diagrams of two model walls (after Fabian, 1990; Resl, 1990).

2.1.3 Load-Elongation Test Devices

The wide width strip tensile test, ASTM D 4595 (ASTM, 1993), has become generally accepted for measuring the load-elongation properties of geosynthetics used as reinforcing in GRS systems. In this test a 100 mm long by 200 mm wide geosynthetic specimen is loaded to failure. Load and deformation data are recorded throughout the test. This method has become accepted primarily because of its relative simplicity, the minimal capital investment required, the reproducibility of test results, and because it is conducted in-isolation (i.e., specimens are not confined in soil). However, numerous researchers have shown that the strength and load-elongation properties of some geosynthetics when confined in soils differ from the properties obtained from in isolation tests (McGown, et al., 1982; El-Fermaoui and Nowatzki, 1982). The load-elongation properties may be influenced by the type of soil, its gradation and density, the confining pressure and the properties of the geosynthetic itself. Many attempts have been made to develop load-elongation test apparatus, but no device has gained wide acceptance.

McGown, et al. (1982) developed the first in-soil load-elongation test apparatus, Figure 2.3. Tests using this device showed definite increases in the initial modulus and the total strength of the geosynthetics, especially for nonwoven geotextiles, Figure 2.4. This device has been used to perform creep tests as well as short term loading tests (Andrawes, et al., 1986) and has become one of the most often cited examples of a confined in-soil tension test apparatus. Wilson-Fahmy, et al. (1993) conducted a systematic confined strength testing program using a modified version of this device, in which the specimen was oriented horizontally. The modifications were made to simplify sample preparation but did not alter the device operation. Wilson-Fahmy, et al. (1993) concluded that confined testing was warranted only for nonwoven geotextiles.

Modified direct shear devices were used by El-Fermaoui and Nowatzki (1982) and Siel, et al. (1987) to perform confined load extension tests, Figure 2.5. In both cases the specimens were laid horizontally and clamped at the back of the device. Tensile load

was applied directly to the sample via a clamp extending into the soil at the front. As was demonstrated by McGown, et al. (1982), geotextile strengths increased over in-isolation values. Necking of the geotextile specimen during load application was significant in nonwoven geotextiles tested by El-Fermaoui and Nowatzki. Leshchinsky and Field (1987) developed an analogous device but placed the geosynthetic on a lubricated rigid bottom plate instead of on soil, Figure 2.6. This modification eliminated out-of-plane bending of the geosynthetic due to settlement of soil below the sample when the normal load was applied. These tests also showed increased in-soil strengths for nonwoven geotextiles, Figure 2.7. These authors concluded that the frictional coefficient between the geotextiles and the soil did not vary significantly with confining pressure; the load-elongation properties of the confined geotextiles were influenced by confining pressure; and the failure strain was about the same regardless of confining pressure.

Christopher, et al. (1986) attempted to simulate the confining soil by using clamps with roughened surfaces and performing a "zero span" test. At the start of the test the clamps butted up against each other with a "zero span" between them. The tests showed an increase in the geosynthetic modulus in this "confined" condition when compared with unconfined (in isolation) wide width tensile tests. The test was simple to perform and required minimal capital investment but had two significant drawbacks. First, as the load was applied the clamps moved apart, deforming the geosynthetic. The portion of the sample between the clamps became unconfined and the test no longer modeled the conditions under which it started. Second, interpretation of the significance of the test proved difficult, especially with regard to the proper gauge length to use for strain calculations (B.R. Christopher, 1991, personal communication).

Wu and Arabian (1990) used a modified triaxial apparatus to apply tensile loads to a rectangular geosynthetic sample confined in a cylindrical column of soil, Figure 2.8. The soil and geosynthetic elongated vertically when the reinforcing was subjected to tension. The tensile force in the geosynthetic was measured via a load cell at one end of the device and was assumed to be constant along the length of the sample. The test was

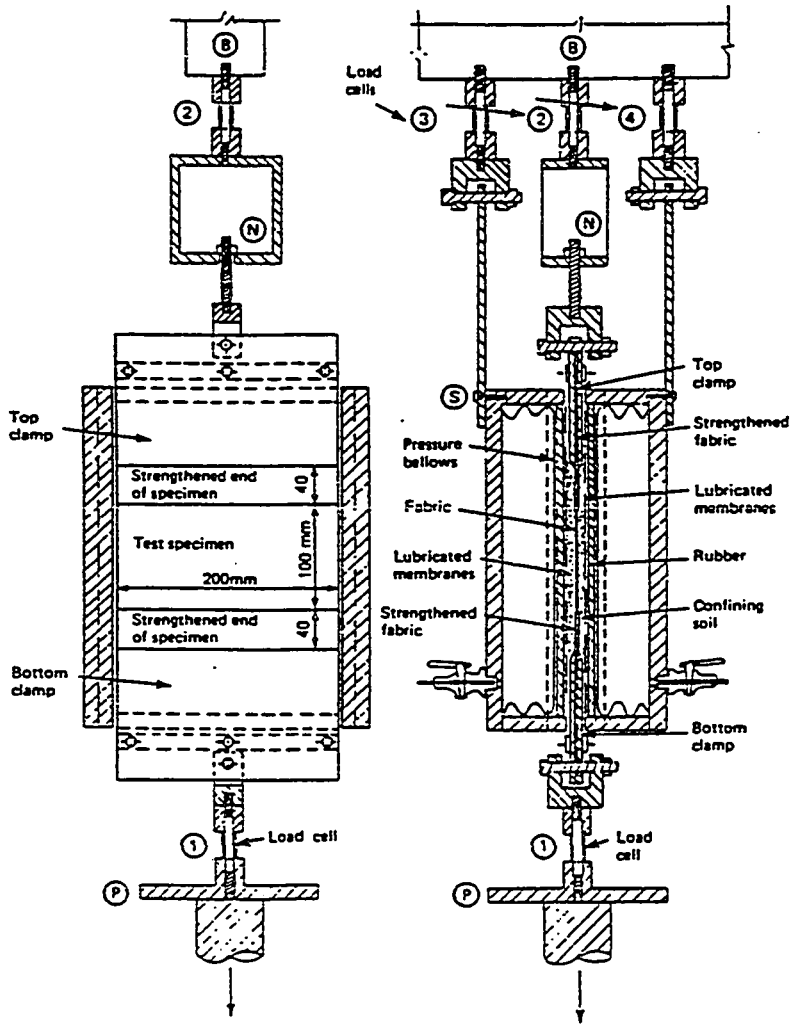

Figure 2.3: In-soil load-elongation test apparatus (after McGown, et al., 1982).

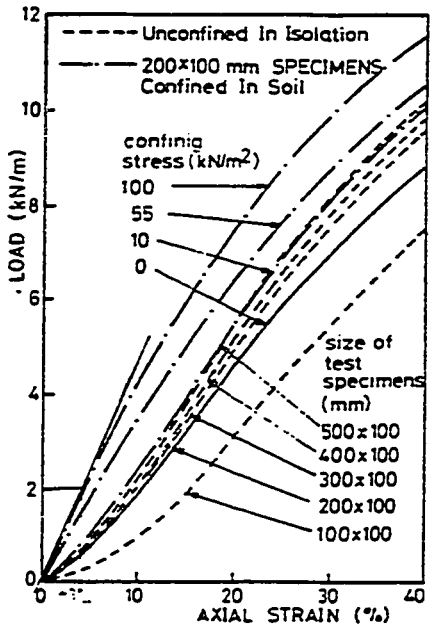

Figure 2.4: In-isolation and in-soil load-elongation data for a nonwoven needle-punched goetextile (after McGown, et al., 1982).

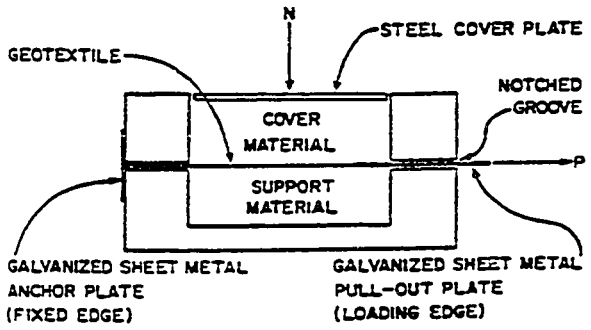

Figure 2.5: Modified direct shear device for in-soil load-elongation testing (after El-Fermaoui and Nowatzki, 1982).

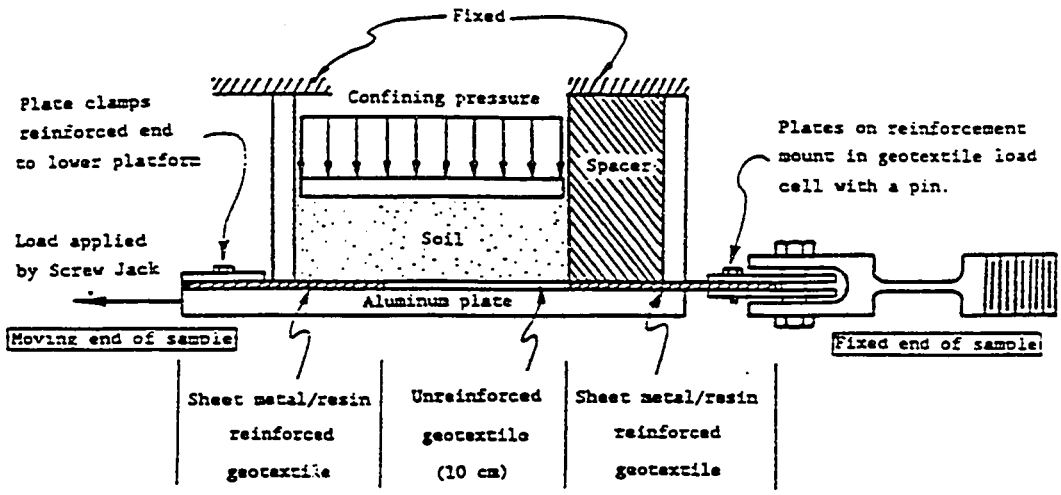

Figure 2.6: Modified direct shear device for in-soil load-elongation testing (after Leshchinsky and Field, 1987).

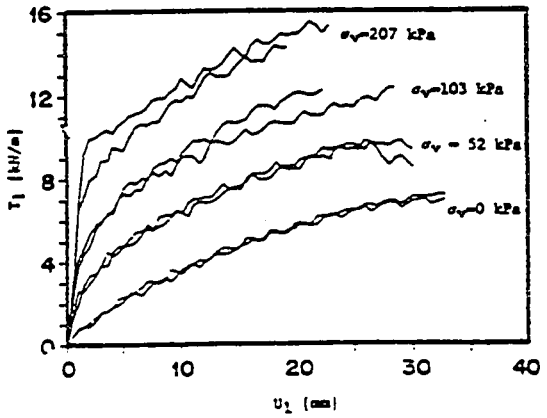

Figure 2.7: Load-displacement curves for a nonwoven geotextile for various confining pressures (after Leshchinsky and Field, 1987).

reported to provide conservative and repeatable results. This test is appealing since it uses available geotechnical laboratory equipment. Installation of a load cell to measure the geosynthetic load experienced at the base and attachment of displacement measurement instruments along the sample may improve this device. The non-uniform confinement condition resulting from radial application of pressure to the cylindrical confining soil increases the complexity of interpreting the data obtained from this test and precludes direct correlation between the results and field observations. Modification of the shape of the confining soil to a rectangular section may also improve interpretation of data from this device.

Ling, et al. (1991, 1992) reported on the results of a confined load-elongation device in which the geosynthetic was loaded by applying tension to both ends and permitting the soil to move with the geosynthetic, Figure 2.9. This test differs from the tests by McGown, et al. (1982) in which the soil remained stationary, although similar results were obtained (i.e., nonwoven geotextiles tested under confinement showed an increase in initial modulus and total strength). The strain at failure for both confined and in isolation tests was essentially identical. Ling, et al. concluded the device was appropriate for load-elongation tests of geosynthetics confined in soil and in isolation. In fact, using only a membrane for confinement, with no soil between the membrane and sample, produced results essentially identical to those where 8 mm of soil separated the membrane and geosynthetic, Figure 2.10. The similarity between the results obtained using only a membrane for confinement and using soil for confinement suggest that confinement and confining pressure on geotextiles, not the interaction of the soil with the geosynthetic, may be the major factor influencing the apparent increase in initial modulus and total strength of the geosynthetic. An alternate interpretation might suggest that boundary effects introduced by this particular device may be significant. The similarity between data recorded with and without the 8 mm of soil cover could be a result of membrane effects dominating the response even when the thin soil layer is utilized. These possibilities should be investigated further.

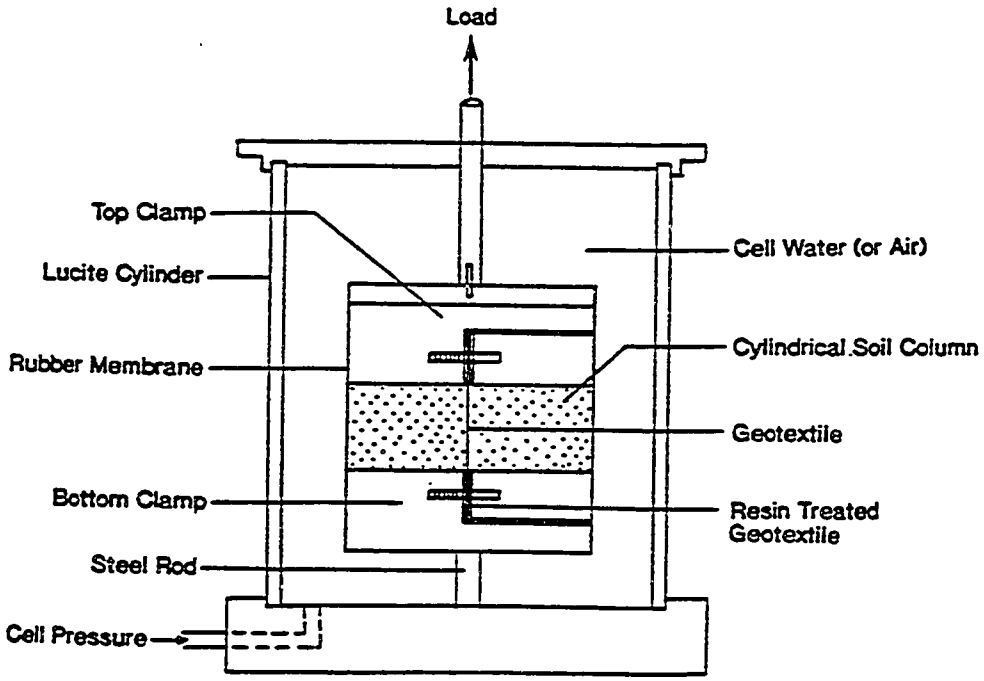

Figure 2.8: In-soil load-elongation apparatus (after Wu and Arabian, 1990).

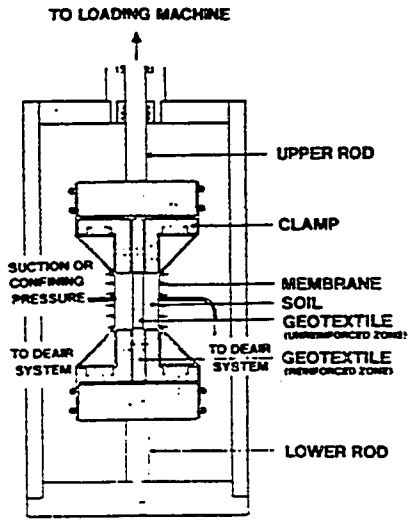

Figure 2.9: In-soil load-elongation apparatus (after Ling, et al., 1992).

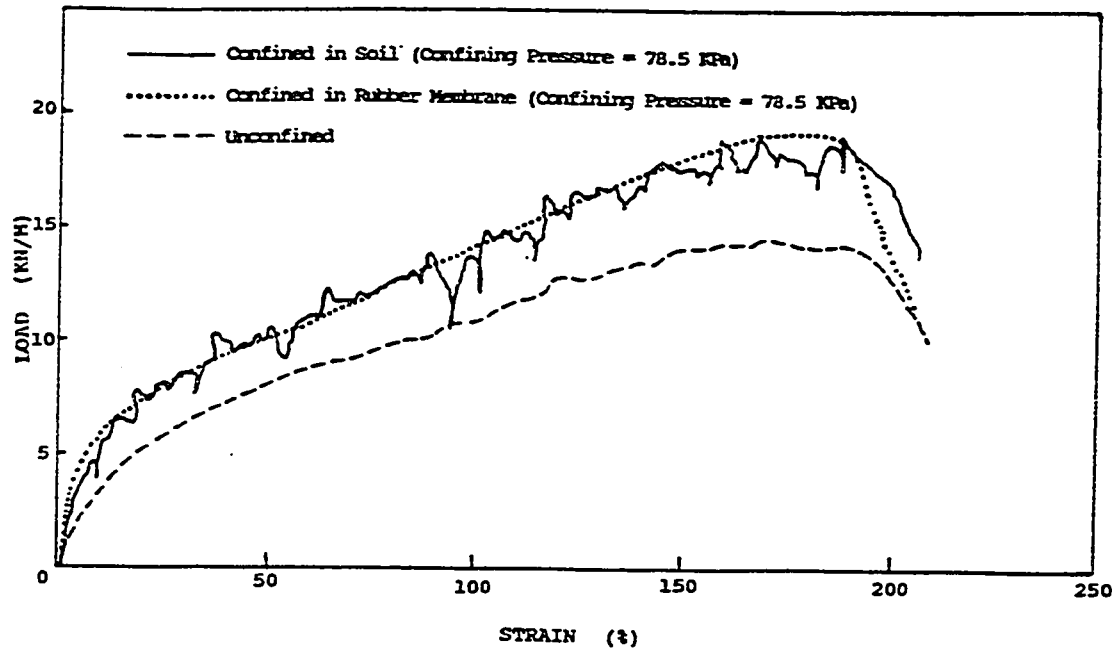

Figure 2.10: Load-elongation relationships of a spun-bonded nonwoven geotextile (after Ling, et al., 1992).

Wu (1991) presented a discussion of the individual in-soil load-elongation devices reviewed in this section and the assumed stress distributions in the geosynthetics. He stated that during deformation of GRS walls, failure of the frictional contact between the soil and geosynthetic does not occur. Wu discounted the modified direct shear type devices and the McGown device as not modeling the conditions which exist in the field because in actual installations "until a 'failure condition' is approached, the geotextile deforms essentially 'with' the confining soil without relative movement at the interface. Consequently, using such test methods, which hold the confining soil stationary and enforce mobilization of adhesive resistance at the interface as the geotextile deforms, is not simulating the predominant operational condition of the geotextile in most geotextile-reinforced structures." (Wu, 1991)

Wu (1991) contends that the devices presented by Wu and Arabian (1990) and Ling, et al. (1992) better simulate the operational, pre-failure condition of extensible

geotextiles, where there is little relative movement between the geotextile and the confining soil. The deformation may in fact be a combination of mechanisms dependent upon the soil properties, the soil-geosynthetic interface friction capacity, the maximum deformation experienced, and the strain compatibility of the soil and geosynthetic. Furthermore, the variation in load-elongation properties, measured using these methods, may not be significant at low strains (less than 5%) apparently experienced by GRS walls under working loads. The magnitude of the difference for the measured in-soil properties cannot be determined without a program in which a direct comparison is made of the test results using the various devices with the same soil and geosynthetic.

With the possible exception of the Wu and Arabian (1990) in-soil load-elongation apparatus, Figure 2.8, only very thin soil layers were placed on either side of the geotextiles in the in-soil tests reviewed in this section, e.g., 10 mm for McGown, et al. (1982), 8 mm for Ling, et al. (1992). The inability of these tests to reproduce the field densities and gradations for the confining soil raises questions concerning the accuracy of the results obtained, particularly with either the McGown, et al. or Ling, et al. devices. Moreover, all of the load-elongation devices discussed directly induce load into the reinforcing via clamps attached at each end of the sample. Loading of the reinforcing by interaction of the confining soil and the geosynthetic is not simulated in these tests, Figure 2.1 (mode A). However, at low strains, the load-elongation properties measured in a test with confining soil of the same gradation and density as experienced in the field may not be significantly different than the results obtained when using the test methods presented in this section. Thus, although the ability of the devices to model the soil-geosynthetic interaction may be in question, the ability of the tests to determine in-soil properties of the geosynthetic may not be adversely affected at low strain. Again, further study is required.

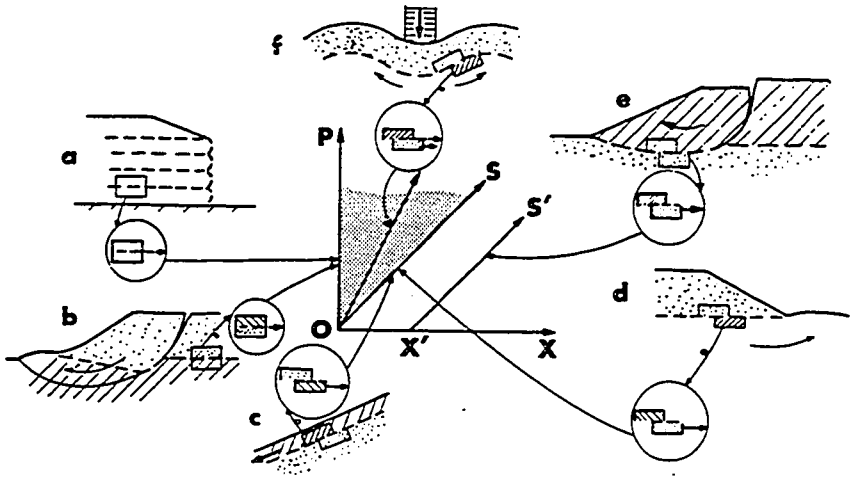

Figure 2.11: Typical soil-geotextile kinematics in the field (after Collios, et al., 1980).

2.1.4 Pull-out Test Devices

Collios, et al. (1980) identified the pull-out and direct shear tests as the most appropriate for modeling the failure mechanisms observed in GRS systems, Figure 2.11. The pull-out test was indicated as the most appropriate for GRS walls (Figure 2.1 mode D) and it has since become popular for determining soil-reinforcing interaction for all types of extensible and inextensible reinforcements. Diagrams of two pull-out box arrangements are shown in Figures 2.12 and 2.13. Juran, et al. (1988) and Rao and Pandey (1988) state that the conditions under which pull-out tests are performed are more representative of field conditions than direct shear tests, and should therefore be used to determine the frictional soil-geosynthetic interaction properties for GRS embankments. Unfortunately, pull-out test devices tend to be relatively large and require significant effort to prepare samples for testing, making them both costly and time consuming.

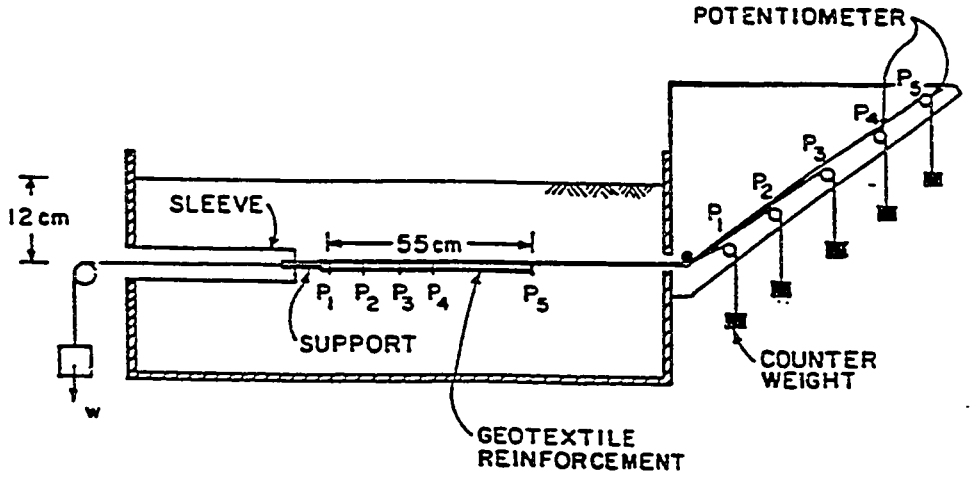

Figure 2.12: Schematic of pull-out box with instrumentation (after Juran and Chen, 1988).

A number of studies have been performed to identify the factors which affect the results of pullout tests and to isolate test apparatus boundary effects (Juran, et al., 1988; Palmeira and Milligan, 1989; Farrag, 1990). These studies conclude that boundary effects may be significant in pull-out tests and identify methods which may be used to reduce the boundary influence. Juran, et al. (1988) present an extensive qualitative discussion on the many soil, geosynthetic and device parameters which may influence test results. Farrag (1990) provides recommendations as to specific dimensions, loading rates, etc. Farrag further recommends a standard device and procedure be established for performing pull-out tests so results may be reproduced in different laboratories. The Geosynthetic Research Institute has proposed standard test methods, GG5, Geogrid Pullout, and GT6, Geotextile Pullout, that incorporate many of these recommendations (Geosynthetics Research Institute, 1991b, 1992b).

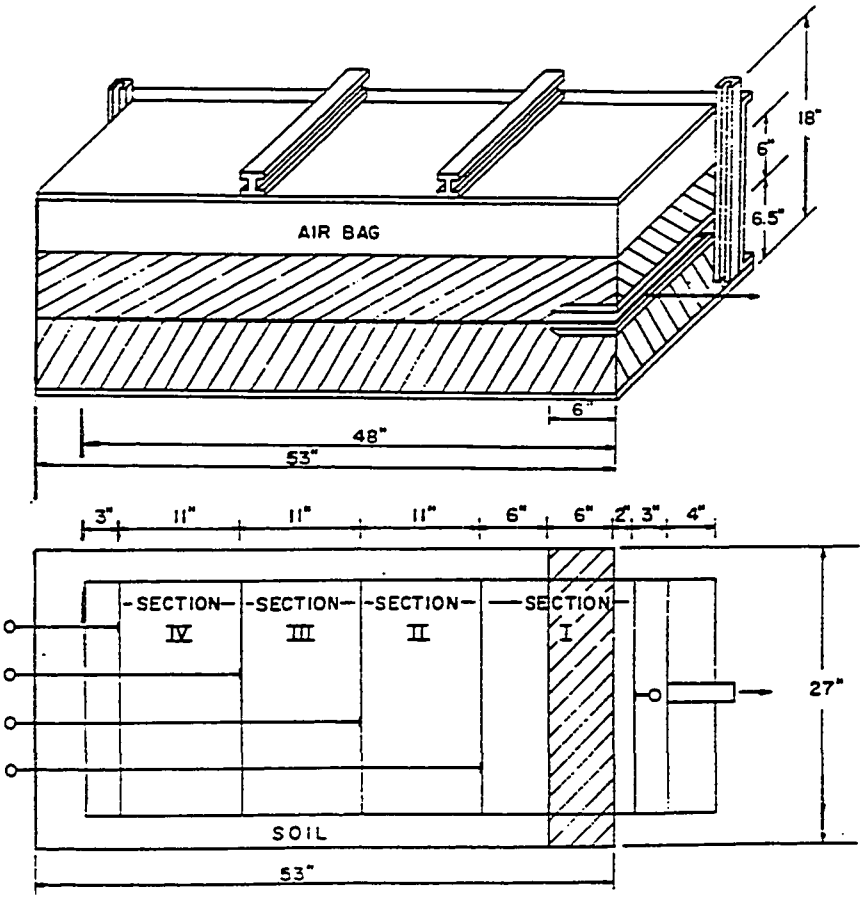

Figure 2.13: Cross-section and plan view of pull-out box (after Bonczkiewicz, et al., 1988).

Pull-out devices were initially developed to determine the soil-geosynthetic friction interface properties and the potential for the reinforcing to pull out of the backfill. They have proven successful for this application. Determination of load-extension properties of geosynthetics confined in soils has also been attempted with these devices, but has been less successful. In either case, pull-out test results on extensible reinforcements have been found to be difficult to interpret (Palmeira and Milligan, 1989; Juran and Chen, 1988; Juran, et al., 1988; Farrag, 1990). The difficulty is primarily a function of the nonuniform stress distribution over the length of the reinforcing. "When a pulling force is applied to the geotextile specimen, the movement initiates at the clamped-end and gradually propagates toward the free-end as the force increases. The deformation of the geotextile is the largest at the clamped-end and becomes smaller toward the free-end. The rate of reduction in deformation increases as the force increases" (Tzong and Cheng-Kuang, 1987). Figure 2.14 illustrates the variation in displacement of points on the reinforcing during a typical test.

Determination of soil-geosynthetic interface friction is complicated because the large displacements cause soil particles to rotate so their surfaces are aligned with the moving sample, resulting in lower friction values (Collios, et al., 1980). The differences in the displacement of the reinforcing results in nonuniform interface friction along the length of the reinforcing until a minimum movement has occurred along the entire specimen length (Holtz, 1977). This nonuniformity increases the difficulty involved in quantifying the soil geosynthetic interface friction. Juran, et al. (1988) discuss other factors which may influence the distribution of shear force development. They summarize by stating: "the concept of a uniformly mobilized limit interface shear is not appropriate for interpreting the results of pull-out tests on extensible reinforcements. An appropriate load transfer model is therefore needed to determine the relevant interaction design parameters."

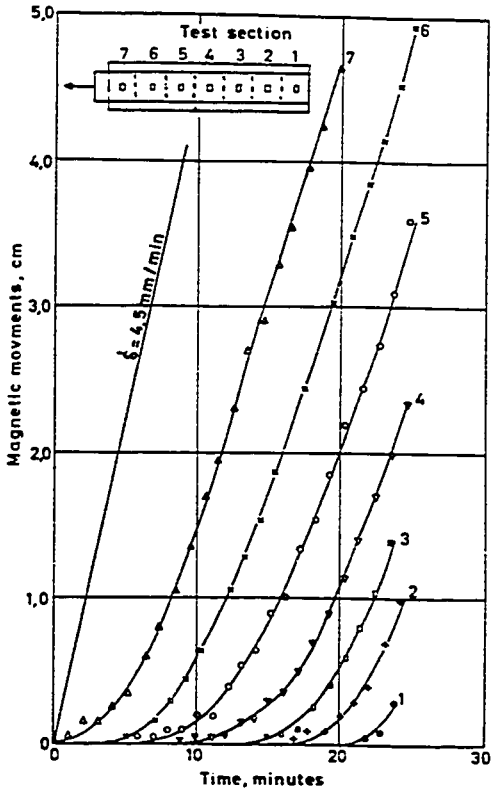

Figure 2.14: Variation of displacement with time during typical pullout test on a high strength polyester geotextile (after Holtz, 1977).

Methods for interpretation of load-elongation properties have been presented by Holtz (1977), Collios, et al. (1980), Salomone, et al. (1980), Bonczkiewicz, et al. (1988) and Juran and Chen (1988). Juran and Chen (1988) conclude that "the effect of extensibility on the shear stress distribution and the front edge displacements raises major difficulties with regard to current use of pull-out tests on extensible reinforcements to obtain relevant interaction design parameters." Nonetheless, they do develop two mathematical models and provide suggestions for using pull-out test results to predict reinforcement response.

From this review the conclusion may be reached that significant experience may be required to predict soil-geosynthetic interface properties or geosynthetic in-soil load-elongation properties utilizing pull-out tests. Although pull-out tests may continue to be utilized for failure prediction, they are of questionable use as practical laboratory tests for load-elongation characterization of geosynthetics confined in soil because the in-soil load-elongation properties of the geosynthetics are required for interpretation of the pull-out test results.

2.1.5 Direct Shear Test Devices

The direct shear test, with the reinforcing oriented parallel to and at the shear plane, may be the simplest test to perform and interpret. In many cases, soil laboratory direct shear devices may be modified to perform soil-geosynthetic interface friction tests. The results of direct shear tests have most often been reported in terms of an efficiency factor, $\tan\delta/\tan\phi$. Efficiency factors for direct shear tests have been reported to typically fall in the range 0.60 to 1.00 (Richards and Scott, 1985; Juran, et. al., 1988; Takasumi, et al., 1991). Collios, et al. (1980) measured efficiency factors as high as 1.16 when the diameter of the openings in the geosynthetic exceeded the soil particle size and the failure surface was forced to occur at the contact of the soil with the reinforcing. However, Collios, et al. warn that when a contact efficiency greater than 1.00 occurs, an actual system would fail in the soil and thus factors greater than 1.00 should not be used for design purposes. The aforementioned papers also present the results of comprehensive investigations of the factors which affect the contact efficiency of the soil and geosynthetic. The most influential characteristics were reported to be the ratio of soil particle size to geosynthetic opening size, the soil gradation, the density of the soil and the type of geosynthetic (woven, nonwoven, geonet, geogrid, etc.). Juran, et al. and Richards and Scott also investigated the effects of the style of the direct shear devices on the results, Figure 2.15. Both studies concluded that maintaining a constant shear surface area during the tests produced more repeatable results.

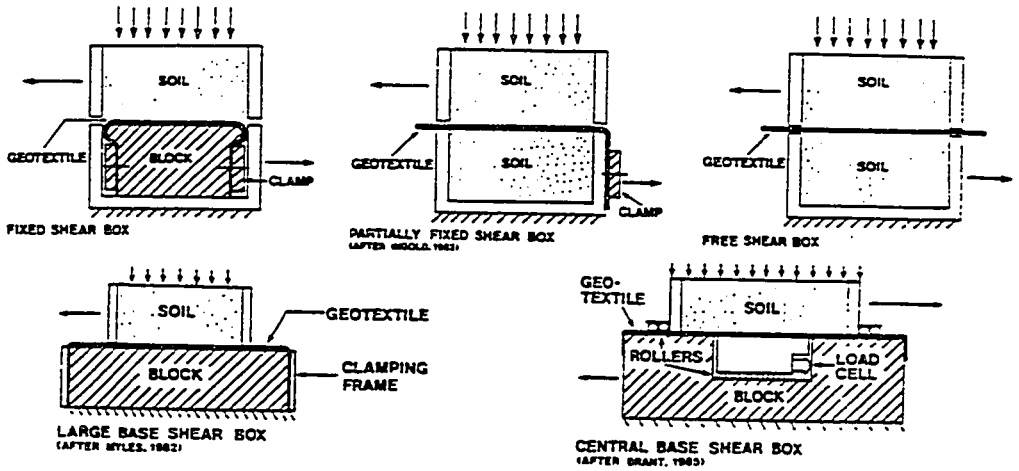

Figure 2.15: Various arrangements of direct shear geosynthetic test apparatus (after Richards and Scott, 1985).

Use of the direct shear device has not proven successful for determination of in-soil load-elongation properties. However, it has been shown to be practical for determination of soil-geosynthetic interface friction properties, and it models an important mode of soil-geosynthetic interaction which must be quantified, Figure 2.1 (mode C) and Figure 2.11. ASTM method D 5321 (ASTM, 1993) has been developed to standardize the testing of soil-geosynthetic and geosynthetic-geosynthetic interface friction using a direct shear device.

Direct shear tests, with the reinforcing crossing the shear plane, have also been performed (Gray and Ohashi, 1983; Athanasopoulos, et al., 1990; Chen and Lee, 1990), Figure 2.1 (mode B). The orientation of the reinforcing with respect to the failure plane has been shown to significantly influence the strength of the sample. It has also been shown that the most efficient use of reinforcement is to orient it in the direction of

maximum tensile strain in the soil mass (McGown, et al., 1978; Gray and Ohashi, 1983; Chen and Lee, 1990). These tests have not been shown to be applicable to advancing our understanding of soil-geosynthetic load-elongation properties. They may, however, prove appropriate in developing the full understanding of GRS retaining wall deformation and/or failure mechanisms.

2.1.6 Cylindrical Triaxial Test Devices

A number of researchers have investigated the response of cylindrical samples of soil reinforced with horizontal layers of geosynthetics (Broms, 1977, 1988; Holtz, et al., 1982; Mandal, 1986; Chandrasekaran, et al., 1989; Futaki, et al., 1990). In each study the introduction of geosynthetic reinforcing increased the ultimate strength of the soil specimens beyond that of unreinforced specimens subject to the same test conditions, Figure 2.16. Chandrasekaran, et al. and Futaki, et al. presented deformation data for the reinforcing and soil and made general conclusions regarding the influence of reinforcing strength, stiffness, and spacing on the behavior of the soil. The axisymmetric strain introduced into the reinforcing increases the difficulty in correlating results to the plane strain conditions experienced in GRS walls. Furthermore, not utilizing the directional nature of the reinforcing elements may invalidate the results obtained when woven geotextiles or geogrids are tested. The information presented in the referenced papers is primarily qualitative and has not been utilized for load-elongation prediction.

2.1.7 Hollow Cylinder Extension Test

Shen, et al. (1988) developed a hollow cylindrical triaxial extension test in which a hollow cylinder of geosynthetic was sandwiched between two 14 mm thick layers of soil, Figure 2.17. By increasing the radial confining pressures on the soil, the geosynthetic would elongate vertically, parallel to the axis of the cylinder. The test attempted to model plane strain conditions for the reinforcing. The sample length

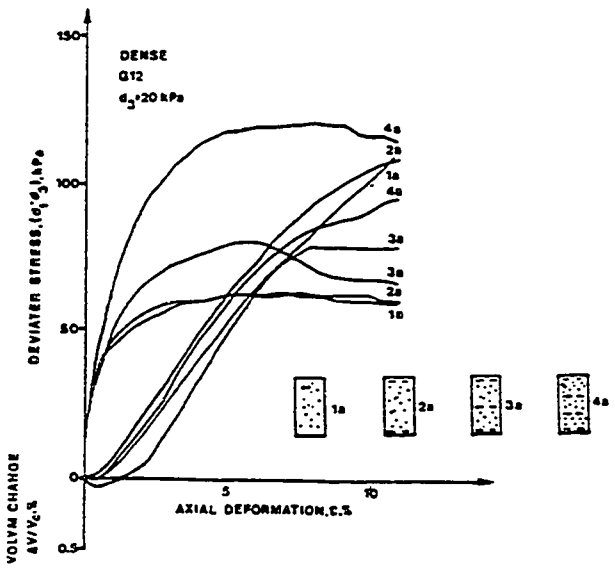

Figure 2.16: Results of test on horizontally reinforced cylindrical specimen (after Broms, 1977).

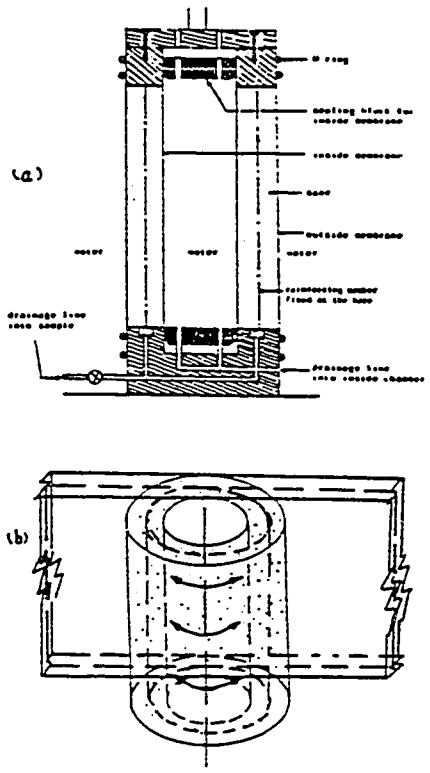

Figure 2.17: Hollow cylinder extension test (after Shen, et al., 1988).

required for the geosynthetic and soil to elongate without relative slippage was determined. The soil was said to be "pushing" on the geosynthetic to introduce load, as opposed to pulling directly on the geosynthetic as is done in pull-out and in-soil load elongation tests.

Direct measurement of loads in the reinforcing in the hollow cylinder extension tests was not performed but would be required for true load-extension relationships to be developed. The difficulty in preparing the samples makes this test less than desirable. Although this test may provide satisfactory empirical strength data, gaining acceptance of this test from practitioners may prove difficult since it does not physically resemble field installations of GRS.

2.1.8 Plane Strain Tests

A plane strain unit cell device that models the horizontal deformation which results from vertical overburden pressures within the reinforced soil wall (Figure 2.1 mode A) may be used for characterizing not only the geosynthetic but also the composite response. (McGown and Andrawes, 1977; McGown, et al., 1978; Fabian, 1990; Ling, 1992; Ling and Tatsuoka, 1994; Helwany and Wu, 1993). Romstad, et al. (1976) defined a unit cell as a fundamental building block which can be isolated from a material that has a regular reinforcing pattern and which completely exhibits the composite characteristics of the material. Romstad, et al. and Shen, et al. (1976) used the unit cell to investigate, on a theoretical basis, soils reinforced with inextensible steel straps, but they did not conduct unit cell tests.

The plane strain unit cell, postulated by Hausmann (1976) and Hausmann and Lee (1976) and later constructed by McGown and Andrawes (1977), McGown, et al. (1978) and by Ling (1992), was deformed laterally due to application of a vertical surcharge, Figure 2.18a. Load was induced in the reinforcement solely through frictional shear forces which develop at the soil-reinforcing contact. Shear stress developed along the length of the reinforcing, decreasing from the periphery to the center, Figure 2.18b. The

strain in the reinforcing peaked in the center of the cell and decreased towards the ends, Figure 2.18c. The nonuniform shear stress distribution and reinforcement strain complicate the evaluation of test results, and the inability to directly measure the force in the reinforcing at the center of the sample precludes identification of the true load-elongation properties of the reinforcing. However because this type of device permits duplication of soil gradations and densities, as well as deformation under plane strain conditions predominant within a reinforced soil wall, the stress-strain behavior of reinforced-soil may be obtained and the influence of soil and reinforcing evaluated.

McGown and Andrawes and their coworkers constructed a unit cell device to physically test the effect of inclusion (reinforcement) properties on the behavior of sand (McGown and Andrawes, 1977; McGown, et al., 1978). This device was also used to measure the effect of the orientation of the geosynthetic reinforcing on the strength of the geosynthetic reinforced soil. The tests showed that inclusion of tensile reinforcement made soils more ductile. Orienting the inclusions in the direction of maximum tensile strain provided the greatest benefit. Note that positioning the geosynthetic in any location other than at midheight and parallel to the top and bottom of the device violates the principle of the unit cell. No direct measurement of the load in the reinforcement was made.

Ling (1992) conducted plane strain deformation tests using clays reinforced with various geosynthetics, Figure 2.19. With this device Ling was able to investigate both drained and undrained response of reinforced clay specimens subjected to a constant rate of vertical strain. The device was operated using a sophisticated automated control system capable of following specified stress paths. No direct measurements of the load induced in the reinforcement were made during the tests. Drained, partially drained, and undrained tests on reinforced and unreinforced clays were performed with this device. Initial consolidation of the clay resulted in a shortening of the reinforcement from its initially placed, "zero strain" position. When vertical loads were applied the reinforced

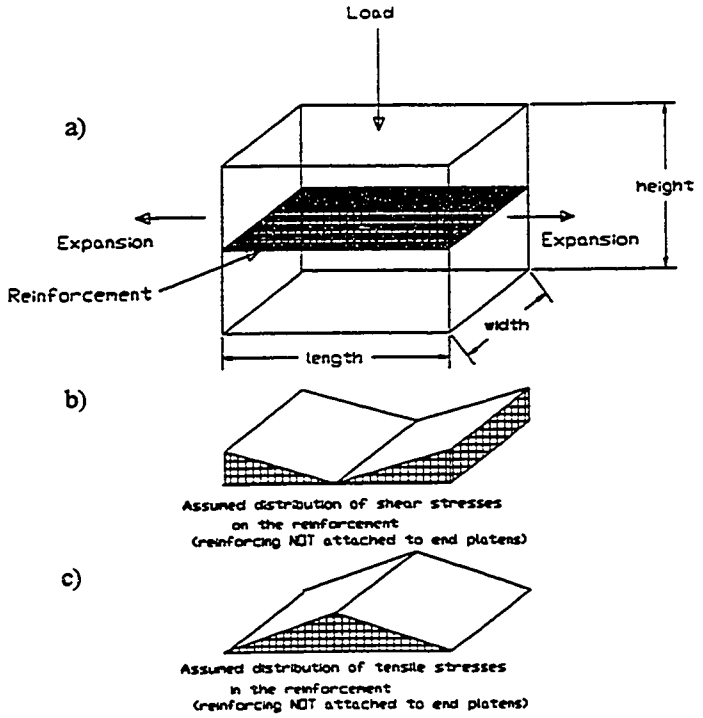

Figure 2.18: a) Unit cell; b) assumed distribution of shear stresses on reinforcement; c) assumed distribution of tensile stresses in reinforcement (after Hausmann, 1990).

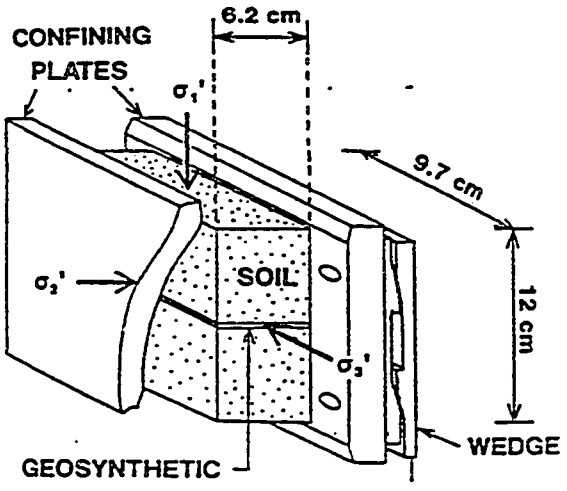

Figure 2.19: Plane strain unit cell apparatus (after Ling, 1992).

specimen first had to deform until the geosynthetic elongated back through the "zero strain" position before tensile loads developed in the reinforcing. Thus, only measurements made after passing though this "zero strain" position indicated the response of reinforced clay.

Helwany and Wu (1993) developed a plane strain device in which, to ensure strain compatibility of the soil and geosynthetic, the reinforcing was attached to each end of the apparatus in the direction of lateral strain. Loading the soil induced strain in the reinforcing due to lateral strain of the specimen which resulted from the Poisson effect. Creep tests were performed on reinforced sand and reinforced clay specimens subjected to sustained constant load. Helwany and Wu concluded that both creep characteristics and the interaction of the soil and reinforcing affected the long term deformation of the composite but provided little additional information. As with the McGown, et al. (1978) and Ling (1992) devices, no direct measurements of the load induced in the reinforcement were made during the tests.

A different style plane strain device has been used to evaluate the in-soil properties of geosynthetic reinforcings, Figure 2.20. The device developed by Whittle, et al. (1993), the Automated Plane Strain Reinforcement cell is quite ingenious with regards to load application and control and solves part of the problem with measuring load in the geosynthetic in plane strain tests. A clamp connected to the non-moving end of the geosynthetic permitted direct measurement of peak reinforcing load. The device is primarily intended to permit determination of shear stress distribution and load transfer properties, not reinforcement strength properties, through measurement of strain along the length of the reinforcement. Only limited data from tests using this device have been published.

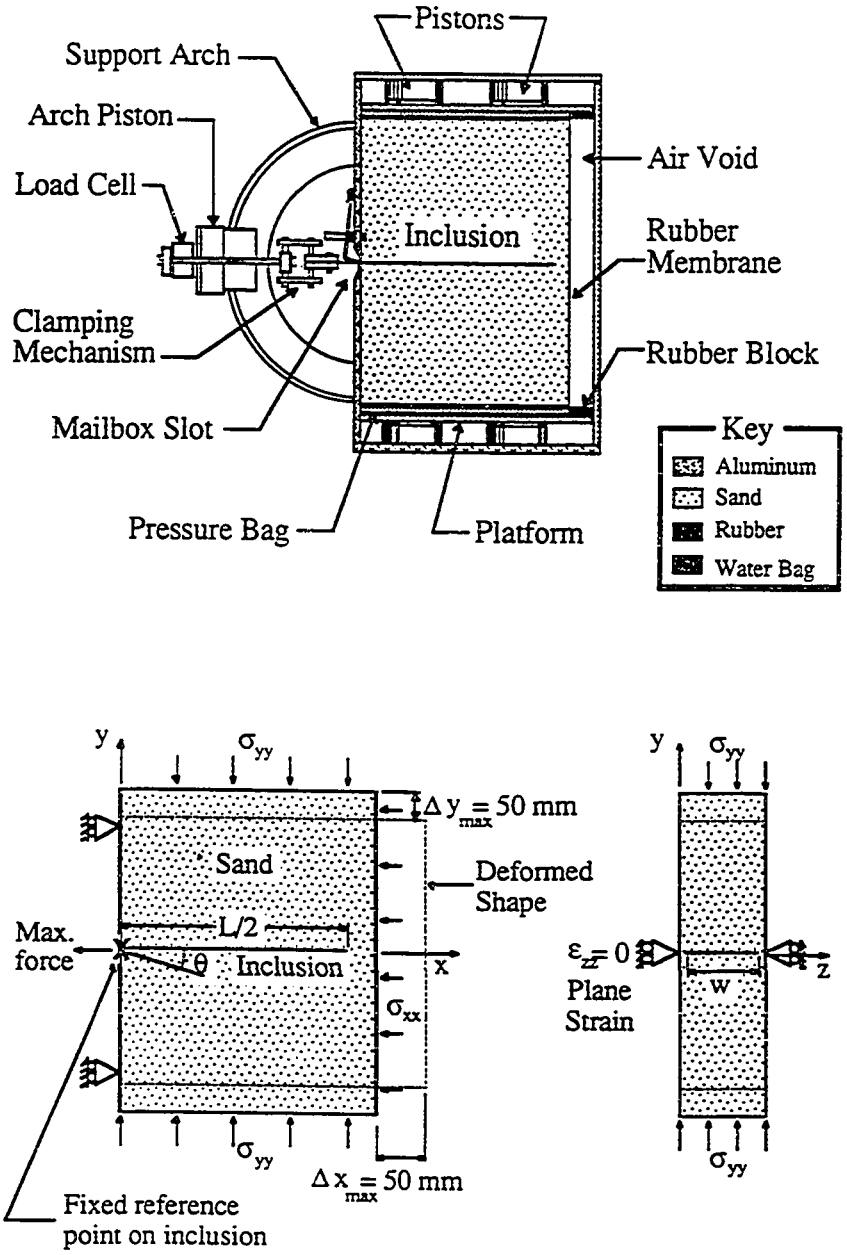

Figure 2.20: Automated Plane Strain Reinforcement cell (after Whittle, et al., 1992).

2.1.9 Summary

A variety of in-soil geosynthetic test apparatus have been developed and reported in the literature. Some of the devices were originally developed for the prediction of failure conditions and may not model the mechanisms acting in GRS walls under working loads. Others were developed to advance the qualitative, rather than quantitative, understanding of GRS behavior. Because there are many modes of soil-geosynthetic interaction which exist in GRS walls and other GRS structures, it may be necessary to develop multiple and distinct test procedures for characterization of the various mechanisms at work in these systems. None of the existing test methods has been universally accepted for determination of in-soil geosynthetic load-elongation properties or for soil-geosynthetic composite behavior characterization: soil gradation and densities could not be reproduced using the existing load-elongation devices; pull-out tests were found to be difficult to interpret; direct shear tests do not measure load-extension properties; and the unit cell tests did not directly measure reinforcing loads. The plane strain test apparatus developed by Whittle, et al. (1993) does permit measurement of reinforcing loads but insufficient information was available to properly assess this device.

Of the test apparatus reviewed, a unit cell device was thought to be the most appropriate device for measuring in-soil behavior of geosynthetics because the soil-geosynthetic interaction mechanism and mode of deformation for the reinforced soil within the wall is modeled. Furthermore, soil densities and gradations used in field applications can be reproduced in such a device. A unit cell device similar to those reviewed in Section 2.1.6 but modified to permit direct measurement of the reinforcing loads would overcome the greatest short-coming of these devices. Such a device would permit determination of both in-soil geosynthetic strength properties and composite reinforced-soil behavior. Based upon this review a Unit Cell Device (UCD), modified to permit direct measurement of reinforcing tensile loads, was designed and manufactured for this project. This device and the accompanying testing program are described in Chapter 6 and Appendix A.

2.2 Creep of Geosynthetics

2.2.1 Introduction

Long term deformation of GRS walls and other GRS structures depends on the long term stress-strain properties, and/or the creep potential, of the geosynthetics. Creep refers to the continued elongation of materials under sustained constant load. The polymers most commonly used for fabrication of geosynthetics (polyester, polypropylene, and polyethylene) have been shown to be susceptible to creep. The creep rate and total creep which can be expected for a geosynthetic are functions of the polymer, manufacturing process for the polymer, structure and manufacturing process for the geosynthetic, strain (applied load), temperature, and time. This potential for creep is one of the major difficulties with using geosynthetics in critical and permanent applications. Any design procedure which attempts to address long term safety or deformation of GRS structures, must consider creep. Without understanding and allowing for creep in geosynthetics, their use in permanent applications will continue to be restricted (Fannin and Hermann, 1989; McGown, et al., 1989; Allen and Holtz, 1991; Allen, 1991; Rimoldi and Montanelli, 1993).

2.2.2 Creep Testing

Laboratory tests to determine creep characteristics of geosynthetics have been performed and standard procedures developed (Andrawes, et al., 1986; Geosynthetics Research Institute, 1991a, 1992a; Rimoldi and Montanelli, 1993). Just as confinement has been found to affect short term strength properties of geosynthetics (See Section 2.1), confinement has also been found to affect geosynthetic creep, Figure 2.21. Creep testing of geosynthetics should, therefore, be conducted under confinement when appropriate (Holtz, et al., 1982; Andrawes, et al., 1986). In creep tests, a geosynthetic specimen is clamped at both ends and a constant load applied. Figure 2.22. Specimen deformation is

measured immediately after loading and at intervals thereafter. A standard wide width test procedure, ASTM D 5262 (ASTM, 1993), has been developed for evaluating the in-isolation tension creep behavior of geosynthetics.

Creep studies tend to concentrate on three controllable parameters which have been shown to affect creep: temperature, initial load (as a percent of ultimate load), and initial strain. The initial applied load, and resulting initial strain, are easily controlled variables. Depending upon the properties of the polymer from which the geosynthetic is constructed, even very low initial loads and initial strains may result in substantial creep over time, Figure 2.23. Polyester geosynthetics have been found to have fairly low creep potential, whereas geosynthetics manufactured with polypropylene and polyethylene are much more susceptible to creep.

Increases in temperature result in increases in the creep rate and decreases in the strength and modulus, Figure 2.24 (Andrawes, et al., 1986; Rimoldi and Montanelli, 1993). Creep tests must therefore be performed in temperature controlled environments. ASTM D 5262 (ASTM 1993) specifies the temperature be maintained at 21°C ± 2°C. When using creep data for GRS design, the temperature at which the creep tests were performed and the anticipated ambient temperature of the proposed GRS structure must be known if the effect of temperature is to be properly considered.

Creep test data have typically been presented graphically by plotting strain or load versus time or via isochronous curves on figures of load versus strain, Figure 2.25. Plotting time on a logarithmic scale has been used to aid in extrapolation to times much greater than the actual testing period. Extrapolation beyond one log cycle of time is not recommended (Andrawes, et al., 1986). Herein lies one of the greatest problems with prediction of long term strain. For permanent structures with anticipated useful lives of 50 to 120 years, test data extending over periods of 50,000 to 100,000 hours would be required. Because this type of data is not available, substantial safety factors are recommended for use in GRS design procedures (Allen, 1991). Allen (1991) and Rimoldi and Montanelli (1993) advocate using an understanding of the temperature

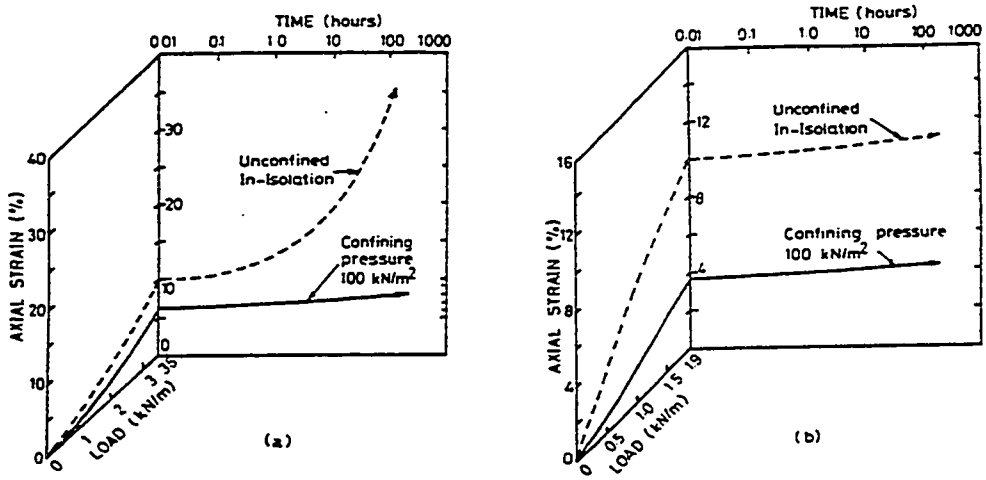

Figure 2.21: Creep test curves for geotextiles in-isolation and in confinement: a) nonwoven melt-bonded polypropylene; b) nonwoven needle-punched polyester (after McGown, et al., 1982).

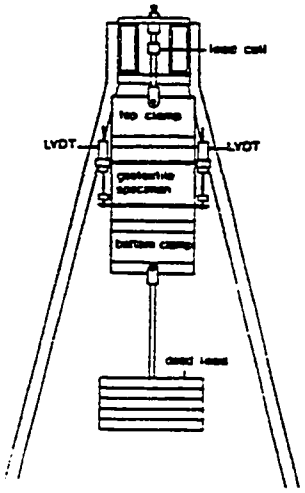

Figure 2.22: Creep test apparatus (after Andrawes, et al., 1986).

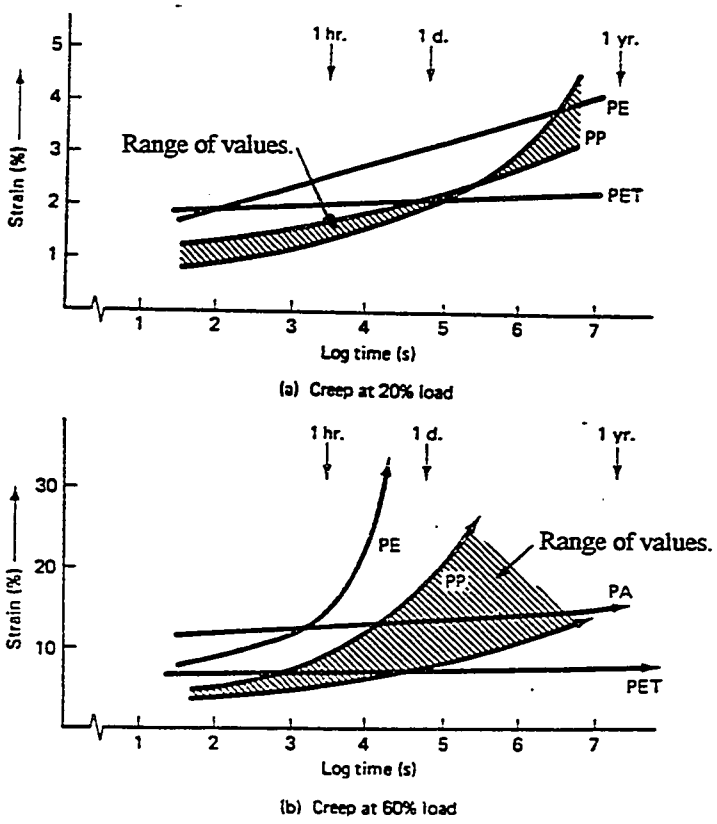

Figure 2.23: Results of creep tests on various yarns of different polymers (after den Hoedt, 1986).

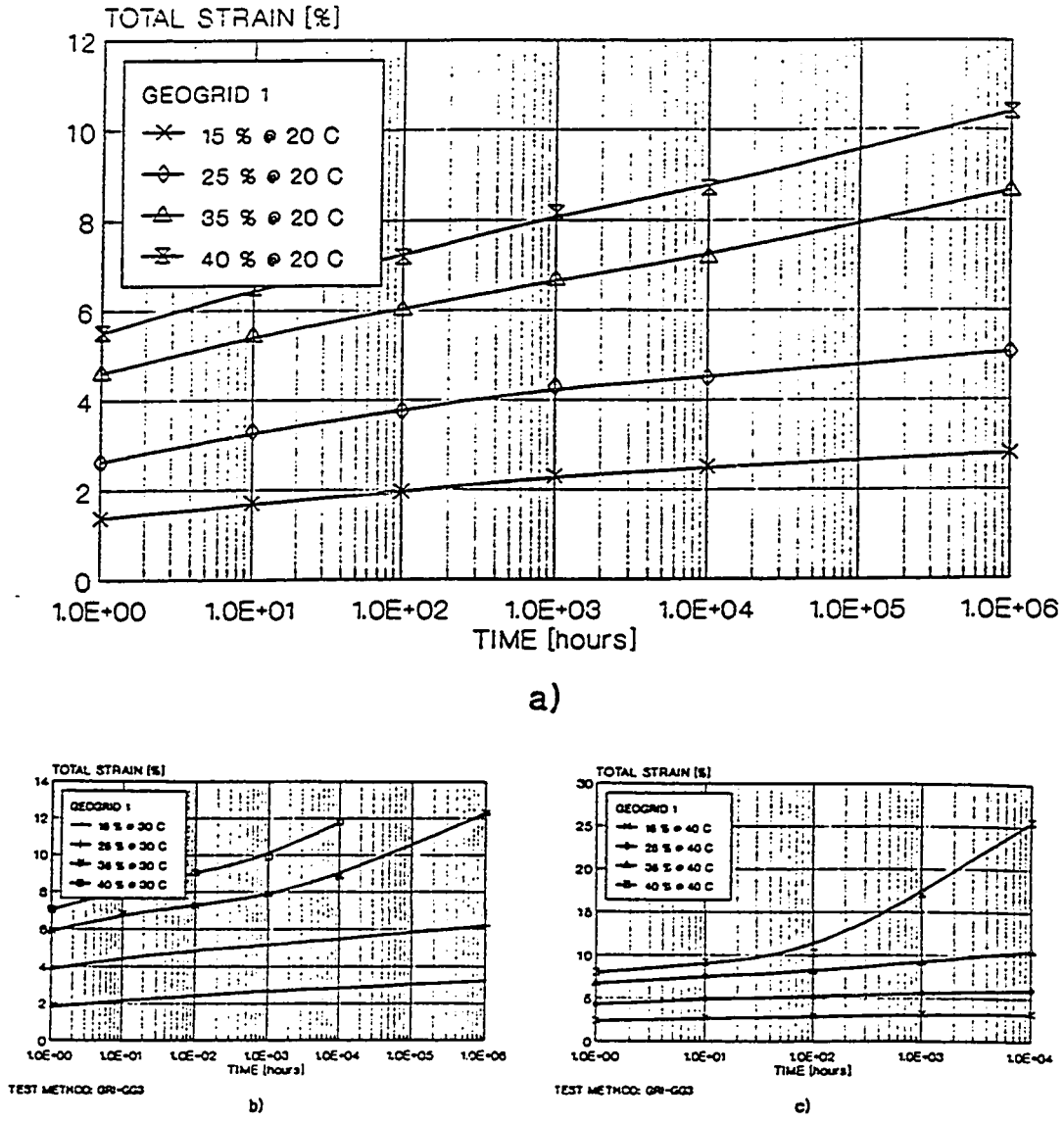

Figure 2.24: Elongation versus log time curves for a geogrid: a) at 20°C; b) at 30°C; and c) at 40°C (after Rimoldi and Montanelli, 1993).

dependence of creep to accelerate the creep process and permit extrapolation across more than one time log cycle.

Creep also affects the strength properties of reinforcings when they are tested at different strain rates. Creep is characterized by realignment of polymer chains in the geosynthetics when they are loaded. If creep occurs rapidly in a particular polymer, relative to the strain rate, it may affect the apparent modulus determined during load-elongation testing (Nothdurft and Janardhanam, 1994; Nothdurft, 1995). Creep effects result in decreases in modulus and peak strength with decreasing strain rate, Figure 2.26 (Cheok, 1985, Anjiang, et al., 1986; and Rowe and Ho, 1986; Nothdurft and Janardhanam, 1994; Nothdurft; 1995). Thus, the creep potential of a geosynthetic affects not only the long term strain but also strength and modulus determined from short term tests.

2.2.3 Creep in GRS Walls

Excessive deformation of existing GRS walls due to creep has not been problematic because current procedures for designing GRS walls have limited initial strain of the reinforcing, following construction and application of surcharges, to less than 1% (Allen and Holtz, 1991; McGown, et al., 1993). Nonetheless, creep has been observed in instrumented geosynthetic reinforced walls and slopes (Bathurst, et al., 1988; Allen, et al., 1992; Fannin and Hermann, 1991). Creep measured in these cases was not substantial. This may have been due to the low initial strain and relatively short time periods over which measurements were taken, Figure 2.27.

Although the influence of creep on GRS has been recognized for some time (Andrawes, et al., 1986; McGown, et al., 1989) in very few cases has it been considered when predicting GRS wall deformations (e.g., Ebeling, et al., 1992a; Chew and Mitchell, 1994). The omission of creep considerations from deformation calculations is due to the lack of creep data and the difficulties associated with incorporating time dependent

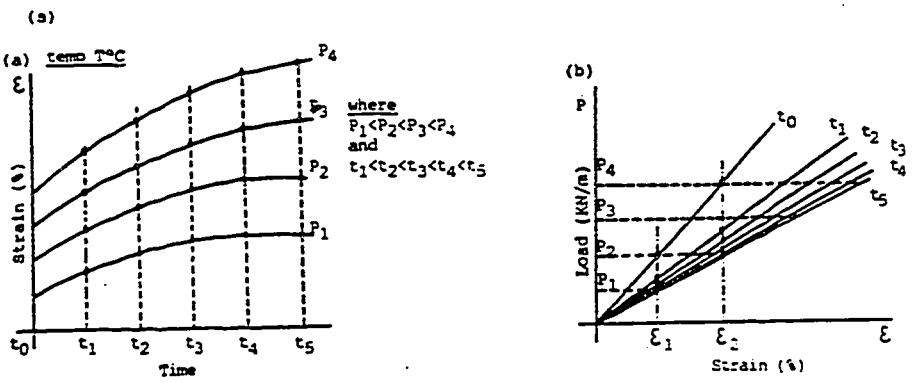

Figure 2.25: Creep test data: a) strain vs. time; b) load vs. strain (after Allen, 1991).

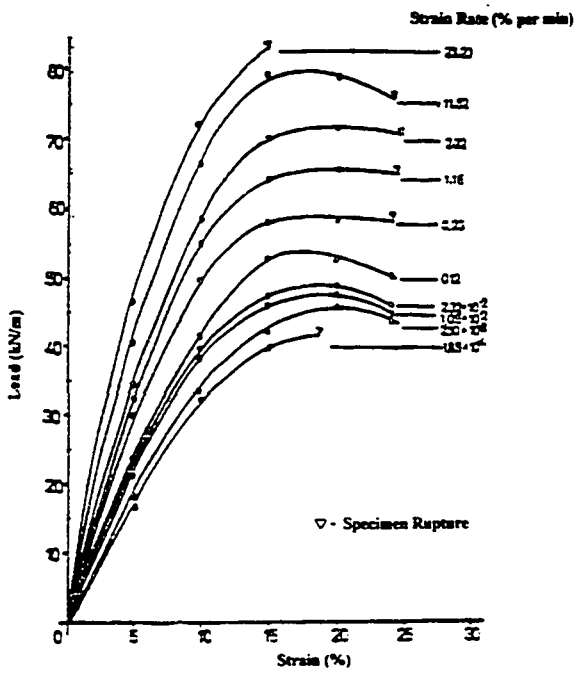

Figure 2.26: Influence of extension rate on load-strain behavior of Tensar SR2 at 20°C (after Nothdurft and Janardhanam, 1994, attributed to Cheok, 1985).

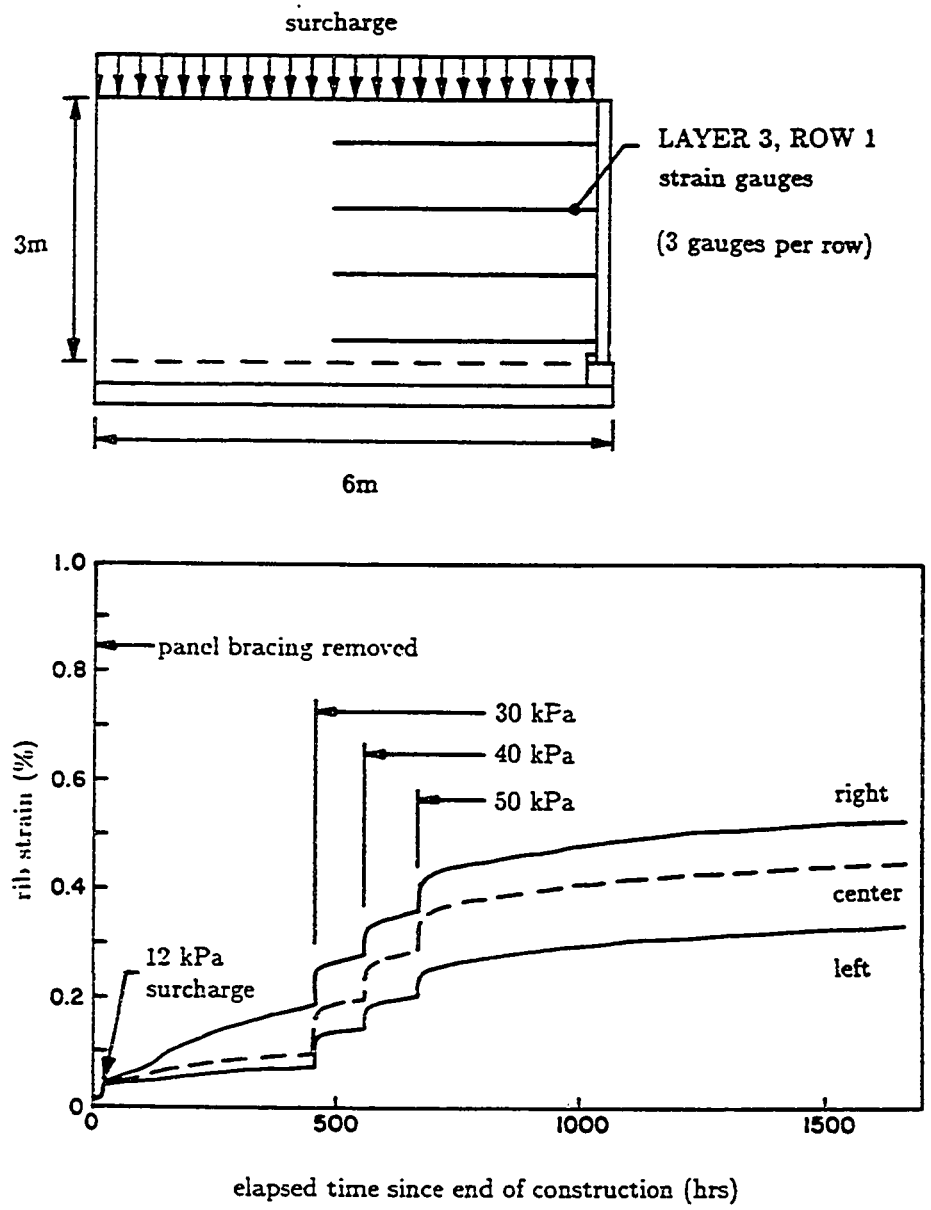

Figure 2.27: Creep strains of geogrid in GRS test wall (after Bathurst, et al., 1988).

properties in limit equilibrium and FEM models. Addressing creep in GRS wall deformation prediction is thus a two part problem. First, creep data must be obtained for the reinforcements of interest. Second, an accurate means of modeling these data in deformation prediction procedures must be developed.

2.2.4 Summary

Characterizing the creep tendency of polymeric reinforcements is necessary since creep has been shown to influence measured geosynthetic properties, and the deformation of GRS walls depends upon both short and long term geosynthetic behavior. Prediction of GRS wall behavior should, ideally, take these time effects into consideration. As more experience is gained with each of the factors affecting geosynthetic strength, and in the pursuit of more economical designs, the partial factors of safety used in the design of GRS walls may be reduced (Allen, 1991; Allen and Holtz, 1991). When these factors are reduced deformations due to creep may increase due to increases in initial strains and initial loads (as a percent of ultimate load) induced in the geosynthetics. In the meantime, characterization of geosynthetic creep potential and a means to incorporate creep into deformation prediction procedures should be pursued.

2.3 Conclusion

A review of existing in-soil geosynthetic test devices determined that none were completely acceptable for determination of in-soil geosynthetic load-elongation properties or for soil-geosynthetic composite behavior characterization as desired for this research project. Of the test apparatus reviewed, a unit cell device was thought to be the most appropriate device for measuring in-soil behavior of geosynthetics because the soil-geosynthetic interaction mechanism and mode of deformation for the reinforced soil within the wall is modeled, and soil densities and gradations used in field applications can

be reproduced in such a device. Consequently, a modified unit cell device, capable of directly measuring reinforcement loads was designed and manufactured for this project.

The tendency for polymeric reinforcements to creep was identified as a factor which may influence the short- and long-term behavior of geosynthetics. The creep response of geosynthetics as well as the short term behavior generally determined in laboratory tests must be understood for predicting GRS wall deformations.

CHAPTER 3
LITERATURE REVIEW - GRS RETAINING WALL DEFORMATION

3.1 Introduction

Predicting geosynthetic reinforced soil (GRS) wall deformations is not an easy process. Behavior is affected by soil in and behind the wall, reinforcement, wall facing, foundation soil, construction method and equipment, wall dimensions, and external loads which the retaining wall must support, Table 3.1. These factors may occur in an almost endless number of possible combinations. Understanding how each of these factors affects GRS wall deformations is necessary if accurate predictions of deformations are to be made. To aid in developing this understanding, a review of previous research which addressed reinforced soil behavior and reinforced soil retaining wall deformation was performed. The findings of this literature review are presented in this chapter. The chapter has been divided into three parts: behavior of reinforced soils, deformation mechanisms, and methods used for predicting deformations.

TABLE 3.1: Factors influencing GRS wall behavior (after Jones, 1988).

REINFORCEMENT	SOIL	CONSTRUCTION
Composition	Particle Size	Construction System
Durability	Grading	Compaction
Form	Index Properties	Facing
Surface Properties	Mineral Content	
Dimensions	Durability	
Strength	Availability	
Stiffness		
REINFORCEMENT DISTRIBUTION	**SOIL STATE**	**STRUCTURE**
Location	Density	Geometry
Spacing	Confinement	End Use
Orientation	State of Stress	Aesthetics
	Degree of Saturation	
	Drainage	

3.2 Behavior of Reinforced Soils

The addition of reinforcement to soil provides a means of resisting tensile stresses that soil alone is otherwise unable support. For tension to develop in the reinforcing, energy introduced to the reinforced soil system, due to applied loads, must transfer between the soil and reinforcing. Energy can be transferred between soils and reinforcements by a combination of friction and passive soil resistance acting along the length of the reinforcing, Figures 3.1 and 3.2. Furthermore, as is illustrated in Figure 3.2, tensile loads can be induced directly into the reinforcing by attachment to wall facing or anchor blocks. The relative contribution from each energy transfer mechanism for a particular soil-reinforcement combination is difficult to assess (Mitchell and Villet, 1987). However, an understanding of these mechanisms is important in evaluating the efficiency of various soil-reinforcement combinations. Some of the testing apparatus which have been employed for this purpose were presented in Chapter 2 of this dissertation. For additional information the reader is referred to Mitchell and Villet (1987) and Hausmann (1990), who have consolidated much of the research in which these mechanisms are evaluated.

Incorporating tensile reinforcement in soil may alter its behavior and, if the reinforcing has sufficient strength and extensibility, increase the soil capacity even at large strains, Figure 3.3. Schlosser and Long (1972) explained the increase in strength observed in reinforced soils as resulting from an apparent cohesion provided to the soil by the reinforcing, Figure 3.4a. The apparent cohesion increases the maximum principal stress supported by the composite for a given minor principal stress. The friction angle for the composite is the same as for the unreinforced soil. Yang and Singh (1974) hypothesized that the increase in maximum principal stress resulted from an "effective" increase in the lateral confining pressure experienced by the soil, Figure 3.4b. The resulting strength of the composite is the same for both hypotheses. Further research into the reinforced soil failure mechanisms (Hausmann, 1976; Hausmann and Lee, 1976; Gray and Ohashi, 1983) found that at low confining pressures failure occurred by slippage at the soil-reinforcing interface. At higher confining pressures failure occurred due to reinforcement breakage, Figure 3.5.

The stress-strain characteristics of reinforced soils depend on the properties of the soils and reinforcing, Figure 3.3. For a given soil, the maximum load supported by the reinforced-soil composite is a function of the concentration (vertical and horizontal

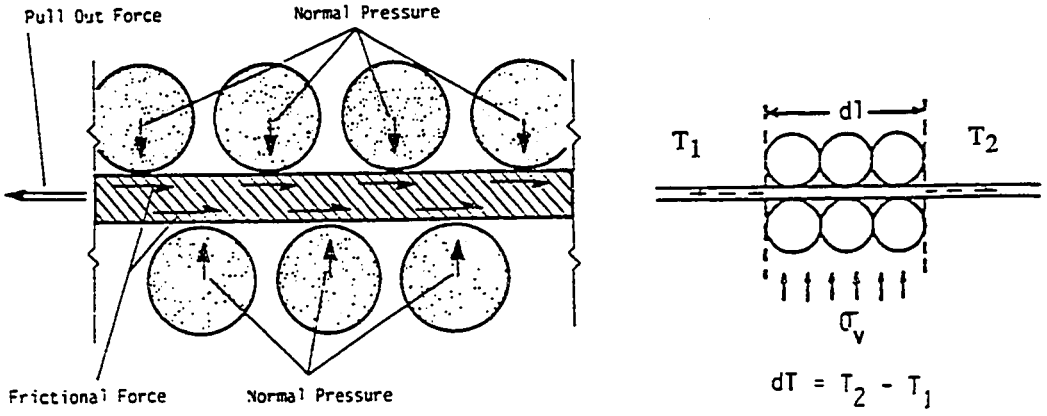

Figure 3.1: Frictional transfer between soil and reinforcement (after Mitchell and Villet, 1987).

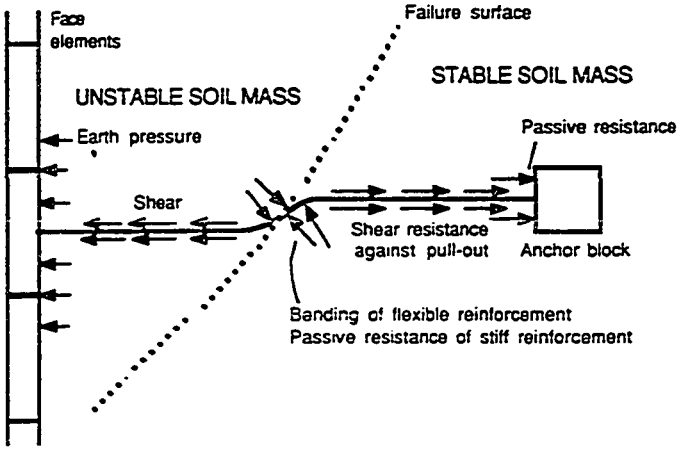

Figure 3.2: Schematic illustrating discrete soil-reinforcement action (after Hausmann, 1990).

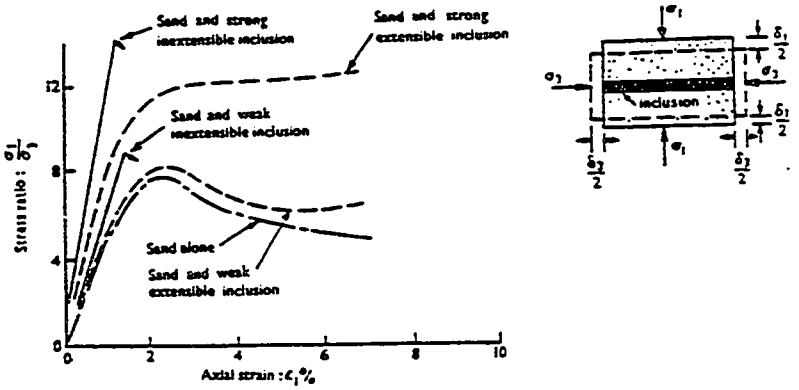

Figure 3.3: Postulated behavior of dense sand and reinforced dense sand in a unit cell (after McGown, et al., 1978).

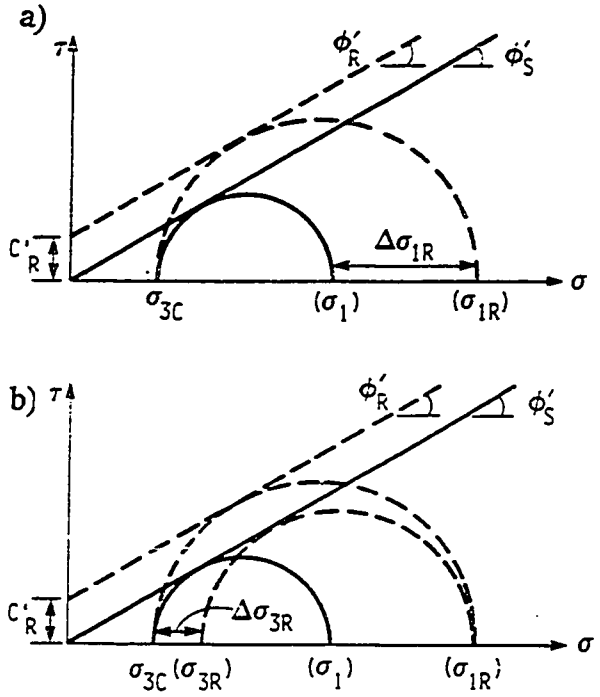

Figure 3.4: Reinforcement action: a) apparent cohesion concept (after Schlosser and Long, 1972), b) increased confining pressure concept (after Yang and Singh, 1974) (figures from Mitchell and Villet, 1987).

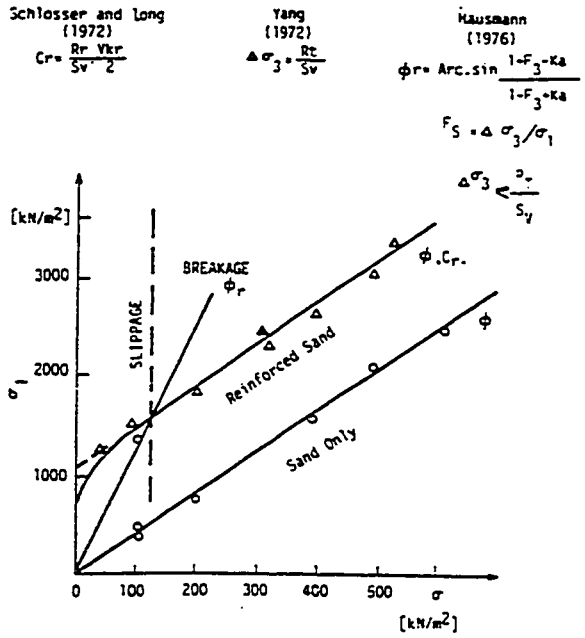

Figure 3.5: Strength envelopes for sand and reinforced sand (after Mitchell and Villet, 1987).

spacing between reinforcing elements) and capacity of the reinforcing. The deformation experienced by the composite differs depending upon the extensibility and modulus of the reinforcing used. When inextensible, high modulus reinforcing is used, the composite may be expected to undergo little lateral deformation under a given load. Under the same load the lateral deformation would be greater for extensible reinforcing having a lower modulus. The amount of deformation required for the reinforcing to develop adequate stress to resist the applied load is used to classify reinforcements into one group or the other. Reinforcements which yield at strains less than the strain at which the soil develops its peak strength would be classified as inextensible (McGown, et al., 1978).

3.3 GRS Wall Deformations

3.3.1 Introduction

The limit equilibrium procedures used for designing GRS walls have been found to be very conservative (Allen, 1991; Allen, et al., 1992). Strains experienced by the reinforcement in instrumented GRS walls have generally been very low, less than 1%, and have been less than predicted (Bathurst and Koerner, 1988; Allen, 1991; McGown, et

al., 1993). In addition to experiencing low strains, GRS structures designed using current standards experience only limited deformations. For typical GRS walls maximum displacements at the wall face at the end of construction have been found to be approximately 0.9% to 1.5% of the height (Christopher, et al., 1990). Despite the recognition of the conservativeness of limit equilibrium design procedures and the knowledge that geosynthetic reinforcements could be safely subjected to larger strains, practitioners have been reluctant to adopt less conservative procedures or to use GRS walls in long term permanent applications. This reluctance stems from a lack of information regarding structure deformations or long term geosynthetic performance (Allen and Holtz, 1991; Allen, 1991). Long term geosynthetic performance with regard to creep was discussed briefly in Section 2.2. An investigation of the factors which influence GRS wall deformations is the subject of this section.

3.3.2 External Deformation Factors

Various factors external to the wall may affect total deformations. Principal among these are foundation settlement, loads applied by the retained soil, and loads applied to the top of the GRS wall or retained soil, Figure 3.6. It has been proposed that foundation settlement be estimated using conventional methods. The calculated settlement could then be superimposed on the deformation of the wall itself to obtain the total deformation (Christopher, et al., 1990). Assumed pressure distributions below the wall are used to compute settlements, Figure 3.7. A difficulty with this approach is that the assumed pressure distributions do not always reflect the conditions measured below actual walls, Figure 3.8. The actual pressure distribution and the foundation material itself may influence settlement and affect lateral deformations and reinforcing strains. Chou and Wu (1993) used the finite element method to analyze reinforced soil retaining walls assumed to be constructed on rigid, stiff clay, medium dense sand and soft clay foundations. Their analysis, confirmed by Xi (1992), demonstrated that the foundation soil may significantly influence wall performance and affect the deformed shape, Figure 3.9.

In limit equilibrium design procedures forces applied to the back of the reinforced soil are computed to check resistance to overturning and sliding, while forces applied to the top of the wall are used to compute increases in lateral earth pressures which must be resisted by the reinforcement. Although these forces are easily applied in limit

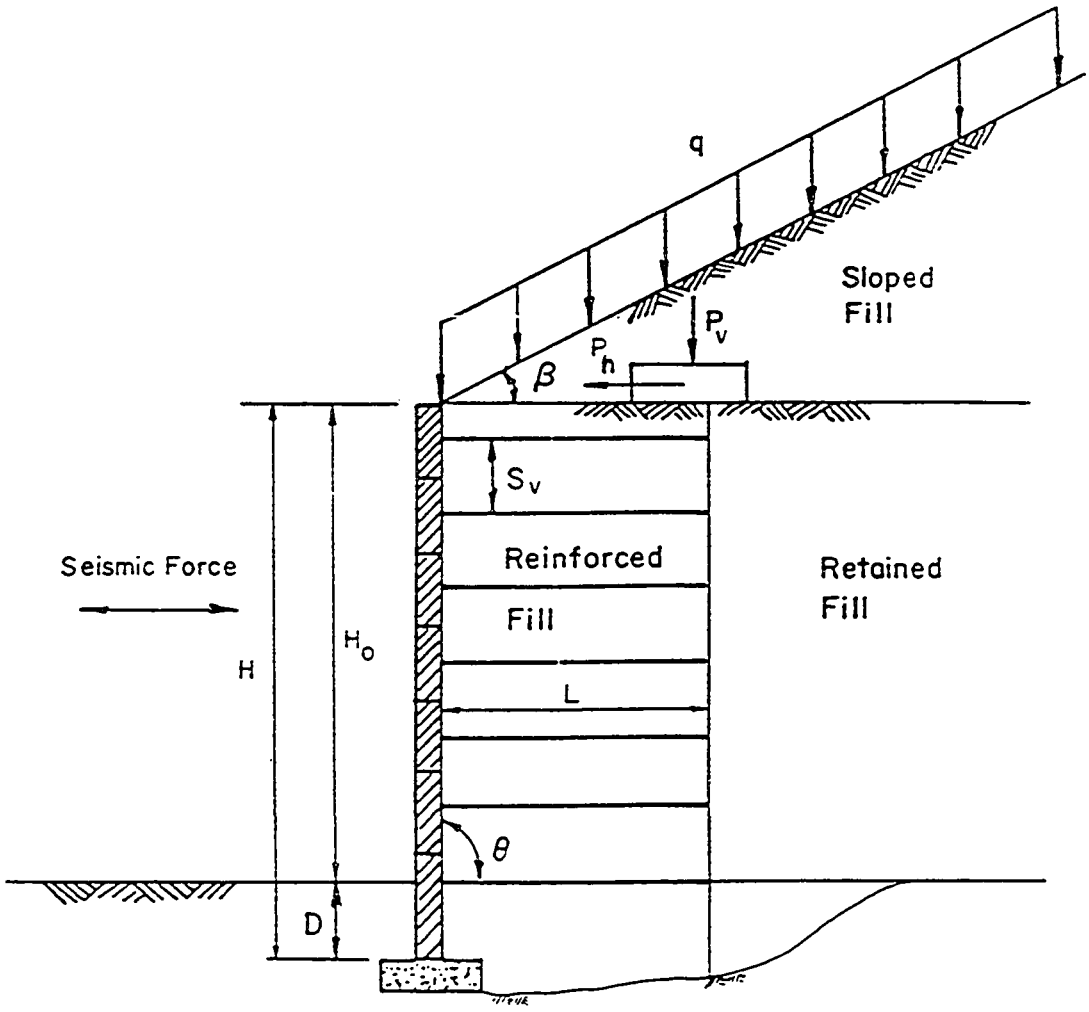

Figure 3.6: Geometric and loading characteristics of a reinforced soil wall (after Christopher, et al., 1990).

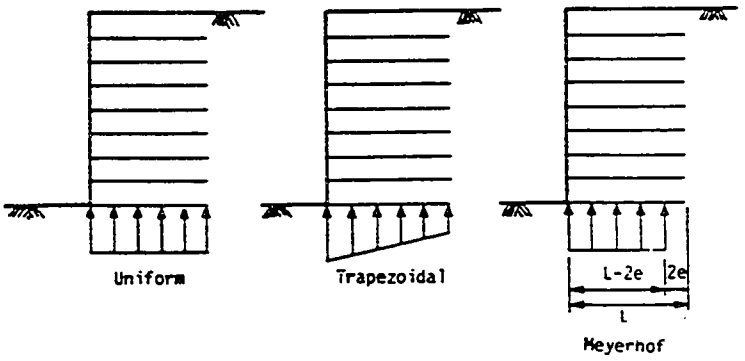

Figure 3.7: Assumed pressure distribution under an earth wall (after Mitchell and Villet, 1987).

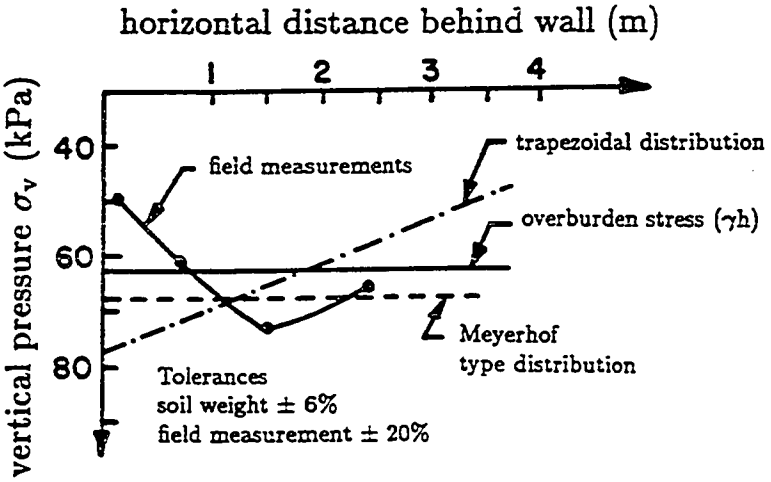

Figure 3.8: Comparison of measured vertical soil pressures to predicted values - Tuscon Wall (after Berg, et al., 1986).

equilibrium design procedures they are not as easily incorporated in simplified procedures for predicting deformations. The variety of load types (e.g., sloping, uniform surcharges, strip footings, etc.) and their potential wide range of magnitudes complicate development of universally applicable simplifying procedures. These difficulties have resulted in numerous researchers applying finite element methods to study the effects of these loads on GRS response (e.g., Collin, 1986; Chew, et al., 1991; Ebeling, et al., 1992b; Ling and Tatsuoka, 1992; Chew and Mitchell, 1994; Ho and Rowe, 1993; Karpurapu and Bathurst, 1992; Rajagopal and Bathurst, 1994; Zornberg and Mitchell, 1993, 1994). The only generalizations that can be made from these studies is that larger loads cause greater deformation and the location of the load and area of application influence the final deformed shape, Figure 3.10. Chew and Mitchell (1994) used the finite element method to perform a parametric study of the effect of sloping and uniform surcharges and strip loads on reinforced soil wall deformations. The design chart procedure which they developed from this analysis is discussed in Section 3.4.4.

3.3.3 Internal Deformation Factors

There are numerous other factors, that could be considered internal to the wall, that influence overall GRS wall behavior: soil strength properties and unit weight, reinforcing strength, length, spacing, arrangement and creep, soil-reinforcement interface properties, construction technique, compaction energy, and wall facing type. The individual contribution of these factors on GRS wall deformations have been investigated by numerous researchers, principally through FEM and centrifuge studies. A few references and the area they investigated are listed below:

a) reinforcement length (Christopher, et al., 1990; Chandrasekaran, 1992; Chou, 1992; Xi, 1992; Christopher, 1993; Ho and Rowe, 1993; Chew and Mitchell, 1994).

b) reinforcement strength, stiffness, spacing and arrangement (Schmertmann, et al., 1989; Chew, et al., 1991; Schlosser and de Buhan, 1991; Chou, 1992; Xi, 1992; Christopher, 1993; Huang, et al., 1993; Miyata and Kawasaki, 1994).

c) facing material (e.g., gabion, modular block, full height face panel) and rigidity; and facing construction technique (Adib, 1988; Graf and Studer, 1988; Christopher, et al., 1990; Allen, et al., 1992; Xi, 1992; Tatsuoka, 1993; Miki, et al., 1994; Kanazawa, et al., 1994).

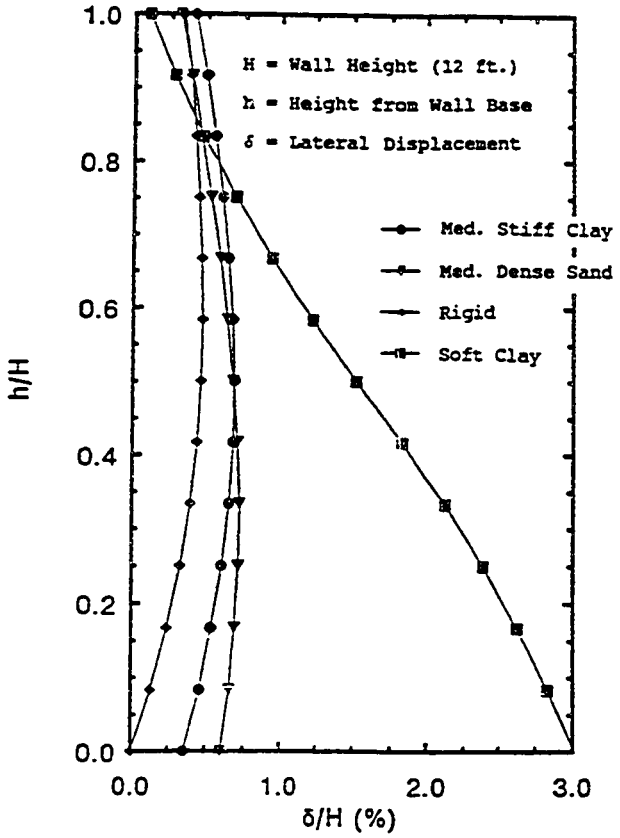

Figure 3.9: Effect of foundation stiffness on lateral wall displacement (after Chou and Wu, 1993).

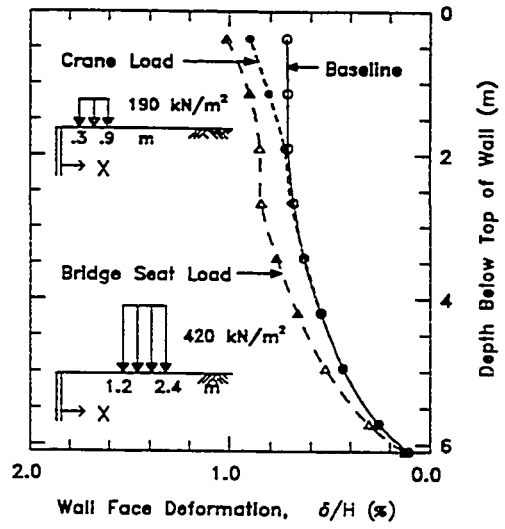

Figure 3.10: Effect of magnitude of strip load on wall face deformation (after Chew, et al., 1990).

d) compaction, compaction stresses (Collin, 1986; Mitchell, 1987; Adib, 1988; Schmertmann, et al., 1989; Chou, 1992; Yogarajah and Andrawes, 1994).

e) soil-reinforcement interface friction and relative motion between the soil and reinforcement (Herrmann and Al-Yassin, 1978; Naylor, 1978; Milligan and Palmeira, 1987; Xi, 1992).

The interested reader is directed to these references for specific details. The consensus from these studies is presented below:

a) The finite element method is an appropriate means of investigating GRS wall deformation and behavior.

b) The deformed shape of reinforced soil walls is very sensitive to the ratio of reinforcing length (L) to wall height (H), for $L/H < 0.7$. As L/H decreases, lateral deformations increase. This ratio has been identified as a primary indicator of total deformations.

c) Increasing the vertical spacing between layers or decreasing the reinforcement strength for a given spacing increases deformations.

d) Greater face element rigidity decreases wall deformation.

e) Compaction energy and compaction induced soil stresses influence deformations which occur during construction and stresses in the reinforcing at the end of construction.

f) Wall face deformations cannot be accurately estimated by integrating reinforcing strains since these strains do not include factors external to the wall (e.g., foundation settlement or global wall rotation).

Although recognized as a variable in GRS walls, the effect of soil properties on wall performance is noticeably missing from the list of factors studied. This can be primarily attributed to the difficulty associated with obtaining representative soil data and difficulties in modeling the soil. The FEM studies cited, in this section and in Section 3.3.2, utilized soil data obtained from, or intended to model, cylindrical triaxial test results. Triaxial soil properties were used even though it has been recognized for some time that plane strain soil behavior would be more representative of actual conditions in

GRS walls (McGown, et al., 1978 and 1989; Ho and Rowe, 1993). Despite this recognition, few authors (e.g. Chandrasekaran, 1992; and Ho and Rowe, 1993) even note in their discussion that the plane strain friction angle can be expected to be higher than the triaxial friction angle, result in smaller deformations and less reinforcing strain, and should be used for analyzing GRS walls. Before plane strain soil properties can be used for GRS wall analysis it is necessary to perform plane strain tests on soil to develop a better understanding of this behavior and to determine material parameters to be used in soil models. Determining the relationship between plane strain soil behavior and the more commonly obtained triaxial soil behavior would also be helpful. With these data, parametric studies could be conducted to investigate differences in GRS wall performance due to differences in assumed soil behavior.

3.3.4 Summary

A large number of factors, both external and internal, influence GRS wall performance, Table 3.1. Their relative importance and contribution to total deformations have been investigated using finite element and centrifuge studies. The finite element approach has proven the most versatile. While each of the factors are important, the ratio of reinforcement length to wall height has been identified as a primary indicator of total wall face deformation. Additional study is required of plane strain soil behavior and its effect on GRS wall deformations.

3.4 Deformation Prediction Methods

3.4.1 Introduction

A number of methods have been developed for designing GRS walls. Most of the methods concentrate on the internal and external stability of the structure with little, if any, emphasis on deformation. Internal stability methods generally use limit equilibrium analysis techniques to determine the forces which must be resisted to ensure a state of equilibrium. Each possible mode of failure must be considered, Figure 2.1. Safety factors are then applied to the assumed material properties to avoid failure. Reviews of these methods have been performed by others and will not be repeated here (Christopher and Holtz, 1985; Mitchell and Villet, 1987; Claybourn and Wu, 1991; Allen and Holtz, 1991). The design procedures themselves can be found in the references cited by these authors as well as Koerner (1990) and Christopher, et al. (1990). External stability of

GRS structures may be verified using conventional retaining wall and slope stability analysis. The potential for the GRS wall to slide along its base, overturn about its toe, or cause a bearing capacity failure of the foundation should be checked. GRS wall design manuals and traditional geotechnical engineering sources should be consulted to review these methods.

The shortage of instrumented reinforced soil wall case histories is one reason deformation is not addressed by most design methods. Although many GRS retaining walls have been constructed, deformation data are available for only a limited number of cases (Yako and Christopher, 1988; also see Section 3.4.4). Furthermore, as was discussed in Section 3.3, predicting GRS wall deformation is difficult because total deformation is a combination of foundation settlement, deformation occurring during construction, deformation due to surcharge loads and earth pressures behind the wall, and deformation due to soil and geosynthetic creep (Graf and Studer, 1988, Allen, et al., 1992). Even in cases where GRS walls were constructed on rigid foundations in laboratories, thereby eliminating foundation deformations as a variable influencing total deformation, deformation predictions have been relatively unsuccessful without the use of the finite element method (FEM) (Bathurst and Koerner, 1988). This difficulty arises because deformation is also influenced by the wall design and construction method: compaction intensity; reinforcement strength, length, spacing, and arrangement; slack in reinforcement-to-facing connections; and type and deformability of the facing system (Graf and Studer, 1988; Jewell, 1988a; Jones, 1988; Christopher, et al., 1990; Chew, et al., 1991).

Deformation prediction is, therefore, quite complicated. Three basic approaches to predicting GRS wall deformations have been advocated:

1) Compute reinforcing strains using assumed stress states obtained from limit equilibrium methods, limit equilibrium methods modified to match empirical data, or working stress methods. Integrate the strains in the reinforcing to compute the deformations of the wall face.

2) Compute wall deformations and reinforcing strains by performing a finite element analysis.

3) Predict wall deformations using design charts which have been developed from empirical data, analytical methods, computer simulations, or combinations thereof.

The effectiveness of each of these three approaches are discussed below.

3.4.2 Limit Equilibrium Methods

Currently, most reinforced soil walls are designed using limit equilibrium based procedures. In fact, although at least two working stress design methods have been proposed (Juran and Chen, 1989; Juran, et al., 1990; Ehrlich and Mitchell, 1994), the author is not aware of any GRS walls that have been constructed that were designed using other than limit equilibrium procedures. With only a couple exceptions, discussed below, limit equilibrium procedures do not implicitly address wall deformation. However, because they are widely used, expansion of these procedures to include prediction of wall deformations would probably speed acceptance by practitioners. (Since working stress methods have not been widely accepted, and because the salient features of the discussion below are also applicable to working stress methods, only limit equilibrium methods will be discussed.)

Most limit equilibrium design methods use assumed or computed soil stress states to select reinforcements which will ensure internal wall stability, Figure 3.11. After the soil stress state is determined, the reinforcement tension necessary to resist these stresses at each depth can be computed using Eq. 3.1.

$$T = \sigma_v K S_h S_v \qquad (3.1)$$

where:

- T = tension in the reinforcing,
- σ_v = vertical overburden stress,
- K = lateral earth pressure coefficient,
- S_h = horizontal spacing of reinforcing elements,
- S_v = vertical spacing of reinforcing elements.

The calculated tension and the load-elongation properties of the reinforcement (i.e., the reinforcing modulus) are used to compute the strains necessary to develop those

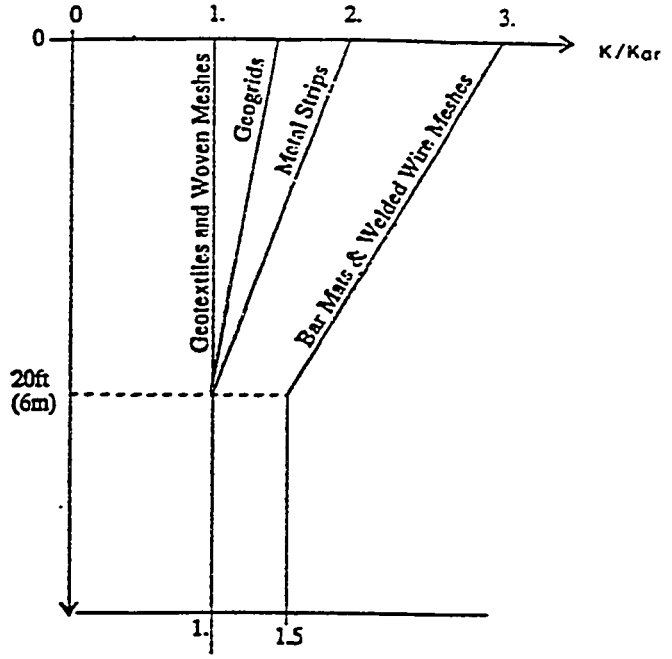

Figure 3.11: Assumed horizontal pressure distribution in a reinforced soil wall (after Christopher, et al., 1990).

forces. The total elongation of the reinforcement at each level in the wall is then computed by integrating the strains over the length of reinforcement over which the soil pressures are acting. Displacement of the wall face at each level, using this approach, would equal the total elongation in the corresponding layer of reinforcement.

If the assumptions implicit in the limit equilibrium design procedures were correct, the tension in the reinforcing would be constant along its entire length. However, instrumentation of reinforced soil walls has indicated that this is not the case and that reinforcing tensions follow the general pattern observed in the Rainier Avenue wall, Figure 3.12. That is, the tension is a maximum at some distance behind the face and decreases on either side of that maximum. At the free end of the reinforcing at the back of the wall the tension must be zero. At the connection to the facing the tension will depend upon the reinforcement type, facing style, and construction technique. To account for this deviation from true limit equilibrium conditions, predicted reinforcing strains and wall deformations are reduced in proportion to the reduction in tensile forces on either side of the maximum.

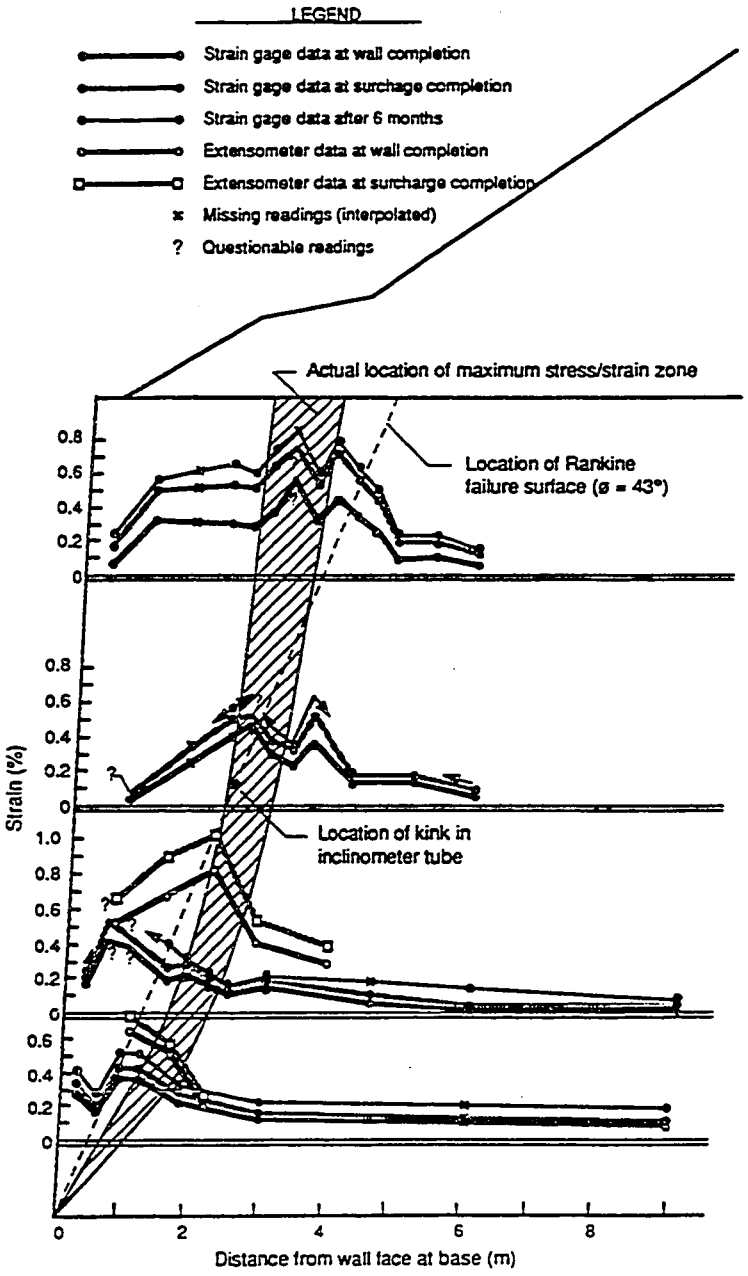

Figure 3.12: Plot of reinforcing strain in a typical GRS wall (after Allen, et al., 1992).

The above procedure is similar to, although not exactly, the approach used by Jewell (1988a) and Jewell and Milligan (1989) for the development of a limit equilibrium design procedure and a series of design charts intended to predict wall deformations. Their procedure is somewhat involved, and will not be presented here. The significance of their approach is that it provides a means to predict horizontal and vertical deformations for a variety of soil friction angles and is said to bound the solution by predicting both maximum and minimum wall deformations, as well as the actual anticipated deformations. The method uses nondimensionalizing factors to permit application of the charts to walls of various heights and using various reinforcing strengths, Figure 3.13. This procedure was applied, with some success, to predict the deformation of full scale walls constructed in a laboratory (Jewell, 1988b, Bathurst and Koerner, 1988) and to predict deformations of model walls (Palmeira and Lanz, 1994). It has not, however, become widely used.

A second limit-equilibrium design procedure, the so-called "displacement" method developed by Gourc, et al, (1986 and 1988) and expanded by Fidler (1993), is also claimed by its developers to be capable of predicting deformations. As with the Jewell (1988a) and Jewell and Milligan (1989) method, consideration for deformations is implicit in this design procedure. The underlying assumption on which this method is based assumes a moving block of reinforced material in front of a defined slip plane, Figure 3.14. Deformation is assumed due to block motion and resulting strains induced in the reinforcement. This method has not become widely used, nor has it been applied to predict deformations of GRS walls.

Limited success has been realized using limit equilibrium design methods for predicting GRS wall deformations. As part of a workshop held at the Royal Military College of Canada in 1987, class A (i.e., before construction) predictions were made concerning the performance of two full scale reinforced soil walls (Jarrett, 1988, Bathurst, et al., 1988; Bathurst and Koerner, 1988). Bathurst and Koerner (1988) summarized the results of the prediction exercise as follows: Seven of the eight prediction methods used limit equilibrium methods with modifications to account for the fact that the walls were not at limiting states throughout the tests. The limiting equilibrium methods did not fare well in predicting response and over-estimated connection loads, facing displacements and strains in the reinforcement. They were, however, found to be inherently safe. The authors noted that if avoidance of catastrophic failure is the only concern, then from the

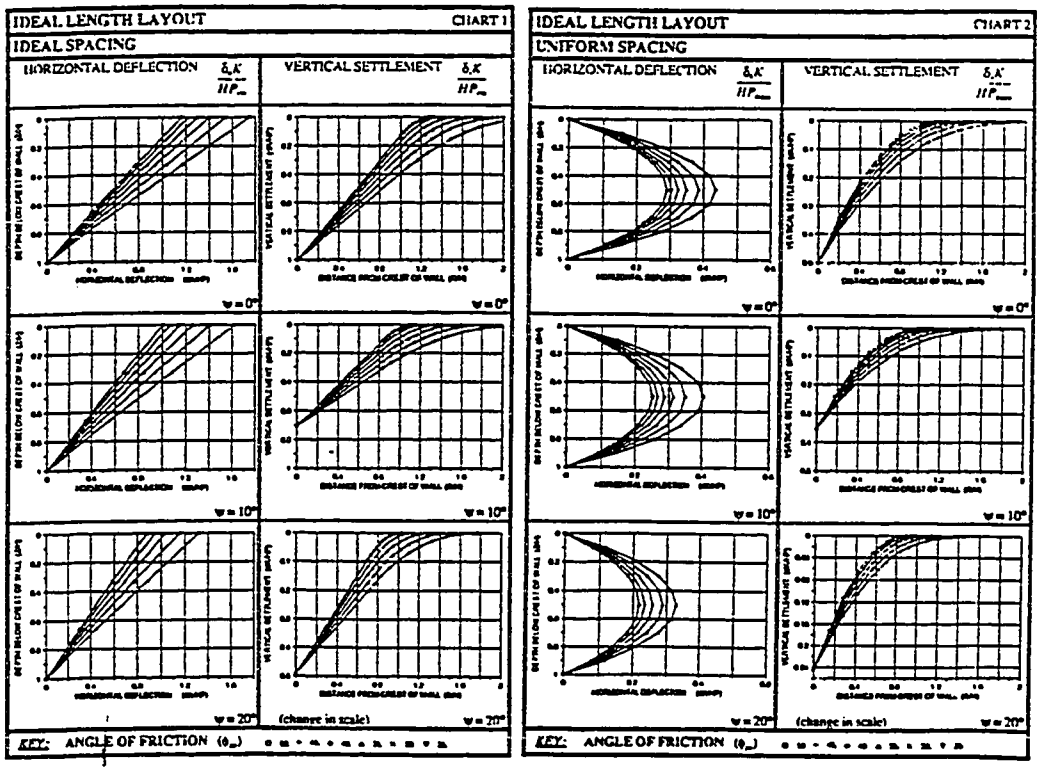

Figure 3.13: Non-dimensional graphs for predicting horizontal and vertical movements of GRS walls (after Jewell and Milligan, 1989).

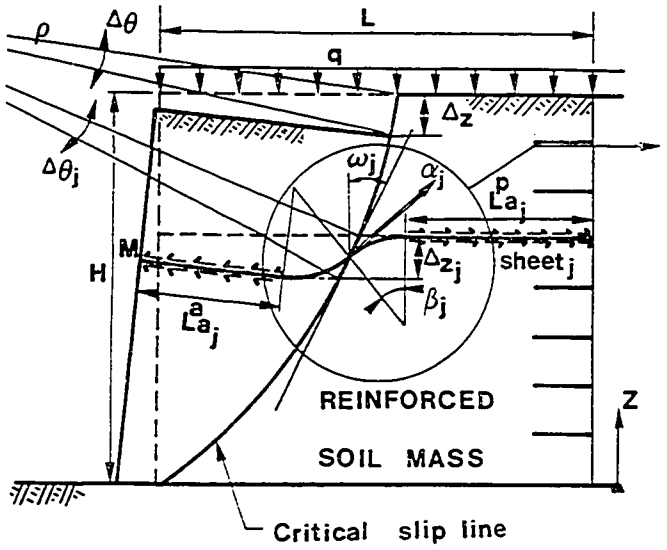

Figure 3.14: Displacement method general principle (after Gourc, et al., 1986).

practitioner's perspective there are strong arguments for the continued used of limit equilibrium methods.

Ho and Rowe (1993) address some of the problems with predicting deformations of GRS walls using assumed stress states in the soil and measured strains and tensile forces in the reinforcement. Their FEM analysis showed that "the force developed in the reinforcement is directly related to the strain developed in the reinforcement and the reinforcement stiffness; and is significantly affected by the stiffness of the foundation. While for a soil element under active condition(s), the state of stress is independent of both the soil strain and the foundation stiffness. The implication of this finding is *that it is generally not valid to assume the tensile force in the reinforcement equal to the equivalent soil force under an assumed stress state*" (emphasis added). This finding, as well as the need to consider external deformation factors, necessitates that limit equilibrium methods used for deformation prediction of GRS walls be correlated with empirically developed data and with calibrated analytical models.

3.4.3 Finite Element Analysis

3.4.3.1 Introduction

Reinforced soil wall design and analysis procedures have been based on limit equilibrium techniques since the first commercial application of reinforced earth (Vidal, 1969; Schlosser and Vidal, 1969). Finite element techniques were first applied to reinforced earth in the mid 1970's, primarily for developing an understanding of reinforced earth behavior (Romstad, et al., 1976; Shen, et al., 1976; Herrmann and Al-Yassin, 1978; Al-Hussaini and Johnson, 1978; Schlosser and Elias, 1978). While FEM has since been applied in numerous parametric studies and for analysis of GRS walls, it is not used routinely in GRS wall design. The widest application of FEM has been in predicting reinforcing strains and wall face deformations of research walls (e.g., Bathurst and Koerner, 1988; Wu, et al., 1992) or for parametric analysis (See Section 3.3.3). In recent years confidence with defining material properties and formulating models has permitted FEM application to more general GRS problems (e.g., Ebeling, et al., 1993; Chandra, et al., 1993).

There are two basic representations for modeling reinforced soils in finite element analysis: composite element and discrete element.

3.4.3.2 Composite Elements

Treating a large body constructed of reinforced soils, or of layered rocks and soils, as a single material having the combined, or composite, elastic properties of the constituent materials has been proposed (Westergaard, 1938; Salamon, 1968; Harrison and Gerrard, 1972; Romstad, et. al., 1976, Shen, et al., 1976). In these references elastic theory was used to develop composite material properties. Harrison and Gerrard (1972) applied the theory directly to the case of reinforced soil and developed a series of equations by which the equivalent elastic properties, Young's modulus, shear modulus, and Poisson's ratio, could be developed. A number of assumptions are necessary for this application to be successfully applied, the most important being that the materials be perfectly bonded at their interface. Sawicki (1983a, b, c), Sawicki and Lesniewska (1988, 1991, 1993), and Sawicki and Kulczykowski (1994) expanded the general formulation for linear elastic materials to include elasto-plastic behavior. The composite material formulations developed by Harrison and Gerrard (1972) and Sawicki and his co-workers have not been incorporated directly into finite element programs and the effectiveness of these models for this application has not been assessed.

Composite materials defined with other formulations have been utilized for evaluating reinforced soil wall behavior, Figure 3.15a. Romstad, et al. (1976), Shen, et al. (1976), and Herrmann and Al-Yassin (1978) compared the results of finite element analyses of Reinforced Earth (steel strap reinforcement) using discrete elements with finite element analysis using composite elements. They determined that composite elements could be used to determine the response of the reinforced soil mass, including peak reinforcing tension, just as well as when discrete elements were used. The benefit is that significantly less computational effort was involved. One criticism of the composite approach is that slip at the soil-reinforcing interface is not normally accounted for. However, Herrmann and Al-Yassin (1978), Naylor (1978) and Naylor and Richards (1978) have developed special methods for permitting slip at the soil-reinforcing interface within composite elements, thus including this parameter but still reducing computational requirements.

The composite material approach has not generally been adopted for GRS wall analyses because of the assumption of perfect bonding and the incompatibility of strains

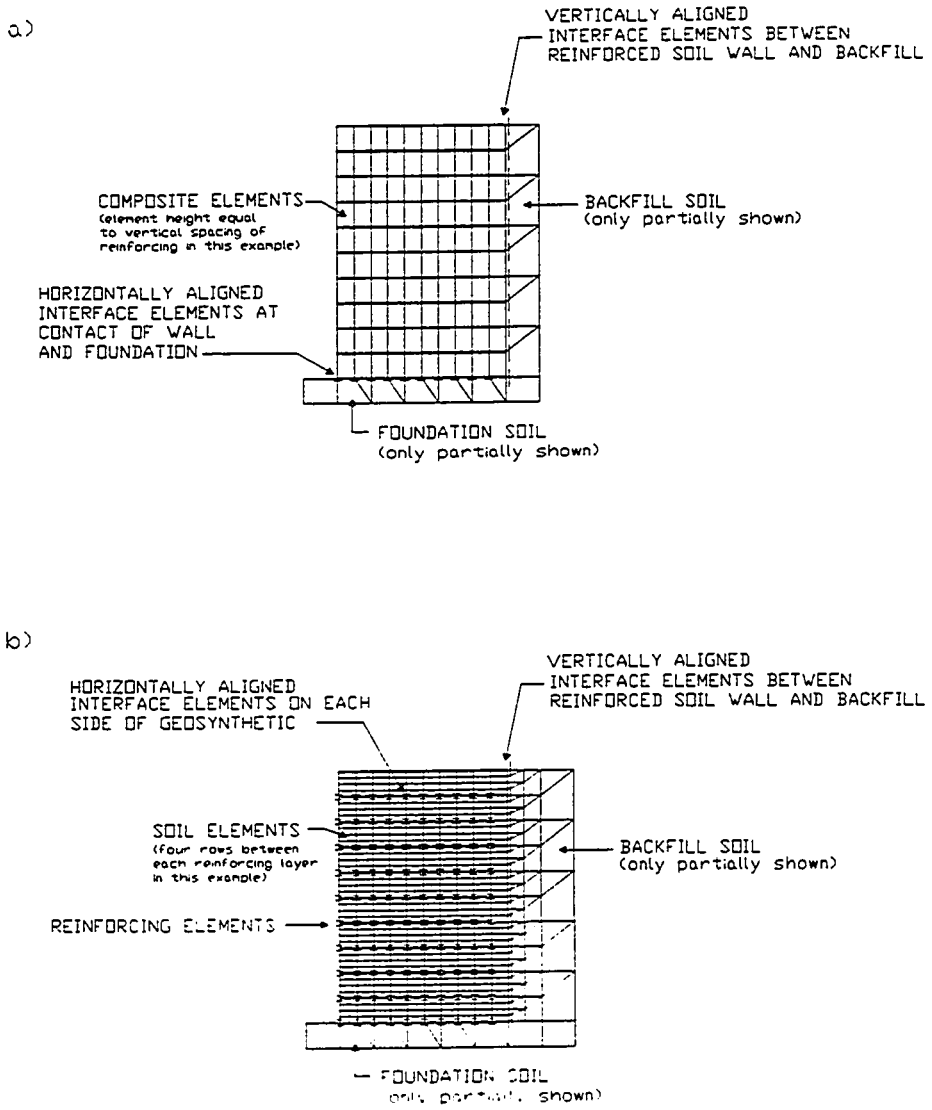

Figure 3.15: Finite element model of a reinforced soil wall: a) with composite elements, b) with discrete elements.

of adjacent elements. Additionally, this approach does not provide direct information concerning the stress and strains at the soil-reinforcing interface, nor does it provide information on localized deformations at the edges of the reinforced soil mass (Rowe and Ho, 1988). A further limitation is in modeling pullout. However, a number of researchers have concluded that slip at the soil-reinforcement contact is insignificant, or does not occur, for most reinforcements in GRS walls at working loads (Xi, 1992; Zornberg and Mitchell, 1993). Ebeling, et al. (1992b) conclude the composite approach is appropriate, and significant computation time is saved, if there is no potential for exceeding the shear transfer capacity between the soil and reinforcement (i.e., no pullout). On the other side of the discussion, Rowe and Ho (1988) argue that with the advanced computing capabilities now available, computational difficulties or time are no longer reasonable arguments for using this approach instead of the more detailed discrete element approach.

3.4.3.3 Discrete Elements

The soil, reinforcing, facing elements and interface boundaries between elements may be individually represented using appropriate types of discrete finite elements, that is, individual elements to represent each different material, Fig 3.15b. This approach to FEM has been found to be acceptable for predicting GRS wall deformations (Bathurst and Koerner, 1988; Wu, et al., 1992), and has been used extensively in parametric studies and evaluation of actual walls (Collin 1986; Adib, 1988; Schmertmann, et al., 1989; Chou, 1992; Xi, 1992; Chandrasekaran, 1992, Karpurapu and Bathurst, 1992; Ho and Rowe, 1993; Zornberg and Mitchell, 1993; Miyata and Kawasaki, 1994). Rowe and Ho (1988) state that the only disadvantages to using this approach are the requirement for more computing resources, and the effort required to prepare input data. They go on to state that the advantages of potentially more accurate analysis outweigh these disadvantages when performing a detailed investigation of reinforced soil wall behavior.

Rowe and Ho (1988) emphasize that to obtain accurate results "it is necessary to ensure that the choice of finite element (type) and the distribution of finite elements (particularly between layers of reinforcement) provide sufficient 'freedom' for realistic stress and strain distributions to be developed. To capture these details, a number of bays of elements should be provided between layers of reinforcement." Thus, a very large number of elements may be required for large structures. Ho and Rowe (1993) use a very

fine mesh of eight-noded isoparametric elements "to minimize the effect of mesh dependency on the numerical modeling, and to enable the use of the same mesh in cases involving a change in geometry of the problem (e.g. an increase in the number of layers of reinforcement or an increase in the reinforcement length, etc.). The findings regarding GRS wall deformation and reinforcement strain distribution reported by Ho and Rowe are not, however, substantially different from those obtained by others who used fewer elements in their models (e.g. Adib, 1988; Chou, 1992; Xi, 1992; Chandrasekaran, 1992). Soil deformation and activity at the interface (the stated reason for using a large number of elements) were not extensively discussed by Ho and Rowe (1993).

A number of finite element programs have been used for analyzing reinforced soil wall performance. With the exception of those papers referenced in Section 3.4.5.2 in which composite "unit cell" element properties were used, finite element analyses of reinforced soils have been performed using discrete elements to represent the reinforcing and soil. A partial list of finite element programs which have been used for analysis of GRS walls is presented in Table 3.2. These programs use a variety of element types and formulations for modeling the soil, reinforcing, facing and material interfaces.

3.4.3.4 Summary

Finite element techniques have been successfully employed for evaluating GRS retaining walls. Both composite and discrete element formulations have been utilized, with the discrete element approach the most widely accepted and applied. At the workshop held at the Royal Military College of Canada in 1987 the prediction of the response of the GRS walls using FEM proved the most accurate, although it was not perfect (Bathurst and Koerner, 1988). The paper concluded that "FEM approaches hold great promise as the analytical tool of choice for polymeric reinforced retaining walls of the type constructed for the prediction exercise. FEM are particularly attractive if predictions of wall performance at non-failure state are the goal."

In the GRS wall prediction exercise held at the University of Colorado, Denver, in 1991 (Wu, 1992a, b, c), the finite element method was used by 11 of the 15 predictors (Wu, et al., 1992). The predictors met with varied success on the multiple aspects of the wall performance they were asked to predict. For prediction of working stress deformations and prediction of soil stress states, FEM was recommended as appropriate. FEM was found to be less effective for prediction of failure loads and deformations

Table 3.2: FEM programs used for GRS wall analysis.

FEM Program	Reference	Notes
AFENA	Ho and Rowe (1993)	Deformation of GRS walls. Used rigid foundation, large number of elements.
	Ho and Rowe (1994)	Deformation of centrifuge model walls.
CRISP	Yeo, Yogarajah and Chan (1992)	Denver wall Prediction*
	Andrawes and Saad (1994)	Full scale walls subject to controlled lateral deformation.
	Yogarajah and Andrawes (1994)	Investigated construction effects of full scale walls.
DACSAR	Chou (1992)	Investigated effects of various factors on performance of GRS walls. Evaluated and compared four FEM programs: SSCOMP, COND2D-86, CRISP, DACSAR.
	Chou and Wu (1993)	Evaluate effects of foundation rigidity on wall deformations.
	Helwany (1992)	Denver wall prediction
GEOFEM	Karpurapu and Bathurst (1992), Rajagopal and Bathurst (1994).	Denver wall and RMC wall** predictions
GRSWALL	Chandrasekaran (1992)	Evaluation of model walls and parametric study
M-CANDE	Ling and Tatsuoka (1992)	Denver wall prediction
REA	Herrmann and Al-Yassin (1978)	Compare discrete and composite analysis
	Xi (1992)	Parametric analysis of GRS walls
SAFE	Chalaturnyk, et al. (1990)	Evaluation of GRS steep slopes
SOILSTRUCT	Ebeling, et al. (1992a,b, 1993)	Denver wall, Red River lock and dam
SSCOMP	Collin, 1986	Evaluated steel reinforced soil walls
	Adib, 1988	Evaluated steel reinforced and GRS walls
	Schmertmann, et al. (1989)	Parametric study of reinforced soil walls
	Chew, et al. (1991)	Parametric study of reinforced soil wall deformations.
	Jaber, et al. (1992)	Denver wall prediction
	Zornberg and Mitchell (1993)	Evaluated Rainier Avenue wall. Did parametric study on effect of surcharge on deformations.
	Chew and Mitchell (1994)	Developed design charts for reinforced soil walls.
SSTIPNH	Mylleville and Rowe (1991)	Study effect of compressible zone between GRS wall and rigid abutment.

* Full scale test walls constructed at the University of Colorado, Denver; See Wu (1992a, b, c).

** Full scale test walls constr. at the Royal Military College of Canada; See Bathurst and Koerner (1988).

at failure because of the difficulties in establishing post-peak soil properties (Jewell, 1992).

The major drawbacks for using FEM analysis, versus limit state analysis, are the greater time required to perform the design and the experience required to properly develop the non-linear material properties for input to the analysis. Other than for projects where deformations could influence the serviceability, it is not anticipated that FEM will become routinely used for GRS wall design. However, FEM may be used to provide a better understanding of the behavior of a system and for the development of design aids (Graf and Studer, 1988; Koerner, 1990; Adib, et al., 1990; Chew, et al., 1991; Christopher, et al., 1990; Allen and Holtz, 1991; Ho and Rowe, 1993; Chou and Wu, 1993; Christopher, 1993; Chew and Mitchell, 1994).

3.4.4 Design Charts

Empirically developed design charts may be a practical alternative to performing FEM studies or complicated limit equilibrium calculations for each wall to be designed. Limit equilibrium design procedures have been used to develop charts that simplify the design of GRS walls (Polyfelt, 1987; Leshchinsky and Perry, 1987; Leshchinsky and Boedeker, 1989; Huesker, undated). However, similar design aids that permit prediction of deformations of the GRS walls designed using those charts are not widely available. Those that have been produced have only recently become available. The Jewell (1988a) and Jewell and Milligan (1989) design charts, Figure 3.13, which are tied to a particular design procedure, were briefly discussed in Section 3.4.2. Two other design chart based deformation prediction procedures, which are not directly tied to a specific design and analysis procedure, have been developed. They are discussed in this section.

Christopher, et al. (1990) presented a graph for estimating the lateral displacement which can be anticipated during construction of simple GRS structures constructed on firm foundations, Figure 3.16. This figure was developed empirically from full scale tests, FEM computer simulations of 6 m high walls, and centrifuge models. Its applicability to walls of other heights is uncertain although Holtz, et al. (1991) found the design chart only slightly overpredicted the wall face movements of the 12.6 m high Rainier Avenue wall. Only the ratio of reinforcing length to wall height and the general classification of the reinforcing material, extensible or inextensible, are needed to use this

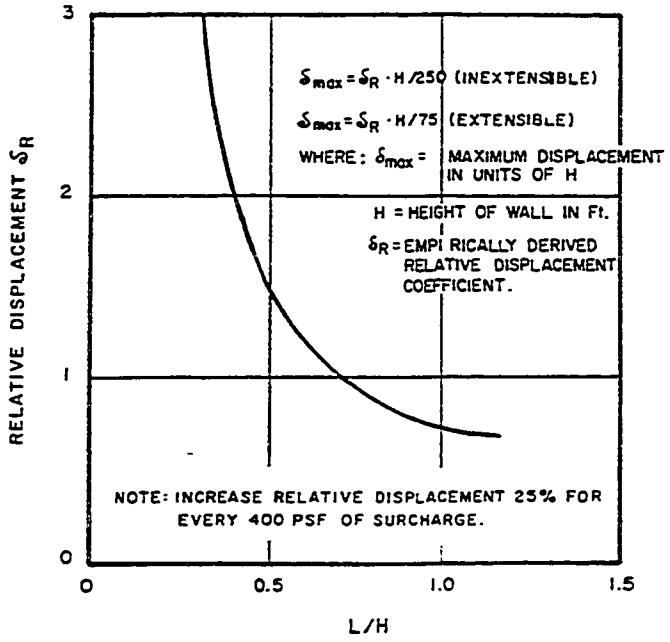

Figure 3.16: Empirical curve for estimating lateral displacement that occurs during construction of reinforced soil structures (after Christopher, et al., 1990).

chart. The chart predicts walls reinforced with extensible reinforcement (geosynthetics) to undergo three times more displacement at the wall face than those constructed with inextensible reinforcements (steel). Christopher (1993) expanded the method to account for differences in geosynthetic reinforcing material modulus properties and vertical spacing of layers. With these modifications, deformations predicted for extensible reinforcements based on Figure 3.16 use the following formula:

$$\delta_{max} = \delta_R \left(\frac{H}{75 \log S_r} \right) \tag{3.2}$$

where S_r is the global stiffness in kips/ft^2 defined as:

$$S_r = \frac{JR_c}{S_v} \tag{3.3}$$

and where:

J = reinforcing modulus per unit width (i.e., normalized with respect to thickness),

R_c = reinforcement coverage ratio (b/S_h) with b equal to the width of the reinforcement and S_h equal to the horizontal spacing, and

S_v = average vertical spacing of reinforcement layers, H/n, with H equal to the wall height and n equal to the number of reinforcement layers.

Chew and Mitchell (1994) presented a series of design charts for predicting GRS wall deformation that were developed using detailed finite element analysis, Figure 3.17. The charts include consideration for the reinforcement length to wall height ratio, L/H, the effect of overall wall height, H, the global stiffness ratio, S_r (as defined in Eq. 3.3), the effect of uniform and sloping surcharges, and strip loads. Deformation of a wall is predicted by first estimating the deformation of a "baseline" wall and adjusting the estimated deformations for differences between this baseline and the wall being evaluated. The baseline case represents a 6 m high wall with L/H equal to 0.7, uniform reinforcement spacing, moderate compaction, level backfill and no external loading. Soil friction angle was assumed between 35° and 40°. To demonstrate the applicability of the charts, Chew and Mitchell (1994) compared deformations predicted using their system with two case histories and obtained favorable results.

Chew and Mitchell (1994) propose the following design methodology for using these charts:

1. Design the basic reinforced soil wall using current design methods.
2. Compute the stiffness ratio, S_r for this wall.
3. Determine $(d/H)_{base}$ for this wall using Figure 3.17b.
4. Determine the deformation index factors, DI, for the wall being evaluated:
   a) $DI_{L/H}$, for the L/H ratio, Figure 3.17c,
   b) DI_H, for the wall height, H, Figure 3.17d,
   c) DI_q, for uniform surcharges (See Chew, et al, 1991),
   d) DI_{slope}, for sloping surcharges, Figure 3.17e,
   e) DI_{other}, to account for other influences.
5. Compute the wall face deformation, d, using Equation 3.4:

$$\frac{\delta}{H} = \left(\frac{\delta}{H}\right)_{base} \cdot DI_{L/H} \cdot DI_H \cdot DI_q \cdot DI_{slope} \cdots \qquad (3.4)$$

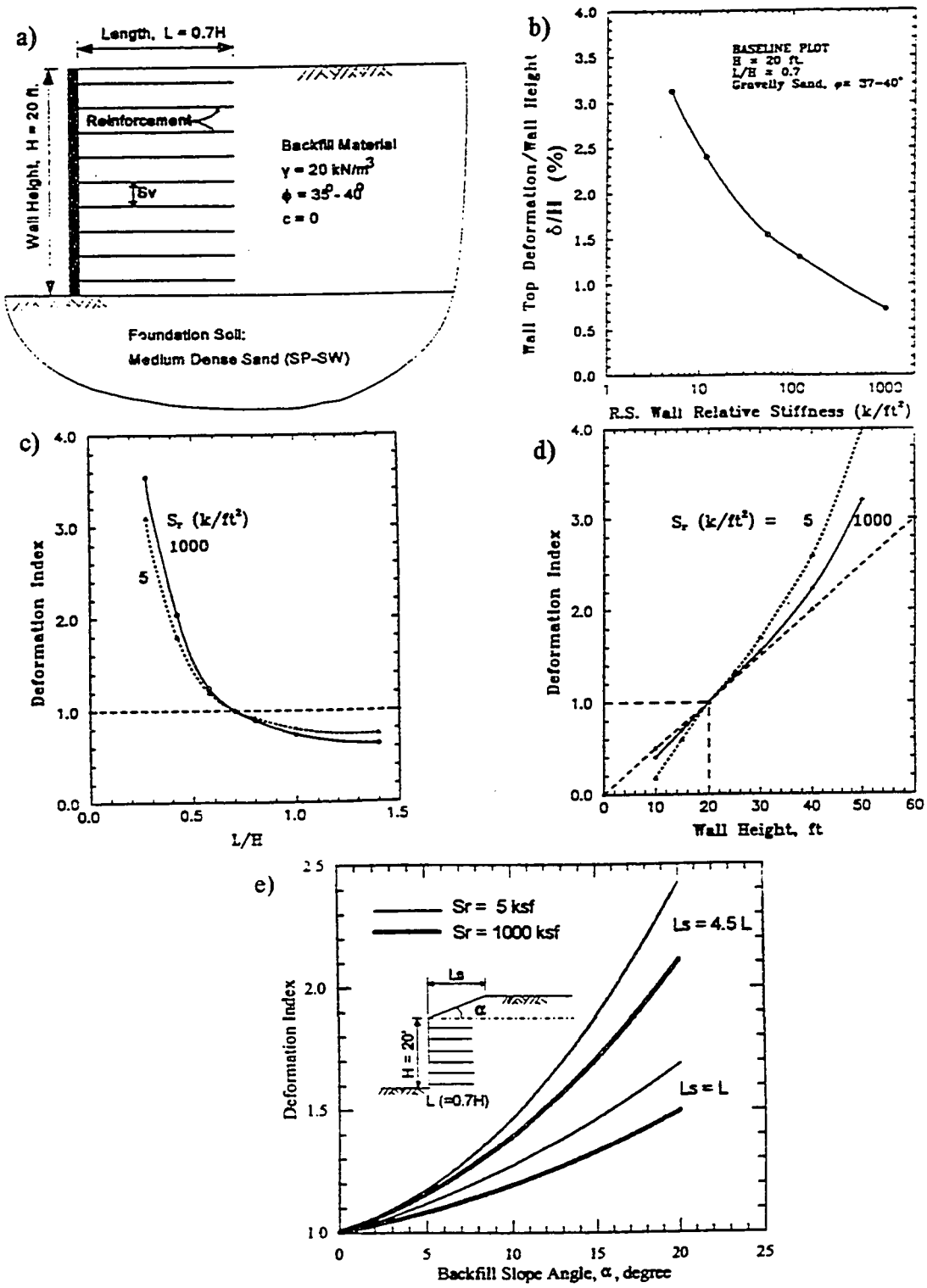

Figure 3.17: GRS wall deformation prediction charts: a) baseline configuration, b) $(\delta/H)_{base}$ vs. S_r, c) $DI_{L/H}$, d) DI_H, and e) DI_{slope} (after Chew and Mitchell, 1994).

6. Evaluate the reduced system stiffness due to material creeping and corrosion, if any. The long term d/H could be evaluated by using a $(d/H)_{base}$ based upon a reduced stiffness ratio, S_r, estimated using reduced reinforcement strength properties which account for creep (Chew and Mitchell, 1994).

Both the Christopher method, [Christopher, et al. (1990) as modified by Christopher (1993)], and the Chew and Mitchell (1994) procedure are simple to apply and may be used to obtain approximate estimates of maximum displacement of the wall face for walls designed using any of the currently used design procedures. To evaluate the accuracy of these procedures a comparison of the displacements predicted using these methods with those measured in instrumented walls was made. Results are presented in Table 3.3. The reader is reminded that the soils and facing materials used in these walls as well as the construction methods may differ from those for which the deformation prediction methods were developed. Except for those walls included in the list which were part of the program used to develop the Christopher (1993) chart [Adib (1988), walls 1 - 6] an exact match of predicted and actual deformations should not be expected.

Both procedures typically predicted wall deformations within -50% to +100% of the deformations measured. With the exception of the two walls which Chew and Mitchell (1994) used as examples of the applicability of their procedure [Gaspe seawall (Berg, et al., 1987) and Mur Ebal wall (Balzier, et al., 1991)] and the three walls reported by Djarwadi and Wong (1994), the Christopher (1993) method more closely predicted wall deformations. The Chew and Mitchell procedure was more likely to overpredict deformations, and by a greater magnitude, than the Christopher method. Even for what could be considered ideal situations: inextensible reinforcement in walls with L/H ratios equal to the baseline case of 0.7 [Adib (1988), walls 1, 3, 4, and 5], the Chew and Mitchell procedure overpredicted deformations by approximately 100%. For walls higher than the 6 m baseline case the amount of overprediction using the Chew and Mitchell procedure increased substantially, predicting deformations 2.6 and 4.25 times greater than those measured for the Malaysian wall (Hajiali, 1991) and the Rainier Avenue wall (Holtz, et al., 1990), respectively. The Christopher (1993) procedure did a better job of predicting deformations of these high walls, with predictions within 5% and 30% of the measured deformations, respectively.

Table 3.3: Predicted deformations for reinforced soil wall case histories using Chew and Mitchell (1993) and Christopher, et al. (1990), as modified by Christopher (1993), procedures.

Description	Reference	H(m)	L/H	ϕ_{tx}	$S_R(k/ft^2)^1$	$\delta_{meas.}$(mm)	$\delta_{C\&M}$(mm)	$\delta_{Christ.}$(mm)
Tuscon wall	Berg, et al. (1986)	4.65	0.80	34	120	65	44	26
Lithonia wall		6.0	0.60	40	120	65	96	44
Gaspe seawall	Berg, et al. (1987)	5.3	0.70	?	120	40	45	71
Wall 1	Adib (1988) and	6.1	0.70	40	1500	24	43	24
Wall 2	Christopher (1993)	6.1	0.70	40	56	25-50	91	46
Wall 3		6.1	0.70	40	1000	23	43	24
Wall 4		6.1	0.70	40	1000	20	43	24
Wall 5		6.1	0.70	40	1000	23	43	24
Wall 6		6.1	0.70	40	10	100	152	74
Malaysa wall	Hajiali (1991)	7.5	0.80	40	1000	25	63	24
Rainier wall	Holtz, et al (1990)	12.6	0.77	43	30	100-130	550	100
Mur Ebal	Balzier, et al. (1991)	2.9	0.70	39	6-12	11	14-17	38
Websol wall	Won, et al. (1994)	8.4	0.64	41-44	≈50?	50-100	240	36
Apron wall	Djarwadi and Wong	8.0	1.11	15	95	100	115	37
Chute wall	(1994)	4.75	1.11	c=16kN/m^2	95	90	34	22
Stilling wall		10.8	1.11	"	95	160	230	50

[1]Stiffness Ratio, S_R, in kips/ft^2 to permit direct application of this ratio in the Chew and Mitchell (1994) and Christopher (1993) procedures.

The Chew and Mitchell (1994) charts were developed using only numerical methods. This required the modeling of material properties, construction effects, foundation conditions, etc. Errors in modeling any of these parameters may have influenced the solutions obtained. The somewhat better performance of the Christopher (1993) method, which also used numerical methods in its development, may result from the correlations that were made with empirical data collected from field and laboratory studies. Thus, errors in modeling material properties may have been compensated for when the computed solutions were "adjusted" to equal the measured values.

Both procedures were found to be simple to use and have identified the L/H ratio and stiffness ratio, S_r, as principal factors affecting deformations. The Christopher (1993) method better predicted deformations but provides no method for accounting for sloping surcharges or strip loads above the wall. The Chew and Mitchell (1994) procedure includes these factors but does not do a better job at predicting wall deformations even when surcharge and strip loads are not applied. Additional work on these or other chart based deformation prediction procedures appears warranted.

3.5 Conclusion

The increase in the load supporting capacity of reinforced soils can be described as resulting from the addition of an apparent cohesion to the soil or from an increase in the effective confining pressure acting on the soil. Reinforced soil behavior is dependent on the soil properties and the modulus and extensibility of the reinforcement.

Through parametric studies a multitude of factors which influence GRS wall deformation have been identified. These include soil and reinforcement properties, construction technique, facing materials, foundation conditions and applied loads. Plane strain soil properties have not been used in the parametric studies conducted using FEM. The effect on GRS wall deformations from using triaxial instead of plane strain soil properties has not been investigated.

Simple design procedures which consider all of these factors and accurately predict deformations of GRS walls are not available. Limit equilibrium methods, which have proven successful in producing safe designs, have not been effectively adapted for deformation prediction. Use of the finite element method has met with mixed success in class A predictions, has been used extensively in parametric studies, and has been found to hold substantial promise as a deformation prediction tool. The design chart presented

by Christopher, et al. (1990) and modified by Christopher (1993) is simple to use and (reportedly) produces acceptable results. The charts developed by Chew and Mitchell (1994) address more loading conditions but were not as accurate for even simple cases. For explicit consideration of GRS wall deformations at the design stage development of new deformation prediction methods, use of the finite element method, or creation of additional design charts is necessary.

An investigation of the plane strain behavior of reinforced soil is required to permit the plane strain conditions to be properly considered when designing and evaluating GRS walls. The reinforcement length to height ratio has been identified as one of the most influential factors affecting GRS wall behavior. Additional study into why this relationship has such a great influence on wall deformations also is warranted. These two factors, plane strain reinforced soil behavior and wall dimensions, were investigated as part of this research project. The results of laboratory tests using the plane strain Unit Cell Device are presented in Chapter 6. Finite element evaluations of reinforced soil walls assumed constructed from elastic materials were conducted to investigate the influence of wall dimensions, Chapter 7.

CHAPTER 4
RESEARCH OBJECTIVES AND PROGRAM SUMMARY

4.1 Research Objectives

The specific goals of this project are to:

1. expand our knowledge of the in-soil load-deformation response of geotextiles, and
2. develop methods for predicting GRS wall deformations under working conditions.

Before a reliable deformation prediction method can be developed it is important to understand the fundamental behavior of geosynthetic reinforced soil. Since both the geosynthetic and the soil contribute to defining this behavior, a literature review was conducted of methods for strength testing reinforcement geotextiles and reinforced soil specimens, Chapter 2. This review identified confinement in soil, simulation of field loading conditions, and polymer creep as factors which may influence measured geosynthetic strength properties. The importance of measuring soil properties at simulated field density and confinement pressures, and under plane strain conditions was also emphasized in the literature. Since no single in-soil geosynthetic testing device met these conditions, a unit cell test device (introduced in Chapter 6) was specially constructed for this project.

A review of the literature on geosynthetic reinforced soil wall behavior, Chapter 3, reemphasized the importance of geosynthetic and soil properties in predicting deformations. Reinforcement length, spacing and arrangement, facing method, facing rigidity, compaction energy, soil-reinforcement interface properties, external applied loads, and foundation conditions were identified as additional factors contributing to deformations. Because of the large number of variables which influence GRS walls, deformation prediction has proven difficult. Current methods for predicting deformations were found to be unreliable (limit equilibrium methods), complicated (FEM), or capable of only producing rough approximations. Additional research into deformation prediction methods is warranted.

4.2 Program Summary

This research program, in working toward the two goals stated above and in light of the findings of the literature reviews, was divided into four principal sections:

1. Performance of in-isolation load-elongation tests on six geotextiles selected for this project. The strain rate dependency and creep characteristics of four woven geotextiles were evaluated. The effect of specimen gage length on the strength properties of two nonwoven needle-punched geotextiles was also investigated. (Chapter 5)

2. Performance of in-soil load-elongation tests using these same six geosynthetics. Evaluation of the geotextile properties and the response of two sands when reinforced with these materials. The unit cell device was used to conduct these tests. (Chapter 6)

3. Investigation of general behavior of reinforced soil retaining walls using linearly elastic materials and the finite element method. (Chapter 7)

4. Combining what was learned in Chapters 5 - 7 and using it to evaluate the measured behavior of the Rainier Avenue wall. Combining the literature review and research findings to make recommendations for predicting GRS wall deformations. (Chapter 8)

Because this project is a follow-on to a field study of the Rainier Avenue wall (Christopher, et al., 1991; STS, 1990; Holtz, et al., 1991; Allen, et al., 1992), the geotextiles and soil used in the construction of the Rainier Avenue wall were included in the testing portion of this research.

Conclusions reached through this research program and recommendations for further study are presented in Chapter 9.

CHAPTER 5
GEOSYNTHETIC CHARACTERIZATION - IN-ISOLATION TESTS

5.1 Introduction

The wide width test, ASTM D 4595 (ASTM 1993), is the most widely used procedure for obtaining the ultimate strength and modulus of geosynthetic reinforcements. To perform this test a 100 mm long by 200 mm wide geosynthetic reinforcement specimen is loaded to failure at a strain rate of 10%/min. This is an in-isolation test, i.e., the specimen is not confined in soil. When this project was conceived, a limited number of standard ASTM D 4595 tests were to be performed on the geotextiles included in this program for comparison with the results obtained from in-soil tests using the Unit Cell Device (UCD) (see Chapter 6). However, early in the UCD testing program it was discovered that the responses of the woven geosynthetics were very sensitive to strain rate, more so than anticipated after performing the literature review (see Section 2.2). These geosynthetics also showed evidence of rapid creep at very low stress and strain levels. Additionally, the increasing normal stress conditions to which the nonwoven geotextiles were subjected during UCD tests made correlation with in-isolation wide width test results difficult. Thus, the in-isolation testing program was expanded for more detailed characterization of the geosynthetics. This expanded program included (1) a series of wide width tests on the woven geotextiles, conducted at various strain rates, to study the strain rate effect; (2) a series of wide width tests on the nonwoven geotextiles, with gage lengths from 25 mm to 115 mm, to determine if an in-isolation zero gage length test would be appropriate for predicting the confined, in-soil modulus; and (3) in-isolation creep tests on the woven geotextiles with an initial strain near 1%., a typical maximum geotextile strain observed in GRS walls (See Section 3.3). Additionally, tests were conducted with strain gages attached to the geotextile specimens to determine if a correlation between strain gage readings and overall strain could be established.

Results of this program are presented in this chapter. The tests were conducted, under the direction of the author, by Mr. Matthew Gallagher while pursuing a masters degree in Civil Engineering at the University of Washington. Comprehensive details of the program are presented in Gallagher (1995). To minimize repetition, only limited discussion of the in-isolation test results is presented in this chapter. The significance of

the in-isolation test results and their relationship to the in-soil tests are discussed in Chapter 6 in conjunction with the UCD test results discussion.

5.2 Materials

The geosynthetic reinforcements used for the in-isolation wide width tests included three polypropylene woven slit-film geotextiles (Reinforcements PP1, PP2 and PP3), one polyester woven multi-filament geotextile (Reinforcement PET2), and two polyester nonwoven needle-punched geotextiles (Reinforcements NW1 and NW2), Table 5.1. Reinforcements PP2 and PP3 were manufactured by stitch-bonding together 2 and 3 layers of Reinforcement PP1, respectively. Reinforcements PP1, PP2, PP3, and PET1 are the same materials which were used in the construction of the Rainier Avenue wall (Allen, et al., 1992). Geotextile PP1 specimens were cut from material which had been exhumed from the Rainier Avenue wall during its demolition. Tests with PP2 and PP3 were conducted with new material. Geotextile PET2 was manufactured of the same materials and by the same procedures as was the polyester reinforcement used in the Rainier Avenue wall, PET1. However, PET2 was used in the in-isolation tests because geotextile PET1 was no longer being manufactured and insufficient quantities had been exhumed from the wall to permit its use for both UCD and in-isolation tests.

Nonwoven geotextiles were included in the laboratory program because they have been effectively used in field applications and full scale GRS test walls (Bell and Steward, 1977; Bell, et al., 1983; Werner and Resl, 1986; Adib, 1988; Delmas, et al., 1988) and are less expensive than other geosynthetic reinforcements. If their behavior and reinforcement characteristics could be better quantified, the economies associated with using nonwoven geotextiles could be recognized more often in GRS wall applications. Nonwoven NW2 was selected because its unit weight, 532 g/m^2, was considered typical of a needle-punched nonwoven which might be selected for application in a GRS wall. The 268 g/m^2 nonwoven geotextile, NW1, was selected as representative of the lightest weight nonwoven which would be considered for this application (T.M. Allen, 1992, personal communication).

5.3 Test Apparatus, Instrumentation, and Sample Preparation

The wide width tests were performed using an MTS 810 testing machine with an 89 kN load cell. Hydraulically operated clamps, Curtis "Sure Grip", Inc. Geo-Grips, were

used to hold each end of the geotextiles during testing. Elongation of the geotextiles was measured using a "scissors" type displacement measuring device, Figure 5.1. The scissors were attached to the geotextiles by pushing needles, mounted at the end of each arm, through the reinforcement. The distance between the needles when the tensile load in the geotextile at the beginning of each test started to increase (approximately 60 - 75 mm for 100 mm gage length specimens) was used as the initial gage length for calculating strains in the woven geotextiles. For the geotextiles tested, no measurable reduction in strength resulted from insertion of the needles. An LVDT was mounted at the opposite end of the scissor arms to measure displacements. To maximize the accuracy of displacement measurements, LVDT's with maximum range of motion as close as practicable to the total displacement anticipated for each material type were selected. Lucas/Schaevitz 500 MHR LVDT, maximum total stroke 25.4 mm, and 1000 MHR LVDT, maximum total stroke 50.8 mm, were used when testing the woven and nonwoven geotextiles, respectively. Load and displacement data signals were converted to digital form using a Metrobyte 16F data acquisition board. Labtech Notebook data acquisition software was used to store the data on an IBM 286 personal computer. Strains in the nonwoven geotextiles were computed using cross-head displacement data, because of erratic and unreliable readings obtained from the "scissors" when used with these reinforcements, and difficulty using the scissors for specimen gage lengths less than 75 mm.

Strain gages were attached to the woven geotextiles for some of the tests to determine the relationship between strains measured with strain gages and overall specimen strain. The purpose for including strain gages in this study was to permit evaluation of strain gage measurement data recorded in the Rainier Avenue wall. Consequently, the strain gages were made by the same manufacturers and of the same models as those used in the Rainier Avenue wall instrumentation program. The same adhesives used for attaching the gages to the geotextiles in the Rainier Avenue wall were also used in this program (see Christopher, et al., 1991 and Allen, et al., 1992). YL-20 gages, manufactured by Tokyo Sokki Kenkyujo Co., LTD (TSK) were attached to the polypropylene geotextiles with CN adhesive. However, because the gages would not stay bonded, it was necessary to pretreat the polypropylene specimens with Aron Polyprimer surface preparation compound, also manufactured by TSK, before applying the CN adhesive. This type of surface preparation was not reported as part of the gage

Table 5.1: Geotextiles tested.

Reinforcement No.	Manufacturer and Product Name	Material	Description	Wide Width Strength (kN/m) -Elongation (%)[1] ASTM D 4595
PP1	Exxon GTF 200	Polypropylene	woven, slit-film	26 - 15[2]
PP2	Exxon GTF 375	Polypropylene	woven, slit-film, 2 layer stitch-bonded	49 - 15[2]
PP3	Exxon GTF 500	Polypropylene	woven, slit-film, 3 layer stitch-bonded	77 - 15[2]
PET1	Exxon GTF 1225T	Polyester	woven, multi-filament	215 / 10[4]
PET2	Exxon GTF 1000	Polyester	woven, multi-filament	175 / 10[2]
NW1	Polyfelt TS700	Polypropylene	nonwoven, needle-punched	16 / 95[3]
NW2	Polyfelt TS1000	Polypropylene	nonwoven, needle-punched	26 / 95[3]

[1]Manufacture published data from *Geotechnical Fabrics Report Specifiers Guide*, 1990, 1993.
[2]Minimum average roll values.
[3]Average roll values.
[4]Average value from Allen, et al., 1992a.

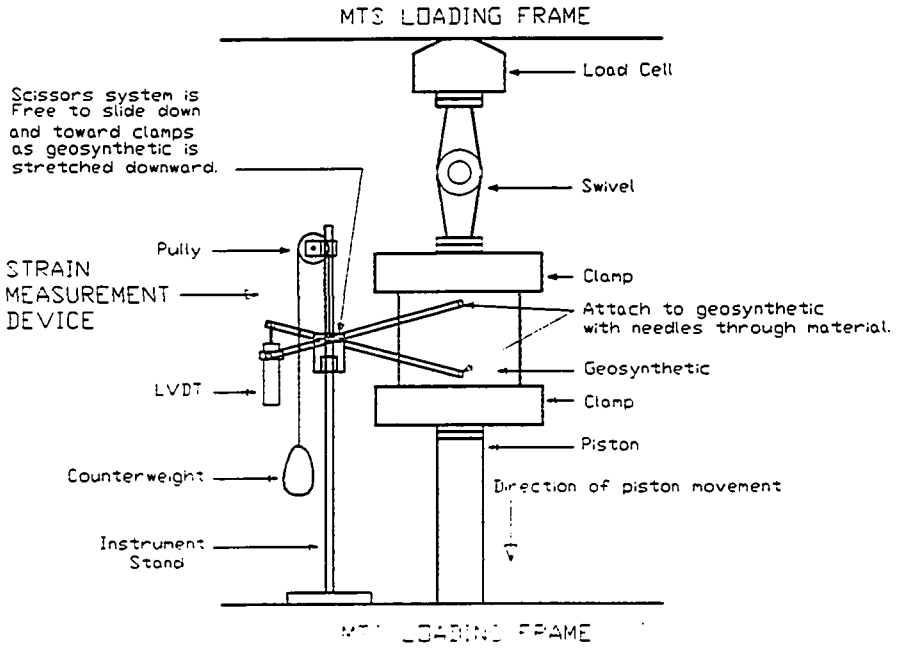

Figure 5.1: In-isolation test setup and displacement measurement "scissors".

attachment procedure by Christopher, et al. (1991) and Allen, et al. (1992). BLH Electronics PA-3 gages were attached to PET2 using SR-4 adhesive. No special surface preparation was required for the polyester geotextile. The waterproofing and other coatings used to protect the gages used in the Rainier Avenue wall were not applied over the gages for these tests. A Micromeasurements 2110A/2120A strain gage conditioner powered the strain gages and amplified their signals. Their signals were then converted to digital form and recorded using the same equipment and software as was used for the load cell and LVDT's.

Polypropylene woven geotextile specimens were cut to 200 mm wide by 200 mm long. The 50 mm on both ends of each specimen, where they were held by the clamps, were reinforced with an epoxy resin to prevent damage by the clamps. This resulted in a test specimen 200 mm wide with a 100 mm gage length between the clamps as required by ASTM D 4595 (ASTM, 1993).

Testing of the high strength polyester woven geotextile, PET2, presented some difficulties. Full 200 mm wide specimens could support loads exceeding the capacity of the clamps. Additionally, slip between the clamps and the specimen occurred at these large loads. To reduce the maximum load, specimen widths were reduced for the high strength polyester woven, PET2. This approach was taken based on the recommendations of Leshchinsky and Fowler (1990) and Paulson (1993). These authors reported that specimen widths could be reduced with no effect on measured wide width properties for materials of this type; i.e., filaments oriented in the direction of loading and little interaction between these filaments and cross-weave fibers. With the exception of two 50 mm wide specimens, PET2 specimens were 100 mm wide. No difference in strength or modulus, per unit width of geotextile, was measured for the different width specimens. Because the polyester filaments were easily damaged, in addition to impregnating the ends of each specimen with epoxy resin, a 0.3 mm thick sheet of stainless steel was glued on the outside of the epoxy for additional protection from the clamp teeth. Specimen gage length between clamps was 100 mm.

All nonwoven geotextile specimens had widths of 200 mm. Because these were low strength materials, it was not necessary to apply epoxy to the ends which were held by the clamps to prevent slippage. However, so that filaments would not be cut, clamps with only a roughened surface, instead of a deeply knurled "toothed" surface, were used.

5.4 Variable Strain Rate Tests

Typical load-elongation results for the woven geotextiles (Table 5.1), tested at 10% strain per minute in accordance with ASTM D 4595, are shown in Figure 5.2. The shapes of these curves are characteristic of the in-isolation tests conducted at 10%/min on these geotextiles. The polypropylene geotextile curves had a near linear or a slight concave downward bend until failure was approached. The curve for the polyester geotextile was more complex; the slope started off flat, steepened near 0.3%-0.5%, flattened again near 3% strain, and increased again near 7% strain. In this program the average strength and the average corresponding elongation measured for the woven geotextiles were less than those reported by Allen, et al. (1992). In fact, the strengths were nearer to, and the corresponding strains were less than (with the exception of Reinforcement PET2), the minimum average roll values reported by the manufacturers, Table 5.1.

The decrease in strength below those reported by Allen, et al. (1992) and the manufacturer may, at least partially, be attributed to difficulties gripping the reinforcements in a manner which did not damage them. As mentioned above, the ends of the specimens were coated with an epoxy resin to prevent damage to the fibers. Additional protection for the multi-filament polyester fibers was provided by overlaying the epoxy with a 0.3 mm steel sheet. However, this protection may not have been sufficient as these geotextiles typically failed near the clamps. Although different types of end protection and grips with smaller teeth were tried, the method used proved to be the best. The application of the epoxy may itself have influenced the failure mode of the specimens by causing a stress concentration at the transition point from epoxy coated reinforcing to the uncoated specimen. A better means of gripping these high strength reinforcements is needed and a program comparing tests performed with roller clamps is recommended.

The differences in strain measurements at failure may also be attributed to failure of the geotextiles near the clamps. This failure zone, which would correspond to the zone of highest localized strain, was outside the region measured by the displacement measurement scissors, Figure 5.1. The scissors did not, therefore, measure overall specimen strain at failure, but only measured the strain between the two needles. Not including this failure zone would result in underrecording of the overall specimen strain

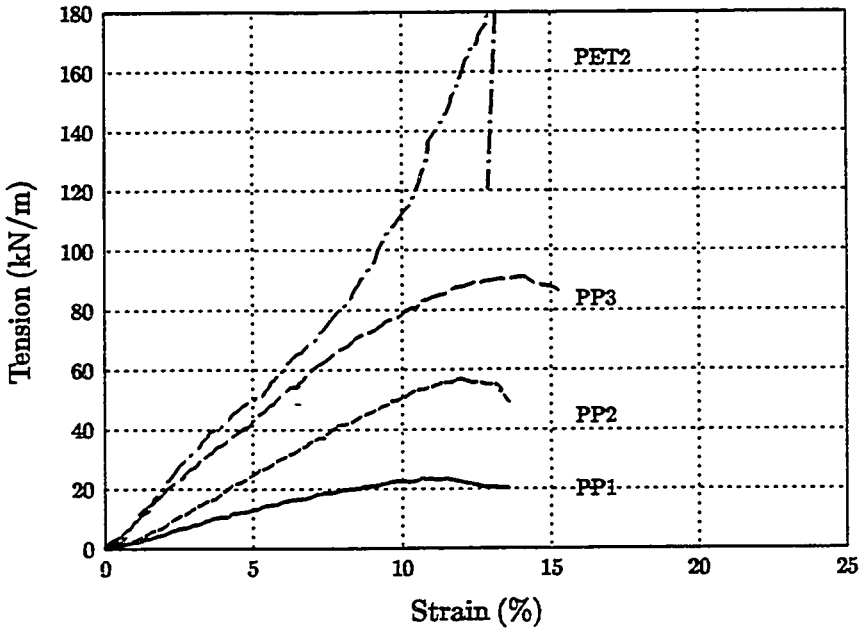

Figure 5.2: Tension vs. strain for the woven geotextiles at a strain rate of 10%/min.

Table 5.2: Comparison of wide width test results (ASTM D 4595) performed by Gallagher (1995) with those reported by Allen, et al. (1992a) for the woven geotextiles.

	Gallagher (1995)			Allen, et al. (1992a)		
Reinforcing	Strength (kN/m)	Strain at failure (%)	5% Secant Modulus (kN/m)	Strength (kN/m)	Strain at failure (%)	5% Secant Modulus (kN/m)
PP1	24.3	10.5	260	31 (21)[1]	21 (15)[1]	198 (181)[1]
PP2	53.3	12.7	470	62	16	453
PP3	77.6	13.6	780	92	17	662
PET1	na	na	na	186	18	1068
PET2	162	12.4	1000	na	na	na

[1]Values in parenthesis are for tests on specimens exhumed from Rainier Avenue wall.

Table 5.3: Number of tests conducted at each strain rate on woven geotextiles.

	Strain Rate (%/min.)				
Reinforcing	10.0	1.0	0.1	0.01	Creep
PP1	7	3	6	6	0
PP2	10	5	4	7	2
PP3	11	5	4	8	2
PET2	10	2	2	5	3

at failure. Again, a better means of clamping these geotextiles is needed so that the failure zone would fall in the region bounded by the strain measurement device needles.

Although the strengths measured in the wide width tests were less than those reported by Allen, et al. (1992) the modulus measured for the three polypropylene geotextiles were greater, Table 5.2. (The modulus of PET2 could not be compared since it was not used in the wall and no manufacturer's data were available for it.) Since the modulus was determined at strains much less than failure, damage to the geotextiles by the clamps should not be a factor. The overall specimen strain should also be more closely measured by the scissors since stress concentration effects should have less effect at the lower stress state associated with these strains. Therefore, the modulus values measured in this program should be closer to the modulus that would be obtained were clamp damage not a factor.

The effect of strain rate on the strength properties of the four woven geotextiles, PP1, PP2, PP3, and PET2, was investigated through a series of wide width tests conducted at strain rates of 10%/min, 1%/min, 0.1%/min and 0.01%/min, Table 5.3. The modulus and strength of the woven polypropylene geotextiles were found to be very sensitive to strain rate and followed the same general pattern as was reported by Cheok (1985), Figure 2.26. With decreasing strain rate a decrease in strength and modulus was observed, Figures 5.3 to 5.5. The woven polyester geotextile, PET2, although still affected, was not as sensitive to strain rate as were the woven polypropylene geotextiles, and it was sometimes difficult to distinguish between tests conducted at different strain rates, Figure 5.6. The 5% modulus (secant modulus determined at 5% strain) decreased by approximately 50% for all three polypropylene woven geotextiles when the strain rate was decreased from 10%/min to 0.01%/min, whereas the 5% modulus for PET2 decreased by only 15% to 20% for the same decrease in strain rates, Figure 5.7.

The in-isolation tests on these woven geotextiles suggest that using the ASTM D 4595 wide width test procedure, conducted at the specified 10%/min strain rate, is not appropriate for measuring geosynthetic strength properties. The procedure should be modified to account for the strain rate dependency of geosynthetics. However, any procedure for determining the load-elongation properties of reinforcement geosynthetics should also, ideally, account for the effects of confinement in soil (see Section 2.2). The influence of confinement in soil on these woven geotextiles is discussed in Section

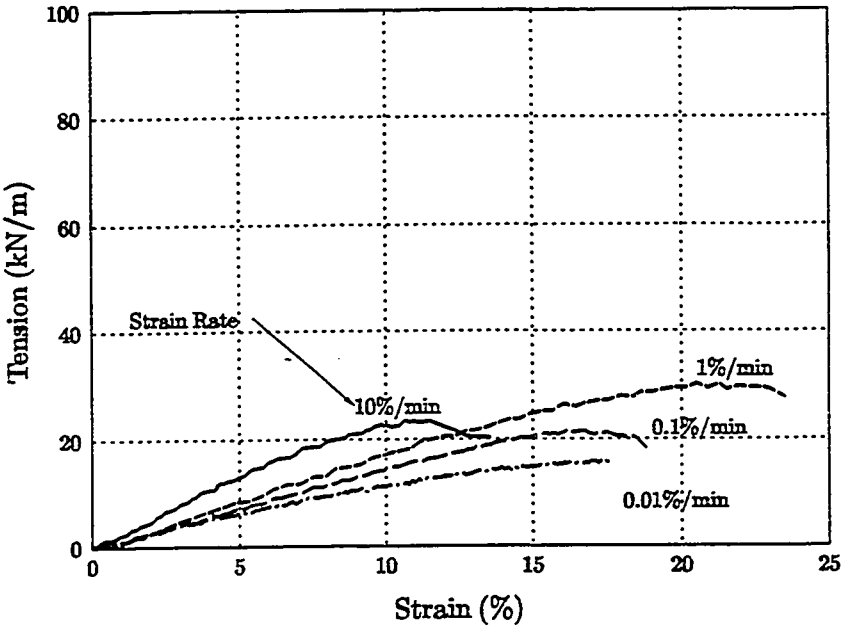

Figure 5.3: Tension vs. strain for Reinforcing PP1.

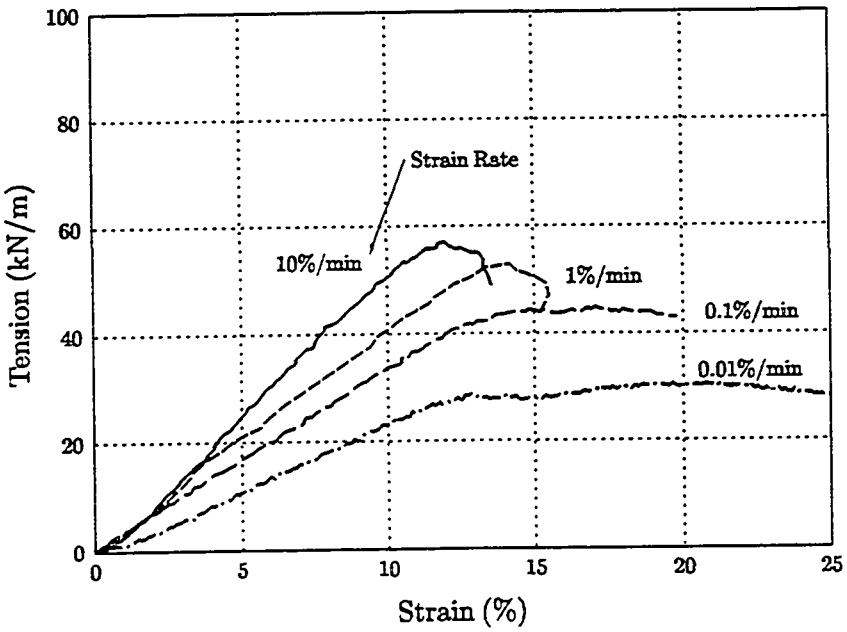

Figure 5.4: Tension vs. strain for Reinforcing PP2.

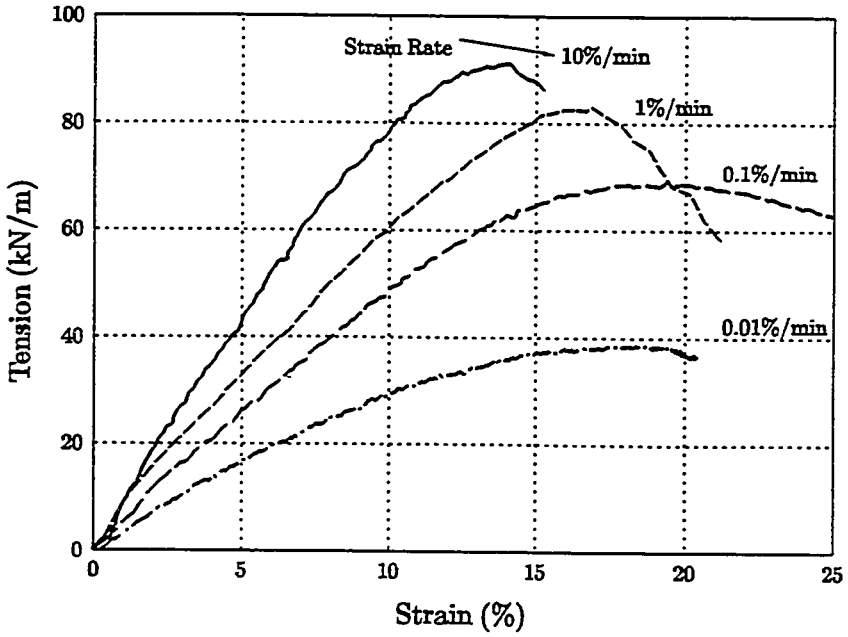

Figure 5.5: Tension vs. strain for Reinforcing PP3.

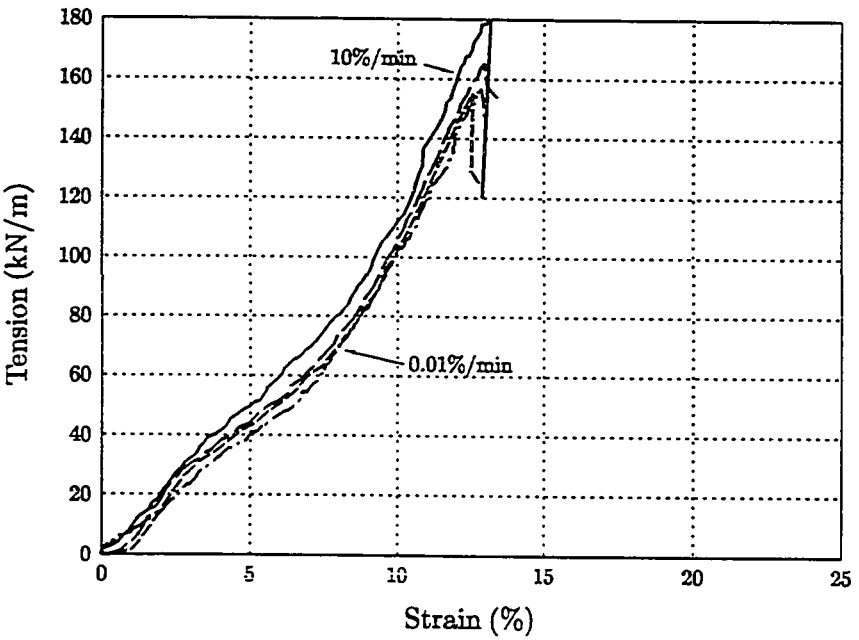

Figure 5.6: Tension vs. strain for Reinforcing PET2.

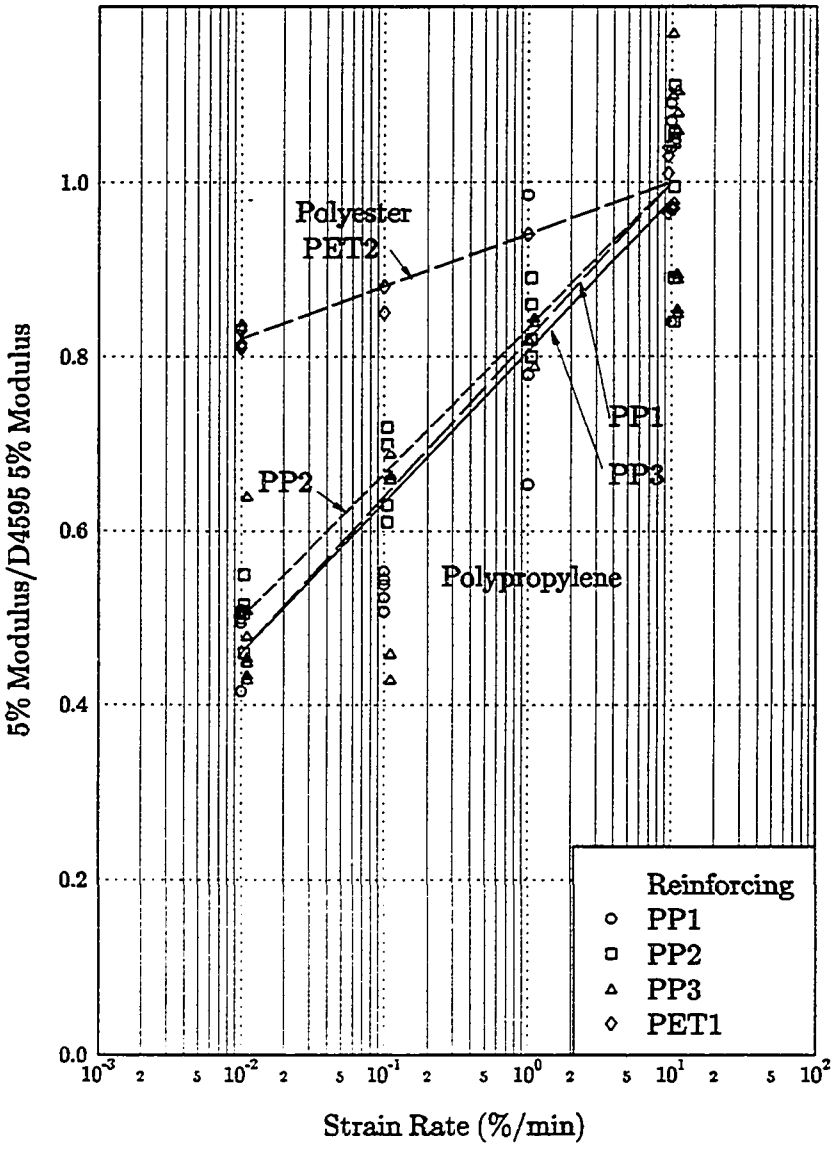

Figure 5.7: Normalized modulus vs. strain rate for the woven geotextiles.

6.4.2.1.3. An assessment of ASTM D 4595, and recommended modifications of this procedure, are presented in Section 6.6.

5.5 Variable Gauge Length Tests

Wide width tests were conducted on 200 mm wide specimens of the nonwoven needle-punched geotextiles, Reinforcements NW1 and NW2, at gage lengths of 25 mm, 50 mm, 56 mm, 75 mm, 100 mm and 115 mm, Table 5.4. All tests were conducted at strain rates of 10%/min by adjusting the loading piston displacement rate for the specimen length. Typical results are presented in Figure 5.8. These tests were performed to determine if a correlation could be established between in-isolation and confined, in-soil stress-strain behavior. If such a relationship could be established it would simplify testing of nonwoven geotextiles by eliminating the need for researchers and practitioners to perform confined tests (see Section 2.1.3). The premise under which these tests were performed assumed that the shorter gage lengths would more closely approximate the plane strain conditions of confinement in soil and would approach the near "zero" gage length between soil particles in GRS systems (Christopher, et al, 1986; Resl, 1990). Anjiang, et al. (1986) and Resl (1990) had shown increases in strength with decreases in gage length of nonwoven geotextiles. However, neither had performed both in-isolation and in-soil tests to determine if a correlation between these test results could be made.

No increase in strength with decrease in gage length was confirmed for the two nonwovens tested, Figure 5.9. Geotextile strength was approximately the same for all gage lengths. This is counter to the results reported by Anjiang, et al. (1986) and Resl (1990). Anjiang, et al. (1986) reported strength increases of 25% to 33% for decreases in length from 200 mm to 50 mm. Resl (1990) reported increases in strength from 65% to greater than 130% for decreases in gage length from 200 mm to 3 mm. One possible explanation for the difference between the results obtained here and those reported by these authors is the rate of strain. The strain rate for tests conducted for this program remained constant at 10%/min regardless of specimen length; therefore the filaments (if their random orientation is ignored) were strained at the same rate regardless of specimen length. Anjiang, et al. (1986) maintained a constant loading piston *displacement* rate, not a constant *strain* rate. Thus, for a decrease in gage length from 200 mm to 50 mm the strain rate would increase by a factor of four. Although Resl (1990) does not indicate if

Table 5.4: Number of tests conducted at each gage length on nonwoven geotextiles.

	Gage Length (mm)					
Reinforcing	25	50	56	75	100	115
NW1	5	5	2	4	6	5
NW2	5	4	4	4	4	3

the strain rate or loading piston displacement rate were held constant, the similarity between Resl (1990) and Anjiang, et al. (1986) data and the 30% increase in strength of woven geotextiles tested by Reŝl using the same procedure suggests Resl also held the displacement rate constant. If the polypropylene filaments in nonwovens NW1 and NW2 behave similarly to the woven polypropylene geotextiles tested in this program (see Section 5.4), an increase in strength with increasing strain rate should be expected. Anjiang, et al. (1986) and Resl (1990) were thus combining variable strain rate tests with variable gage length tests, and their results should not be used for projecting a "zero" gage length strength. The test method chosen for this program, where strain rate was constant regardless of specimen length, would more closely model an in-soil load-elongation test conducted at that same strain rate (see Section 2.1.3) and is the more appropriate test method for comparison of in-isolation and in-soil results.

Although no increase in nonwoven geotextile strength was recorded, the modulus appears to have increased with decreasing gage length, Figure 5.10. The 5% modulus for NW1 and NW2 increased by approximately 100% and 55%, respectively, when the gage length was reduced from 115 mm to 25 mm. Since neither Anjiang, et al. (1986) nor Resl (1990) had reported modulus data, no comparison with their results could be made. The extrapolated "zero" gage length 5% modulus for NW1 and NW2 were approximately 55 kN/m and 105 kN/m, respectively. These correspond to increases in modulus of 100% and 60% for NW1 and NW2, respectively, for a decrease in gage length from the ASTM D 4595 specified length of 100 mm to the assumed "zero" gage length for reinforcings installed in GRS walls. These increases are much less than the 200% to 300% increase in modulus of nonwoven geotextiles with confinement in soil reported by McGown, et al. (1982), Figure 2.3. Further discussion on the relationship between the "zero" span modulus and the in-soil modulus for these same reinforcements is presented in Section 6.4.2.1.2.

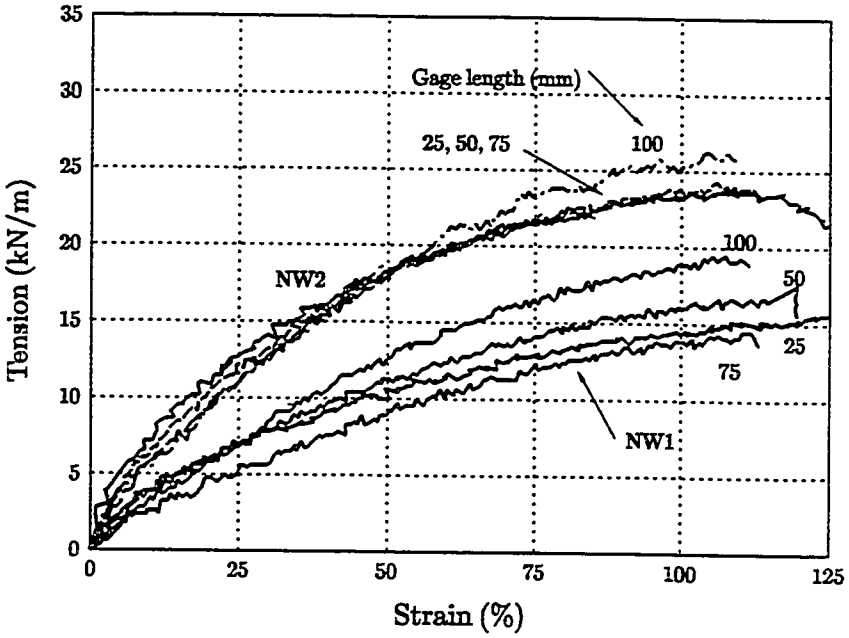

Figure 5.8: Tension vs. strain for the nonwoven geotextiles.

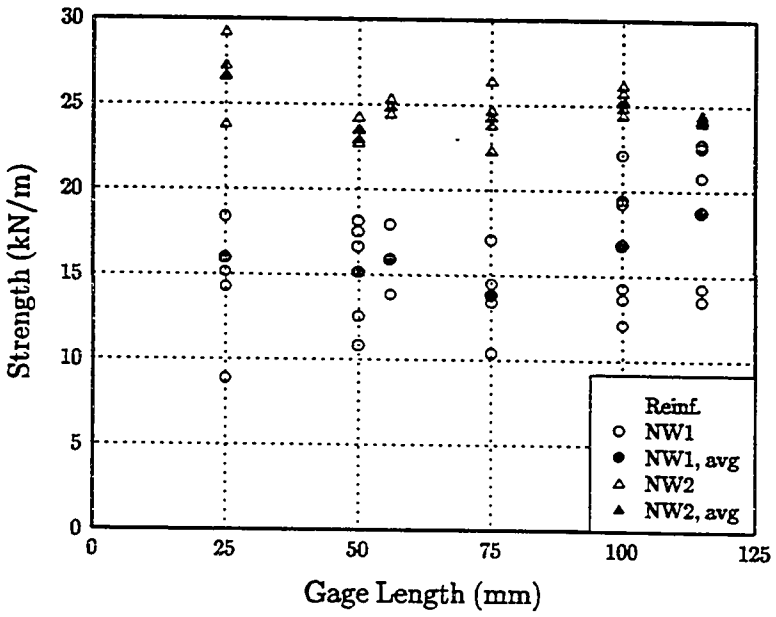

Figure 5.9: Strength vs. gage length for the nonwoven geotextiles.

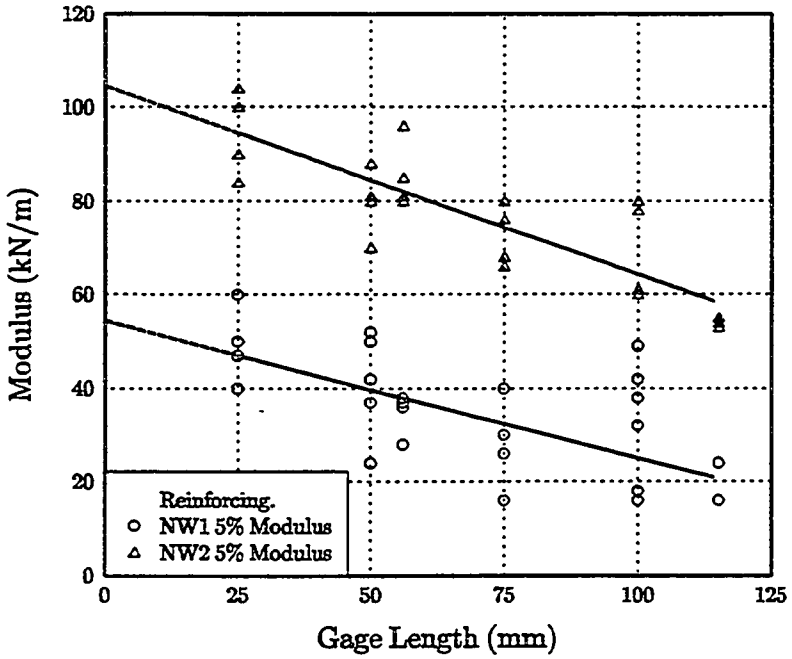

Figure 5.10: Modulus vs. gage length for the nonwoven geotextiles

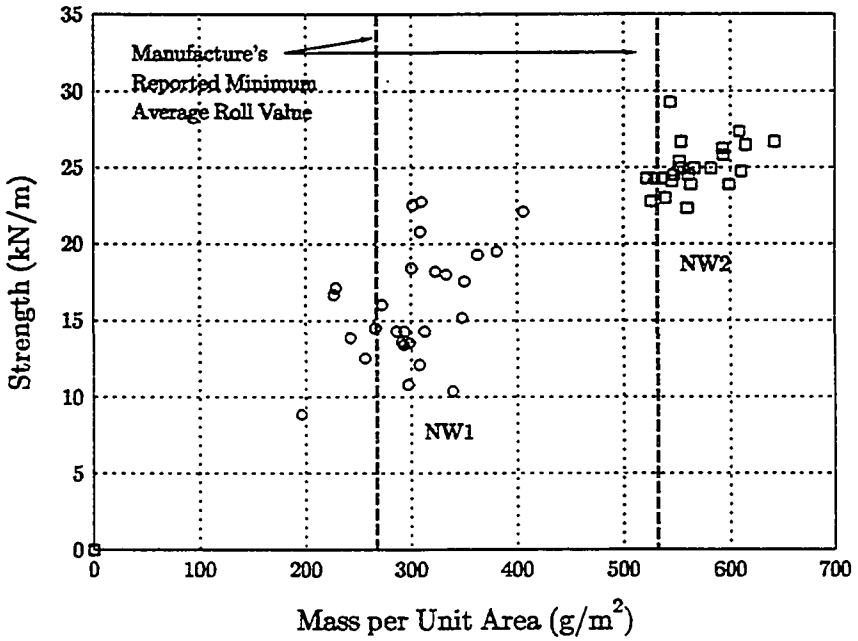

Figure 5.11: Strength vs. mass per unit area for the nonwoven geotextiles. (Minimum average roll value mass per unit area corresponds to the value two standard deviations below the mean determined in accordance with ASTM D 5361 (ASTM, 1993)

There was significant scatter in the test results for the nonwoven needle-punched geotextiles, Figures 5.8 to 5.10. This scatter was more pronounced with Reinforcement NW1, the lighter weight geotextile, than with Reinforcement NW2, which had approximately twice the mass per unit area. Some of this scatter can be attributed to test method variability or inaccuracies in the testing and response measurement of the nonwoven geotextiles. However, much of this scatter may be attributed to material variability. Despite both geotextiles being produced by the same manufacturer, supposedly by the same process, visual inspection and weighing of individual specimens found substantial variability in the density and distribution of fibers. Variation in unit weight had a noticeable influence on the measured geotextile strength. A general trend of strength decreasing with decreasing unit weight was identified, Figure 5.11. There was significantly more variability in unit weight for NW1 specimens, which also showed more variability in strength, than was observed for NW2. This variation in geotextile properties could create difficulties if the wide variability is not considered when these products are specified for use in GRS wall, or other, applications.

5.6 Creep Tests

An abbreviated creep test program involving only Reinforcements PP2, PP3, and PET2 was undertaken to establish the creep susceptibility of the woven geotextiles, Table 5.2. This program was initiated because of the substantial creep effects observed in UCD tests (see Section 6.4.2.2) and the creep observed in the Rainier Avenue walls (Allen, et al., 1992), Figure 3.10. Specimens were suspended from a small hoist and loaded with a known weight for a minimum of 72 hours, Figure 5.12. The weight was selected, using the wide width test results to correspond with the load associated with 1% strain on a 10%/min wide width test. The 72 hour test duration was deemed to be sufficient to establish the primary creep curve (T. Allen, 1993, personal communication). Due to variability in wide width test results, strain rate effects, creep, and material variability, it was difficult to select a weight which met the 1% strain criterion. Consequently, there was substantial variation in the initial strain and creep test results, for each reinforcement.

Significant creep was measured for both polypropylene geotextiles. Initial creep occurred quickly but decreased with time throughout each test. Strain at the end of the tests was over three times the strain immediately after load application for PP2, Figure

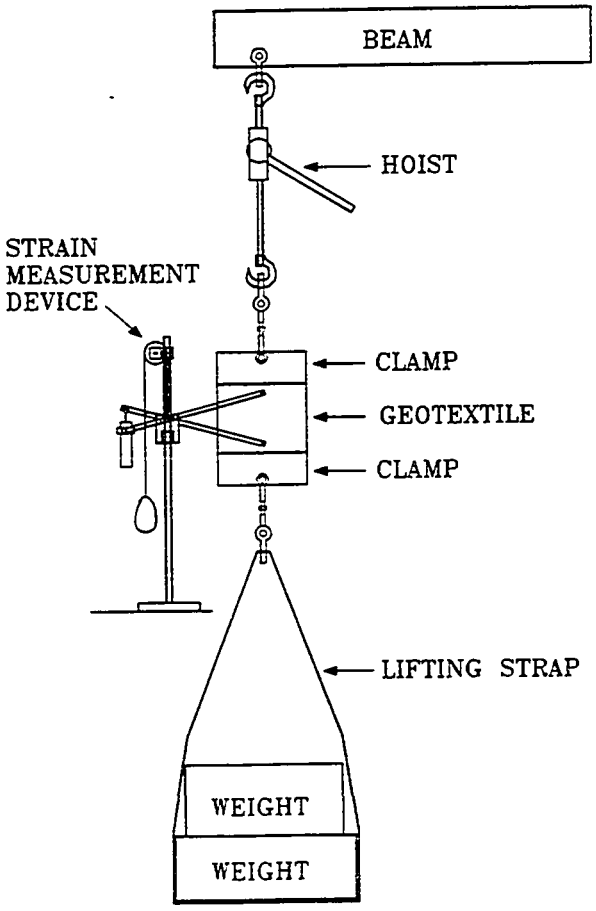

Figure 5.12: Creep test setup.

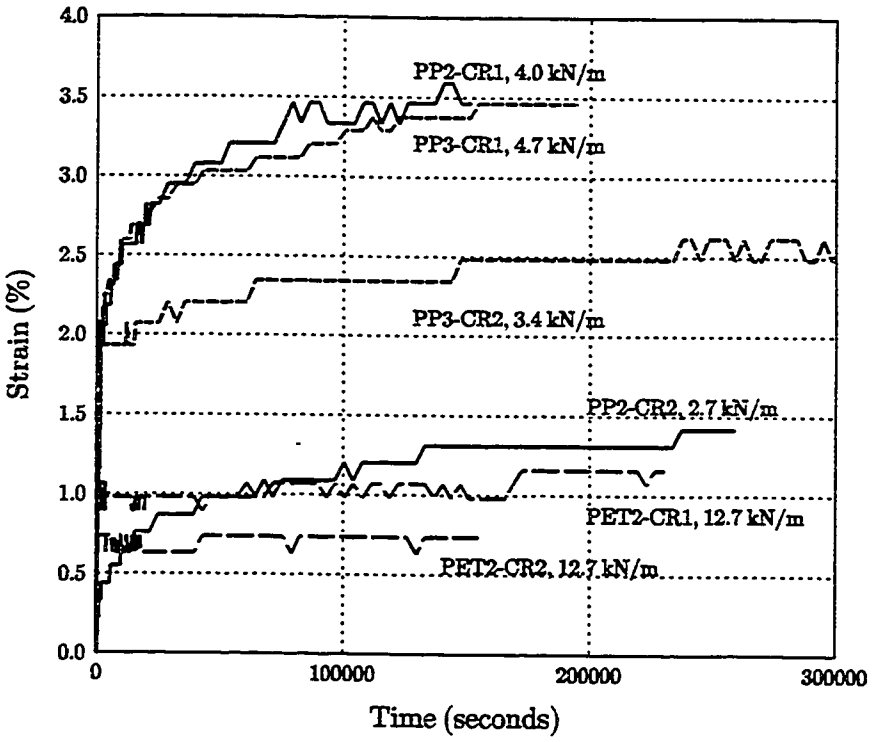

Figure 5.13: Strain vs. creep for woven geotextiles PP2, PP3 and PET2.

5.13. After about 2000 minutes the creep rate had slowed substantially but creep was still occurring when the tests were discontinued. For PP3 the strain at the end of the tests was less than two times the strain immediately after loading, but the creep rate had not slowed as much after 2000 minutes as it had for PP2, Figure 5.13. The polyester geotextile, PET2, did creep, but not as noticeably as did the polypropylenes, with increases in strain less than 20% beyond the initial strain, Figure 5.13.

This limited creep testing did little more than confirm the substantial difference in the creep potential of these two material types. Because of the greater creep potential of the polypropylene geotextiles and the substantial influence of strain rate on modulus, selecting a load to apply in the creep test from a 10%/min strain rate test, as was done here, is obviously inappropriate. Even when the initial load was reduced substantially below the 1% strain load determined from a standard wide width test (e.g., creep test PP2-CR2), the strain at the end of the test was more than 1%, Figure 5.13. This is much different from what occurred during the two tests performed on PET2; creep and strain rate effects were minimal despite a higher initial strain than was induced in PP2 for creep test PP2-CR2.

5.7 Strain Gage Tests

Some of the in-isolation wide width tests on woven geotextiles tested at various strain rates (Section 5.4) were conducted with strain gages attached to the reinforcing. The purpose for performing these tests was to determine if a correlation between overall reinforcing strain and that recorded by the strain gage could be established. The gages were positioned as near the center of the specimen as possible and aligned with the loading direction. The gages selected and the adhesives used for attaching them to the geotextiles were described in Section 5.3.

Strain gages attached to the polypropylene slit-film woven geotextiles, PP1, PP2, and PP3, reported less strain than was recorded for the overall specimen. The ratio of strain gage strain to total specimen strain (measured with the "scissors" device) changed during each test. After the first 1% strain this ratio generally increased to a maximum between 3% and 8% overall strain, Figure 5.14. Sensitivity of the calculation of this ratio to the low absolute initial magnitudes of both the total overall and strain gage strains resulted in significant variability of the calculated ratio of strain gage strain to overall strain for the first 1% overall strain. This sensitivity also affected the absolute magnitude of this ratio for the complete test. Therefore, the results were normalized to remove the effect of initial strain gage and overall strain readings from the analysis. Normalization entailed dividing the increase in strain gage strain by the corresponding increase in overall specimen strain which occurred during the same period of the test, Eq. 5.1.

$$NISR = \frac{\varepsilon_{sg}(t_2) - \varepsilon_{sg}(t_1)}{\varepsilon_{total}(t_2) - \varepsilon_{total}(t_1)} \qquad (5.1)$$

where:

NISR = normalized incremental strain ratio

$\varepsilon_{sg}(t)$ = strain gage strain at time t

$\varepsilon_{total}(t)$ = total overall strain at time t

The normalized incremental strain ratio, NISR, was computed at increments of 0.5% overall strain for the polypropylene geotextiles, and at smaller increments for the polyester geotextile. The pattern of NISR versus overall strain for the three polypropylene geotextiles followed the same general trend, Figures 5.15 to 5.17. The NISR increased to a maximum between 3% and 8% overall strain and then decreased after the yield strain of the gage was reached. Values near or beyond the gage yield

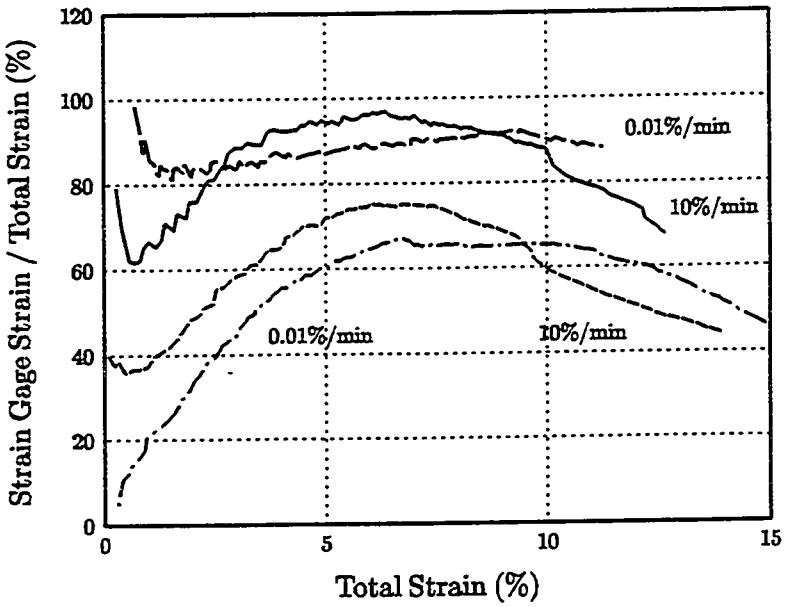

Figure 5.14: Normalized gage strain vs. overall specimen strain for PP2.

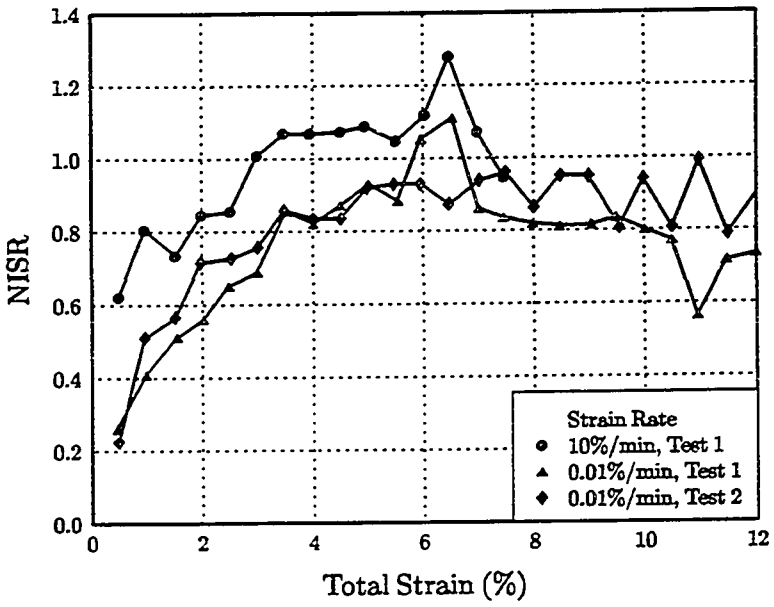

Figure 5.15: NISR vs. overall specimen strain for PP1.

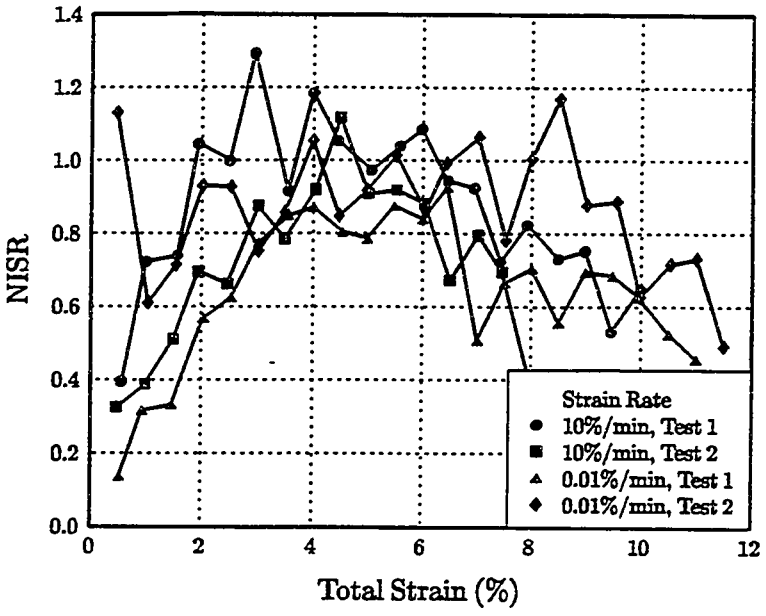

Figure 5.16: NISR vs. overall specimen strain for PP2.

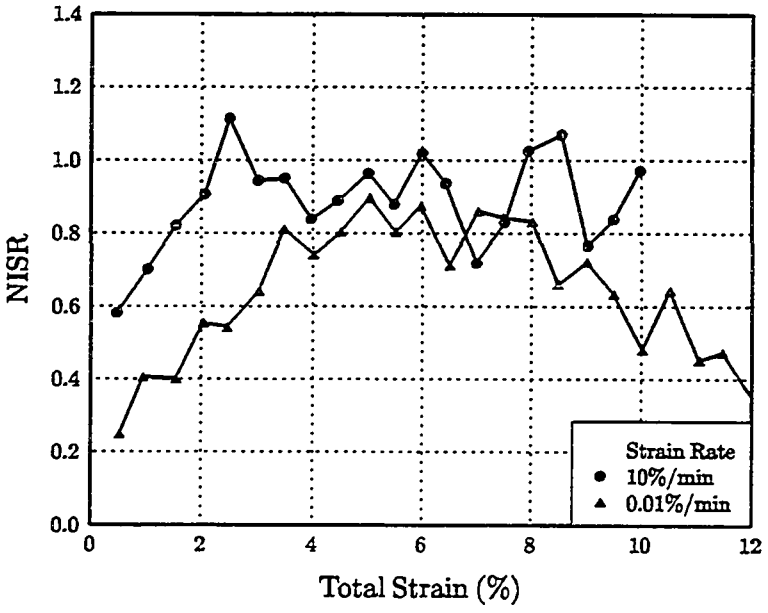

Figure 5.17: NISR vs. overall specimen strain for PP3.

strain, identifiable by the decrease in NISR at strains between 6% and 10%, should not be relied on. Ignoring the scatter of individual data points, it can be seen that the maximum incremental strain gage strain was typically between 80% and 100% of the incremental total strain. However, before reaching this maximum the gages significantly underrecorded overall strain.

Strain gage tests with PA-3 gages attached to Reinforcement PET2 met with limited success. Only two tests with strain gages produced reasonable NISR values, between 0.78 and 1.10, Figure 5.18. NISR values for one other test, shown in the figure, were very erratic and ranged from approximately 1.0 to greater than 1.6. Because the PA-3 gages would debond from the geotextile at low strains, 1 to 3%, evaluation of strain gage performance at higher strains was not possible.

This study confirmed that attaching strain gages to geotextiles may be an acceptable technique for measurement of geotextile strain, although they have been shown to underrecord overall geotextile strain. Provided the gages are properly calibrated and adjustments to the measurements are made to account for this underrecording, using strain gages for measuring geotextile strains in field installations may be adequate. The high variability of strain gage strain at low total strains may present some difficulties in geotextile walls where strains less than 1% have been measured (Allen, et al., 1992). This topic is discussed further in Section 6.4.5.2 in conjunction with the evaluation of in-soil tests with strain gages attached to the geotextiles.

5.8 Summary

a) In-isolation wide width tests on the woven geotextiles conducted at various strain rates determined that the strength and modulus of these materials decreased with decreasing strain rate. The decrease in 5% modulus associated with a decrease in strain rate from 10%/min to 0.01%/min was approximately 50% and 15% for the polypropylene and polyester geotextiles, respectively.

b) No increase in strength was observed with decreases in specimen length for the nonwoven geotextiles, although the modulus of these materials did increase. The "zero" span 5% modulus for NW1 and NW2 increased by approximately 100% and 60%, respectively, above the modulus measured using the standard 100 mm gage length.

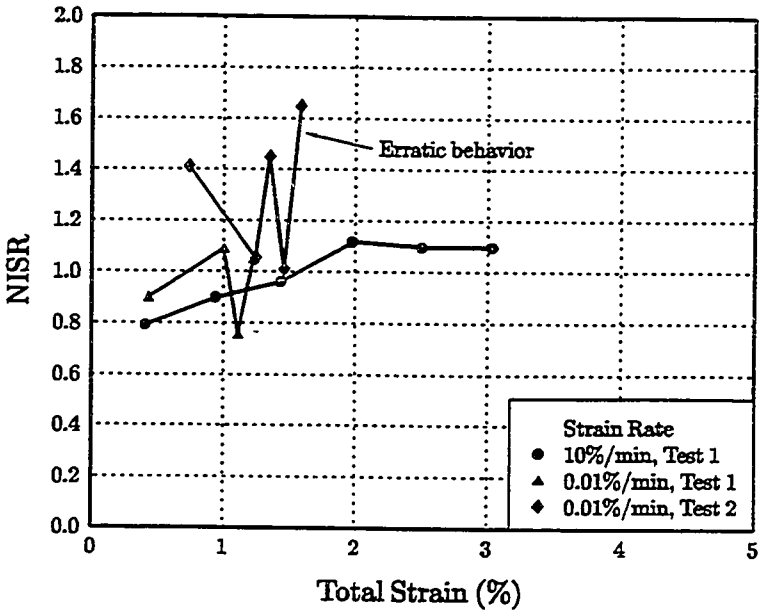

Figure 5.18: NISR vs. overall specimen strain for PET2.

c) The limited creep tests performed illustrated that the woven geotextiles do have a tendency to creep and that the creep rate decreased over time. The polypropylenes were particularly susceptible to creep with ultimate strains as much as three times the strain immediately after loading, even when the initial strain was much less than 1%.

d) In-isolation tests using strain gages determined that the YL-20 strain gages would underpredict the overall strain of the polypropylene geotextiles. PA-3 strain gages predicted nearly 100% of the overall strain of the woven polyester geotextile.

Additional evaluation of the results reported in this chapter will be presented in the next chapter where they are discussed in relation to the in-soil test results.

CHAPTER 6
UNIT CELL TESTS

6.1 Introduction

Soil and reinforcement are principal factors which affect the deformation response of GRS walls. While they are not the only factors, or perhaps the most important (see Chapter 3), a better understanding of GRS wall deformation will be possible only if the properties of the soil and reinforcement used in the walls and their composite behavior are defined. To accurately measure the soil, reinforcement, and composite properties, it is preferable to do so with a device that models the conditions existing in GRS walls. These conditions include plane strain soil deformation and strain of the reinforcement due to horizontal deformation of the soil. Since only small reinforcing strains have been measured in GRS walls subjected to working loads (Allen, et al., 1992; McGown, et al., 1993) the soil and reinforcing properties should be measured at low strain levels.

A review of existing in-soil geosynthetic characterization tests, presented in Chapter 2, found existing tests to be less than ideal. Full or large scale model wall tests are too time consuming and expensive to be routinely used for determination of material properties prior to GRS wall design. Pull-out tests, direct shear tests, horizontally reinforced cylindrical soil specimens, and hollow cylinder extension tests do not model the mechanisms causing deformation of GRS walls and were shown to be inappropriate for evaluation of load-elongation properties. Existing confined load-elongation devices may not properly model the interaction of soil and geosynthetics within GRS walls. In these devices the reinforcing is loaded in tension. No load is transferred to the reinforcing from the surrounding soil; instead, load is transferred to the soil from the reinforcing. Reproduction of field densities for the soil is not possible in any of the in-soil load-elongation devices identified. Of the methods reviewed only a plane strain unit cell type device was believed to have the potential for accurate and economic characterization of in-soil geosynthetic properties and determination of the soil-

geosynthetic composite response. A unit cell device was, therefore, selected as the most appropriate device for use in this project. The unit cell device and testing program are described and results presented in this chapter.

6.2 The Unit Cell Device

The unit cell device (UCD) designed and manufactured for this research project (Figures 6.1 and 6.2) differs from the devices used by McGown and Andrawes (1977), McGown, et al. (1978) and Ling (1992) (see Section 2.1.8) in four fundamental ways. First, the device is load controlled, instead of strain rate controlled. Second, only one end of the specimen is permitted to strain laterally. This ensures the peak strain in the reinforcement occurs at one end of the reinforcement and not in the middle as was the case with previous unit cell devices, Figure 2.18. Third, the end platens of the specimen in the σ_3 direction are rigid, ensuring that adjacent sides of the specimen remain orthogonal during loading. And finally, each end of the reinforcing is held in clamps which are mechanically linked to the end platens of the UCD which retain the soil. This feature permits direct measurement of the load induced in the reinforcing and maintains the integrity of the unit cell by ensuring that the reinforcing displaces horizontally a distance equal to the soil displacement.

The UCD permits testing of a 100 mm gage length by 200 mm wide reinforcing specimen confined above and below by approximately 100 mm of soil. The reinforcing is situated at midheight of the soil and held in position by clamps at each end. Load is applied to the reinforced soil via flexible bladders located above and below the soil. The left instrument box rests on bearings and is free to displace horizontally, a maximum of 8 mm, when vertical compression causes lateral expansion of the soil element. Lateral strain of the soil is resisted by loads induced in the reinforcing element. A clamp connecting the geotextile to the left instrument box ensures the reinforcing elongates with the deforming soil *even if the soil-geosynthetic contact friction is exceeded.* The load application bladder between the left instrument box and the reaction frame provides

lateral confinement pressure. Constant confining pressure is maintained by increasing the pressure in the end bladder to compensate for vertical straining of the soil specimen and for changes in top and bottom bladder pressures. The rigid vertical faces of the device force the soil to maintain its shape, with all faces mutually perpendicular, Figures 6.1 and 6.2.

The UCD and its integral reaction frame were constructed of steel. The plates which surround the specimen and the reaction frame were sized to minimize device deformations which might affect specimen behavior. The load application bladders are manufactured of latex rubber. Bladder pressure was manually controlled using regulators installed in a control panel situated next to the UCD. The unit cell and geosynthetic were instrumented to measure and record the data necessary for characterization of the soil, geosynthetic and GRS composite specimen, Table 6.1. Locations of load cells and LVDT's are shown in Figure 6.1. Pressure transducers for recording bladder pressures are not shown, nor are strain gages which were attached to the geosynthetics for a few of the tests. Sensotec SA-10 controllers powered the instruments and conditioned and amplified the return signals. Strain gages were powered and their signals amplified using a Micromeasurements 2110A/2120A strain gage conditioner. The amplified signals were converted to analog DC and sent to a Metrobyte analog-to-digital converter installed in an IBM 286 PC computer, Figure 6.3. Labtech Notebook data acquisition software was used to control the data collection and storage operations. Specifics on the UCD, including design rationale and fabrication drawings, are presented in Appendix A.

6.3 Test Program

6.3.1 Materials

Tests performed using the unit cell device involved two sands, four woven geotextiles, two nonwoven geotextiles, and sheet steel reinforcing. Uniformly graded steel beads were used in lieu of soil in one test. Because the sponsor of this project, the Washington State Department of Transportation, was specifically interested in furthering

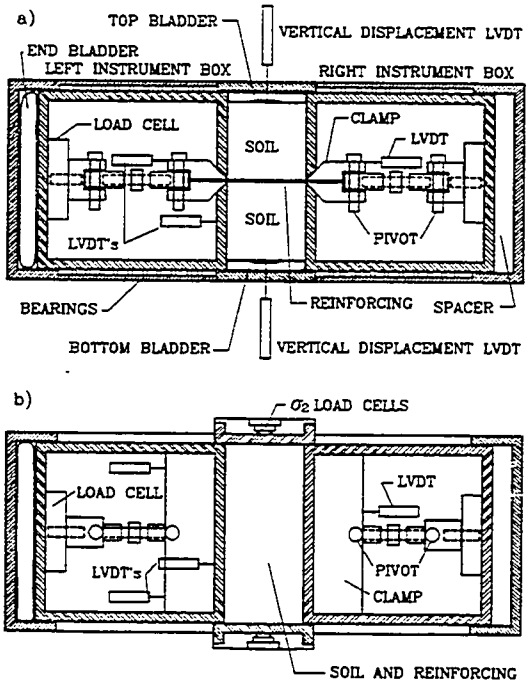

Figure 6.1: Schematic of Unit Cell Device: a) profile, and b) plan view section. Reaction frame not shown.

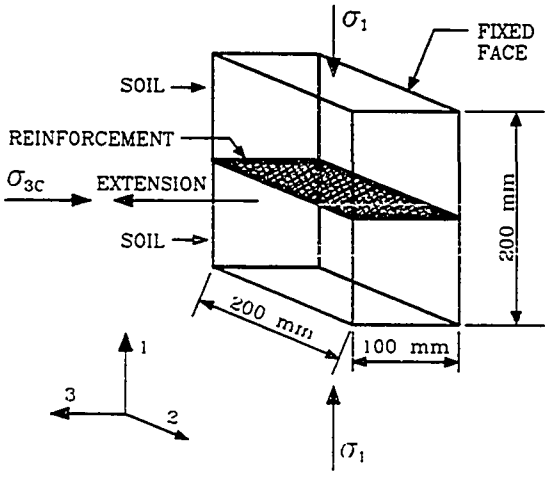

Figure 6.2: UCD principle of operation and specimen dimensions.

Table 6.1: Unit Cell Instrumentation.

Instrument	Manufacturer and Model	Full Scale Range	Location and Function
Tension Load Cell	Sensotec Model 41	17.8 kN	Installed between the clamps and the instrument boxes. Measure load in reinforcement
Compression Load Cell	Sensotec Model 53	8.9 kN	Installed between reaction frame and the vertical confining plates in direction perpendicular to sample elongation. Measure load in restrained direction.
Pressure Transducer	Sensotec Model LM	1390 kPa	Monitor pressure in bladders applying vertical load.
Pressure Transducer	Sensotec Model LM	695 kPa	Monitor pressure in bladder applying lateral confining load.
LVDT	Scheavitz Model 250 MHR	± 6.35 mm	Measure displacement of instrument box and clamps.
LVDT	Scheavitz Model 500 MHR	± 12.70 mm	Measure vertical movement of soil.
Pressure Gauge		1390 kPa, 3.5 kPa divisions	Redundant pressure monitoring system for visual verification of bladder pressures.

their understanding of the Rainier Avenue wall, the soil and geotextiles used for constructing that wall were tested as part of this program.

Soil O was a uniformly graded Ottawa sand. Soil R was a poorly graded sand obtained from the Rainier Avenue wall. Due to device size limitations, particles greater than the No. 4 US standard sieve (4.75 mm) were removed. The steel beads were designated Soil S. Soil properties are presented in Table 6.2, Figures 6.4 and 6.5, and Appendix B.

The four woven geotextiles tested, Reinforcements PP1, PP2, PP3 and PET1, were the same geosynthetics used in the Rainier Avenue wall. All of the UCD tests using Reinforcements PP2 and PET1 were performed on specimens exhumed from the wall. Both new and exhumed specimens of Reinforcements PP2 and PP3 were used in the tests. All specimens of Reinforcements NW1 and NW2, the nonwoven needle-punched geotextiles, were from new material. Reinforcement SS specimens were cut from 0.051 mm thick stainless steel shim material. With the exception of Reinforcement SS the

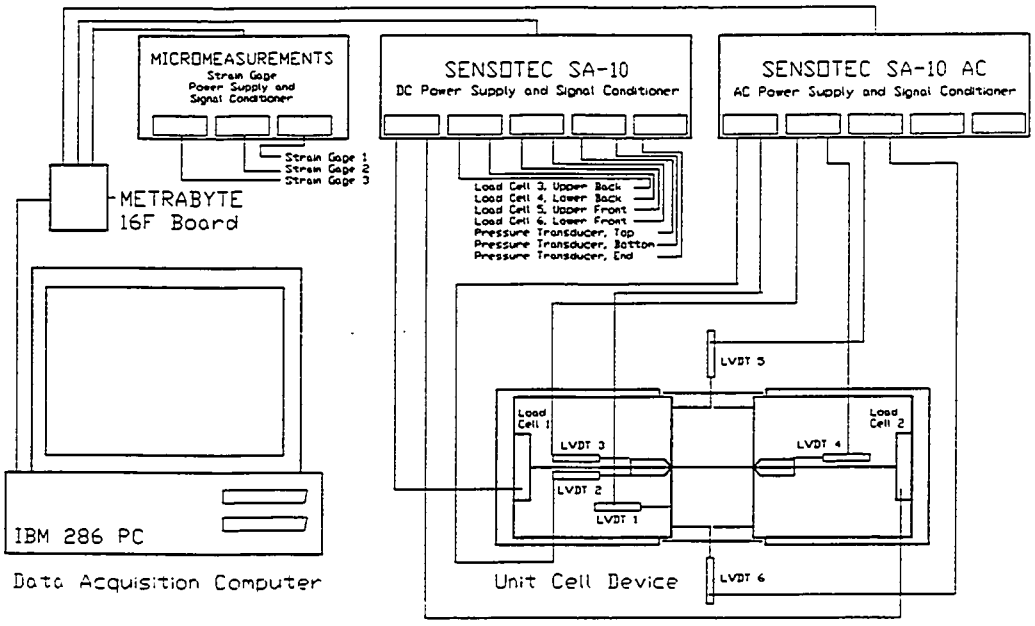

Figure 6.3: Schematic of instrumentation and data acquisition system.

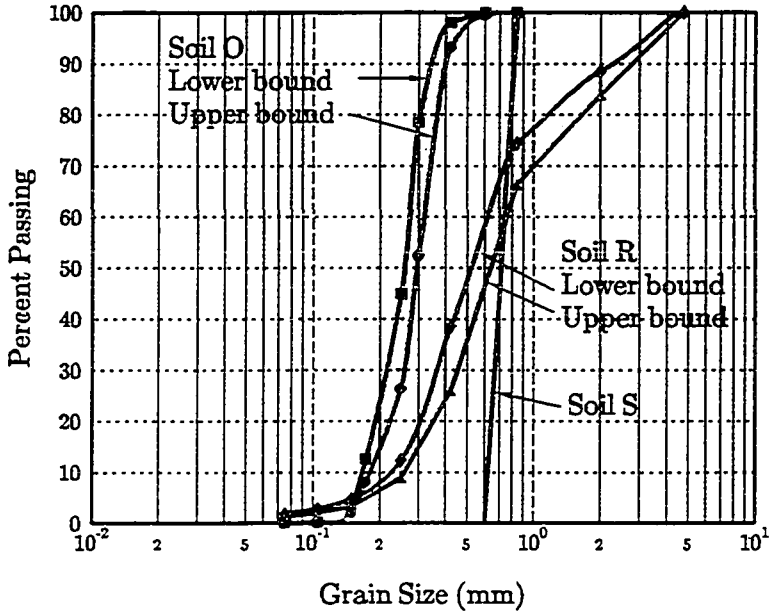

Figure 6.4: Grain size distribution for Soils O, R, and S.

Table 6.2: Maximum and minimum density and void ratios for Soils O, R, and S per ASTM D 4253.

SOIL	Maximum Density (kN/m^3)	Minimum Density (kN/m^3)	Specific Gravity	Min. Void Ratio (%)	Max. Void Ratio (%)
Soil O	17.2	14.8	2.65	51	75
Soil R	18.3	15.2	2.73	46	76
Soil S	47.0	42.5	7.2	50	66

Table 6.3: Reinforcement material, type and ASTM D 4595 wide width test data.

Reinforcement No.	Manufacturer and Product Name	Material and Description	ASTM D 4595 test results: Strength (kN/m) - Elongation (%)[1]	ASTM D 4595 test results: 5% modulus (kN/m)[2]
PP1	Exxon GTF 200	woven, slit-film, polypropylene	26 - 15[3]	260
PP2	Exxon GTF 375	woven, slit-film, 2 layer stitch-bonded, polypropylene	49 - 15[3]	470
PP3	Exxon GTF 500	woven, slit-film, 3 layer stitch-bonded, polypropylene	77 - 15[3]	780
PET1	Exxon GTF 1225T	woven, multi-filament, polyester	215 - 10[5]	1068[5]
NW1	Polyfelt TS700	nonwoven, needle-punched, polypropylene	16 - 95[4]	30
NW2	Polyfelt TS1000	nonwoven, needle-punched, polypropylene	26 - 95[4]	70
SS	Precision Brand	0.051 mm stainless steel, type 321	8 - 0.23[6]	3500[6]

[1]Manufacture published data from *Geotechnical Fabrics Report Specifiers Guide*, 1990, 1993.
[2]Average modulus values from Gallagher (1995) (see Chapter 5), unless otherwise noted.
[3]Minimum average roll values.
[4]Average roll values.
[5]Average value from Allen, et al., 1992a.
[6]Yield strength, strain, and preyield modulus provided.

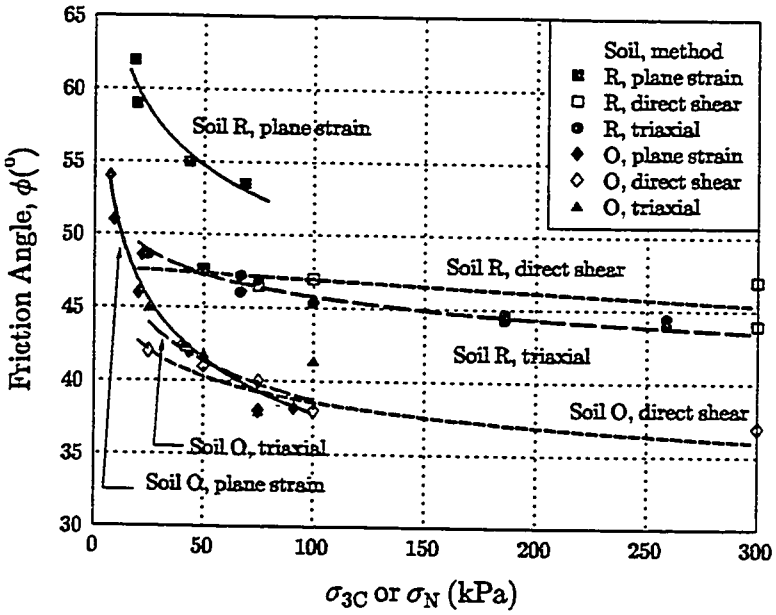

Figure 6.5: Plane strain, triaxial, and direct shear friction angles for Soils O and R. (σ_{3C} = confining pressure, σ_N = direct shear normal pressure, kPa). Triaxial results for Soil R at 70, 190, 260 and 310 kPa from STS (1990).

specimen ends were coated with an epoxy adhesive to prevent damage to the specimen when the clamps were tightened. Although the geosynthetic reinforcement properties were presented in Table 5.1, they are also included in Table 6.3, which includes the properties of the steel sheet to permit direct comparison.

6.3.2 Unit Cell Tests

Unit cell tests performed on reinforced soil specimens are summarized in Table 6.4. Results for specific tests are presented in Appendix C. Because the UCD is a load control device, with load applied vertically to the soil specimen, neither the vertical nor horizontal (reinforcing) strain rate could be controlled. The lateral confining pressure applied to the soil-geosynthetic composite could be controlled and was maintained constant for each test. Lateral confining pressure applied for any given test was between

10 kPa and 100 kPa. This range of pressures was selected because it was thought to be of the magnitude that existed in the Rainier Avenue wall.

Prior to placing specimens in the UCD the interior was lubricated with a silicon grease and lined with a 0.3 mm latex membrane. Specimens were constructed by placing two approximately equal weight layers of soil below the reinforcing, installing the reinforcing, and placing two more equal weight soil layers above the reinforcing. Since the soil used in GRS walls are generally compacted, Soils O and R were compacted in the UCD, to relative densities of 96% and 101%, respectively (relative density was determined in accordance with ASTM D 4253). Each soil layer was compacted by 25 blows of a 2.27 kg mass dropped from 300 mm. All specimens were constructed with dry soils.

Before loading, each specimen was anisotropically consolidated by applying a vertical pressure, σ_1, equal to the lateral confining pressure, σ_{3C}, to be applied to the composite during the test. Pressures acting in the σ_2 and σ_{3C} directions during consolidation could not be controlled and were dependent upon the applied vertical pressure, σ_1, and the soil properties. After a minimum consolidation period of 150 seconds, the vertical pressure on the specimen was manually increased in 10 kPa increments every 30 seconds until the reinforcing failed, the lateral displacement limit of the UCD was reached, or the limits of the measurement devices were approached. In some tests, loading was discontinued prior to reaching one of the above conditions and the vertical pressure held constant so that the response of the composite under sustained loading could be monitored. Complete details of sample preparation and test procedures are provided in Appendix A.

After a major portion of the test program had been completed, up to Test No. 118, it was discovered that at low pressures the end bladder, which applied confining pressure, was not fully inflating to fill the cavity in which it was housed, Figure 6.1. With increasing pressure the bladder expanded into the corners of the cavity and increased the area over which the bladder acted. The actual confining pressure was, therefore, not

Table 6.4: List of UCD tests. (Results for each test on reinforced soil specimens are presented in Appendix C in the order they appear in this table. Results for tests on unreinforced specimens are presented in Appendix B).

SOIL	REINF.[1]	σ_{3C}	Test No.	Notes:
O	None	12.5	118	
O	None	12.5	117	
O	None	25.0	113	
O	None	25.0	114	
O	None	50.0	20	
O	None	50.0	21	
O	None	100.0	22	
O	PP2*	50.0	48	
O	PP2*	75.0	47	
O	PP2*	100.0	46	
O	PP2*	100.0	45	
O	PP3*	50.0	43	
O	PP3*	75.0	41	
O	PP3*	75.0	42	
O	PP3*	100.0	44	
O	PET1	12.5	108	
O	PET1	25.0	107	
O	PET1	50.0	109	
O	PET1	50.0	110	
O	NW1	12.5	88	
O	NW1	25.0	89	
O	NW1	50.0	93	
O	NW2	12.5	90	
O	NW2	12.5	91	
O	NW2	50.0	92	
O	SS	12.5	96	
O	SS	25.0	95	
O	SS	50.0	97	
R	None	12.5	115	
R	None	25.0	112	
R	None	25.0	116	
R	None	50.0	49	
R	None	75.0	50	
R	None	100.0	51	
R	PP1	12.5	79	
R	PP1	12.5	131	YL-10 Strain Gages, Clear Face
R	PP1	25.0	65	
R	PP1	25.0	67	

Table 6.4 cont.: List of UCD tests.

SOIL	REINF.[1]	σ_{3C}	Test No.	Notes:
R	PP1	25.0	74	
R	PP1	25.0	81	
R	PP1	25.0	129	YL-10 Strain Gages, Clear Face
R	PP2	12.5	77	
R	PP2	12.5	128	YL-10 Strain Gages, Clear Face
R	PP2*	20.0	132	YL-10 Strain Gages, Clear Face
R	PP2*	20.0	135	Creep Test
R	PP2	25.0	70	
R	PP2*	25.0	73	
R	PP2*	25.0	123	YL-2 Strain Gages
R	PP2	25.0	124	YL-2 Strain Gages
R	PP3	12.5	76	
R	PP3	12.5	125	YL-2 Strain Gages
R	PP3	12.5	126	YL-20 Strain Gages
R	PP3*	20.0	130	YL-10 Strain Gages, Clear Face
R	PP3*	25.0	68	
R	PP3	25.0	71	
R	PP3*	25.0	122	YL-2 Strain Gages
R	PET1	12.5	98	
R	PET1	12.5	134	PA-7 Strain Gages
R	PET1	20.0	133	PA-7 Strain Gages
R	PET1	25.0	99	
R	PET1	25.0	100	
R	PET1	25.0	111	
R	PET1	50.0	106	
R	NW1	12.5	84	
R	NW1	25.0	85	
R	NW1	50.0	87	
R	NW2	12.5	82	
R	NW2	12.5	83	
R	NW2	25.0	72	
R	NW2	50.0	86	
R	SS	12.5	101	
R	SS	25.0	102	
R	SS	50.0	104	
S	PP2	50.0	94	

[1] Reinforcements 1-4 obtained from Rainier Ave. wall except when marked with "*", in which case new materials were used.

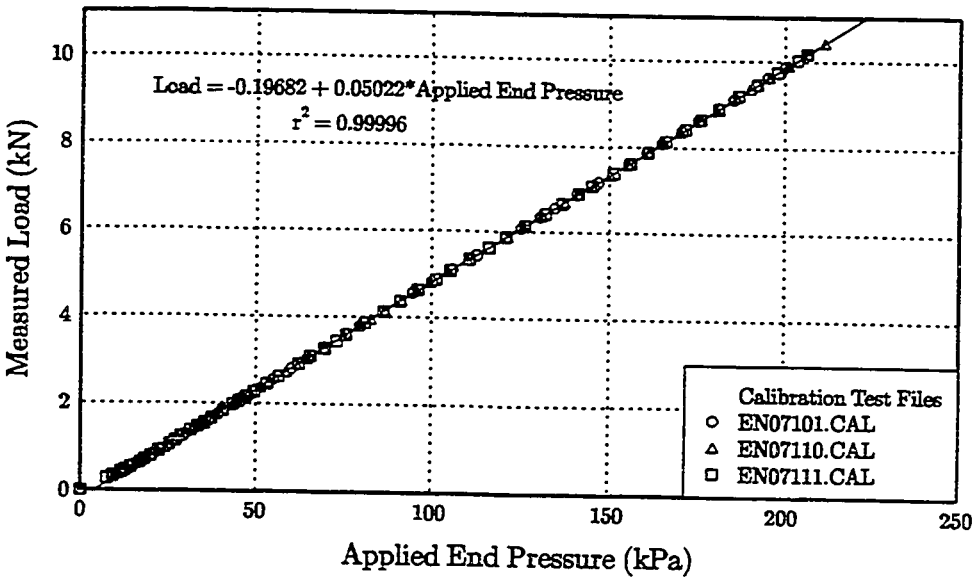

Figure 6.6: UCD calibration test results and equation.

equal to the confining pressure thought to have been applied in the tests. To determine the actual confining pressure the device was calibrated by measuring the horizontal load applied to the left instrument box for given end bladder pressures, Figure 6.6. This calibration curve was used for controlling end bladder pressure in tests numbered greater than 118 and was used for analysis of *all* test results to ensure the actual confining pressures were accurately computed when the results were analyzed. This error in calibration, once accounted for in the reduction of recorded test data, should not invalidate any of the tests.

6.4 Discussion of Results

6.4.1 Soil Behavior

6.4.1.1 Unreinforced Soil

Unreinforced specimens of Soils O and R were tested in the UCD to determine their plane strain response and friction angle at various confining pressures. These results were compared with those obtained from direct shear and cylindrical triaxial tests, Figure 6.5. The friction angle increased with decreasing confining pressure for both soils and all

test methods. The plane strain value was higher than the triaxial value, as expected, Figure 6.7a (Cornforth, 1964; Lee and Seed, 1967; Marachi, et al., 1981). It is unclear why the triaxial and plane strain friction angles for Soil O were so similar as the plane strain friction angle of Ottawa sand was anticipated to exceed the triaxial value by 2° to 6° (Lee, 1970). The triaxial and plane strain friction angle for Soil R agree within reason for the limited test data available, with the relationship attributed to Lade and Lee (1976) by Holtz and Kovacs (1981), Equation 6.1.

$$\phi_{ps} = 1.5\,\phi_{tx} - 17^{\circ} \qquad (\phi_{tx} > 34^{\circ}) \qquad \textbf{(6.1)}$$

$$\phi_{tx} = \phi_{tx} \qquad (\phi_{tx} \leq 34^{\circ})$$

where: ϕ_{tx} = triaxial friction angle and ϕ_{ps} = plane strain friction angle.

Similar relationships have been published by others for estimating the plane strain friction angle of sands from the triaxial friction angle (e.g., Lee, 1970; and Hanna, et al., 1987). There is, however, no method to permit the shape of the plane strain stress-strain curve to be predicted using triaxial stress-strain relations. A dense cohesionless sand can be expected to reach its peak strength at a greater strain in a triaxial test than it would in a plane strain test, and have a higher peak value, Figure 6.7b. This same pattern was observed in this program. Dense specimens of Soils O and R peaked between 3% and 6% axial strain in triaxial tests and between 0.5% and 3% axial strain (2% to 3% lateral strain) in plane strain tests (see Appendix B). The strains at which the plain strain peaks occurred are in the same range as the soils tested by Cornforth (1964) and Marachi, et al. (1981) but are slightly lower than the strains reported by McGown, et al. (1989) in their review of biaxial and triaxial test data on sand. For a wide range of initial soil densities and mean stresses, McGown, et al. found the peak angle of friction was typically mobilized within 3% to 6% lateral strain. The large strain (constant volume) friction angle was mobilized after 8% to 12% lateral strain. Since post peak behavior and constant volume strain could not be determined with the UCD, no comparison of the constant volume strain with those reported by McGown, et al. can be made. Because of

the limited number of tests performed, the lack of post peak data, and the different emphasis being pursued, no attempt has been made in this program to develop a method to estimate the plane strain curve shape from triaxial data. Such a procedure may be useful, since triaxial tests are more commonly performed than plane strain tests, and could be a topic for future research.

6.4.1.2 General Response of Reinforced Soil

The reinforced soil composite behaved as postulated by McGown et al. (1978), Figure 3.4. Deformation of reinforced soil composites was dependent on both soil and reinforcing properties, as well as the applied confining pressure. As would be expected, composites constructed with Soil R, $\phi_{ps} \cong 55^{o}$, experienced less horizontal deformation than did those constructed with the same reinforcing and Soils O or S, $\phi_{ps} \cong 42^{o}$, when subjected to identical loads, Figure 6.8. Similarly, when higher modulus reinforcing was used with a particular soil, the composite supported a greater load, Figure 6.9. The load supported by the reinforced soil also increased with increased confining pressure, Figure 6.10. Since the rupture strain of the geotextiles was much greater than the strain at which the peak friction angle occurred (2% to 3%), the sudden failure characteristic of dense cohesionless soil was replaced by a more ductile response when the soil was reinforced. The reader will have noticed that the results have been plotted in terms of lateral strain, ε_3, and not the more commonly used vertical (i.e., axial) strain, ε_1. This has been done because horizontal deformation of GRS walls is the parameter of principal interest and because it permits direct correlation with reinforcing strain, which occurs in the horizontal direction.

Initial tests using the UCD were conducted on reinforced specimens of Soil O, the Ottawa sand, Figures 6.9c and 6.10a. The "slip-stick" behavior of Soil O seemed unusual and, since the UCD was a newly developed apparatus, the possibility that it might be a function of the UCD design or operation was considered. Subsequent tests using Soil R

a)

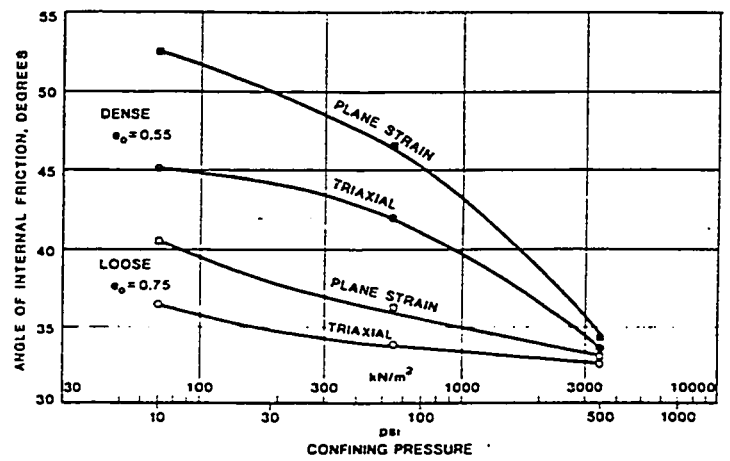

b)

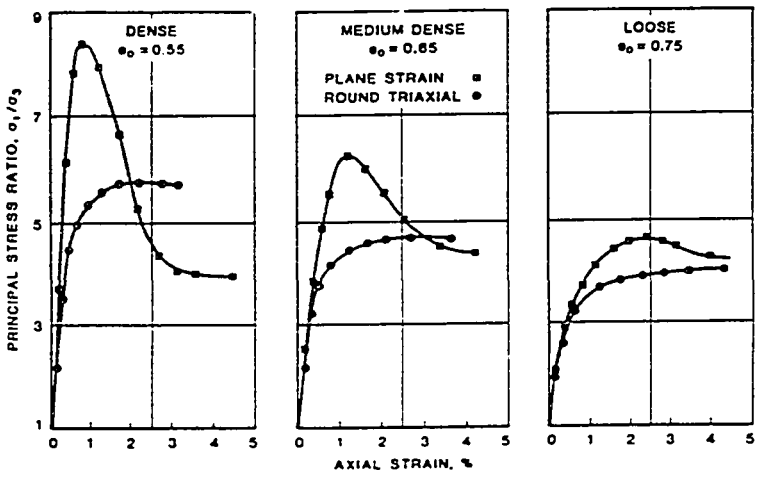

Figure 6.7: a) Comparison of plane strain and triaxial friction angles, b) stress-strain relationship for plane strain and triaxial specimen, σ_3 = 70 kPa (after Marachi, et al., 1981).

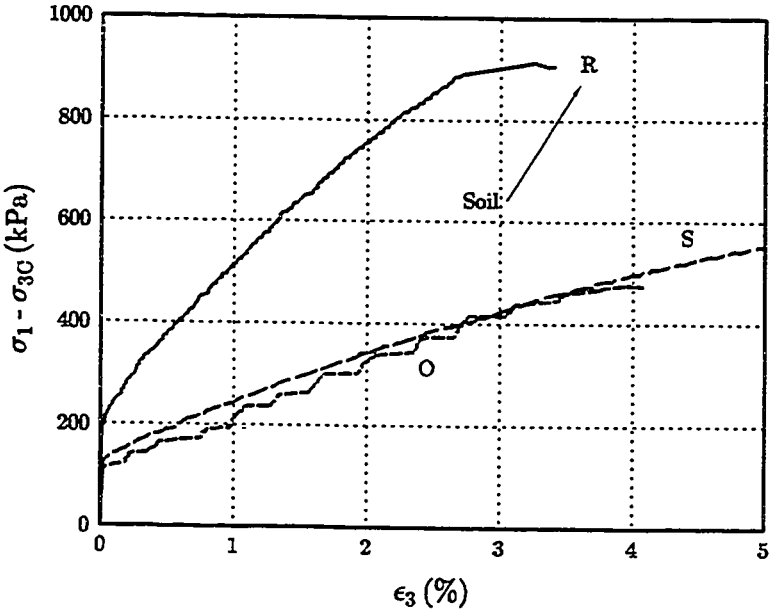

Figure 6.8: Specimen stress-strain behavior for different soils, Reinforcement PP2, $\sigma_{3C} = 50$ kPa.

did not exhibit this behavior, Figures 6.9b and 6.10b. The high friction angle and less uniform gradation of this soil were suspected of possibly suppressing the response. Therefore, a third more idealized soil was sought for testing. Spherical, nearly uniform diameter steel beads, designated Soil S, were selected, Figure 6.4 and Table 6.2. A single test was conducted with this soil and Reinforcement PP2. Slip-stick behavior was not observed, Figure 6.8. It was concluded that the UCD was operating correctly and the slip stick behavior was a function of the characteristics of Soil O, perhaps associated with particle shape or roughness. Testing was continued with no modifications to the UCD. [When the testing program was nearing completion the author learned that researchers at Washington State University had also observed this slip-stick behavior of Ottawa sand in triaxial tests (Dr. C. Ho and Mr. D. Running, 1994, personal communication)].

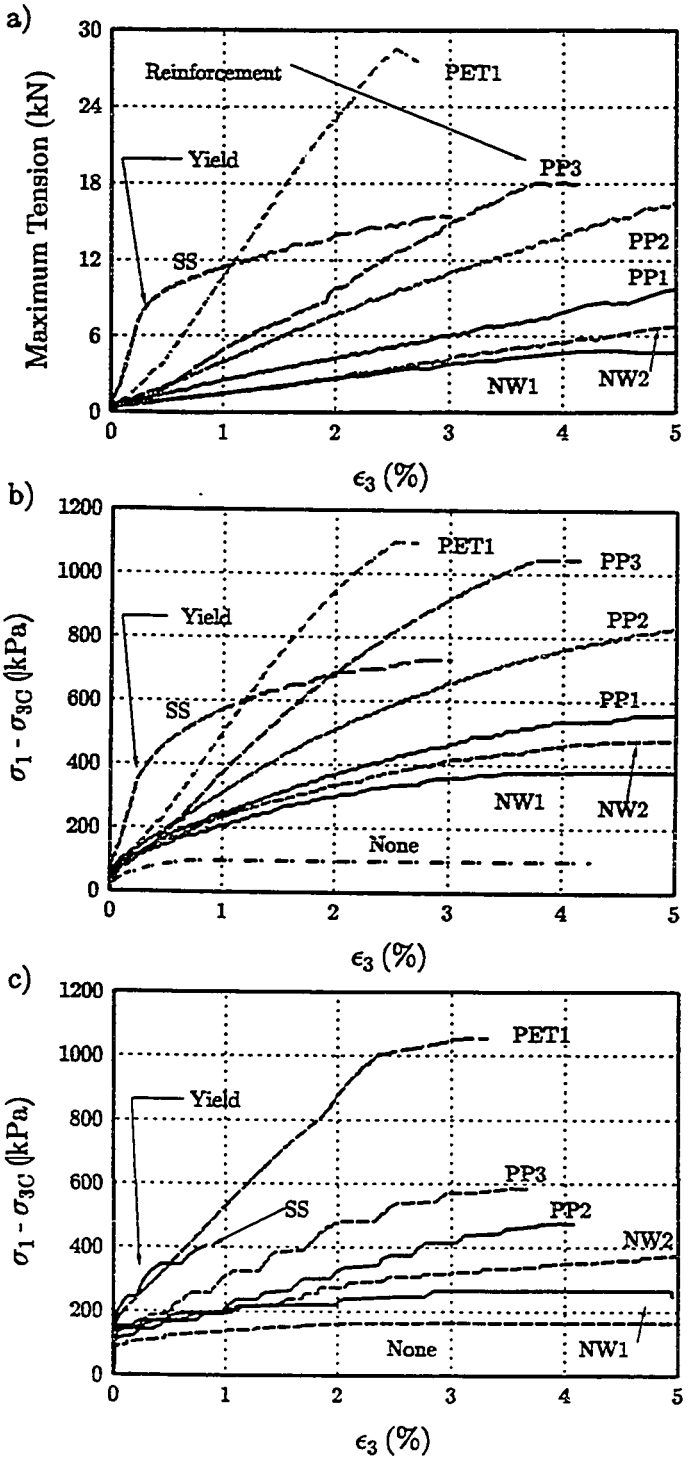

Figure 6.9: a) Reinforcement Tension vs. Strain (Soil R, σ_{3C} = 10 kPa) and Specimen stress-strain behavior for different reinforcings: b) Soil R, σ_{3C} = 10 kPa, c) Soil O, σ_{3C} = 50 kPa.

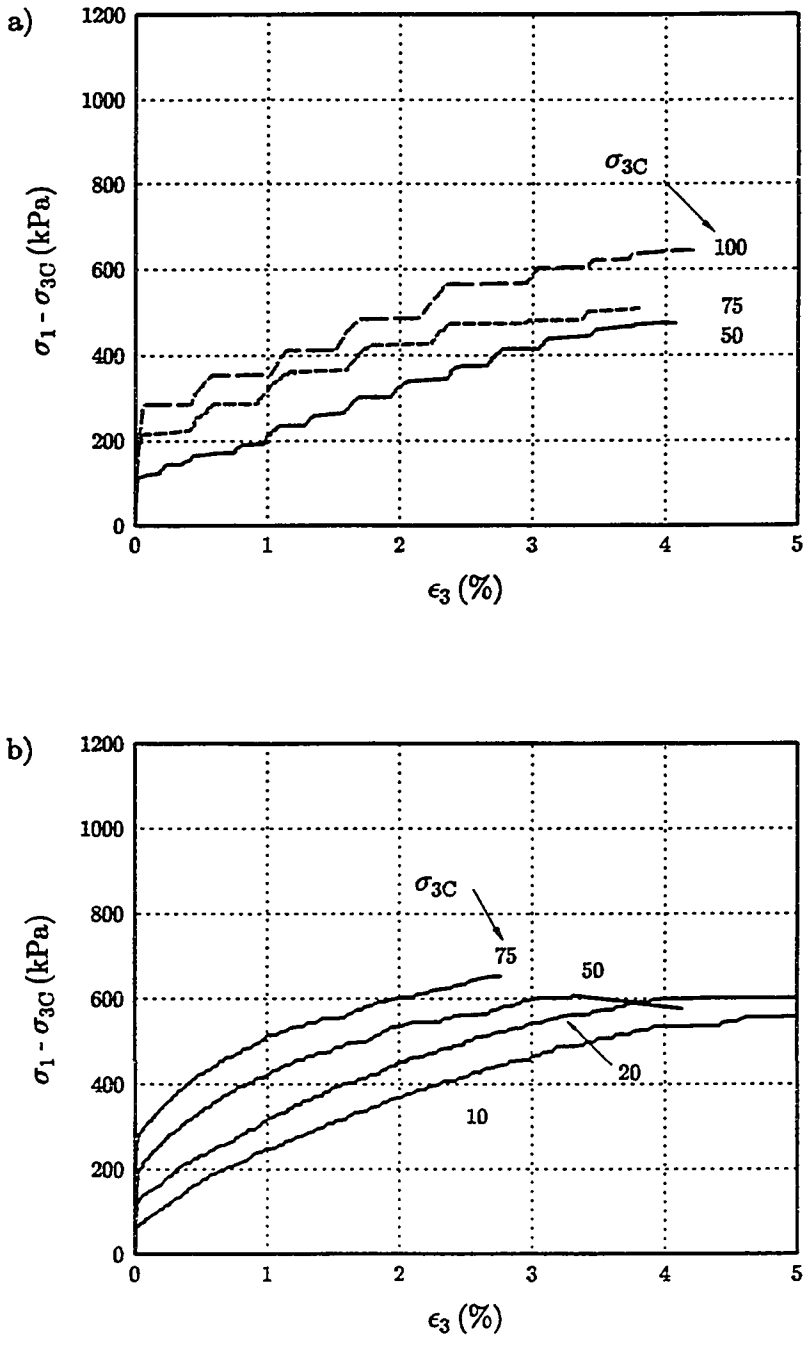

Figure 6.10: Specimen stress-strain behavior for different confining pressures: a) Soil O, Reinforcement PP2, and b) Soil R, Reinforcement PP1.

6.4.1.3 Increased Confining Pressure Concept

Two hypothesis have been proposed to explain the mechanisms by which reinforcing improves the load supporting capability of soil: (1) the reinforcing provides an apparent cohesion to the soil (Schlosser and Long, 1972), and (2) the effective confining pressure experienced by the soil increases due to tension which develops in the reinforcement when it is elongated (Yang and Singh, 1974), Figure 3.4. The resulting strength of the composite is the same for both interpretations. Previous research efforts had not verified either hypothesis because the tests had been performed in cylindrical triaxial apparatus, a device which does not permit direct measurement of reinforcing loads. However, reinforcing tension could be measured in UCD tests.

The UCD tests have verified the Yang and Singh hypothesis--the tension which develops in the reinforcing during straining of the reinforced soil increases the lateral pressure acting on the soil, thus increasing the soil strength. Since in the UCD the end area of the specimen was known and the load in the reinforcing was measured, the effective lateral confining stress acting on the soil, σ_{3E}, could be computed using Equation 6.2.

$$\sigma_{3E} = \sigma_{3C} + \frac{T}{B \cdot H} \qquad \textbf{(6.2)}$$

where:

σ_{3E} = effective lateral confining pressure action on the soil,

σ_{3C} = lateral confining pressure acting on the composite,

T = tension in the reinforcement,

B = width of the composite,

H = height of the composite.

Strain in the higher modulus reinforcements resulted in greater effective lateral confining pressures acting on the soil, permitting the soil to support greater vertical loads than would be possible with lower modulus reinforcements, Figures 6.11 and 6.12. To

facilitate comparison of UCD tests a non-dimensional effective stress ratio was computed by dividing the vertical pressure, σ_1, by the effective lateral pressure acting on the soil, σ_{3E}, Figures 6.13 and 6.14. With the exception of composites constructed with Reinforcing PET1, the change in effective stress ratio with lateral strain followed the general trend, but with widely variable peak values, established for each soil when unreinforced. The effective stress ratio reached a maximum between 1% and 3% strain and then decreased with increasing strain as the soil reached an active state. Reinforcement PET1, the high strength polyester, changed the way both soils behaved. The slip-stick deformation mode of Soil O was suppressed, Figure 6.13. For Soil R, the shape of the effective stress ratio versus lateral strain curve was changed dramatically in comparison to results obtained when the other geotextile reinforcements were used, Figure 6.14. The steel sheet, Reinforcement SS, yielded at 0.23% strain, long before the soil could attain an active state. A review of the results of effective stress ratio and effective lateral stress versus lateral strain for a variety of soils, reinforcings, and lateral confining pressures, σ_{3C}, found that:

a) Both soils, when reinforced with the lower modulus reinforcings (all reinforcings except PET1 and SS), generally reached their maximum effective stress ratio between 1% and 3% lateral strain (Figures 6.13 and 6.14).

b) The use of a high strength multi-filament polyester geotextile, Reinforcement PET1, altered the response of Soils O and R from that observed when other geosynthetic reinforcements were used. Specimens constructed with Soil O and Reinforcement PET1 did not experience the slip-stick, saw-tooth response which occurred when Soil O was unreinforced or reinforced with the other geotextiles (Figures 6.9c, 6.10a and 6.13). In two tests with Soil O and Reinforcement PET1 the effective stress ratio reached a maximum at less than 1% lateral strain, remained constant for 1% to 2.5% lateral strain, then decreased, Figure 6.13b. When Reinforcement PET1 was used in Soil R the maximum effective stress ratio

was reduced to approximately 8.5 and occurred at less than 1% lateral strain, Figure 6.14. After reaching the maximum, the effective stress ratio decreased with increasing strain.

The effect of this substantial reduction in soil stress ratio when PET 1 was used can be observed in Figure 6.12b. Until lateral strains exceeded 1% the capacity of the reinforced soil composite was greater when Soil R was reinforced with PP3 than when reinforced with PET1.

c) Prior to yield of the steel sheet, Reinforcement SS, at 0.23% strain, Soils O and R had reached stress ratios of only 4.5 and 7, respectively. At this low horizontal strain the soil was nearer at-rest than fully active conditions. As a result the reinforcing was carrying proportionately more of the applied vertical load than would be necessary if the soil had been able to fully mobilize its strength.

d) An increase in lateral confining pressure generally resulted in a decrease in the maximum effective stress ratio, as would be expected for cohesionless soils (Lee and Seed, 1967; Marachi, et al., 1981). The relationship between the maximum effective stress ratio and effective confining pressure at which it occurred followed the same trend as that for unreinforced soils, Figure 6.15. When extensible geotextile reinforcements were used, the effective confining pressure corresponding to the maximum stress ratio was, with the notable exception of the Soil R-Reinforcement PET1 combination, equal to or greater than the maximum stress ratio for the unreinforced soil. When Reinforcement PET1, the high strength polyester, was used in Soil R, the peak stress ratio was reduced to approximately 8.5 for all effective confining pressures, Figure 6.15b.

Why the stress ratio is higher for soil specimens reinforced with the lower modulus geotextiles than it is for unreinforced specimens is not clear. One possible explanation is that soil mobilization began at the low effective confining pressures to which the soil was initially subjected. This may permit the soil to

establish failure planes along the steeper angles associated with those lower confining pressures before the ultimate effective confining pressure acting on the soil is attained. However, inspection of the results did not identify any clear correlation between initial confining pressures and maximum stress ratio. Because of the relatively large number of data points falling above or on the unreinforced soil line, other factors such as inaccuracies in UCD control and calibration or frictional interaction of the soil with the reinforcement (reducing the measured reinforcement load), while also possible explanations, are not likely to be the sole cause of this behavior.

e) Once lateral strain commenced, the intermediate stress ratio, σ_1/σ_2, remained essentially constant for the duration of the test, Figure 6.16. The intermediate stress ratios were approximately 2, 3, and 2 for Soils O, R and S, respectively. As with the principal effective stress ratio, σ_1/σ_{3E}, the intermediate stress ratio reached a peak between 1% and 3% lateral strain. However, it was unaffected by confining pressure or reinforcement properties.

f) The reinforcing influenced the soil response as soon as lateral strain was initiated. In Figure 6.17 the contribution of the reinforcing can be identified as the difference between the stress ratio of the composite, σ_1/σ_{3C}, and that of the soil, σ_1/σ_{3E}. The greater the reinforcing modulus the less horizontal strain required for an increase in soil capacity to be realized. Reinforcement SS, the steel sheet, had a much greater influence at very low strains than did the geosynthetic reinforcements.

In Figure 6.17a, Reinforcing PP2 is contributing very little to the soil at these small strains, however, it is making a contribution. The influence of this reinforcement is related to reinforcement tension and resulting increase in effective lateral confining pressure acting on the soil (Eq. 6.2), which are small at the strains plotted. So, while this reinforcement does increase soil capacity, its

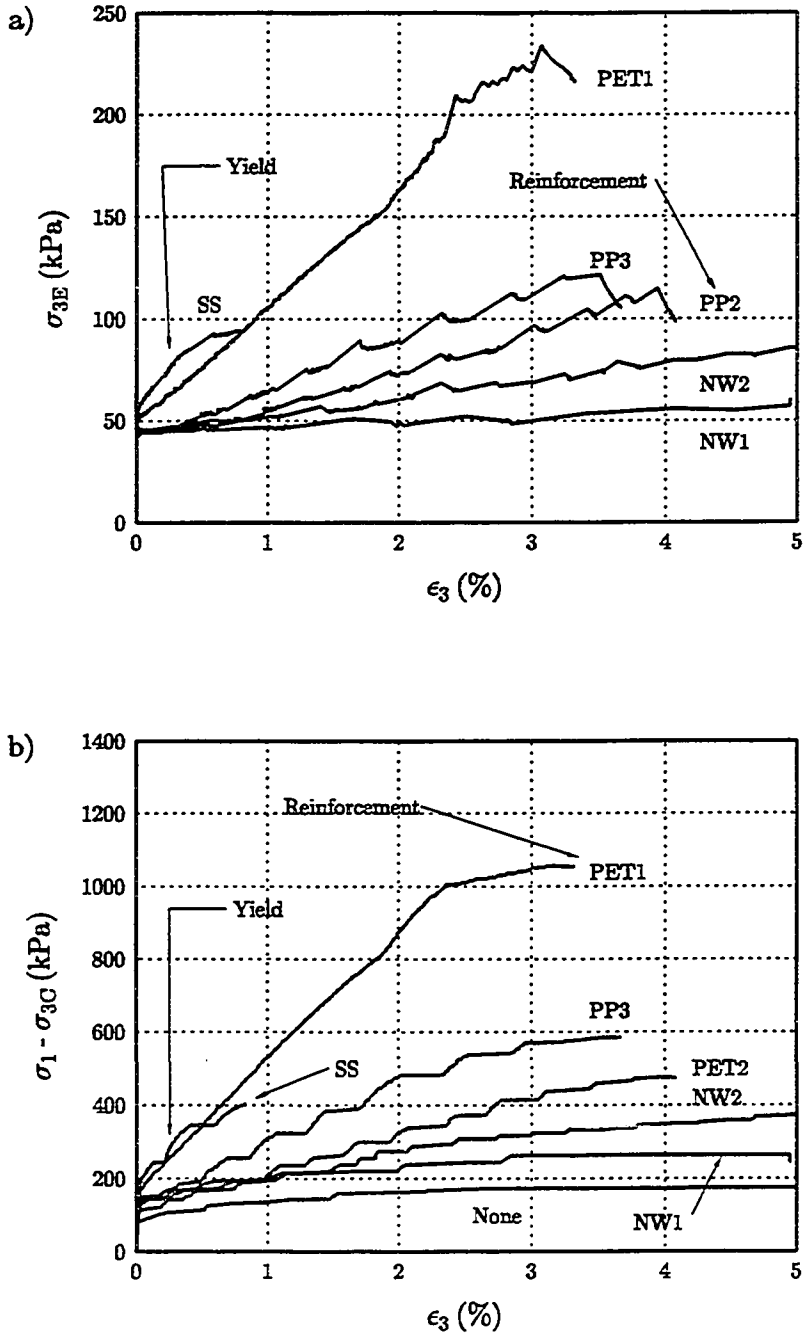

Figure 6.11: a) Effective confining pressure vs. lateral strain, and b) corresponding principal stress difference vs. lateral strain, Soil O, $\sigma_{3C} = 50$ kPa.

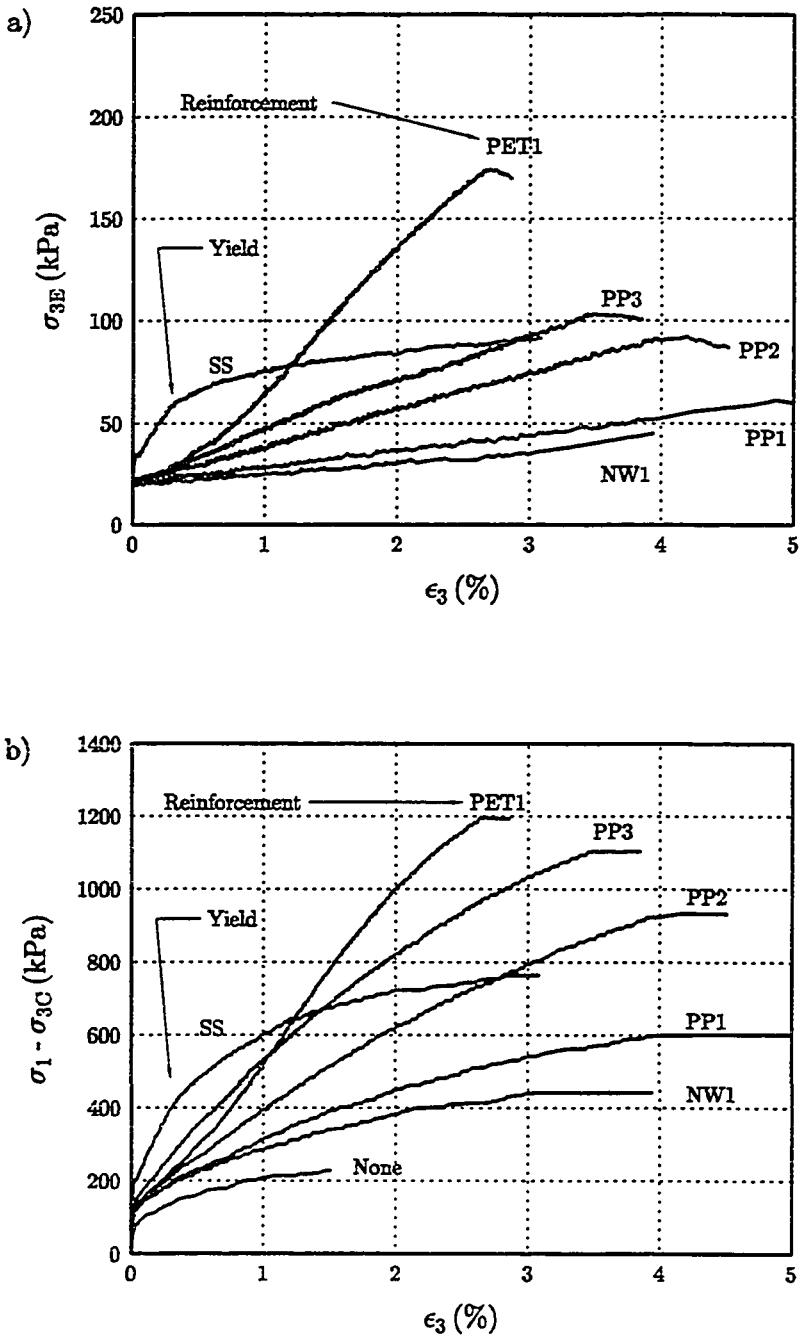

Figure 6.12: a) Effective confining pressure vs. lateral strain, and b) corresponding principal stress difference vs. lateral strain, Soil R, $\sigma_{3C} = 20$ kPa.

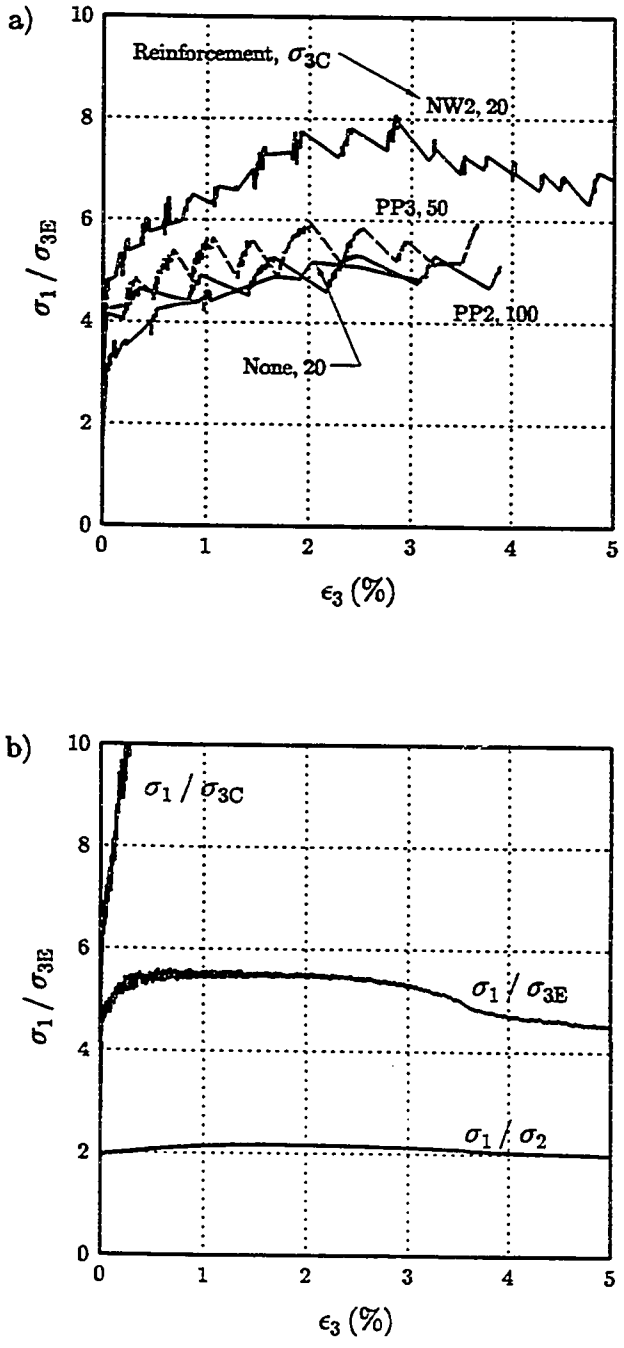

Figure 6.13: Effective stress ratio vs. lateral strain for Soil O: a) various reinforcements and confining pressures, and b) Reinforcement PET1, $\sigma_{3C} = 20$ kPa.

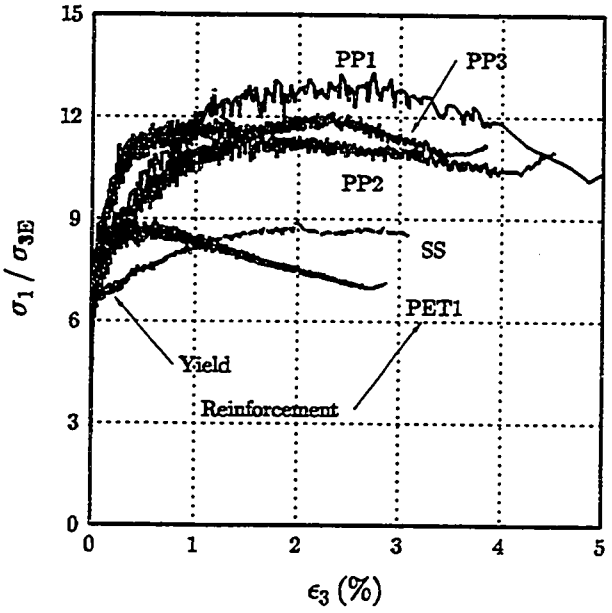

Figure 6.14: Effective stress ratio vs. lateral strain for Soil R, $\sigma_{3C} = 20$ kPa.

contribution is not significant *relative* to the contribution to total capacity associated with the composite confining pressure, σ_{3C}. This relationship between composite confining pressure and effective confining pressure due to reinforcing tension is discussed further in Section 6.4.3.4.

A comparison of 6.17d and 6.17e would lead to the conclusion that the lower modulus woven slit-film polypropylene geotextile, PP3, increased soil capacity more than the higher modulus woven multi-filament polyester geotextile, PET1. And, for these reinforcings, at these strains, this conclusion would be correct. The geotextiles have been classified by secant modulus values determined at 5% strain, Table 6.2. However, they are not linear elastic materials and behave differently at very low strains. As was discussed in Section 5.4, the shape of the polyester load-elongation curve is fairly complex: starting out fairly flat the slope increases near 0.3% strain, flattens again near 3% strain, and steepens again near 7% strain, Figure 5.2. Because of this behavior, the initial secant modulus for PET1 is less than the initial secant modulus for PP3. As is

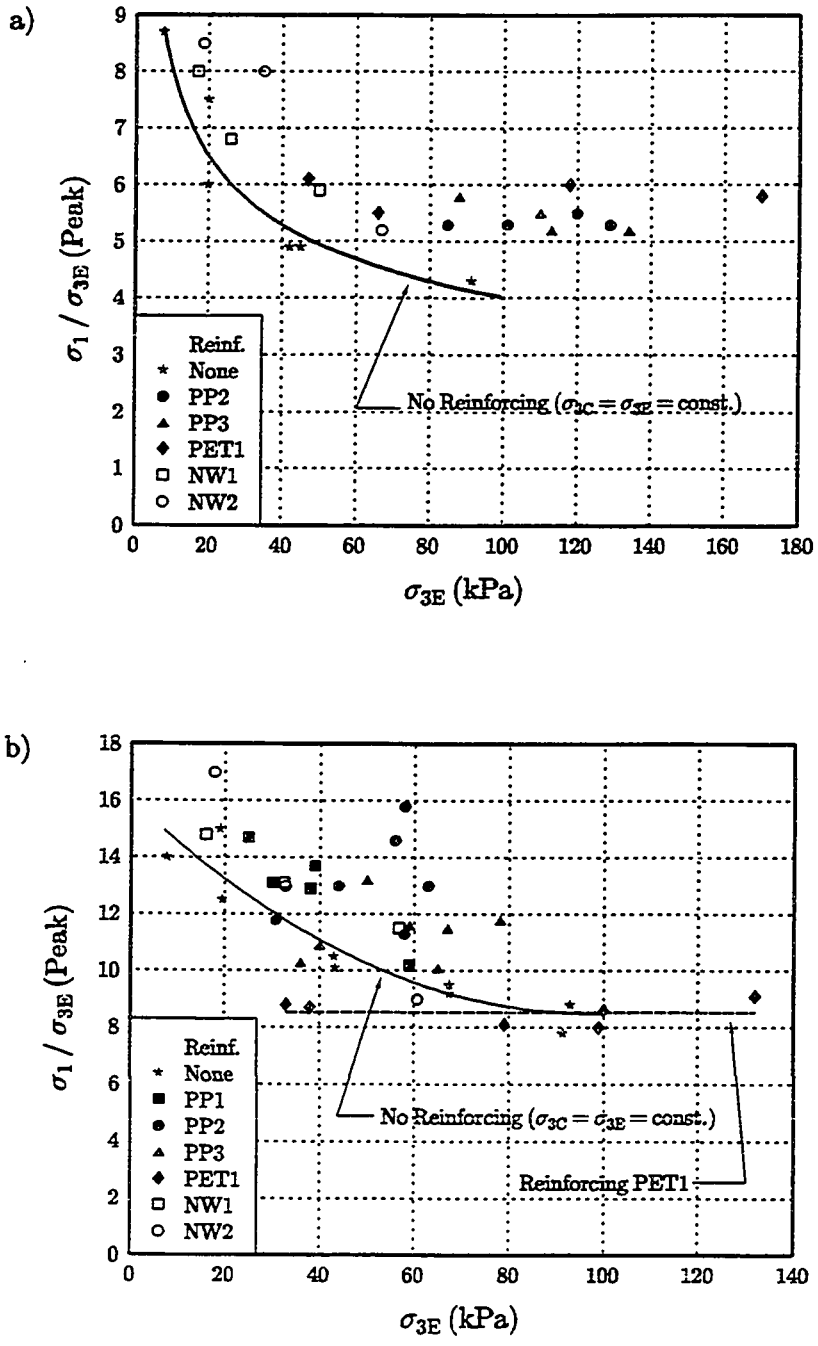

Figure 6.15: Peak effective stress ratio vs. corresponding effective confining pressure for: a) Soil O, and b) Soil R.

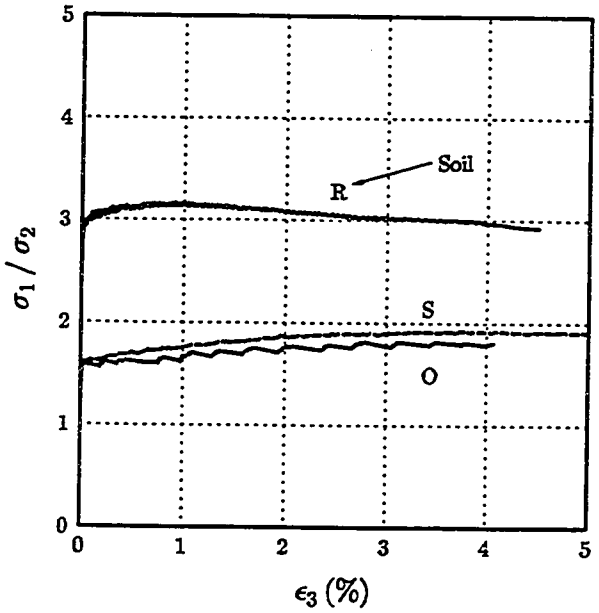

Figure 6.16: Intermediate principal stress ratio for Soils O, R, and S.

illustrated in Figure 6.12a, the effective confining pressure acting on Soil PP2 due to Reinforcement PET1 did not exceed that for Reinforcement PP3 until lateral strain exceeded 0.4%. Thus, at these strains the soil reinforced with PP3 should have a greater capacity than it would if reinforced with PP4.

6.4.1.4 Soil Dilation

It is well known that dense cohesionless soils dilate during drained shear at low confining pressures (Holtz and Kovacs, 1981). Since Soils O, R, and S were tested at relative densities of 96%, 101% and 100%, respectively, with initial confining pressures below 100 kPa, it is not surprising that soil dilation played a significant role in the composite response measured. The specimens in the UCD compressed vertically before dilating, Figures 6.18 to 6.23. The vertical strain was approximately 0.3% to 0.5% and the corresponding lateral strain approximately 0.02% when the rate of volumetric

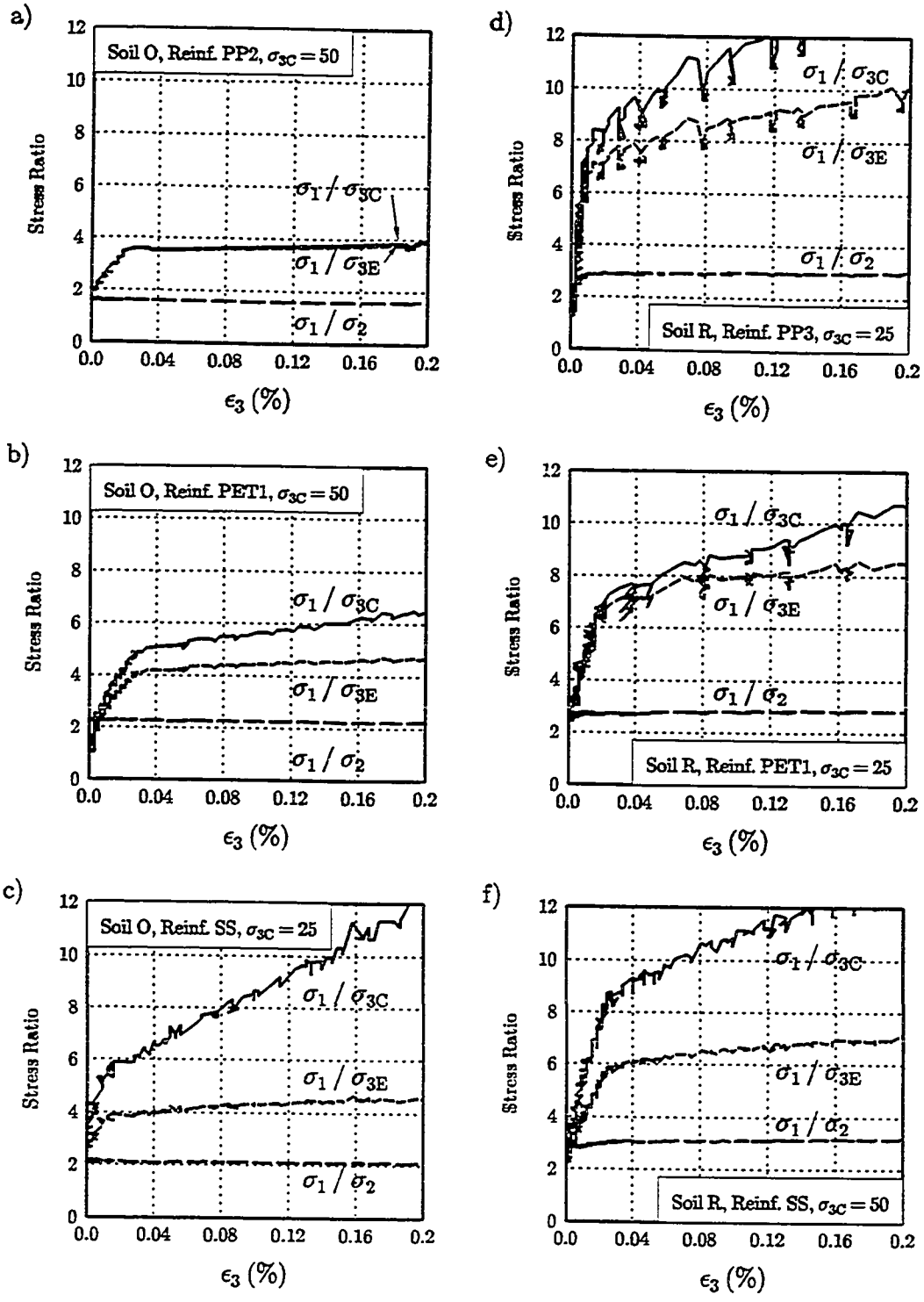

Figure 6.17: Composite and soil stress ratios showing influence of reinforcement in first 0.2% lateral strain for Soils O and R with extensible and inextensible reinforcements.

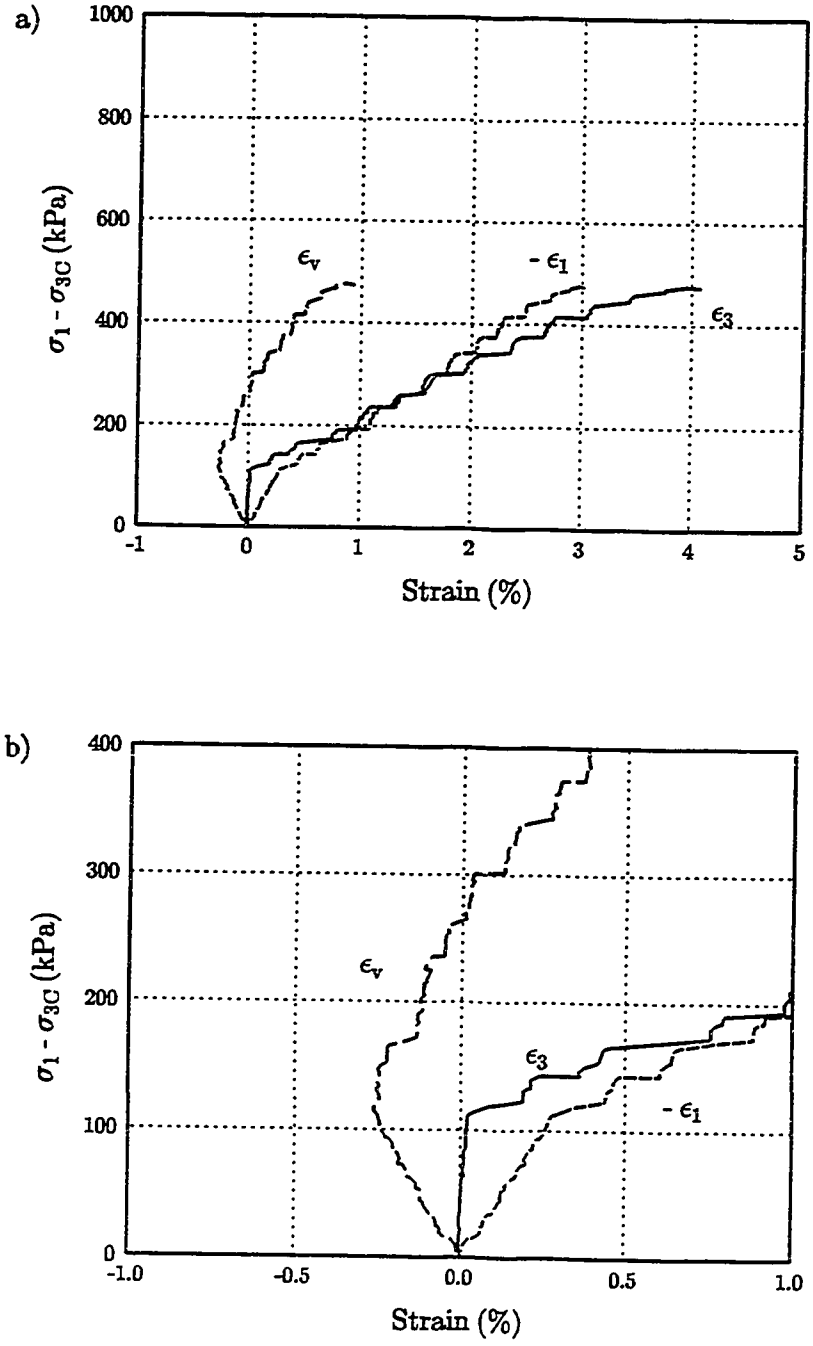

Figure 6.18: Principal stress difference vs. vertical, horizontal and volumetric strains for test and close-up of initial strains for Soil O with Reinforcement PP2, $\sigma_{3C} = 50$ kPa.

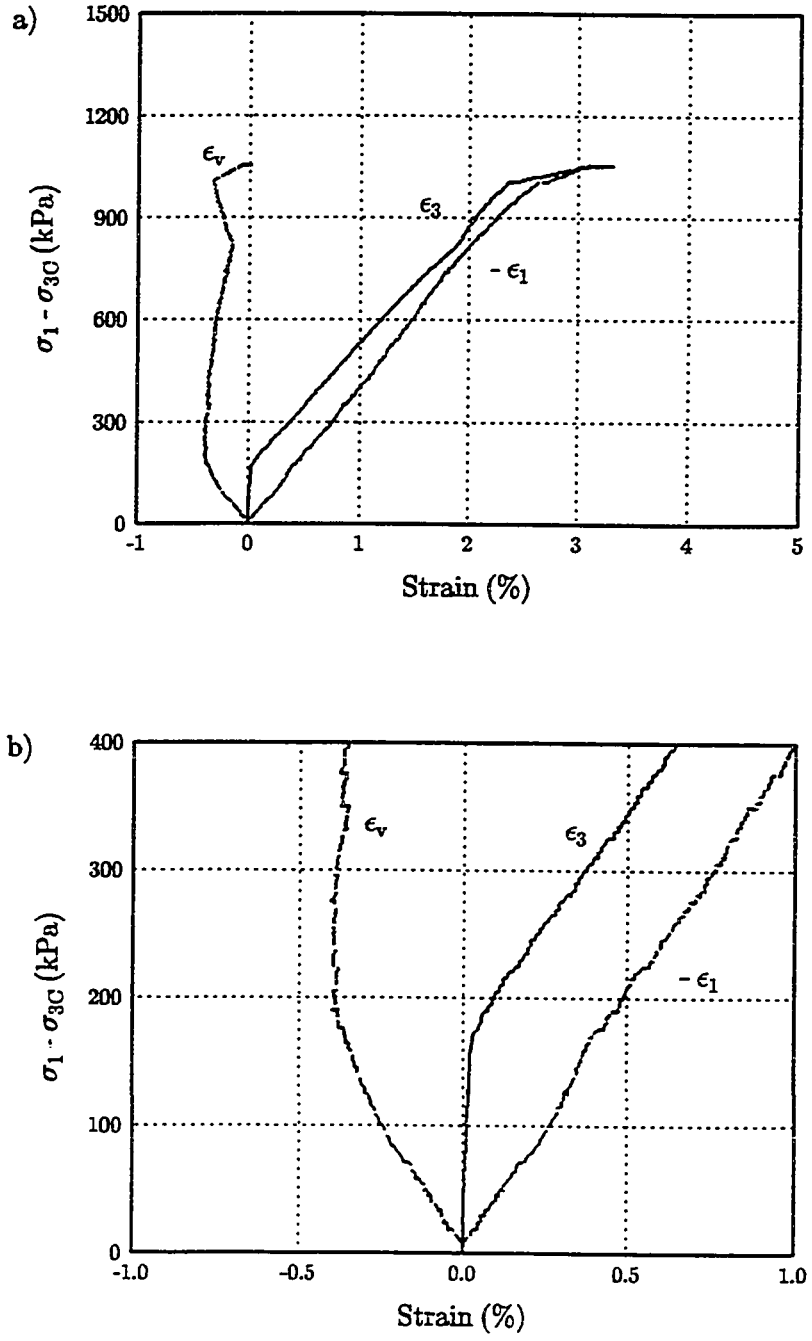

Figure 6.19: Principal stress difference vs. vertical, horizontal and volumetric strains for complete test and close-up of initial strains for Soil O with Reinforcement PET1, σ_{3C} = 20 kPa.

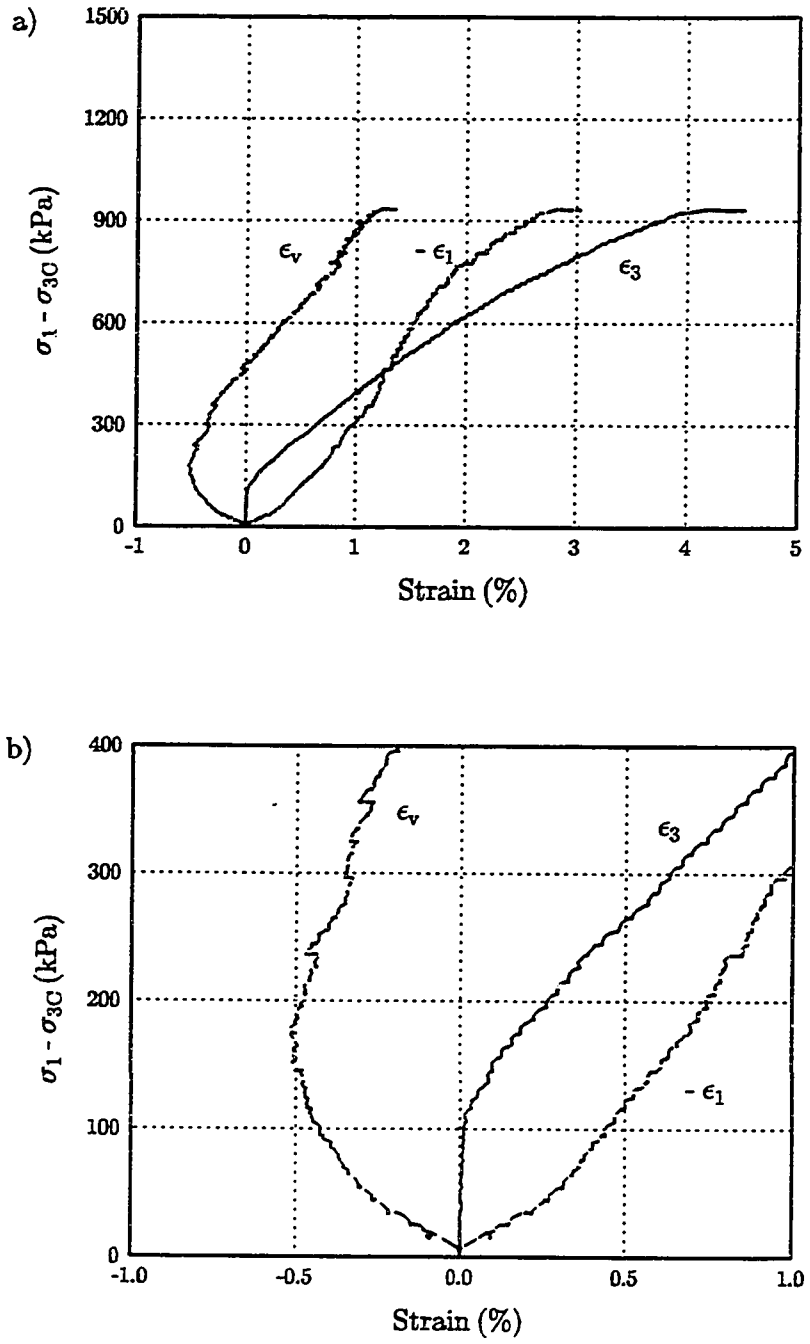

Figure 6.20: Principal stress difference vs. vertical, horizontal and volumetric strains for complete test and close-up of initial strains for Soil R with Reinforcement PP2, σ_{3C} = 20 kPa.

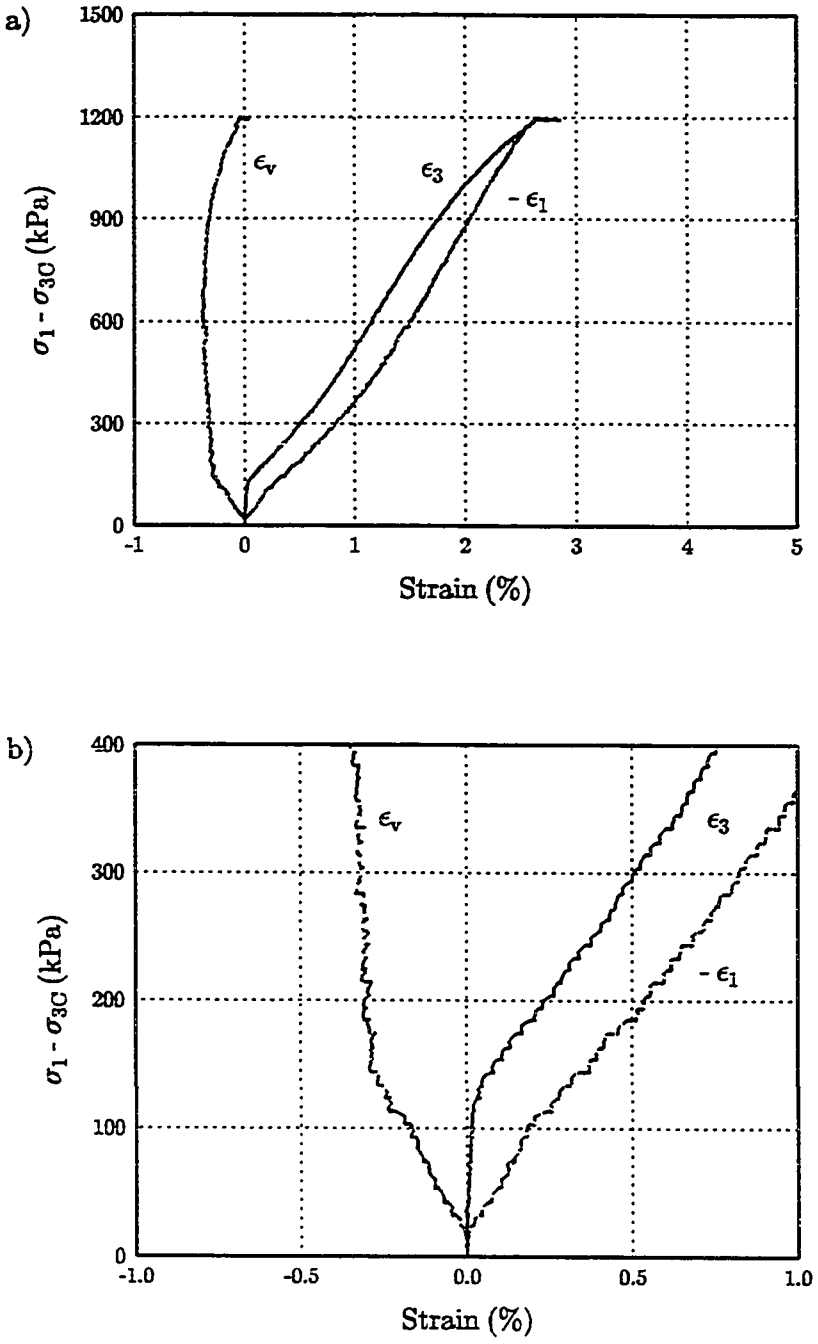

Figure 6.21: Principal stress difference vs. vertical, horizontal and volumetric strains for complete test and close-up of initial strains for Soil R with Reinforcement PET1, σ_{3C} = 20 kPa.

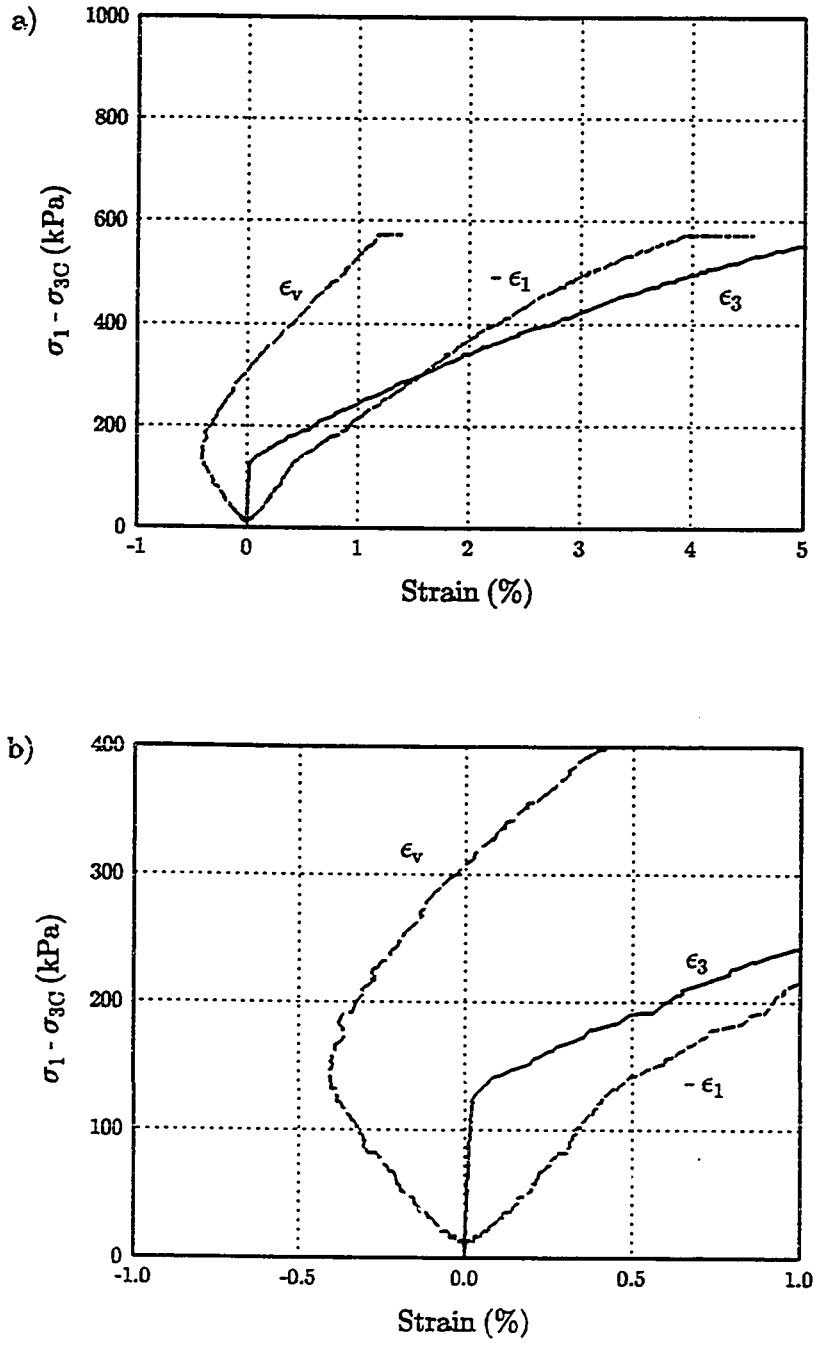

Figure 6.22: Principal stress difference vs. vertical, horizontal and volumetric strains for complete test and close-up of initial strains for Soil S with Reinforcement PP2, σ_{3C} = 50 kPa.

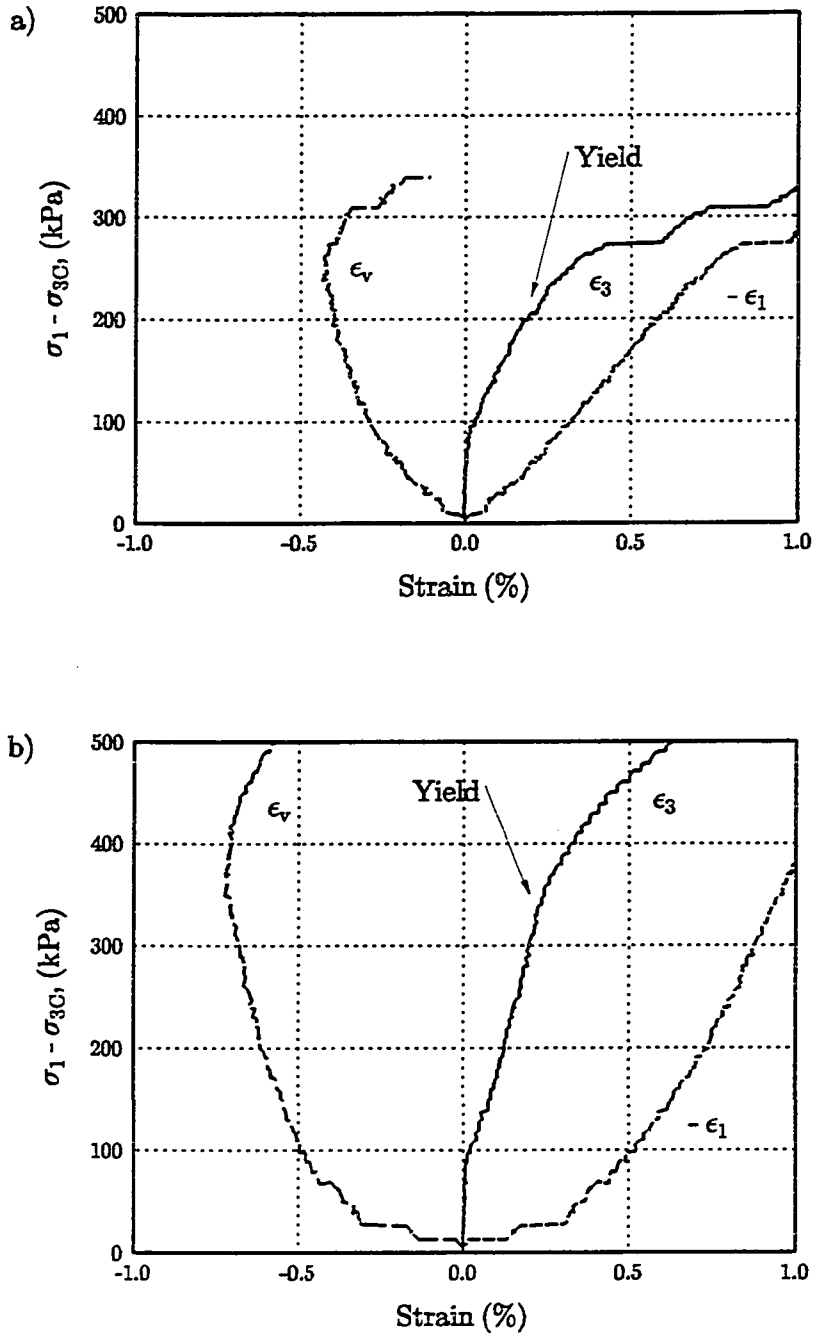

Figure 6.23: Principal stress difference vs. vertical, horizontal and volumetric strains; close-up of initial strains for Reinforcement SS with: a) Soil O, σ_{3C} = 20 kPa, and b) Soil R, σ_{3C} = 10 kPa.

compression decreased and the lateral expansion rate increased. It was not until after dilation was initiated that significant lateral expansion of the soil occurred.

Lateral strains of 0.02% represent nearly 10% of the yield strain (corresponding to 10% of the yield capacity) of the steel sheet, Reinforcement SS. Reinforcement SS had, therefore, developed significant loads, which had increased the effective lateral confining pressure and soil strength (Figures 6.17c and f), when the lateral expansion rate increased relative to the vertical compression rate. However, the soil was still compressing when the steel's yield strain of 0.23% was reached, Figures 6.23 and 6.24. Thus, while the tendency for the soil to dilate influences the response of steel-reinforced soil, no increase in volume is possible prior to yielding of the steel.

At the much greater strains possible with geosynthetic reinforcements dilation of the soil could occur. There is little difference in the behavior of steel reinforced soil and geosynthetic reinforced soil at the very low strains at which steel yields. The soil initially compresses approximately 0.5% and the rate of lateral expansion increases substantially at about 0.02% lateral strain. As with the steel-reinforced soils, those reinforced with geosynthetics were still compressing at 0.23% strain. It was not until greater lateral strains had been attained that the soil could begin to dilate, Figures 6.18 to 6.22. At these strain levels the geosynthetic reinforcings had not developed significant tension and had not increased the capacity of the composite much above the unreinforced strength, Figure 6.17. In fact, it is not until lateral expansion of the soil begins in earnest that much tension develops in the reinforcing, Figure 6.9a. Since dilation is associated with lateral expansion, if not primarily responsible for it, the conclusion could be reached that the dilation of the dense cohesionless soils is necessary for the lower modulus geosynthetics to develop tensile loads.

Very different volumetric responses were observed for specimens constructed with Reinforcement PET1, the high strength polyester, and those constructed with the other geosynthetics, Figures 6.18 to 6.21. When reinforced with the lower modulus geotextiles, the soils began to dilate almost immediately after the initial 0.5% vertical

compression. When Reinforcement PET1 was used dilation was prevented altogether, or substantially reduced. After initial compression, near constant volume deformation accompanied the first 1% to 3% lateral strain. The overall trend of reduced dilation with increasing reinforcing modulus is evident in Figure 6.25. As the modulus of the reinforcements increase, the lateral strain is greater for any given volumetric strain. Volumetric strain of composites constructed with the lower modulus reinforcements, PP2, PP3, NW1 and NW2, appear least affected by reinforcement strength properties and those constructed with the higher modulus reinforcements, PP3 and PET1, most affected. UCD specimens constructed with the nonwoven needle-punched geotextiles experienced a reduction in volume equal to, or greater than, those constructed with the woven geotextiles, Figure 6.25. Compression of the geotextile is the suspected cause of this, not a change in soil behavior. Variability of specimen construction may explain why specimens with woven geotextiles, which should have been less compressible in general, sometimes experienced as much reduction in volume as did specimens constructed with the nonwoven geotextiles.

Reinforcement compressibility (especially for the nonwovens, NW1 and NW2), specimen preparation, UCD operation, and variation of soil and reinforcement properties introduce sufficient variability in the results which prevent determination of the exact relationship between reinforcement modulus and restriction of dilation. However, the influence of Reinforcement PET1 on the behavior of Soils O and R (Figures 6.13, 6.14, and 6.18 to 6.21) and the somewhat different volumetric strain versus lateral strain behavior when higher modulus reinforcements were used (Figure 6.25) provides substantial evidence that soil dilation is being restricted and that the soil response is modified as a result. Of course, as was discussed in Section 6.4.1.3, it is not the reinforcement modulus which is actually affecting the soil behavior. The increase in confining pressure which is accompanying lateral strain is responsible for the modification of soil behavior. It should, therefore, be possible to study this phenomenon by conducting plane strain tests on unreinforced soil where an increase in lateral

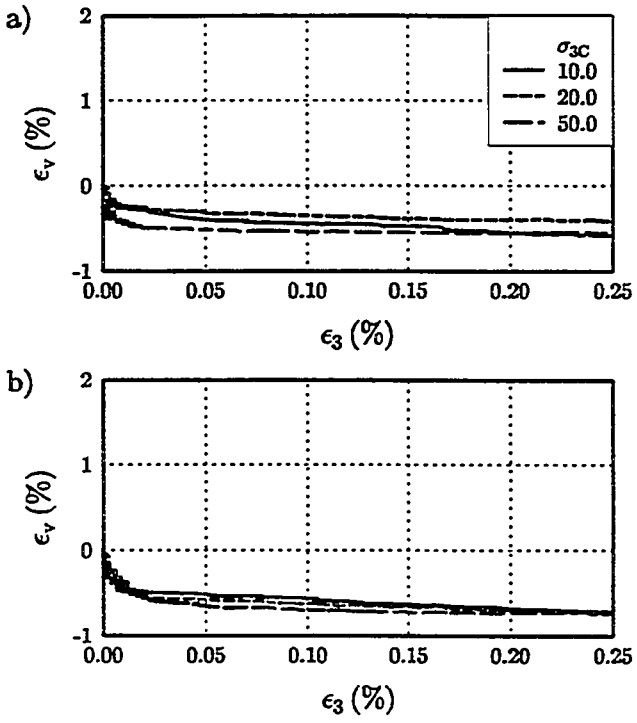

Figure 6.24: Volumetric strain vs. lateral strain for Reinforcement SS: a) Soil O, and b) Soil R.

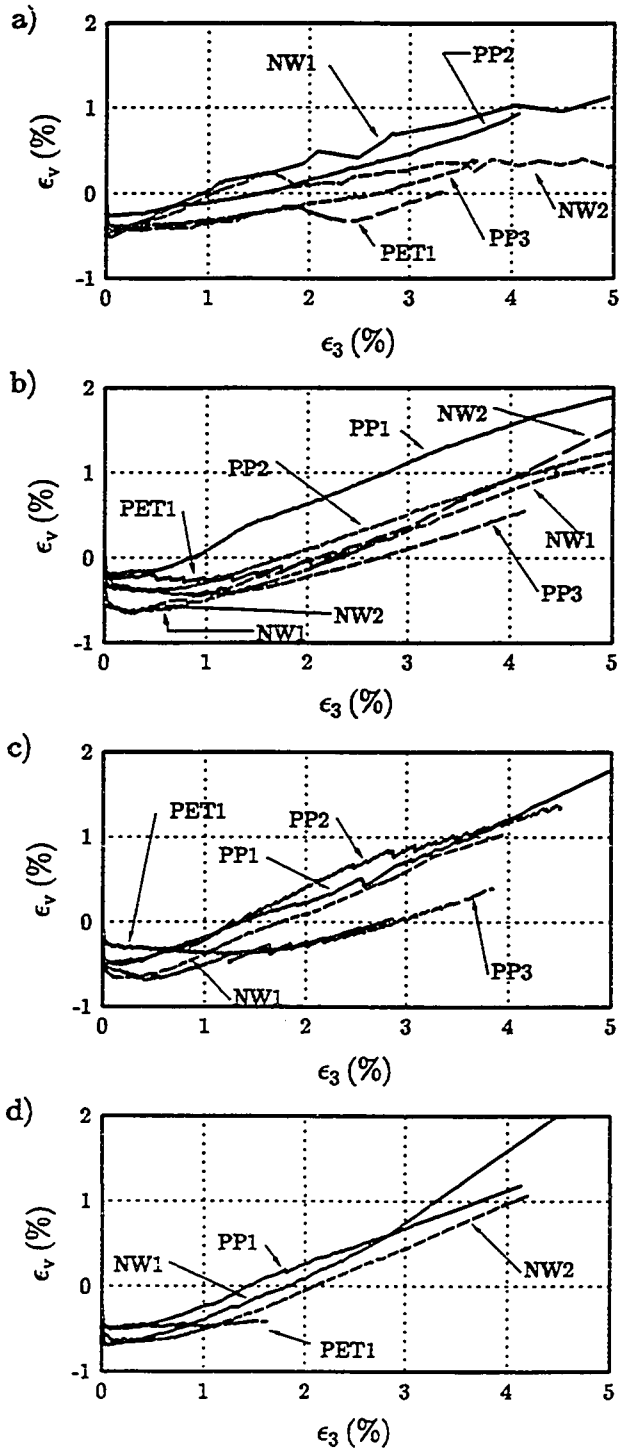

Figure 6.25: Volumetric strain vs. lateral strain for various extensible reinforcements a) Soil O, σ_{3C} = 50 kPa, b) Soil R, σ_{3C} = 10 kPa, c) Soil R, σ_{3C} = 20 kPa, d) Soil R, σ_{3C} = 50 kPa.

confining pressure accompanies lateral strain. Such a study could prove very worthwhile, since it can be concluded from this discussion that dilation is an important factor which defines the relationship between vertical and horizontal deformations of geosynthetic reinforced dense cohesionless soils at lateral strains greater than 0.25%.

The UCD was designed for measuring the response of reinforced soil composites at low lateral strains and subjected to vertical pressures anticipated in field applications. Unfortunately, these limitations restricted maximum lateral strain to less than 8% and maximum applied vertical pressure to less than 1300 kPa. Thus, the soils were still dilating at the completion of the tests and constant volume deformation could not be reached. The UCD cannot, therefore, be used to measure two conceivably very important properties of the soil: the constant volume effective stress ratio and the strain required to attain constant volume deformation. Modifications to this or future unit cell test apparatus may be appropriate to facilitate acquisition of these properties.

6.4.1.5 Summary

a) The importance of measuring soil properties using tests which simulate the conditions in the field was highlighted. An increase in friction angle was measured for the two sands when tested under plane strain instead of triaxial conditions.

b) The Yang and Singh (1974) hypothesis was confirmed - when the reinforcing is strained an increase in soil capacity results from the increase in effective confining pressure acting on the soil.

c) Soil dilation played an important role in defining geosynthetic reinforced soil behavior. Higher modulus reinforcements were able to modify the dilative behavior of the soils.

d) The increase in effective confining pressure which accompanied lateral strain modified the soil behavior when compared with tests performed at constant lateral confining pressures.

6.4.2 Geosynthetic Behavior

6.4.2.1 Modulus

6.4.2.1.1 General

In addition to measuring the soil response the UCD also measures the tension in each end of the reinforcement throughout each test. The "apparent" in-soil reinforcing modulus may be computed by dividing the tension by the corresponding strain. Due to frictional interaction of the soil and reinforcement, the loads measured at each end were not necessarily equal throughout each test, Figures 6.26 to 6.32. The difference between the two loads increased with decreasing reinforcing modulus, increasing soil friction and lateral strain. The confined modulus was computed by averaging the tensile forces measured in each end of the reinforcement. Unfortunately, because of its mode of operation, direct comparison of the modulus obtained from tests in the UCD with the modulus obtained from tests in other in-soil devices may be difficult for the following reasons:

a) The confined modulus of geosynthetics has often been measured using devices which apply a constant pressure normal to the reinforcement during load application (e.g., McGown, et al., 1982, and Ling, et al., 1992). For UCD tests the normal pressure on the reinforcement was not constant but increased continually during each test. This process models the conditions which occur during the construction of reinforced soil walls. However, the apparent modulus of confinement-sensitive geosynthetics changed as the normal pressure increased during testing. Arriving at a single modulus value for these reinforcements from UCD test results is difficult since for each test the reinforcing strain and normal

pressure differ depending on the soil properties and the effective lateral confining pressure.

b) Other in-soil reinforcement testing devices maintain a constant strain rate throughout each test (McGown, et al., 1982; Wu, 1991; Ling, et al., 1992). With the UCD the load is applied to the soil and the rate of lateral expansion is dependent on the soil response and may vary during testing. Any variation in the reinforcing strain rate may cause the apparent modulus of strain-rate-sensitive reinforcements to vary during a test.

6.4.2.1.2 Nonwoven Needle-Punched Geotextiles

Although more than 17 tests were conducted with Reinforcements NW1 and NW2, a meaningful modulus could not be determined for all of those tests. No modulus was computed if the difference in tension measured at the two ends was deemed excessive or if the reinforced soil specimen exhibited odd (i.e., very different than that observed in other tests) behavior during the test. The low geotextile tensile loads, variability of specimen strength due to the manufacturing process (discussed in Section 5.5), variability in specimen preparation, and the nonuniform tension in the geotextiles made determining a modulus difficult. Consequently, no single in-soil modulus could be computed for either nonwoven geotextile.

However, even with the limited data it can be implied that the apparent modulus increased above the modulus attained from ASTM D 4595 standard wide width tests on 100 mm specimens when these reinforcements were confined in soil, Figure 6.33. Nonwoven needle-punched geotextiles had confined moduli 1 to 4 times the standard, 100 mm gage length, in-isolation tests. This increase in modulus for the nonwoven geotextiles due to confinement in soil and application of normal pressure was anticipated since this effect had been reported by others (e.g., McGown, et al., 1982). The "zero" span in-isolation 5% modulus values were on the order of 55 kN/m and 115 kN/m for

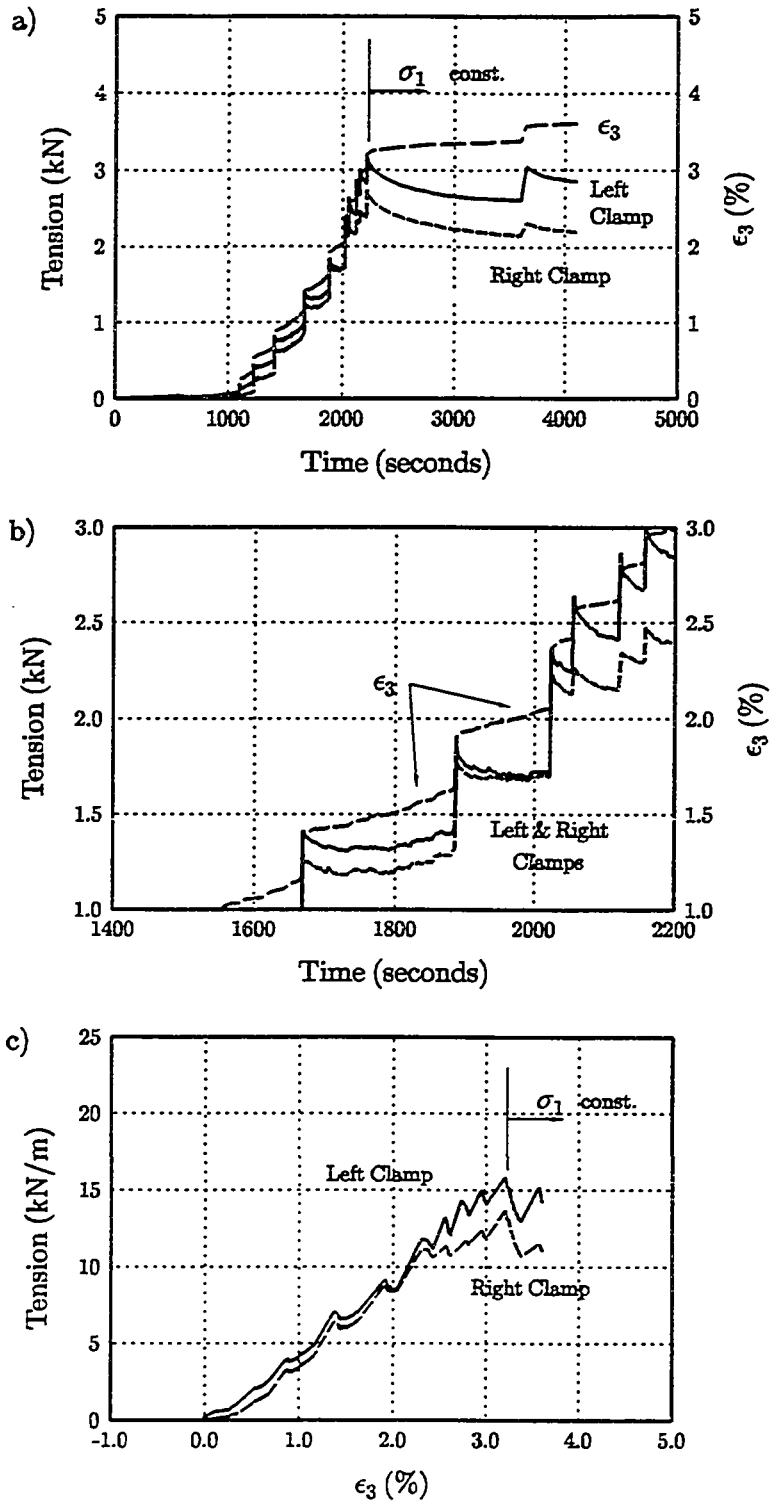

Figure 6.26: Tension vs. time and lateral strain: a) full test and b) portion of test; and c) tension vs. lateral strain. Soil O, Reinforcement PP3, σ_{3C} = 75 kPa.

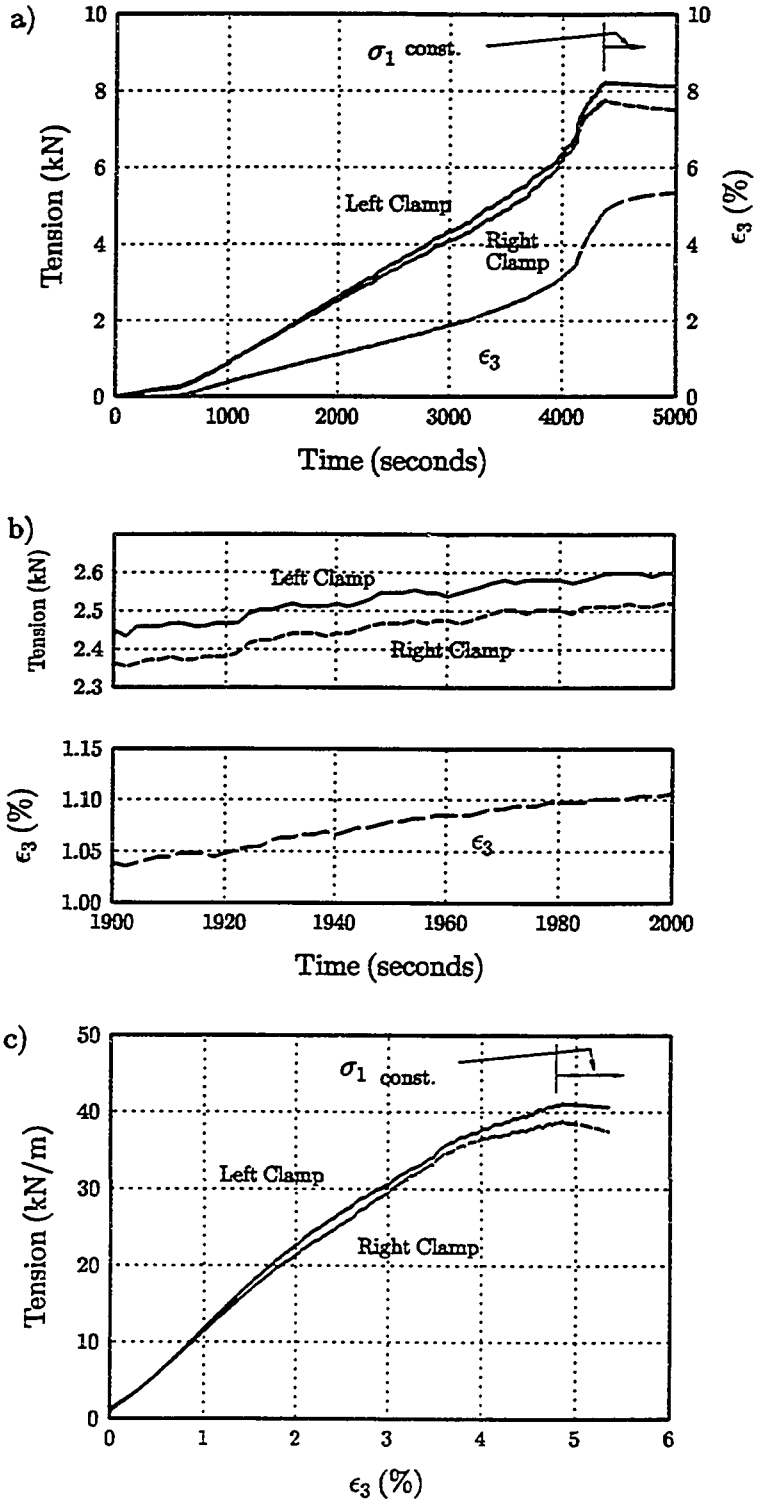

Figure 6.27: Tension vs. time and lateral strain: a) full test and b) portion of test; and c) tension vs. lateral strain, Soil O, Reinforcement PET1, $\sigma_{3C} = 20$ kPa.

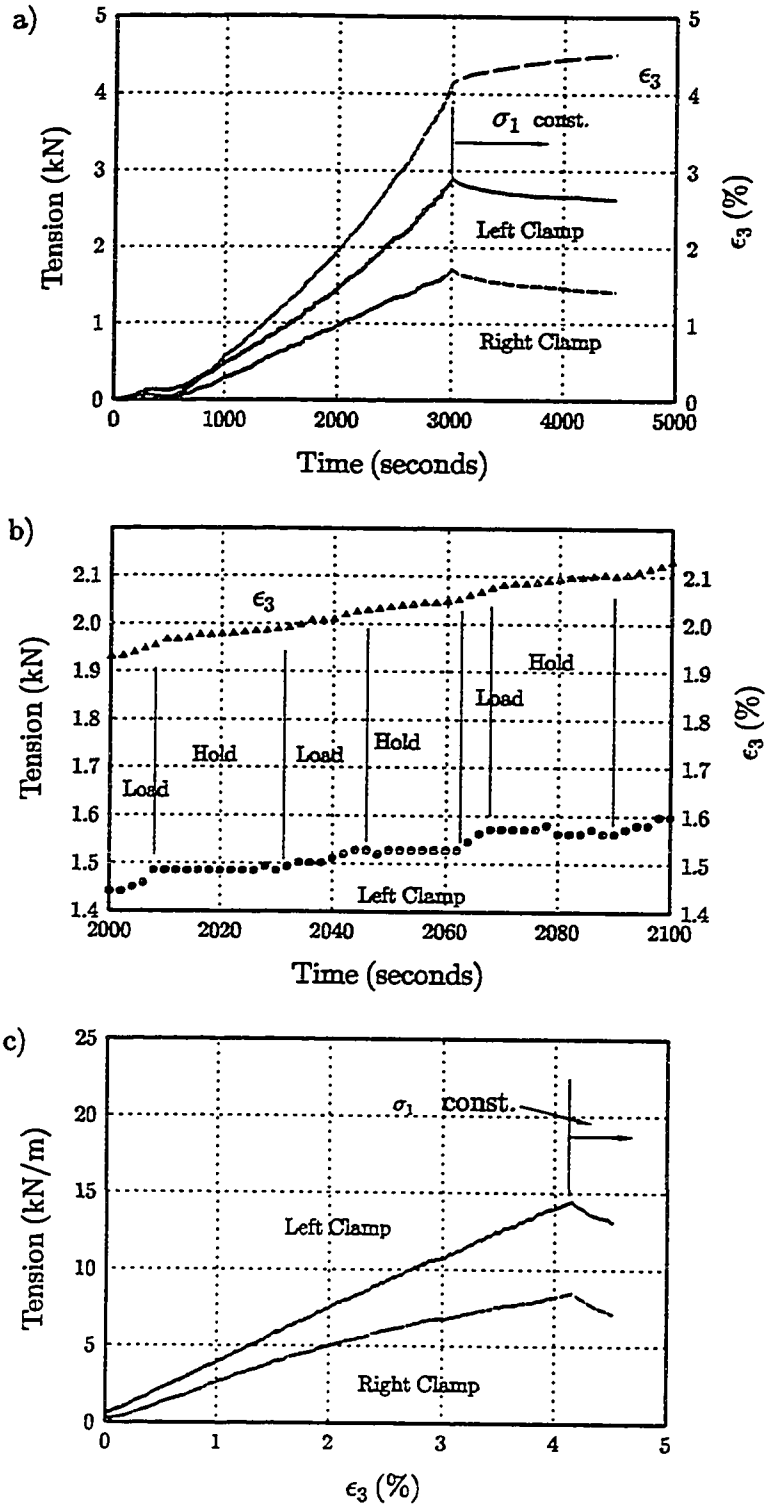

Figure 6.28: Tension vs. time and lateral strain: a) full test and b) portion of test; and c) tension vs. lateral strain, Soil R, Reinforcement PP2, $\sigma_{3C} = 20$ kPa.

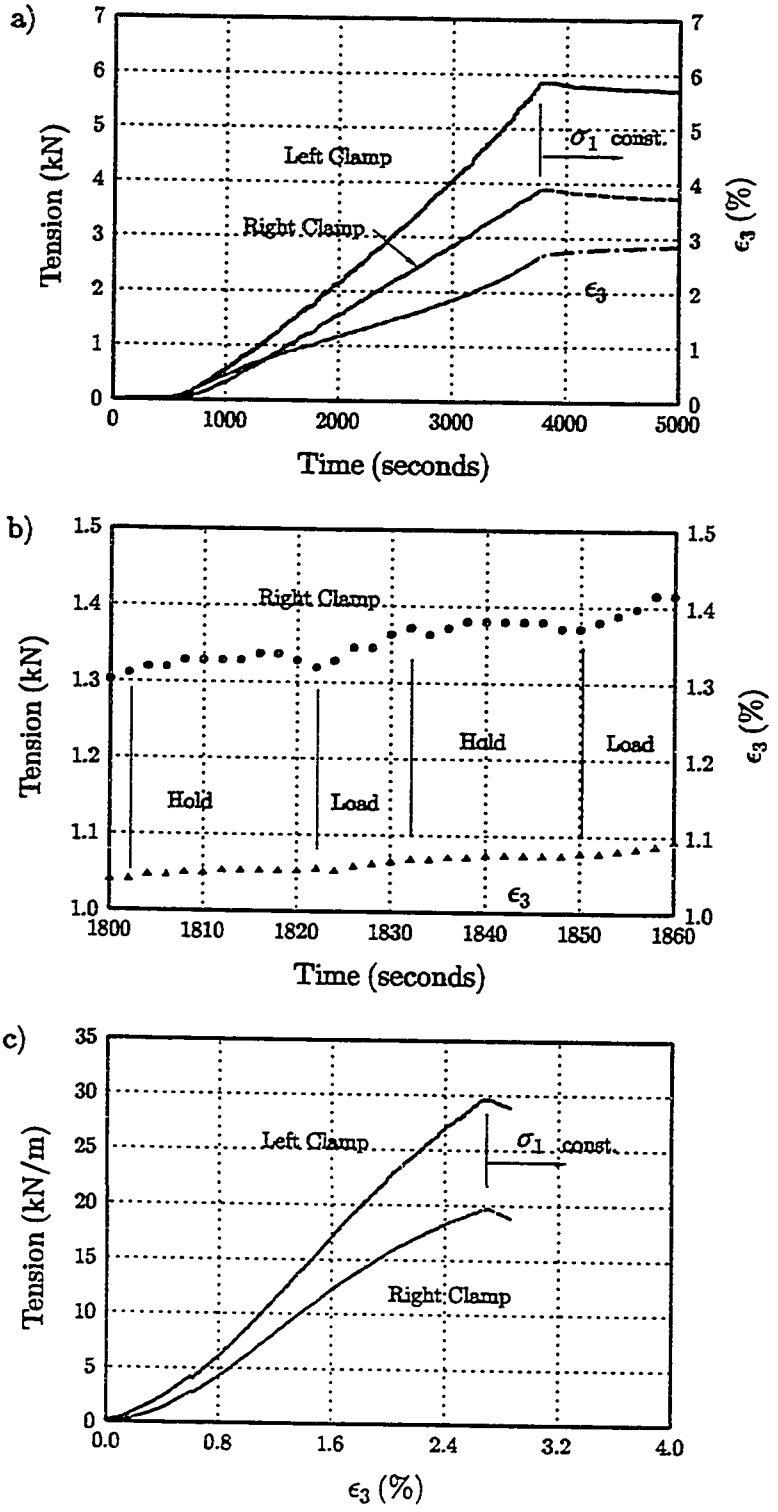

Figure 6.29: Tension vs. time and lateral strain: a) full test and b) portion of test; and c) tension vs. lateral strain, Soil R, Reinforcement PET1, σ_{3C} = 20 kPa.

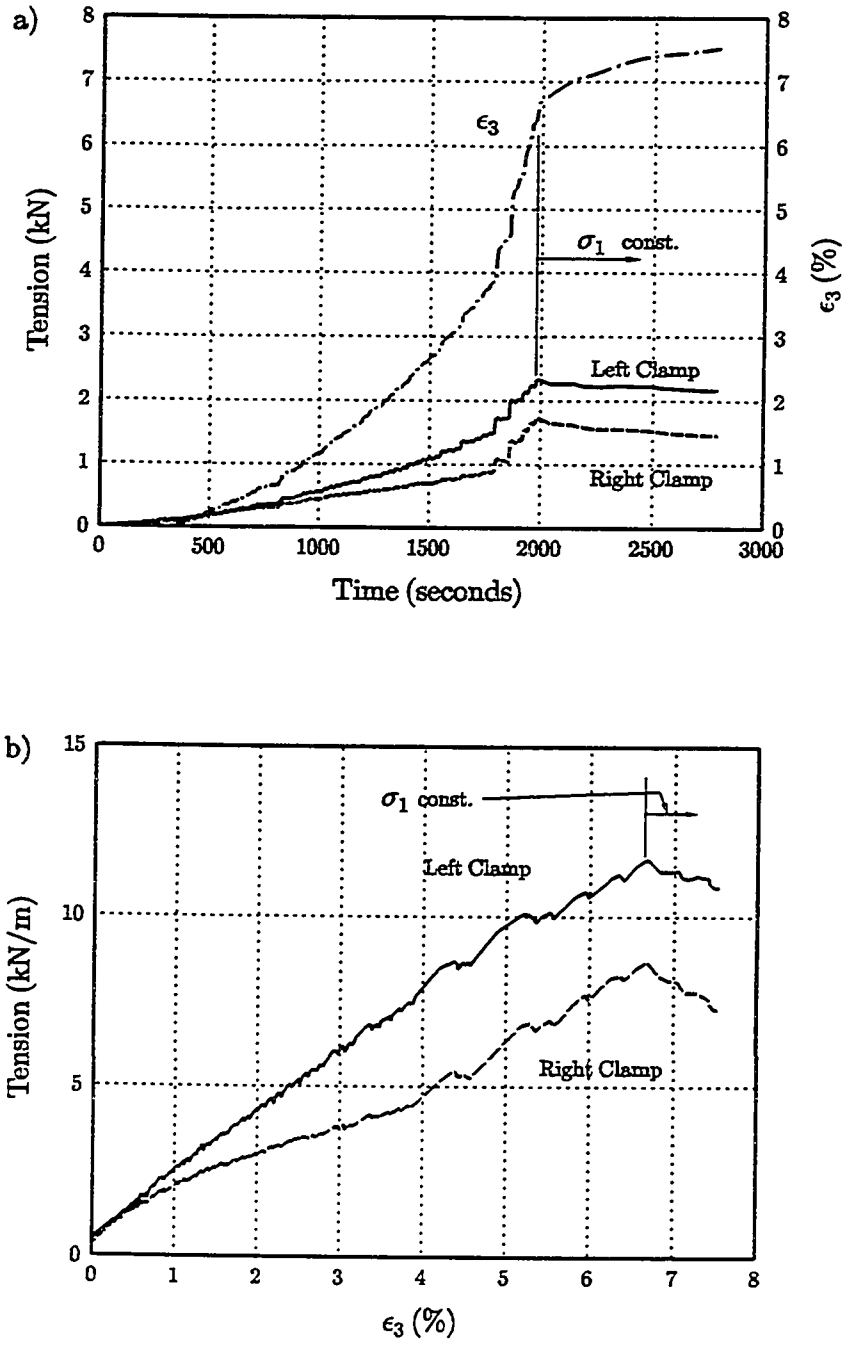

Figure 6.30: a) Tension vs. time and lateral strain, and b) tension vs. lateral strain, Soil R, Reinforcement PP1, σ_{3C} = 10 kPa.

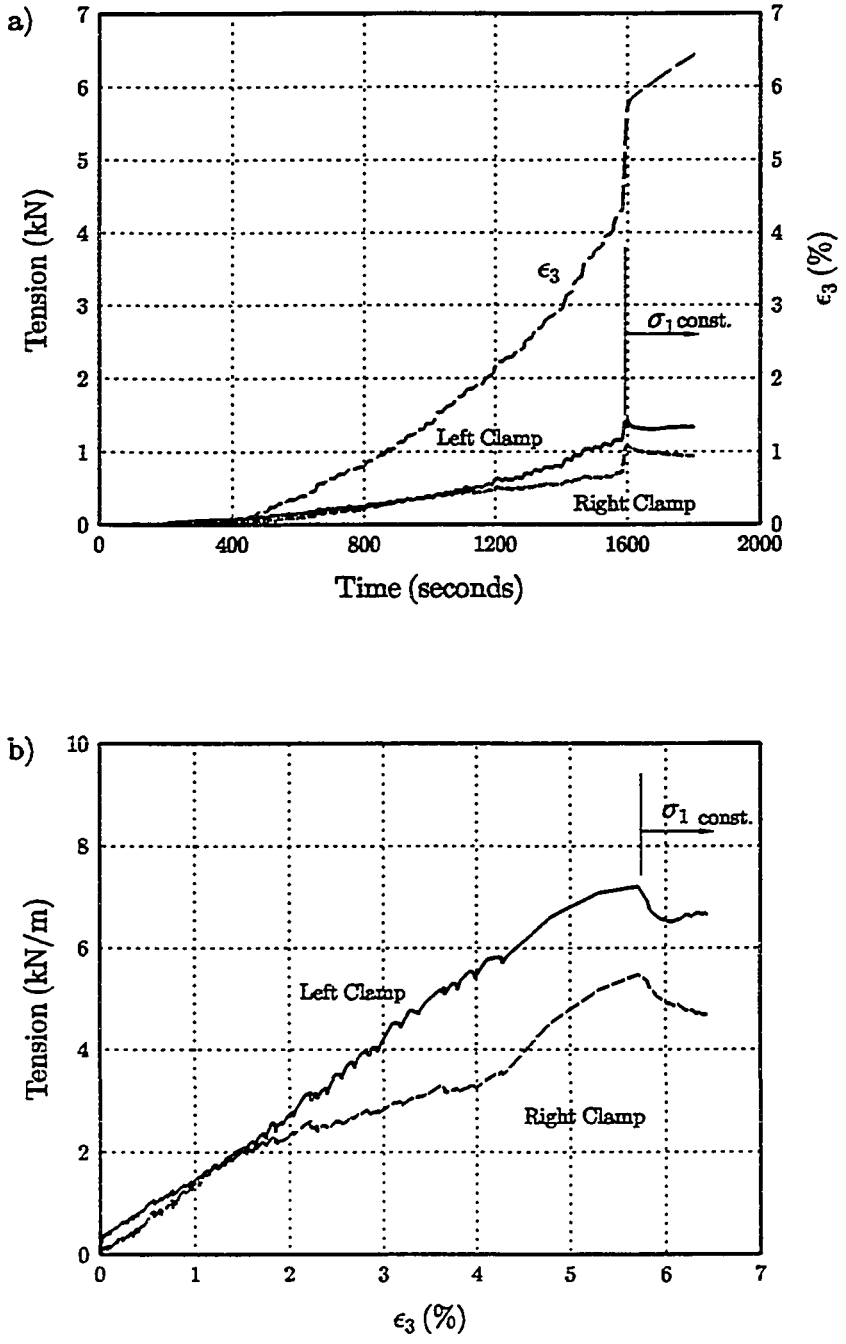

Figure 6.31: a) Tension vs. time and lateral strain and b) tension vs. lateral strain, Soil R, Reinforcement NW2, σ_{3C} = 10 kPa.

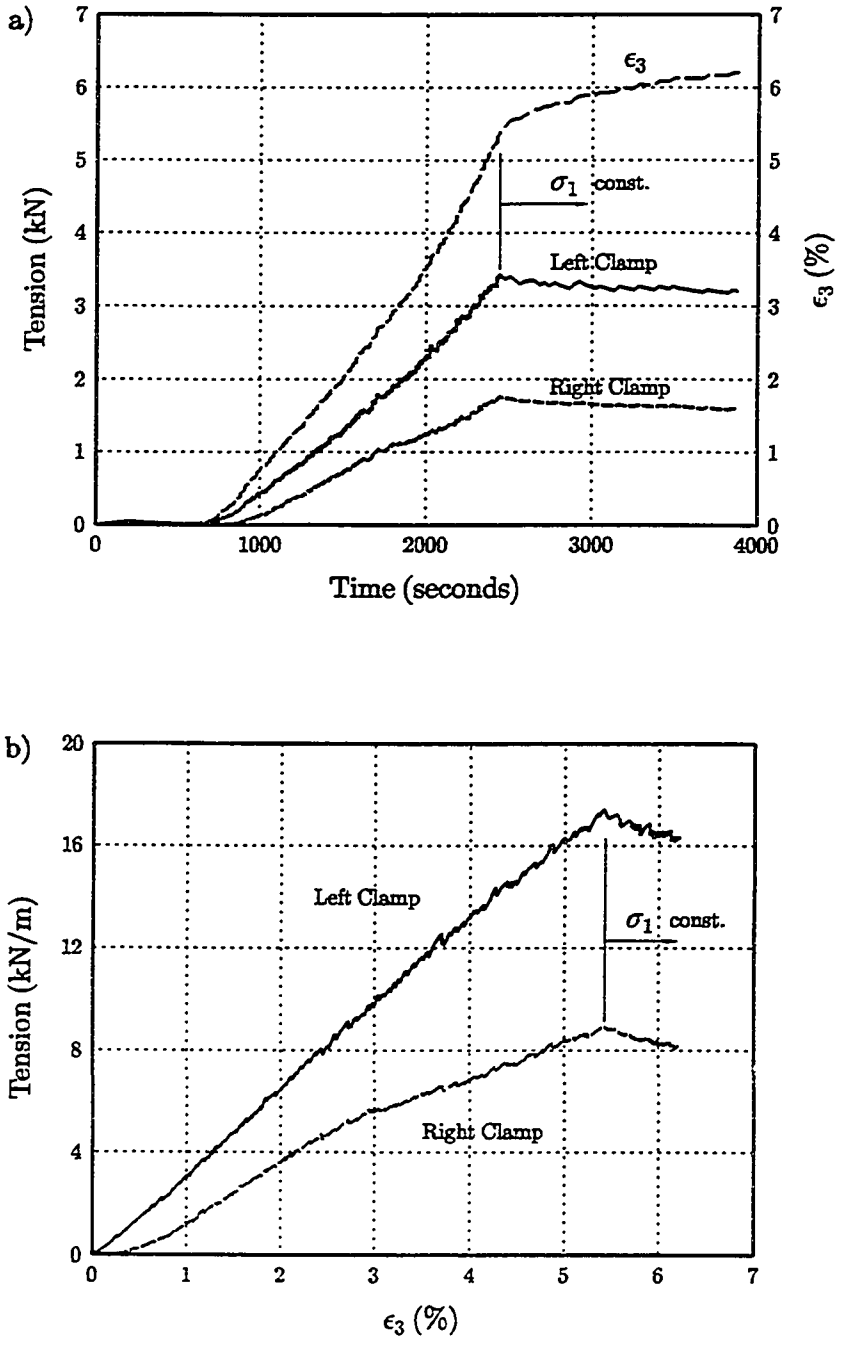

Figure 6.32: a) Tension vs. time and lateral strain, and b) tension vs. lateral strain, Soil 3, Reinforcement PP2, σ_{3C} = 50 kPa.

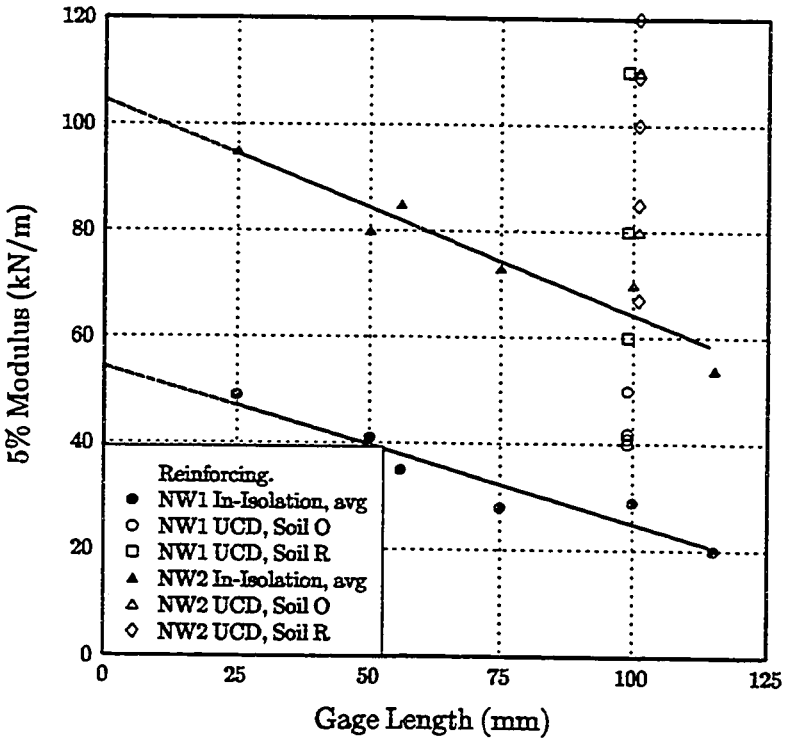

Figure 6.33: Comparison of modulus of nonwoven geotextiles determined from UCD tests with those determined from in-isolation tests (Figure 5.10).

Reinforcements NW1 and NW2, respectively. These are within the range of in-soil modulus values determined from the UCD tests, Figure 6.33.

However, developing a correlation between in-isolation and "the" in-soil modulus is difficult because the UCD normal pressure is dependent on the soil strength and effective confining pressure experienced by the soil. This relationship between nonwoven needle-punched geotextile modulus and normal pressure, and not simply to a "zero" gage length, prevents the development of an exact correlation between UCD determined modulus and the projected "zero" span modulus of nonwoven geotextiles determined through in-isolation tests (Section 5.5). A different confined testing program, perhaps utilizing one of the devices discussed in Section 2.1.3, is recommended for determining the confined modulus of needle-punched nonwoven geotextiles, at specific normal

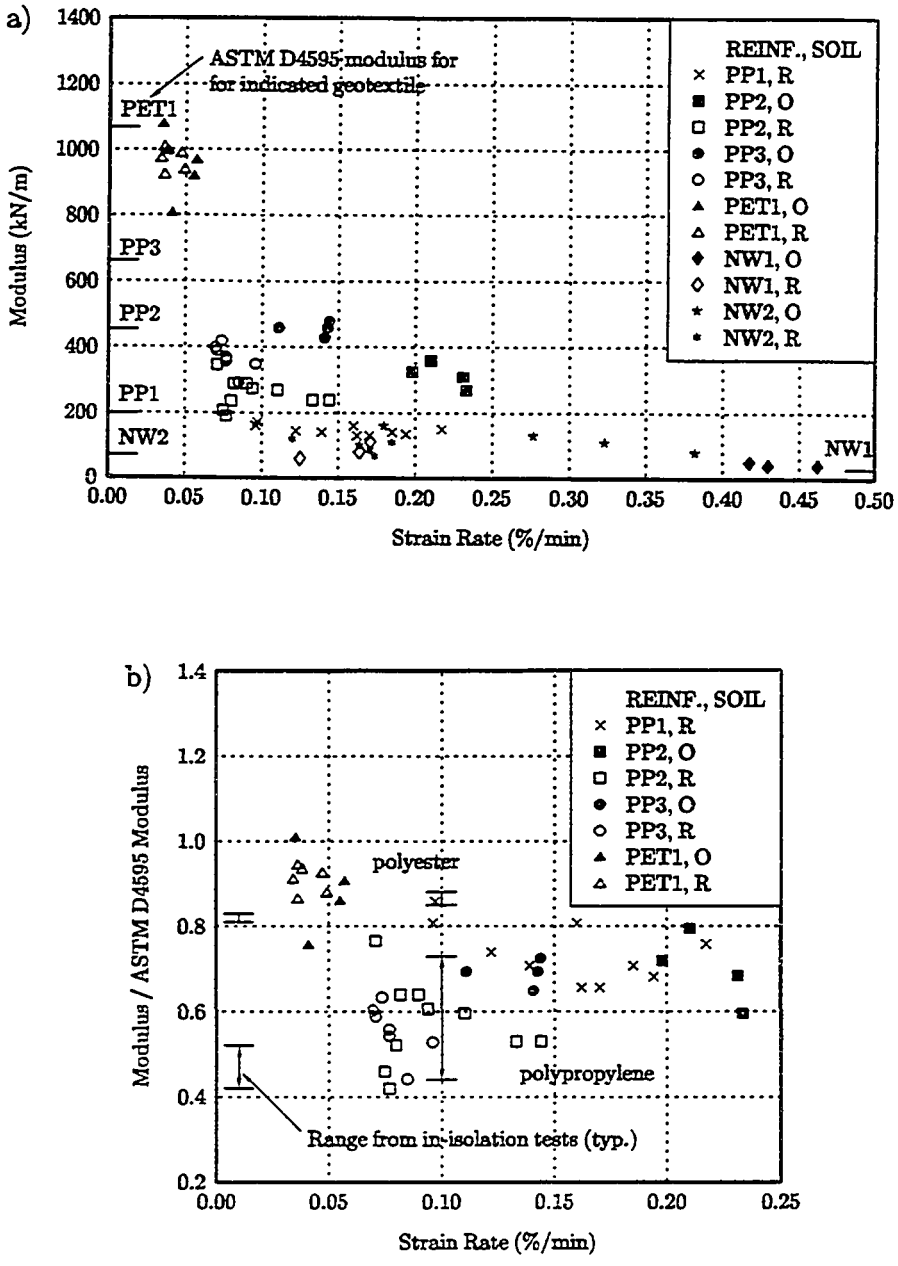

Figure 6.34: a) Modulus vs. strain rate for all geotextiles tested and b) normalized modulus vs. strain rate for the woven geotextiles only.

pressures. The projected "zero" span modulus could be compared to the confined modulus to determine how closely it approximates, if at all, the confined modulus and for what normal pressures. The limited tests performed for this project, and the scatter in the data, are insufficient to confirm or rule out the potential for a "zero" span test to adequately predict the in-soil modulus for nonwoven needle-punched geotextiles. Further research in this area is recommended as the savings in both time and money associated with performing in-isolation tests instead of in-soil tests would be significant. Any research undertaken for this purpose, using nonwoven needle-punched geotextiles similar to NW1 and NW2, should use a large number of specimens because of the high degree of variability of manufacture observed in these geotextiles (see Section 5.5).

6.4.2.1.3 Woven Geotextiles

An increase in modulus with confinement was not observed for the woven geotextiles; instead the modulus decreased significantly in comparison to the in-isolation ASTM D 4595 wide width test values, Figure 6.34a. The modulus computed for the polypropylene woven geotextiles, Reinforcements PP1, PP2, and PP3, were between 40% and 80% of the 5% secant modulus (modulus determined at 5% strain) determined from standard in-isolation ASTM D 4595 tests. The woven polyester geotextile, Reinforcement PET1, was not as greatly affected; its modulus was near 90% of the ASTM D 4595 5% secant moduli. One notable difference between tests conducted in the UCD, other than confinement, and standard wide width tests (ASTM D 4595) is the rate at which the reinforcing is strained. Standard wide width tests are conducted at strain rates of 10%/min while UCD specimens experienced average strain rates between 0.5 and 0.035%/min. These strain rates are 20 to 300 times slower than the standard test, Figure 6.34a. (The apparent increase in nonwoven geotextile modulus with decreasing strain rate, shown in this figure, is misleading, as this increase is probably related to normal pressure as discussed in Section 6.4.2.1.2.)

A reduction in modulus of geosynthetics with decreasing strain rate had been reported by Rowe and Ho (1986), Anjiang, et al. (1990) Nothdurft and Janardhanam (1994), and Nothdurft (1995) and is the suspected cause of the reduction in modulus observed in this program. The increase in the rate at which tension developed in the geotextiles when the lateral strain rate increased verifies that these materials display substantial strain rate dependencies, Figures 6.24 to 6.30. The in-isolation tests conducted on the woven geotextiles, Section 5.4, also found that the "apparent" modulus increased with increasing strain rate, Figure 5.6. The results of that portion of this study have been superimposed on the normalized modulus values determined for woven geosynthetics tested in the UCD in Figure 6.34b. The fairly close relationship, especially for the slit-film polypropylene geotextiles, suggests that the modulus of the woven geotextiles measured in the UCD were not influenced by confinement, but were related directly to strain rate. The slight difference in strength reduction with decreasing strain rate for PET1, when compared with the in-isolation tests, may be due to confinement in soil but is more likely due to differences between the polyester geotextile tested in-isolation, PET2, and PET1, which had been exhumed from the Rainier Avenue wall. Provided the strain rate effects are known, this decoupling of woven geotextile modulus from confinement effects should simplify testing of these materials, since only in-isolation testing is required. This is in agreement with the in-soil load-elongation tests reported by Wilson-Fahmy, et al. (1993) where they concluded that only nonwoven geosynthetics need be tested in confinement. The in-isolation testing should be performed to define the relationship of strength and modulus to strain rate. Further discussion on measuring the load-elongation properties of woven geosynthetics is presented in Section 6.6

6.4.2.2 Creep

Creep (strain under constant stress) and stress relaxation (stress reduction at constant strain) of the geosynthetics occurred in UCD tests at low stress and low strain

levels and over short time intervals. For convenience, and since the same mechanism is involved in both phenomenon, creep and stress relaxation will be referred to as creep in the discussion which follows.

In several tests, after initial straining of the specimens, loading was discontinued and the vertical pressure held constant. With constant load applied to the composite the reinforcement continued to strain and simultaneously experienced a reduction in tension, Figures 6.24 - 6.30. The creep rate decreased with time with the most significant effects occurring relatively quickly. For the tests presented in Figures 6.26, 6.28, and 6.29, when loading was discontinued reinforcing tensions were at 18%, 34%, and 16%, of the in-isolation ASTM D 4595 wide width test strength for Reinforcements PP3, PP2, and PET1, respectively. The potential for creep at these stress levels has been reported previously (den Hoedt, 1986; Andrawes, et al., 1986).

For composites constructed with Soil O and the polypropylene geotextiles, each "slip" was accompanied by a lateral displacement which caused the tension in the reinforcement to increase suddenly, Figure 6.26. During each "stick" phase, tension in the reinforcing decreased noticeably while the unit cell continued to experience lateral displacement. Near the end of the test presented in Figure 6.26a, a significant decrease in reinforcement load, while vertical pressure was held constant, resulted in a critical reduction in the effective lateral confining pressure acting on Soil O. The soil then experienced a sudden slip, reached a new equilibrium state with higher stresses in the reinforcing, and immediately began creeping again. This cycle of slip-stick-creep was typical of tests on Soil O for all geosynthetic reinforcings except PET1.

Creep also occurred between loading increments. Each 10 kPa pressure increase took approximately 10 seconds to apply (indicated by "Load" in Figures 6.28 and 6.29). The pressure was then held constant for 20 seconds until the next increment was applied (indicated by "Hold" in the figures). While the vertical pressure was held constant the geosynthetic specimens continued to strain without experiencing a corresponding increase in tension (Figures 6.27 - 6.30). Creep of Reinforcement PET1 was surprising

given the reported low creep potential of polyesters (Figure 2.23, den Hoedt, 1986), and since it occurred over a short time interval with the reinforcement experiencing 1.1% strain. While in some tests with Reinforcement PET1 the strain rate during "Load" cycles was obviously greater than the strain rate during "Hold" cycles (Figure 6.28b), in some tests this change in strain rate was not so obvious, if in fact it did occur (Figure 6.27b). The speed at which creep occurred suggests that the creep mechanism is responsible for the decrease in modulus with decreasing strain rate observed in the woven geotextiles, Figure 5.6. By permitting the specimen to continue to strain at no increase in load, the modulus computed using this increased length would be less than it would otherwise be.

The tendency for the woven polypropylene geotextiles to experience substantial creep, even at small initial strains, was previously discussed in Section 5.6, Figure 5.13. The in-isolation creep tests presented in that figure illustrated that creep occurred rapidly after initial loading, similar to that observed in the UCD tests. As with the UCD tests, the in-isolation creep rate also decreased with time. The in-isolation creep tests on the polyester geotextile, Figure 5.13, while also indicating creep did occur, did not show the creep to occur as quickly as was indicated in the UCD tests. This difference may possibly be due to failure to accurately record the strains in the few seconds immediately after application of load in the in-isolation tests, the lower precision of the displacement measurement "scissors" used in the in-isolation tests, or the longer time interval between instrument readings at the beginning of the in-isolation creep tests. Another explanation could be that creep simply did not occur as rapidly in the in-isolation tests, although the approximately 20% increase in overall in-isolation specimen strain recorded over the duration of these tests makes this explanation unlikely.

6.4.2.3 Summary

a) Confinement of nonwoven geotextiles in soil resulted in an increase in modulus above the in-isolation values measured on 100 mm gage length specimens using the standard ASTM wide width test.

b) The modulus of woven geotextiles decreased with decreases in strain rate. This reduction in modulus was attributed to the tendency for these materials to creep.

c) Creep and stress relaxation of the geotextiles occurred over short time intervals and at low strains.

6.4.3 Composite Behavior

6.4.3.1 Composite Creep

During some of the UCD tests, after some lateral strain had been induced in the specimen, loading was discontinued and the vertical load held constant for an extended period of time, typically 1000 to 2500 seconds. During this period, as was discussed earlier, the load in the reinforcing decreased and the strain increased. For the vast majority of the UCD tests, with the possible exception of some conducted using Soil R and Reinforcing PET1, the soil had reached a fully active state prior to discontinuing loading. At UCD lateral strains greater than 3% the reinforcing strain exceeded 15% of the failure strain. Creep of the reinforcing would be expected at these levels. The decreasing rates of lateral strain and stress relaxation during each of these periods suggests that an equilibrium condition might be reached if the specimens were allowed to sit for an extended period of time. Such an equilibrium condition was observed in the in-isolation creep tests, Section 5.6.

To evaluate the long term response of a reinforced composite, at typical maximum reinforcing strains observed in the field, a single long term UCD test was conducted. The specimen, constructed with Soil R and Reinforcing PP2, was loaded until reaching 1% lateral strain and then monitored for 69 hours, Figure 6.35. For the first 1500 seconds instrument readings were taken at 1 second intervals. Reading intervals were increased to 1 every 5 minutes at 1500 seconds and again to 1 per hour at 19,500 seconds.

As was observed in the short term UCD tests, the load in the reinforcing decreased and the lateral strain continued to increase after loading of the UCD specimen was discontinued. At 9600 seconds into the test, after substantial reduction in reinforcing

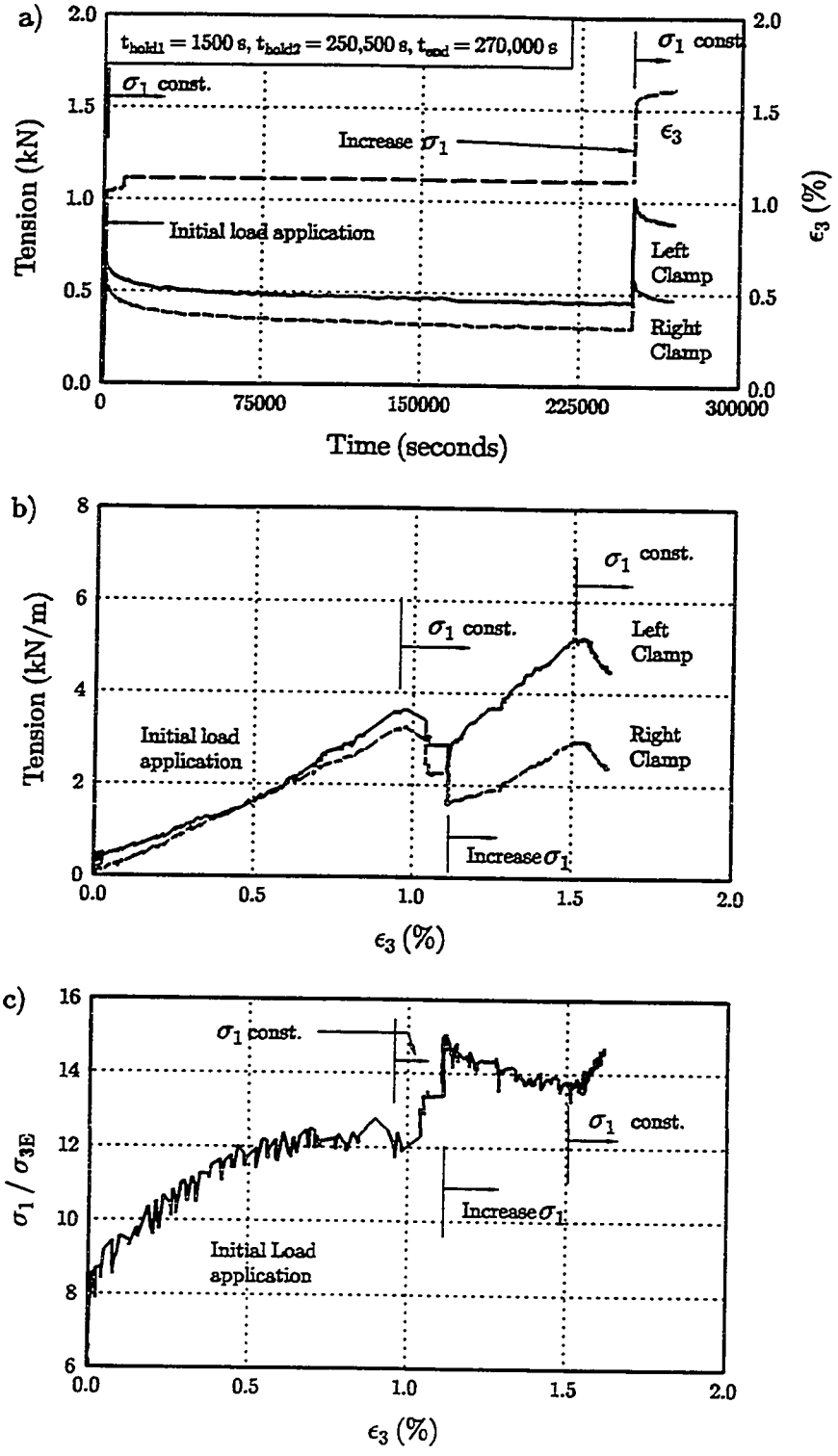

Figure 6.35: Composite creep test: a) tension vs. time, b) tension vs. lateral strain, and c) stress-ratio vs. lateral strain, Soil R, Reinforcement PP2, σ_{3C} = 20 kPa.

tension, the specimen experienced a sudden lateral displacement. This is similar to what occurred when Soil O and Reinforcement PP3 were used, Figure 6.26. Although this increase in strain should be accompanied by an increase in reinforcement tension no increase was observed. It is probable that there was sufficient time between instrument readings for this increase in tension to itself be relieved due to stress relaxation. After the lateral displacement at 9600 seconds, stress relaxation continued on the same curve. Although the load in the reinforcing decreased substantially, and continued to decrease throughout the test, the specimen did not continue to experience lateral strain. At 249,900 seconds the vertical pressure was increased until overall lateral strain reached 1.5%. Vertical load was then held constant for 19,500 seconds during which the same pattern of simultaneous creep and stress relaxation was again observed.

A decrease in the effective lateral confining pressure, and corresponding increase in the effective stress ratio, accompanied the reduction in reinforcing tensile load, Figure 6.35c. For the initial loading, the maximum stress ratio that the soil stress state slowly approached was still below the maximum stress ratio recorded for Soil R in some tests. The total lateral strain which the soil experienced was also below the lateral strain associated with active soil conditions. It could be that the soil was stable in this arrangement since it still had available residual capacity. If this is the case, additional strain should not be expected. This does not explain why the soil is apparently stable under decreasing confining pressure conditions after the second load application. With lateral strains over 1.5% the soil was past peak stress ratio, as is indicated by the reduction in effective stress ratio that accompanied lateral strain during the second period of load application, Figure 6.35c. Yet, decreases in effective confining pressure due to reduction in tension did not result in continued straining. Possible explanations for this behavior include "locking" together of soil grains and transfer of some energy to the UCD at the specimen boundaries. Because boundary effects may not be ruled out, it would be premature to conclude reinforced cohesionless soils will not creep.

Since only one long term UCD test was conducted only speculation can be made concerning the true reasons for this soil behavior. Before the effects of geosynthetic creep and stress relaxation on the response of reinforced soil can be fully understood, additional long term plane strain tests on cohesionless soils subjected to decreasing lateral confining pressure under constant vertical pressure are recommended.

6.4.3.2 Strain Gage Tests

Strain gages were attached to the geosynthetic reinforcing in a few tests to determine (1) the strain distribution along the length of the reinforcing specimen, (2) the adequacy of using strain gages for measuring geotextile strain, and (3) the correlation between overall specimen strain and strain reported by the strain gages. Strain gages were located as indicated in Figure 6.36. The gages used were high elongation strain gages of similar type, and by the same manufacturers, as those used in the Rainier Avenue wall (see Appendix A). To facilitate connection to and spacing along the relatively small specimens, the gages selected had shorter overall dimensions.

For the woven polypropylene geotextiles either two YL-20 gages, three YL-10 gages, or three YL-2 gages were applied using the procedure described in Section 5.3. Only two strain gage tests were conducted with Reinforcement PET1, the multi-filament polyester: one with two PA-7 gages and one with three PA-7 gages. The gages were attached using an SR-4 adhesive. Although an MB-4 rubber cement was applied over the strain gages and their lead wires to protect them during soil compaction and load application, as was done in the Rainier Avenue wall, no polysulfite sealant was applied (see Allen, et al., 1992). Soil R was the only soil used in tests that included attachment of strain gages to geotextiles.

The reinforcing specimens were placed in the unit cell with the strain gages on the top surface. Wires connecting the strain gages to the signal conditioner passed out of the unit cell between the right end clamp and the steel end plate above it. A small sheet of 0.3 mm latex rubber was placed over the strain gages, providing additional protection,

TEST	REINF.	GAGE	a	b	c	d	e	f
122*	PP3	YL-2	100.0	13.0	115.0	45.5	100.0	78.0
123*	PP2	YL-2	98.5	15.0	113.0	40.0	101.0	80.0
124	PP2	YL-2	86.0	18.0	114.0	43.0	93.0	78.0
125	PP3	YL-2	94.0	12.0	109.0	43.0	94.0	83.0
126	PP3	YL-20	31.0	112.0	75.0	98.0	----	----
127	PP3	YL-10	25.0	89.5	52.0	95.5	77.0	108.0
128	PP2	YL-10	29.0	99.5	55.0	114.5	76.0	103.5
129	PP1	YL-10	25.0	125.0	50.0	105	78.0	92.5
130	PP3	YL-10	18.0	121.0	47.0	109.5	75.0	90.0
131	PP1	YL-10	22.0	121.5	46.0	105.5	75.0	82.0
132	PP2	YL-10	20.0	115.5	43.5	105.5	75.0	91.0
133	PET1	PA-7	23.0	110.0	68.0	93.0	----	----
134+	PET1	PA-7	21.0	120.0	42.0	105.0	75.0	85.0

* Elements in cross-machine direction removed under gages.
+ Gage at location "a" - "b" rotated 7° clockwise from machine direction.

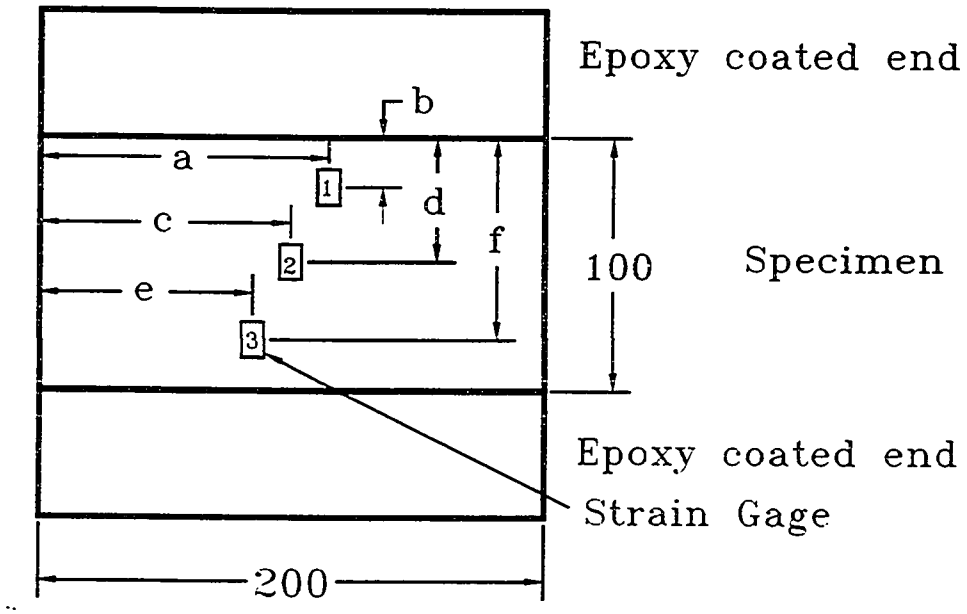

Figure 6.36: Strain gage locations (all dimensions in mm).

before placing and compacting soil over the reinforcing. Prior to application of initial vertical consolidation pressure the strain gage outputs were zeroed. The same test procedure used for all other UCD tests was used for loading the specimens in the strain gage tests. Unlike previous discussions, where similarities existed between multiple tests, there was substantial variation in the strain gage data. Because of the limited number of tests performed and the variability between them, these tests will be referred to by test number when a specific situation is described or when referred to in a figure label (see Figure 6.36).

The pattern of strain reported by the strain gages, including creep strain after discontinuing loading, closely followed the pattern for overall lateral strain, Figures 6.37a. However, in all of the strain gage tests the gages recorded less than the overall specimen strain, ε_3, Figures 6.37 to 6.40 and Appendix C. For Reinforcings PP1, PP2, and PP3 the ratio of strain recorded using strain gages to overall strain typically fell between 30% and 100%, with the ratio increasing as overall strain increased. For Reinforcing PET1 this ratio was between 30% and 70% (Figure 6.40). This underreporting of strain by strain gages attached to geosynthetics had also been reported by Farrag, et al. (1994). In their study strain gages attached to the ribs of high density polyethylene geogrids underreported global strain by 20% to 35%.

Investigation of the strain gage behavior using the normalized incremental strain ratio (NISR), as defined by Eq. 5.1, found the strain gage behavior to be less erratic in UCD tests than in the in-isolation tests. This is likely due to zeroing of the gage reading after confining the geotextile in soil, pretensioning of the reinforcing, and elimination of specimen flexibility by confining it in soil. As with the in-isolation tests, the NISR tended to increase with increasing overall specimen strain, Figures 6.37 to 6.40, and Appendix C. The NISR values for the three different length YL gages were generally greater than 0.6, and some values were greater than 1.0.

This underrecording by strain gages of overall specimen strain and NISR values less than 1.0 was also observed in the in-isolation tests performed with gages, Section

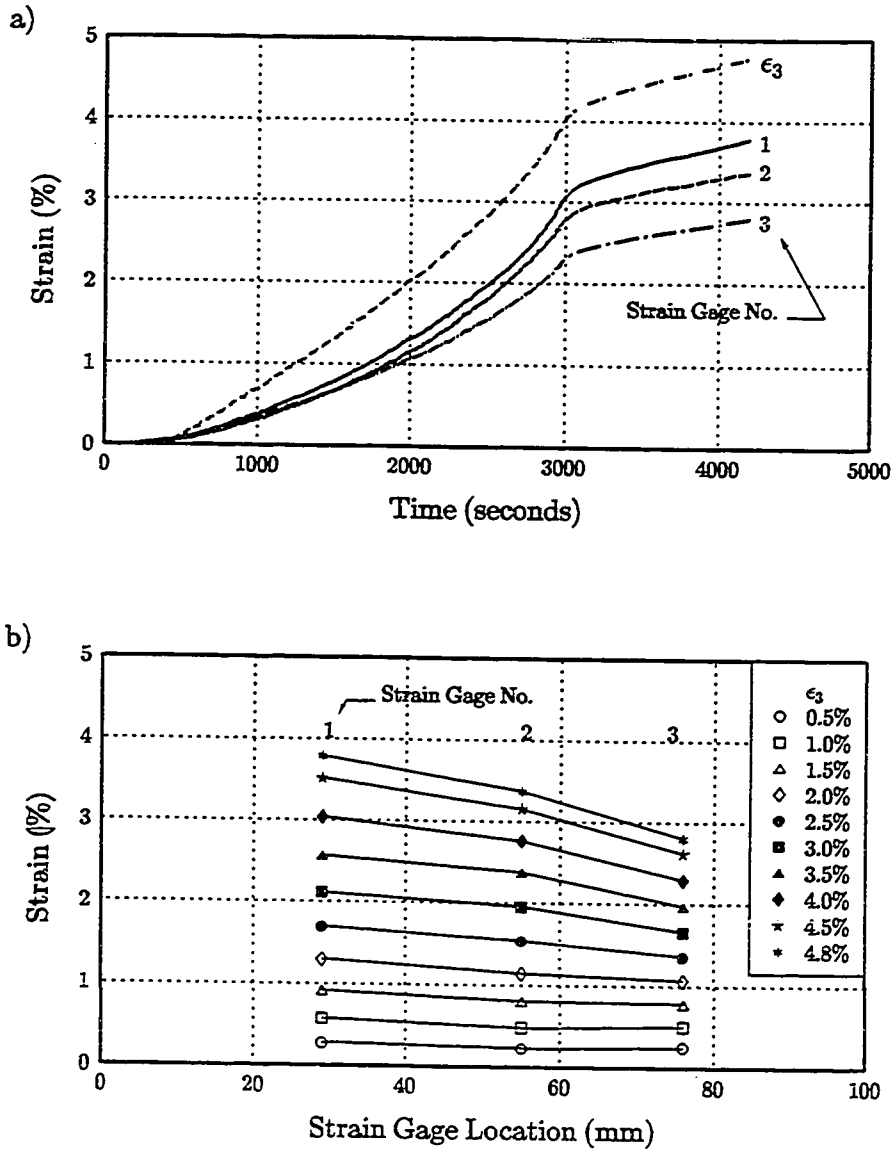

Figure 6.37: a) Overall lateral strain (ε_3) and gage strain vs. time, b) gage strain distribution along specimen, Gage YL-10, Reinforcing PP2, Test 128.

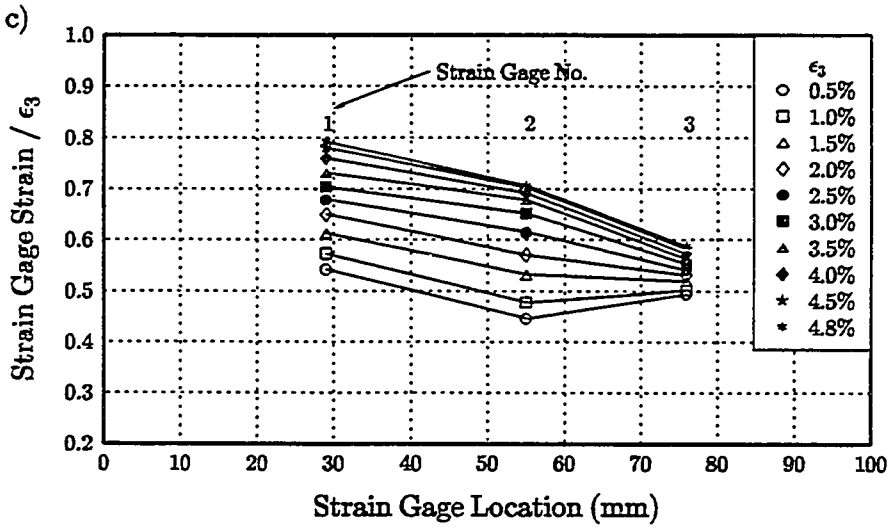

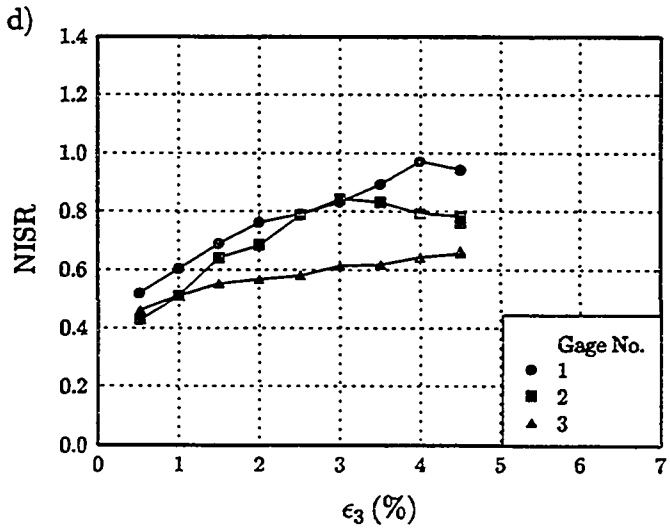

Figure 6.37, cont: c) normalized gage strain along specimen, and d) NISR vs. overall lateral strain; Gage YL-10, Reinforcing PP2, Test 128.

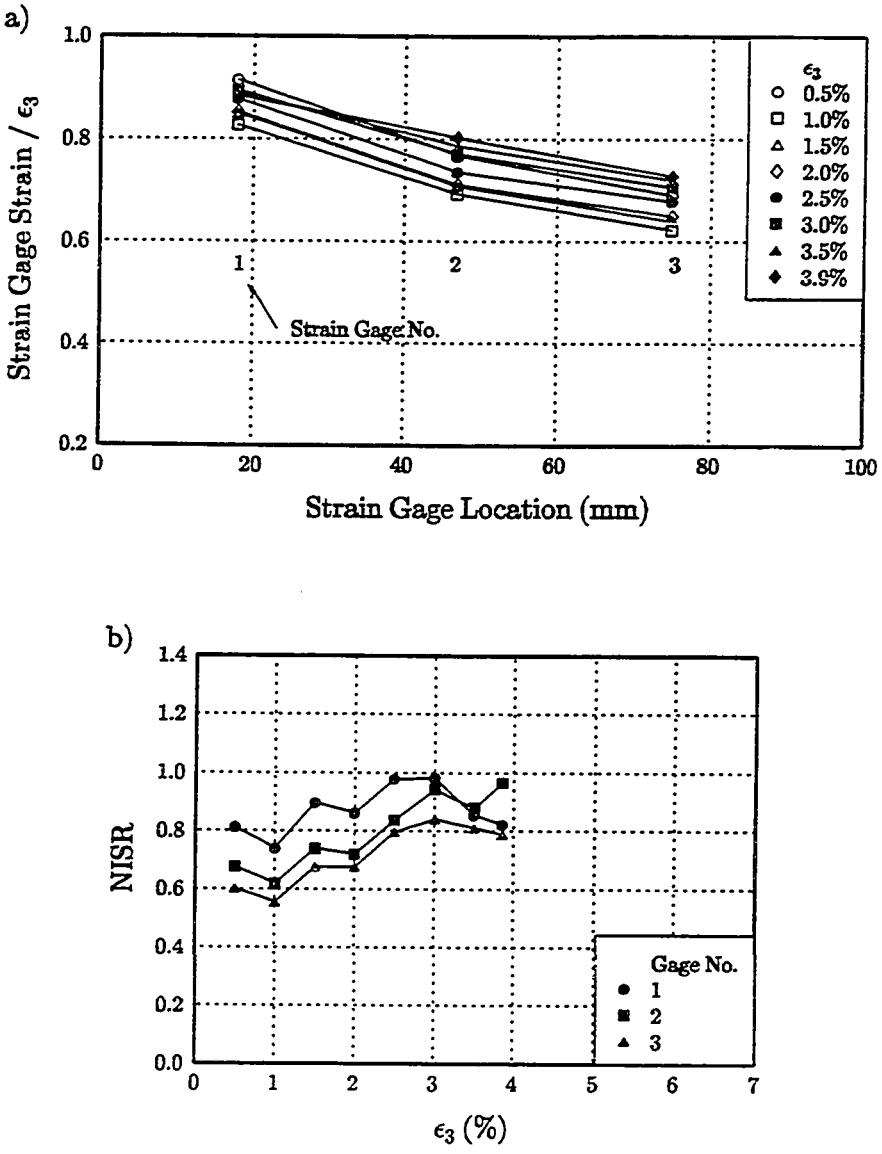

Figure 6.38: a) normalized gage strain along specimen, and b) NISR vs. overall lateral strain; Gage YL-10, Reinforcing PP3, Test 130.

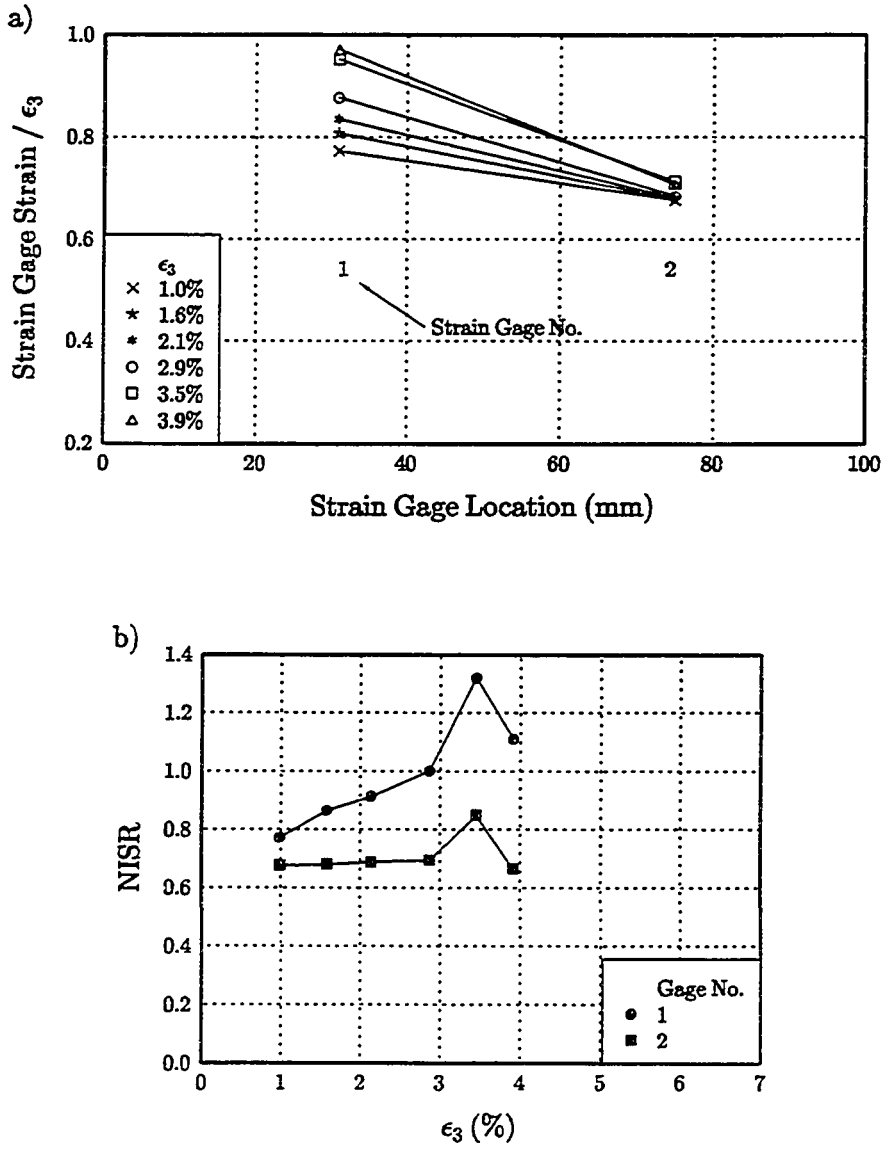

Figure 6.39: a) normalized gage strain along specimen, and b) NISR vs. overall lateral strain; Gage YL-20, Reinforcing PP3, Test 126.

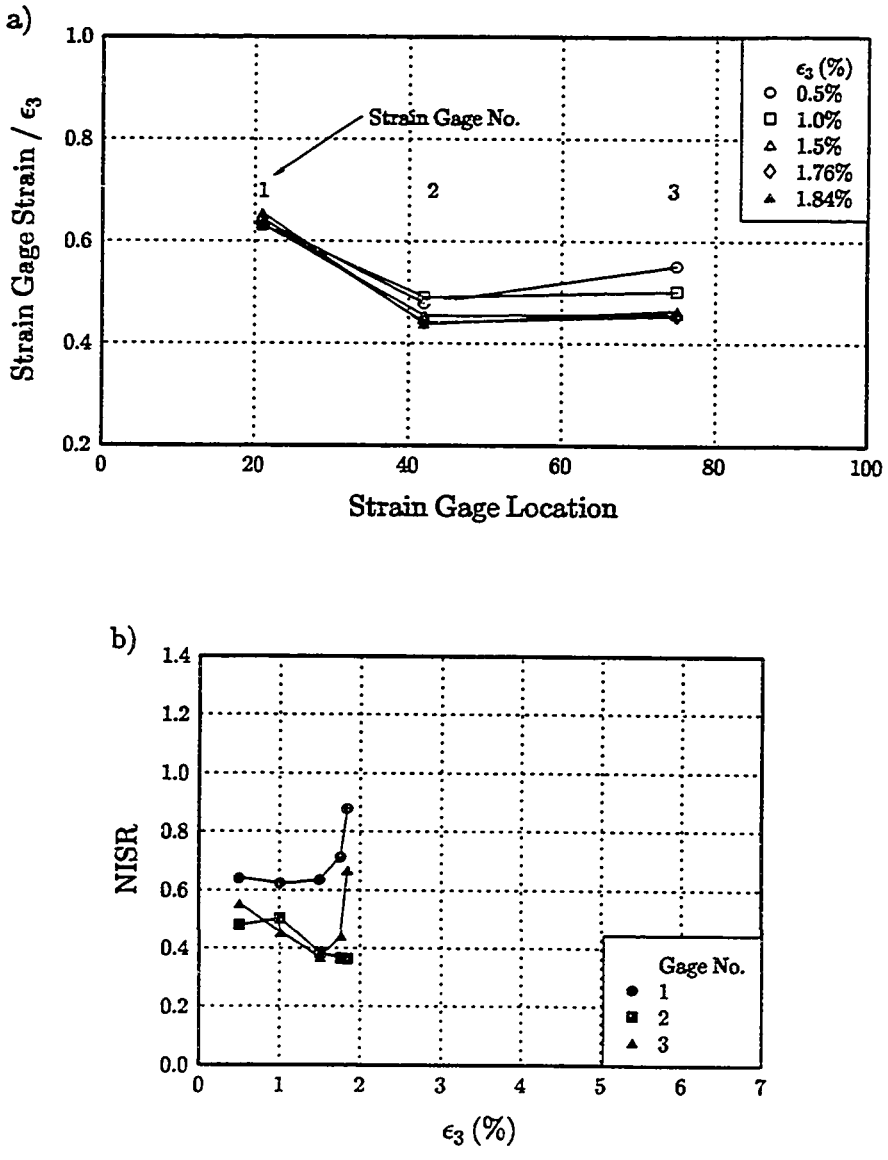

Figure 6.40: a) normalized gage strain along specimen, and b) NISR vs. overall lateral strain; Gage PA-3, Reinforcing PET1, Test 134.

5.7. A number of factors may contribute to the strain gages recording strains less than the overall strain:

a) Overall strain includes global rearrangement of the fibers and tightening of the weave. Since the reinforcing was slightly pre-tensioned during specimen construction, removal of wrinkles, a concern when instrumenting full scale walls, is not thought to be a factor in these tests.

b) Since there is soil both above and below the reinforcing, it is possible (even likely) that the reinforcing initially has a slight arch to it. During straining this arch may be increased, removed, or reversed, depending upon specimen behavior. Any change in the reinforcement orientation would influence the gage reading.

c) Strain gages are intended for application to smooth, flat surfaces. Because of the weave in the geotextiles the gages were not flat but had rises and depressions in them depending on whether the weave was going over or between the fibers (elements) oriented perpendicular to the gages. The height of these bumps could be expected to change throughout the test as the reinforcing is strained and the weave tightened. This could affect the gage response by changing the degree of flatness of the gage, which would register as a change in resistance. Tests conducted with the cross weave fibers removed reported even lower ratios of gage strain to overall strain because the fibers parallel to the direction of strain were initially loose and had no cross weave fibers with which to tighten up on.

d) The strain gages were not attached to a single geosynthetic fiber oriented in the direction of straining. For both types of geotextiles the gages were attached to three parallel fibers or filament bundles. Additionally, the cross fibers oriented perpendicular to the direction of strain, and over which the gages passed, probably do not behave in the same manner as the fibers oriented in the direction of strain. These factors could affect gage behavior. Accuracy of the gages may be related to the number of weaves the gages extended over, the more the better. This is

suspected to be a significant contributor to the low ratio of strain gage strain to overall strain and low NISR values recorded by the PA-7 gages used on Reinforcing PET1, Figure 6.40. While the overall length of the PA-7 strain gage backing was near 30 mm the gage itself was only 7 mm. Compatible PA gages with longer backing could not be used due to the specimen length.

Similar patterns of underrecording were observed when YL-2 strain gages were attached to Reinforcements PP1, PP2 and PP3 (see Appendix C). These gages had overall lengths of 7.6 mm but the actual gage was only 2.5 mm long. The YL-10 (12.5 mm gage length, 20.5 mm backing length) and the YL-20 (20.5 mm gage length, 30.5 mm backing length) recorded strains more closely representative of the overall strain than did the YL-2 and PA-7 gages. The ratio of gage strain to overall lateral strain for the YL-2, YL-10, and YL-20 gages fell in the ranges 0.30 to 0.70, 0.45 to 0.90, and 0.65 to 1.0, respectively. It would appear that longer gages provide more accurate correlation with overall strains. The results for the YL-20 gages compare well with the in-isolation wide width tests with these gages. Those tests reported strains 50% to 100% of overall strain, Section 5.7.

The NISR values for the YL gages were typically greater than 0.6 and typically increased with increasing overall specimen strain. With the limited data available, concluding that the longer YL gages performed better than the shorter ones in obtaining NISR values closer to 1.0 would be premature.

e) Large strains of the gages, when attached to a material of unknown, or possibly variable, Poisson ratio may result in a change in the gage factor (i.e. resistance) of the strain gages, resulting in different readings than would otherwise be expected. This possibility is supported by the results reported by Farrag, et al. (1994) where strain gages were attached to the smooth flat surface of a geogrid rib. It might be possible to calibrate the gage for this effect, although attachment of the gage to

three individual parallel elements, as was the case in these tests, may complicate calibration.

The findings of the in-isolation wide width tests with strain gages attached to the reinforcing (Section 5.7) were similar to the UCD findings: the proportion of total strain reported by the strain gages increased with increasing total strain. Gages attached to Reinforcings PP1, PP2, and PP3 tended to underpredict overall specimen strain on the order of 20%. The PA-3 strain gages used for the in-isolation tests on Reinforcing PET1 were longer than the PA-7 gages used for the UCD tests. The PA-3 gages reported strains very near the global strain (Figure 5.18) - a much more favorable result than obtained with the PA-7 gages in the UCD.

Because of the limited number of tests and numerous complicating factors associated with interpretation of the UCD results, only general conclusions may be stated: (1) longer gages, which cross more weaves, more closely predict the overall strain, (2) YL-20 and YL-10 gages attached to Reinforcements PP1, PP2 and PP3 can be expected to report strains of 45% to 100% of the overall strain and 60% to 100% of incremental strains, (3) PA-3 gages attached to Reinforcement PET1 report near 100% of overall strain, and (4) PA-7 gages are probably too short to permit reliable conversion of strain gage data to overall reinforcement strain.

Despite the limitations of using the strain gages to accurately measure overall specimen strain, they are probably relatively accurate predictors of strain distribution along the geotextile in UCD tests. A single pattern of strain distribution was not observed for the tests, Figures 6.37 to 6.40 and Appendix C. Some of the tests indicated a fairly uniform strain along the specimen while others indicated higher or lower strains at one end or in the middle of the specimen. In no case did the strain gages indicate uniform strain along the specimen as would be required for a true "unit cell" condition to exist. The strain distribution was, however, much more uniform than it would have been if the UCD had been designed similar to the McGown, et al. (1978) and Ling (1992)

devices (see Section 2.1.8). For those devices the reinforcing strain would have followed the pattern shown in Figure 2.18c. Clamping the reinforcing at both ends of the specimen and permitting movement of only one vertical face appears to have served its intended purpose; to increase uniformity of strain and to ensure the peak reinforcing load occurred at one end.

6.4.3.3 Visual Observation

To facilitate visual observation of soil behavior a clear plexiglass plate was installed in the front face of the UCD for the strain gage tests conducted with Reinforcings PP1, PP2 and PP3. No photographs were taken of specimens constructed with Soil R and Reinforcing PET1 because the maximum strains were anticipated to be very small and reliable interpretation of the photographs would be questionable. Millimeter scales were attached directly to the clear face place on the right and bottom edges. Slide photographs were taken during loading of the composite: at the end of consolidation, at initiation of lateral displacement, and at approximately 0.5% lateral strain increments. To facilitate tracking and identification of soil grains, the soil placed next to the clear plate was dyed purple and orange and particles smaller than the No. 20 US sieve (0.85 mm) were removed. The 0.3 mm latex membrane normally used to line the UCD was replaced by a 0.1 mm transparent polyethylene membrane inside the plexiglass plate. Installation of the plexiglass plate necessitated removal of the two load cells which measured intermediate stresses on the front side of the UCD (see Figures 6.1 and 6.3). The two load cells on the back side of the UCD, which also measured intermediate stresses, were not affected. Because fines migrated to the face through the coarser dyed grains during compaction and inhibited the ability to distinguish individual grains, only photographs taken during Tests 128 through 131 (see Figure 6.36) produced usable images. Because of damage to the polyethylene liner, the silicone grease, and the slight blurring of the image through the polyethylene, movement for only a small percentage of the sand grains could be measured reliably.

To evaluate particle movements occurring in these tests, the slide images were projected onto a white sheet of paper such that the image was enlarged by a factor of five. Particle locations at the end of consolidation and at the end of the tests were compared to produce particle movement plots, Figures 6.41 to 6.44. Particles near the left face, the moving face in the UCD, experienced the greatest horizontal displacement in all the tests photographed. Horizontal displacement appears to have been uniformly distributed from a maximum at the left to no displacement at the right. Vertical displacement was not identical above and below the reinforcing in the tests, as was hoped for and as was intended by use of independently controlled top and bottom pressure bladders and compensation for soil weight during load application. The soil above the reinforcing and (by inference since it was not visible) the reinforcing, moved upward slightly during tests 128, 130 and 131, Figures 6.41, 6.43 and 6.44, respectively. This vertical movement of the reinforcing may be a contributing factor in the difference between strain gage readings and global strain readings. However, the strain gages still under predicted overall strain despite the fact that upward arching of the reinforcing should, theoretically, increase the gage length and the strain gage readings should be closer to the overall lateral strain than would otherwise be reported.

No distinct failure plane was observed in any of the tests photographed. While not noticeable in these photos, a failure plane was very well defined in one UCD test (which was video taped but not photographed) constructed with Soil O and Reinforcing PP3, and which experienced 7% lateral strain. Once a failure plane develops the assumptions of the unit cell, i.e. uniform stress and strain conditions throughout, are no longer valid. Thus, the most reliable data are those recorded at low strains, say less than 3%. Fortunately, this is well within the limit of interest for reinforced soil in GRS wall applications and was the region where most of the test data for the high strength reinforcements were recorded.

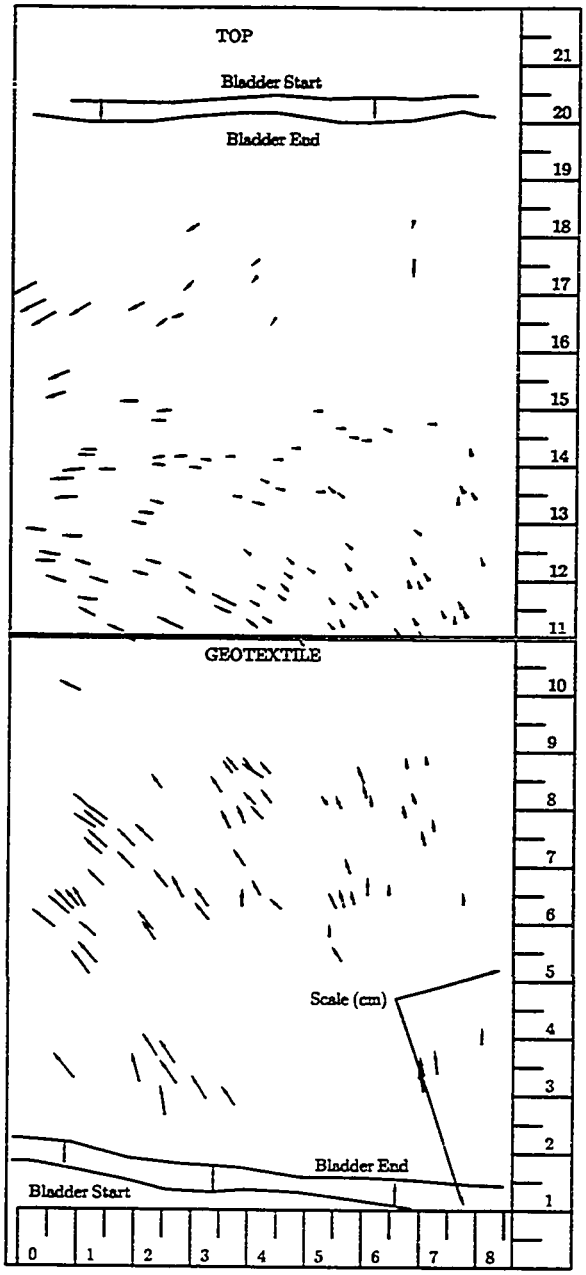

Figure 6.41: Soil particle movement, Test 128.

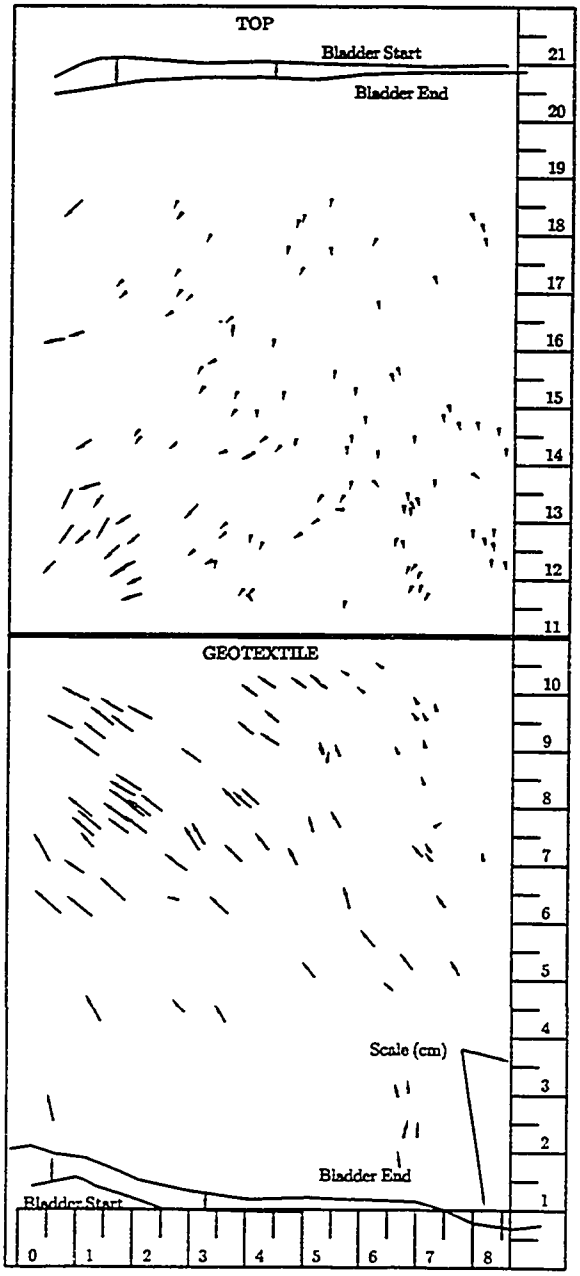

Figure 6.42: Soil particle movement, Test 129.

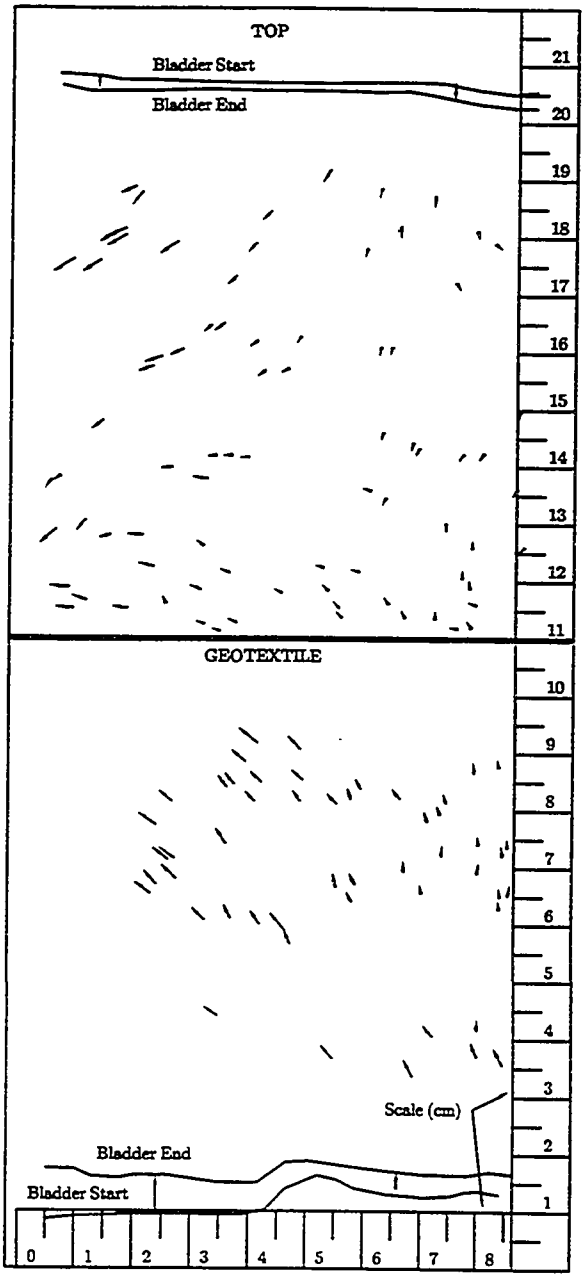

Figure 6.43: Soil particle movement, Test 130.

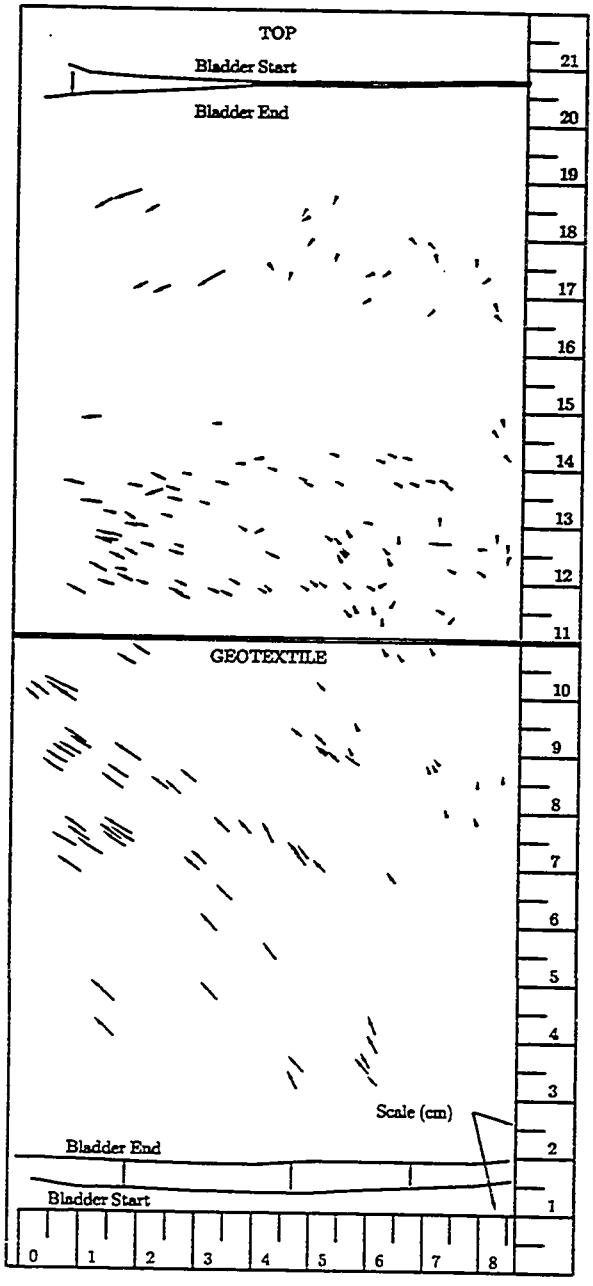

Figure 6.44: Soil particle movement, Test 131.

Although dying the soil, removing the fines, and using a transparent polyethylene membrane helped to produce photographs which could be used for soil particle movement tracking the method could use improvements:

a) During placement and compaction of the soil, fines often worked their way to the face and individual grains could not be distinguished in the photographs. Removal of all smaller particles from the entire soil specimen would prevent this, but might also modify the soil response.

b) The polyethylene liner, underlain by silicone grease, resulted in a blurry image, preventing certain identification of smaller particles.

c) The polyethylene liner often was torn or wrinkled during compaction of the soil. A thicker polyethylene, less susceptible to damage, should possibly have been used. Use of a thicker liner, however, may decrease the ability to distinguish individual soil particles.

d) The small (0 to 5 mm) displacements through which the soil particles moved caused some difficulty in identifying the actual displacement when the image was projected onto a screen.

In spite of these difficulties the use of a clear panel in the UCD permitted tracking of the soil particles and a general understanding of the deformation pattern experienced by the soil. The soil just above the reinforcing, and thus the reinforcing itself, moved upward in three of the four tests photographed. Thus, the geotextile did not remain in a plane, but instead arched upward. This pattern of deformation may increase the tension in the reinforcing above that which would occur, for a given lateral strain, if the reinforcing remained horizontal. Although this increase may be minimal it is unclear what effects it has on the measurement of reinforcement and composite response. No reason for the under reporting of overall strain by the strain gages associated with soil movement was found.

6.4.3.4 Hypothesis for Composite Behavior

For a true "unit cell" composite element the stress and strain state should be uniform throughout. However, as shown in Figures 6.26 to 6.32, it was rarely the case that the reinforcing supported the same load on each end of the specimen, with the difference increasing with lateral strain. Further evidence of non-uniformity in UCD specimens was verified by measuring the distribution of reinforcement strains, Figures 6.37 to 6.40, and the displacements experienced by the soil during testing, Figures 6.41 to 6.44. Since the unit cell device did not produce a true unit cell element, care must be applied when interpreting the results. Soil mobility, soil-geotextile friction and boundary effects of the UCD may contribute to producing this non-uniform behavior. To what degree these factors influence the measured response is not known. However, a simplified analysis which utilizes the effective confining pressure concept and assumed soil and reinforcing properties may be performed as a check as to how each parameter (shape of the soil stress-strain curve, modulus of the reinforcement, and lateral confining pressure, σ_{3C}) could be expected to influence an ideal unit element which did not suffer from non-uniform mobility and boundary effects.

To study the expected composite response for various possible soil behaviors and reinforcement strengths the increased confining pressure concept (see Section 6.4.1.3) was applied using four different hypothetical soil stress-ratio versus lateral strain curves, four different hypothetical extensible reinforcements, and one inextensible reinforcement, Figure 6.45. The hypothetical soil curves are composite formulations of the measured and computed response for the soils used in this project. Soil OH approximates the effective stress-ratio versus lateral strain for Soil O. Soils RHA and RHB are intended to simulate the response of Soil R reinforced with lower modulus geotextiles at low (less than 25 kPa) and higher (greater than 25 kPa) initial confining pressures, respectively. Soil RHC is based on Soil R with Reinforcement PET1. All of the soils were assumed to reach a condition of constant effective stress ratio at 6% strain. The actual strain associated with this condition is not known and the 6% strain was chosen for

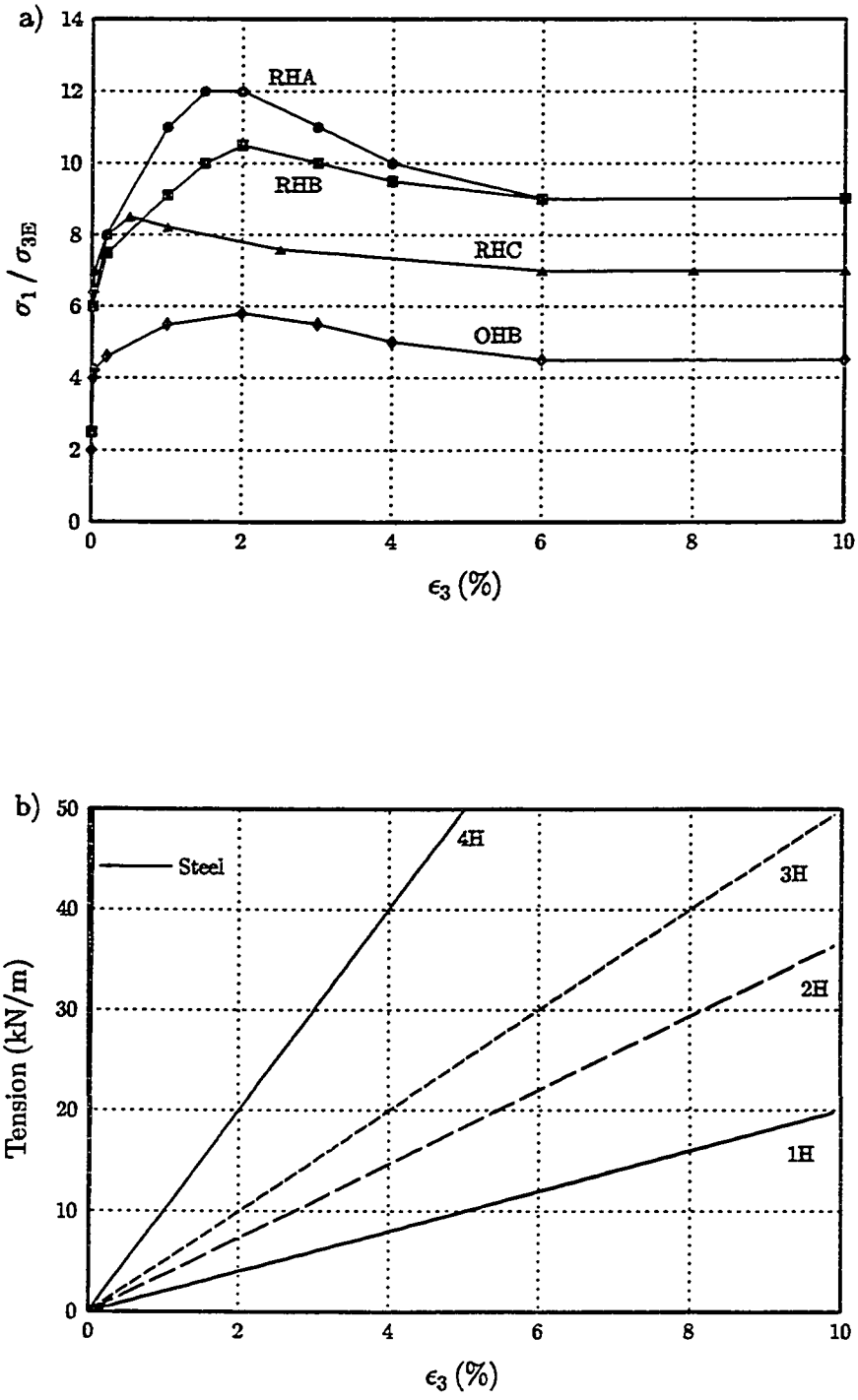

Figure 6.45: Hypothetical materials: a) soil effective stress ratio vs. lateral strain, and b) geotextile tension vs. lateral strain.

convenience. Reinforcements 1H through 4H are linearized approximations of Reinforcements PP1, PP2, PP3 and PET1, respectively, as measured in the UCD. The hypothetical steel reinforcement was selected to approximate the equivalent modulus per unit width of wall for 5 mm by 100 mm steel straps (E_{steel} = 200,000,000 kN/m^2) at a horizontal spacing 750 mm, and then rounding to a convenient value. An equivalent modulus of 100,000 kN/m was selected for the steel, and was computed via the following formula (Christopher, et al., 1990):

$$E_m = \frac{E_r \cdot A}{S_h} \tag{6.3}$$

where:

E_m = equivalent modulus (kN/m),

E_r = reinforcing modulus (kN/m^2),

A = cross sectional area of element (m^2),

S_h = horizontal spacing of elements (m).

Application of the formula for effective lateral confining pressure, Eq. 6.2, using these hypothetical soils and reinforcements (Figure 6.45) at confining pressures of 12.5, 50, 100 and 200 kPa at assumed reinforcement spacings of 200 mm (750 mm for the steel) results in hypothetical composite response curves similar to those obtained from UCD tests, Figures 6.46 to 6.50. Compare these composite stress-strain figures with those from UCD tests presented in Figures 6.8 to 6.12. The effect of changing the vertical spacing of the reinforcing is not presented in this analysis since this effect could be determined by simply changing the assumed reinforcing modulus in proportion to the assumed change in spacing, Eq. 6.2 (see also Christopher, et al. 1990). A benefit of evaluating reinforced soil using the hypothetical material approach and the effective confining pressure concept is the elimination of material variability, specimen construction, UCD operation effects, and boundary conditions, from the computed

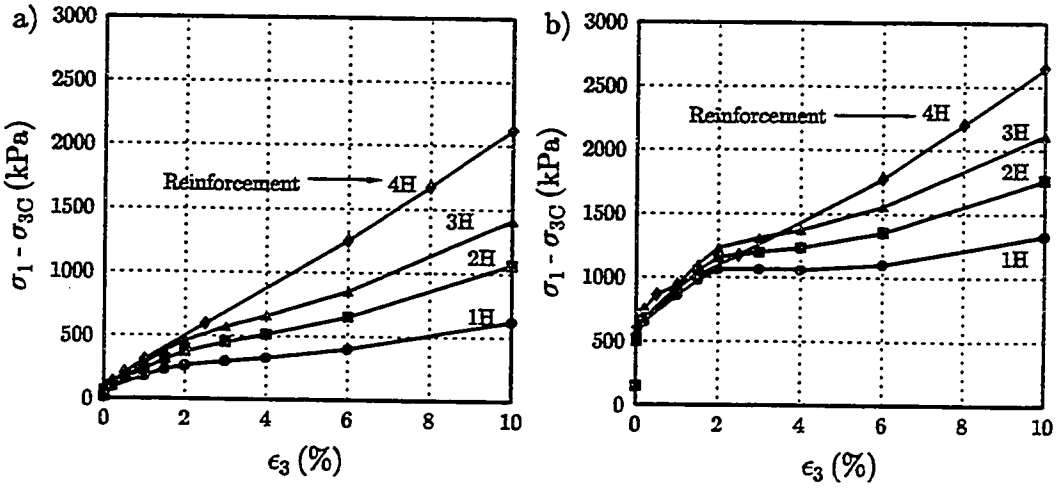

Figure 6.46: Composite principal stress difference vs. lateral strain: a) Soil RHA with Reinforcements 1H, 2H and 3H, and Soil RHC with Reinforcement 4H, σ_{3C} = 12.5 kPa, and b) Soil RHB with Reinforcements 1H, 2H, and 3H, and Soil RHC with Reinforcement 4H, σ_{3C} = 100 kPa.

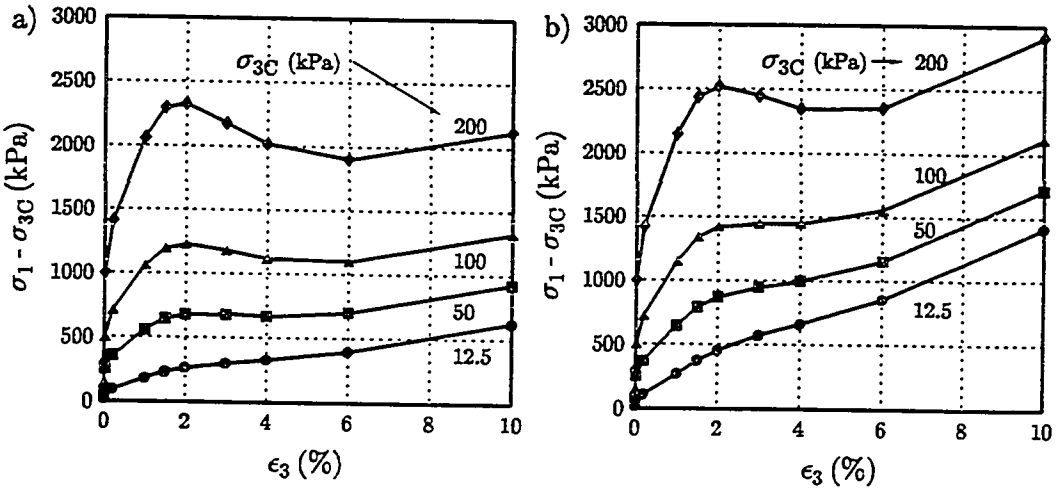

Figure 6.47: Composite principal stress difference vs. lateral strain at various confining pressures, Soil RHA: a) Reinforcement 1H, and b) Reinforcement 3H.

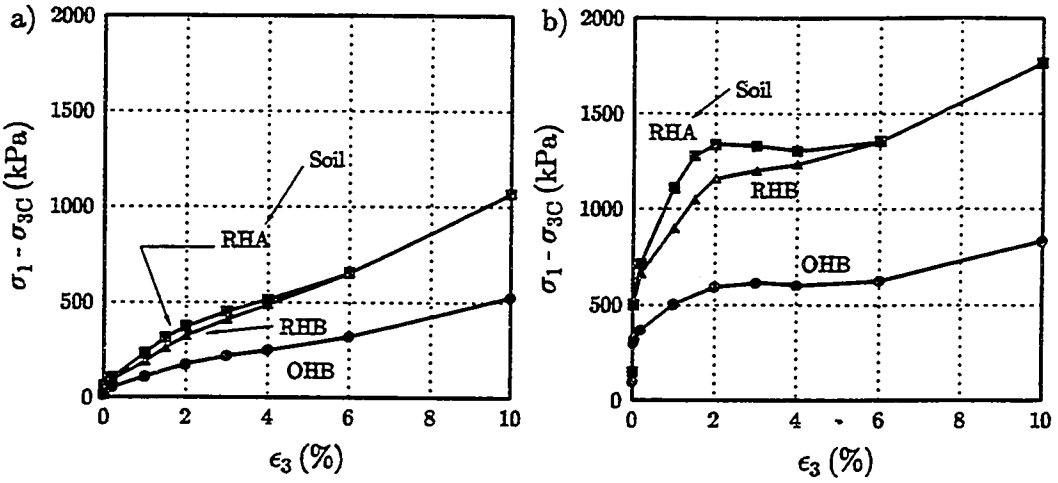

Figure 6.48: Composite principal stress difference vs. lateral strain for various soils, Reinforcement 2H: a) σ_{3C} = 12.5 kPa, and b) σ_{3C} = 100 kPa.

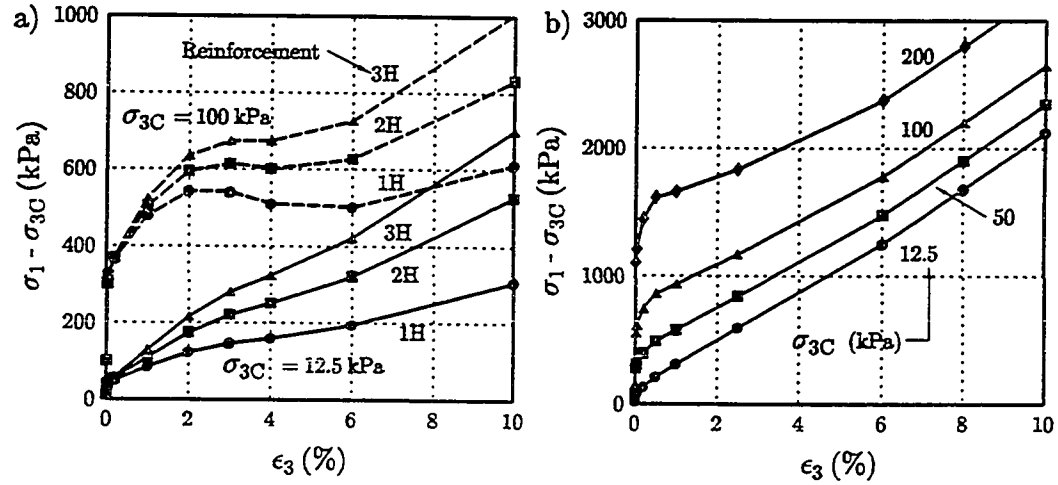

Figure 6.49: Composite principal stress difference vs. lateral strain: a) Soil 1HB, Reinforcements 1H, 2H, and 3H, at σ_{3C} = 12.5 kPa and σ_{3C} = 100 kPa, and b) Soil RHC, Reinforcement 4H at various confining pressures.

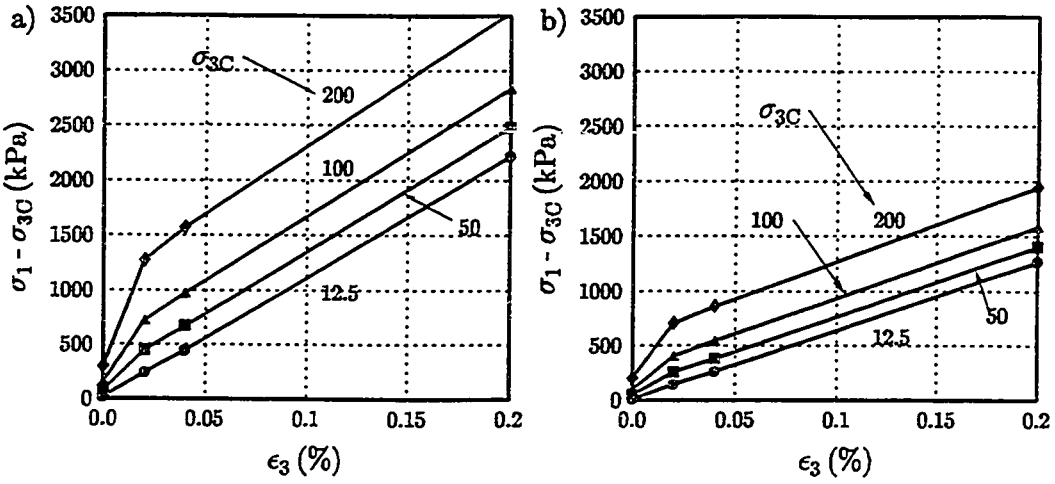

Figure 6.50: Composite principal stress difference vs. lateral strain, hypothetical steel reinforcement (100,000 kN/m): a) Soil RHC, and b) Soil OHB.

response. Additionally, post peak behavior, which could not be obtained using the UCD, may be predicted with this hypothetical formulation. A review of the "composite" response produced using this method illustrates a number of properties of reinforced-cohesionless soil behavior:

a) The composite response is affected by: soil stress-strain behavior, reinforcement modulus and density (vertical spacing), and confining pressure acting on the composite.

b) Figures 6.46 to 6.49 confirm the observation made from UCD tests, and the intuitive conclusion, that, all other factors being equal, the vertical load supported by the composite increases with increasing reinforcing modulus, with increasing confining pressure, and with increasing soil stress-ratio.

c) The shape of the soil stress-strain curve greatly influences the shape of the composite stress-strain curve. The greater the maximum effective stress ratio attained by the soil during straining, the greater the load supported by the reinforced soil composite for any given lateral strain prior to reaching the strain that corresponds to the maximum effective stress ratio of the soil, Figure 6.48.

d) Soil behavior is the controlling factor in defining the composite response at very low strains (less than 0.23%, the yield strain of steel) for both extensible and inextensible reinforced soils. [Reinforcements which yield at strains less than the strain at which the soil develops its peak strength would be classified as inextensible (McGown, et al., 1978; see Section 3.2)] At these strains extensible reinforcements have not developed enough force to significantly affect the composite response. As the strains increase and the soil stress ratio versus strain curve flattens, the influence of different reinforcements is more noticeable, Figures 6.45, 6.46 and 6.49a.

e) When steel reinforcement is used, at the pre-yield strain of 0.2%, increasing the confining pressure applied to the composite from 12.5 kPa to 100 kPa results in only a 50% increase in the capacity of the composite, Figure 6.50. This relatively small increase in composite capacity for an eight fold increase in confining pressure can be attributed to: (1) much of the initial capacity of the composite is due to the steep soil stress-strain curve in the first 0.02% lateral strain, and (2) for inextensible reinforcements, e.g., steel straps, the increase in effective confining pressure due to reinforcement strain is large relative to the confining pressure applied to the composite (see Eq. 6.2).

f) At low strains, say 1%, when extensible reinforcements are used, the load supporting capacity of the reinforced soil composite is more greatly affected by lateral confining pressure acting on the composite than by reinforcing tension. Consider a composite constructed of Soil RHA and Reinforcing 1H, Figure 6.47.

At 1% lateral strain, increasing the confining pressure applied to the composite from 12.5 kPa to 100 kPa increases the load supported by the composite by 580%. As an alternative to increasing the confining pressure acting on the composite, σ_{3C}, consider replacing Reinforcement 1H with Reinforcement 3H. Although Reinforcement 3H has a modulus 250% greater than Reinforcement 1H, the capacity of the composite at 1% strain increases, above the case when Reinforcement 1H was used, by only 60% for σ_{3C} = 12.5 kPa and 8% for σ_{3C} = 100 kPa. At higher strains, where the contribution of reinforcement tension to the overall effective lateral confining pressure acting on the soil increases, the relative influence of the reinforcing increases (see Eq. 6.2 and Figure 6.45).

These observations are in agreement with the Unit Cell test results presented in Section 6.4.1. Removal of test and soil variability permits simpler quantification of the effects of changes in soil or geosynthetic properties or confining pressure. The UCD test results and those developed using the hypothetical soils and reinforcements are similar. This similarity suggests that the non-uniform stress state in the unit cell specimens does not adversely influence the measured UCD behavior to any significant extent, nor does it invalidate the conclusions reached in Section 6.4.1. It may be concluded that the observed UCD response is the response which should be expected. These similarities also suggest that where the composite capacity decreases after reaching a maximum, some degree of confidence may be placed in the post peak behavior predicted using the hypothetical materials:

a) Post peak behavior of the composite depends on the slope of the soil curve after passing the soil peak stress ratio, the ultimate post peak magnitude of effective stress ratio, the confining pressure acting on the composite, and the modulus of the reinforcing.

b) The increase in effective confining pressure acting on the soil with increasing reinforcing strain may be sufficient to offset any decrease in soil strength, thus preventing the composite from displaying a "peak" strength. This is the case for higher modulus reinforcements for both the hypothetical materials assumed here (Figure 6.49b) and the UCD tests (Figure 6.19b). It is also the case for the other reinforcements at lower confining pressures, Figures 6.47, 6.48a, and 6.49a. Increases in σ_{3C} may change the behavior of the composite from one of increasing strength with lateral strain to one which exhibits a decrease in strength after the soil stress ratio has peaked. This change in response is illustrated in Figures 6.47, 6.48, and 6.49a.

c) If the reinforcing has a breaking strain sufficiently larger than the strain at which the soil achieves a constant stress ratio it is possible that a composite which exhibits a peak behavior may reach a strain at which it will again increase in capacity, Figures 6.47 and 6.49a. At lower composite confining pressures, where the confining pressure due to reinforcement strain represents a significant portion of the total effective confining pressure acting on the soil, the composite is more likely to reach a condition where the final load supported exceeds the load supported when the soil stress ratio was at its peak, Figure 6.46a. This ductile response is more desirable in most civil engineering works than the catastrophic type failure normally associated with unreinforced dense sands.

d) After the soil reaches a condition in which it displays a constant stress-ratio with increasing strain ($\varepsilon_3 > 6\%$ for the hypothetical soils assumed here), for a particular soil-reinforcement combination, the tangent modulus of the composite is identical for all confining pressures, σ_{3C}. That is, the composite stress-strain curves become parallel to each other, Figures 6.47 and 6.49.

The above discussion provides some insight into the large strain behavior of geosynthetic reinforced soils. At low confining pressures the composite can be expected to increase in capacity until rupture of the reinforcement occurs. At higher confining pressures, relative to the increase in confinement provided by each increment of reinforcing strain, the composite tangent modulus may decrease dramatically or a peak may be exhibited in the composite stress strain curve. Even if a peak does occur, high rupture strains of geosynthetic reinforcements may be sufficient to regain some or all of the capacity lost prior to ultimate failure of the reinforcing. Thus when high elongation geosynthetic reinforcements are used, large deformations, providing visible evidence of reinforced soil wall distress, could occur before collapse.

This study also has implications for prediction of reinforced soil wall deformations:

a) If steel reinforcements are used, the behavior of the soil past the yield strain of the steel need not be considered. Elaborate modeling of the soil or reinforced soil behavior is not necessary. Errors would probably not be overly significant, given the other variables which may affect reinforced soil wall deformation (see Chapter 3) and the substantial increase in effective confining pressure resulting from straining of steel reinforcements, if the soil were modeled with a single curve selected at an intermediate confining pressure to which the soil might be subjected in a reinforced soil wall. Although the soil model could be simply a secant modulus value or a hyperbolic model, a bilinear curve breaking near 0.02% lateral strain may be an adequate compromise, Figure 6.50.

b) The shape of the soil stress-strain curve and the magnitude of the peak stress-ratio can significantly affect the predicted composite response. While this is true for all reinforcements, the effect may be more significant for extensible reinforcements capable of experiencing large strains. For discussion purposes, assume that the curves for Soils OHB and RHB (Figure 6.45) represent triaxial and plane strain

responses of the same soil. The very different strains predicted for these soils in Figure 6.48 provides an example of how the use of triaxial test data in GRS wall prediction exercises could grossly over estimate lateral displacements. At a principal stress difference, $\sigma_1 - \sigma_{3C}$, of 600 kPa the triaxial soil data would predict lateral strains of 2%, but the plane strain soil data would predict a lateral strain of approximately 0.2%.

c) The confining stress acting on reinforced soil elements plays an important role in defining the behavior of the composite. GRS wall deformation prediction methods which fail to account for pressures resulting from tension in the reinforcing and interaction of the soil with adjacent elements will have difficulty producing accurate results.

d) The modulus of the reinforcement affects the composite response. For extensible reinforcements the effect of an increase in modulus increases with increasing strain. If strains are kept fairly small, say less than 0.5%, little benefit is gained by increasing the modulus of the reinforcing used or by decreasing the vertical spacing of the reinforcement.

6.4.3.5 Stiffness of Reinforced Soil Specimens

For evaluating the deformation of a structure it is necessary to know a material's response to various forms of loading. In conventional structural mechanics material behavior has traditionally been defined using relationships between principal strains and principal stresses, shear strain and shear stress, and volumetric strain and volumetric stress. If the material is isotropic and follows Hooke's Law, Young's modulus, E, Poisson's ratio, ν, shear modulus, G, and bulk modulus, B, may be used to define these relationships (Ugural and Fenster, 1995):

$$\varepsilon_3 = \frac{1}{E}\left(\sigma_3 - \nu\sigma_2 - \nu\sigma_1\right), \qquad \gamma_{32} = \frac{\tau_{32}}{G} \tag{6.4}$$

$$\varepsilon_2 = \frac{1}{E}\left(\nu\sigma_3 + \sigma_2 - \nu\sigma_1\right); \qquad \gamma_{21} = \frac{\tau_{21}}{G} \tag{6.5}$$

$$\varepsilon_1 = \frac{1}{E}\left(-\nu\sigma_3 - \nu\sigma_2 + \sigma_1\right); \qquad \gamma_{31} = \frac{\tau_{31}}{G} \tag{6.6}$$

$$G = \frac{E}{2(1+\nu)} \tag{6.7}$$

$$\varepsilon_v = \varepsilon_1 + \varepsilon_2 + \varepsilon_3 \tag{6.8}$$

$$B = \frac{-p}{\varepsilon_v} = \frac{-(\sigma_1 + \sigma_2 + \sigma_3)}{3 \cdot \varepsilon_v} \tag{6.9}$$

where:

ε_i = strain in the *i* direction when *i* = 1, 2, or 3,

ε_v = volumetric strain,

γ_{ij} = shear strain in the *i-j* plane,

τ_{ij} = shear stress in the *i-j* plane

σ_i = stress in the *i* direction,

p = volumetric stress;

Assuming plane strain conditions, $\varepsilon_2 = 0$, these terms may be redefined as (Atkinson, 1981):

$$\varepsilon_3 = \frac{1+\nu}{E}\left[(1-\nu)\sigma_3 - \nu\sigma_1\right] \tag{6.10}$$

$$\varepsilon_1 = \frac{1+\nu}{E}\left[-\nu\sigma_3 + (1-\nu)\sigma_1\right] \tag{6.11}$$

$$\gamma_{31} = \varepsilon_1 - \varepsilon_3 \tag{6.12}$$

$$\varepsilon_v = \varepsilon_1 + \varepsilon_3 \tag{6.13}$$

$$p_{ps} = \frac{1}{2}(\sigma_1 + \sigma_3) \tag{6.14}$$

$$\tau_{31} = q_{ps} = \frac{1}{2}(\sigma_1 - \sigma_3) \tag{6.15}$$

$$G = \frac{\tau_{31}}{\gamma_{31}} = \frac{(\sigma_1 - \sigma_3)}{2(\varepsilon_1 - \varepsilon_3)} \tag{6.16}$$

$$B = \frac{-p_{ps}}{\varepsilon_v} = \frac{-(\sigma_1 + \sigma_3)}{2(\varepsilon_1 + \varepsilon_3)} \tag{6.17}$$

Unfortunately, neither soil nor reinforced soil are isotropic and, therefore, do not follow these equations. Although similar formulations could be presented for transverse isotropic materials, which may better approximate the reinforced soil specimen, the "elastic" properties could still not be adequately defined because: (1) specimen loading was applied only in the vertical direction and it is not possible to determine all the material properties for a transverse isotropic material subject to plane strain deformation from a single loading condition (Bowles, 1988); and (2) the Poisson's ratio of soil varies during loading, and in fact, becomes greater than 0.5 once the soil has begun to dilate. It would still be useful, for discussion purposes and for use in numerical modeling, to define a stress-strain relationship for the plane strain tests given that neither the soil or the reinforced soil composite strictly adheres to Hooke's law. Therefore, in addition to using the equations for plane strain shear modulus, G (Eq. 6.16), and bulk modulus, B (Eq. 6.17), the following terms will be defined for relating vertical stress to vertical strain, vertical stress to lateral strain, and lateral strain to vertical strain, respectively:

$$E_{11} = \frac{\sigma_1 - \sigma_3}{\varepsilon_1} \tag{6.18}$$

$$E_{31} = \frac{\sigma_1 - \sigma_3}{\varepsilon_3} \tag{6.19}$$

$$\nu_{ps} = \frac{\varepsilon_3}{\varepsilon_1} \tag{6.20}$$

The values of G, B, E_{11}, E_{31}, and ν_{ps} may be determined graphically from test results as is illustrated in Figure 6.51. Values for G, E_{11}, and E_{31} obtained in this manner for the UCD tests are presented in Table 6.5. Tangent values have been reported to illustrate how these properties change with increasing strain. Because UCD specimens represent reinforced soil with layers spaced at 200 mm, the modulus values reported in the table for geosynthetic reinforced soil specimens should be larger than for actual conditions where spacings of 300 mm to 1 m would be typical. Poisson's ratio and Bulk modulus have not been tabulated because dilation of the soil makes determination of these coefficients difficult and violates the constitutive and energy conservation laws fundamental to Hooke's Law. Increases in volume result in improper values of Poisson's ratio and Bulk modulus [i.e.,$\nu_{ps} > 1.0$ ($\nu > 0.5$), $B > 0$].

Shear strain plots had the most consistent form, typically exhibiting a fairly steep initial modulus, G_i, until the shear strain reached 0.4% to 1%, then exhibiting a distinct break, after which the shear modulus was substantially lower. The break point corresponded to lateral strains near 0.02%. The shear modulus continued to decrease with decreasing strain, Figure 6.52. Values for the shear modulus computed for unreinforced and reinforced soil specimens tested in the UCD are tabulated in Table 6.5. Typical initial shear modulus values ranged from 1500 kN/m^2 to 30,000 kN/ m^2 for Soil O and from 5000 kN/m^2 to 46,000 kN/ m^2 for Soil R. The initial shear modulus was highly dependent on the lateral confining pressure. Shear modulus values after the break point (2nd tangent modulus, G_2) varied over a narrower range, from 500 kN/m^2 to 9300 kN/ m^2 for Soil O and from 3200 kN/m^2 to 15,000 kN/ m^2 for Soil R. After the break point the shear modulus seemed to be related to the modulus of the reinforcing. Composites constructed with higher modulus reinforcing, in general, had a higher shear modulus after the break point.

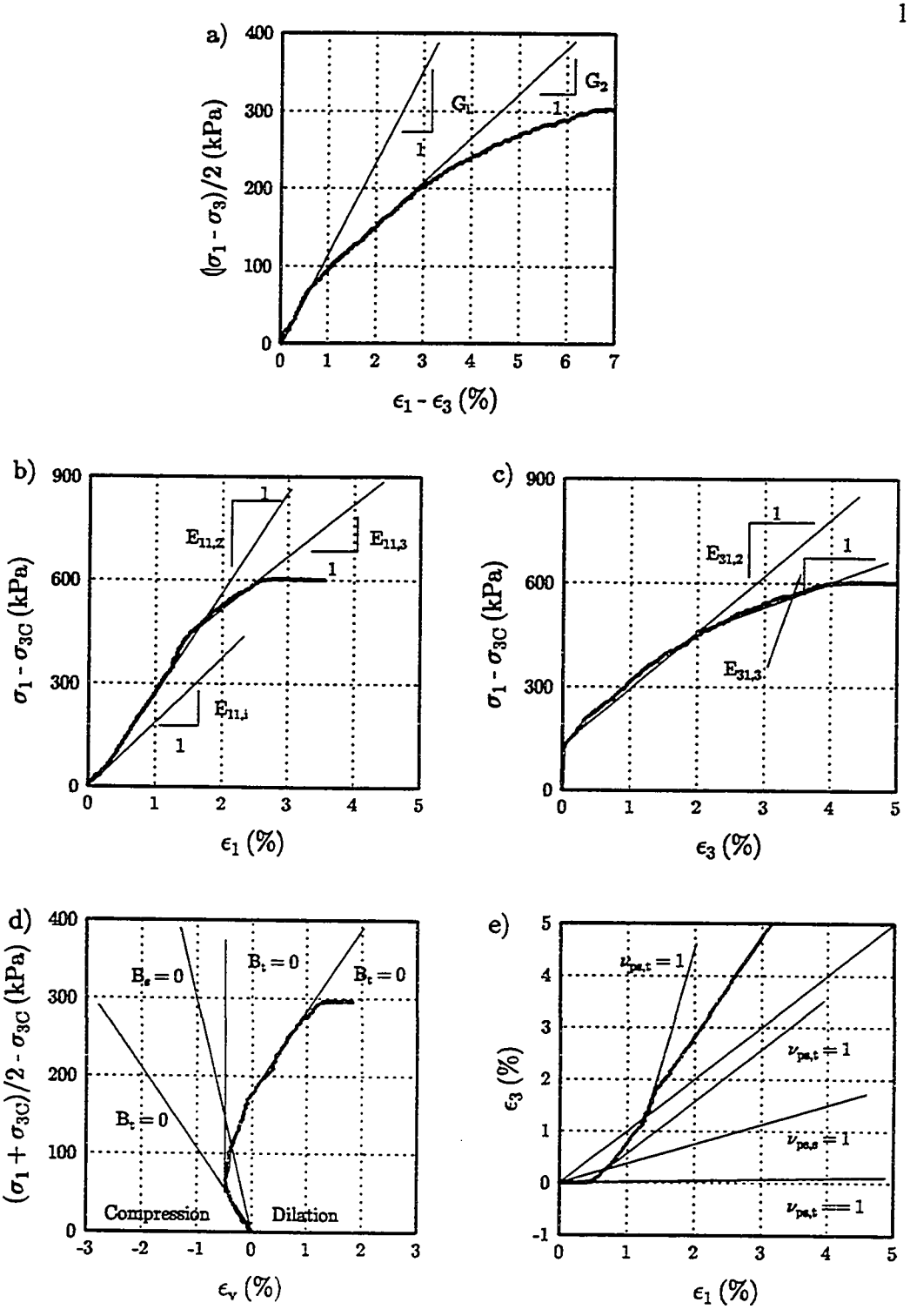

Figure 6.51: Examples for determining "elastic" properties from UCD test data: a) G, b) E_{11}, c) E_{31}, d) B, and e) ν_{ps}.

Table 6.5: Composite stiffness properties.

		σ_{3C}		E_{11} (kN/m^2)			G (kN/m^2)		E_{31} (kN/m^2)	
SOIL	REINF	kN/m^2	TEST	$E_{11,i}$	$E_{11,2}$	$E_{11,3}$	G_i	G_2	$E_{31,2}$	$E_{31,3}$
O	PP2	50.0	48	30000	15300	---	20000	3000	10900	---
O	PP2	75.0	47	49000	14400	---	24000	3500	12500	4800
O	PP2	100.0	45	50000	15700	---	23000	4000	11700	11700
O	PP2	100.0	46	50000	18700	---	23000	3700	12400	4000
O	PP3	50.0	43	24000	21000	---	16300	4300	17200	10800
O	PP3	75.0	41	42000	18600	---	20000	3250	16700	5000
O	PP3	75.0	42	43000	19800	---	18300	6600	17700	---
O	PP3	100.0	44	56000	25500	---	28000	5300	20700	6000
O	PET1	12.5	108	14000	28000	42000	7000	8700	30000	---
O	PET1	25.0	107	36000	36000	54000	25000	9200	33000	---
O	PET1	25.0	109	53000	41000	---	30000	9300	36000	---
O	PET1	25.0	110	40000	40000	---	20000	9300	34000	---
O	PET1	50.0	111	24000	30000	54000	14000	---	64000	---
O	NW1	12.5	88	7500	4000	3000	5700	500	3500	2000
O	NW1	25.0	89	---	---	---	---	940	4500	2100
O	NW2	25.0	90	10000	6000	5500	5000	1200	4900	3600
O	NW2	25.0	91	15000	8000	4000	8000	1800	6700	3800
O	NW2	50.0	92	25000	10000	4000	12700	2300	6800	3600
O	NW2	50.0	93	24000	5000	---	12500	2300	5100	2500
O	SS	12.5	96	10000	---	---	8900	---	80000	---
O	SS	25.0	95	35000	---	---	13800	---	66000	---
O	SS	50.0	97	38000	---	---	15000	---	53000	---

Table 6.5 cont: Composite stiffness properties.

		σ_{3C}		E_{11} (kN/m^2)			G (kN/m^2)		E_{31} (kN/m^2)	
SOIL	REINF	kN/m^2	TEST	$E_{11,i}$	$E_{11,2}$	$E_{11,3}$	G_i	G_2	$E_{31,2}$	$E_{31,3}$
R	PP1	12.5	79	25000	25000	---	16000	5100	14500	7800
R	PP1	25.0	74	26000	32000	20000	13600	6100	17300	7800
R	PP1	25.0	81	20000	31600	15600	12700	5200	15200	8000
R	PP1	50.0	80	37000	37000	10700	18600	6100	19500	6700
R	PP2	25.0	70	16000	36000	---	18000	7900	26100	14800
R	PP2	25.0	73	8000	15000	---	12700	6700	24200	10200
R	PP2	25.0	77	18700	30000	20000	8900	6300	20600	12900
R	PP3	12.5	76	16600	37000	---	7300	11400	32000	20400
R	PP3	25.0	71	24000	39000	---	13000	9700	34800	18000
R	PET1	12.5	98	17000	46000	60000	10000	12900	45000	---
R	PET1	25.0	99	37000	45000	---	13900	---	48000	---
R	PET1	25.0	100	34000	52000	---	22000	9400	44000	---
R	PET1	50.0	106	46000	61000	---	26000	15000	58000	---
R	NW1	12.5	84	8000	16000	---	5500	3200	16000	7500
R	NW1	25.0	85	13000	23600	---	9400	4300	22900	10200
R	NW1	50.0	87	24000	49000	27000	17300	6600	23700	10000
R	NW2	12.5	82	8000	20800	---	6000	4000	15200	7500
R	NW2	12.5	83	10000	16600	---	5000	4000	17200	6500
R	NW2	25.0	72	24000	24000	---	---	5400	18900	11300
R	NW2	50.0	86	30000	24800	14000	16700	4800	21200	7600
R	SS	12.5	101		---	---	15000	---	107000	---
R	SS	25.0	102	23000	---	---	15000	---	83000	---
R	SS	50.0	104	32000	---	---	24000	---	90000	---
S	PP2	50.0	94	26000	16000	10000	7500	1500	11000	7500

The E_{31} modulus, defined for horizontal strain associated with vertical stress, was also well behaved; for all reinforcings except PET1, E_{31} continually decreased with increasing horizontal strain, Figure 6.53 [if the soil had been able to reach constant effective stress ratio conditions, the tangent modulus might have ceased to decrease or even increased, see Section 6.4.3.4)]. The initial tangent value of E_{31} is not reported in Table 6.5 because until lateral soil strain reached approximately 0.02%, the first break point in the soil deformation curve, the vertical stress value was primarily dependent on the composite confining pressure (see Sections 6.4.1 and 6.4.3.4). Furthermore, it did not seem prudent to rely on differences in measured values at this very low strain for computing the initial E_{31} modulus given the sensitivity of the computed value to the actual break point strain and the variability in specimen preparation. Therefore, only the tangent modulus values for the approximate range of lateral strains of 0.2% to 2.0% (2nd tangent modulus, $E_{31,2}$) and from 2.0% to 4% (3rd tangent modulus, $E_{31,3}$) are reported in the table. While the overall range of E_{31} values for each soil was quite broad, for each soil-reinforcing combination the E_{31} modulus values typically fell within fairly narrow ranges, Table 6.5.

Plots of vertical stress versus vertical strain, used for computation of modulus E_{11}, were the least consistent in shape, Figure 6.54. Initial compression, soil dilation, and the increase in the contribution of geosynthetic reinforcements with increasing strain are responsible for the slightly "S" shaped vertical stress versus vertical strain curve in some tests, Figure 6.51. The lateral confining pressure and initial compression of the soil defined the E_{11} modulus in the first 0.5% vertical strain (initial tangent modulus, $E_{11,i}$). The modulus computed for vertical strains between 0.5% and 2% (2nd tangent modulus, $E_{11,2}$) may be greater or less than the initial modulus depending upon the initial confining pressure and the strength of the reinforcement. The tangent E_{11} modulus decreased after 2% vertical strain (3rd tangent modulus, $E_{11,3}$) except when Reinforcement PET1 was used, in which case the modulus of the composite increased with increasing strain, Figure 6.54.

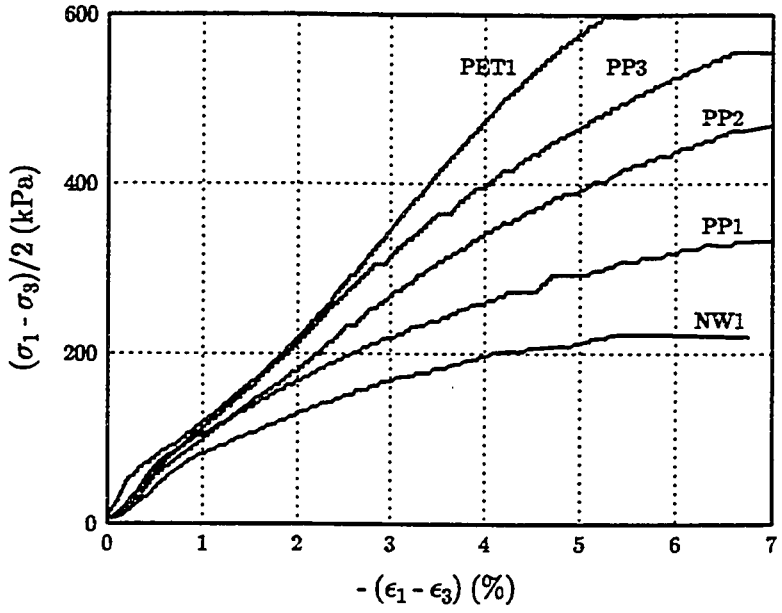

Figure 6.52: Shear stress vs. shear strain for Soil R with various reinforcings, $\sigma_{3C} = 20$ kPa.

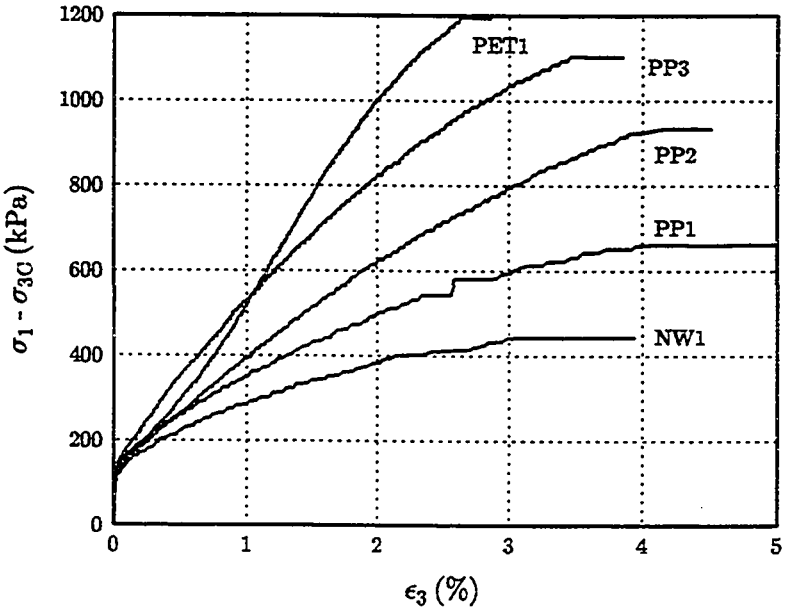

Figure 6.53: Principal stress difference vs. lateral strain for Soil R with various reinforcings, $\sigma_{3C} = 20$ kPa.

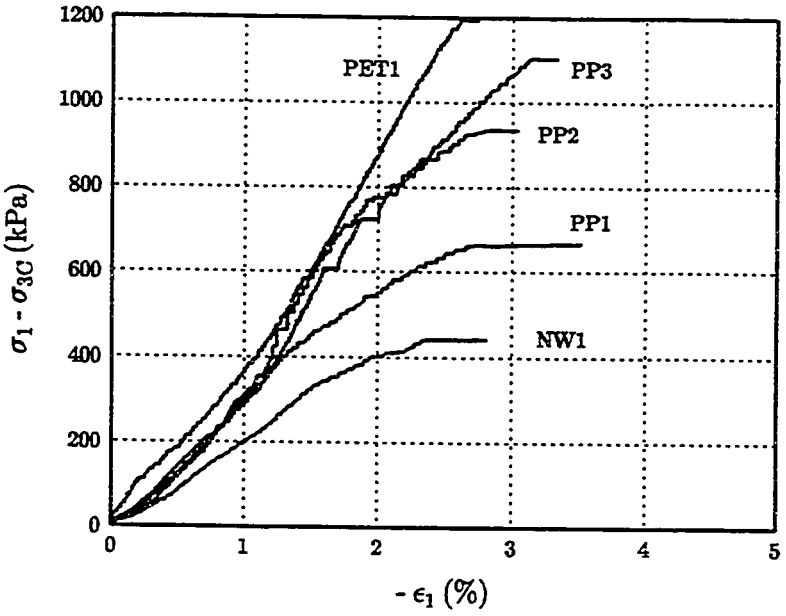

Figure 6.54: Principal stress difference vs. vertical strain for Soil R with various reinforcings, $\sigma_{3C} = 20$ kPa.

Because the cohesionless soil is not a continuum which obeys Hooke's law, the shear modulus, G, cannot be computed from a knowledge of Young's modulus and the Poisson ratio as indicated for an isotropic material in Equation 6.7. The initial Poisson ratio for the soils in plane strain, ν_{ps}, is approximately 0.04. This very small value results from the minimal lateral expansion associated with the first 0.5% compression. Beyond this point the plane strain Poisson ratio rapidly increases, reaching 1.0 ($\nu = 0.5$) when volume expansion commences. Additional lateral strain causes the tangent Poisson's ratio to equal or exceed 0.5. This condition is difficult to handle in numerical analysis.

If the secant value is used, instead of the tangent value, the computed Poisson ratio (and Bulk modulus) will be valid, for numeric analysis, until total lateral strain exceeds total vertical strain (most of which is associated with initial compression), Figure 6.51e. In the UCD tests this condition typically occurred between 0.25% and 3% lateral

strain, Figure 6.23. Composites constructed with higher modulus reinforcements capable of suppressing dilation correspond to the higher end of this range (see Section 6.4.1.4). Using a secant modulus formulation would, therefore, permit more accurate estimates of reinforced soil deformation by extending the range of numerical calculation beyond the point where the soil starts to dilate, a very small lateral strain, to strains more typical of those observed in reinforced soil walls, approximately 1% (Allen, et al., 1992; McGown, et al., 1993).

This presentation on the determination of, and the patterns associated with, the "elastic" properties of geosynthetic reinforced soil has been made to give the reader an idea of the complex nature of reinforced soil. The values presented should also provide an idea of the expected order of magnitude for these parameters.

6.4.3.6 Summary

a) The single long term test on a reinforced soil specimen did not exhibit continued lateral strain under constant vertical load (i.e., creep) despite substantial reductions in the reinforcing tension.

b) Strain gages attached to the geosynthetics underreported both overall lateral strain and incremental strains.

c) The tests with strain gages verified the maximum reinforcing tension occurred at the clamps. Reinforcing tension was not, however, uniform across the unit cell specimen.

d) Visual observation of reinforced soil specimens during loading confirmed that true unit cell conditions were not attained. In three of the four tests in which visual observations were made, soil particles immediately above the reinforcing, and by inference the reinforcing, moved upward.

e) An evaluation of reinforced soil behavior using hypothetical soils and reinforcements and the effective confining pressure concept predicted results similar to those obtained from UCD tests. Composite behavior at large strains for

conditions that result in a peak in the composite stress-strain curve could be predicted using these hypothetical materials and the effective confining pressure concept.

f) Values for "elastic" material parameters were determined for the UCD tests. The values determined should be larger than those for actual situations in which the layers of reinforcement are spaced at distances greater than the 200 mm vertical spacing simulated in the UCD. The tendency for the dense sands to dilate resulted in invalid values of Poisson's ratio, ν, and bulk modulus, B, at low lateral strains.

6.5 An Improved Approach for Measuring Reinforced Soil Behavior

The Unit Cell Device designed and manufactured for this project has proven to be effective for measuring the response of reinforced soil subjected to vertical loading. It was also capable of measuring the tension which developed in the reinforcement. Direct measurement of the reinforcing tension permitted verification, as opposed to acceptance based on circumstantial evidence, that the increase in effective confining pressure associated with reinforcing strain is responsible for the increase in capacity when the soil is reinforced. The UCD tests also determined that increasing the effective confining pressure while the soil is experiencing strain results in a very different soil response than would be obtained from constant confining pressure tests. When the increase in confining pressure with lateral strain is significant, the dilation of the soil may be reduced or prevented.

While the effective confining pressure concept was verified and restriction of dilation could positively be identified, variability between UCD tests caused difficulty for more explicit quantification of these effects on the soil response. This variability may be attributed to a number of factors:

a) Soil variability - density, grain sizes, specimen preparation,

b) Reinforcement variability - manufacturing, specimen preparation,

c) Creep of geosynthetics and strain rate effects,

d) Geosynthetic compressibility,

e) UCD design and method of operation.

Reduction or removal of the influence of these factors from tests on reinforced soil specimens would increase repeatability of tests. Increased repeatability might permit the behavior of reinforced soil to be more accurately defined and possibly correlated with the behavior of unreinforced soil. Removal of many of these factors from the tests may be possible since this program showed that the woven reinforcements were not affected by confinement in the soil and the UCD was an inappropriate device for characterizing the in-soil modulus of nonwoven geotextiles. Since it was determined that the increasing confining pressure concept is valid, obtaining reinforced soil stress-strain behavior may be possible without installing reinforcing in the soil specimens tested under plane strain conditions. Instead, the composite response could be simulated by increasing the lateral confining pressure acting on an unreinforced soil specimen by an amount equal to that which would result due to elongation of the reinforcing had it been installed, Eq. 6.21.

$$\sigma_3 \text{ (applied)} = \sigma_{3E} = \sigma_{3C} \text{ (modeled)} + \frac{E_r \cdot \varepsilon_3}{B \cdot H} \qquad \textbf{(6.21)}$$

where:

σ_3 (applied) = lateral confining pressure applied to device,

σ_{3E} = effective lateral confining pressure on soil,

σ_{3C} (modeled) = confining pressure on composite element,

E_r = reinforcing modulus (force/length),

ε_3 = lateral strain,

B = specimen width, and

H = specimen height.

The reinforcing properties would be obtained from a separate appropriate test which accounted for strain rate and creep effects as well as normal pressure. Use of this technique for testing "reinforced soil composite" behavior would:

a) reduce the number of tests required,

b) reduce the time required to perform each test by eliminating the need to prepare and install reinforcing specimens,

c) eliminate variability in the response resulting from variability in reinforcing specimens,

d) permit control of the rate of increase in confining pressure with lateral strain, and thereby permit simulation of any reinforcement or reinforcement vertical spacing,

e) eliminate the effect of strain rate or normal pressure on geotextile modulus as uncontrolled variables in the tests,

f) permit simulation of stress relaxation in the reinforcement through a controlled decrease in confining pressure,

g) eliminate non-uniform stress conditions in the specimen resulting from friction at the soil-reinforcing contact,

h) permit undrained testing (since there would be no reinforcement to extend to clamps located outside the soil boundaries),

i) eliminate problems associated with installing the reinforcing in the soil and attaching it to the clamps while maintaining the soil density near the clamps and where the clamps penetrate the side wall,

j) eliminate material compressibility from consideration when investigating the volumetric behavior of soil subjected to increasing confining pressure during lateral strain.

A simple plane strain unit cell device which permits the lateral confining pressure to be increased at a rate which is coupled to the rate of lateral strain would suffice for this purpose. If this device is strain rate controlled and capable of large lateral deformations, even post peak behavior of reinforced soil could be obtained. It is recommended that in future studies on the behavior of reinforced soils, the effective confining pressure concept be utilized and reinforcing be eliminated from the soil specimen. This approach should work in most cases except perhaps in partially drained tests on low permeability soils where the contribution of the reinforcement to soil drainage is being investigated. Greater control plus removal of a number of factors which complicate testing and data interpretation make this proposed method superior to the current UCD design and current practice.

6.6 Assessment of ASTM D 4595 Wide Width Test

The standard wide width test, ASTM D 4595 (ASTM 1993), specifies that strength and modulus of geosynthetics be determined, regardless of material properties and manufacture technique, by conducting an in-isolation load-elongation test on 100 mm gage length by 200 mm wide specimens strained at 10%/min. The tests conducted on both the woven and nonwoven geotextiles for this project illustrate the problem with applying such a universal standard to materials which are manufactured using a variety of materials and techniques. Material properties, manufacturing method, specimen size, and strain rate affect the measured performance of these materials. While such a universal standard may be appropriate for quality control testing by manufacturers, it appears that the ASTM D 4595 standard is inappropriate, in its current form, for obtaining engineering properties of reinforcement geosynthetics.

The effect of strain rate on the computed modulus implies that the modulus determined from wide width tests is actually an "apparent" modulus and is not an intrinsic property of the material (Nothdurft and Janardhanam, 1994; Nothdurft, 1995). For strain rate susceptible geosynthetics which are not influenced by confinement in soil,

a better approach to obtaining the engineering strength properties would be to perform a series of in-isolation tests at various strain rates and generate a plot similar to Figure 5.7. When designing or evaluating a GRS wall the "apparent" modulus, which would depend on the strain rate anticipated during construction, could be obtained from interpolation or extrapolation of the strain rate test data. Because these tests take less time to perform than creep tests the engineering data could be obtained fairly quickly for any particular geosynthetic reinforcement. While each designer could commission the testing to be performed for each geosynthetic, it would be easier, and reduce repetition, if manufacturers or suppliers of reinforcement geosynthetics provided charts or tables specific to each geosynthetic which address the influence of strain rate on the strength properties.

A similar situation exists for testing of nonwoven geosynthetics which have apparent modulus dependent on gage length, strain rate, and normal pressure. ASTM D 4595 wide width tests may be appropriate for manufacturer quality control, and while conservative if used directly in design, are all but useless for obtaining actual engineering properties without some sort of correlation to account for these factors. Furthermore, when testing these products to determine engineering properties or as part of quality assurance or control programs, the substantial variation in unit weight of the nonwoven geotextiles tested in this program suggests that a statistically significant number of tests, not the minimum six tests required by ASTM D 4595, must be run. The large number of tests are required to determine the minimum average strength and modulus (two standard deviations below the mean) for these materials so that sufficiently conservative values may be used in design.

The importance of developing a clear understanding of the behavior of geosynthetic reinforcing and the behavior of reinforced soil when modeling or predicting GRS behavior can be illustrated by comparing the findings reported in Section 6.4 with the conclusions reached by Zornberg and Mitchell (1993, 1994) through their FEM study of the Rainier Avenue wall. This GRS wall is the same wall from which Soil R and

Reinforcements PP1, PP2, PP3 and PET1 were obtained. For their study Zornberg and Mitchell used the triaxial test results for Soil R and reinforcing properties determined from standard ASTM D 4595 wide width tests (as reported by STS, 1990) to model the soil and reinforcing behavior. Increases in the reinforcing modulus were required for Zornberg and Mitchell to calibrate their FEM model such that it would predict the behavior observed in the Rainier Avenue wall. From this they concluded that the modulus of the reinforcements must have increased due to confinement.

The results of this laboratory investigation refute their conclusion. The Rainier Avenue wall was constructed over a period of approximately 85 days and the reinforcing generally experienced strains of less than 1% (Allen, et al., 1992). Strain rates were, therefore, on the order of 0.00001 %/min -- 1 million times slower than the ASTM specified strain rate. Extrapolating the data presented in Figures 5.6 to 5.8, 5.9 and 6.34b, the modulus for this strain rate would fall between 25% to 40% and 60% to 90% of the ASTM D 4595-determined modulus for the polypropylene and polyester woven geotextiles, respectively. It is unlikely that confinement resulted in *doubling* of the ASTM D 4595 strength values as Zornberg and Mitchell (1993, 1994) concluded. Instead, the plane strain soil behavior is probably responsible for the reduction in deformations below those computed by Zornberg and Mitchell with the unadjusted reinforcement properties. As was shown earlier, the plane strain friction angle is greater than the triaxial friction angle, Figure 6.5. Dense granular soils also reach their peak strain sooner in plane strain tests than in triaxial tests, Figure 6.7b. Both of these factors would contribute to a higher initial soil modulus and account for the decreased deformations (see Section 6.4.3.4). Thus, the conclusion reached by Zornberg and Mitchell (1993, 1994) that the modulus of the woven geotextiles must increase with confinement is incorrect.

It should be acknowledged that adjustment of the soil data, instead of the reinforcement data, would have been much more involved since no plane strain soil data were available to these researchers and no such technique is available, as was discussed in

Section 6.4.1.1. Furthermore, Zornberg and Mitchell did not have access to variable strain rate test results for the four woven geotextiles which have been produced as part of this program, Section 5.4.

6.7 Conclusions

The unit cell device was developed to expand our understanding of reinforced soil by permitting measurement of soil, reinforcement and composite properties under conditions similar to those which would be experienced in the field. It has proven successful in meeting this objective. Tests were conducted using two different sands, uniformly graded steel beads, four woven geotextiles, two nonwoven geotextiles, and a steel sheet reinforcement. The soils and reinforcings were used in various combinations in an attempt to quantify the influence of the reinforcements on the soils. As expected, the deformation of the reinforced soil composite decreased with increasing soil friction angle and with increasing reinforcement modulus. However, the significant change in soil response when subjected to increasing confining pressure during strain and the severity of rate effects on the reinforcing modulus in these short duration tests was not expected.

The testing program confirmed the Yang and Singh (1974) hypothesis, that the reinforcing increases the confining pressure acting on the soil, thereby increasing its load supporting capacity. Dilation of the dense cohesionless sands, which accompanied lateral deformation, played an important role in defining the composite behavior. Dilation was restricted or prevented when high modulus extensible reinforcements were used. When reinforced with sheet steel, dilation was not an major issue since the soil was still compressing when the steel yielded.

The importance of using plane strain soil behavior in predicting GRS response was illustrated. When lower modulus reinforcements were used, it was shown that the peak effective stress-ratio, σ_1/σ_{3E}, attained by the reinforced soil equaled or exceeded the value derived from constant confining pressure plane strain tests on unreinforced soils.

Stress-strain curves obtained from triaxial tests on cohesionless soils underpredict the soil strength at any given strain. Their use, while conservative, overpredicts GRS deformations.

It was shown in both the UCD tests and the simplified study of composite behavior using hypothetical materials that confining pressure, soil stress-strain behavior, reinforcing modulus and vertical spacing of reinforcement all affect the composite behavior. The relative importance of these factors varies with the degree of lateral strain undergone by the soil and the shape of the soil stress-strain curve. Post peak behavior could be predicted using the hypothetical soil properties.

Geotextile strength properties were found to be influenced by test conditions. The modulus of nonwoven needle-punched geotextiles increased with increasing normal pressure. Because the normal pressure acting on the geotextile increases throughout each unit cell test (i.e., the normal pressure is not constant during reinforcement straining) and because of the high degree of variability in the measured behavior, no recommendations could be made for obtaining the "correct" in-soil modulus to use for these geotextiles from UCD tests. For the same reason, correlation with the "zero" span in-isolation modulus could not be made. The modulus of woven geotextiles were not influenced by confinement but were very much affected by strain rate. Decreasing the strain rate reduced the "apparent" modulus. It was concluded that woven geotextiles similar to those used in this program need not be tested in confined conditions but their strain rate dependency should be quantified using a program similar to that presented in Chapter 5.

Creep of the woven geotextiles occurred rapidly and at low strains. The rate of creep and stress relaxation decreased with increasing time. In two UCD tests the reduction in reinforcing tension after vertical loading had been discontinued was sufficient to permit the soil to expand laterally. In the single long term UCD test performed, the specimen did not continue to strain laterally despite the continued reduction in reinforcement tension and the soil having already reached active conditions. Long term geosynthetic creep, and the effect of creep on the apparent modulus is an issue

which must be considered in designing GRS walls and when modeling GRS wall behavior. Additional research on the creep characteristics of geosynthetics and the effect of slowly decreasing confining pressure on reinforced soils is necessary.

Additional research is also required on the plane strain behavior of reinforced dense cohesionless soils. To simplify performance, control, and interpretation it was suggested that reinforcement not be used in these tests. Instead, the increase in effective confining pressure which would result from elongation of reinforcement could be simulated by increasing the applied lateral confining pressure during lateral straining of the soil specimen. The magnitude of the increase could be controlled to model any particular reinforcement. Performing the tests in this manner would simplify sample preparation, eliminate non-uniform stress distributions caused by inclusion of the reinforcement, eliminate the influence of reinforcing specimen variability, eliminate the effects of strain rate on reinforcing modulus, remove the effect of reinforcement compression on volumetric behavior, and permit undrained tests to be conducted. Greater control, plus removal of a number of factors which complicate testing and data interpretation, make this proposed approach superior to the continued use of the UCD as currently designed. Removal of these variables should also permit a reduction in the number of tests which must be conducted to confidently define the soil behavior for a given reinforcement.

CHAPTER 7
REINFORCED SOIL WALLS TREATED AS ELASTIC BODIES SUBJECT TO SELF WEIGHT

7.1 Introduction

In the previous two chapters geosynthetic and reinforced soil properties were investigated through laboratory studies on individual specimens. A knowledge of the material behavior is necessary for designing reinforced soil structures and predicting their response to loads. In addition to understanding the material properties it is also necessary to understand the general behavior of structures constructed using these materials. Each type of structure can be expected to respond to applied loads in a certain manner irrespective of the material from which it is constructed. For structures constructed of linear elastic materials, the deformed structure would have the same shape regardless of material properties, only the absolute magnitudes of displacements and strains would be material dependent. For structures constructed with non-linear materials, which have moduli that decrease with increasing strain, the shape of the deformed structure as well as the magnitude of displacements and strains are dependent on the degree of material nonlinearity. However, the *general, overall* deformed shape would be similar to the deformed shape which would have resulted had the structure been constructed from elastic materials.

Non-linear material properties have been utilized in parametric studies performed to identify factors which affect reinforced soil retaining wall behavior (see Sections 3.3 and 3.4). While these studies have identified numerous factors which influence the response of reinforced soil retaining walls, none have looked at the general behavior which should be expected due to geometry, loading, and boundary conditions. That is, the expected response for such a structure has not been separated from the influences of the soil and reinforcing. The study reported on in this chapter was undertaken to identify which of the factors influencing deformations are functions of the problem being

evaluated (i.e., a rectangular mass subjected to loads) and not functions of the specific soil and reinforcing properties assumed.

7.2 Analysis

To develop a general understanding of reinforced soil retaining wall behavior and how various factors may affect this behavior, a study was made of the deformations, strains, and stresses experienced by an elastic rectangular soil mass subject to plane strain deformation under its own weight. Although it is well known that soils, polymeric reinforcing materials, and reinforced soil composites typically exhibit nonlinear stress-strain properties (e.g., McGown and Andrawes, 1977, McGown, et al., 1978 and 1982; and Chapters 5 and 6 of this dissertation), linearly elastic material properties were assumed for this study. This approach was considered appropriate because (1) previous work, wherein soils were assumed elastic, had proven effective for identifying the pattern of stresses, strains, and deformations in soil systems (Goodman and Brown, 1963; Clough and Woodward, 1967; Poulos, et al., 1972); (2) the strains measured in reinforced soil walls have been very small -- less than 0.25% and 1% for steel and polymeric reinforced structures, respectively (Anderson, et al, 1987; Christopher, et al., 1990; Allen, et al., 1992; McGown, et al., 1993); and (3) the maximum face deformations for steel and polymeric reinforced walls have been observed to be less than 0.8% and 2% of the wall height, respectively (Christopher, et al., 1990; Holtz, et al., 1991).

A review of the literature revealed that in reinforced soil walls, the location of maximum horizontal strain in the reinforcing followed the general pattern shown in Figure 3.12. Schlosser and Elias (1978) showed that this same pattern would occur if the constituent materials of the reinforced wall were linearly elastic, Figure 7.1. The deformed shape of reinforced earth walls and the stress distribution within them was also observed to be similar to the pattern observed by Richards and Schmid (1968) in photoelastic studies of gelatin models, Figure 7.2. These observations suggest, that although geosynthetic reinforced soil may not meet the strict definition of a composite

material (Romstad, et al., 1976; Rowe and Ho, 1988), it would be useful to consider the soil and reinforcing as an elastic composite to increase our understanding of reinforced soil wall behavior.

The simplified model used for this study consisted of a wall of height, H, length, L, material unit weight, γ, and shear modulus, G, Figure 7.3. A Poisson's ratio, ν, equal to 0.498 was selected as a compromise between the volumetric compression that occurs upon initial loading of reinforced cohesionless soil and the dilation at greater strains (see Section 6.4.1.4). Since the material was assumed linear elastic, the deformation, strains and stresses of the wall could be determined by summing effects of self weight, pure bending and pure shear, as shown in Figure 7.4.

Solutions for horizontal displacement, u_x, of the face due to pure bending, u_{xb}, and pure shear, u_{xs}, may be derived by assuming the wall to be a cantilever rectangular beam of unit width, having a depth equal to the length of the reinforcing, L, and a length equal to the height of the wall, H (see Appendix D). The governing equations are presented in Equations 7.1 and 7.2 for bending and shear, respectively. The terms used in the equations have been defined in Figure 7.3 or in the text above.

$$u_{xb}(z) = \frac{K_r \gamma H^2}{30G}\left(\frac{H}{L}\right)^3\left\{\left(\frac{z}{H}\right)^5 - \frac{5z}{H} + 4\right\} \tag{7.1}$$

$$u_{xs}(z) = \frac{-K_r \gamma H^2}{6G}\left(\frac{H}{L}\right)\left\{\left(\frac{z}{H}\right)^3 - 1\right\} \tag{7.2}$$

Because closed form solutions for elastic bodies under self weight, for even this simple geometry, are difficult to derive (Goodman and Brown, 1963; Richards and Schmid, 1968), it was necessary to utilize the finite element method to evaluate the contribution of body forces to deformations, stresses, and strains.

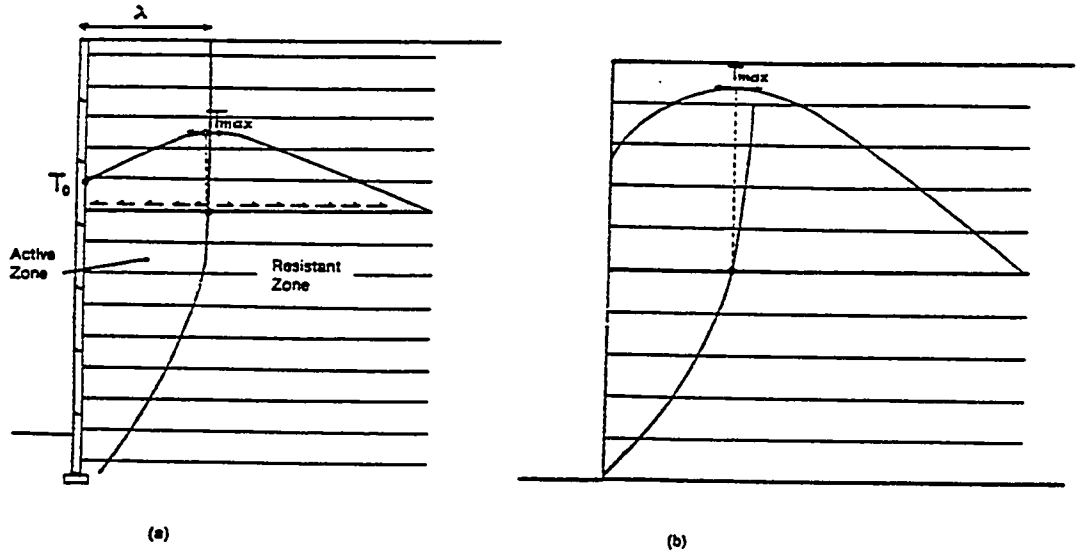

Figure 7.1: Tensile force distribution along reinforcements: a) in Reinforced Earth wall, b) using finite element analysis and assuming purely elastic materials (after Schlosser and Elias, 1978).

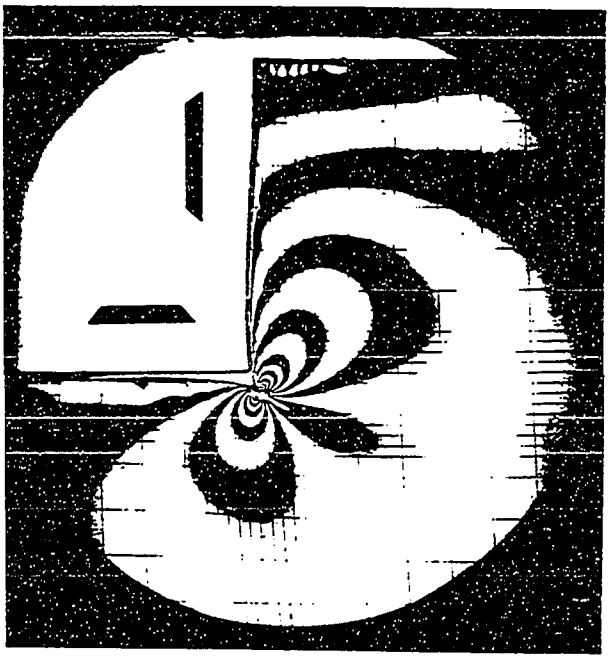

Figure 7.2: Deformed shape and lines of equal maximum shear stress from photoelastic studies of a gelatin model for a vertical slope deforming under self weight (after Richards and Schmid, 1968).

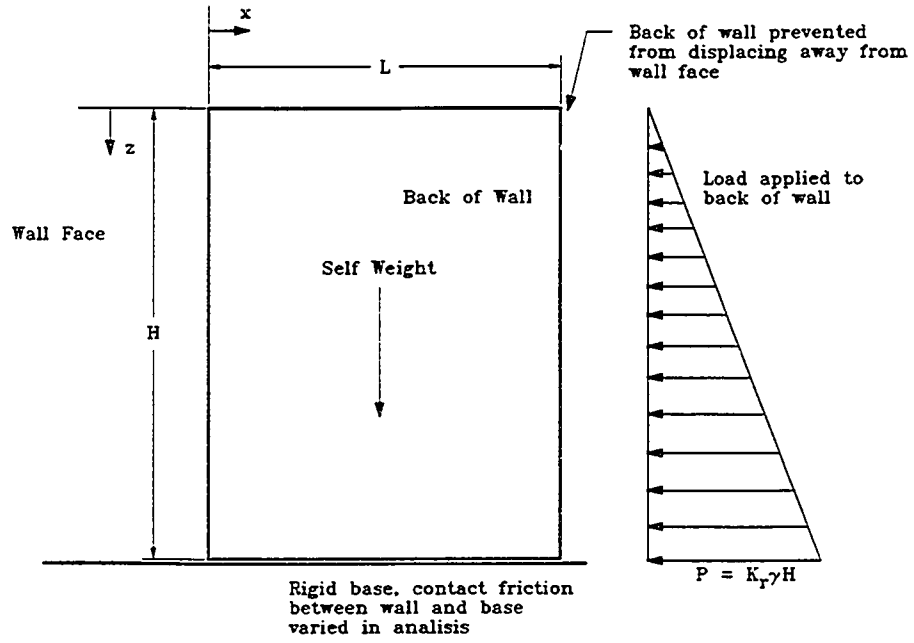

Figure 7.3: Model used for this study.

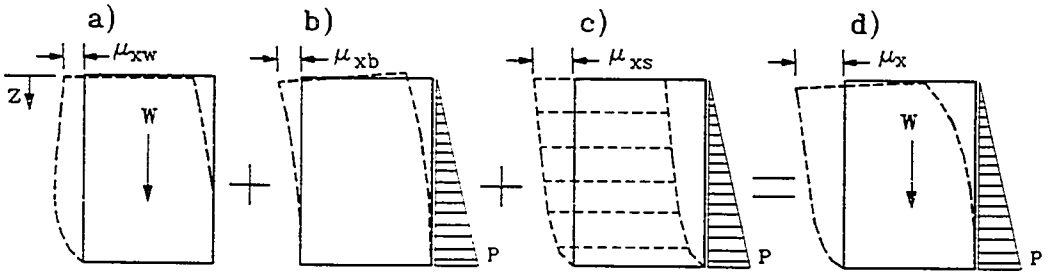

Figure 7.4: Contribution of a) self weight, b) pure bending, and c) pure shear to d) total deformation of the body.

In the model evaluated (Figure 7.3), the wall was free to displace outward but the back of the wall was prevented from displacing away from the wall face. This restraint approximates the conditions for actual walls where the retained soil and the wall would be simultaneously constructed, thereby preventing displacement of the wall into the retained soil. To isolate the effects of the material mass, shear modulus, and applied loads from the effects of foundation material properties, a rigid foundation with a horizontal upper surface was assumed. Base friction, μ_b, values of infinity (fixed base), 0.6 (stiff foundation soil), 0.2 (soft foundation soil) and 0 (no friction) were selected to permit deformations resulting from various foundation conditions. Since previous studies of reinforced retaining walls have shown that most deformation occurs during construction (Christopher, et al., 1990; Allen, et al., 1992), and that incremental loading affects the solution (Goodman and Brown, 1963; Clough and Woodward, 1967), the body was incrementally constructed in the FEM analysis. Length to height (L/H) ratios from 0.4 to 1.0 were considered. The load applied to the back of the wall was assumed to increase linearly with depth and have a value of $K_r\gamma z$. Values for the lateral earth pressure coefficient for the retained soil, K_r, of 0, 0.17 and 0.27 were used, corresponding to cases for no soil retained behind the wall (or a soil with $\phi = 90^o$), $\phi = 45^o$, and $\phi = 35^o$, respectively. Unrealistic cases where loading caused vertical tensile forces to develop at the heel of the wall were not considered. Material shear moduli and unit weight assumed to be typical for reinforced soil applications were selected: 3000 kN/m^2 < G < 20000 kN/m^2 and 16 kN/m^3 < γ < 22 kN/m^3.

A general purpose finite element analysis package, ANSYS 5.0 (Swanson Analysis Systems, 1992), was used for this study. To model the wall and the base friction between the foundation and the wall, respectively, linear quadrilateral elements and Coulomb friction interface elements were utilized. Downdrag due to friction between the wall and retained soil was not considered so as to reduce the number of variables in the analysis.

Some of the results obtained from this analysis are presented in Figures 7.5 through 7.16. The results have been non-dimensionalized using factors derived from equations developed by Goodman and Brown (1963) for an infinite elastic quarterspace subject to deformation under its own weight (see Appendix D). The factors derived for loading due to body weight only do not truly non-dimensionalize the solution for the cases where loading was applied behind the wall; however, the error introduced by using these same factors was less than 1% for the range of γ and G assumed, and was considered insignificant.

Inspection of the results reveals:

a) The deformed shape of the reinforced mass varied with L/H, applied horizontal load, and boundary conditions, Figures 7.5-7.9. The back of the walls tilted outward, toward the face, even when no lateral loads were applied, Figure 7.5b.

b) An increase in the lateral load applied to the wall (i.e., retained soils with lower friction angles) increased the deformation experienced at both the face and the back of the wall, Figures 7.5-7.8. As the ratio of L/H decreased (i.e., slender walls) the *shape* of the wall face was most noticeably changed, while the *magnitude* of deformation at the back of the wall increased most significantly. For walls with larger L/H values, the point of maximum horizontal displacement of the face moved upward as the load behind the wall increased. The magnitude of horizontal displacement of the top of the wall increased substantially with decreasing L/H and increasing applied lateral load, Figure 7.9.

c) Displacement of the wall face increased near the toe of the wall when slip was permitted between the foundation and the wall, Figure 7.8. The displaced shape of the face was not substantially altered when the base friction coefficient, μ_b, was reduced from infinity (fixed condition) to 0.6 (stiff foundation soil). When the base friction coefficient was reduced to 0.2 (soft foundation) and 0.0 the displaced shape was noticeably affected.

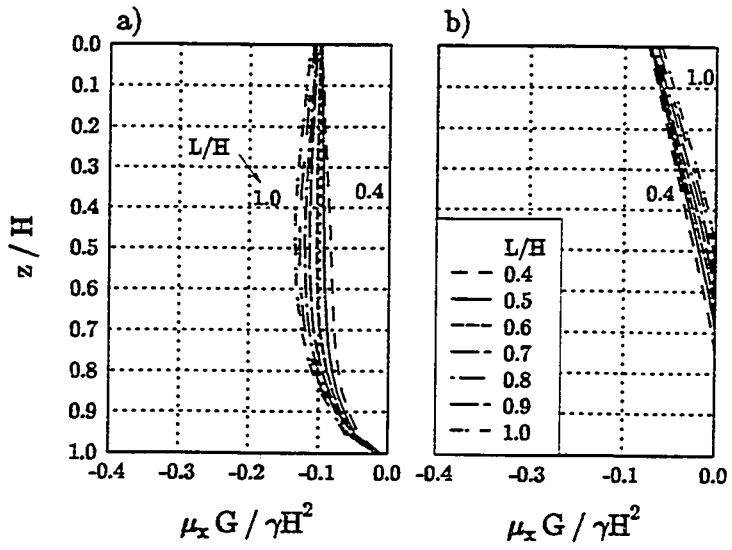

Figure 7.5: Displaced shape of body for various L/H, $\mu_b = 0.6$, $K_r = 0.0$ ($\phi = 90^o$): a) front face, b) back face.

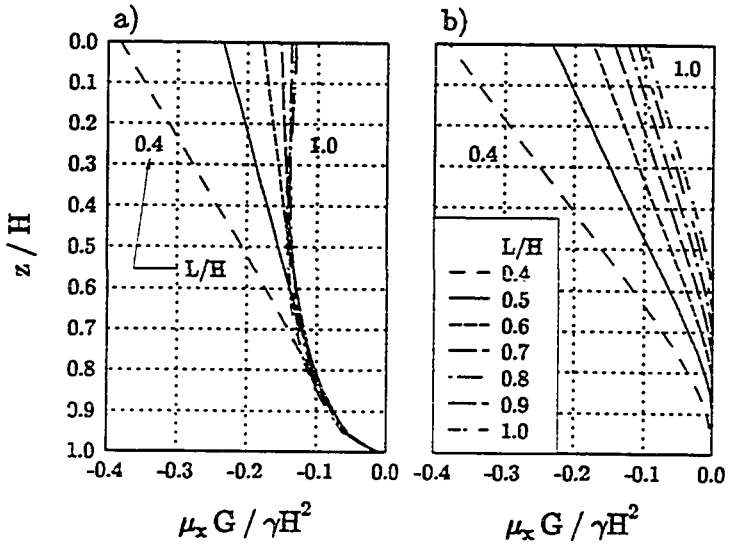

Figure 7.6: Displaced shape of body for various L/H, $\mu_b = 0.6$, $K_r = 0.17$ ($\phi = 45^o$): a) front face, b) back face.

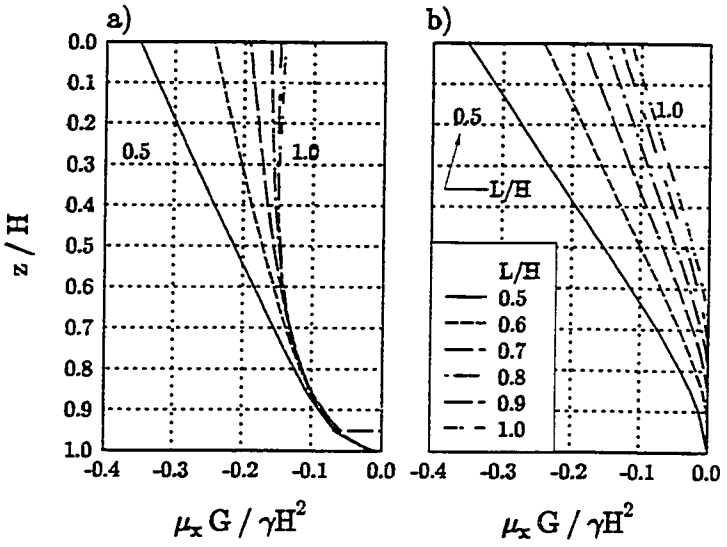

Figure 7.7: Displaced shape of body for various L/H, $\mu_b = 0.6$, $K_r = 0.27$ ($\phi = 35^\circ$): a) front face, b) back face.

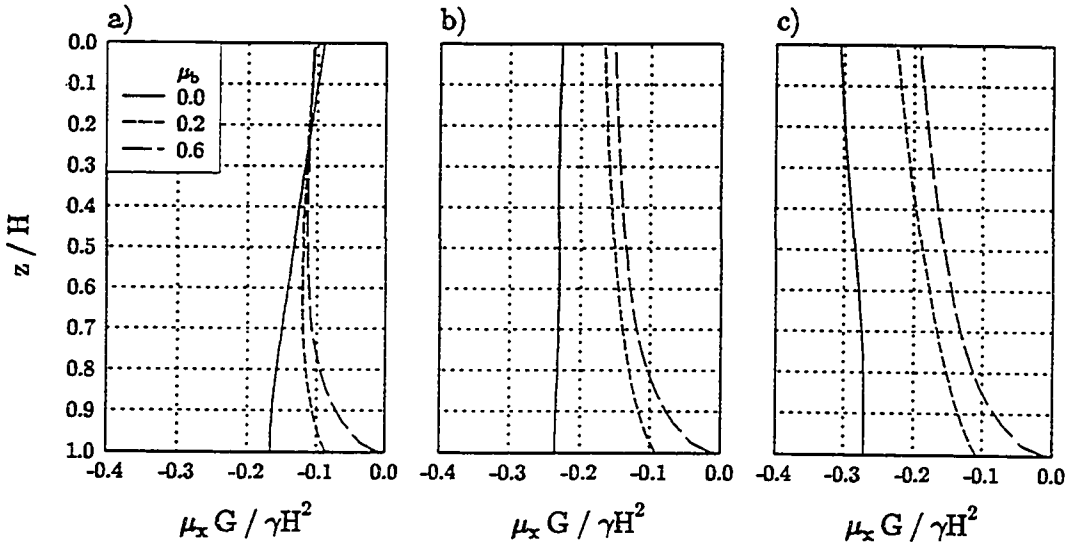

Figure 7.8: Displaced shape of face for various base friction coefficients, L/H = 0.7: a) $K_r = 0.0$ ($\phi = 90^\circ$), b) $K_r = 0.17$ ($\phi = 45^\circ$), c) $K_r = 0.27$ ($\phi = 35^\circ$).

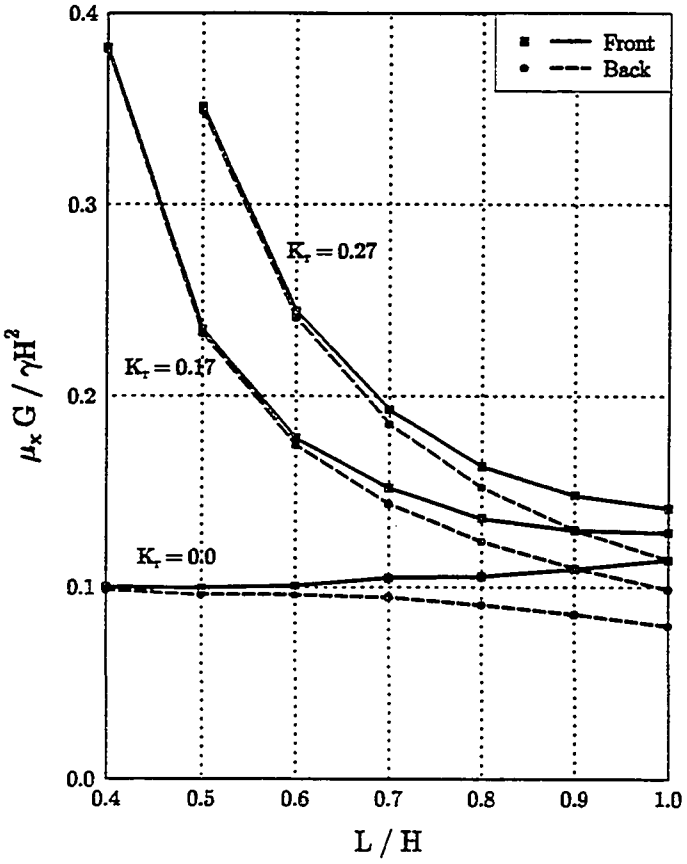

Figure 7.9: Displacement of top point on front and back wall faces vs. L/H ratio.

d) The magnitude of the maximum horizontal strain for elements in the top portion of the wall did not change substantially with L/H, with applied lateral load, or with interface friction between the wall and foundation, Figures 7.10-7.12. This phenomenon occurred despite the significant change in wall deformation associated with variation of these factors. The magnitude of maximum horizontal strain increased with increasing depth below the top of the wall, increasing applied lateral load, decreasing base friction, and decreasing L/H ratio.

e) Except near the wall toe, the case with no base friction, $\mu_b = 0$, resulted in maximum horizontal strains equal to or greater than the maximum horizontal strains resulting when there was base friction, Figure 7.11. The magnitude of maximum horizontal strain increased linearly with depth, until very near the toe, only when no lateral load (or an unlikely case where $\phi = 90^o$) was applied behind the wall.

f) The loci of maximum horizontal and shear strains moved closer to the wall face with increasing applied lateral load (i.e., lower friction angle of the retained soil), Figure 7.13. The locus of maximum horizontal strain did not coincide with the locus of maximum shear strain.

g) The distribution of strain in the reinforcing became more uniform as the distance from the toe increased, Figure 7.14. That is, the absolute magnitude of the difference between the maximum and minimum strains for a specific layer decreased as the distance from the toe increased.

h) The horizontal stresses along the locus of maximum horizontal strain were positive, indicating tension, near the top of the wall, Figure 7.15. The distribution of horizontal stress at any depth, z, within the wall was a function of depth, L/H ratio, and lateral load applied to the back of the wall, Figure 7.16.

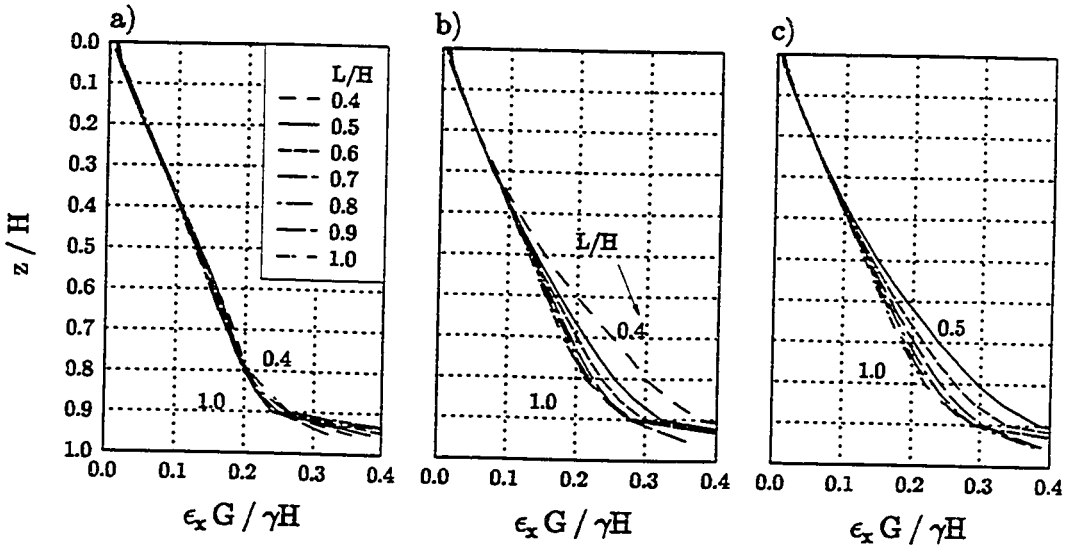

Figure 7.10: Maximum horizontal strain vs. depth for various L/H, $\mu_b = 0.6$: a) $K_r = 0.0$, b) $K_r = 0.17$, c) $K_r = 0.27$.

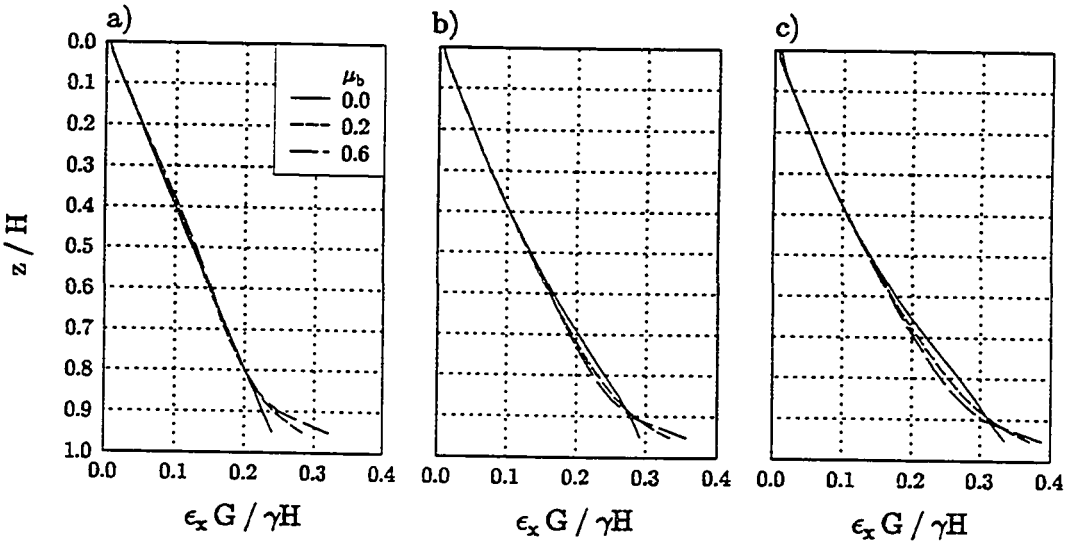

Figure 7.11: Maximum horizontal strain vs. depth for various base friction coefficients, L/H = 0.7: a) $K_r = 0.0$, b) $K_r = 0.17$, c) $K_r = 0.27$.

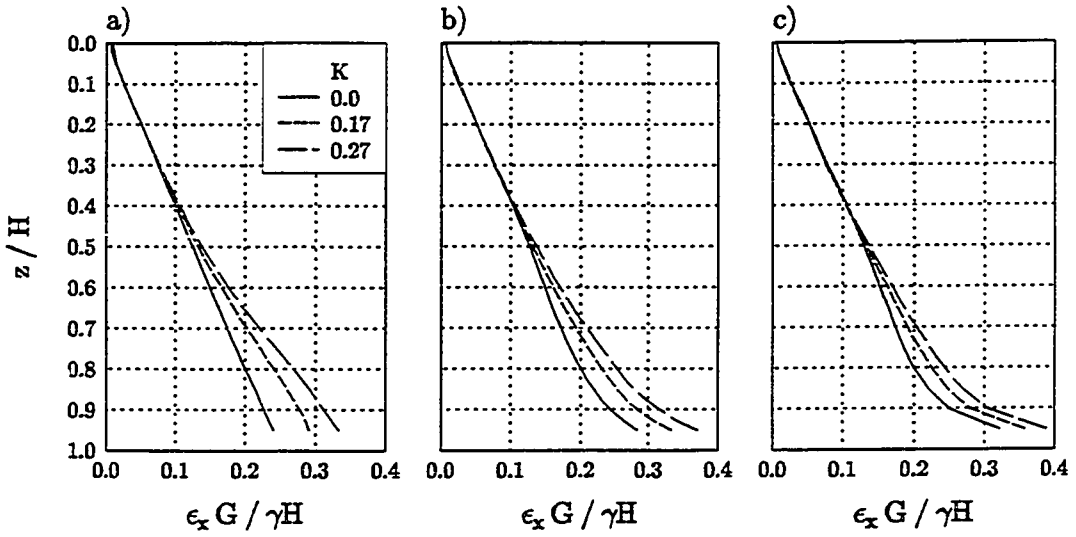

Figure 7.12: Maximum horizontal strain vs. depth for various applied lateral loads, L/H = 0.7: a) $\mu_b = 0.0$, b) $\mu_b = 0.2$, c) $\mu_b = 0.6$.

7.3 Discussion

7.3.1 General

The patterns of deformation and horizontal strain within the walls analyzed here resemble those observed in actual reinforced earth walls and in more rigorous FEM studies, Figures 3.12 and 3.16 (Anderson, et al., 1987; Christopher, et al., 1990; Adib, et al., 1990; Holtz, et al., 1991; Chandrasekaran, 1992; Xi, 1992; Chou and Wu, 1993; Ho and Rowe, 1993; Zornberg and Mitchell, 1993). The displacement of the back of the wall was similar to that reported by Chandrasekaran (1992) and Ho and Rowe (1993). The relationship between the maximum displacement of the wall face for various L/H, Figure 7.9, followed the same pattern determined by Christopher, et al. (1990) and Chew and Mitchell (1994), Figures 3.16 and 3.17c. These similarities suggest that although the assumptions of linear elasticity and composite behavior may not represent actual

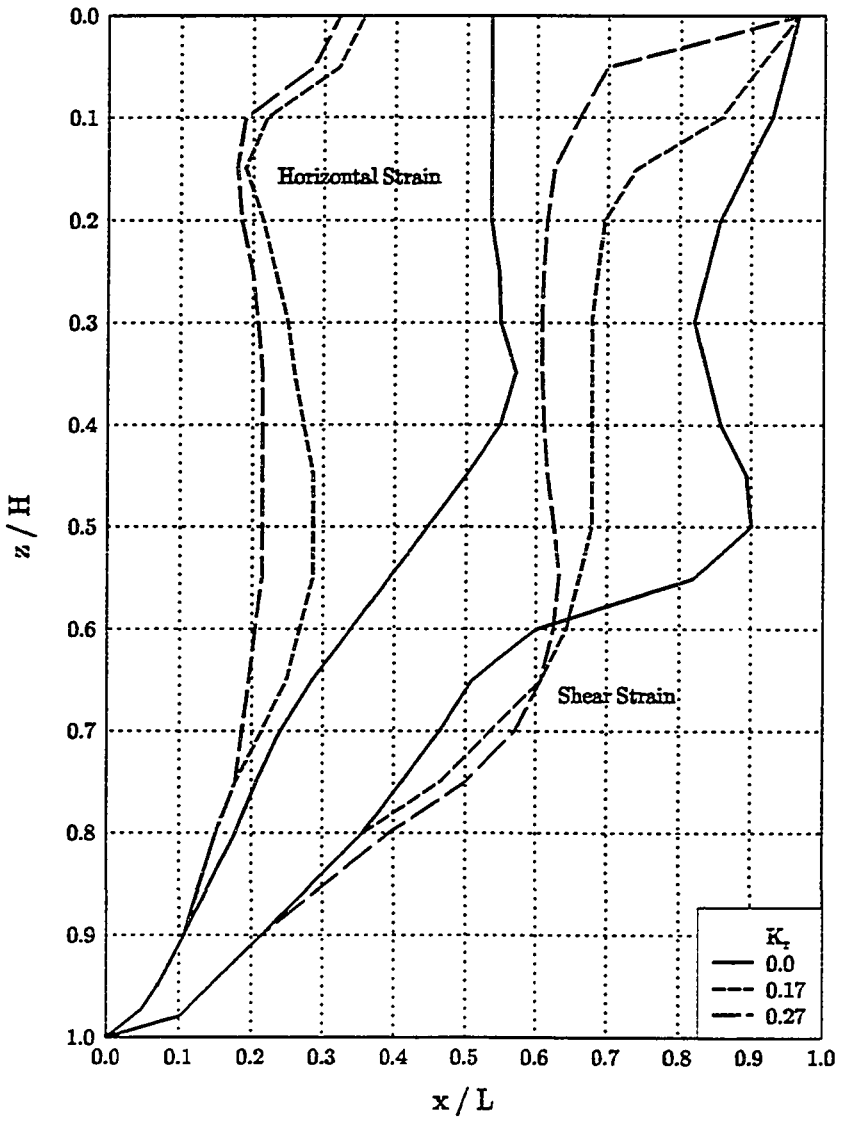

Figure 7.13: Locus of maximum horizontal strains and maximum shear strains, L/H = 0.7, $\mu_b = 0.6$.

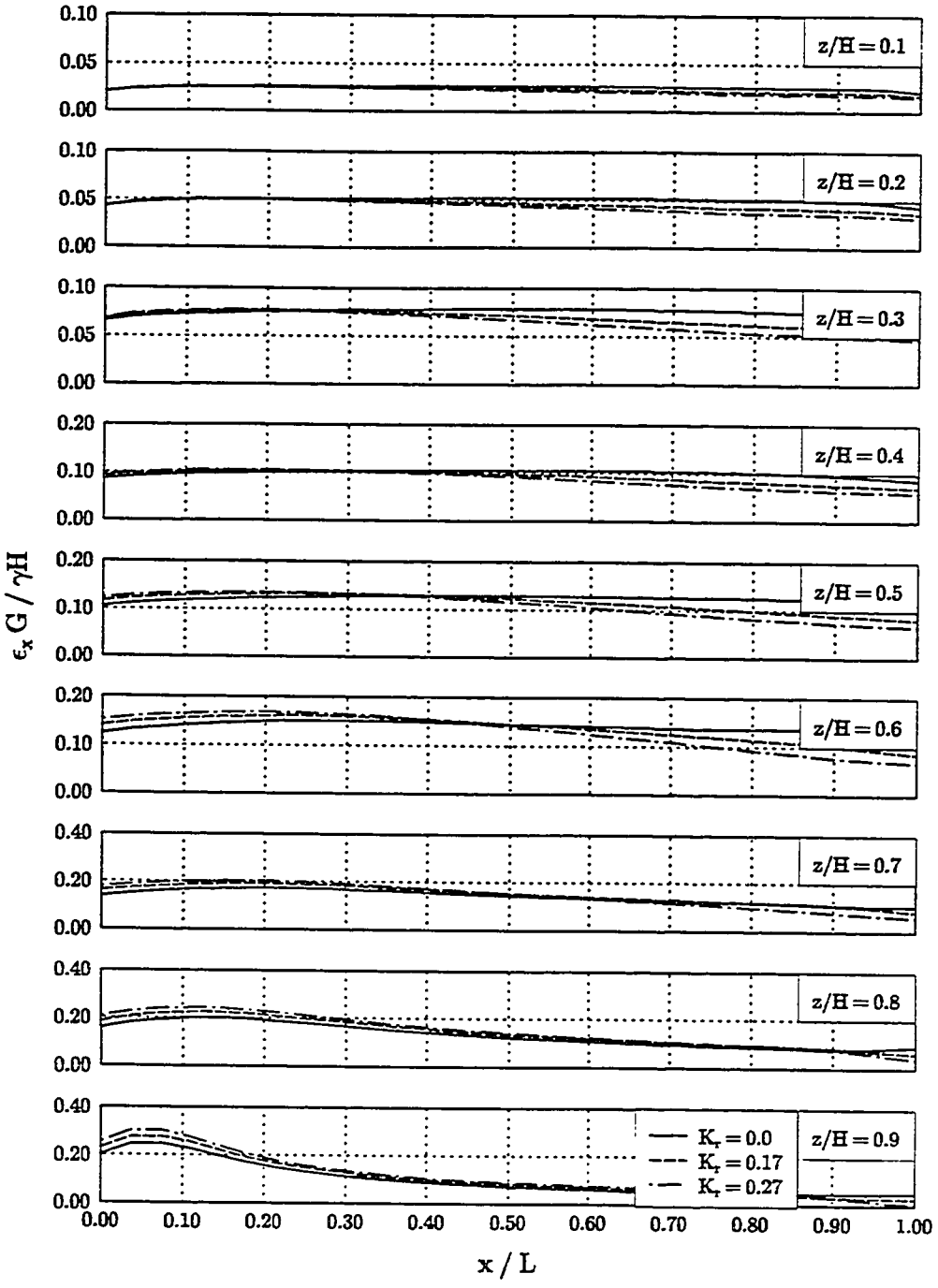

Figure 7.14: Distribution of horizontal strain throughout body, L/H = 0.7, $\mu_b = 0.6$.

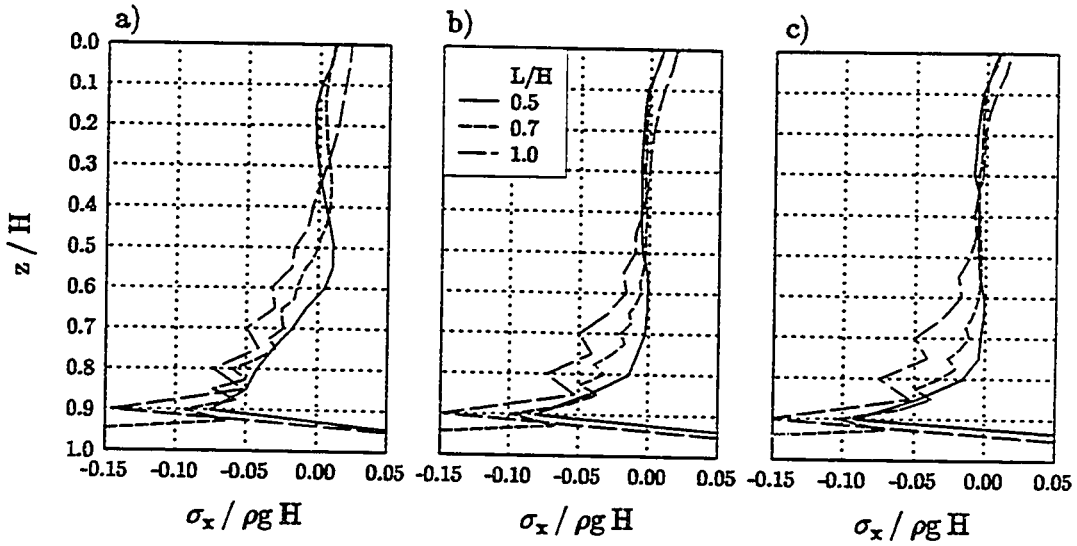

Figure 7.15: Horizontal stress at locus of maximum horizontal strain for various L/H, $\mu_b = 0.6$: a) $K_r = 0.0$, b) $K_r = 0.17$, c) $K_r = 0.27$.

conditions experienced by reinforced soil retaining walls, a general understanding of the expected response of reinforced soil walls may be obtained through such an analysis.

With this in mind, the results of the FEM analysis described above are discussed in more detail below with regard to deformations, strains, and stresses. The discussion is extended to include the implications of these results to actual reinforced soil structures.

7.3.2 Deformed Shape

Bending, shear, and material weight all contribute to the total deformation. Their relative contribution to the horizontal displacement at the top front face of the wall is illustrated in Figure 7.17. For each K_r, the lateral earth pressure coefficient of the backfill, the relative importance of shear to total deformations remains fairly constant over the range of L/H ratios studied. This is not the case for bending and material weight where their relative importance appears to be inversely related. Comparison of the displaced shape of the front and back wall faces, with and without lateral load application behind the wall, illustrate the importance of material weight in overall deformations,

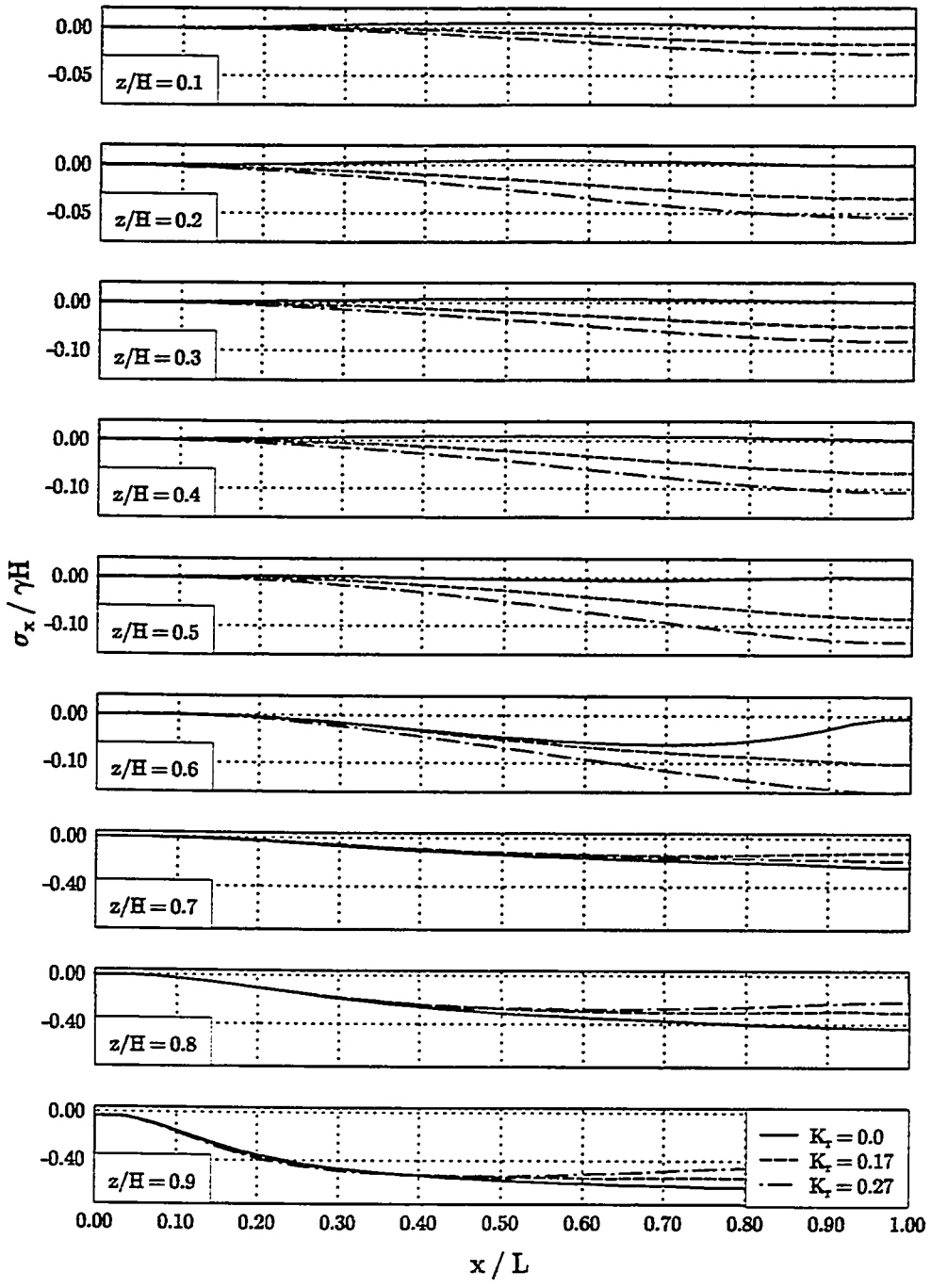

Figure 7.16: Distribution of horizontal stress throughout body, L/H = 0.7, $\mu_b = 0.6$.

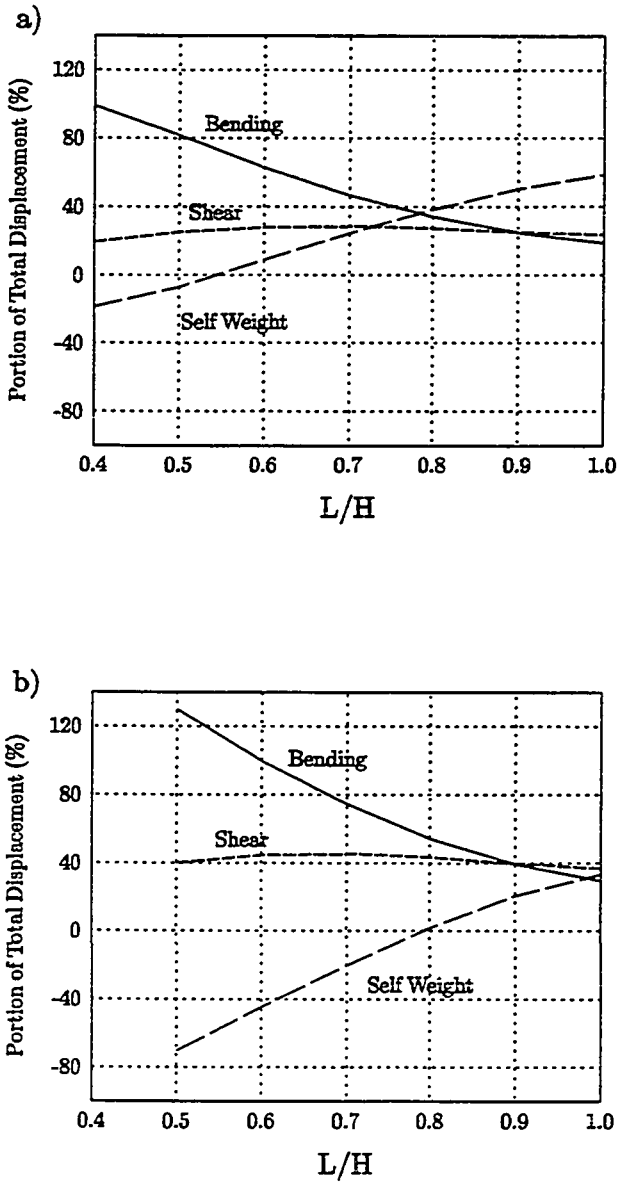

Figure 7.17: Relative contribution of bending, shear and self weight to total displacement at top front wall face: a) $K_r = 0.17$, b) $K_r = 0.27$.

TABLE 7.1: Maximum Displacement of a Reinforced Soil Wall, H = 6 m, and Shear Modulus Required for an Elastic Body to Experience Identical Maximum Displacement, $\gamma = 20$ kN/m^3.

L/H	Extensible Reinforcement			Inextensible Reinforcement		
		G (kN/m^3)			G (kN/m^3)	
	μ_x (mm)	$K_r = 0.17$	$K_r = 0.27$	μ_x (mm)	$K_r = 0.17$	$K_r = 0.27$
0.4	160	1710		48	5700	
0.5	120	1380	2100	36	4600	7000
0.6	96	1350	1800	29	4470	5960
0.7	80	1350	1760	24	4500	5850
0.8	70	1390	1750	21	4630	5830
0.9	64	1485	1690	19	5000	5680
1.0	58	1500	1740	18	5200	5600

Figures 7.5-7.7. For larger L/H ratios and lower values of K_r (i.e., higher friction angles of the retained soil), much of the total deformation can be attributed to wall material weight, γ, alone, although bending and shear still contribute. The relative importance of material weight to total displacement at the top of the wall decreases as L/H decreases and with increases in K_r. This decrease in the importance of body weight is more than offset by an increase in the contribution of bending to total displacement. At the lower L/H ratios (i.e., more slender walls) the material weight counteracts bending forces, reducing the total displacement instead of contributing to it. As L/H decreases, most of the total deformation results from bending forces.

In fact, the bending forces and wall dimensions may be more important than the material properties in predicting the displaced shape of the wall. Equation 7.1 shows that at the top of the wall, z = 0, displacement varies with K_rH^2 (bending force factor) and inversely with $(L/H)^3$ (wall dimension factor) but only linearly with shear modulus, G and material weight, γ. This may partially explain the substantial increase in horizontal displacement with decreasing L/H, which have been observed in actual GRS walls, as well as the relatively small difference (a factor of 3) in displacement when high modulus

extensible reinforcements are used instead of lower modulus inextensible reinforcements, Figures 3.16. The substantial increases in wall face displacement with decreasing L/H is a function of the problem being investigated and should, therefore, be expected.

Although wall dimensions may substantially influence wall performance the material properties cannot be totally ignored. Since soil and reinforced-soil strength parameters are much more variable and more difficult to ascertain than the weight of compacted soils, with typical values of 19 $kN/m^2 \pm 20\%$, more care should be taken in establishing these parameters than in determining soil weight. When selecting soil and reinforcing to be used in retaining structures it would be beneficial to know the order of magnitude required for the shear modulus for the retaining structure to behave adequately. As an example the anticipated maximum displacements for a 6 m high wall for various L/H ratios were computed (Table 7.1) using the Christopher, et al. (1990) chart (Figure 3.16). The predicted displacements were relatively small, less than 1.5% of the wall height, even for low L/H ratios. Shear moduli required for an elastic body to undergo identical displacements, assuming $\gamma = 20\ kN/m^2$, were calculated by applying the results for the FEM evaluation performed herein (Figure 7.9) to the displacements computed using Figure 3.16. The low values of shear moduli obtained suggest that reinforced soil retaining walls should not be expected to experience large deformations for loading by self weight and retained soil, even if the shear modulus is very low.

In addition to shear modulus, the FEM analysis also showed that loads applied to reinforced soil walls must be considered when predicting deformations, Figure 7.9. However, the empirically developed design chart presented by Christopher, et al. (1990), Figure 3.16, does not address variability in applied loads. It is based solely on L/H ratio and material extensibility (which is related to the reinforced soil shear modulus). Therefore, the displacement predicted when Figure 3.16 is applied to actual walls should be assumed approximate since the properties of the retained soil are not considered. Similarly, Figure 3.17c may also over predict deformations if the retained soil's friction angle is greater than the 30° to 40° friction angle used to develop the chart. It should also

be noted that Figure 3.17c was developed using soil properties obtained from cylindrical triaxial tests instead of the more appropriate plane strain test (see Marachi, et al., 1981 and Chapter 6). This, too, may result in overprediction of deformations when this chart is used.

Displacements at the back of the wall must also be understood to permit an appreciation of the overall problem of reinforced soil wall behavior. The analysis performed herein showed that these displacements should be expected simply due to the problem dimensions, material weight and boundary conditions. The observation that the back face of the wall would lean toward the front face, with or without applied lateral loads, has implications for field monitoring of walls, Figures 7.5b, 7.6b, and 7.7b. Specifically, integration of horizontal strains *within* the wall should not be expected to correlate with the overall deformed shape of the structure, although this has been attempted in some field studies (e.g., Berg, et al., 1987; Allen, et al., 1992). Leaning of the back wall also has implications for interpreting observed or predicted horizontal deformations of GRS walls. Ho and Rowe (1993) use the concept of a zero force line to try and explain wall deformations, Figure 7.18a. They attribute the deformation which occurs in the wall above the zero force line to the presence of a large amount of soil strain in the "unreinforced" retained fill. While the properties of the reinforced soil and backfill are functions of the soil strength, the tendency for the wall to deform is highly dependent on the L/H ratio and would result in front and back face deformed shapes similar to that observed by Ho and Rowe (Figure 7.18b) even without application of load behind the wall (Figure 7.5). Thus, the large amount of strain in the retained fill did not cause the wall deformation but rather occurred, in part at least, because the wall tends to deform in the manner observed by Ho and Rowe (1993), even without application of loads and regardless of the material "friction angle". The apparent correlation, reported by Ho and Rowe, between the location of the point at which the back of the wall began displacing toward the face with the "zero force line" must be considered coincidental and result from a liberal interpretation of the results.

7.3.3 Horizontal Strain

7.3.3.1 Horizontal Strains Near the Toe of the Wall

In current practice anticipated reinforcing tension is computed assuming that each layer of reinforcement must resist tensile forces caused by lateral earth pressures acting on a tributary area, Eq. 7.3.

$$T_{req} = K_1 \gamma \; z \, S_h S_v \tag{7.3}$$

where:

T_{req} = required reinforcing tensile capacity,

K_1 = lateral earth pressure coefficient of the soil within the reinforced zone,

γ = soil unit weight,

z = depth below top of wall to layer being evaluated,

S_h = horizontal spacing of reinforcement,

S_v = vertical spacing of reinforcement layers.

The lateral earth pressure coefficient in Eq. 7.3 depends upon the extensibility of the reinforcing material and is selected from empirically developed charts similar to that presented in Figure 3.11 (Christopher, et al., 1990) or simply assumed to be equal to K_a or K_o. Attempts to predict strains in the reinforcement have been made by dividing the computed tensile force by the modulus for the selected reinforcement (see Section 3.4.2). No consideration or adjustments are made to account for adjacent layers of reinforced soil or boundary conditions.

Failure to account for boundary conditions may partially explain why this method of predicting reinforcing strains has proven unsuccessful. Figures 7.10 to 7.12 and 7.14 provide evidence that strains within an elastic body may be significantly affected by the boundary conditions. For any depth the magnitude of maximum horizontal strains increased with decreasing contact friction, with decreasing L/H, and with increasing

applied load behind the wall. For any given L/H and applied lateral load the influence of boundary rigidity was found to have the least influence on horizontal strain within the wall, Figure 7.11, while changes in the L/H ratio or lateral loading significantly affected the maximum horizontal strains, Figures 7.10 and 7.12. These influences are not dealt with in current design procedures. However, failure to explicitly address these factors may not be a cause for immediate concern because:

1) The chart for selection of K_1 (Figure 3.11) has been non-dimensionalized as a function of soil and reinforcement properties, and the retained soil is typically the same material as that used in the wall itself. It is possible the effect of lateral loading may be implicitly, if unintentionally, incorporated in the chart; and

2) The vast majority of walls already constructed have L/H ratios of 0.6 or greater. The influence on the magnitude of maximum horizontal strains, for a given loading condition, did not appear to be as greatly influenced for these L/H ratios as it was for smaller L/H ratios.

7.3.3.2 Horizontal Strains Near the Top of the Wall

While the magnitudes of maximum horizontal strains near the base of the wall were significantly influenced by foundation rigidity, applied load, and the L/H ratio, the maximum horizontal strains in the upper portion of the wall were relatively unaffected by these factors, Figures 7.10 to 7.12. Although a reduction in the influence of the boundary conditions should be expected as the distance from boundaries increases, the convergence of the curves may also be related to the horizontal stresses that develop between elements in this portion of the wall, Figures 7.15 and 7.16.

Goodman and Brown (1963) demonstrated for an infinite quarterspace that the horizontal and shear stresses between adjacent elements would equal zero. These stresses would also equal zero if, treating reinforced soil as a composite material, all of the horizontal strain in the reinforcing of a unit element was due to the weight of the

overlying soil. The wall considered for this analysis (Figure 7.3) had finite dimensions, L and H, and horizontal tension developed in the upper layers of the elastic body, Figure 7.15. This tension between composite elements results in greater horizontal strain than that which would occur if lateral strain was due solely to the Poisson effect caused by overburden pressures. The magnitude of horizontal tensile stresses between elements in the upper portion of the wall was also influenced by application of loads behind the wall, with the greatest tension occurring when no load was applied. Increased magnitude of applied load decreased the tensile forces between elements.

This observation may provide partial explanation for the larger lateral earth pressure values recommended for reinforced soil wall design in the upper regions of walls, Figure 3.11. Charts of this type were developed by measuring strain induced in instrumented full scale walls, or computed in FEM studies, and back calculating the lateral earth pressure, K_l, using an equation similar to Eq. 7.3. K_l is thus an "apparent" lateral pressure, as the actual pressures have not been measured or computed. Some studies, typically those involving inextensible reinforcements, have found the apparent lateral earth pressure near the top of the wall to be greater than either K_a or K_o (Anderson, et al., 1986, Adib, 1988; Schmertmann, et al., 1989). The reason for this larger lateral earth pressure has sometimes been attributed to locked in compaction stresses (Adib, 1988; Zornberg and Mitchell, 1993; Ehrlich and Mitchell, 1994). Ho and Rowe (1993), in a finite element analysis of a reinforced earth wall having extensible reinforcements, also reported the back-calculated apparent lateral earth pressure to be greater than K_a. However, compaction effects had not been incorporated into their analysis. They suggested that the apparently large lateral earth pressure may be attributable to something other than compaction, such as interaction between the soil, the reinforcement, and the wall facing. The horizontal tensile forces which developed in the elements simply due to the nature of the structure being evaluated may also be a contributing factor. The findings of Ho and Rowe (1993) and the occurrence of horizontal tensile stresses that cannot be attributed to overburden pressures indicate that the back-calculated "apparent"

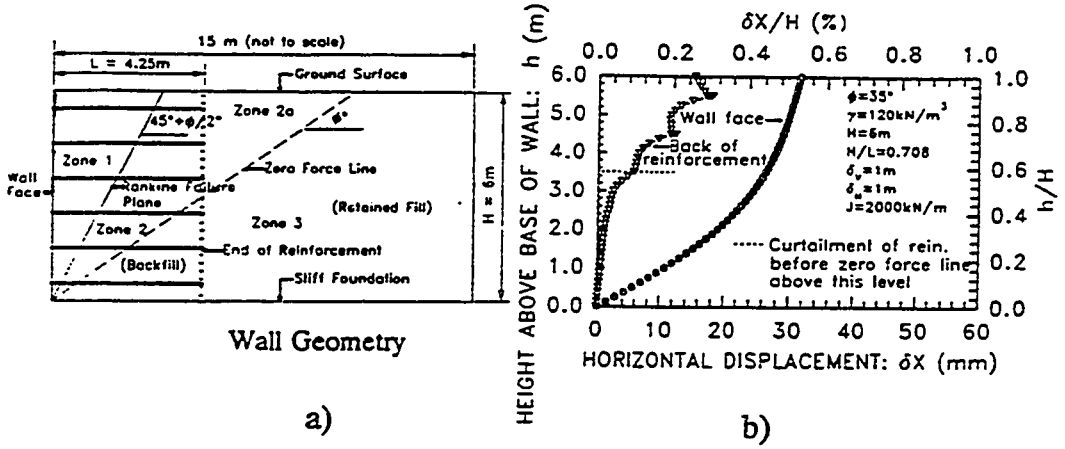

Figure 7.18: Lateral displacement of GRS wall: a) Wall geometry; b) Horizontal deformation of wall face and at back of reinforced soil mass (after Ho and Rowe, 1993).

lateral earth pressures are just that -- apparent, and should not be used as indicators of the true stress state of the soil.

7.3.3.3 Locus of Maximum Horizontal Strain

Determination of the locus of maximum reinforcing tension has been the subject of much discussion in the literature. This curve is the critical surface defining the location of probable failure of the reinforced soil; it has occasionally been referred to as a slip plane. Studies by Mitchell and Villet (1987), Anderson, et al. (1987), Christopher, et al. (1990), and Bathurst, et al. (1992) have shown that the locus of points approximates a log spiral or, for design purposes, a bilinear curve, Figure 7.19. A log spiral or bilinear curve could also effectively approximate the curves presented in Figure 7.13. This similarity suggests that reinforced soil walls may be more closely approximated by an elastic composite than has previously been acknowledged. For inextensible reinforcements, where maximum strains are limited to less than the yield strain of steel,

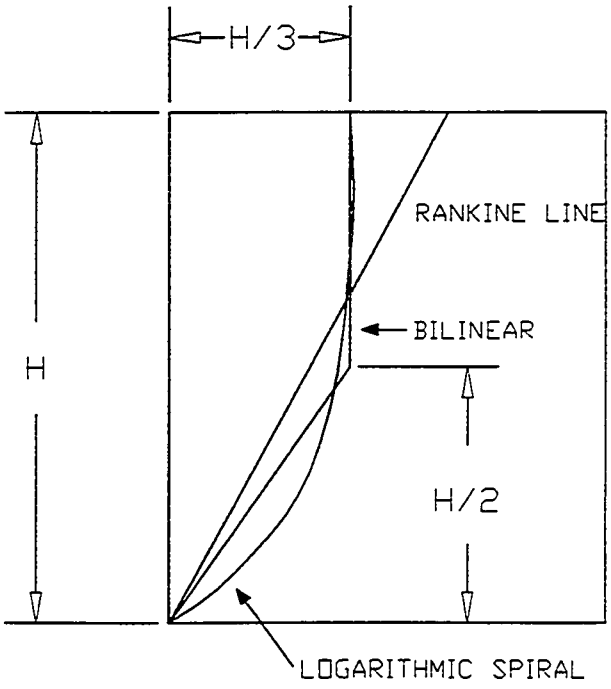

Figure 7.19: Methods of predicting locus of maximum horizontal strain.

this may be especially true. The locus of maximum horizontal strain predicted for elastic materials, Figure 7.13, is very similar to the locus of maximum strains which was recorded in a 17 m high welded wire reinforced soil wall, Figure 7.20 (Anderson, et al., 1987).

Although not a perfect match, some authors (e.g., Allen, et al., 1992; Figure 3.12) have used the Rankine failure plane to approximate the locus of maximum horizontal strain. While this may be true in some cases, this study and an understanding of soil behavior leads to the conclusion that the similarity is coincidental for the following reasons:

a) The analysis presented in this chapter assumed elastic, not plastic, material properties; yet the locus of maximum horizontal strain observed is similar to that observed in reinforced earth walls.

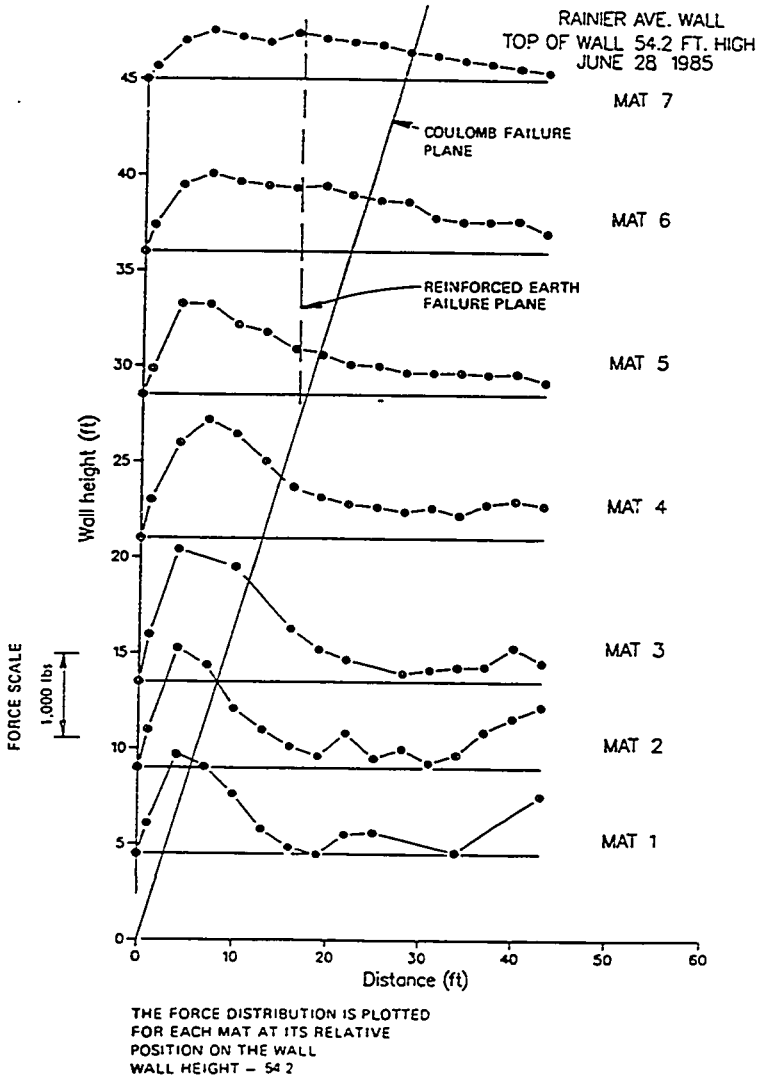

Figure 7.20: Measured strain distribution in 17 m high welded wire mesh reinforced soil wall (after Anderson, et al., 1987).

b) It is generally acknowledged that plane strain conditions prevail in reinforced soil retaining walls. It is also known that the plane strain angle of internal friction for cohesionless soil is greater than that obtained in cylindrical triaxial tests (Cornforth, 1964; Lee, 1970; Marachi, et al., 1981). However, the friction angle used to establish the Rankine plane is rarely, if ever, adjusted to account for plane strain conditions, nor are the friction angles adjusted to account for the low lateral earth pressures actually existing in the walls.

c) Rankine's (1857) theory for lateral earth pressure was developed for the case of a mass composed of separate grains whose stability "arises wholly from the mutual friction of those grains, and not from any adhesion amongst them." However, studies have shown that soil reinforcement has the effect of introducing an "apparent" cohesion to the soil (Schlosser and Long, 1972; Yang and Singh, 1974; Chapter 6 of this dissertation). This apparent cohesion is a direct violation of Rankine's most basic assumption.

d) Rankine (1857) showed that failure of a purely frictional material would occur on the plane in the mass where the induced shear stresses overcome the frictional resistance provided by normal stresses on that plane. The failure is a shear stress induced failure and is unrelated to horizontal strains. For Rankine's assumptions, strains in the direction of minor principal stress would be uniform. For the case of an elastic body subject to deformation under its own weight horizontal strains are not uniform. Furthermore, the locus of maximum horizontal strains, along which the *reinforcing* is most likely to fail, does not coincide with the locus of maximum shear strains, along which the *soil* is most likely to fail, Figure 7.13.

Therefore, the practice of attempting to approximate the location of maximum horizontal strains within a reinforced soil mass with a Rankine line should be discontinued. This is an inappropriate application of Rankine's theory, and it is both erroneous and misleading. Instead, reliance should be placed on appropriate empirically,

theoretically, or numerically developed relations. Additional research may be required to obtain relations which properly consider the effect of the L/H ratio of the wall, the properties of the soil and reinforcement, the foundation conditions, and the loads applied to the wall on the locus of maximum strain.

7.4 Application to Reinforced Soil Wall Design

It has been observed, in this study and by others (e.g., Christopher, et al., 1990; Allen, et al., 1992), that the majority of reinforced soil wall deformation occurs during wall construction and depends greatly on the L/H ratio. That deformation occurs during construction makes sense since that is when the loads get applied to the wall. It has been suggested that unsightly deformations at the wall face may be eliminated by compensating for anticipated final deformations during the construction process (Christopher, et al. 1990). If the magnitude of final deformations may be predicted and compensated for during construction any stable wall, regardless of L/H ratio, could be constructed to the desired face batter. Making use of construction experience, and analyses similar to that presented above, charts could be constructed which indicate how much the face location must be adjusted during placement of each layer. Because of the interaction of each layer, boundary effects, body forces, applied loads, and the influence of material properties and structure dimensions, the finite element method must be utilized to construct these charts.

Such a chart has been constructed for retained soil lateral earth pressure coefficients, K_r, of 0.17 ($\phi = 45^o$) and 0.27 ($\phi = 35^o$) for a wall with L/H ratio of 0.6, Figure 7.21. The setback at which the next layer of reinforcing must be placed is computed by subtracting the ultimate computed horizontal position of the wall face at that elevation predicted from an FEM analysis from its position when it was first placed. The computed setback is the absolute horizontal distance behind the desired final face location for that layer. Using this technique, horizontal displacements which occur after placement of that layer, due to overlying layers and loads applied to the structure, could

be compensated for. An example of the progression of face displacement with increasing height during construction for a wall where this compensation is not made is shown in Figure 7.22a, where "h" corresponds to the vertical distance from the toe of the wall. The uppermost point on each line in the figure corresponds to the height of the wall associated with that displaced shape. The progression of face displacement when deformations are compensated for in this same wall are presented in Figure 7.22b. The face of the wall after construction is vertical instead of outward leaning. Charts for any L/H and K_r may be constructed using this same technique. When constructing similar charts for actual use, material properties that more closely resemble the materials to be used for constructing the particular wall of interest should be used.

In non-critical, temporary installations where deformation of the face is not a concern, the relatively small displacements which may be expected for lower L/H ratios (Table 7.1) may not adversely affect the performance of the walls, thus eliminating the need to compensate for them during construction. In these situations and when final deformations may be compensated for, reduction of the length of the reinforcement has the potential for substantial material and cost savings, especially on large projects. Proper interaction of the reinforcing and soil must be ensured to avoid a pull-out failure and external stability must still be verified.

Decreasing the L/H ratio may increase the magnitude of maximum horizontal strain in a structure, Figure 7.10. As was stated earlier, the charts similar to Figure 3.11, for determining the lateral earth pressure coefficient to be used in Eq. 7.3, do not consider the L/H ratio and were developed empirically based on walls constructed using current design procedures, which typically have L/H ratios near 0.7. Thus, while this analysis indicates that the reinforcement length could be decreased, it may be necessary to compensate for the expected increased stress levels by decreasing the vertical spacing of reinforcement layers or increasing the reinforcing strength to obtain a structure which behaves satisfactorily. Of course, before dramatic decreases in the L/H ratio or alternate

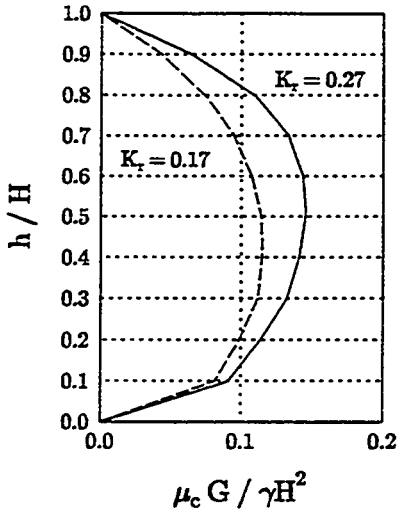

Figure 7.21: Chart for determining horizontal setback distance, μ_c, for L/H = 0.6, μ_b=∞.

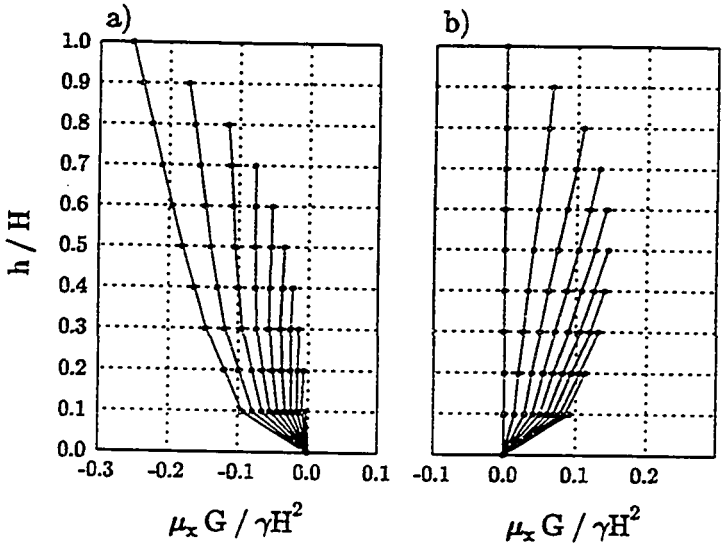

Figure 7.22: Displaced shape of wall face during construction, L/H = 0.6, μ_b = ∞, K_r = 0.27: a) Without compensation for deformations, b) With compensation for deformations.

reinforcing schemes are adopted, additional analyses using more appropriate material models and proper field testing are required.

Actual reinforced walls have nonlinear stress-strain properties, whereas this study was performed using linear elastic material properties. For nonlinear materials, with modulus decreasing with increasing strain, the lower portion of the walls could be expected to strain more than would linearly elastic materials having the same initial modulus under the same stress conditions. This could result in greater horizontal tensile stresses developing between elements near the top of the wall. However, this potential increase in strains may be partially offset by the increase in modulus associated with the increase in confining pressure which occurs due to interaction of adjacent elements as the wall is constructed.

Although walls designed to date have been shown to behave adequately, some of this success may be attributable to the substantial factors of safety which are applied to the reinforcement and soil parameters during design. This study found that wall dimensions and boundary conditions influence horizontal strains in the lower portion of walls and that there is a tendency for horizontal tensile forces to develop in the upper portion of walls. These two factors are not considered in current design procedures. Therefore, existing design procedures should not be applied to walls having substantially different dimensions and loading conditions than those which were used to develop the design procedure.

7.5 Summary

The deformed shapes and distribution of horizontal strains observed for elastic bodies evaluated in this study were shown to be similar to those observed in reinforced walls and in more rigorous FEM studies. The occurrence of these similarities were used as justification for extending the discussion of results obtained from the elastic analysis to the case of reinforced soil retaining walls. The conclusions reached through this study may be summarized:

7.5.1 Wall Deformations

a. Self weight is a major contributor to displacements and strains for larger L/H ratios.

b. Total displacement at the top of the wall is inversely related to $(L/H)^3$. As L/H decreases the contribution to total displacement due to bending forces increases dramatically.

c. The deformation is affected by the applied lateral loading, a factor which is not incorporated in the design chart presented by Christopher, et al., (1990), Figure 3.16.

d. The magnitude of expected displacement, based upon previously published design charts, are small relative to the wall height (less then 3%) for the L/H ratios investigated.

e. The results of this study agreed with the findings of others that wall deformation due to soil weight and the retained soil can be expected to occur during construction.

7.5.2 Reinforcing Strains

a. The magnitude of peak horizontal strains in the lower 70% of the walls are influenced by the L/H ratio, boundary conditions, and applied lateral load.

b. The horizontal strains near the top of the walls are nearly independent of the boundary conditions and the L/H ratio.

c. Tension developed between adjacent elements near the top of the walls. This was suggested as a factor which may contribute to the relatively large "apparent" lateral earth pressures back-calculated from instrumented case histories.

7.5.3 Location of Maximum Horizontal Strains

a) The Rankine failure plane should not be used for prediction of the location of maximum horizontal strain in the reinforcing. This plane was developed and defined for an entirely different purpose and is unrelated to horizontal strains in the reinforced soil mass.

7.5.4 Wall Design

a) Some of the mechanisms which have been shown to affect performance are not explicitly addressed in the current procedures. Caution is advised if attempts are made to apply existing empirically developed design aids to situations dissimilar to those from which they were developed.

b) Additional research and analysis should be performed prior to, or as part of, any program in which reinforced soil retaining walls are designed less conservatively than would be the case using current methods.

CHAPTER 8
USING THE FINDINGS OF THIS PROJECT

8.1 Applicability to the Rainier Avenue Wall

8.1.1 Introduction

This project was initiated by the Washington State Department of Transportation (WSDOT) to advance the understanding of geosynthetic reinforced soil and geosynthetic reinforced retaining walls. WSDOT was motivated to sponsor this project by the potential economic savings that could be realized by using GRS walls as permanent structures. Furthermore, GRS wall designs were recognized as being overly conservative. Additional savings, even in temporary applications, could be realized if the safety factors used in GRS wall design procedures could be decreased. The inability to accurately predict reinforcing strains and wall deformations using current design procedures and the potential for geosynthetic reinforcements to creep under sustained loading are two factors preventing GRS walls from being used in permanent applications. It was the need to understand these factors which lead to the investigation into the behavior of geosynthetics, geosynthetic reinforced soil, and GRS walls presented in the previous three chapters.

This was not the first GRS research wall project in which WSDOT has been involved. In the late 1980's a series of GRS walls were constructed at the intersection of Interstate 90 and Rainier Avenue in Seattle, Washington to preload bridge abutment foundations. One of these walls exceeded 12.6 meters in height and supported a 5.3 meter high 2:1 sloping surcharge, Figure 8.1. Because of its unprecedented height and location next to a busy intersection this wall was heavily instrumented to monitor its behavior. Since it was being monitored and was only a temporary structure, WSDOT applied lower safety factors than design procedures dictated for permanent GRS structures. Despite its height, the sloping surcharge, and the reduced safety factors the wall experienced little deformation and measured reinforcing strains remained below 1%,

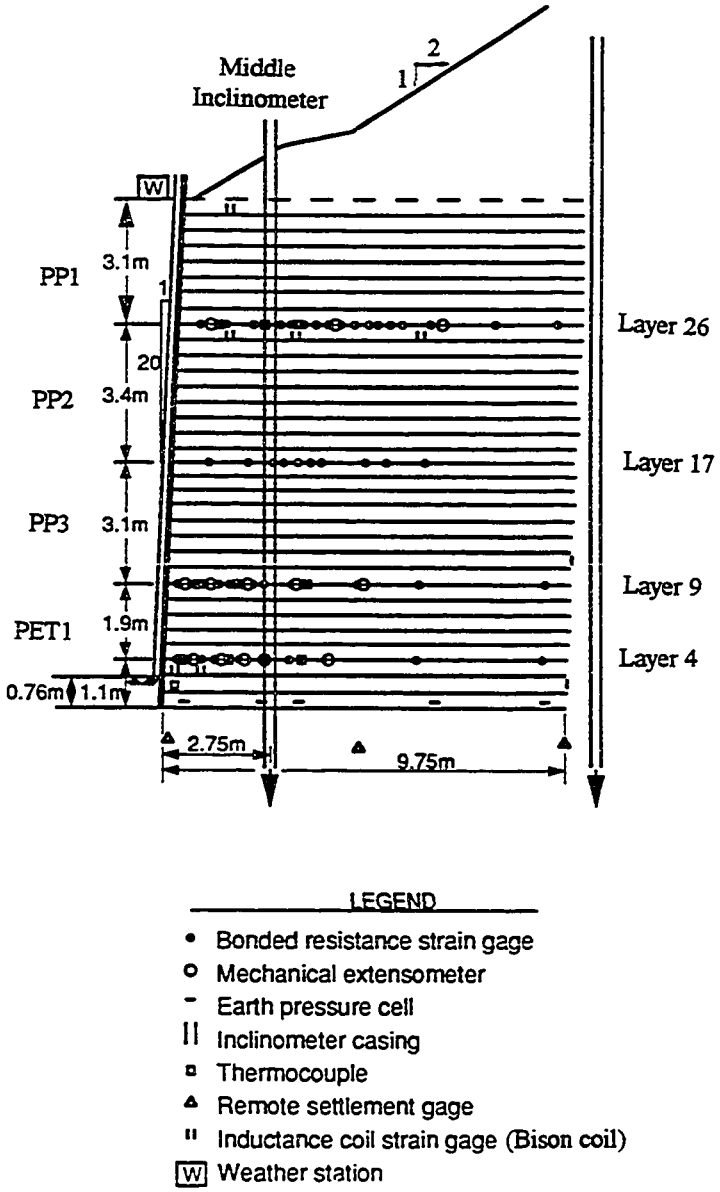

Figure 8.1: Vertical cross section of Rainier Avenue wall showing reinforcement and instrumentation (after Allen, et al., 1992).

Figure 8.2. The results of the monitoring program for the Rainier Avenue wall have been reported by Christopher, et al. (1991), Holtz, et al. (1991), and Allen, et al. (1992).

Since the deformations and strains measured in the Rainier Avenue wall were much less than had been expected it was realized that the behavior of GRS walls was not well understood, which led to the project reported on in this dissertation. To take advantage of the Rainier Avenue wall instrumentation program and to permit comparison of the full scale response with laboratory measured material behavior, the geotextile reinforcements and the soil used in the wall were included in the testing program. The remainder of this section will discuss the significance of the findings of the laboratory testing program (Chapters 5 and 6) and the FEM study (Chapter 7) in relation to the observed behavior of the Rainier Avenue wall. Specifics on the Rainier Avenue wall design, construction, materials and observed behavior included in this discussion have been obtained from Christopher, et al. (1991), STS (1990), Holtz, et al. (1991), and Allen, et al. (1992). In the discussion these documents will be lumped together and referred to as the Rainier Wall Papers.

8.1.2 Soil Properties

A soil friction angle of 36° and unit weight of 20.4 kN/m^3 were assumed for the design of the Rainier Avenue wall. Triaxial tests on the gravelly sand actually used in the wall indicated friction angles from 43° to 47° and field densities of 21.1 kN/m^3. These triaxial tests were conducted at lateral confining pressures ranging from 69 kPa to over 300 kPa. These pressures were intended to simulate the pressures anticipated in the wall and corresponded to the approximate overburden pressure at the uppermost and lowermost instrumented geotextile layer in the wall, respectively. However, because the lateral earth pressure coefficient, K, for cohesionless soils (i.e., the ratio of lateral stress to overburden stress, σ_3/σ_1) was less than 1.0, the lateral confining pressure experienced by the soil at any depth in the wall should be less than the overburden pressures. More

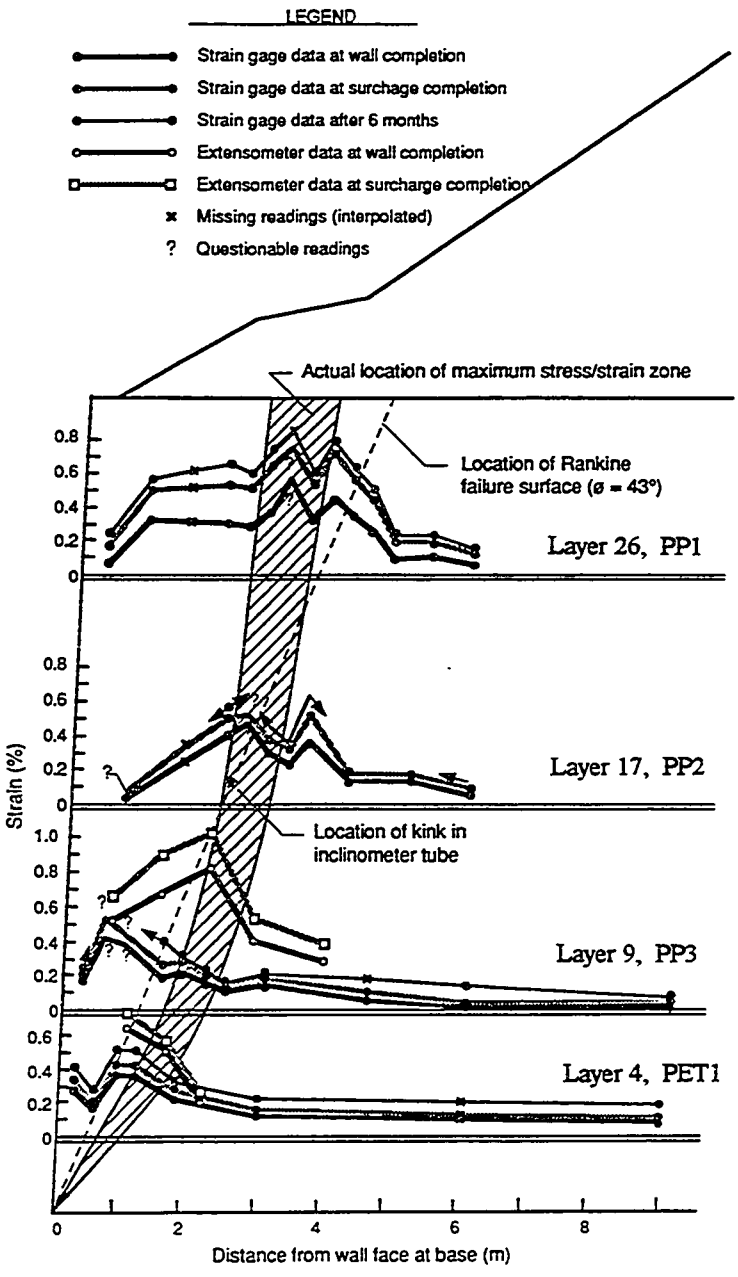

Figure 8.2: Distribution of strains in each instrumented layer at various times, Rainier Avenue wall (after Allen, et al., 1992).

appropriate confining pressures to use in these tests would have been on the order of the at rest, K_o, and active, K_a, lateral earth pressures associated with these *overburden* stresses. Assuming $\phi = 43^\circ$ and applying Eqs. 8.1 and 8.2 (Holtz and Kovacs, 1981) with overburden pressures of 70 kPa to 300 kPa the confining pressures to be used in these tests would have been in the range 22 kPa to 95 kPa, for K_o conditions, and 13 kPa to 57 kPa, for K_a conditions. The soil friction angle for these confining pressures would be between 50° and 46°, Figure 6.5.

$$K_o = 1 - \sin\phi \tag{8.1}$$

$$K_a = \frac{1-\sin\phi}{1+\sin\phi} \tag{8.2}$$

The lower friction angles also would have overpredicted the lateral earth pressures to which the soil would be subjected in the wall. Because plane strain conditions prevail in GRS walls and plane strain friction angles are larger than triaxial friction angles, anticipated lateral earth pressures should also decrease. For the soil used in the Rainier Avenue wall the plane strain friction angle at these low confining pressures was between 63° and 53°, Figure 6.5. If the plane strain friction angle developed by the soil in the wall was on the order of 55° instead of the 36° assumed in the design or the 43° determined from triaxial tests, the lateral earth pressure would be reduced by 73% and 47%, respectively, Figure 8.3. These are substantial reductions in the lateral earth pressure which must be resisted by the reinforcing and may partially explain the low lateral strains measured in the Rainier Wall.

The 43° friction angle obtained from triaxial tests at 300 kPa confining pressure was used to define the Rankine failure line for the Rainier Avenue wall. This line has been superposed on a plot of measured reinforcing strains in Figure 8.2. Since this friction angle was determined from triaxial tests and since Rankine's assumption of no cohesive interaction in the soil mass has been violated (see Section 7.3.3.3) the apparent correlation between the "kink" in the inclinometer tube with the "theoretical failure

plane" must be assumed coincidental. Furthermore, if the "kink" was related to the Rankine failure plane, when the inclinometer passed from the region behind the plane into the "failure wedge", the rate of horizontal displacement would have increased with increasing wall height and would have increased in relative importance with increasing applied loads. This action would have resulted from the greater motion of the failure wedge compared to the region behind the wedge. Instead, the inclinometer readings indicated a decrease in horizontal displacement associated with passing through the failure plane, Figure 8.4. No explanation for this kink in the inclinometer can be determined from the evaluations reported in Chapters 6 or 7. It is possible that it was inadvertently induced in the inclinometer during construction of the wall.

8.1.3 Geotextile Modulus

One of the factors suggested in the Rainier Wall Papers as possibly contributing to the very low strains measured in the Rainier Avenue wall was an assumed increase in modulus of geotextiles when confined in soil above the in-isolation modulus. This conclusion was partially based upon reports of an increase in modulus due to confinement in soil for some geotextiles (see Section 2.1.3). Zornberg and Mitchell (1993, 1994) in a finite element analysis of the Rainier Avenue wall also concluded the modulus of the reinforcing must have increased due to confinement in the soil. However, the UCD testing program (Chapter 6) determined the woven geotextiles were not influenced by confinement in soil. In fact, it was found that the apparent modulus of the woven geotextiles were probably lower in the Rainier Avenue wall than was predicted from the ASTM D 4595 standard wide width test. In the test program a reduction in strain rate from 10%/min. to 0.01%/min. resulted in a corresponding reduction in the apparent modulus for the polyester and polypropylene geotextiles of approximately 20% and 50%, respectively, Figure 6.32. In the Rainier Avenue wall the average strain rate for the geotextiles was on the order of 10^{-6} %/min., Table 8.1. The apparent modulus for the geotextiles at these loading rates would be even less than those determined in the testing

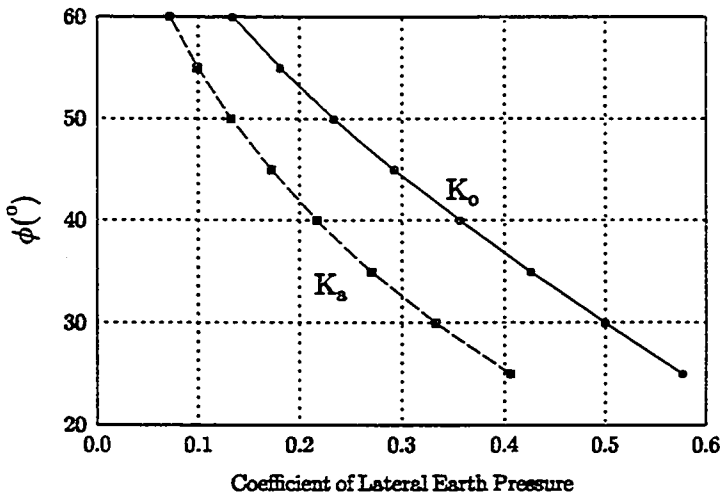

Figure 8.3: Lateral earth pressure coefficients for various friction angles.

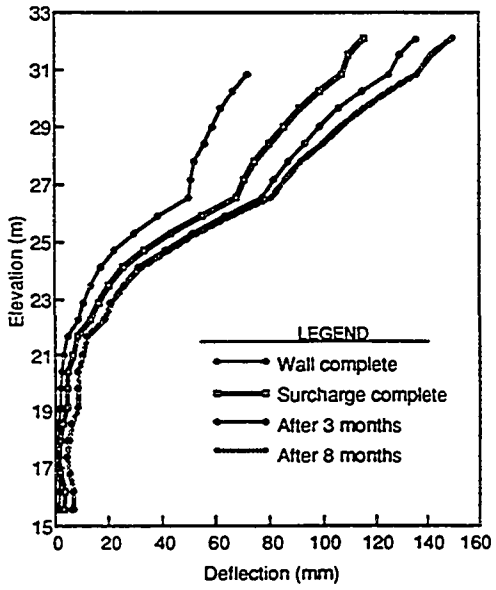

Figure 8.4: Deflection perpendicular to the Rainier Avenue wall face obtained from the inclinometer in the middle of the reinforced backfill. Base of wall is at 19.7 m (after Allen, et al., 1992).

Table 8.1: Approximate strain rates at location of peak strain and corresponding geotextile modulus as percentage of ASTM D 4595 modulus for Rainier Avenue wall (STS, 1990; Allen, et al., 1992; Gallagher, 1995).

Reinf. No.	Layer No.	No. Days	Total Strain (%)	Strain Rate (%/min)	Approx. % of ASTM D 4595 Modulus (see Figure 5.7)
4	4	56	0.40	0.5×10^{-6}	70% - 80%
3	9	43	0.55	0.9×10^{-6}	30% - 40%
2	17	26	0.60	1.6×10^{-6}	30% - 40%
1	26	13	0.70	3.7×10^{-6}	30% - 40%

program presented in Chapters 5 and 6 if the data in Figure 5.7 were projected to these lower rates. This reduction in modulus should result in an increase in horizontal strain in the wall, not a decrease, and therefore cannot be a factor contributing to the low strains observed in the Rainier Avenue wall.

8.1.4 Geotextile Creep

In the Rainier Avenue wall the polypropylene geotextiles in the upper portions of the wall experienced more creep than those near the bottom of the wall, Figure 8.2. The Rainier Wall Papers attribute the increased levels of creep which occurred in the upper portions of the wall to the reduced confining pressures acting on the geotextiles and the increased stress level in the upper geotextiles. The confining pressure argument can be discarded for the reasons discussed in Section 8.1.3. The conclusion that increased stress levels, associated with higher strains, would result in increased creep strains is supported by the in-isolation creep tests and the UCD tests. Reinforcings strained to greater levels at initiation of creep testing experienced greater creep strains.

The testing program also determined that creep was influenced by the strain rate at which the reinforcing was loaded prior to suspension of loading. Specimens loaded quickly experienced more creep, which occurred more rapidly, than those that were

loaded more slowly. This may also be a factor in the greater creep recorded in the upper layers of reinforcement of the Rainier Avenue wall where Layers 17 and 26 were initially strained 2 and 4 times faster than Layer 9, respectively, Table 8.1. However, this possibility is not supported by the data recorded in the Rainier Avenue wall where all three layers experienced similar creep strains immediately after completion of the surcharge fill, Figure 8.5. It is during this initial period that the majority of total creep should take place and during which creep should occur the fastest. This is also the time period during which the effect of different stress levels in the reinforcings and the different initial strain rates should be the most obvious. These patterns of creep strain development were not observed in the Rainier Avenue wall. The creep strains in the polypropylene reinforcements were nearly identical, despite different initial strain rates and total strain, during the first 22 days after completion of the surcharge. The creep rate was then increased substantially for the next 100 days after which it began to level off. Thus, while initial strain rate was shown to influence creep in the laboratory tests, an increase in creep with increasing initial strain rate cannot conclusively be identified as a factor which contributed to the different magnitudes of creep in the Rainier Avenue wall. As was concluded in the Rainier Wall Papers, the difference in stress levels in the polypropylene geotextiles is most likely responsible for the different creep strains recorded.

This does not explain why the creep strain measured in the high strength polyester geotextile (Reinforcing PET1, Layer 4) was of the same order of magnitude as that measured in the weakest polypropylene geotextile (Reinforcing PP2, Layer 26). The results of the laboratory test program suggest the polyester geotextile should have experienced the smallest creep strains since it was determined to have been the least susceptible to creep, it was strained significantly slower than any of the other geotextiles, and the total strain in the polyester was lower than in the other reinforcings, Table 8.1. The research program reported in this dissertation provides no explanation for this apparent anomaly based solely on the creep test results. One contributing factor may be

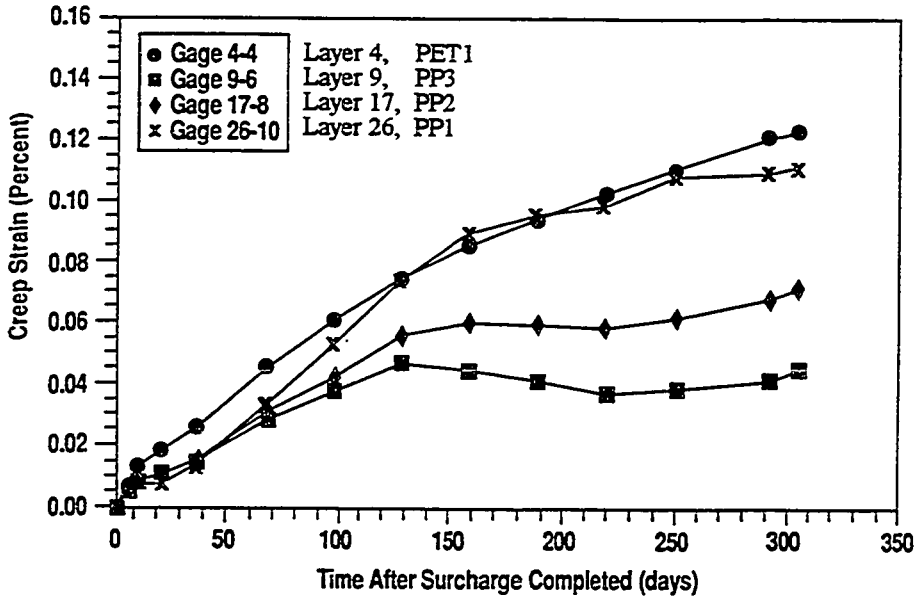

Figure 8.5: Geotextile creep after surcharge construction as measured by strain gages, Rainier Avenue wall (after Allen, et al., 1992).

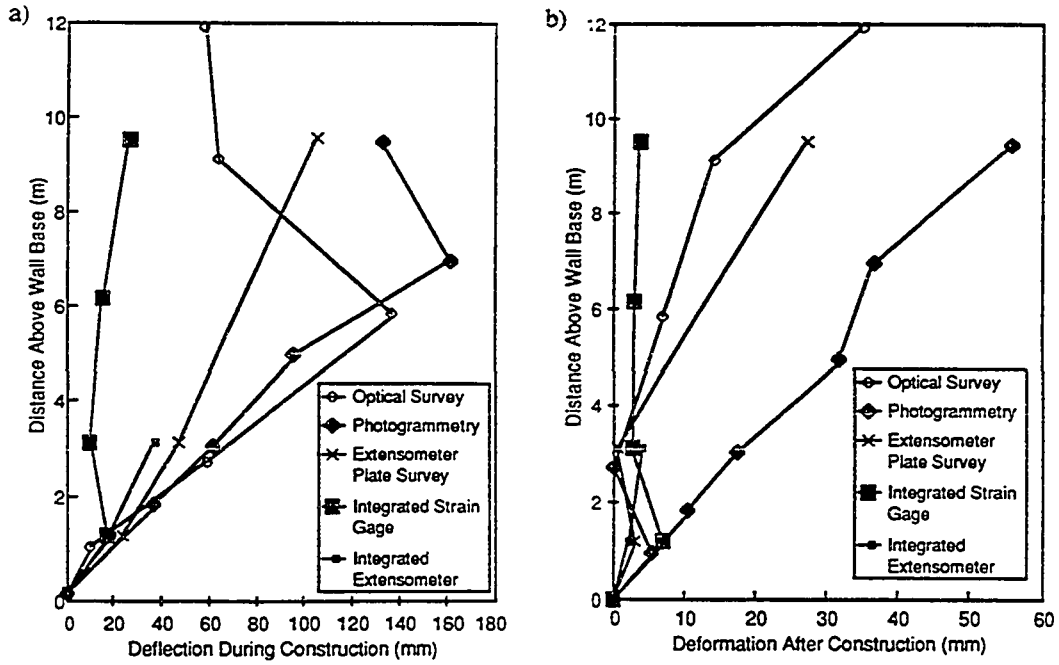

Figure 8.6: Rainier Avenue wall face deformation determined from various methods: a) during construction, b) after construction (photogrammetry data void for post construction period) (after Allen, et al., 1992).

the proximity of reinforcing layer 4 to the stress concentration at the wall toe, Figure 7.1. At this location slight changes in strains would likely cause greater redistribution of energy between adjacent layers than would slight changes in strains in layers in the upper portions of the wall.

An additional contributing factor to the relatively large strain recorded in the polyester reinforcing may be related to soil stress state. The two Bison inductance coil strain gages, used to measure soil strains, installed just below reinforcing Layer 4 (Figure 8.1) indicated the soil may have reached active conditions at this location. When preload construction was complete, the Bison gages indicated soil strains of 7.3% and 2.2% at the face and 0.75 meters behind the face, respectively. At the end of the instrumentation program, 10 months after completion of the preload, the soil strains at these locations had increased by 1.4% and 1.3%, respectively, Table 8.2. The UCD tests indicated that for these soil strains, additional strain would result in a decrease in the portion of total vertical load supported by the soil and a corresponding increase in the load supported by the reinforcing, Figure 6.14. This increase in tensile load in the polyester geotextile, in addition to creep, may have contributed to the total post construction reinforcing strain.

The response of the Bison coils located 5.8 meters and 1.2 meters from the wall face at Layers 26 and 32, respectively, are in agreement with this argument. At completion of surcharge construction the Bison coil at Layer 26 indicated 1.2% strain in the soil. This gage was not working 10 months later and no final soil strain data were reported at this location. At Layer 32 the Bison coil indicated soil strains increased from 0.2% to 1.1% after completion of the preload. At these low soil strains when reinforced with Reinforcement PP1 the soil may not have reached an active state and additional strain would result in additional load transfer to the soil, not to the geotextile, Figure 6.14. Thus, additional strains measured in the polypropylene geotextiles can probably be attributed to creep of the reinforcing and not changing load conditions.

Table 8.2: Summary of Bison magnetic coil instrumentation data (after STS, 1990).

Gage Location	Date of Measurement	Fill Height (m)	% Soil Strain
Layer 4 - at face	3/17/89	0.58	0.0
	3/23/89	2.10	0.7
	3/30/89	3.05	1.1
	4/20/89	6.10	2.3
	5/12/89	12.2	6.3
	5/31/89	Surcharge	7.3
	7/03/89	Surcharge	7.3
	3/12/90	Final	8.7
Layer 4 - 0.76 m from face	3/17/89	0.58	0.0
	3/23/89	2.10	0.4
	3/30/89	3.05	0.3
	4/20/89	6.10	1.0
	5/12/89	12.2	2.2
	5/31/89	Surcharge	2.2
	7/03/89	Surcharge	2.2
	3/12/90	Final	3.5
Layer 26 - 5.79 m from face	5/03/59	9.75	0.0
	5/12/89	12.2	1.2
	5/31/89	Surcharge	1.2
	7/03/89	Surcharge	1.2
	3/12/90	Final	—
Layer 32 - 1.22 m from face	5/12/89	12.2	0.0
	5/31/89	Surcharge	0.2
	7/03/89	Surcharge	0.3
	3/12/90	Final	1.1

8.1.5 Strain Gage Measurements

The strain gages attached to the geotextiles in the Rainier Avenue wall reported strains on the order of 0.5%. Strains measured by the extensometers were somewhat higher, on the order of 0.7% to 1.0%, Figure 8.2. The Rainier Wall Papers attribute the different strains reported by these two methods to the longer gage length of the extensometers. The extensometers could therefore incorporate strain occurring in the geotextile macrostructure, including local effects such as creases and folds. The in-isolation and UCD tests on these geotextiles, wherein strain gages were attached to the reinforcing, also tended to underpredict overall specimen strains, Figures 5.14 and 6.37. In these tests the specimens were pretensioned slightly and no creases or folds were

present. At low strains the strain gages readings were approximately 50% to 80% of the overall strain for the polypropylene geotextiles. The ratio of strain gage strain to overall strain increased with increasing strain. That is, the more the geotextile was strained the more closely the strains reported by the gages reflected the overall strains.

A study of the relationship between the incremental strain reported by the strain gages and the incremental overall strain showed the strain gages to consistently under report overall specimen strain as well as changes in overall strain, Figures 5.15 to 5.18 and 6.37 to 6.40. Attachment of the strain gages to the geotextiles affects their ability to measure true strain in the reinforcing and under reporting of overall strain should be expected. The cross weave in the geotextile and the resulting bumps in the gages as well as tightening of the weave during strain are suspected factors contributing to this phenomenon.

It appears that the strain gages used in the Rainier Avenue wall were working correctly and their data can be relied on for evaluating that wall. However, the strain gage readings should be adjusted upward by 25% to 100% since they underreport overall reinforcing strains. This underreporting of strains is likely due to the characteristic nature of using stain gages for measuring geotextile strains as well as the occurrence of creases and folds observed in the geotextile macrostructure in the Rainier Avenue wall.

8.1.6 Wall Deformation

Deformation of the Rainier Avenue wall increased with increasing height. This is in agreement with the discussion in Chapter 7 where it was determined that deformations increase with decreasing ratio of reinforcing length to wall height, L/H. For a wall with constant length reinforcement, as the wall increases in height during construction the L/H ratio decreases and deformation increases, Figures 7.22a and 8.4.

The analysis in Chapter 7 also explains why most deformations of the Rainier Avenue wall occurred during construction. It is during this period that loads are applied to the structure. Since loads were not increased after completion of the wall and

placement of the surcharge, deformations also should cease to increase. However, after surcharge completion, deformations did continue to increase, Figure 8.4. Approximately 7 mm of the total deformation at the top of the wall measured by the inclinometer in the middle of the wall can be attributed to horizontal motion of the inclinometer at the base of the wall and strains in the reinforcing. Since the majority of the horizontal displacements below elevation 23 m can be attributed to horizontal motion of the inclinometer, the remaining 27 mm of horizontal motion must be associated with additional bending or horizontal shear strain of the wall itself in the upper 9 m. This 27 mm of horizontal motion represents only 0.3% of the upper 9 m of wall. For this increase in deformations to occur the soil itself must have experienced some creep or the loads on the wall must have increased with time. These explanations are both possible since settlement of the foundation did occur, which could change the loads applied to the back of the wall, and the Bison coil strain gages recorded post construction horizontal soil strains on the order of 1%, Table 8.2. Since the in-isolation creep tests showed very little creep occurred at these very low strains (see Section 5.6 and Figure 5.13), and creep of the soil was not observed in UCD tests after geotextile creep ceased (see Section 6.4.3.1 and Figure 6.33a), increased loads on the wall are most likely responsible for the soil strains as well as the wall deformations.

The Rainier Wall Papers noted that the integrated strain gage measurements could not be correlated to the deformed shape of the wall itself, Figure 8.6. As discussed in Section 7.3.2, because the reinforcing strains relate only to deformations within the wall and do not include deformations of the wall itself, this lack of correlation should be expected.

8.2 Predicting Reinforced Soil Wall Deformations

8.2.1 Material Properties

The results of an investigation into the behavior of geosynthetic reinforcement, geosynthetic reinforced soil, and reinforced soil retaining walls have been presented in the previous three chapters. Because soil, geosynthetic reinforcement, and reinforced soil retaining wall behavior have been the subject of investigation for some time, there were few surprises. This research program did, however, reemphasize the importance of measuring geosynthetic and soil properties under the conditions to which they will be subjected. Failure to do so may lead to erroneous solutions or conclusions when these material properties are used in analysis of reinforced soil walls.

Plane strain soil properties should be used for designing and analyzing reinforced soil structures. The higher friction angle associated with plane strain conditions results in lower lateral earth pressures than would be obtained under triaxial conditions, Figures 6.7a and 8.3. Lower lateral pressures mean the reinforcing must resist smaller loads and would be expected to strain less than would be predicted using triaxial data. In addition to having a higher peak capacity under plane strain conditions, this capacity is reached at a lower strain than under triaxial conditions, increasing the initial modulus, Figure 6.7b. This increase in modulus would also result in lower lateral strains for a given vertical load prior to the soil reaching its peak strength. Therefore, the use of triaxial soil properties for the design and analysis of reinforced earth walls would overpredict lateral deformations and required reinforcement strengths.

The UCD test program also showed that it is not enough to simply obtain soil behavior from plane strain conducted at constant confining pressures. Laboratory shear tests on soils, whether cylindrical triaxial, cubical triaxial, or plane strain tests, have historically been conducted at constant confining pressures. For plane strain tests intended to determine reinforced soil behavior the increase in confining pressure with increasing lateral strain, which results from the tension induced in the reinforcing, must

also be simulated during testing. This change in confinement stress during strain affected soil dilation and caused the soil to behave differently than it would had constant confining pressure been maintained (see Section 6.4.1). This further highlights the importance of ensuring that plane strain tests simulate the stress and strain conditions to which the soil will be subjected in actual walls.

Advocating that plane strain tests be performed for determination of soil properties used for the design and analysis of reinforced soil walls presents a practical problem since plane strain test apparatus are not widely available. The scarcity of these devices is the primary reason triaxial soil properties are currently relied on. Some of the conservatism in current design procedures could be removed by adjusting triaxial soil friction angles using the relationships established by Lee (1970), Lade and Lee (1976) (see Eq. 6.1), or Hanna, et al., (1987). While adjustment of the friction angle may suffice for design, accurate analysis requires plane strain stress-strain data. There is, however, no method which permits the shape of the plane strain stress-strain curve to be predicted using triaxial stress-strain relations. Further research is required if such a procedure is to be developed.

The stress conditions to which nonwoven geotextile reinforcements will be subjected in reinforced soil walls should also be modeled when measuring their strength properties in laboratory tests. This is because the moduli of nonwoven geotextiles are sensitive to confining pressures (see Sections 2.1.3 and 6.4.2.1). Unfortunately, modeling field conditions is not easily done, as was demonstrated in the UCD tests. Lateral strain occurs as vertical loads on the reinforced soil are increased. This simultaneously increases the pressure acting normal to the plane of the geotextile, which results in an increase in the geotextile modulus. The geotextile "modulus" is constantly changing. UCD tests are just as unacceptable for measuring the modulus of nonwoven geotextiles as are in-soil load-elongation tests conducted at a single normal pressure. The relationship between normal pressure and modulus of the nonwoven geotextiles must be determined through a series of tests conducted at different normal pressures.

For woven geotextiles, which were shown to be unaffected by confining pressures but sensitive to strain rate (see Section 6.4.2.2), the relationship between strain rate and modulus must be established. A series of tests conducted at different strain rates is necessary to establish this relationship. Geotextile creep and the dependence of creep on the rate at which the geosynthetic is loaded further complicate characterization of geotextile *stress-strain* properties (see Section 6.4.2.2).

8.2.2 Deformation prediction

The dependence of soil properties on lateral confining stress, nonwoven geotextile modulus on normal pressure, and woven geotextile modulus on strain rate complicates the prediction of reinforced soil wall deformations. The stress conditions and strain rate are dependent on the wall dimensions and are constantly changing in each individual element within a reinforced soil wall during construction. Reinforced soil wall deformation prediction is further complicated by boundary conditions, foundation conditions, external loads, construction method, wall facing, and interaction of soil layers. An analysis method that can incorporate all of these factors is necessary if accurate predictions are to be performed. Of the deformation prediction techniques discussed in Section 3.3 the finite element method is the most promising for this application.

If all the factors that influence wall deformations are addressed, performing a FEM analysis could be a difficult and costly task. This would not be practical for most GRS walls. Only in situations where knowledge of the wall behavior was crucial, or in research applications, would such a program be considered. In other situations, where deformations must be controlled, it would probably be more cost effective to not perform this analysis but instead increase the strength or density of reinforcement, increase the ratio of reinforcement length to wall height, or closely monitor and control construction. However, even in these situations some means of estimating deformations would be

required so the wall could be constructed with the proper face batter and the effect of loads applied to the completed wall considered.

The analysis performed in Chapter 7 and the work by Christopher, et al. (1990), Christopher (1993) and Chew and Mitchell (1994) have shown that wall dimensions and loads applied are major factors influencing wall behavior. Wall deformations could be estimated, perhaps within acceptable limits, if soil and reinforcement properties used in the FEM analysis approximated the true conditions. This statement is supported by both the Christopher, et al (1990) chart, Figure 3.16, and the Chew and Mitchell (1994) procedure, Figure 3.17. Only small differences in absolute magnitude of deformations are predicted using these methods for walls constructed with extensible and inextensible reinforcements despite substantial differences in the composite reinforced soil properties, Table 7.1. Furthermore, these deformations occur during construction of the wall and could be compensated for at that time by relying on construction experience or a technique similar to that presented in Section 7.4.

Wall dimensions, applied loads, and soil and reinforcing properties are but a few of the factors known to influence wall deformations, Table 3.1. Foundation conditions, construction technique, facing materials, soil confinement, and reinforcement spacing also affect wall behavior. In Section 3.4.4 wall deformations predicted using the Christopher, et al. (1990) procedure, as modified by Christopher (1993), and the Chew and Mitchell (1994) procedure were compared with deformations measured in actual walls or computed from FEM analysis, Table 3.3. The Chew and Mitchell procedure tended to overpredict deformations to a greater degree than did the Christopher, et al. procedure, especially for high walls. Despite exclusion of a variety of factors that affect wall deformations, predictions made with either procedure were generally within -50% to +100% of the actual or computed deformation. If crude approximations of wall deformations are acceptable then use of the charts and procedures developed by Christopher, et al. (1990), Christopher (1993) and Chew and Mitchell (1994) are recommended.

Because of the substantial influence of geometry on deformations and the relatively small absolute magnitude of deformations recorded in reinforced soil walls, errors resulting from the use of these procedures may be tolerable. In applications where the actual soil and reinforcings are not selected until after the construction contract is awarded or where the expense of accurately measuring the plane strain soil behavior is not warranted, the use of techniques such as these may prove expedient, economical, and adequate. These procedures could also be expanded to include design charts similar to Figure 7.19 which would permit compensation for final deformations during construction.

The FEM analysis presented in Chapter 7 also determined that reinforcing strains were influenced by material properties, wall dimensions, foundation conditions and applied loads. Since in permanent structures strains must be maintained below the creep limit of geosynthetics and the yield strain of steel reinforcements, predicting reinforcing strains is certainly as important as deformation prediction. Without the ability to predict reinforcing strains the real benefits of having procedures which permit prediction of wall deformations, such as optimization of design and reduction of reinforcement quantities, cannot be realized. The Christopher (1993) and Chew and Mitchell (1994) procedures could be especially useful design tools if they could be expanded to predict reinforcing strains and include the effect of changes in geometry and boundary conditions on these strains. Perhaps charts similar to those presented in Figures 7.9 - 7.11 could be utilized.

In summary, if accurate predictions of deformations and strains in a geosynthetic reinforced soil retaining wall are to be made, the finite element method must be utilized. Proper determination and modeling of soil and reinforcing properties, boundary conditions, construction technique, facing material and applied loads is required. If approximate solutions are acceptable then using simplified FEM models, approximate material properties, or design charts for "typical" geosynthetic reinforced walls developed from empirical data or FEM analysis are recommended.

CHAPTER 9
SUMMARY, CONCLUSIONS, AND RECOMMENDATIONS FOR FURTHER STUDY

9.1 Summary

A program to investigate the behavior of geosynthetic reinforced soil and the deformation of geosynthetic reinforced soil retaining walls was undertaken. Since previous research had determined that geosynthetic strength properties could be modified by confinement in soil, a review of various apparatus designed for in-soil geosynthetic testing was conducted. The importance of properly modeling soil conditions and the mode of interaction of the geosynthetic and soil when measuring in-soil geosynthetic properties was stressed in the literature. Because none of the existing in-soil testing devices was determined to adequately model these conditions, a specially designed plane strain unit cell device (UCD) was manufactured for this project.

Reinforced soil specimens, having dimensions 100 mm long by 200 mm wide by 200 mm high, with the reinforcement located at midheight, were tested in the UCD. Soil response as well as geosynthetic load-elongation properties could be measured. The UCD is unique when compared with other unit cell devices described in the literature in that it is a load-controlled device, as opposed to strain rate-controlled, and it permits direct measurement of reinforcing tension. The UCD design limits lateral displacements to less than 8 mm and vertical pressures to less than 200 kPa. Although the UCD was constructed to allow lateral displacement in two opposing directions, movement was permitted in only one direction for the tests conducted for this dissertation. Limiting deformation of the soil specimen in this manner guaranteed that the maximum reinforcing tension would occur at one of the two clamps.

Two sands, two nonwoven needle-punched geotextiles, three polypropylene woven slit-film geotextiles, and a multi-filament polyester woven geotextile were the focus of the testing program. For comparison purposes a "soil" of uniformly sized steel

beads and a steel sheet reinforcement were used in some unit cell tests. Reinforced soil specimens were subjected to lateral confining pressures between 10 kPa and 100 kPa. After consolidation, vertical pressure was increased in 10 kPa increments each 30 seconds. Because loading was manually controlled this procedure resulted in a step loading of the specimen. The 10 kPa increment was actually applied over a period of approximately 10 seconds and the load was then held constant for 20 seconds before the next increase. Each specimen was loaded until the reinforcing failed, the lateral displacement limit of the UCD was reached, or the limits of the measurement devices were approached. The response of the composite under sustained loading was monitored in some tests by discontinuing loading and holding the vertical pressure constant prior to reaching one of the above conditions. Strain gages were attached to woven geotextile reinforcements in a few tests to permit the strain distribution along the specimen to be determined. A clear plexiglass plate was installed on one side of the specimen during these tests so soil particle movement within the specimen could also be monitored.

Because the UCD was a load control device with the load applied directly to the soil, neither the vertical nor horizontal (reinforcing) strain rate could be controlled. Evaluation of the UCD data determined that the woven geotextile modulus decreased with decreasing strain rate. Creep and stress relaxation of these geotextiles was also observed, even at small stress and strain levels. To further study these mechanisms a series of in-isolation wide width tests, conducted at strain rates from 10%/min to 0.01%/min, as well as short term creep tests on the woven geotextiles, were added to this research program. In-isolation wide width tests on the nonwoven geotextiles were also included because the changing normal pressure conditions that occurred in UCD tests complicated determination of the in-soil modulus for these reinforcements. The gage length of 200 mm wide nonwoven geotextile specimens was varied from 100 mm to 25 mm so that the modulus for a zero mm gage length, that would approximate the distance between adjacent soil grains, could be predicted.

In addition to testing geotextiles and reinforced soil specimens to evaluate their behavior, a study of the general behavior of reinforced soil walls was also performed. Wall behavior was known to be influenced by a number of factors including reinforcement and soil properties, foundation materials, construction techniques, and wall geometry. Attempts by other researchers to predict reinforced soil wall behavior using limit equilibrium techniques have proven unsuccessful. Design charts developed using the results of full scale and model wall tests, FEM analysis, and centrifuge modeling have been somewhat successful in predicting wall deformations. However, because of the large number of factors that could influence retaining wall behavior, the finite element method is advocated as the most appropriate for accurately predicting deformations of these structures.

A number of detailed parametric studies of reinforced soil wall behavior have been performed by other researchers. While these studies identified numerous factors that influence reinforced soil retaining wall deformations and strains, none looked at the general behavior that should be expected for these walls due to geometry, loading, and boundary conditions. That is, the expected structure response had not been separated from the influences of the soil and reinforcing. Utilizing linear elastic material properties and the finite element method, a study was made to identify which of the factors influencing wall deformations were functions of the problem being evaluated (i.e., a rectangular mass subjected to loads) and not functions of the specific soil and reinforcing properties assumed. Boundary conditions and applied loads were selected to simulate conditions to which a reinforced soil wall would be subjected. The deformations and strains of this FEM model were similar to those observed in actual reinforced soil walls and walls evaluated with a more realistic representation of the soil and reinforcing. These similarities were used as justification for extending the discussion of results obtained from the linear elastic FEM analysis to the case of reinforced soil retaining walls.

The findings of the laboratory tests and the FEM analysis were applied to the Rainier Avenue wall. Conclusions reached from earlier investigations of this wall were

evaluated. This research supported some of those conclusions and repudiated others. Recommendations for determining soil and geosynthetic properties and using them for predicting reinforced soil retaining wall deformations were also made. Only rough estimates of deformations could be made using existing design chart based deformation prediction procedures. The FEM method was determined to be the best means for accurately predicting deformations of individual walls.

9.2 Conclusions

From this research program it can be concluded:

a) Reinforcing increases cohesionless soil capacity by increasing the confining pressure acting on the soil.

b) Plane strain soil properties should be used for reinforced soil wall design and deformation prediction. Triaxial soil properties underpredict the strength and overpredict lateral deformations.

c) Soil dilation is an important variable influencing the response of geosynthetic reinforced soil. High modulus geotextile reinforcements were able to restrict dilation during deformation. Restriction of dilation modified the soil behavior and reduced the peak stress ratio attained by the soil.

d) Increases in effective confining pressure acting on cohesionless soil while it is being strained may result in a different soil response and peak stress ratio than would be obtained from tests in which a constant confining pressure is applied.

e) Soil capacity increased as tension developed in the reinforcing. The degree of improvement depended on the confining pressure, soil stress-strain behavior, reinforcing modulus, and spacing of the reinforcing. The relative importance of these factors varied with magnitude of lateral strain.

f) Reinforced soil specimens did not exhibit the sudden failure associated with unreinforced dense cohesionless soils. A more ductile response was observed.

g) Depending upon the confining pressure, soil stress-strain behavior, and reinforcement properties, reinforced soil specimens may or may not exhibit a peak capacity at the strains associated with the peak unreinforced soil capacity. Even in situations where a peak composite strength does occur at low strains, the high extensibility of the geosynthetics and the increase in tension in the reinforcement that accompanies increases in strain may be sufficient for the reinforced soil composite to regain or exceed that capacity at higher strains.

h) The moduli of the woven geotextiles were not influenced by confinement in soil. They were, however, affected by strain rate. The apparent modulus of the woven geotextiles decreased with decreasing strain rate. If field conditions simulate those modeled in the UCD test program, there is no need to perform confined load-elongation tests on these geotextiles.

i) The apparent modulus of the nonwoven geotextiles increased with confinement in soil and with decreased specimen gage length. The in-soil modulus determined from UCD tests could not be correlated to a "zero" gage length modulus predicted from in-air tests.

j) Creep and stress relaxation of the woven geotextiles occurred rapidly and at low strains. The rate of creep and stress relaxation decreased with time. The tendency for the woven geotextiles to creep was determined to be the cause of the reduction in apparent modulus that accompanied decreases in strain rate.

k) The magnitude and rate of creep are related to the strain rate before initiation of creep testing. Woven geotextile specimens loaded quickly exhibited more creep, that occurred more rapidly, than specimens loaded more slowly.

l) Strains measured with strain gages attached to the woven geotextiles under reported overall specimen strain. The degree of under reporting varied depending upon reinforcing type, strain gage length and type, and strain in the specimen.

m) Self weight of the material within reinforced soil walls results in wall deformation even if no loads are applied to the back of the wall.

n) Bending of the wall is responsible for the increase in deformations associated with decreases in the ratio of reinforcement length to wall height.

o) The majority of reinforced soil retaining wall deformations occur during construction, when the loads are applied.

p) Horizontal strains in the upper portion of the wall are a combination of strains due to overburden pressures plus strains due to tensile forces.

q) The Rankine failure plane should not be used for predicting the location of maximum horizontal strain in reinforced soil walls. This plane was developed and defined for an entirely different purpose and is unrelated to horizontal strains in the reinforced soil mass.

r) Some of the mechanisms that have been shown to affect performance are not explicitly addressed in current design procedures. Caution is advised if attempts are made to apply existing empirically developed design methods to situations dissimilar to those from which they were developed.

s) The apparently small deformations and strains measured in the Rainier Avenue wall may at least be partly related to the use of triaxial, instead of plane strain, soil properties for selection of reinforcing.

t) The low strains in the woven geotextiles measured in the Rainier Avenue wall did not result from an increase in modulus due to confinement in soil.

u) The polypropylene geotextiles in the Rainier Avenue wall showed signs of creep after completion of the wall. The increase in length of the polyester geotextile at the base of the wall was possibly due to increases in loads supported by the reinforcing as well as creep.

v) The strain gages used in the Rainier Avenue wall were, apparently, operating properly. Under reporting of the strains, when compared with extensometer measurements, is likely related to the tendency for these strain gages to under predict the overall strain of the woven geotextiles in addition to the occurrence of folds and creases observed in the field installation.

w) Because of the large number of variables that may influence reinforced soil retaining wall behavior, the finite element method is recommended for predicting deformations and strains.

x) Accurate prediction of reinforced soil retaining wall behavior during and after construction requires that plane strain soil properties and time dependent geosynthetic properties be included in the analysis. Approximations of these properties may be acceptable in some cases since wall geometry, foundation conditions, and externally applied loads, may be more influential in affecting the general wall response.

9.3 Recommendations for Further Study

Although the research presented in this dissertation should help in understanding the behavior of geosynthetic reinforced soils and geosynthetic reinforced soil retaining wall deformations, it also identified a number of areas where additional research is required. Further research should be conducted to:

a) Develop data on the plane strain behavior of dense cohesionless soils at the low confining pressures that could be expected in GRS walls during construction.

b) Investigate the plane strain behavior of dense cohesionless soils subject to increasing confining pressure during strain. The rate of increase in confining pressure should simulate the increase in confining pressure that the soil would experience if reinforced with a particular reinforcement.

c) Investigate the plane strain behavior of cohesionless soils under conditions that simulate the effect of decreasing lateral confining pressure associated with stress relaxation of geosynthetic reinforcements.

d) Develop data for the plane strain behavior of cohesive and cohesive-frictional soils.

e) Develop creep data and define the strain rate dependency for geosynthetics intended for use as soil reinforcement.

f) Further characterize in-soil nonwoven geosynthetic properties at stresses and operating conditions that would be expected in field applications.

g) Evaluate, probably using FEM, the influence of plane strain soil properties and strain rate dependent geosynthetic properties on geosynthetic reinforced earth wall behavior.

h) Compare results obtained from detailed, multi-element FEM analysis of GRS walls and their foundations with results obtained using simplified FEM models of GRS walls to determine the minimum level of detail required for practitioners to economically apply the FEM method to the design of GRS walls.

i) Develop guidelines and charts that could be used to compensate for anticipated GRS wall deformation during construction.

j) Modify and expand the existing deformation prediction design procedures for a variety of soil friction angles, construction techniques, and boundary conditions.

k) Define the relationship between reinforcing strains and reinforced soil retaining wall material properties, dimensions, and boundary conditions.

REFERENCES

Adib, M. (1988), Internal Lateral Earth Pressure in Earth Walls, PhD. Dissertation, University of California, Berkeley, 376p.

Adib, M., Mitchell, J.K. and Christopher, B. (1990), "Finite Element Modeling of Reinforced Soil Walls and Embankments," Design and Performance of Earth Retaining Structures, P.C. Lambe and L.A. Hansen, eds., ASCE, Geotechnical Special Publication No. 25, pp. 423.

Al-Hussaini, M.M. and Johnson, L.D. (1978), "Numerical Analysis of a Reinforced Earth Wall," Symposium on Earth Reinforcement, ASCE, Pittsburgh, pp. 98-126.

Allen, T.M. (1991), "Determination of Long-Term Tensile Strength of Geosynthetics: A State-of-the-Art Review," Geosynthetics '91, Atlanta, Vol. 1, pp. 351-379.

Allen, T.M., Christopher, B.R., and Holtz, R.D. (1992), "Performance of a 12.6 m high geotextile wall in Seattle, Washington," Geosynthetic-Reinforced Soil Retaining Walls, Proceedings of the International Symposium on Geosynthetic-Reinforced Soil Retaining Walls, Denver, J.T.H. Wu ed., A.A. Balkema Publ., Rotterdam, pp. 81-100.

Allen, T.M. and Holtz, R.D. (1991), "Design of Retaining Walls Reinforced With Geosynthetics," Geotechnical Engineering Congress 1991, F.G. McLean, D.A. Campbell and D.W. Harris eds., ASCE, Geotechnical Special Publication No. 27, Vol 2, pp. 970-987.

Anderson, L.R., Sharp, K.D. and Harding, O.T. (1987) "Performance of a 50-Foot High Welded Wire Retaining Wall", Soil Improvement - A Ten Year Update, Geotechnical Special Publication No. 12, ASCE, J.P. Welsh, ed., pp. 280-308.

Andrawes, K.Z., Loke, K.H., Yeo, K.C. and Murray, R.T. (1991), "Application of boundary yielding concept to full scale reinforced and unreinforced soil walls," Performance of Reinforced Soil Structures, Proceedings of International Reinforced Soil Conference, A. McGown, K.C. Yeo, and K.Z. Andrawes, eds., British Geotechnical Society, Glasgow, pp. 79-83.

Andrawes, K.Z., McGown, A., and Murray, R.T. (1986), "The Load-Strain-Time-Temperature Behavior of Geotextiles and Geogrids," Third International Conference on Geotextiles, Vienna, Vol. 3, pp. 707-712.

Andrawes, K.Z. and Saad, M.A. (1994), "Geogrid Reinforced Soil Walls Subjected to Controlled Lateral Deformation," Fifth International Conferenced on Geotextiles, Geomembranes, and Related Products, Singapore, Vol. 1, pp. 187-192.

Anjiang, W., Zhang, B. and Lihua, L. (1990), "Research of Influence of Test Conditions on the Tensile Strength of Geotextile," Fourth International Conference on Geotextiles, Geomembranes and Related Products, The Hague, Vol. 2, p. 782.

ASTM (1993), ASTM Standards on Geosynthetics, 3rd ed., ASTM Committee D-35, Philadelphia, 129 p.

Athanasopoulos, G.A., Atmatzidis, D.K. and Bousias, P.Z. (1990), "Sand-Geotextile Interaction by Direct Shear Testing," Fourth International Conference on Geotextiles, Geomembranes and Related Products, The Hague, Vol. 2, p. 795.

Atkinson, J.H. (1981), Foundations and Slopes: An Introduction to Applications of Critical State Soil Mechanics, John Wiley, New York, 382 p.

Balzier, E., Matichard, Y., and Thamm, B.R. (1990), "Geotextile Reinforced Abutment: Full Scale Test and Theory," Performance of Reinforced Soil Structures, Proceedings of International Reinforced Soil Conference, A. McGown, K.C. Yeo, and K.Z. Andrawes, eds., British Geotechnical Society, Glasgow, pp. 47-52.

Bathurst, R.J., Karpurapu, R. and Jarret, P.M. (1992), "Finite Element Analysis of a Geogrid Reinforced Soil Wall", Grouting, Soil Improvement and Geosynthetics, Geotechnical Special Publication No. 30., ASCE, pp. 1213-1224.

Bathurst, R.J. and R.M. Koerner (1988), "Results of Class A Predictions for the RMC Reinforced Soil Wall Trials," The Application of Polymeric Reinforcement in Soil Retaining Structures, P.M. Jarrett and A. McGown eds., NATO ASI Series, Series E: Applied Sciences - Vol. 147, Kluwer Academic Publishers, Boston, pp. 127-171.

Bathurst, R.J., Wawrychuk, W.F. and Jarrett, P.M. (1988), "Laboratory Investigation of Two Large-Scale Geogrid Reinforced Soil Walls," The Application of Polymeric Reinforcement in Soil Retaining Structures, P.M. Jarrett and A. McGown eds., NATO ASI Series, Series E: Applied Sciences - Vol. 147, Kluwer Academic Publishers, Boston, pp. 70-126.

Beer, F.P. and Johnston, E.R. (1981), Mechanics of Materials, McGraw-Hill, New York, 616 p.

Bell, J.R. and Steward, J.E. (1977), "Construction and observations of fabric retained soil walls," International Conference on the use of Fabrics in Geotechnics, Paris, Vol. 2, pp. 123-128.

Bell, J.R., Barrett, R.K., and Ruchman, A.C. (1983), "Geotextile Earth-Reinforced Retaining Wall Tests: Glenwood Canyon, Colorado," Transportation Research Record 916: Engineering Fabrics in Transportation Construction, Transportation Research Board, pp. 59-69.

Berg, R.R., Bonaparte, R., Anderson, R.P., and Chourey, V.E. (1986), "Design, Construction and Performance of Two Geogrid Reinforced Soil Retaining Walls," Proceedings of the Third International Conference on Geotextiles, Vienna, Vol. 2, pp. 401-406.

Berg, R.R., La Rochelle, P., Bonaparte, R. and Tanquay, L. (1987), "Gaspe Peninsula Reinforced Soil Seawall," Soil Improvement - A Ten Year Update, ASCE Geotechnical Special Publication No. 12, J.P. Welsh, ed., pp. 309-328.

Bonczkiewicz, C., Christopher, B.R., and Atmatzidis, D.K. (1988), "Evaluation of Soil-Reinforcement Interaction by Large-Scale Pullout Tests," Transportation Research Record 1188: Effects of Geosynthetics on Soil Properties and of Environment on Pavement Structures, Transportation Research Board, Washington, D.C., pp. 1-18.

Bowles, J.E. (1988), Foundation Analysis and Design, 4th ed., McGraw-Hill, New York, 1004 p.

Broms, B.B. (1977), "Triaxial tests with fabric-reinforced soil," International Conference on the use of Fabrics in Geotechnics, Paris, Vol. 3, pp. 129-133.

Broms, B.B. (1988), "Fabric Reinforced Retaining Walls," International Geotechnical Symposium on Theory and Practice of Earth Reinforcement, Fukuoka, Japan, pp. 3-31.

Chalaturnyk, R.J., Scott, J.D., Chan, D.H.K. and Richards, E.A. (1990), "Stresses and Deformations in a Reinforced Soil Slope," Canadian Geotechnical Journal, NRCC, Vol. 27, No. 2, pp. 224-232.

Chandra, D., Lay, G.C., and Thielen, D.L. (1993), "Geogrid Reinforcement for Massive Shear Key Applications," Geosynthetics '93, Vancouver, Vol. 1, pp. 245-254.

Chandrasekaran, B. (1992), Behavior of Geotextile Reinforced Soil Retaining Wall, PhD. Dissertation, Nanyang Technological University, Singapore, 508 p.

Chandrasekaran, B., Broms, B.B., and Wong, K.S. (1989), "Strength of Fabric Reinforced Sand Under Axisymmetric Loading," Geotextiles and Geomembranes, Vol. 8, pp. 293-310.

Chen, R.H. and Lee, R.G. (1990), "The Mechanical Effect of Inclination of Geotextiles in Sands," Fourth International Conference on Geotextiles, Geomembranes and Related Products, The Hague, Vol. 2, p. 797.

Cheok, Y.K. (1985), The Behavior of Polymeric Grids for Soil Reinforcement, PhD. Dissertation, University of Strathclyde, Glasgow, Scotland. [As cited by Nothdurft and Janardhanam (1994) and Nothdurft (1995)]

Chew, S.H., Schmertmann, G.R., and Mitchell, J.K. (1990), "Reinforced soil wall deformations by finite element method," Performance of Reinforced Soil Structures, Proceedings of International Reinforced Soil Conference, A. McGown, K.C. Yeo, and K.Z. Andrawes, eds., British Geotechnical Society, Glasgow, pp. 35-40.

Chew, S.H. and Mitchell, J.K. (1994), "Deformation Evaluation Procedure for Reinforced Soil Walls," Fifth International Conference on Geotextiles, Geomembranes and Related Products, Singapore, Vol. 1, pp. 171-176.

Chou, N.N.S. (1992), Performance of Geosynthetic Reinforced Soil Walls, PhD. Dissertation, University of Colorado, Denver, 316 p.

Chou, N.N.S and J.T.H. Wu (1993), "Effects of Foundations on the Performance of Geosynthetic-Reinforced Soil Walls," Geosynthetics '93, Vancouver, Vol. 1, pp. 189-201.

Christopher, B.R. (1993), Deformation Response and Wall Stiffness in Relation to Reinforced Soil Wall Design, PhD. Dissertation, Purdue University, 354 p.

Christopher, B.R., Gill, S.A., Giroud, J.P., Juran, I., Mitchell, J.K., Schlosser, F. and Dunnicliff, J. (1990), Reinforced Soil Structures Volume I. Design and Construction Guidelines and Reinforced Soil Structures Volume II. Summary of Research and Systems Information, Federal Highway Administration, FHWA-RD-89-043, Washington, D.C., Vol. 1, 283 p., Vol. 2, 158 p.

Christopher, B.R. and R.D.Holtz, (1985) Geotextile Engineering Manual, Federal Highway Administration, Report FHWA-TS-86/203, Washington, D.C. 1044 p.

Christopher, B.R., Holtz, R.D., and Allen, T.M. (1991), "Instrumentation for a 12.6 m High Geotextile-Reinforced Wall," Performance of Reinforced Soil Structures, Proceedings of International Reinforced Soil Conference, A. McGown, K.C. Yeo, and K.Z. Andrawes, eds., British Geotechnical Society, Glasgow, pp. 73-78.

Christopher, B.R., Holtz, R.D., Bell, W.D. (1986), "New Tests for Determining The In-Soil Stress-Strain Properties of Geotextiles", Third International Conference On Geotextiles, Vienna, Vol. 3, pp. 683-686.

Chu, D. and Poorman, I (1989), "Reinforcement of an Earthen Buttress with a Polymer Geogrid," Geosynthetics '89, San Diego, Vol. 1, pp. 243-254.

Claybourn A.F. and J.T.H. Wu (1991), "Case History Comparison of Geosynthetics-Reinforced Soil Walls," Geosynthetics '91, Atlanta, Vol. 2, pp. 549-559.

Clough, R.W. and Woodward, R.J. (1967), "Analysis of Embankment Stresses and Deformations," Journal of the Soil Mechanics and Foundation Division, ASCE, Vol. 89, No. SM3, pp. 103-134.

Collin, J.G. (1986) Earth Wall Design, PhD. Dissertation, University of California, Berkeley, 289 p.

Collios, A., Delmas, P., Gourc, J.P. and Giroud, J.P. (1980), "Experiments on Soil Reinforcement with Geotextiles", The Use of Geotextiles for Soil Improvement, ASCE National Convention, Portland, ASCE 80-177, pp. 53-73.

Cornforth, D.H. (1964), "Some Experiments on the Influence of Strain Conditions on the Strength of Sand," Geotechnique, ICE, Vol. 14, No. 2, pp. 143-167.

Delmas, P., Blivet, J.C. and Matichard, Y. (1988), "Geotextile-Reinforced Retaining Structures: A Few Instrumented Examples," The Application of Polymeric Reinforcement in Soil Retaining Structures, P.M. Jarrett and A. McGown eds., NATO ASI Series, Series E: Applied Sciences - Vol. 147, Kluwer Academic Publishers, Boston, pp. 285-312.

Dembicki, E. and Alenowitz, J. (1987), "Determination of Frictional Properties of Geotextiles," Geotextiles and Geomembranes, Elsevier, Vol. 6, No. 4, pp. 307-314.

Dembicki, E. and Piotr, J. (1991), "Soil-Geotextile Interaction," Geotextiles and Geomembranes, Elsevier, Vol. 10, No. 3, pp. 249-268.

den Hoedt, G. (1986), "Creep and Relaxation of Geotextile Fabrics," Geotextiles and Geomembranes, Elsevier, Vol. 4, No. 2, pp. 83-92.

Djarwadi, D. and Wong, I.N. (1994) "Construction and Performance of Spillway Walls in Makakuning Dam," Fifth International Conference on Geotextiles, Geomembranes, and Related Products, Singapore, Vol. 1, pp. 289-292.

Ebeling, R.M., Mosher, R.L., Abraham, K., and Peters, J.F. (1993), Soil-Structure Interaction Study of Red River Lock and Dam No. 1 Subjected to Sediment Loading, U.S. Army Corps of Engineers Technical Report ITL-93-3, 283 p.

Ebeling, R.M., Peters, J.F., and Wahl, R.E. (1992a), "Prediction of reinforced sand wall performance," Geosynthetic-Reinforced Soil Retaining Walls, Proceedings of the International Symposium on Geosynthetic-Reinforced Soil Retaining Walls, Denver, J.T.H. Wu, ed., Balkema, Rotterdam, pp. 243-253.

Ebeling, R.M., Peters, J.F. and Mosher, R.L. (1992b), "Finite Element Analysis of Slopes with Layer Reinforcement," Stability and Performance of Slopes and Embankments - II, Geotechnical Special Publication No. 31, ASCE, Vol. 2, pp. 1427-1443.

El-Fermaoui, A. and Nowatzki, E. (1982), "Effect of Confining Pressure on Performance of Geotextiles in Soils," Second International Conference on Geotextiles, Vol. 3, pp. 799-804.

Ehrlich, M. and Mitchell, J.K. (1994), "Working Stress Design Method for Reinforced Soil Walls," Journal of Geotechnical Engineering, ASCE, Vol. 120, No. 5, pp. 625-645.

Fabian, K. (1990), "Time Dependent Behavior of Geotextile Reinforced Clay Walls", Fourth International Conference on Geotextiles, Geomembranes and Related Products, The Hague, Vol. 1, pp. 33-38.

Fannin, R.J. and Hermann, S. (1990), "Performance data for a sloped reinforced soil wall," Canadian Geotechnical Journal, NRCC, Vol. 27, No. 5, pp. 676-686.

Farrag, K.A. (1990), "Interaction Properties of Geogrids in Reinforced-Soil Walls, Testing and Analysis," PhD Dissertation, Louisiana State University, 267 p.

Farrag, K.A., Oglesby, J., and Griffin, P. (1994), "Large strain measurements in geogrid reinforcements," Transportation Research Record No. 1439: Durability of Geosynthetics, Transportation Research Council, pp. 41-45.

Fidler, S.R. (1993), "Working load design methods for reinforced soil sytems," Earth Reinforcement Practice, Proceedings of the International Symposium on Earth Reinforcement Practice, Fukuoka, H. Ochiai, S. Hayashi and J. Otani, eds., Balkema, Rotterdam, Vol. 1, pp. 325-330.

Futaki, M., Suzuki, H. and Yamato, S. (1990), "Super Large Triaxial Compression Tests on Reinforced Sand with High Strength Geogrid," Fourth International Conference on Geotextiles, Geomembranes and Related Products, The Hague, Vol. 2, pp. 759-764.

Gallagher, M. (1995), In-isolation Wide Width Tests on Geotextiles, Submitted in partial fulfillment of the requirements for a Master of Science in Civil Engineering, University of Washington, Seattle.

GFR (1990), "1991 Specifiers Guide," Geotechnical Fabrics Report, IFAI, Vol. 8, No. 7.

GFR (1993), "1994 Specifiers Guide," Geotechnical Fabrics Report, IFAI, Vol. 10, No. 9.

Goodman, L.E., and Brown, C.E. (1963), "Dead Load Stresses and the Instability of Slopes," Journal of the Soil Mechanics and Foundations Division, ASCE, Vol. 89, No. SM3, pp. 103-134.

Gourc, J.P. and Beech, J.F. (1989), "Contribution to discussion: Soil-Reinforcement interaction," Twelfth International Conference on Soil Mechanics and Foundation Engineering, Rio de Janeiro, Vol. 5, pp. 3007-3008.

Gourc, J.P., Ratel, A. and Delmas, P. (1986), "Design of fabric retaining walls: the 'displacement method'," Third International Conference On Geotextiles, Vienna, Vol. 4, pp. 1067-1072.

Gourc, J.P., Ratel, A. and Gotteland, P. (1988), "Design of reinforcec soil retaining walls: Analysis and comparison of existing design methods and proposal for a new approach," The Application of Polymeric Reinforcement in Soil Retaining Structures, P.M. Jarrett and A. McGown eds., NATO ASI Series, Series E: Applied Sciences - Vol. 147, Kluwer Academic Publishers, Boston, pp. 459-506.

Graf, B. and Studer, J.A., (1988) "Geotextile Reinforced Retaining Walls: Discussion of Instrumented Large Scale Test With Respect to the Verification of Design Consepts," The Application of Polymeric Reinforcement in Soil Retaining Structures, P.M. Jarrett and A. McGown eds., NATO ASI Series, Series E: Applied Sciences - Vol. 147, Kluwer Academic Publishers, Boston, pp. 313-337.

Gray, D.H. and Ohashi, H. (1983), "Mechanics of Fiber Reinforcement in Sand," Journal of Geotechnical Engineering, ASCE, Vol. 109, No. 3, pp. 335-353.

Geosynthetics Research Institute (1991a), "GRI GG4, Standard Practice for Determination of the Long-Term Design Strength of Stiff Geogrids," Drexel University, 29p.

Geosynthetics Research Institute (1991b), "GRI GG5, Standard Test Method for Geogrid Pullout," Drexel University, 11p.

Geosynthetics Research Institute (1992a), "GRI GT7, Standard Practice for Determination of the Long-Term Design Strength of Geotextiles," Drexel University, 13p.

Geosynthetics Research Institute (1992b), "GRI GT6, Standard Test Method for Geotextile Pullout," Drexel University, 10p.

Hajiali, F. (1991), "Field behavior of a Reinforce Earth Wall in Malaysian Conditions," Performance of Reinforced Soil Structures, Proceedings of International Reinforced Soil Conference, A. McGown, K.C. Yeo, and K.Z. Andrawes, eds., British Geotechnical Society, Glasgow, pp. 169-173.

Hanna, A.M., Massoud, N. and Youssef, H. (1987), "Prediction of plane strain angles of shear resistance from triaxial test results," Prediction and Performance in Geotechnical Engineering, Proceedings of International Symposium, Calgary, R.C. Joshi and F.J. Griffiths, eds, A.A. Balkema Publishers, Rotterdam, pp. 369-376.

Harrison, W.J. and Gerrard, C.M. (1972), "Elastic Theory Applied to Reinforced Earth," Journal of the Soil Mechanics and Foundations Division, ASCE, Vol. 98, No. SM12, pp. 1325-1345.

Hausmann, M.R. (1976), "Strength of Reinforced Soil," Proceedings of the Eighth Austalian Road Research Board Conference, Perth, Session 13, pp. 1-3.

Hausmann, M.R. (1990), Engineering Principles of Ground Modification, McGraw-Hill, New York, 632 p.

Hausmann, M.R. and Lee I.K. (1976), "Strength Characteristics of Reinforced Soil," International Symposium on New Horizons in Construction Materials, Lehigh, Vol. 1, pp. 165-176.

Helwany, M.B. (1992), "Finite element analysis of geotextile reinforced retaining walls considering creep," Geosynthetic-Reinforced Soil Retaining Walls, Proceedings of the International Symposium on Geosynthetic-Reinforced Soil Retaining Walls, Denver, J.T.H. Wu ed., A.A. Balkema Publishers, Rotterdam, pp. 179-192.

Helwany, M.B. and Wu, J.T.H (1993), "A Performance Test for Long-Term Soil-Geosynthetic Interaction," University of Colorado, unpublished preprint.

Herrmann, L.R. and Al-Yassin, Z. (1978) "Numerical Analysis of Reinforced Soil Systems," Symposium on Earth Reinforcement, ASCE, Pittsburgh, pp. 428-457.

Ho, S.K. and Rowe, R.K. (1993), "Finite Element Analysis of Geosynthetics-Reinforced Soil Walls," Geosynthetics '93, Vancouver, 1993, Vol. 1, pp. 189-201.

Ho, S.K. and Rowe, R.K. (1994), "Predicted Behavior of Two Centrifugal Model Soil Walls," Journal of Geotechnical Engineering, ASCE, Vol. 120, No. 10, pp. 1845-1873.

Holtz, R.D. (1977), "Laboratory Studies of Reinforced Earth Using a Woven Polyester Fabric," International Conference on the Use of Fabrics in Geotechnics, Paris, Vol. 2, pp. 149-154.

Holtz, R.D., Allen, T.M. and Christopher, B.R. (1991), "Displacement of a 12.6 m high geotextile-reinforced wall," Tenth European Conference on Soil Mechanics and Foundation Engineering, Florence, Vol. 2, pp. 725-728.

Holtz, R.D. and Kovacs, W.D. (1981), An Introduction to Geotechnical Engineering, Prentice-Hall, Englewood Cliffs, 733 p.

Holtz, R.D., Tobin, W.R. and Burke, W.W. (1982), Second International Conference on Geotextiles, Las Vegas, Vol. 3, pp. 805-808.

Huang, C.C., Cheng, C.Y., Hsia, S.H. and Hsu, S.P. (1994), "Reinforcement Stiffness on Load-Deformation Characteristics of Reinforcements," Fifth International Conference on Geotextiles, Geomembranes and Related Products, Singapore, Vol. 1, pp. 197-200.

Huesker, Inc. (undated), Fortrac Geogrid Estimating Charts for Reinforced Modular Block Walls, Technical Brochures, Huesker, Inc., Charlotte, NC.

Jaber, M., Collin, J.G. and Schmertmann, G.R. (1992), "Prediction of geosynthetic reinforced wall performance using finite element analysis," Geosynthetic-Reinforced Soil Retaining Walls, Proceedings of the International Symposium on Geosynthetic-Reinforced Soil Retaining Walls, Denver, J.T.H. Wu ed., A.A. Balkema Publishers, Rotterdam, pp. 305-314.

Jarrett, P.M. (1988), "Introduction and Rationale for Prediction Exersize," The Application of Polymeric Reinforcement in Soil Retaining Structures, P.M. Jarrett and A. McGown eds., NATO ASI Series, Series E: Applied Sciences - Vol. 147, Kluwer Academic Publishers, Boston, pp. 69-70.

Jewell, R.A. (1988a), "Reinforced Soil Wall Analysis and Behavior," The Application of Polymeric Reinforcement in Soil Retaining Structures, P.M. Jarrett and A. McGown eds., NATO ASI Series, Series E: Applied Sciences - Vol. 147, Kluwer Academic Publishers, Boston, pp. 365-408.

Jewell, R.A. (1988b), "Analysis and Predicted Behavior for the Royal Military College Trial Wall," The Application of Polymeric Reinforcement in Soil Retaining Structures, P.M. Jarrett and A. McGown eds., NATO ASI Series, Series E: Applied Sciences - Vol. 147, Kluwer Academic Publishers, Boston, pp. 193-235.

Jewell, R.A. (1992), "Panel Discussion," Geosynthetic-Reinforced Soil Retaining Walls, Proceedings of the International Symposium on Geosynthetic-Reinforced Soil Retaining Walls, Denver, J.T.H. Wu, ed., A.A. Balkema Publishers, Rotterdam, pp. 363-370.

Jewell, R.A. and Milligan, G.W.E. (1989), "Deformation calculations for reinforced soil walls," Twelfth International Conference on Soil Mechanics and Foundation Engineering, Rio de Janeiro, Vol. 2, pp. 1257-1263.

Jones, C.J.F.P. (1988), "Predicting the behaviour of reinforced soil structures," International Geotechnical Symposium on Theory and Practice of Earth Reinforcement, Fukuoka, Balkema Press, Rotterdam, pp. 535-540.

Juran, I. and Chen, C.L. (1988), "Soil-Geotextile Pull-out Interaction Properties: Testing and Interaction", Transportation Research Record 1188: Effects of Geosynthetics on Soil Properties and of Environment on Pavement Structures, Transportation Research Board, Washington, D.C., pp. 37-47.

Juran, I. and Chen, C.L. (1989), "Strain Compatibility Design Method for Reinforced Earth," Journal of Geotechnical Engineering, ASCE, Vol. 115, No. 4, pp. 435-456.

Juran, I., Knochenmus, G., Acar, Y.B., Arman, A. (1988), "Pull-out Response of Geotextiles and Geogrids (Synthesis of Available Experimental Data)," Geosynthetics for Soil Improvement, Geotechnical Special Publication No. 18, ASCE.

Juran, I., Ider, H.M. and Farrag, K. (1990), "Strain Compatibility Analysis for Geosynthetic Soil Walls," Journal of Geotechnical Engineering, ASCE, Vol. 116, No. 2, pp. 312-329.

Kanazawa, Y., Ikeda, K., Murata, O., Tateyama, M. and Tatsuoka, F. (1994), "Geosynthetic-reinforced soil retaining walls for reconstructing railway embankment at Amagasaki," Recent Case Histories of Permanenet Geosynthetic-Reinforced Soil Retaining Walls, F. Tasuoka and D. Leshchinsky, eds., Balkema, Rotterdam, pp. 233-242.

Karpurapu, R.G. and Bathurst, R.J. (1992), "Finite element predictions for the Colorado geosynthetic-reinforced soil retaining walls," Geosynthetic-Reinforced Soil Retaining Walls, Proceedings of the International Symposium on Geosynthetic-Reinforced Soil Retaining Walls, Denver, J.T.H. Wu, ed., A.A. Balkema Publishers, Rotterdam, pp 329-342.

Koerner, R.M. (1994), Designing with Geosynthetics, 3rd ed., Prentice-Hall, Englewood Cliffs, 783 p.

Lade, P.V. and Lee, K.L. (1976), "Engineering Properties of Soils," Report UCLA-ENG-7652, 145 pp. [As cited by Holtz and Kovacs (1981)]

Lee, K.L. (1970), "Comparison of Plane Strain and Triaxial Tests on Sand," Journal of the Soil Mechanics and Foundation Division, ASCE, Vol. 96, No. SM3, pp. 901-923.

Lee, K.L. and Seed, H.B. (1967), "Drained Strength Characteristics of Sands," Journal of the Soil Mechanics and Foundation Division, ASCE, Vol. 96, No. SM3, pp. 901-923.

Leshchinsky, D. and Boedeker, R.H. (1989), "Geosynthetic Reinforced Soil Structures," Journal of Geotechnical Engineering, ASCE, Vol. 115, No. 10, pp. 1459-1478.

Leshchinsky, D. and Field, D.A. (1987), "In-Soil Load Elongation, Tensile Strength and Interface Friction of Non-Woven Geotextiles," Geosynthetics '87, New Orleans, pp. 238-249.

Leshchinsky, D. and Fowler, J. (1990), "Laboratory Measurement of Load-Elongation Relationship of High Strength Geotextiles," Geotextiles and Geomembranes, Elsevier, Vol. 9, pp. 145-164.

Leshchinsky, D. and Perry, E.B. (1987), "A Design Procedure for Geotextile Reinforced Walls," Geotechnical Fabrics Report, IFAI, Vol. 5, No. 4, pp. 21-27.

Ling, H.I. (1992), Performance of Geosynthetic-Reinforced Cohesive Soil Mass at Plane Strain Compression, PhD. Dissertation, University of Tokyo, 509 p.

Ling, H.I., and Tatsuoka, F. (1992), "Nonlinear analysis of reinforced soil structures by Modified CANDE (M-CANDE)," Geosynthetic-Reinforced Soil Retaining Walls, Proceedings of the International Symposium on Geosynthetic-Reinforced Soil Retaining Walls, Denver, J.T.H. Wu ed., A.A. Balkema Publishers, Rotterdam, pp. 279-296.

Ling, H.I. and Tatsuoka, F. (1994), "Performance of Anisotropic Geosynthetic-Reinforced Cohesive Soil Mass," Journal of Geotechnical Engineering, ASCE, Vol. 120, No. 7, pp. 1166-1184.

Ling, H.I., Wu, J.T.H., Tatsuoka, F. (1991), "Effectiveness of In-Membrane Test in Simulating Strength and Deformation Characteristics of a Nonwoven Geotextile Under Operational Conditions," Geosynthetics '91, Atlanta, Vol. 2, pp. 601-614.

Ling, H.I., Wu, J.T.H., and Tatsuoka, F. (1992), "Short-term Strength and Deformation Characteristics of Geotextiles Under Typical Operational Conditions," Geotextiles and Geomembranes, Elsevier, Vol. 11, No. 2, pp. 185-219.

Mandal, J.N. (1986), "A Goal for Geotextiles," Third International Conference On Geotextiles, Vienna, Vol 3, pp. 747-750.

Marachi, N.D., Duncan, J.M., Chan, C.K., and Seed, H.B. (1981), "Plane-Strain Testing of Sand", Laboratory Shear Strength of Soil, Standard Technical Publication 740, ASTM, pp. 294-302.

McGown, A. and Andrawes, K.Z. (1977), "The influences of non-woven fabric inclusions on the stress strain behavior of a soil mass," International Conference on the use of Fabrics in Geotechnics, Paris, Vol. 2, pp. 161-166.

McGown, A., Andrawes, K.Z. and Al-Hasani, M.M. (1978), "Effect of Inclusion Properties on the Behavior of Sand," Geotechnique, ICE, Vol. 28, No. 3, pp. 327-346.

McGown, A., Andrawes, K.Z., Kabir, M.H. (1982), "Load-Extension Testing of Geotextiles Confined In Soil," Second International Conference on Geotextiles, Vol. 3, pp. 793-798.

McGown, A., Murray, R.T. and Jewell, R.A. (1989), "General Report/ Discussion session 17: Reinforced Soil Slopes and Walls," Twelfth International Conference on Soil Mechanics and Foundation Engineering, Rio De Janeiro, Vol. 4, pp. 2637-2648.

McGown, A., Yogarajah, I. and Yeo, K.C. (1993), "Choice of soil properties for limit state analysis of reinforced soil retaining structures," Retaining Structures, Proceedings of Conference on Retaining Structures, Cambridge, C.R.I. Clayton, ed., Thomas Telford Publishers, London, pp. 529-540.

Miki, H., Kudo, K., Taki, M., Fukuda, N., Iwasaki, K., and Nishimura, J. (1994), "The facing's retaining effect of steep slope reinforced embankment," Recent Case Histories of Permanenet Geosynthetic-Reinforced Soil Retaining Walls, F. Tasuoka and D. Leshchinsky, eds., Balkema, Rotterdam, pp. 131-140.

Milligan, G.W.E. and Palmeira, E.P. (1987), "Prediction of bond between soil and reinforcement," Prediction and Performance in Geotechnical Engineering, Proceedings of International Symposium, Calgary, R.C. Joshi and F.J. Griffiths, eds, A.A. Balkema Publishers, Rotterdam, pp. 147-153.

Mitchell, J.K. (1987), "Reinforcement for Earthwork Construction and Ground Stabilization," Proceedings of the Eigth Pan American Conference on Soil Mechanics and Foundations, Vol. 1, pp. 349-380.

Mitchell, J.K. and Villet, W.C.B. (1987), National Cooperative Highway Research Program Report 290: Reinforcement of Earth Slopes and Embankments, Transportation Research Board, Washington, D.C., 323 p.

Miyamori, T., Iwai, S. and Makiuchi, K. (1986), "Frictional Characteristics of Non-Woven Fabrics," Third International Conference On Geotextiles, Vienna, Vol. 3, pp. 701-705.

Miyata, K. and Kawasaki, H. (1994), "Reinforced soil retaining walls by FRP geogrid," Recent Case Histories of Permanenet Geosynthetic-Reinforced Soil Retaining Walls, F. Tasuoka and D. Leshchinsky, eds., Balkema, Rotterdam, pp. 253-257.

Mylleville, B.L.J. and Rowe, R.K. (1991), "On the Design of Reinforced Embankments on Soft Brittle Clays," Geosynthetics '91, Vol. 1, pp 395-408.

Naylor, D.J. (1978), "A Study of Reinforced Earth Walls Allowing Strip Slip," Symposium on Earth Reinforcement, ASCE, Pittsburgh, pp. 618-643.

Naylor, D.H. and Richards, H. (1978), "Slipping Strip Analysis of Reinforced Earth," International Journal for Numerical and Analytical Methods in Geomechanics, J. Wiley, Vol. 2, No. 4, pp. 343-366.

Nothdurft, D.B. (1995), Disscussion: "Tensile Reinforcement Effects on Bridge-Approach Settlement," Journal of Geotechnical Engineering, ASCE, Vol. 121, No. 1, pp. 94-96.

Nothdurft, D.B. and Janardhanam, R. (1994), "Influence of Polymer Viscoelasticity in Reinforced Soil Structure Design," Fifth International Conference on Geotextiles, Geomembranes, and Related Products, Singapore, Vol. 1, pp. 247-250.

Palmeira, E.M. and Lanz, D. (1994), "Stresses and Deformations in Geotextile Reinforced Model Walls," Geotextiles and Geomembranes, Elsevier, Vol. 13, No. 5, pp. 331-348.

Palmeira, E.M. and Milligan, G.W.E. (1989), "Scale and Other Factors Affecting the Results of Pull-out Tests of Grids Buried in Sand," Geotechnique, ICE, Vol. 39, No. 3, pp. 511-524.

Paulson, J. (1993), "High Strength Polyester Geotextile Testing and Material Property Evaluation," Geosynthetic Soil Reinforcement Testing Procedures, Standard Technical Publication 1190, ASTM, S.C.J. Chen, ed., Philadelphia, 1993.

Polyfelt, Inc. (1987) Design and Practice, Technical Manual, Polyfelt, Inc., Evergreen, AL.

Poulos, H.G., Booker, J.R. and Ring, G.J. (1972), "Simplified Calculation of Embankment Deformations," Soils and Foundations, JSSMFE, Vol. 12, No. 4, pp. 1-17.

Rajagopal, K. and Bathurst R.J. (1994), "Parametric Finite Element Investigation of Reinforced Soil Retaining Walls," Fifth International Conference on Geotextiles, Geomembranes, and Related Products, Singapore, Vol. 1, pp. 193-196.

Rankine, W.J.M. (1857), "On the Stability of Loose Earth," Philosophical Transactions of the Royal Society of London, Vol. 147. pp. 9-27.

Rao, G.V. and Pandey, S.K. (1988), "Evaluation of Geotextile-Soil Friction," Indian Geotechnical Journal, IGS, Vol 18, No. 1, pp. 77-105.

Resl, S. (1990), "Soil-reinforcing mechanisms of nonwoven geotextiles," Fourth International Conference on Geotextiles, Geomembranes and Related Products, The Hague, Vol. 1, pp. 93-96.

Richards, E.A. and Scott, J.D. (1985), "Soil Geotextile Frictional Properties," Second Canadian Symposium on Geotextiles and Geomembranes, Edmonton, pp. 13-24.

Richards, R., Jr., and Schmid, W.E. (1968), "Body-Force Stresses in Gravity Structures," Journal of the Soil Mechanics and Foundation Division, ASCE, Vol. 94, No. SM1, pp. 205-229.

Rimoldi, P. and Montanelli, F. (1993), "Creep and Accelerated Creep Testing for Geogrids," Geosynthetics '93, Vancouver, Vol. 2, pp 773-787.

Romstad, K.M., Herrmann, L.R., and Shen, C.K. (1976), "Integrated Study of Reinforced Earth -- I: Theoretical Formulation," Journal of Geotechnical Engineering, ASCE, Vol. 102, No. GT5, pp. 457-472.

Rowe, R.K. and Ho, S.K. (1986), "Determination of Geotextile Stress-Strain Characteristics Using a Wide Strip Test," Third International Conference on Geotextiles, Vienna, Vol. 3, pp. 885-890.

Rowe, R.K. and Ho, S.K. (1988), "Application of Finite Element Techniques to the Analysis of Reinforced Soil Walls," The Application of Polymeric Reinforcement in Soil Retaining Structures, P.M. Jarrett and A. McGown eds., NATO ASI Series, Series E: Applied Sciences - Vol. 147, Kluwer Academic Publishers, Boston, p 541-556.

Salamon, M.D.G. (1968), "Elastic Moduli of a Stratified Rock Mass," International Journal of Rock Mechanics and Mineral Science, Pergamon Press, Vol. 5, pp. 519-527.

Salomone, W.G., Boutrup, E., Holtz, R.D., Kovacs, W.D., and Sutton, C.D. (1980), "Fabric Reinforcement Designed Against Pullout," The Use of Geotextiles for Soil Improvement, ASCE National Convention, Portland, ASCE 80-177, pp. 75-85.

Sawicki, A. (1983a), "Engineering Mechanics of Elasto-Plastic Composites," Mechanics of Materials, Elsevier, Vol. 2, No. 3, pp. 217-231.

Sawicki, A. (1983b), "Axisymmetrical Elasto-Plastic Behaviour of Reinforced Earth," International Journal for Numerical and Analytical Methods in Geomechanics, J. Wiley, Vol. 7, No. 4, pp. 493-498.

Sawicki, A. (1983c), "Plastic Limit Behavior of Reinforced Earth," Journal of Geotechnical Engineering, ASCE, Vol. 109, No. 7, pp. 1000-1005.

Sawicki, A. and Kulczykowski, M. (1994), "Pre-failure Behaviour of Reinforced Soil," Geotextiles and Geomembranes, Elsevier, Vol. 13, No. 4, pp. 213-230.

Sawicki, A. and Lesniewska, D. (1988), "Limit Analysis of Reinforced Slopes," Geotextiles and Geomembranes, Elsevier, Vol. 7, No. 3, pp. 203-220.

Sawicki, A. and Lesniewska, D. (1991), "Stability of Fabric Reinforced Cohesive Soil Slopes," Geotextiles and Geomembranes, Elsevier, Vol. 10, No. 2, pp. 125-146.

Sawicki, A. and Lesniewska, D. (1993), "On modelling visco-elastic behaviour of reinforced soil," Earth Reinforcement Practice, Proceedings of the International Symposium on Earth Reinforcement Practice, Fukuoka, H. Ochiai, S. Hayashi and J. Otani, eds., Balkema, Rotterdam, Vol. 1, pp. 163-166.

Schlosser, F. and de Buhan, P. (1991), "Theory and design related to the performance of reinforced soil structures," Performance of Reinforced Soil Structures, Proceedings of International Reinforced Soil Conference, A. McGown, K.C. Yeo, and K.Z. Andrawes, eds., British Geotechnical Society, Glasgow, pp. 1-14.

Schlosser, F. and Elias, V. (1978) "Friction in Reinforced Earth," Symposium on Earth Reinforcement, ASCE, Pittsburgh, pp. 735-763.

Schlosser, F. and Long, N.T. (1972), "Recent Results in French Research on Reinforced Earth," Journal of the Construction Division, ASCE, Vol. 100, No. CO3, pp. 223-237.

Schlosser, F. and Vidal H. (1969), "Reinforced Earth," Bulletin de Liasison Des Laboratories Routiers - Ponts et Chaussees, No. 41 (English Translation).

Schmertmann, G.R., Chew, S.H. and Mitchell, J.K. (1989), Finite Element Modeling of Reinforced Soil Wall Behavior, University of California, Berkeley, Geotechnical Engineering Report No. UCB/GT/89-01, 220 p.

Shen, C.K., Kim, O., Li, X.S. and Sohn, J. (1988), "Soil-Reinforcement Interaction Determined By Extension Test," International Geotechnical Symposium on Theory and Practice of Earth Reinforcement, Fukuoka, Balkema Press, Rotterdam, pp. 165-170.

Shen, C.K., Romstad K.M. and Herrmann, L.R. (1976), "Integrated Study of Reinforced Earth -- II: Behavior and Design," Journal of Geotechnical Engineering, ASCE, Vol. 102, No. GT6, pp. 577-590.

Siel, B.D., Tzong, W.H. and Chou, N.N.S. (1987), "In-Soil Stress-Strain Behavior of Geotextile," Geosynthetics '87, New Orleans, pp. 260-265.

STS Consultants, Inc. (1990), "Final Report of SR-90, Rainier Avenue Interchange," Prepared for the Washington State Department of Transportation.

Swanson Analysis System, Inc. (1992), ANSYS Revision 5.

Takasumi, D.L., Green, K.R., and Holtz, R.D. (1991), "Soil-Geosynthetics Interface Strength Characteristics: A Review of State-of-the-Art Testing Procedures," Geosynthetics '91, Atlanta, Vol. 1, pp. 87-100.

Tatsuoka, F. (1993), "Keynote Lecture: Roles of Facing Rigidity in Soil Reinforcing," Earth Reinforcement Practice, Proceedings of the International Symposium on Earth Reinforcement Practice, Fukuoka, H. Ochiai, S. Hayashi and J. Otani, eds., Balkema, Rotterdam, Vol. 2, pp. 831-870.

Tzong, W.H. and Cheng-Kuang, S. (1987), "Soil-Geotextile Interaction Mechanism in Pullout Test," Geosynthetics '87, New Orleans, Vol. 1, pp. 250-259.

Urgural, A.C. and Fenster, S.K. (1995), Advanced Strength and Applied Elasticity, 3rd ed., Elsevier, New York, 570 p.

Van Leeuwen, J.H. (1977), "New Methods of Determining the Stress-Strain Behavior of Woven and Non-Woven Fabrics in the Laboratory and in Practice," International Conference on the Use of Fabrics in Geotechnics, Paris, Vol. 2, pp. 299-304.

Vidal, H. (1969), "The Principle of Reinforced Earth," Highway Research Record 282: Soil Theories: Reinforced Earth, Displacements, Bearing and Seepage, Highway Research Board, Washington, D.C., pp. 1-16.

Voskamp, W. (1991), "Pull-out Tests and Junction Strengths of Geogrids," Geosynthetics World, pp. 28-33.

Werner, G. and Resl, S. (1986), "Stability Mechanisms in Reinforced Earth-Structures," Third International Conference On Geotextiles, Vienna, Vol. 4, pp. 1131-1135.

Westergaard, H.M. (1938), "A Problem of Elasticity Suggested by a Problem in Soil Mechanics: Soft Material Reinforced by Numerous Strong Horizontal Sheets," Contributions to the Mechanics of Solids, Steven Timeshenko 60th Anniversary Volume, The MacMillian Company, New York.

Whittle, A.J., Germaine, J.T., Larson, D.G. and Abramento, M. (1993), "Measurement and interpretation of reinforcement stresses in the ASPR cell," Earth Reinforcement Practice, Proceedings of the International Symposium on Earth Reinforcement Practice, Fukuoka, Ochiai, Hayashi and Otani eds., Balkema, Rotterdam, pp. 179-184.

Wilson-Fahmy, R.F., Koerner, R.M. and Fleck, J.A. (1993), "Unconfined and Confined Wide Width Testing of Geosynthetics," Geosynthetic Soil Reinforcement Testing Procedures, Standard Technical Publication 1190, ASTM, S.J. Cheng, ed., Philadelphia.

Won, G.W., Hausmann, M.R., Jankulovski, E. "Performance of a Reinforced Soil Wall in Syndey, Australia," Fifth International Conference on Geotextiles, Geomembranes and Related Products, Singapore, Vol. 1, pp. 277-280.

Wu, J.T.H. (1991), "Measuring Inherent Load-Extension Properties of Geotextiles for Design of Reinforced Structures," Geotechnical Testing Journal, ASTM, Vol. 14, No. 2, pp. 157-165.

Wu, J.T.H. (1992a) "Predicting performance of the Denver Walls: General Report," Geosynthetic-Reinforced Soil Retaining Walls, Proceedings of the International Symposium on Geosynthetic-Reinforced Soil Retaining Walls, Denver, J.T.H. Wu ed., A.A. Balkema Publishers, Rotterdam, pp. 3-20.

Wu, J.T.H. (1992b), "Construction and Instrumentation of the Denver Walls," Geosynthetic-Reinforced Soil Retaining Walls, Proceedings of the International Symposium on Geosynthetic-Reinforced Soil Retaining Walls, Denver, J.T.H. Wu ed., A.A. Balkema Publishers, Rotterdam, pp. 21-30.

Wu, J.T.H. (1992c), "Measured Behavior of the Denver Walls," Geosynthetic-Reinforced Soil Retaining Walls, Proceedings of the International Symposium on Geosynthetic-Reinforced Soil Retaining Walls, Denver, J.T.H. Wu ed., A.A. Balkema Publishers, Rotterdam, pp. 31-42.

Wu, J.T.H., ed. (1992d) Geosynthetic-Reinforced Soil Retaining Walls, Proceedings of the International Symposium on Geosynthetic-Reinforced Soil Retaining Walls, J.T.H. Wu ed., A.A. Balkema Publishers, Rotterdam, 375 p.

Wu, J.T.H. and Arabian, V. (1990), "Cubical and Cylindrical Tests for Measuring In-Soil Load Extension Properties of Geotextiles," Fourth International Conference on Geotextiles, Geomembranes and Related Products, The Hague, Vol. 2, p 785.

Wu, J.T.H., X. Qi, N. Chou, I. Ksouri, M.B. Helwany and C.C. Huang (1992), "Comparisons of predictions for the Denver Walls," Geosynthetic-Reinforced Soil Retaining Walls, Proceedings of the International Symposium on Geosynthetic-Reinforced Soil Retaining Walls, Denver, J.T.H. Wu ed., A.A. Balkema Publishers, Rotterdam, pp. 43-60.

Xi, F. (1992), Finite Element Analysis of Geosynthetically Reinforced Walls: A Parametric Study, Masters Thesis, University of Delaware, 141 p.

Yako, M.A. and Christopher, B.R. (1988), "Polymerically Reinforced Retaining Walls and Slopes in North America," The Application of Polymeric Reinforcement in Soil Retaining Structures, Jarrett, P.M. and McGown, A. eds., NATO ASI Series, Series E: Applied Sciences - Vol. 147, Kluwer Academic Publishers, Boston, pp. 541-556.

Yang, Z. and Singh, A. (1974), "Strength and Deformation Characteristics of Reinforced Sand," National Meeting on Water Resources Engineering, ASCE, Los Angeles, Preprint 2189.

Yeo, K.C., Yogarajah, I. and Chan, A.H.C. (1992), "Prediction analysis of two geosynthetic reinforced soil retaining walls using finite element method," Geosynthetic-Reinforced Soil Retaining Walls, Proceedings of the International Symposium on Geosynthetic-Reinforced Soil Retaining Walls, Denver, J.T.H. Wu ed., A.A. Balkema Publishers, Rotterdam, pp. 193-204.

Yogarajah, I. and Andrawes, K.Z. (1994), "Modeling Construction Effects in Polymeric Grid Reinforced Soil Walls," Fifth International Conference on Geotextiles, Geomembranes and Related Products, Singapore, Vol. 1, pp. 177-182.

Zornberg, J.G. and Mitchell, J.K. (1993), Finite Element Analysis of Geosynthetically Reinforced Soil Walls with Sloping Backfills, Geotechnical Engineering Report No. UCB/GT/93-04, Department of Civil Engineering, University of California, Berkeley, 164 p.

Zornberg, J.G. and Mitchell, J.K. (1994), "Effect of Sloping Backfills on Geosynthetically Reinforced Walls," Fifth International Conference on Geotextiles, Geomembranes and Related Products, Singapore, Vol. 1, pp. 201-206.

APPENDIX A:
UNIT CELL APPARATUS

A.1 Design Considerations

A.1.1 Introduction

The rationale for the design of the unit cell device (UCD) and the test procedure are presented in this section of the appendix. This information is intended to address questions with regard to the apparatus dimensions, loading system, testing procedure and consideration of boundary effects as well as provide a historical record of the reasoning behind the device design.

Studies by others have demonstrated the importance of performing tests on geosynthetics in conditions as closely resembling the anticipated field conditions as possible, and of reducing the boundary effects of the test apparatus. The field conditions to consider include: soil type and properties, including gradation, moisture and density; temperature; lateral confining pressures; vertical pressures; geosynthetic material; and strain rate of the geosynthetic. Total strain, creep, and scale and edge effects must also be considered (McGown, et al., 1978, 1982; Salomone, et al., 1980; Andrawes, et al., 1986; Rowe and Ho, 1986; Dembicki and Piotr, 1991; Juran, et al., 1988; Siel, et al., 1987; Miyamori, et al., 1986; Palmeira and Milligan, 1989). The effects on the design of the UCD due to these conditions are addressed, when applicable, below.

A.1.2 Total Strain

Geosynthetics in GRS walls designed according to current procedures have been shown to experience very low strains, typically less than 1% (Allen, 1991; McGown, et al., 1993). If design procedures are modified and the degree of conservatism in GRS walls is reduced, Allen recommends total strain in the reinforcement be maintained at less than 5% to meet serviceability requirements. Prediction of the deformation of GRS walls

under working conditions requires knowledge of the strength properties of geosynthetic reinforcing at these low strains. Therefore, determining the strength properties of reinforcement at strains between 0% and 5% was established as the range of interest for tests to be conducted as part of this project.

A.1.3 Specimen Size

A.1.3.1 General

Ideally a unit cell device intended for testing reinforced soil should be sized to reproduce the same relative concentration of reinforcing in the soil mass as exists in field applications. The spacing of reinforcing layers in GRS walls is determined by wall dimensions, the loads the wall is to experience and the properties of the soil and reinforcing. Layer spacing varies from wall to wall and may exceed one meter (Christopher, et al., 1991a, b; STS, 1990; Koerner, 1990; Allen, et al., 1992a; Fannin and Hermann, 1990). To develop a unit cell device for each potential spacing would require a very adaptable device or many individual devices, some of which would be relatively large.

Determining reinforced soil strength and deformation properties using a unit cell device requires that the improvement to the unreinforced soil provided by the reinforcing be measurable. To ensure the contribution of the reinforcing would be discernible, an increase in the concentration of reinforcing in the test device beyond the field concentration was deemed necessary. Increasing the reinforcement concentration may be accomplished in at least two ways. One option would require adding more sheets of geosynthetic to the center of a soil specimen having a vertical dimension equal to the design layer spacing for the GRS wall being designed. However, since the soil-reinforcement interaction mechanism was of primary interest in this program, increasing the quantity of reinforcement by placing two or more layers of geosynthetic adjacent to each other may have adversely affected the test results.

The concentration of reinforcement can also be increased by decreasing the vertical dimension of the soil specimen without adding more reinforcement. Once the in-soil load-elongation properties of the reinforcings are determined, extrapolation to the anticipated field spacings can be performed. This option was deemed more viable because it reduced the size of the test apparatus and specimen. Furthermore, if only a single apparatus is to be constructed, reliance on extrapolation for spacing of reinforcing different than the spacing selected for the device would have to be relied on at some point anyway. Reducing the test apparatus dimensions decreased space requirements and should have reduced total costs. Specimen preparation time for individual tests was also decreased, thus decreasing the overall time requirements for the testing program.

A.1.3.2 Geosynthetic Specimen Size

Research by McGown, et al. (1982) and Anjiang, et al. (1990) found specimens with dimensions of 200 mm wide by 100 mm long behave satisfactorily in tension tests. Further reducing the gauge length would assist in producing near uniform stress along the length of the reinforcing. However, a specimen gauge length of 100 mm has been found to be the minimum acceptable length for testing nonwoven geotextiles (in-isolation). Research indicates lengths less than 100 mm may report fiber strength instead of fabric strength (Anjiang, et al., 1990).

There has been no consensus by researchers as to the most appropriate aspect ratio to use in tension tests. Ling, et al. (1992) and Rowe and Ho (1986) recommend aspect ratios of 8:1 and 5:1, respectively. These authors reported on research where failure strains, which ranged from 16% to greater than 180%, were of primary interest. Although strains of this magnitude may be appropriate for determination of ultimate strength, they are much larger than the 0% to 5% range of interest. Using the aspect ratios recommended by Ling, et al. and Rowe and Ho may be unnecessary at low strains. McGown, et al. (1982) and Anjiang, et al. (1990) found aspect ratios of 2:1 to be acceptable. Necking of the specimens, subjected to low strains and confined in soil, was

not anticipated to be problematic so little benefit would be realized by increasing the aspect ratio beyond 2:1.

The specimen used for the ASTM D 4595 wide width tensile test has dimensions of 200 mm wide by 100 mm long. Direct correlation between manufacturer published ASTM D 4595 results and the results of tests performed with the unit-cell apparatus may be possible by using a specimen with these dimensions. A 200 mm wide by 100 mm gauge length specimen was therefore deemed appropriate as a starting point for performing the in-soil characterization tests of geosynthetics in the unit cell device.

A.1.3.3 Soil Specimen Dimensions

The necessity of performing in-soil tests with the soil at the same moisture content and density as it is placed in the field has been demonstrated (Dembicki and Piotr, 1991; Juran and Chen, 1988; Siel, et al., 1987; Miyamori, et al., 1986). Soils are generally compacted in field installations. Therefore, to obtain similar densities in laboratory tests, soils must be compacted in test devices. AASHTO method T180-74 (modified proctor compaction test) permits a 19.0 mm maximum particle size for soil to be compacted in a 101.6 mm diameter specimen. For devices with dimensions in excess of 71 mm, AASHTO test procedure T234-74 (triaxial compression test) requires the maximum particle size to be less than one-sixth the minimum dimension of the device. To obtain proper compaction of the soil in the testing device these recommendations seemed appropriate.

Minimizing the total volume of soil required in a given specimen should minimize specimen preparation time and cleanup. However, it was also necessary to ensure sufficient soil coverage to reduced boundary effects and ensure the unit cell concept is not violated. In an evaluation of boundary effects Rao, et al. (1988) found that soil thicknesses above and below geosynthetics in direct shear style tests should be the greater of 50 mm, 15 times the D_{85} of the soil, or 2 times the maximum particle size.

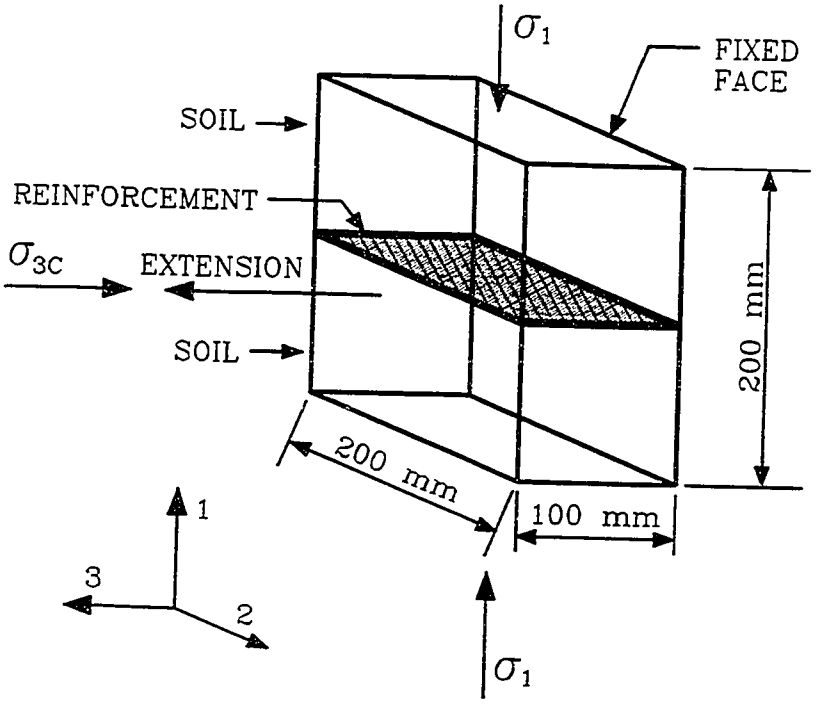

Figure A.1: Unit cell specimen dimensions.

Maximizing the soil depth above and below the geosynthetic should minimize the effect of compressibility and thickness of the reinforcing on specimen preparation and test results (Miyamori, et al., 1986). The potential for repeatable obtaining proper soil density should also be improved. Maximizing the soil cover also increases the distance between the reinforcing and any device boundary effects.

For a maximum soil particle size of 9.5 mm (US 3/8 in. sieve) and minimum soil specimen dimension of 100 mm, all of these recommendations are met. Constructing the unit cell device with a 100 mm gauge length geosynthetic specimen and 100 mm of soil cover above and below the geosynthetic was required, Figure A.1.

A.1.4 Method of Load Application

To simulate the vertical applied loads of high (12.5 meter) GRS walls, as was experienced in the Rainier Avenue Wall (Christopher, et al., 1991), a unit cell device

constructed to simulate the full scale spacing of reinforcing layers (380 mm in the case of the Rainier Avenue Wall) must be capable of applying vertical pressures in excess of 310 kPa. However, the unit cell device, as dimensioned above, has an effective reinforcement layer spacing of only 200 mm. To obtain the same lateral strains as experienced in the Rainier Avenue wall the effective vertical pressure to be applied must be doubled to near 600 kPa. And furthermore, since the Rainier Avenue Wall experienced only very small strains the loading system must be able to apply even greater vertical pressures to induce additional strain in the reinforcing. A peak applied pressure of 1360 kPa was selected. For the selected geosynthetic specimen dimensions of 200 mm by 100 mm, the reaction load per 100 kPa of applied pressure is 2 kN. The unit cell device was constructed heavily enough to resist excessive deformation when loads of this magnitude are applied.

Very few laboratory tests involving geosynthetics for reinforcing applications have been performed with pressures this high. Applying the loads with weights or weights on lever arms could require significant space. Utilizing hydraulic rams to apply the load is another possibility. However, if numerous creep tests are to be performed additional devices may need to be manufactured. This would require many hydraulic load applicators and the additional plumbing, pumps and controllers could become expensive.

Rigid plates have generally been used in geosynthetic test apparatus to transfer energy from weight or hydraulic ram load applicators to the soil. However, to reduce boundary influences and ensure uniform applications of loads to the soil, Palmeira and Milligan (1987) recommend the use of flexible bladders instead of rigid plates. By incorporating flexible bladders into the device, overall space requirements were reduced. Space limitations, as well as financial considerations, encouraged the use of a device as small as practicable.

Thus, flexible bladders were selected as the method of choice for load application. Flexible bladders insure uniform distribution of applied pressures and are able to deform with the specimen as dimensions of the unit cell change during loading. As long as the

bladders remain confined, and are flexible enough to expand to the rectangular shape of the unit cell, the pressure which can be applied to the specimen is limited only by the strength of the reaction frame for the test device and the source of pressurized gas.

Because of the relatively large volume change which the bladders undergo during a test, very flexible load application bladders were required. Furthermore, the edges and corners of the rectangular prism were found to cause problems if the bladder did not readily take the shape of the area in which it was confined. Custom manufactured, thin-wall, latex rubber bladders were ultimately obtained for use in the unit cell device. Silicone rubber "fillet" pieces were put in the corners of the space confining the bladders to prevent the bladders from getting damaged by squeezing into the space between moving parts.

A.1.5 Rate of Load Application

Tests on geosynthetics have shown that the rate of load application influences the measured strength, with modulus and ultimate strength decreasing as strain rate decreases (Rowe and Ho, 1986; Anjiang, et al., 1990, Nothdurft, 1994, 1995). Under field conditions, during the construction of GRS walls, the reinforcing is loaded very slowly. To best simulate field conditions it follows that the geosynthetic should be loaded as slowly as practicable. Rowe and Ho recommend the strain rate not exceed 2% per minute to minimize the difference between strengths measured in the laboratory and those actually obtained in field installations. In the unit cell device the soil, not the geosynthetic will be loaded. Consequently, the reinforcing strain rate cannot be controlled since soils and geosynthetics with various strengths respond differently to the rate of soil loading.

Loading the specimen from the initial confining pressure to the maximum pressure or strain limit of the device in step loadings of 10 kPa each 30 seconds was selected as an appropriate rate. This rate was been selected to maximize the number of tests performed in this program, while allowing the specimens to be loaded slowly.

A.1.6 Temperature

The polymeric reinforcing strength has been found to be temperature sensitive. It has been recommended that laboratory tests on geosynthetics be performed at temperatures simulating those anticipated in field operating conditions (McGown, et al., 1982; Andrawes, et al., 1986; Rowe and Ho, 1986). In many parts of North America this average ambient temperature is within the range 10°C to 25°C. The temperature in the laboratory in which the tests were performed could not be independently controlled. However, the room temperature was fairly stable, typically between 20°C and 22°C.

A.1.7 Boundary Effects

Boundary effects may significantly influence test results if not properly accounted for. Reducing or eliminating boundary effects on the test specimen, due to the test apparatus, is necessary (McGown, et al., 1982; Palmeira and Milligan, 1989; Farrag, 1990). This can be accomplished by removing boundaries from the zone of influence, reducing the contact friction and/or measuring the influence of the boundaries on the test results and "backing out" these effects. Reducing contact friction between the soil and device has been shown to be an effective solution (McGown, et al., 1982; Palmeira and Milligan, 1987).

A finite element analysis was undertaken to evaluate the effects of boundary friction on tests performed in the UCD. The ANSYS® finite element program was used (Swanson Analysis Systems, 1992). The analysis was performed to evaluate the effects of boundary friction on: (1) the distribution of confining stress that would be experienced at the soil-geosynthetic contact; (2) the uniformity of stress in the soil; and (3) the displacements of the soil at the soil-vertical face contact.

The unit cell, measuring 100 mm long by 200 mm wide by 200 mm high, Figure A.1, was modeled as a two dimensional linearly elastic body in cross-section in the

direction of expansion of the cell. In recognition of the symmetry of the problem, only one quarter of the unit cell required modeling, Figure A.2. Two-dimensional isoparametric stress elements defined the soil and two-dimensional interface elements were used to simulate sidewall friction in the analysis. To ensure the soil remained in contact with the device sidewalls during deformation, the nodes along the vertical faces were coupled to undergo equal lateral displacements. Elastic properties for the soil were taken as: $E = 100{,}000$ kPa, $\nu = 0.3$, $G = E/[2(1+\nu)]$. The coefficient of friction was varied from 0.00 to 0.30. Lateral confining pressure, P_h, was applied in the form of point loads at nodes on the vertical faces. Vertical surcharge pressures, P_v, were applied as distributed pressures on the top surface. Both horizontal and vertical pressures were varied from 20 kPa to 280 kPa.

The evaluation of the results of the analysis concentrated on the distribution of vertical pressure experienced at the soil geosynthetic contact, SG_v, and its relation to the applied vertical pressures, P_v. The results of the analysis, for the range of pressures and coefficients of friction investigated are presented in Figures A.3 - A.10. As the coefficient of sidewall contact friction increased, the maximum pressure experienced at the soil-geosynthetic contact decreased. The uniformity of the soil-geosynthetic contact pressure also decreased with increasing sidewall friction. The analysis also showed the ratio of contact pressure to vertical pressure, SG_v/P_v, to be a function of the ratio of horizontal pressure to vertical pressure, P_h/P_v. For any given coefficient of friction, as the ratio of P_h/P_v decreased, the magnitude and uniformity of the soil-geosynthetic contact pressure increased.

Analysis was also performed assuming a length of geosynthetic of 200 mm instead of 100 mm. The uniformity of contact pressure and the maximum value of contact pressure increased above that obtained for a specimen of 100 mm length subjected to identical pressures and sidewall friction. Thus, the uniformity of stress distribution in the specimen increased with decreasing ratio of soil volume to boundary contact area.

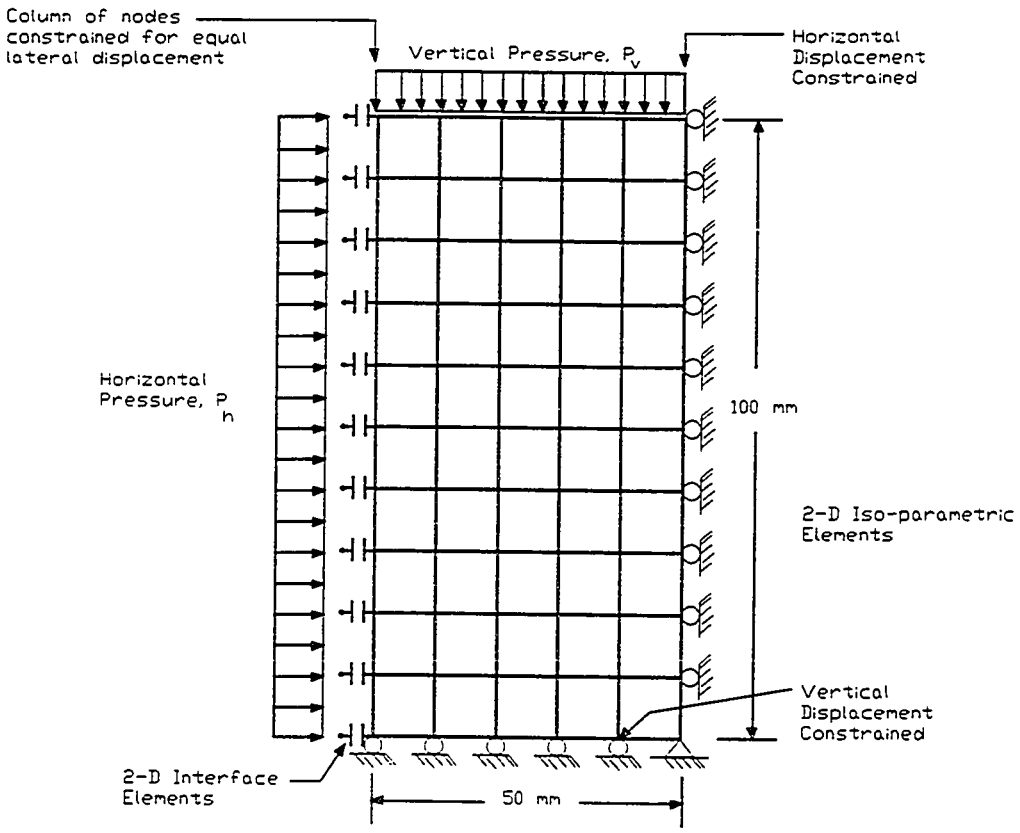

Figure A.2: Finite element model of the UCD for boundary friction analysis.

The maximum degree of non-uniformity of the soil-geosynthetic contact pressure that would not adversely affect the results of tests in the unit cell device may be a matter of opinion. Using this finite element analysis as a basis, Figures A.3 - A.10 suggest that a coefficient of friction as high as 0.10 may be acceptable in some cases. Lower friction coefficients would be more desirable and would have less effect on the stress distribution within the specimen. By lubricating all surfaces and covering them with a flexible membrane, coefficients of contact friction less than 0.03 have been reported (Leshchinsky and Field, 1987; Wu, 1992a).

To confirm that coefficients of friction of this magnitude would be possible, a series of direct shear tests were performed. In a Karol-Warner direct shear device the bottom half of the soil specimen was replaced by a machined steel surface, Figure A.11. The surface extended beyond the limits of the circular soil specimen such that a constant contact area shear test was performed. The friction angle determined from direct shear test for the Rainier Avenue Sand used varied from 55° at 207 kPa normal stress to 49° at 690 kPa normal stress. The various surface conditions evaluated and the results are presented in Table A.1. Coefficients of friction ranging from 0.018 to 0.031 were obtained when silicone spray covered with a 0.3 mm latex membrane separated the soil from the steel. However, the spray is water based and as the water evaporates, as would occur during the time it takes to fully construct a specimen in the unit cell device, the friction angle increases. Tests with silicone grease between the steel surface and a 0.3 mm latex membrane obtained friction coefficients near 0.09. This coefficient is higher than those reported by Palmeira and Milligan (1989) and Wu (1992a) but within the margin of acceptability based upon the finite element analysis performed. Uniformity of soil-geosynthetic contact friction would fall between the conditions presented in Figures A..5 and A.6.

The finite element analysis determined that boundary effects may be significant if efforts are not made to reduce the contact friction. Following the recommendations of Palmeira and Milligan (1989) and Wu (1992a), lubrication of the interior of the unit cell with silicone grease and lining it with a flexible latex membrane should have reduced the influence of boundary friction to acceptable levels. Grease was applied to the neoprene liner used to protect the bladders from the soil to minimize friction at the top and bottom of the specimen.

A.1.8 Apparatus Design

The unit cell apparatus, manufactured for this project, is depicted in Figure A.12. The device, as shown, permits testing of a 100 mm gauge length by 200 mm wide

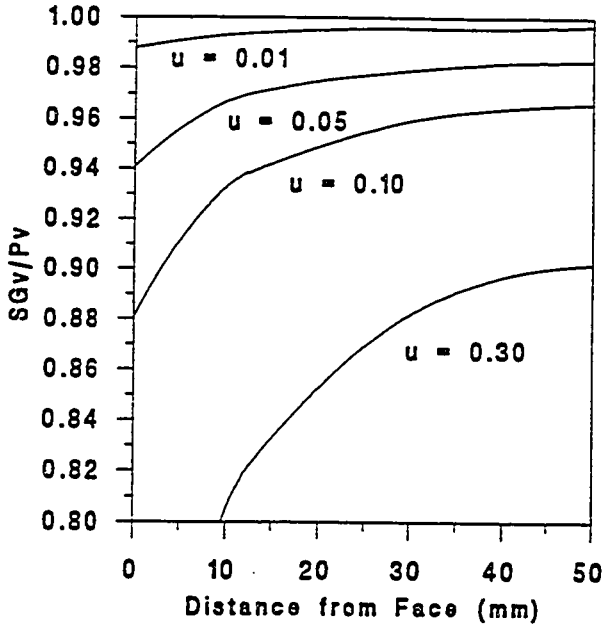

Figure A.3: Contact stress distribution. $P_h = 20$ kPa, $P_v = 70$ kPa.

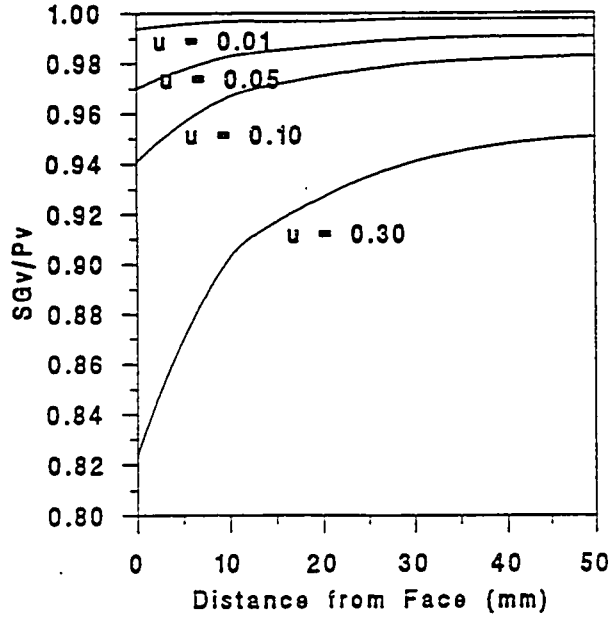

Figure A.4: Contact stress distribution. $P_h = 20$ kPa, $P_v = 140$ kPa.

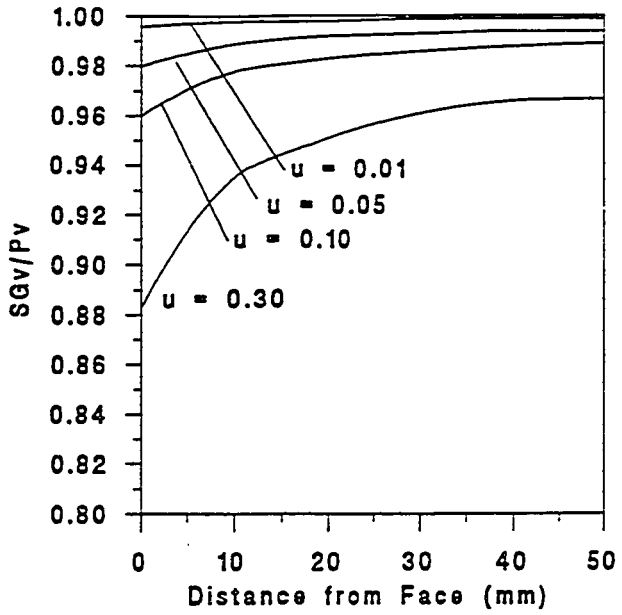

Figure A.5: Contact stress distribution. $P_h = 20$ kPa, $P_v = 210$ kPa.

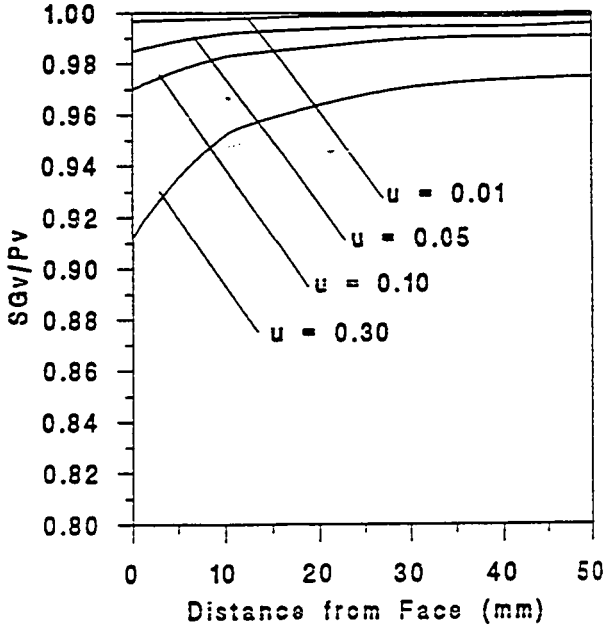

Figure A.6: Contact stress distribution. $P_h = 20$ kPa, $P_v = 280$ kPa.

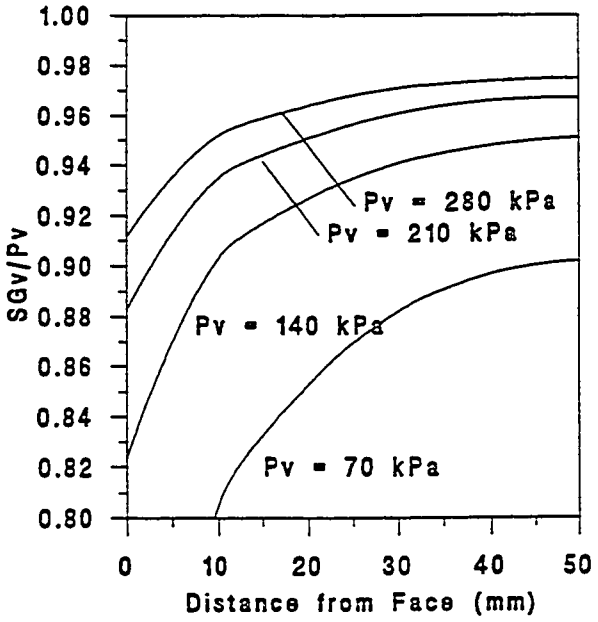

Figure A.7: Contact stress distribution: $P_h = 20$ kPa, $\mu = 0.30$.

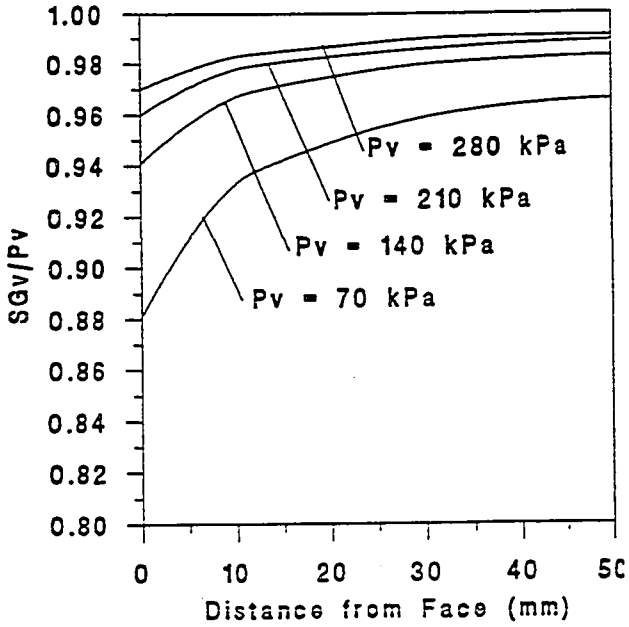

Figure A.8: Contact stress distribution: $P_h = 20$ kPa, $\mu = 0.10$.

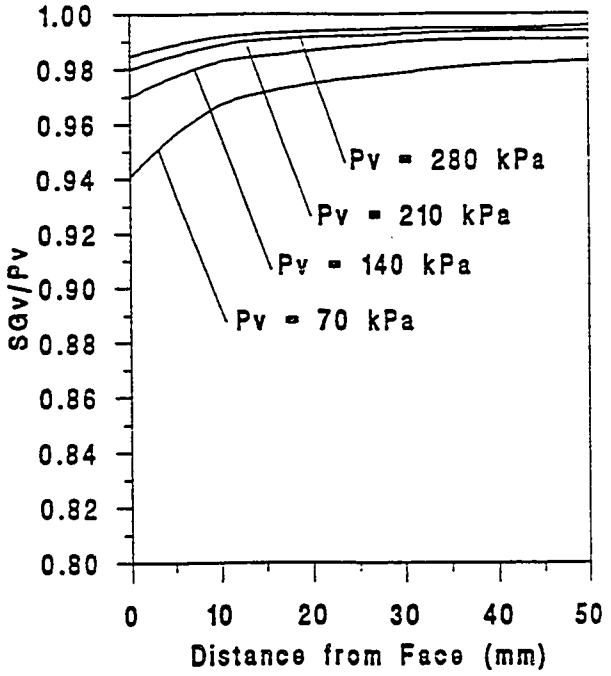

Figure A.9: Contact stress distribution: $P_h = 20$ kPa. $\mu = 0.05$.

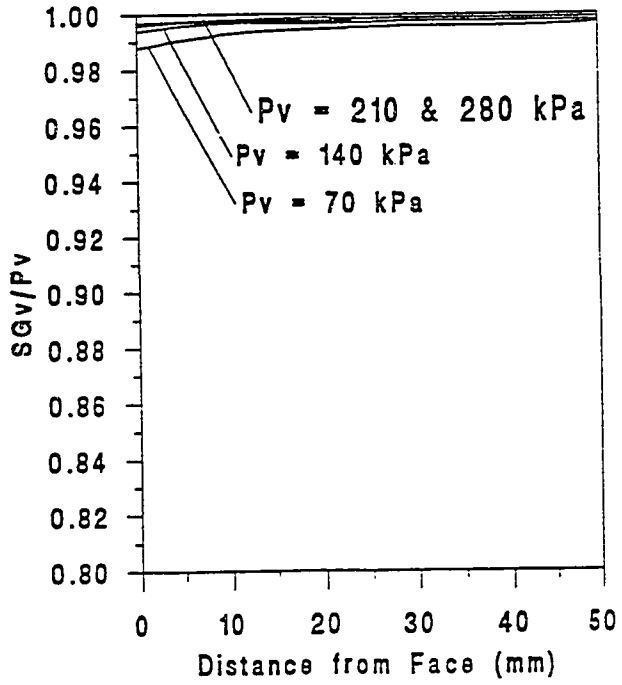

Figure A.10: Contact stress distribution: $P_h = 20$ kPa, $\mu = 0.01$.

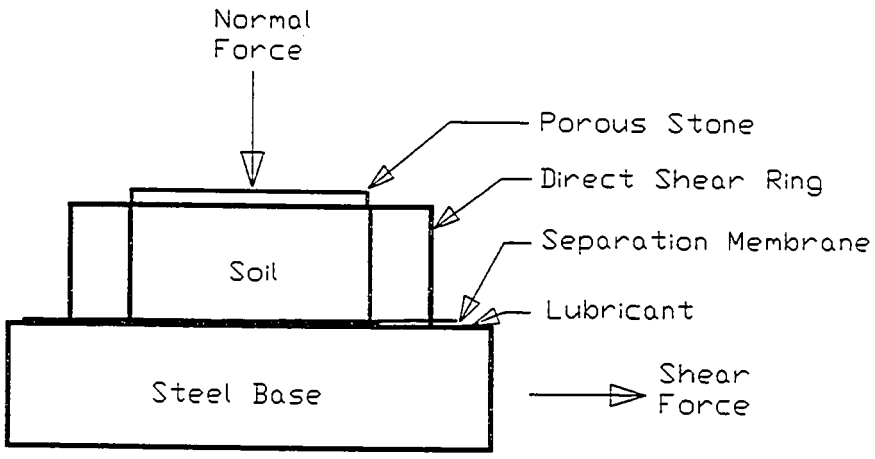

Figure A.11: Modified direct shear device for interface friction tests.

Table A.1: Interface friction test results.

Interface Description	Coefficient of Friction
Steel alone	0.44 +/- 0.03
Steel w/0.1 mm polyethylene sheet, lubricated with silicone grease.	0.21 +/- 0.03
Steel w/ 0.1 mm polyethylene sheet, lubricated with silicone spray.	0.16 +/- 0.02
Steel w/ 0.3 mm latex membrane, lubricated with silicone grease.	0.09 +/- 0.015
Steel w/0.03 mm latex membrane, lubricated with silicone spray.	0.025 +/- 0.007

specimen covered with 100 mm of soil both above and below. The geosynthetic is situated at mid-height of the specimen and held in position by clamps at each end. Vertical pressure is applied to the top and bottom of the reinforced soil via bladders. The Poisson effect from vertical compression of the soil results in lateral expansion of the soil element, Figure A.1. The left instrument box is mounted on bearings and is free to displace horizontally, permitting the soil to strain laterally when loaded. The lateral strain of the soil is resisted by loads induced in the reinforcing element. A clamp connecting the geotextile to the left instrument box ensures the reinforcing elongates with the deforming soil *even if the soil-geosynthetic contact friction is exceeded.* The clamp is connected with a single pin which will permits rotation of the clamp in the horizontal plane. By allowing this rotation, non-uniform stress application across the width of the specimen should be eliminated. The bladder between the left instrument box and the reaction frame provides lateral confining pressure. Constant confining pressure can be maintained by increasing the pressure in the end bladder to compensate for increases in pressure in the top and bottom bladder. The rigid vertical faces of the device force the soil to maintain its shape with all faces mutually perpendicular.

The apparatus was designed as a collection of modules to permit simplified modifications. Testing unit cell elements of greater length or height could be accomplished by designing and manufacturing the necessary components. These modifications are discussed in appendix Section A.5.

A.1.9 Summary

The rationale behind the design of the unit cell apparatus was presented in this section of Appendix A. The discussion concerned issues of total strain, strain rate, specimen size, load application methods, temperature and boundary conditions and how they were considered in the design. Boundary effects were investigated at length. A finite element analysis found that the stress state in the soil should be relatively uniform if the coefficient of friction between the soil and steel side walls could be maintained below

LEGEND

A	REACTION FRAME
B	LEFT INSTRUMENT BOX
C	RIGHT INSTRUMENT BOX
D	LEFT END BLADDER
E	RIGHT END SPACER
F	VERTICAL DISPLACEMENT LVDT's
G	HORIZONTAL DISPLACEMENT LVDT's
H	CLAMP LOAD CELL's
I	PIVOTS
J	CLAMPS
K	TOP AND BOTTOM BLADDERS
L	TURNBUCKLES
M	BEARINGS
N	REINFORCING
O	σ_2 LOAD CELLS

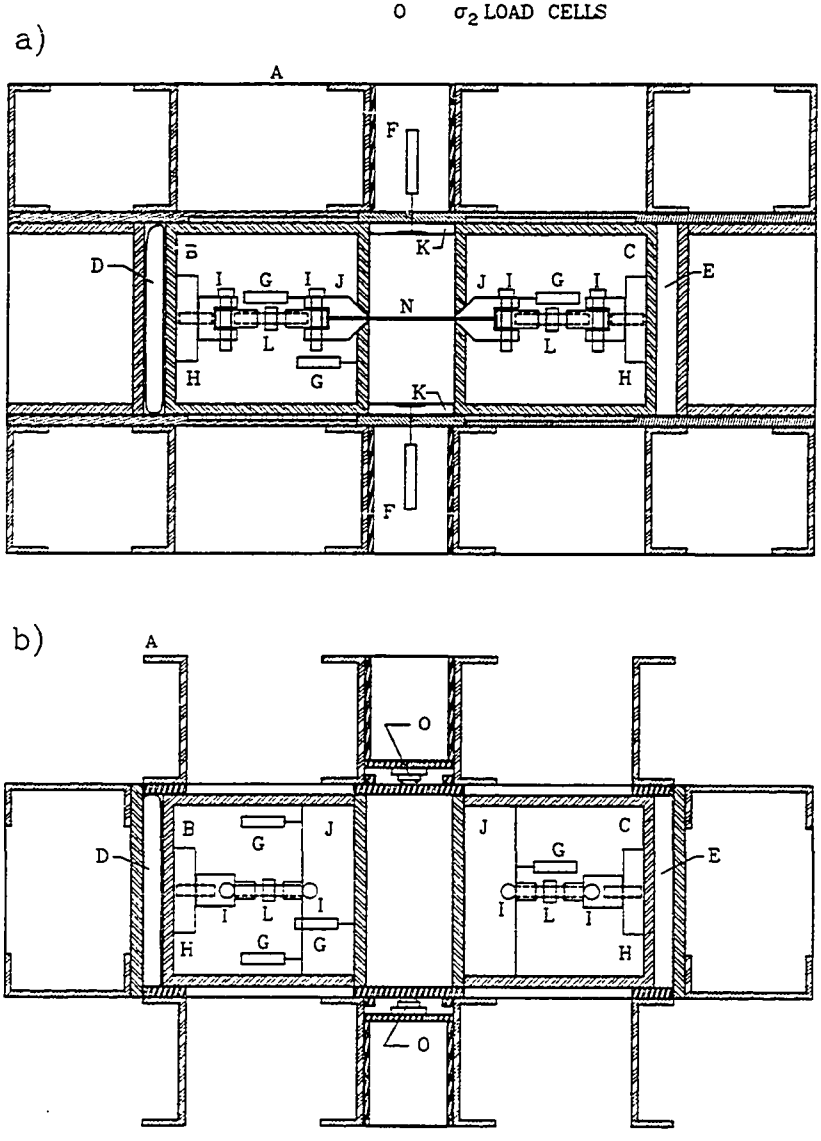

Figure A.12: Schematic of Unit Cell Device, including reaction frame, a) profile cross section, b) plan view cross section.

0.10. Lubricating the steel with silicone grease and covering the grease with a 0.3 mm latex membrane was found to meet this criterion.

A.2 Operating Options

A.2.1 Constant Lateral Confining Pressure on Composite

The lateral confining pressure applied to the composite is governed by Equation A.1. To maintain a constant lateral pressure on the composite throughout the test the pressure applied to the end bladder must be adjusted to offset the increase in horizontal forces applied to the confining plate (clamp/instrument box) due to increases in applied vertical pressures and specimen deformation. This is the mode of operation followed for the test program presented in this dissertation.

$$\sigma_{3C} = \text{Constant} = \frac{P_e H_e W_e - (P_t H_t + P_b H_b) W_s}{H_s W_s} \qquad \textbf{(A.1)}$$

where $P_{e,t,b}$ = pressure in end bladder,

$H_{e,t,b}$ = height of end, top, bottom, bladder,

W_e = width of end bladder,

W_s = width of soil specimen,

H_e = height of soil specimen.

A.2.2 Effective Confining Pressure Concept - Tests without Reinforcing

It may be possible to obtain the plane strain composite response of reinforced soil without including reinforcing in the soil specimen, as advocated in Section 6.5. The composite response may be simulated by increasing the lateral confining pressure acting on an unreinforced soil specimen by an amount equal to that which would result due to elongation of the reinforcing had it been installed, Eq. 6.21. The UCD may be used to perform tests in this manner. To do so it is necessary to replace the end plates, through which the reinforcing passes to the clamps, with the solid plates used for testing

unreinforced soil. Because the UCD is a load control device the post-peak behavior of reinforced specimens could not be obtained. Modifying the UCD to be a strain controlled apparatus would facilitate measurement of the post-peak response and would permit verification of the post-peak behavior hypothesized in Section 6.4.3.4.

A.2.3 Stress Relaxation of Unconfined Specimens

Stress relaxation tests may be conducted using the UCD. It is possible to install a geosynthetic specimen in the unit cell device without encapsulating it in soil and to load the specimen using the turnbuckles on the clamp-load cell connecting rods, Figure A.12. Stress-relaxation tests on various geosynthetics could be performed by applying a known strain or load to a reinforcing specimen and monitoring the load in the specimen for an extended duration. Stress relaxation tests, where known strains are applied, may be used to estimate the load supported by a reinforcing specimen at a given strain. The results of stress relaxation tests of this type would provide a more direct means of assessing the long term stress condition in reinforcement in an actual wall than could be obtained by converting measured strains to stresses using load-elongation correlations obtained from wide width, pull-out, or creep test results.

A.2.4 Bi-directional Displacement of Specimen

The unit cell device, as configured for the tests performed as part of this study, only permitted lateral deformation of the specimen from one end, Figure 6.12. By replacing the spacer plate behind the right end instrument box with a load application bladder lateral deformation of the specimen can occur in both directions. The primary advantage of permitting bi-directional displacement is that deformation of the specimen could exceed 10% lateral strain. The primary disadvantage would be that the maximum load carried by the fabric would not occur at one of the clamps, Figure 2.18.

A.2.5 Different Size Specimens

The dimensions of unit cell specimens tested in the device could be varied by modifying the apparatus. Testing specimens with greater lengths, e.g., 200 mm instead of 100 mm, could be accomplished by manufacturing new side plates and top and bottom center frames. Increasing the specimen length to an even multiple of the current 100 mm would permit use of existing top and bottom bladders. For other lengths, additional bladder molds and bladders would have to be manufactured.

To test taller specimens would require modifications to the heights of the instrument boxes or installation of a spacer, of 1/2 the height change, below the boxes as well as modifying the face plates on the boxes. In either case, the end of the reaction frame would have to be increased in height. Spacers could be used, and longer vertical members manufactured for the sides. Testing shorter specimens may be possible with the current arrangement by stretching the load application bladders further than they are in the tests performed as part of this program.

A.3 UCD Specimen Preparation and Test Procedure

A.3.1 UCD Specimen Preparation

Prior to constructing a specimen in the UCD the interior space was wiped clean and the bottom bladders installed. The left instrument box was then clamped in the zero displacement position. A 0.8 mm neoprene rubber sheet, lubricated on both sides with silicone grease, was placed over the bladders to prevent damage during compaction of the soil or when the bladders were pressurized. Silicone grease was then applied to the interior face of the UCD steel plates and overlain with a 0.3 mm latex rubber membrane liner. One quarter of the soil specimen (by weight) was then placed in the UCD and compacted by dropping a 2.3 kg mass through a distance of 300 mm 25 times. Because of the rectangular shape of the UCD and the circular cross-section of the weight used for compaction the weight was dropped on a 97 mm by 40 mm steel plate that was in contact

with the soil surface. Use of this plate improved compactibility of the dry sands and ensured the soil near the device corners and boundaries was properly compacted. The next quarter of the soil specimen was then similarly compacted in the UCD.

After compacting the soil in the lower half of the UCD the reinforcing specimen was installed over the soil and clamped at both ends. [To facilitate installation of the reinforcing and prevent damage due to the clamps, the ends of the geosynthetic reinforcements were coated with epoxy. Holes were punched through the epoxy to match the clamp bolt pattern.] Once the clamps had been tightened the reinforcing was pretensioned to remove slack by turning the turnbuckles located between the clamps and their load cells, Figure A.12. The remaining soil was then placed above the reinforcing in two more lifts. Each lift was compacted as described above. Once the soil was in place another 0.8 mm neoprene rubber sheet, lubricated on both sides, was placed over the soil so soil particles would not puncture the top bladders when they were inflated. The top of the UCD, to which the top bladders were attached, was then positioned over the soil and tightened in place.

A.3.2 UCD Test Procedure

Tests were begun by applying vertical and lateral confining pressures to the specimen that were equal to the lateral confining pressure to be applied to the composite during the test, σ_{3C}. The clamp holding the left instrument box was then removed and the specimen permitted to consolidate for a minimum of 150 seconds. Because the soils tested were dense sands longer consolidation periods were not necessary. Upon completion of consolidation, the specimens were loaded by increasing the vertical pressure, σ_1, by 10 kPa every 30 seconds. This pressure increase was manually controlled using pressure regulators. To maintain conditions of constant lateral confining pressure on the composite during each test, the pressure in the end bladder was increased to compensate for pressure from the top and bottom bladders that acted on the left instrument box in accordance with Equation A.1. Electronic instruments and a

computerized data acquisition system were used to measure and record applied pressures, displacements, and reinforcing loads.

A.4 Equipment and Material Supplier List

The companies which supplied or manufactured equipment and materials that were used in the UCD testing program are presented in Table A.2.

Table A:2: Equipment and Material Supplier List.

Item and Use or Purpose	Product Description	Manufacturer and/or Supplier
Steel beads used for Soil 3	0.42 mm - 0.84 mm steel shot	Abrasives NW 1114 Andover Park West Seattle, WA 98188
Stainless Steel Sheet Reinforcement	Stainless steel Type 321 Tool Wrap -- MFR Code: 698158 NIDA/SIDA: 20110 GAGE: 0.002	Precision Brand Downers Grove, IL.
Epoxy for preparing ends of geotextile specimens	Epibond epoxy adhesive 1526-A/B	Ciba-Geigy Corp. 5121 San Fernando Road West Los Angeles, CA 90039
Lubricant for greasing inside of UCD	Marson K-2 Silicone Compound No. 35008	Marson Corp. 130 Cressent Ave. Chelsea, MA 02150
Woven Geotextiles	GTF 200, 375, 500, 1000 and 1225. (GTF 375, 500, and 1225 no longer manufactured.)	Exxon Chemical Corp. (Now LINQ Industrial Fabrics) 2550 W. 5th N. Street Summerville, SC 29483
Nonwoven Geotextiles	TS700, TS1000	Polyfelt, Inc. 1000 Abernathy Rd. Building 400, Ste. 825 Atlanta, GA 30328
Pressure Gauges for UCD Control Panel	0-100 psi pressure gage Cat No. G-68800-49 0-200 psi pressure gage Cat No. G-68800-44	Cole Palmer Instrument Co. 7425 N. Oak Park Ave. Niles IL 60714
Pressure Regulators for UCD	2-250 psig pressure regulator 10162BP 3-200 psig pressure regulator 10172	Fairchild Industrial Products Co. 3920 West Point Blvd. Winston-Salem, N.C. 27103
Displacement measurement LVDT's for UCD and in-isolation "scissors"	250 MHR LVDT, ± 6.35 mm 500 MHR LVDT, ± 12.7 mm 1000 MHR LVDT, ± 25.4 mm	Lucus-Schaevitz 7905 N. Route 130 Pennsauken, NJ 08110-1489
Power supplies, amplifiers, and signal conditioners for UCD instruments	AE312 SA-10 -- Power Supply AE321 SA-B -- DC Card AE325 SA-AC -- AC Card	Sensotec 1200 Chesepeake Ave. Columbus, Ohio 43212-2237
Pressure transducers for UCD bladders	BP211 Model LM, 200 psi BP211 Model LM, 100 psi	Sensotec 1200 Chesepeake Ave. Columbus, Ohio 43212-2237
Load cells for measuring clamp load and intermeadiate principle stress in UCD	AL111 Model 41, 4000 lb AL131 Model 53, 2000 lb	Sensotec 1200 Chesepeake Ave. Columbus, Ohio 43212-2237

Table A.2, cont: Instrument and Material Suppliers List

Item and Use or Purpose	Product Description	Manufacturer and/or Supplier
Latex Liner for UCD	0.3 mm latex sheeting	McMaster-Carr Supply Co. P.O. Box 54960 Los Angeles, CA 90054-0960
Bladders for load application in UCD	Custom fabrication	California Latex, Inc. 748 E. Bonita Ave. #205 Pomona, CA 91767
Strain gages, primer and adhesive used on woven polypropylene geotextiles.	YFLA-2, YL-10 and YL-20 strain gages. Aron polyprimer and CN adhesive.	Texas Measurements, Inc. P.O. Box 2618 College Station, TX 77841
Strain gages and adhesive used on woven multi-filament polyester geotextiles.	PA-3 and PA-7 strain gages. SR-4 cement.	BLH Electronics Shawmut Road. Canton, MA 02021
Dye for Ottawa Sand (Soil O)	Methylthymol Blue ($C_{37}H_{39}N_2Na_5O_{13}S$)[blue dye]	Eastman Kodac Co. Rochester, NY 14650
Dye for Rainier Sand (Soil R)	Alizarin [orange dye] Thymol Blue (Thymol Sulfonphthalein) [blue dye]	Allied Chemical 40 Rector Street New York 6, NY

APPENDIX B
SOIL TEST RESULTS

This appendix contains information on soil shear strength and deformation properties. Triaxial test results are presented in the form of stress ratio, σ_1/σ_3, versus axial strain, ε_1, and volumetric strain, ε_v, versus axial strain. Plane strain test results, which were performed on unreinforced soil specimens in the unit cell device, are presented in the form of stress ratio, σ_1/σ_3, versus *lateral* strain, ε_1, and volumetric strain, ε_v, versus lateral strain. Lateral strain is plotted to permit comparison with the results for reinforced specimens presented in Chapter 6 and in Appendix C. Because the UCD is a load control device post peak behavior of the soil could not be obtained. Therefore, unlike the triaxial test results, post peak soil behavior is not presented on the figures in this appendix.

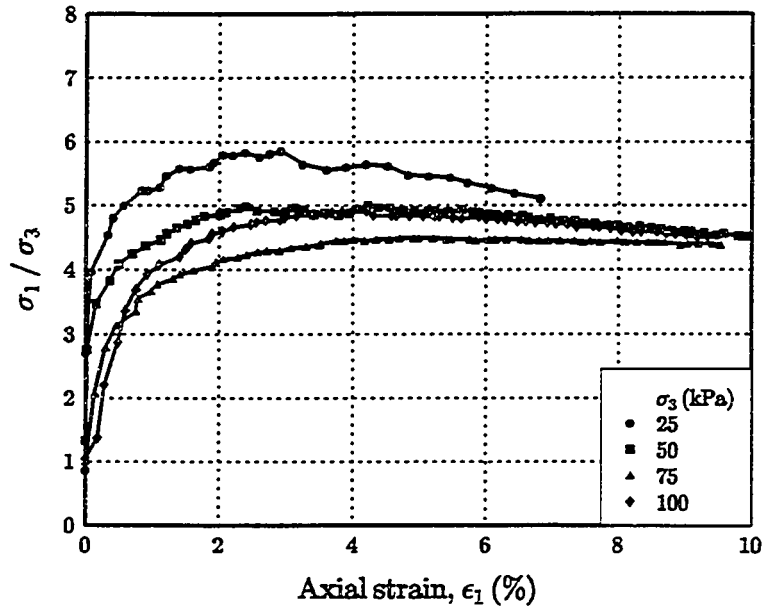

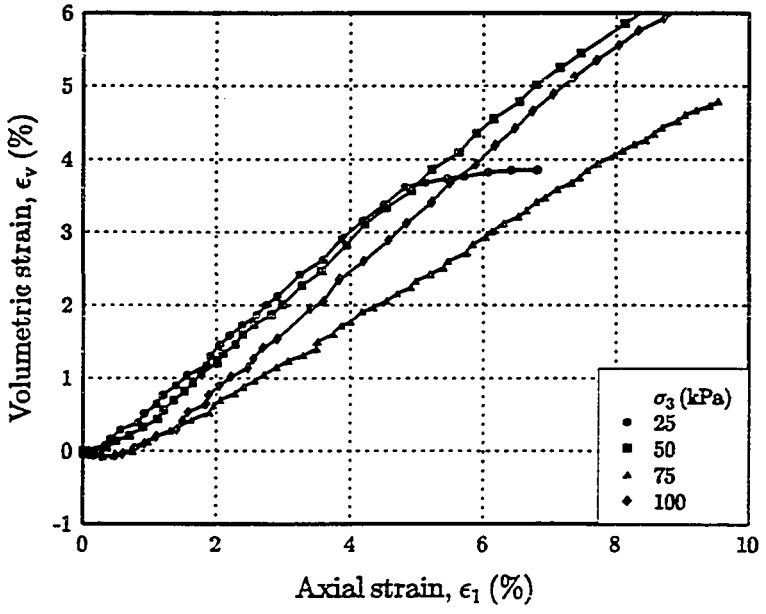

Figure B.1: Triaxial test results for Soil O.

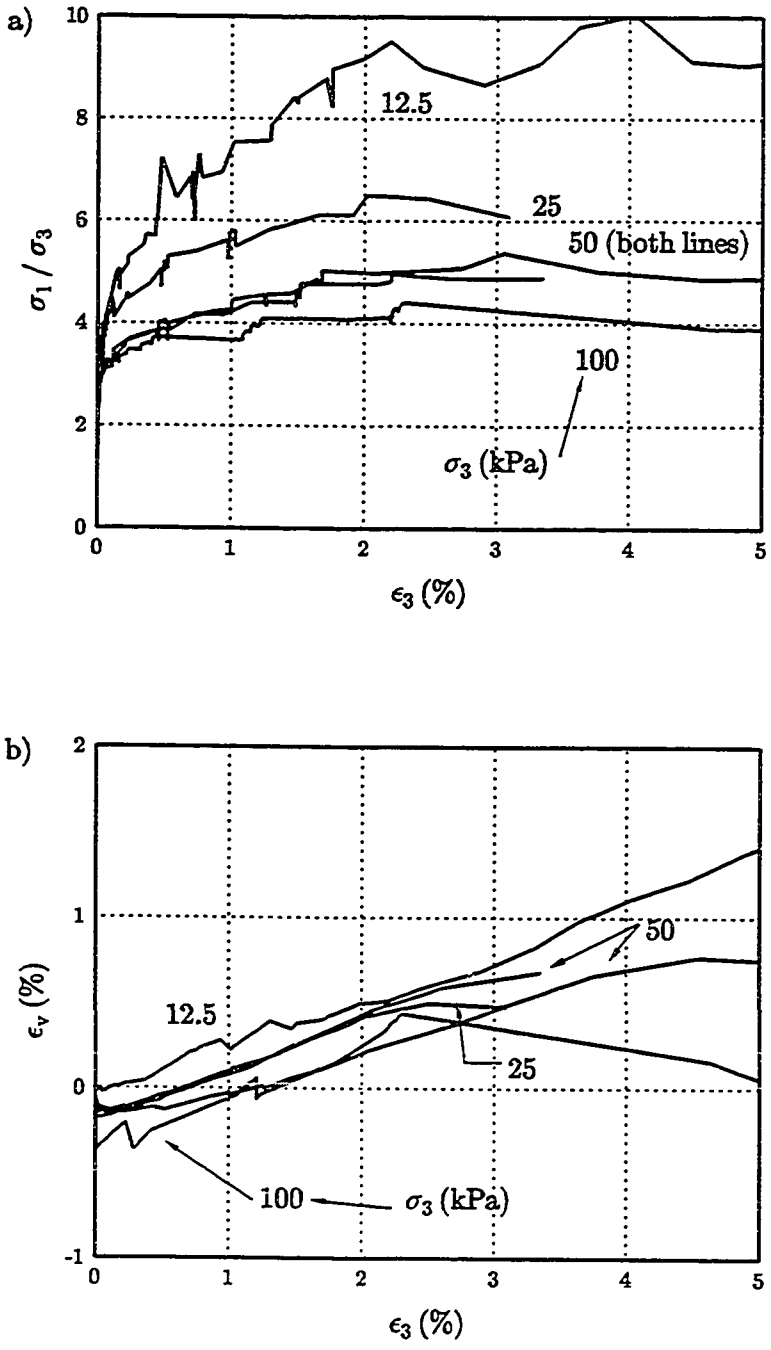

Figure B.2: Plane strain test results for Soil O.

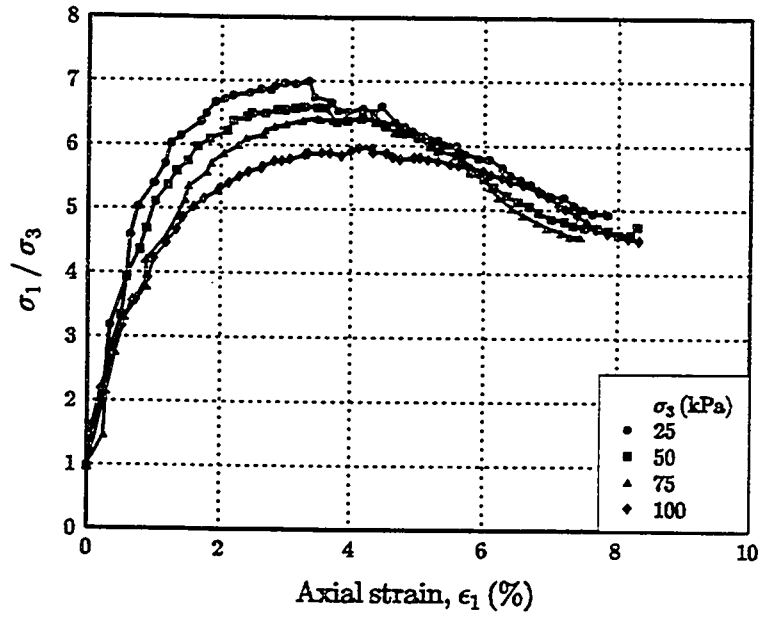

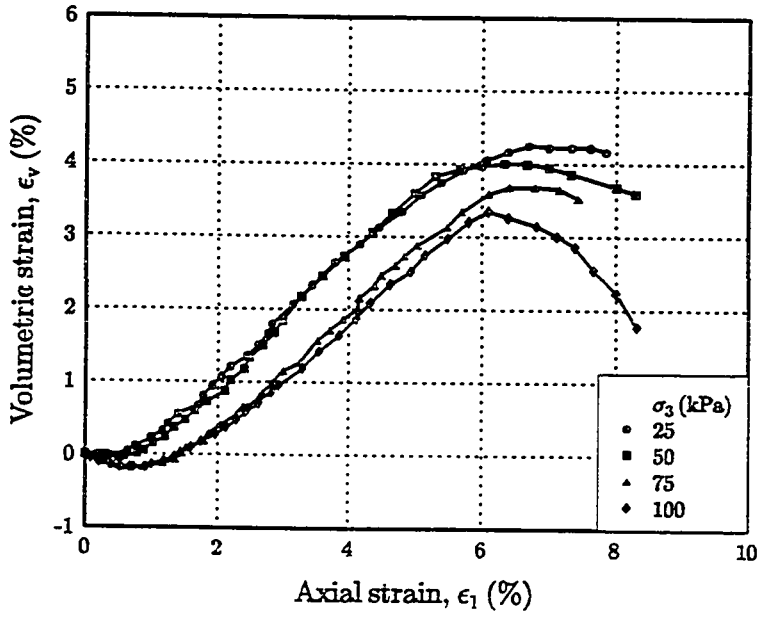

Figure B.3: Triaxial test results for Soil R.

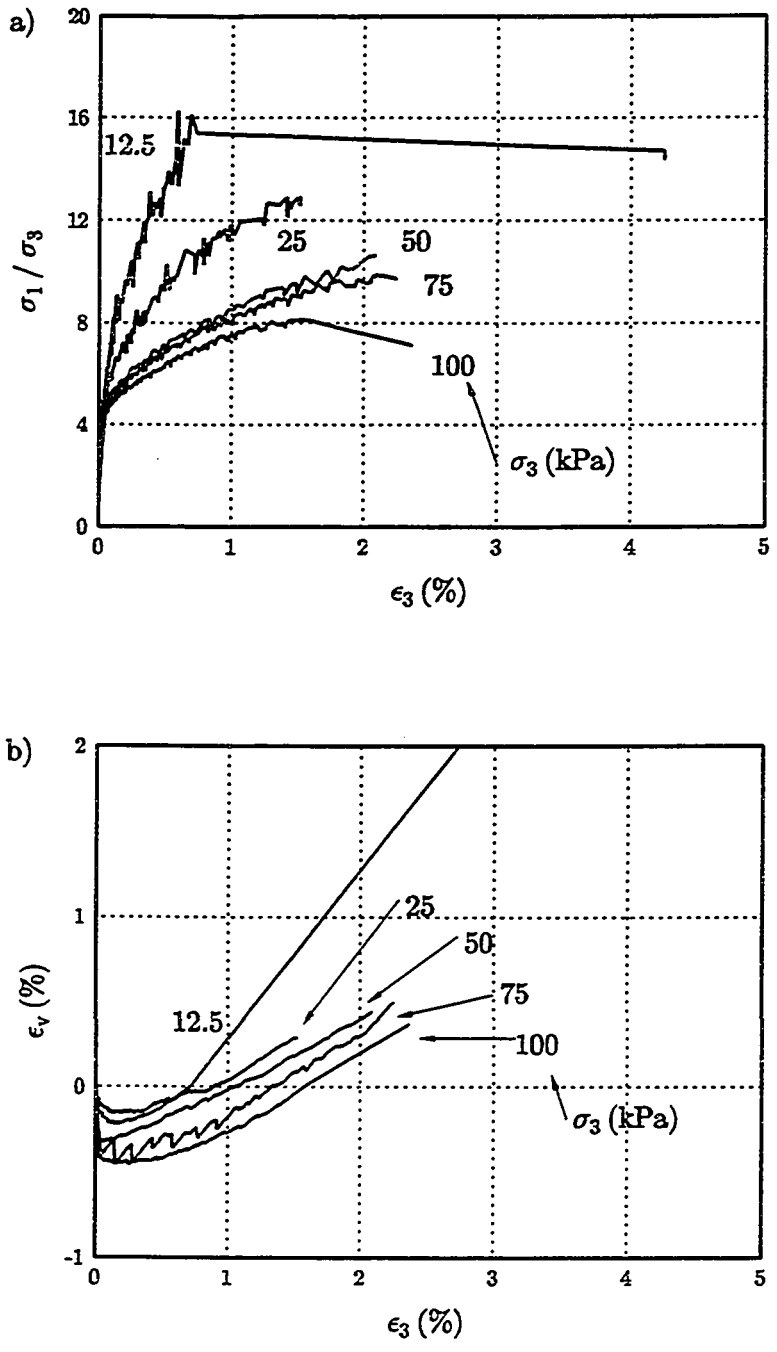

Figure B.4: Plane strain test results for Soil R.

APPENDIX C
UNIT CELL TEST RESULTS

This appendix contains plots of results from each of the unit cell tests on reinforced soil specimens listed in Table 6.4. The test results are grouped by soil type, subgrouped by reinforcing type, and further subgrouped by applied lateral confining pressure, σ_{3C}, in the order in which they appear in Table 6.4.

The results for a single test, in the form of three plots is presented on each page. Plot "a" for each test is a plot of principal stress difference, $\sigma_1 - \sigma_{3C}$, versus vertical, lateral, and volumetric strain, ε_1, ε_3, and ε_v, respectively. Composite and effective stress ratios, σ_1/σ_{3C} and σ_1/σ_E, versus lateral strain, ε_3, are presented in plot "b". Finally, reinforcing tension versus lateral strain, ε_3, are presented in plot "c". To provide an idea of the time span over which creep and stress relaxation occurred during those tests in which the vertical stress, σ_1, was held constant at the end of the test, the time at which loading was discontinued, t_{hold}, and the time at which the test was discontinued, t_{end}, are also provided.

At the end of this appendix the results of strain gage tests are presented for those tests not presented in Figures 6.37 - 6.40, see Figures C.62 to C.69. These tests are grouped by type of strain gage used and are presented in order of increasing test number (See Figure 6.36). Plots of normalized strain versus gage location and NISR versus overall lateral strain, ε_3, are included.

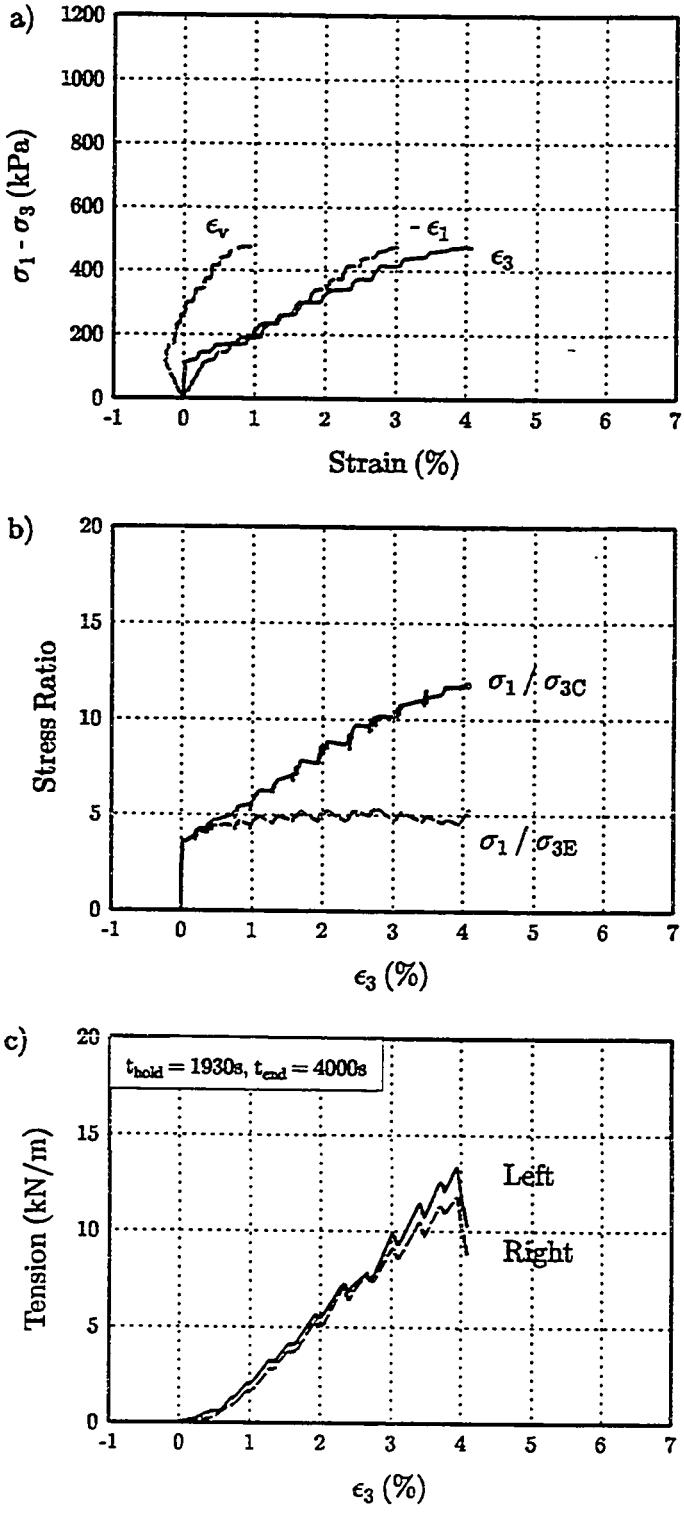

Figure C.1: Soil O, Reinforcing PP2, σ_{3C} = 50 kPa, Test 48.

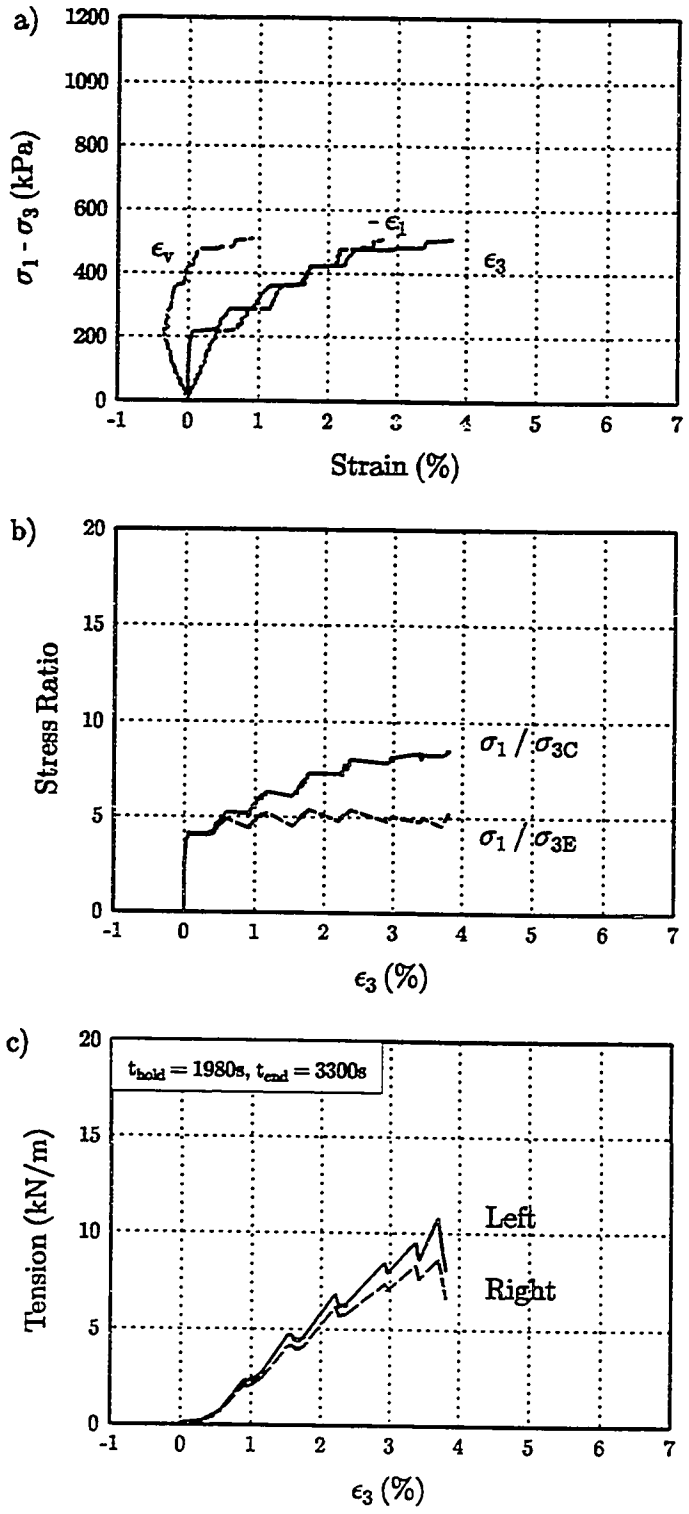

Figure C.2: Soil O, Reinforcing PP2, σ_{3C} = 75 kPa, Test 47.

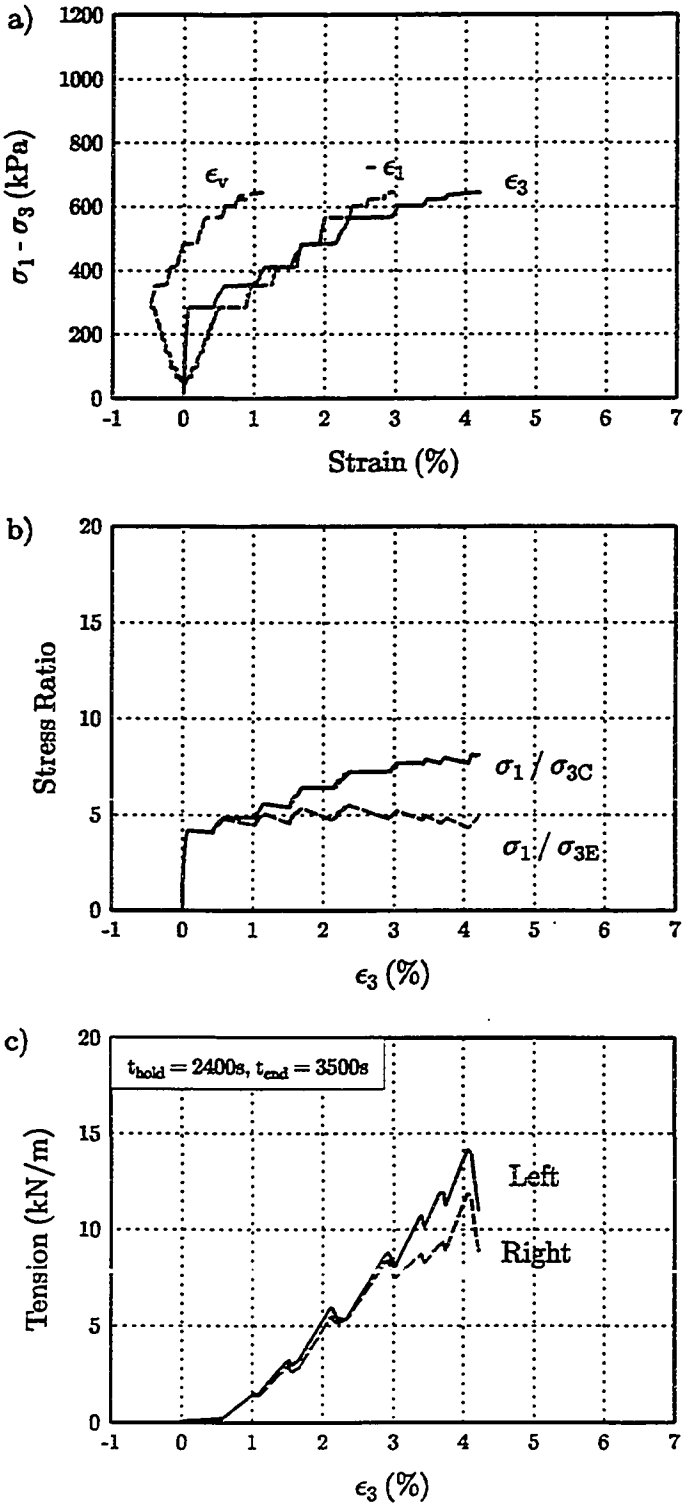

Figure C.3: Soil O, Reinforcing PP2, σ_{3C} = 100 kPa, Test 46.

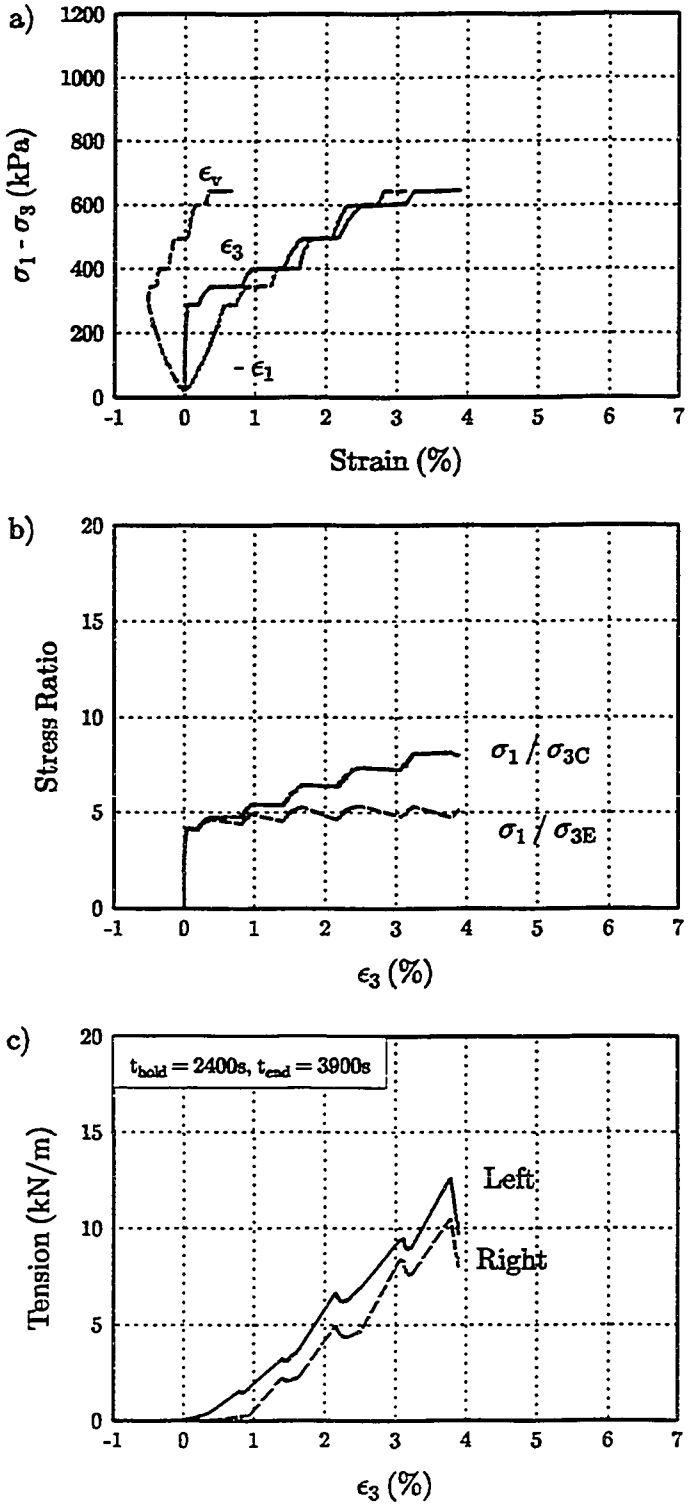

Figure C.4: Soil O, Reinforcing PP2, σ_{3C} = 100 kPa, Test 45.

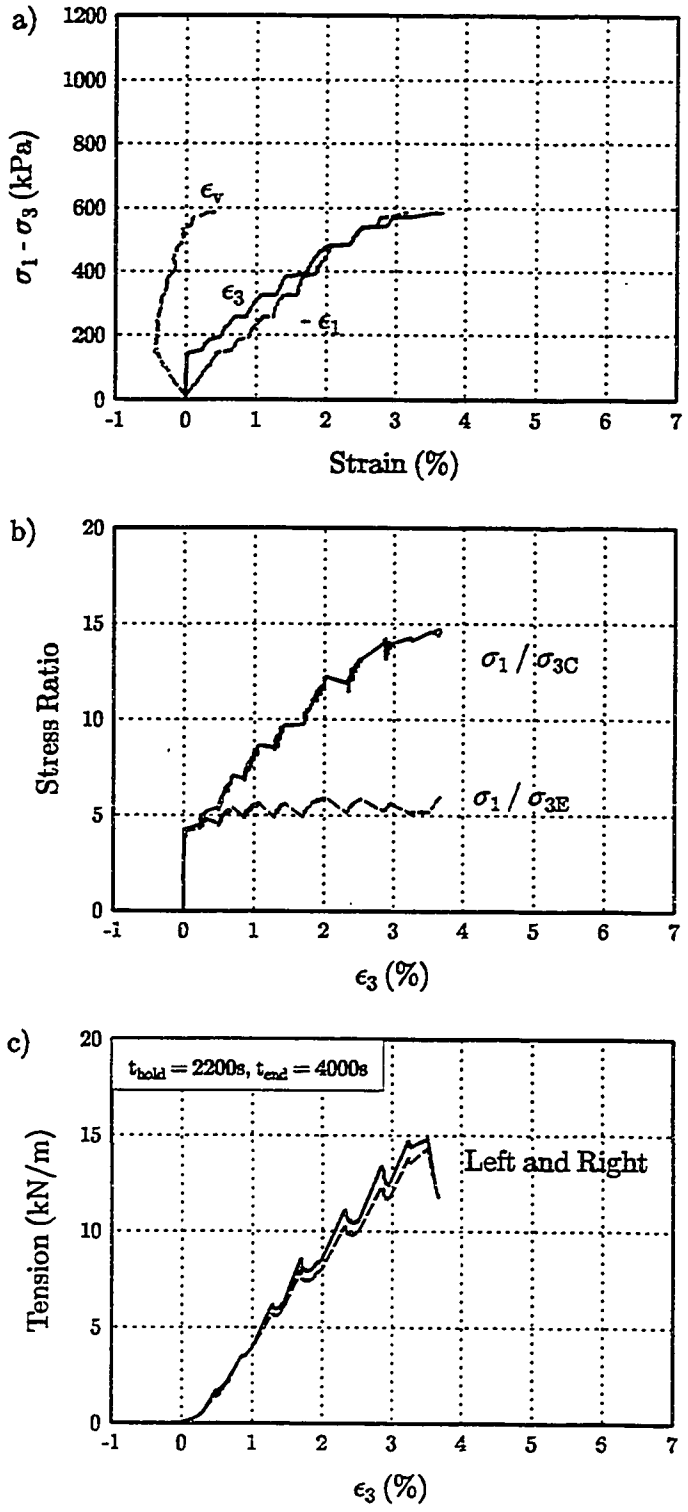

Figure C.5: Soil O, Reinforcing PP3, $\sigma_{3C} = 50$ kPa, Test 43.

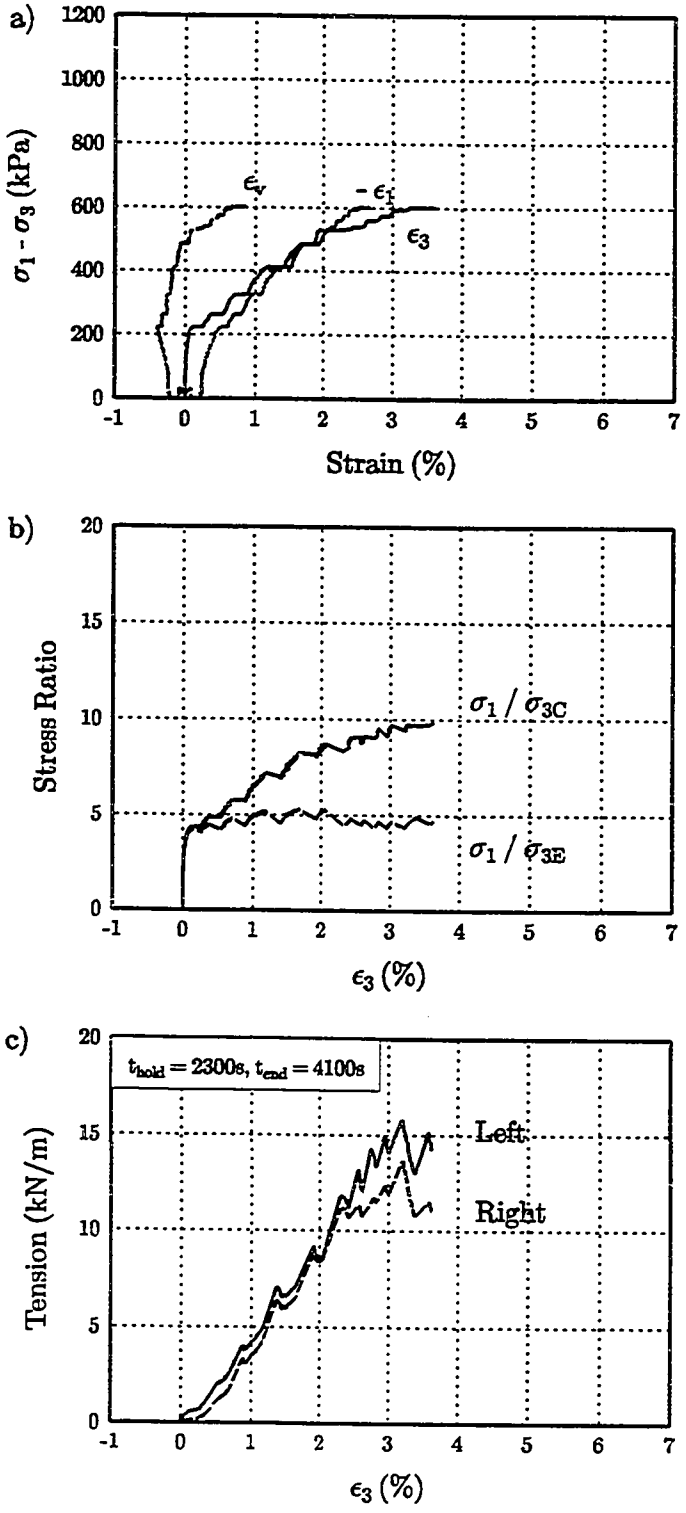

Figure C.6: Soil O, Reinforcing PP3, σ_{3C} = 75 kPa, Test 41.

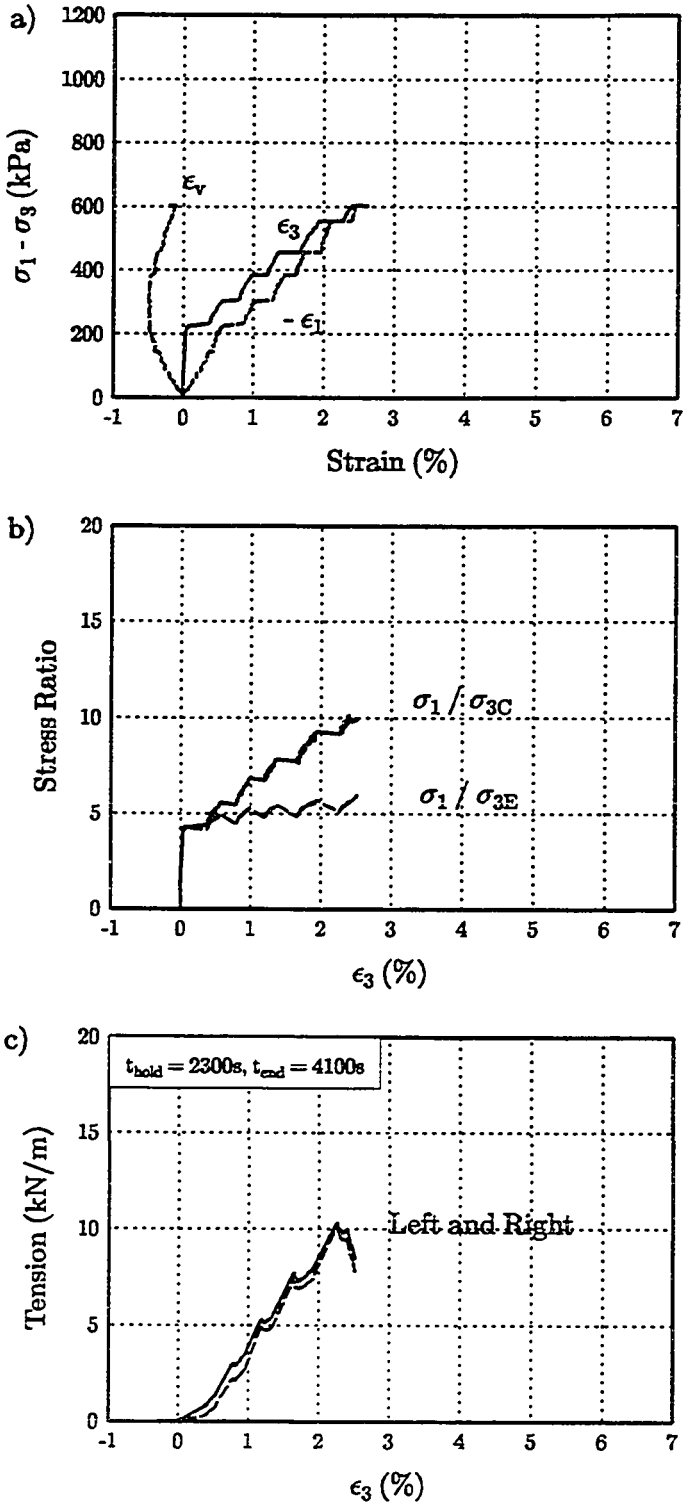

Figure C.7: Soil O, Reinforcing PP3, $\sigma_{3C} = 75$ kPa, Test 42.

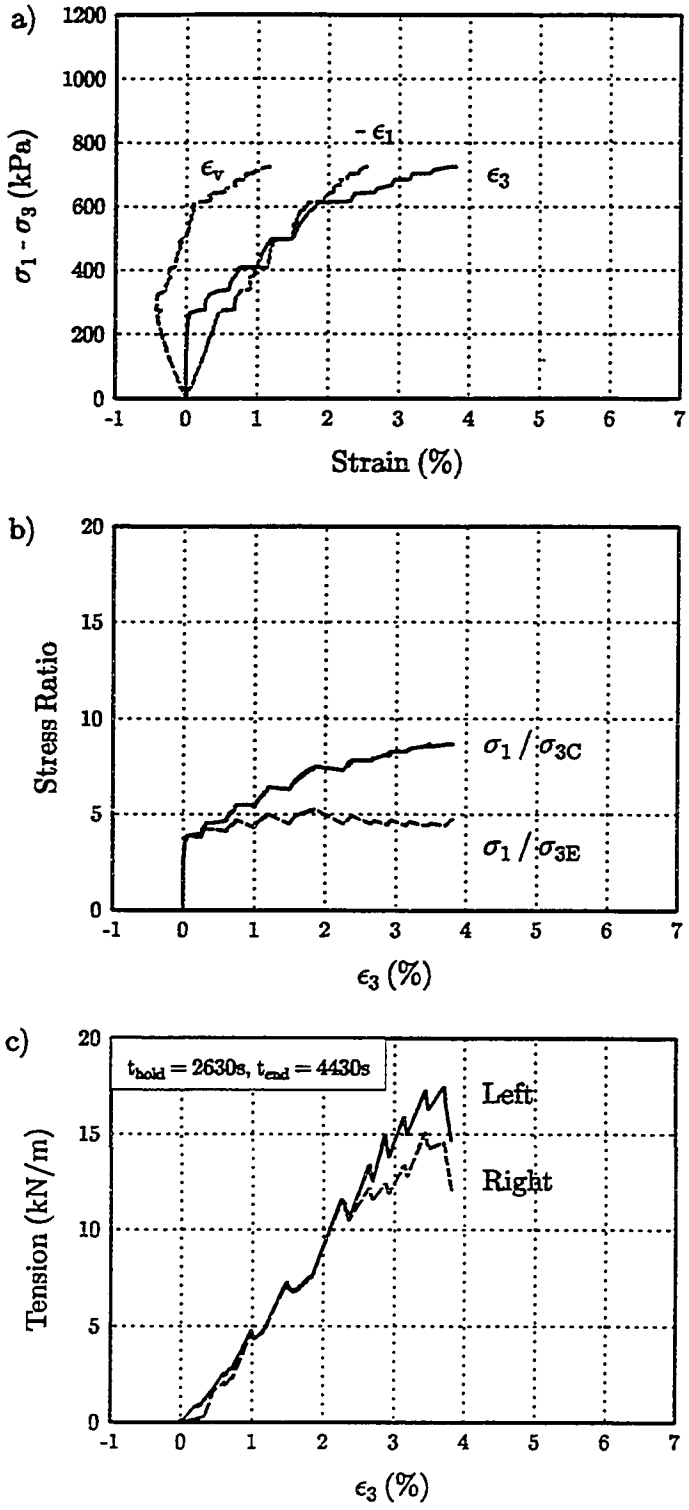

Figure C.8: Soil O, Reinforcing PP3, σ_{3C} = 100 kPa, Test 44.

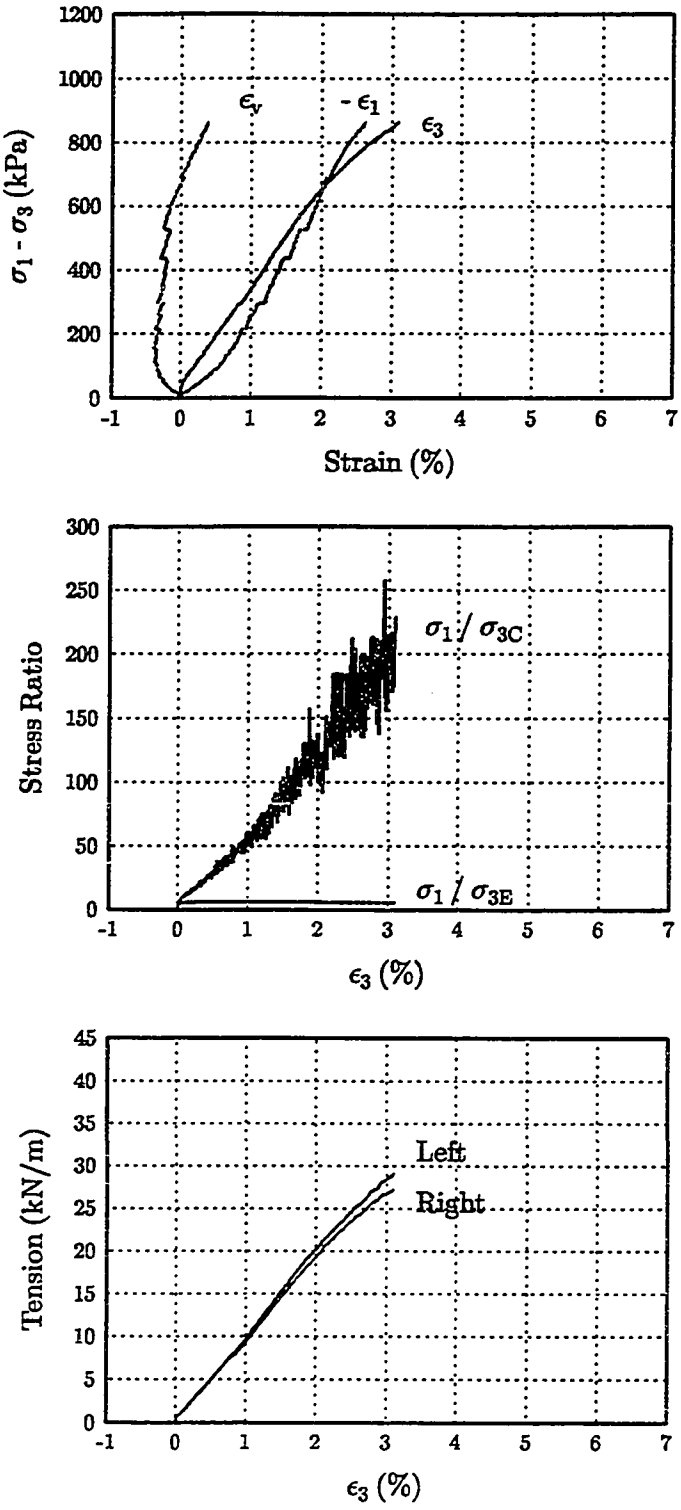

Figure C.9: Soil O, Reinforcing PET1, σ_{3C} = 12.5 kPa, Test 108.

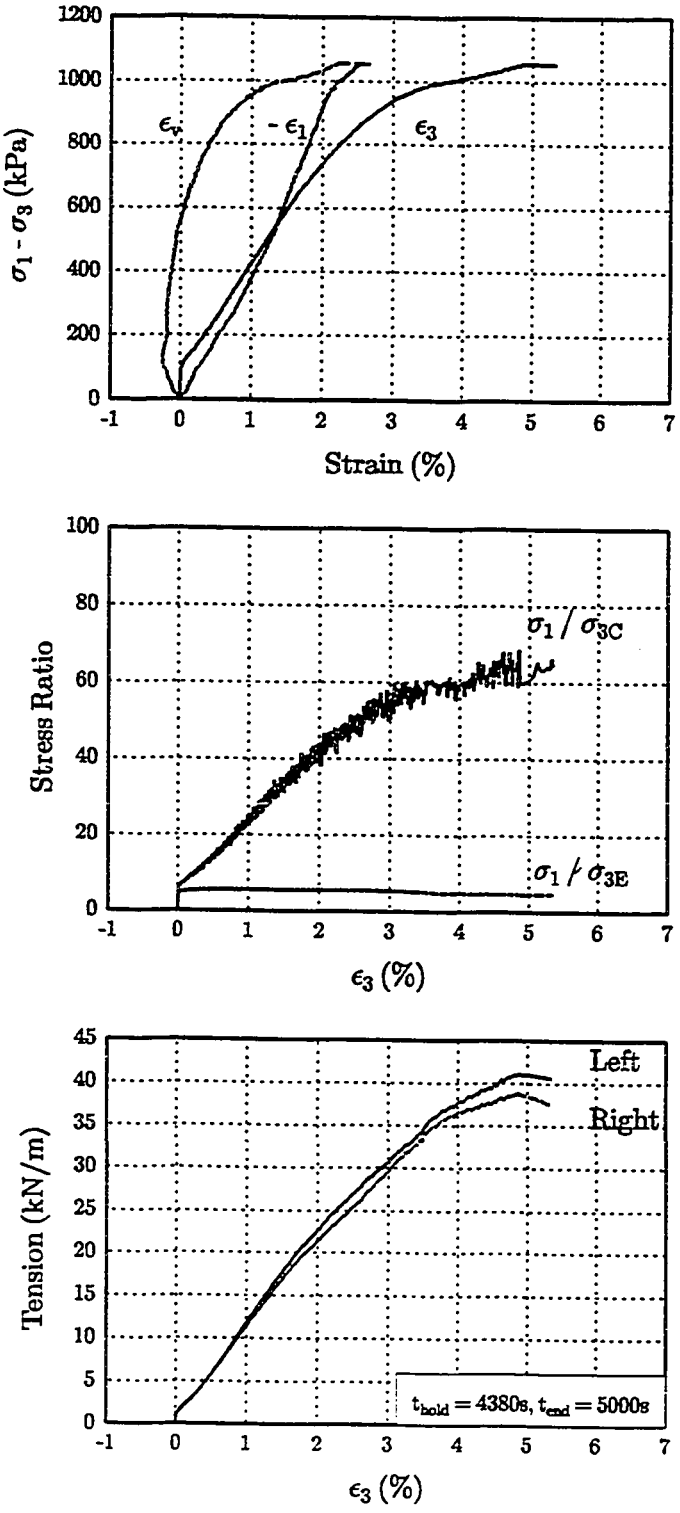

Figure C.10: Soil O, Reinforcing PET1, $\sigma_{3C} = 25$ kPa, Test 107.

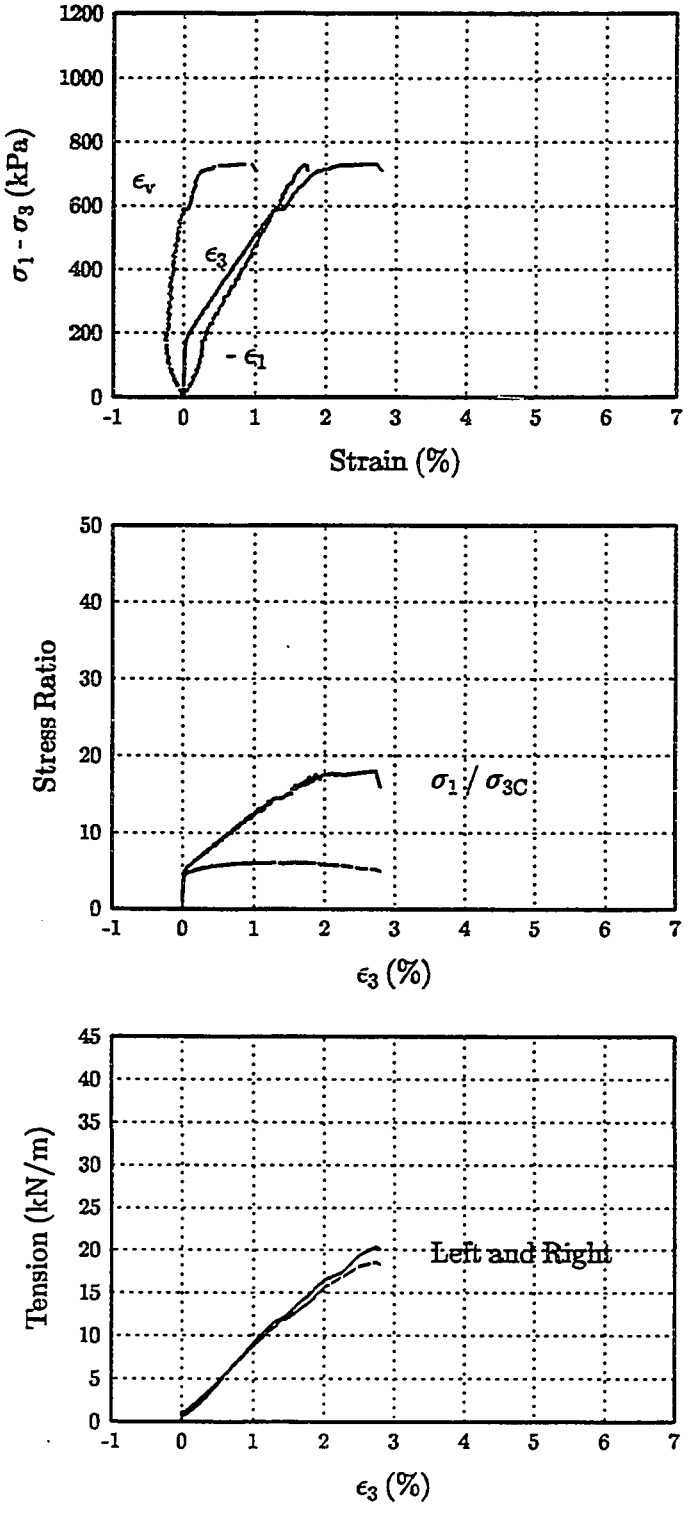

Figure C.11: Soil O, Reinforcing PET1, σ_{3C} = 50 kPa, Test 109.

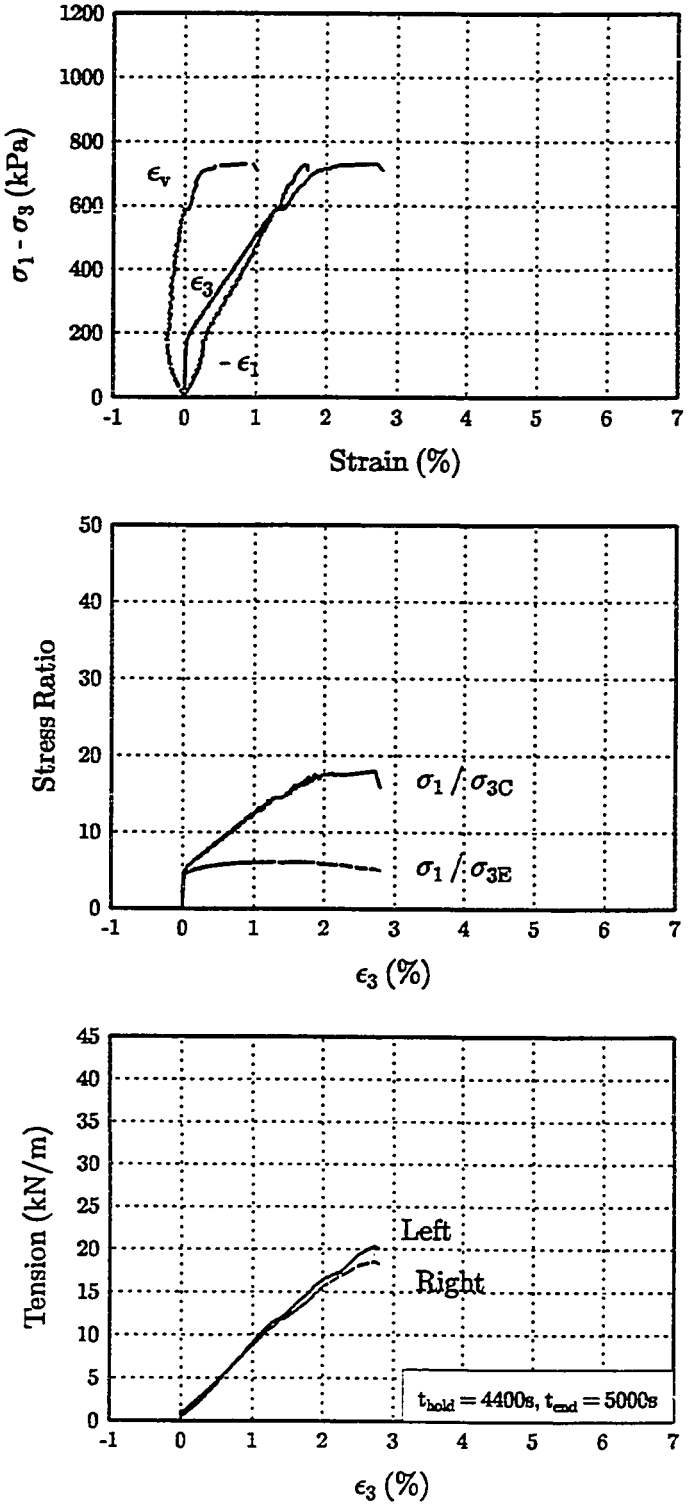

Figure C.12: Soil O, Reinforcing PET1, $\sigma_{3C} = 50$ kPa, Test 110.

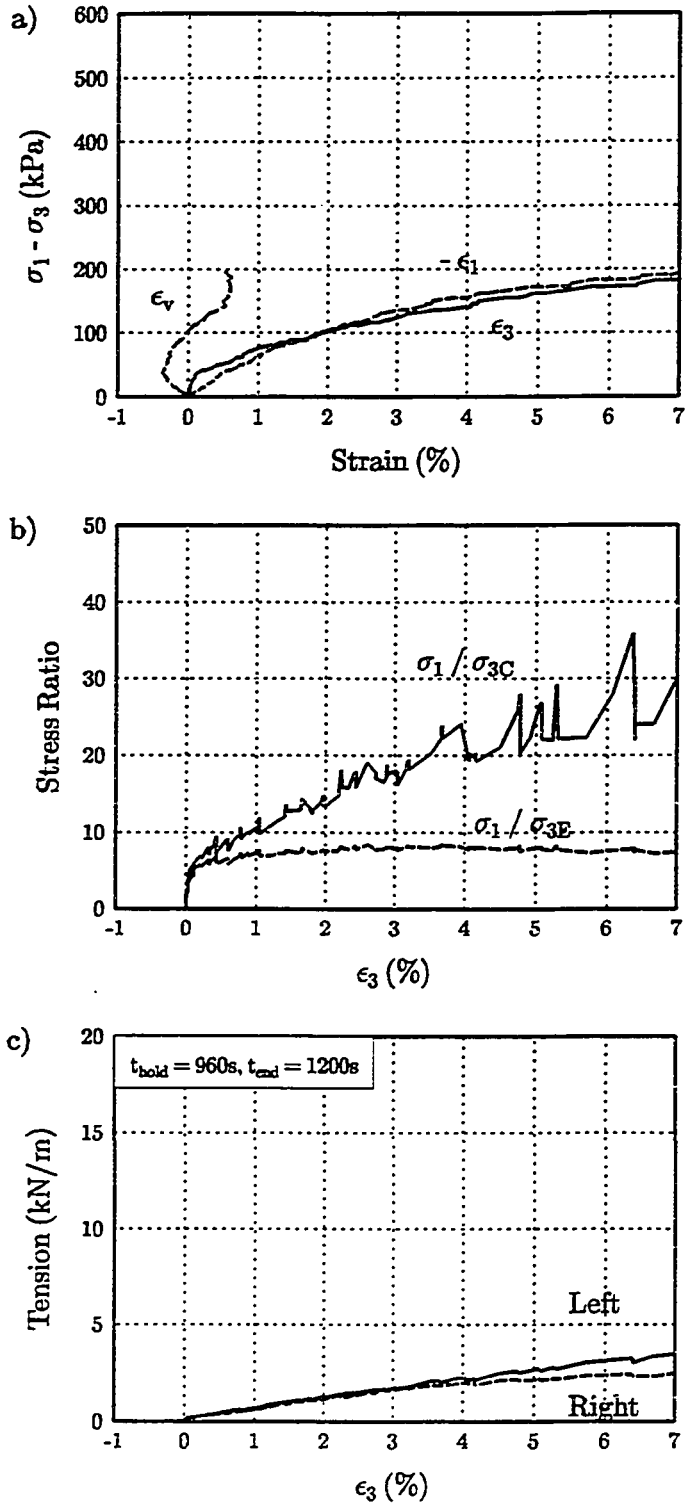

Figure C.13: Soil O, Reinforcing NW1, σ_{3C} = 12.5 kPa, Test 88.

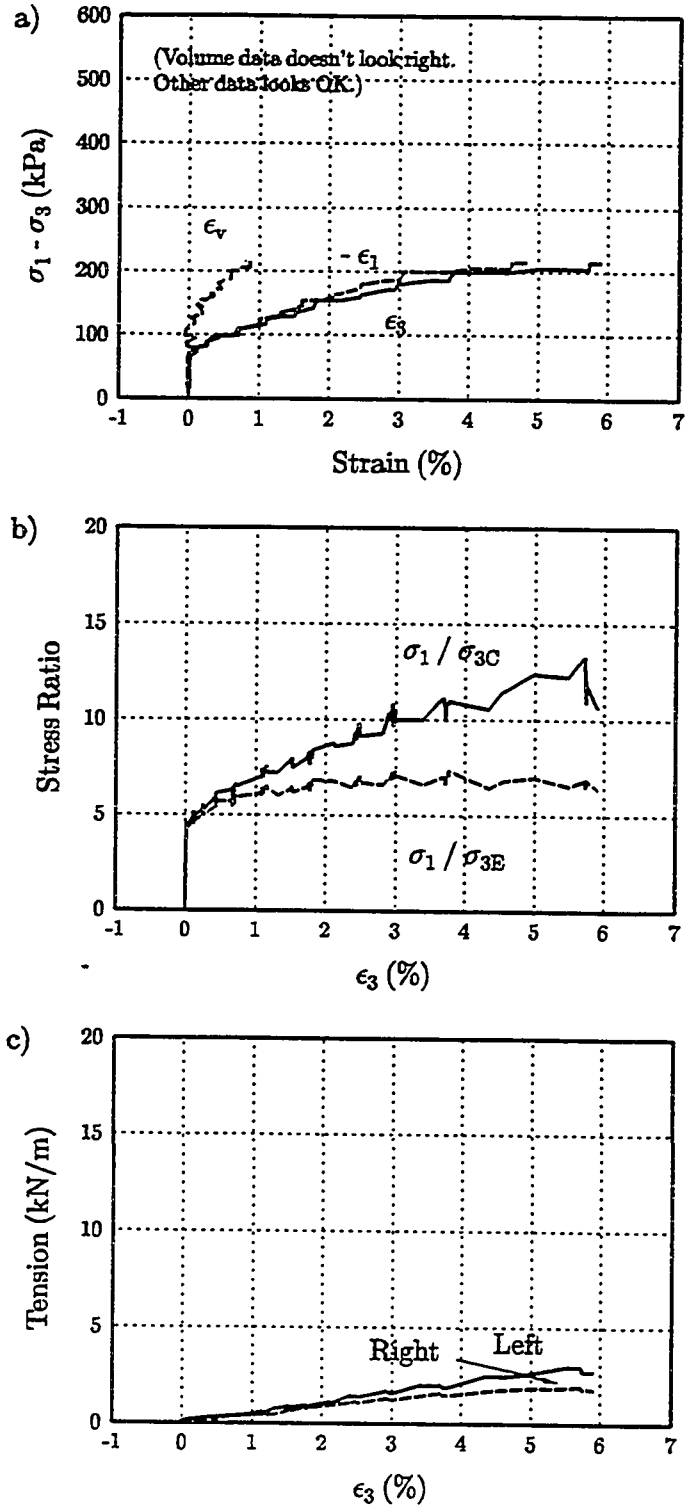

Figure C.14: Soil O, Reinforcing NW1, $\sigma_{3C} = 25$ kPa, Test 89.

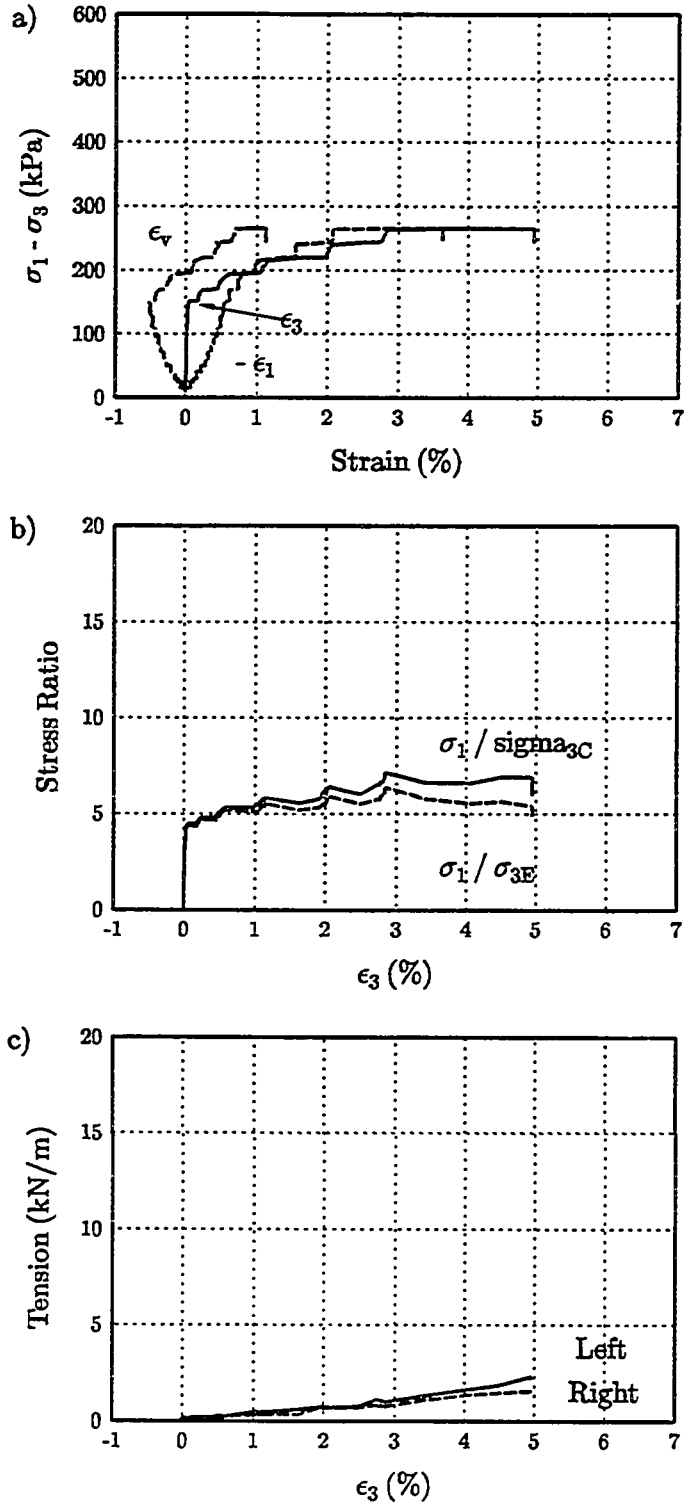

Figure C.15: Soil O, Reinforcing NW1, σ_{3C} = 50 kPa, Test 93.

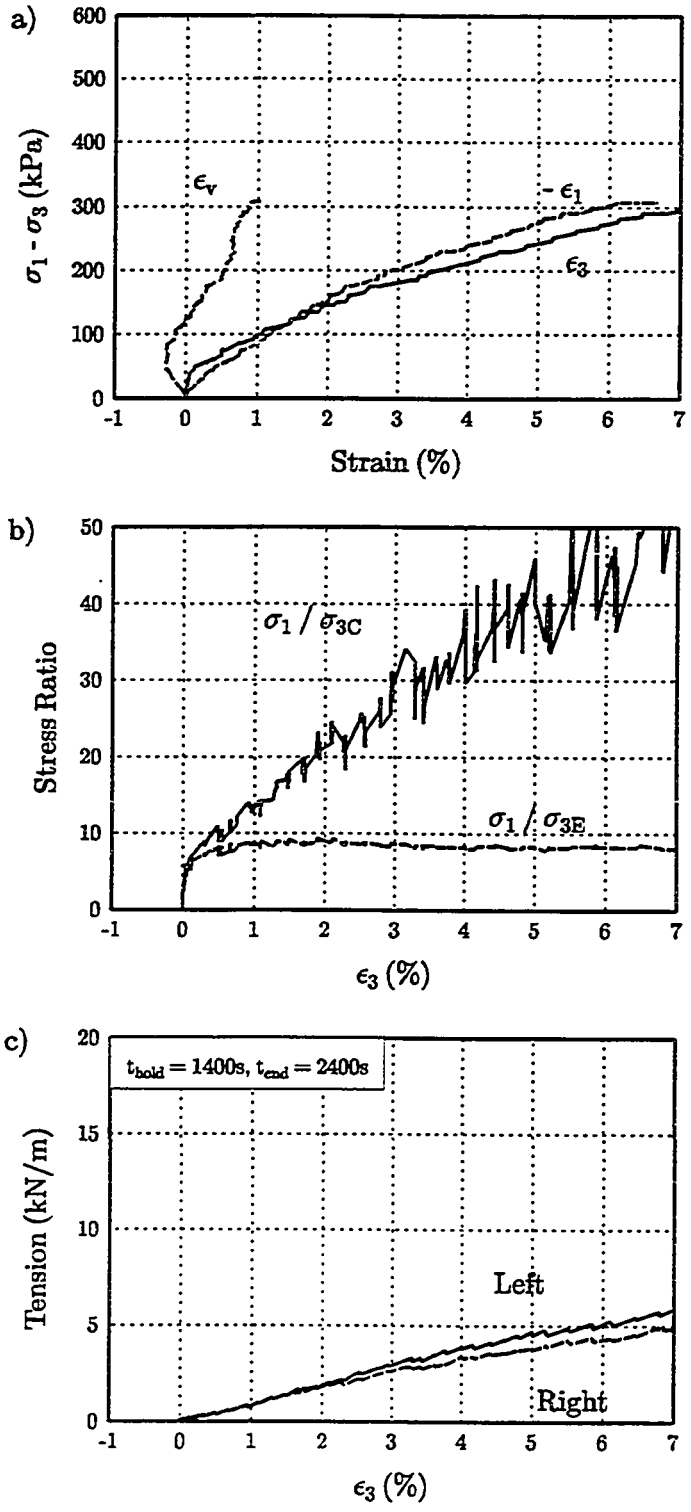

Figure C.16: Soil O, Reinforcing NW2, σ_{3C} = 12.5 kPa, Test 90.

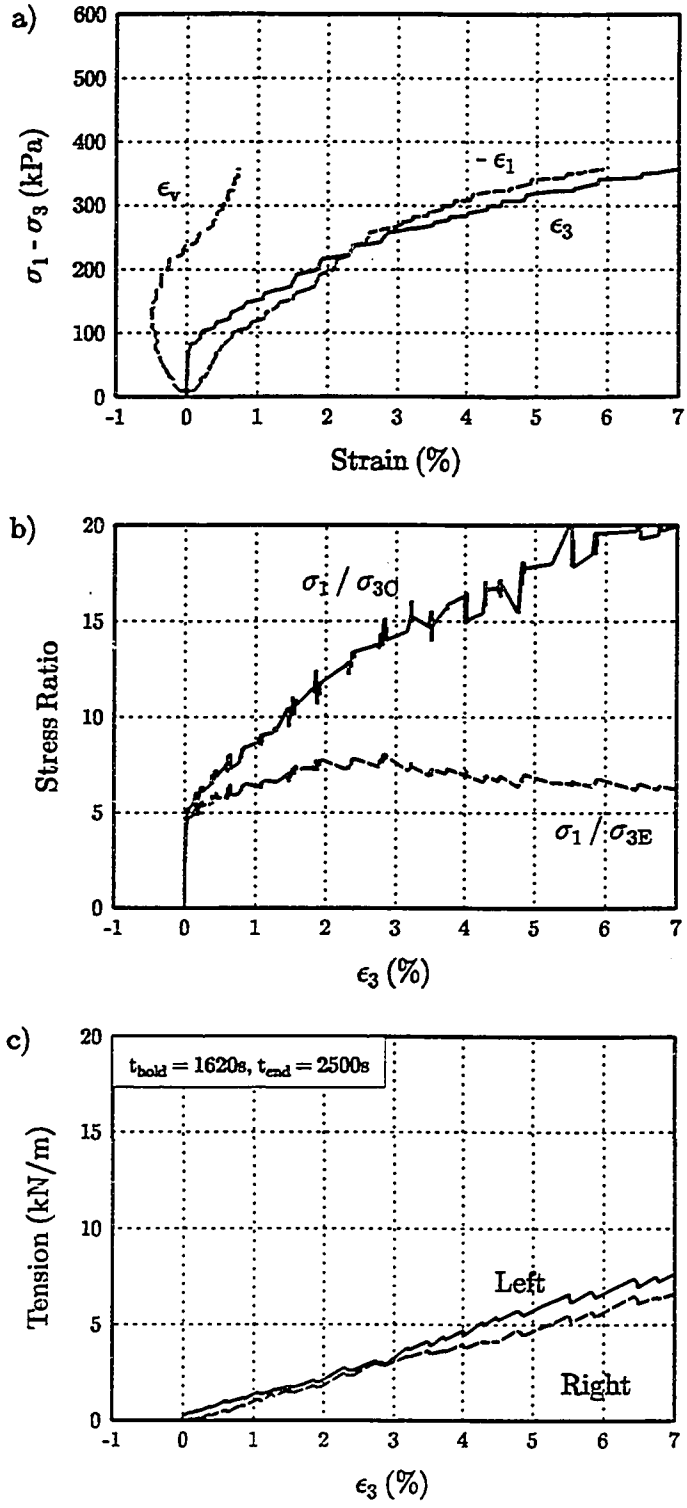

Figure C.17: Soil O, Reinforcing NW2, σ_{3C} = 12.5 kPa, Test 91.

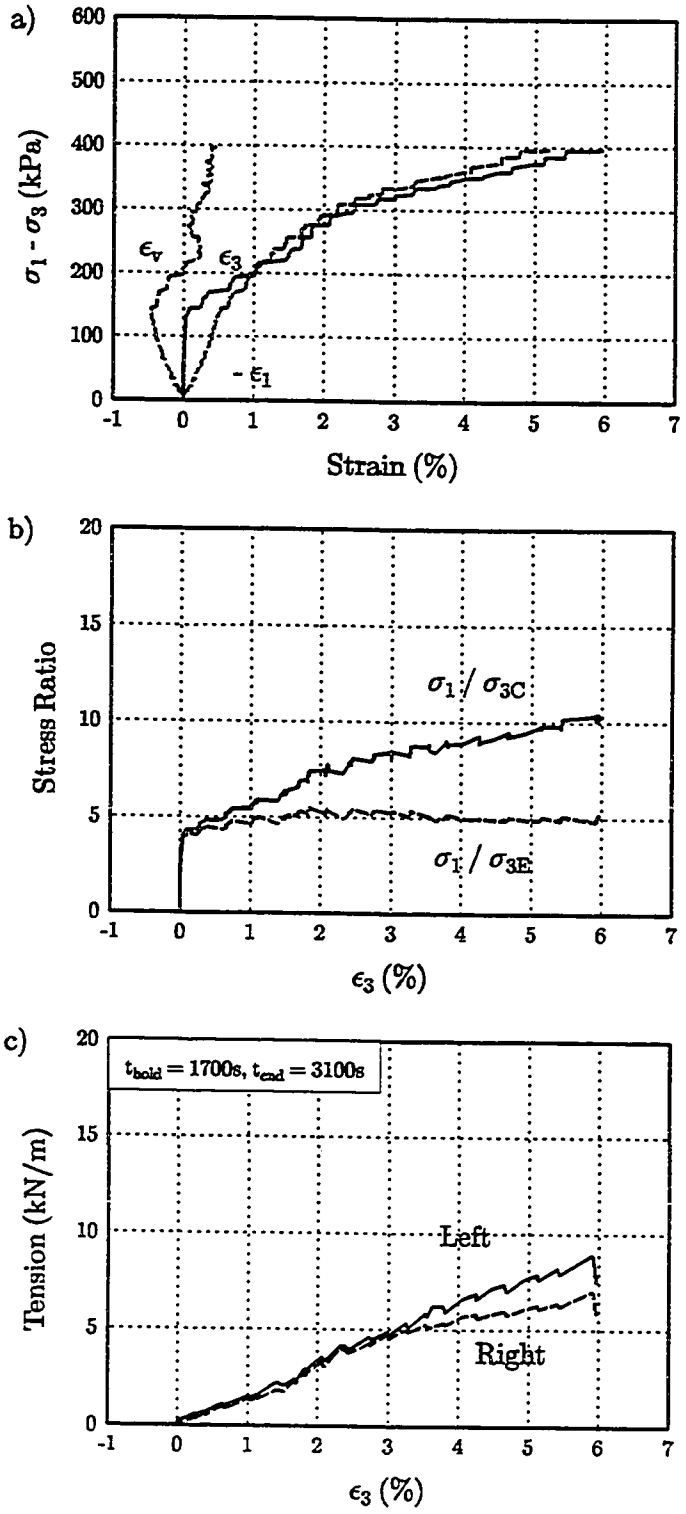

Figure C.18: Soil O, Reinforcing NW2, σ_{3C} = 50 kPa, Test 92.

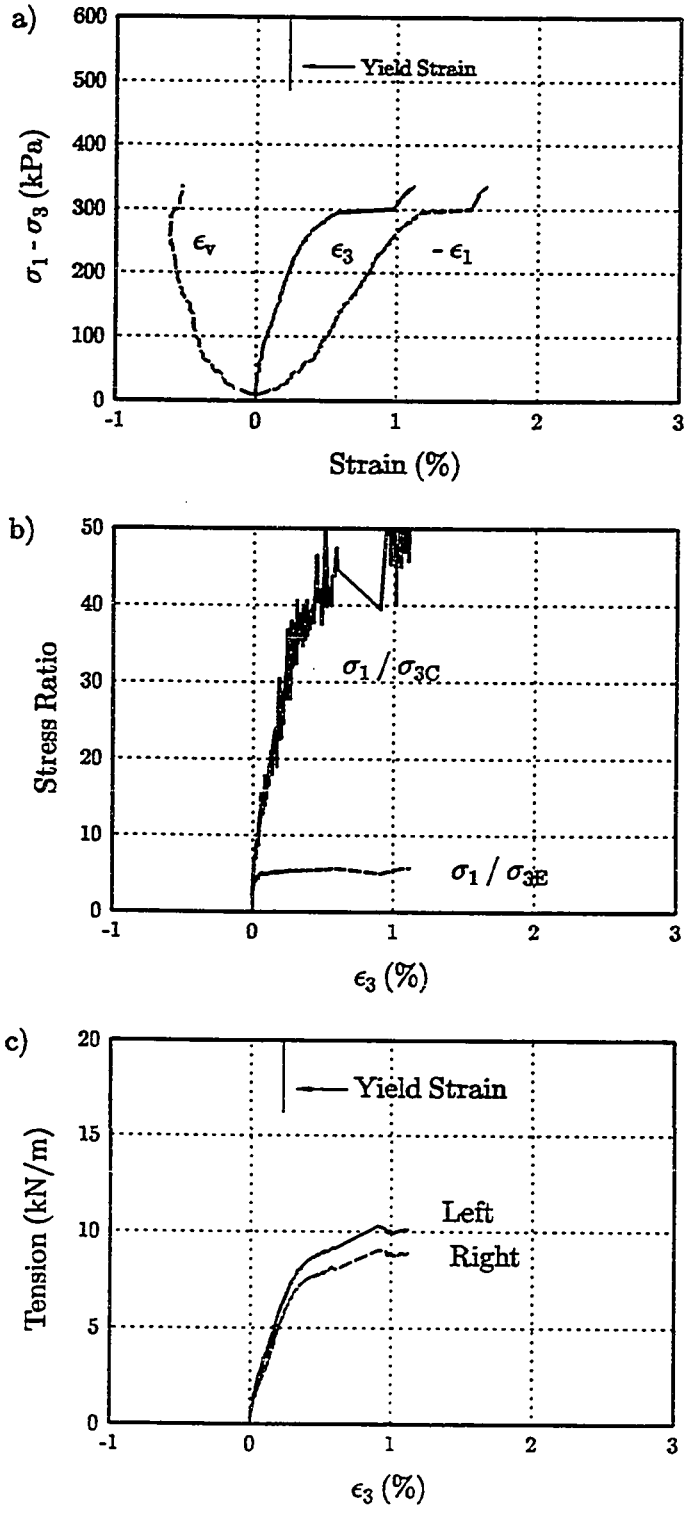

Figure C.19: Soil O, Reinforcing SS, σ_{3C} = 12.5 kPa, Test 96.

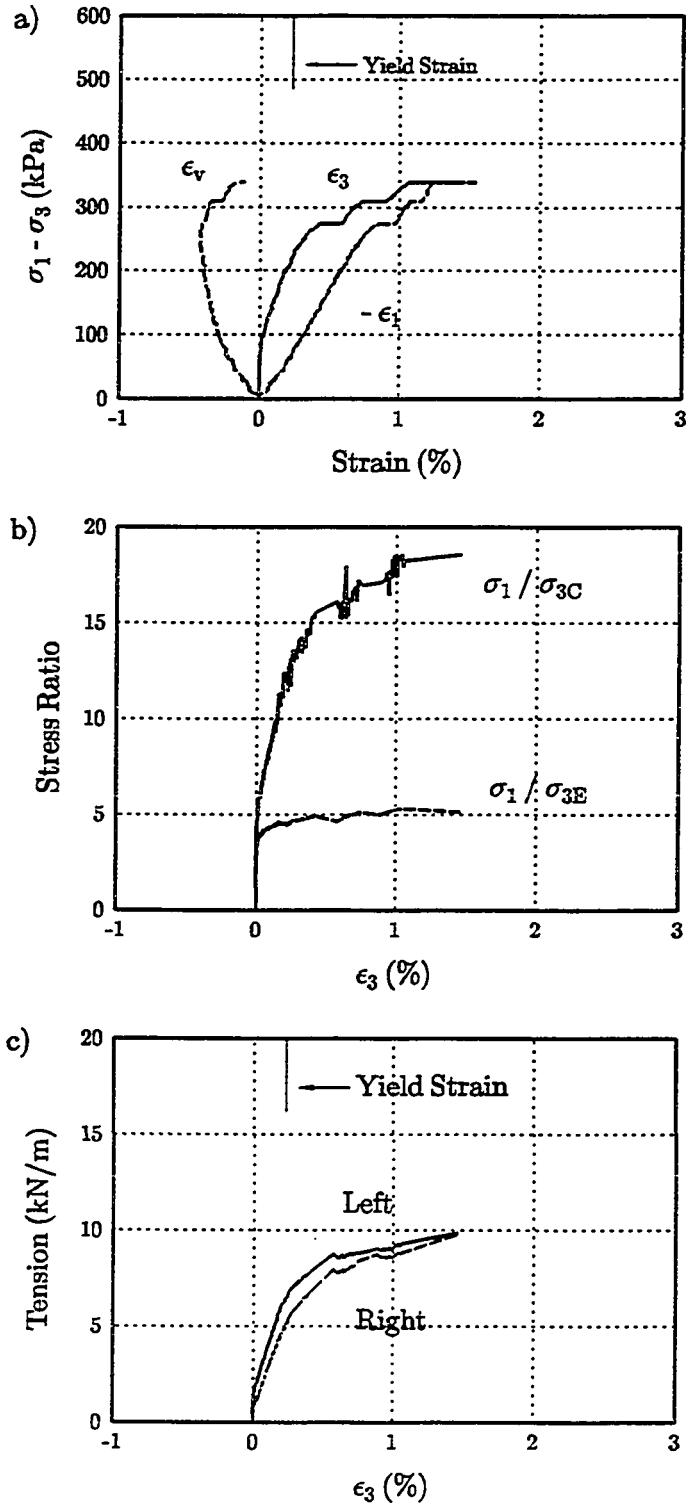

Figure C.20: Soil O, Reinforcing SS, σ_{3C} = 25 kPa, Test 95.

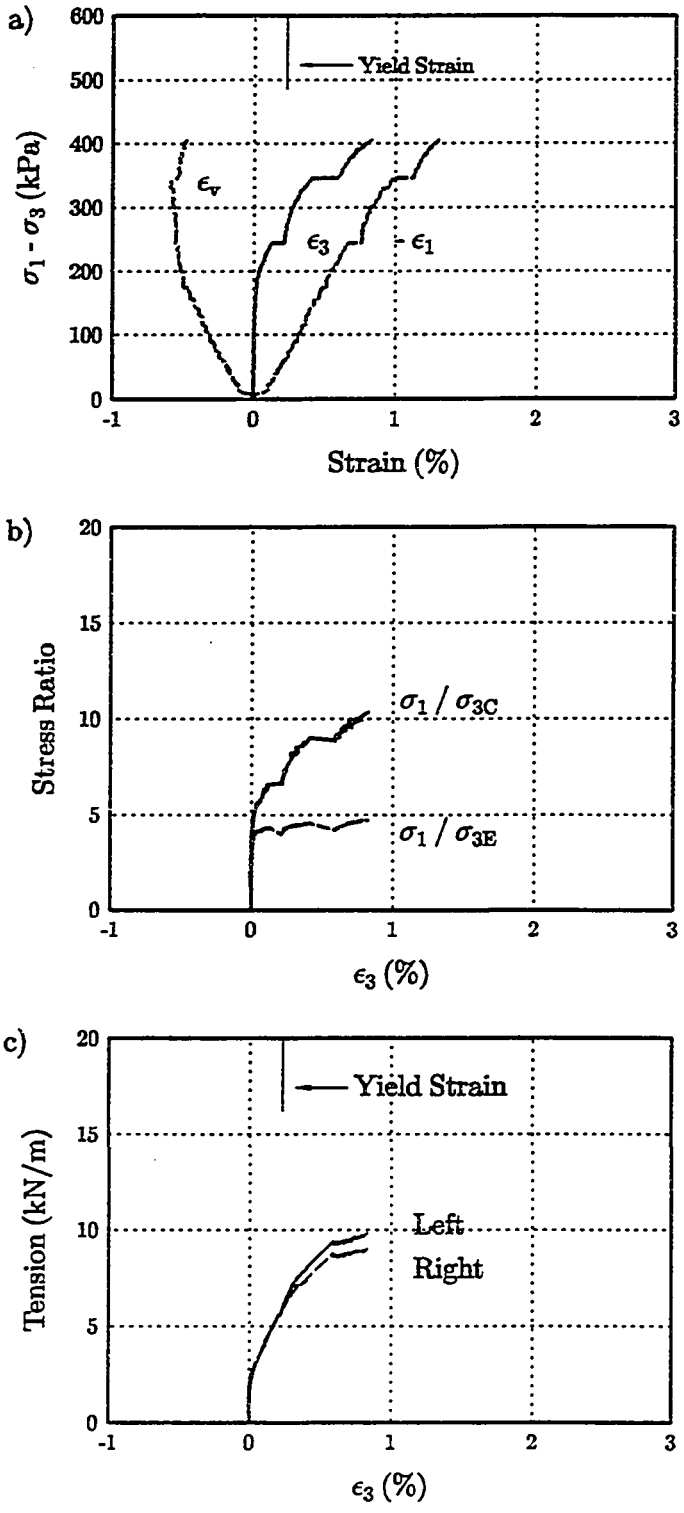

Figure C.21: Soil O, Reinforcing SS, σ_{3C} = 50 kPa, Test 97.

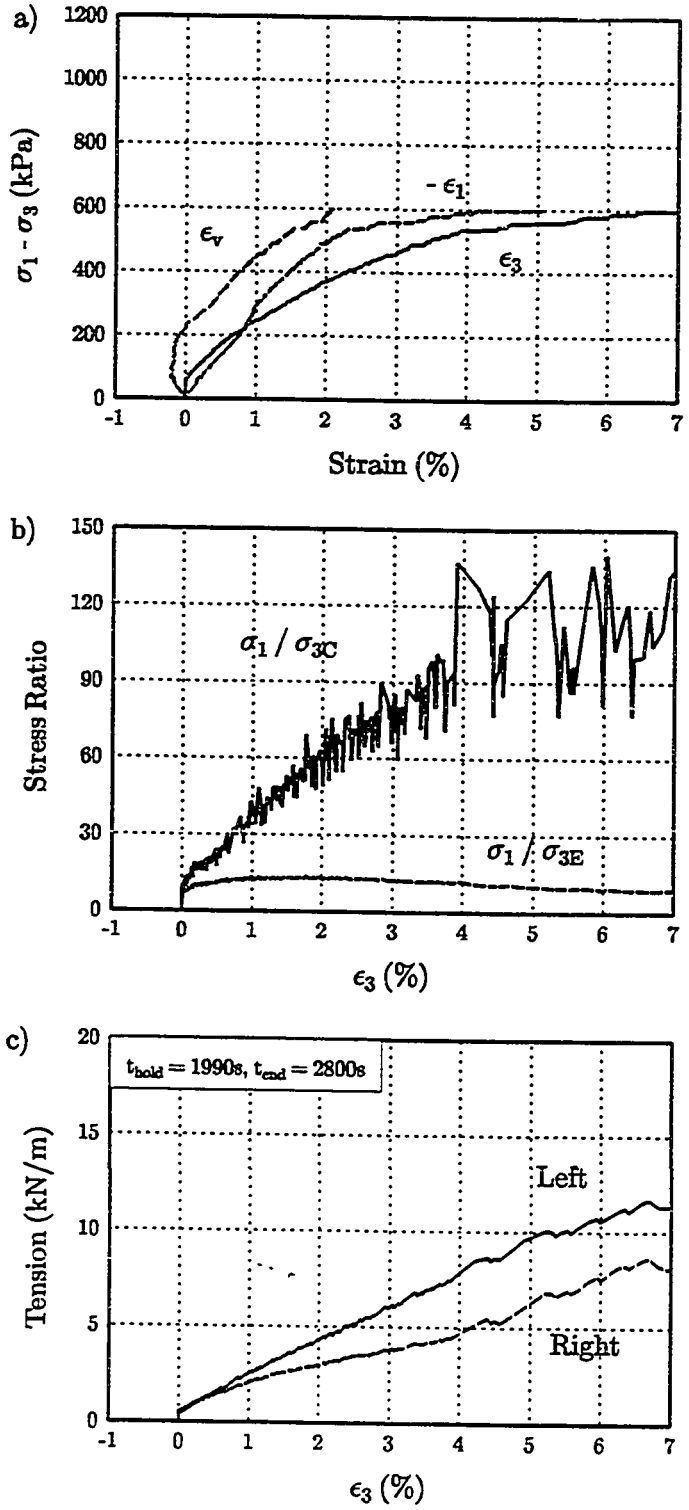

Figure C.22: Soil R, Reinforcing PP1, $\sigma_{3C} = 12.5$ kPa, Test 79.

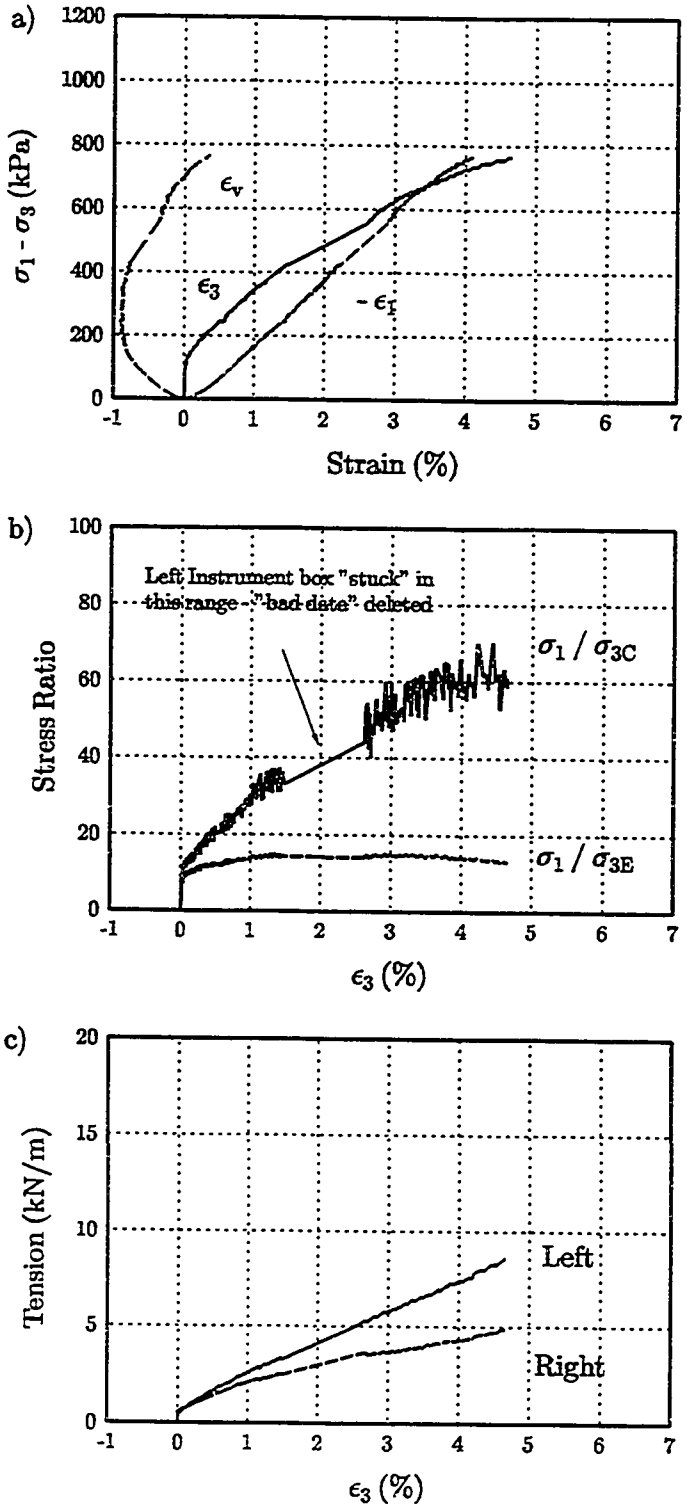

Figure C.23: Soil R, Reinforcing PP1, σ_{3C} = 12.5 kPa, Test 131.

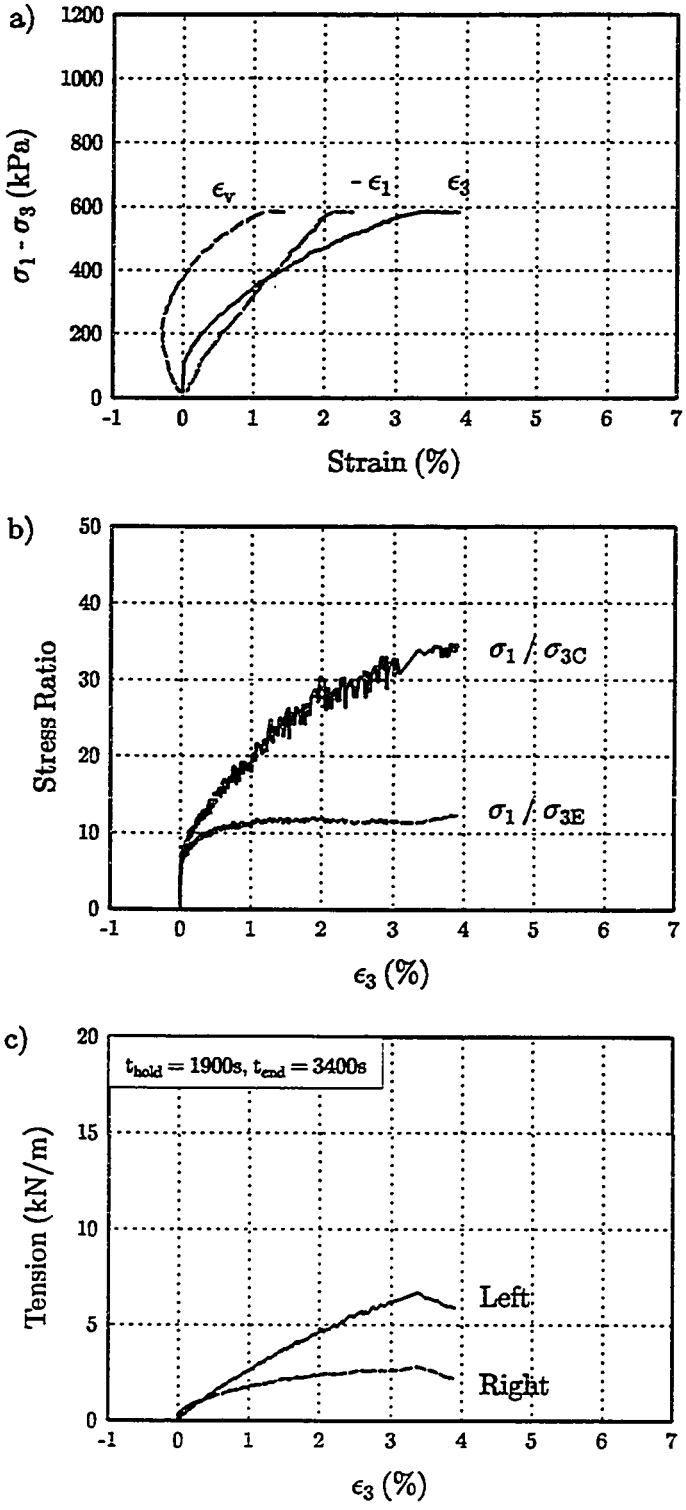

Figure C.24: Soil R, Reinforcing PP1, $\sigma_{3C} = 25$ kPa, Test 65.

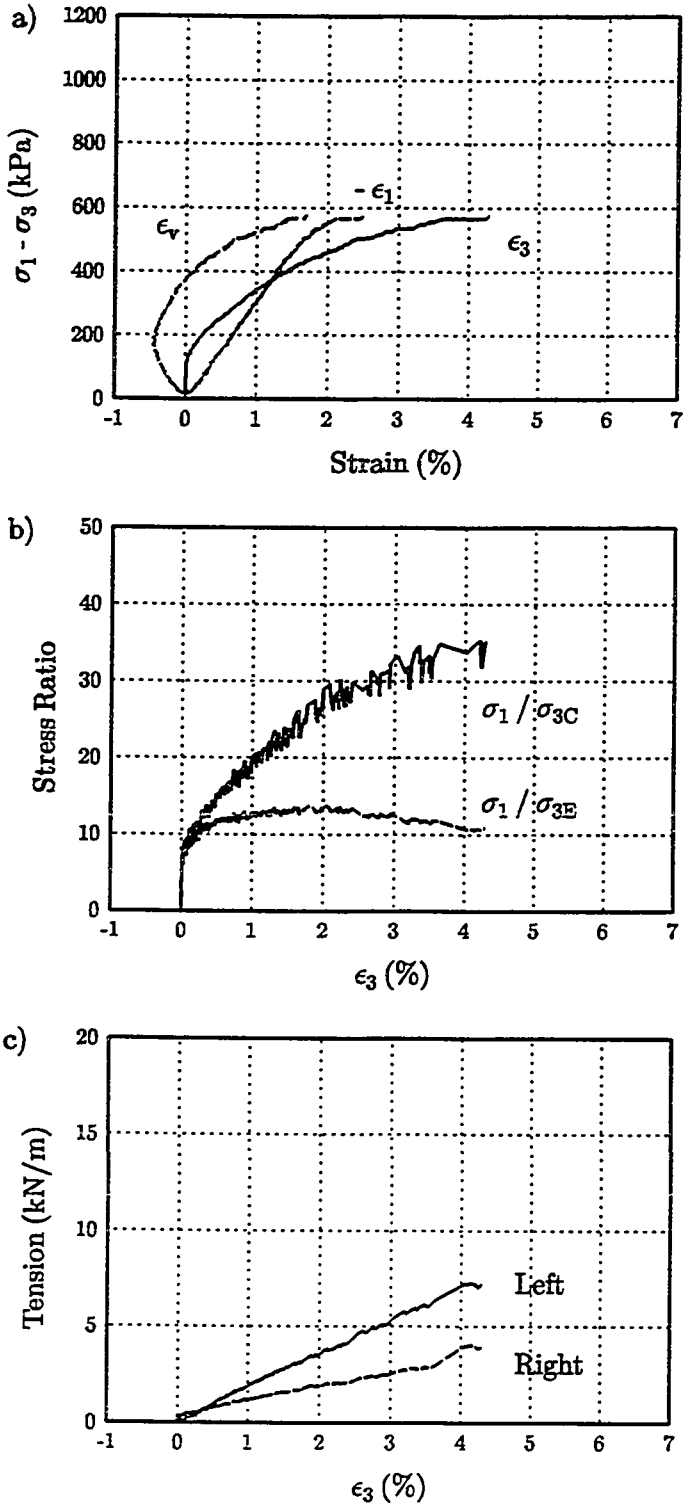

Figure C.25: Soil R, Reinforcing PP1, $\sigma_{3C} = 25$ kPa, Test 67.

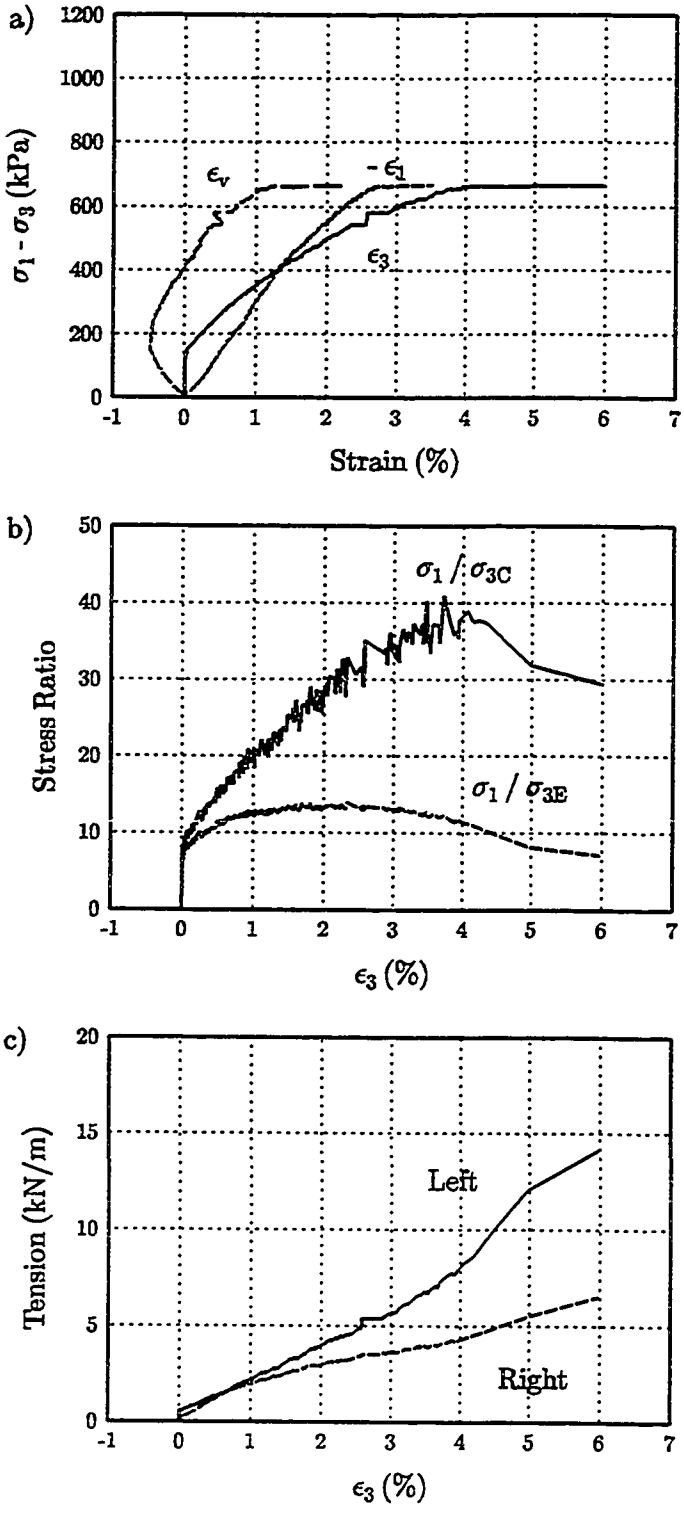

Figure C.26: Soil R, Reinforcing PP1, $\sigma_{3C} = 25$ kPa, Test 74.

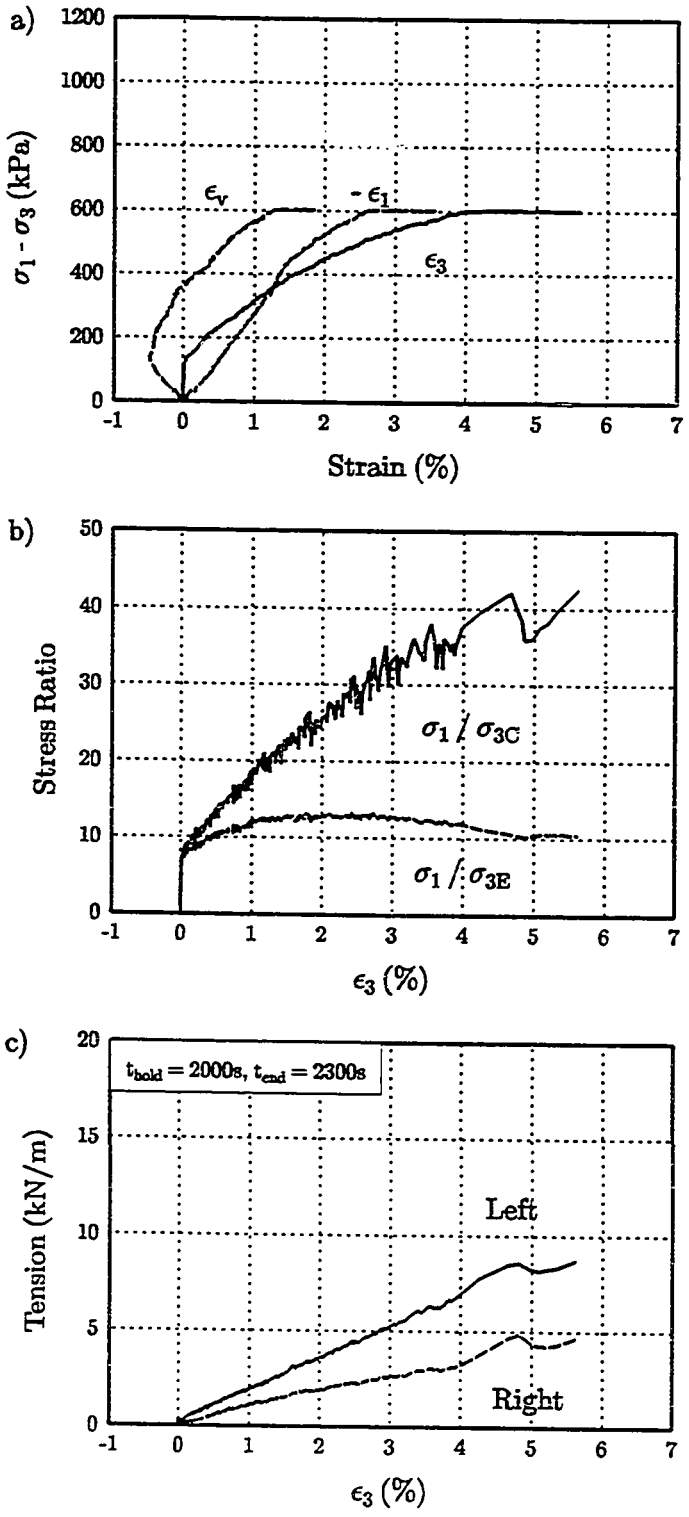

Figure C.27: Soil R, Reinforcing PP1, $\sigma_{3C} = 25$ kPa, Test 81.

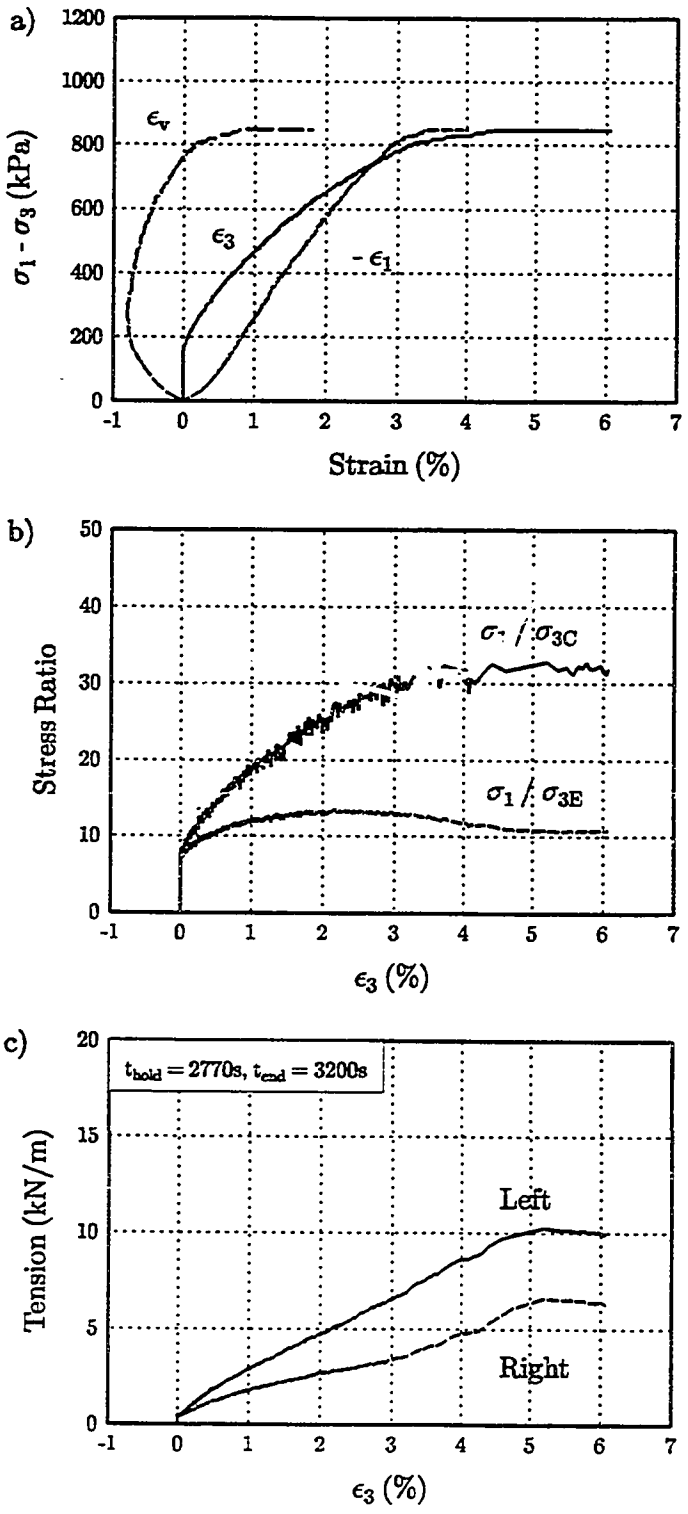

Figure C.28: Soil R, Reinforcing PP1, $\sigma_{3C} = 25$ kPa, Test 129.

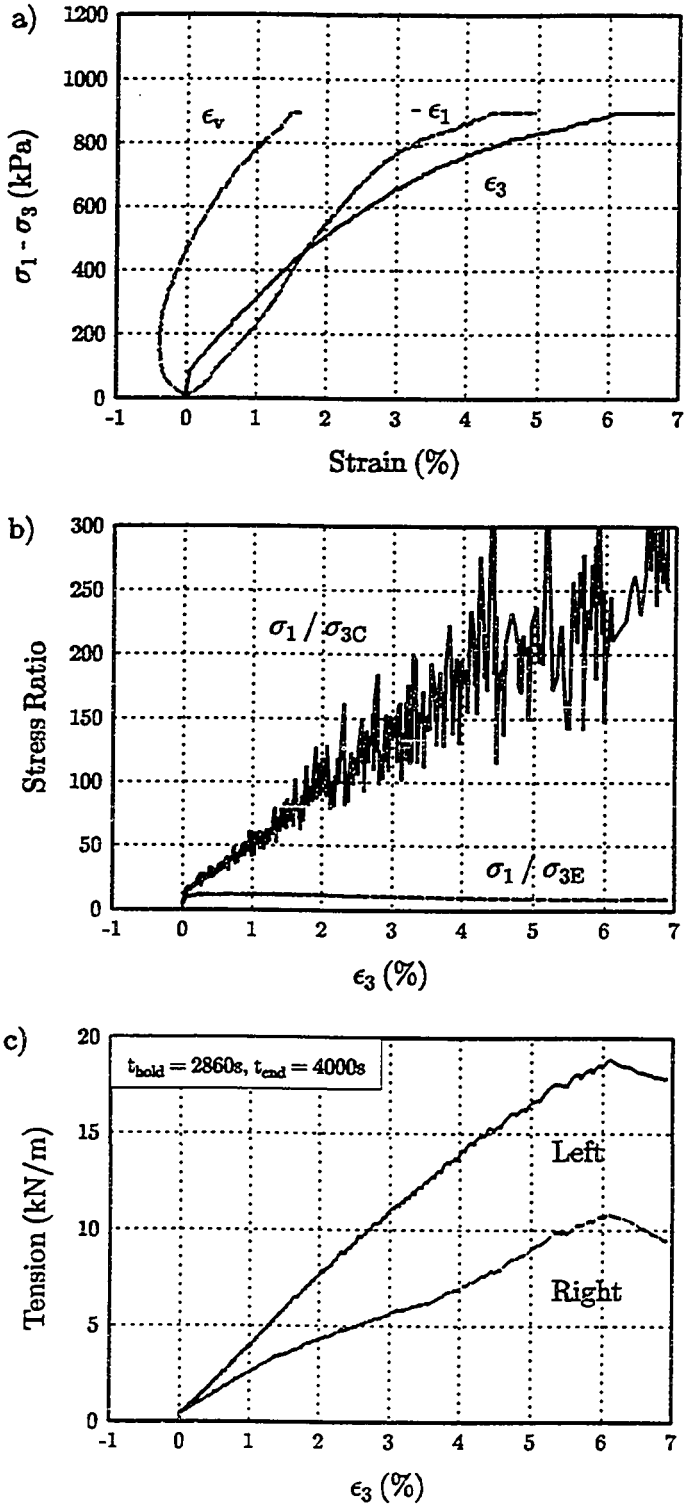

Figure C.29: Soil R, Reinforcing PP2, σ_{3C} = 12.5 kPa, Test 77.

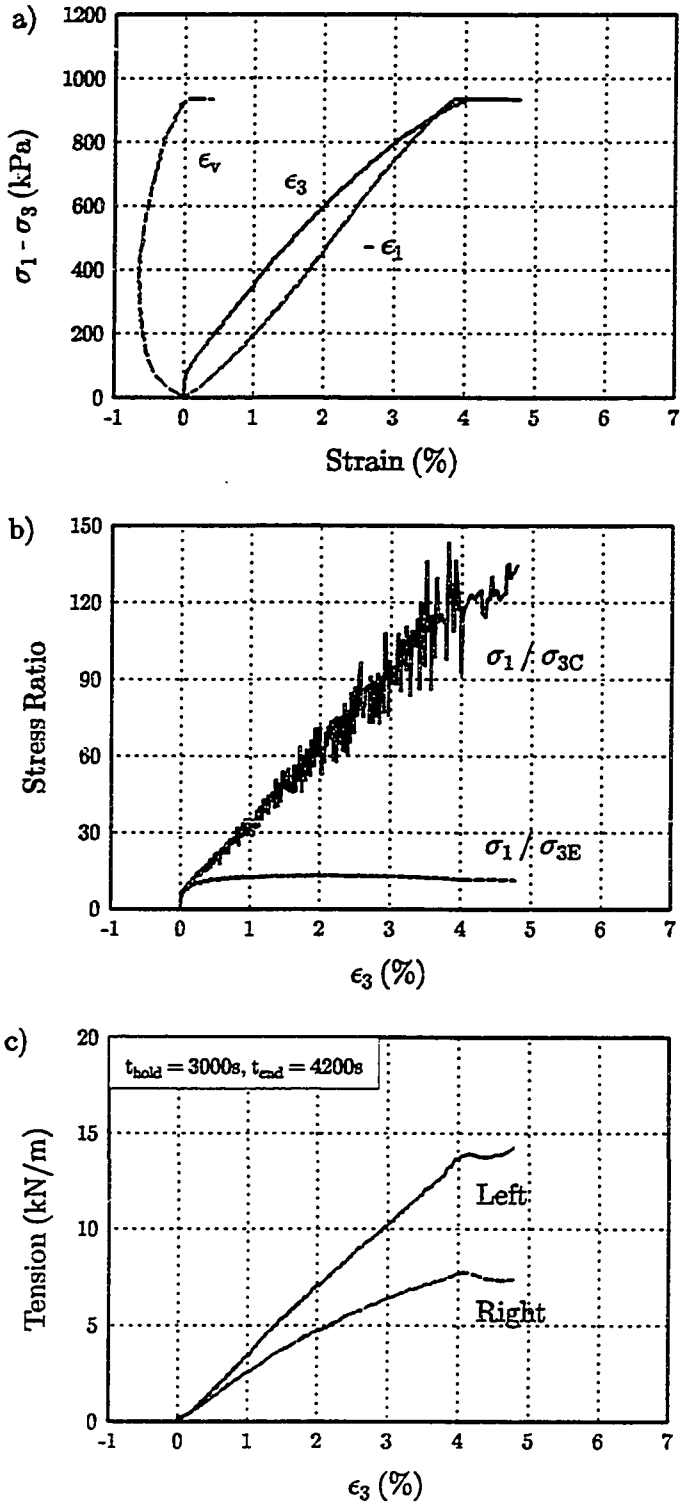

Figure C.30: Soil R, Reinforcing PP2, σ_{3C} = 12.5 kPa, Test 128.

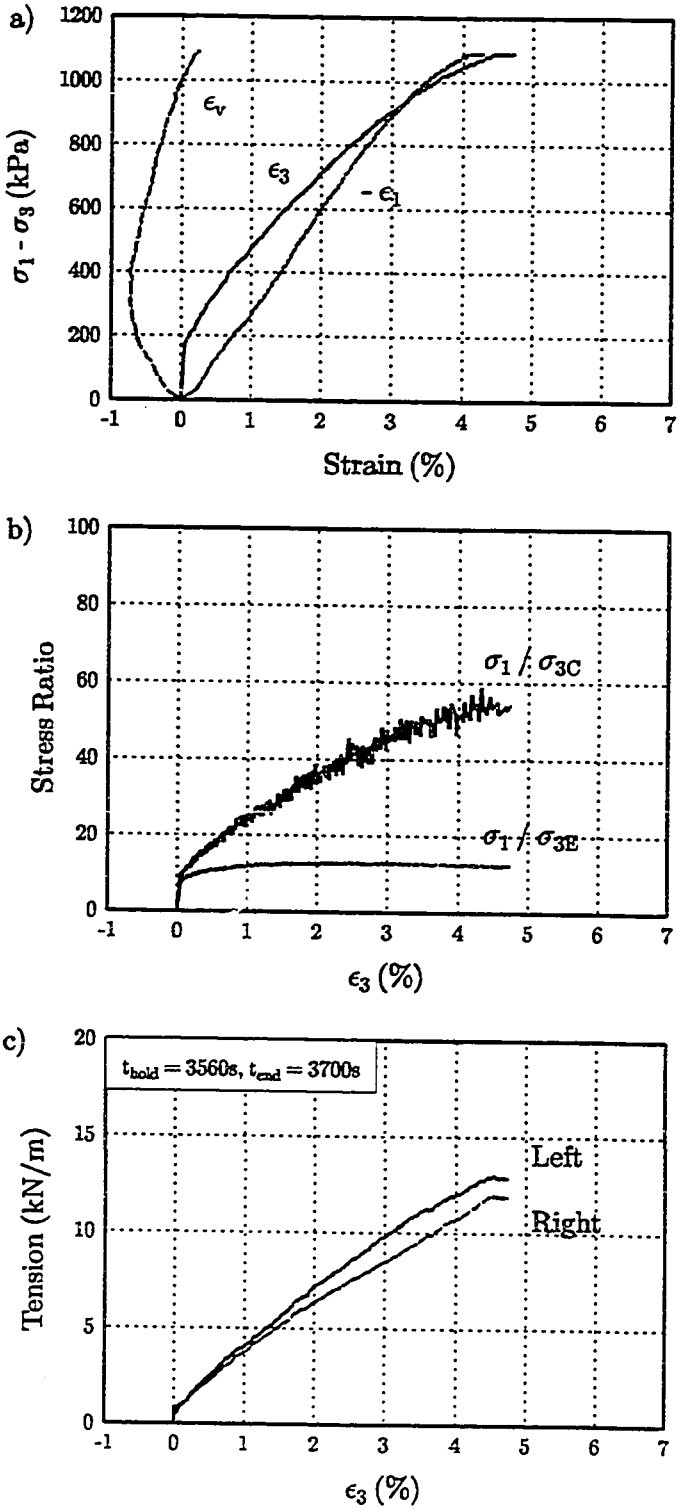

Figure C.31: Soil R, Reinforcing PP2, $\sigma_{3C} = 20$ kPa, Test 132.

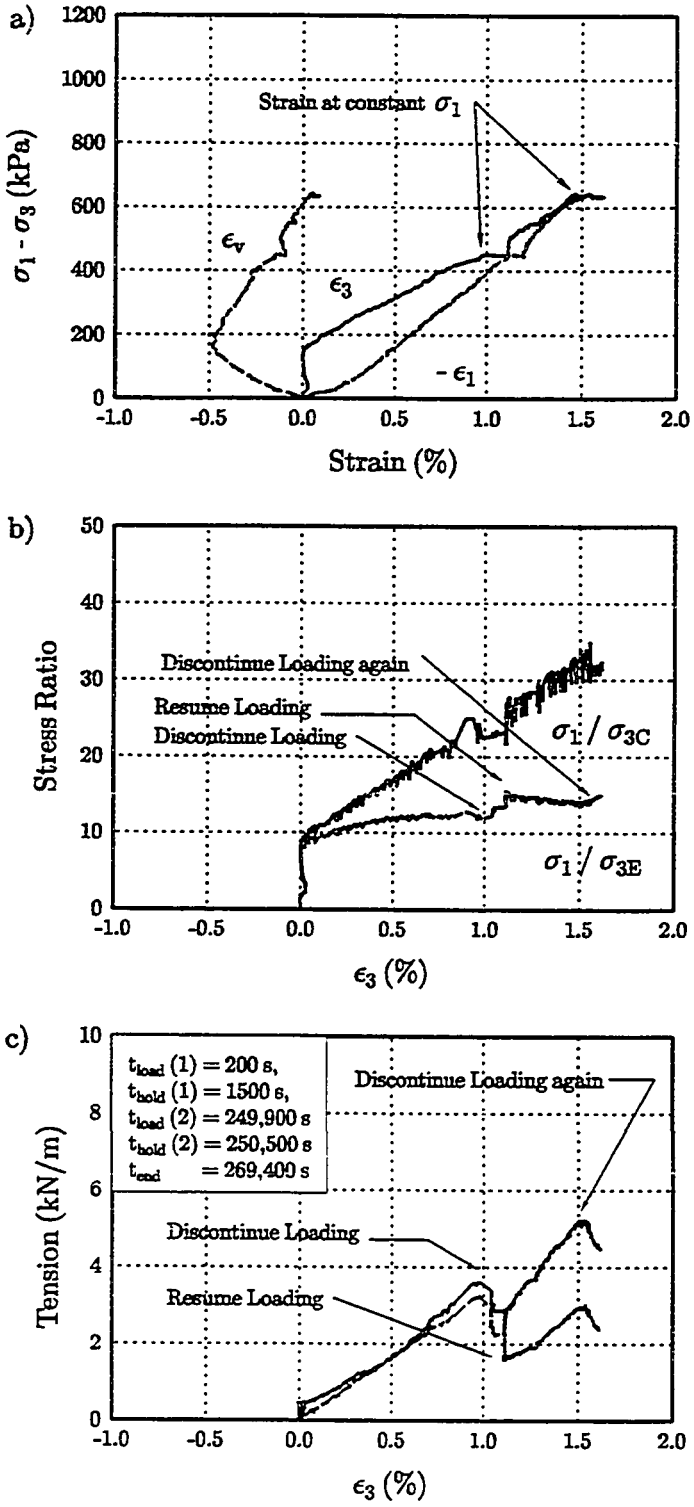

Figure C.32: Soil R, Reinforcing PP2, σ_{3C} = 20 kPa, Test 135.

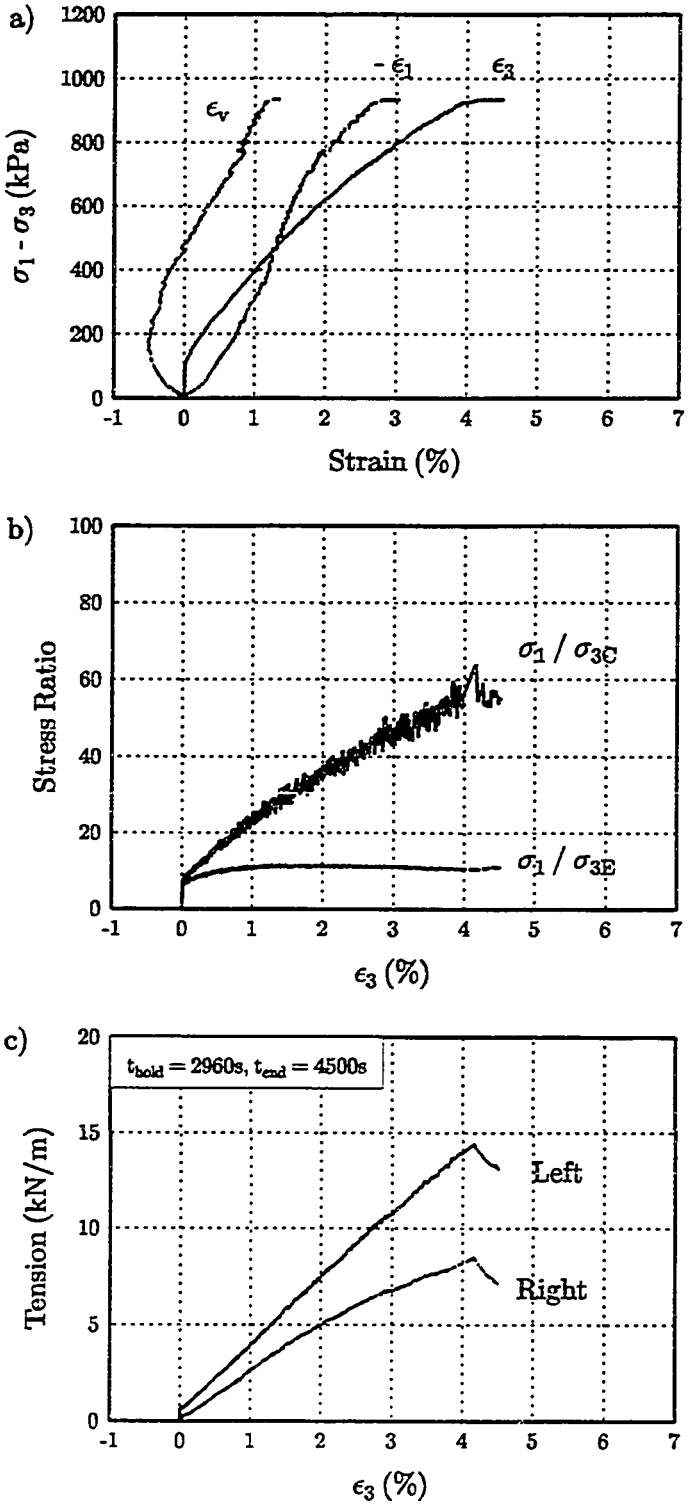

Figure C.33: Soil R, Reinforcing PP2, $\sigma_{3C} = 25$ kPa, Test 70.

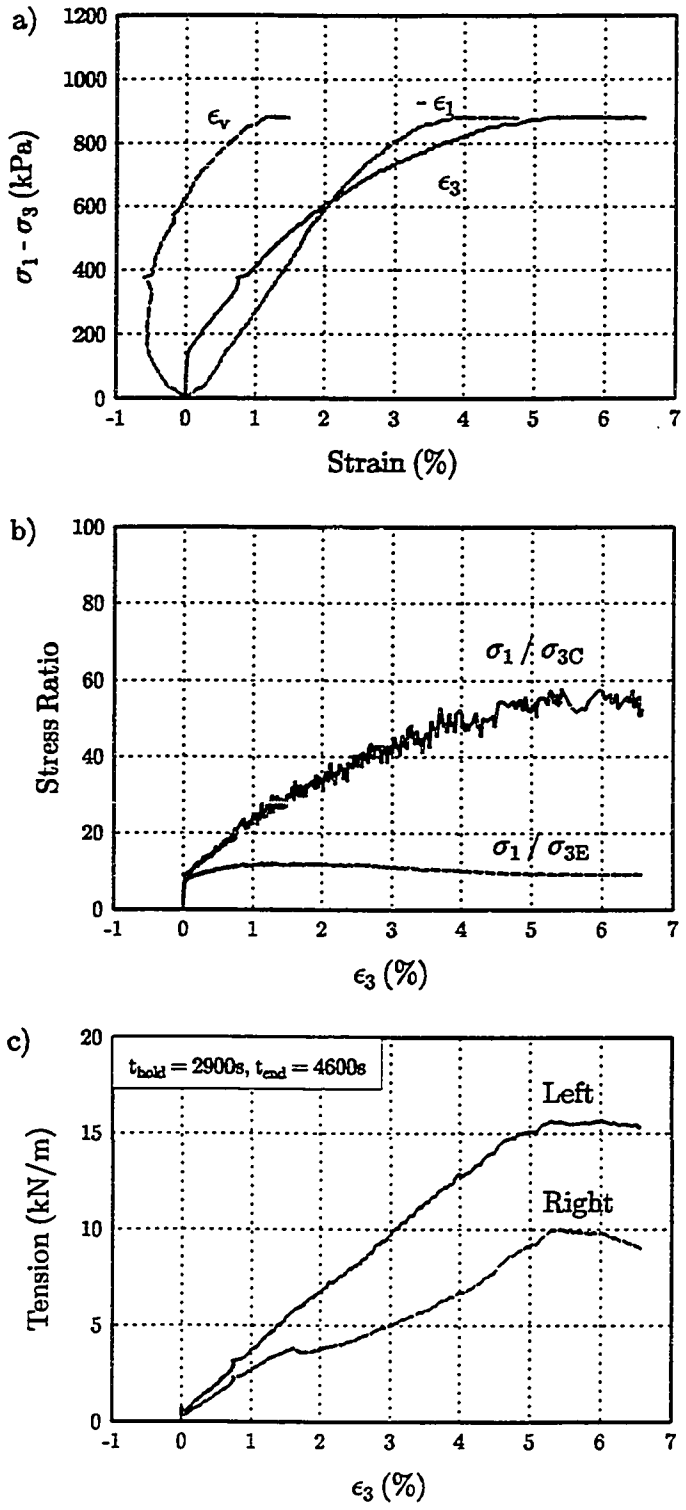

Figure C.34: Soil R, Reinforcing PP2, $\sigma_{3C} = 25$ kPa, Test 73.

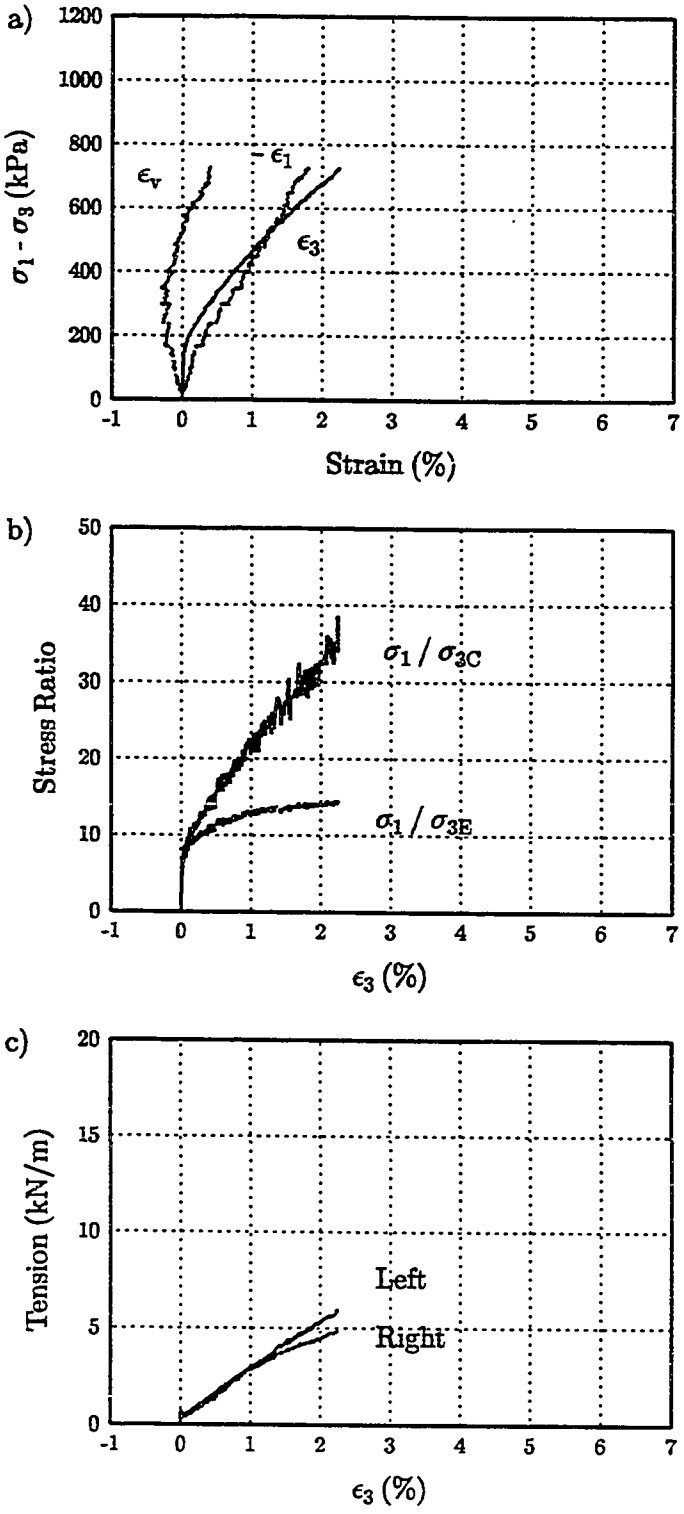

Figure C.35: Soil R, Reinforcing PP2, $\sigma_{3C} = 25$ kPa, Test 123.

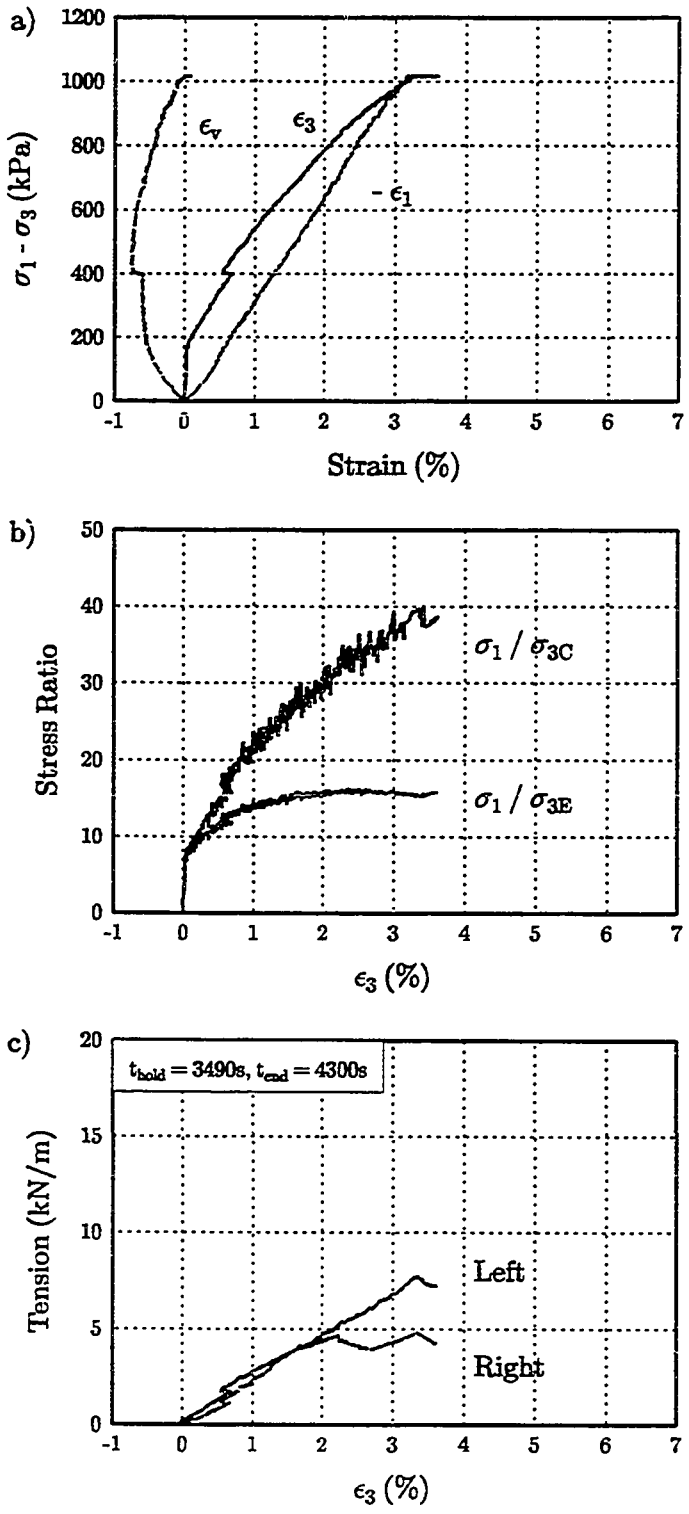

Figure C.36: Soil R, Reinforcing PP2, $\sigma_{3C} = 25$ kPa, Test 124.

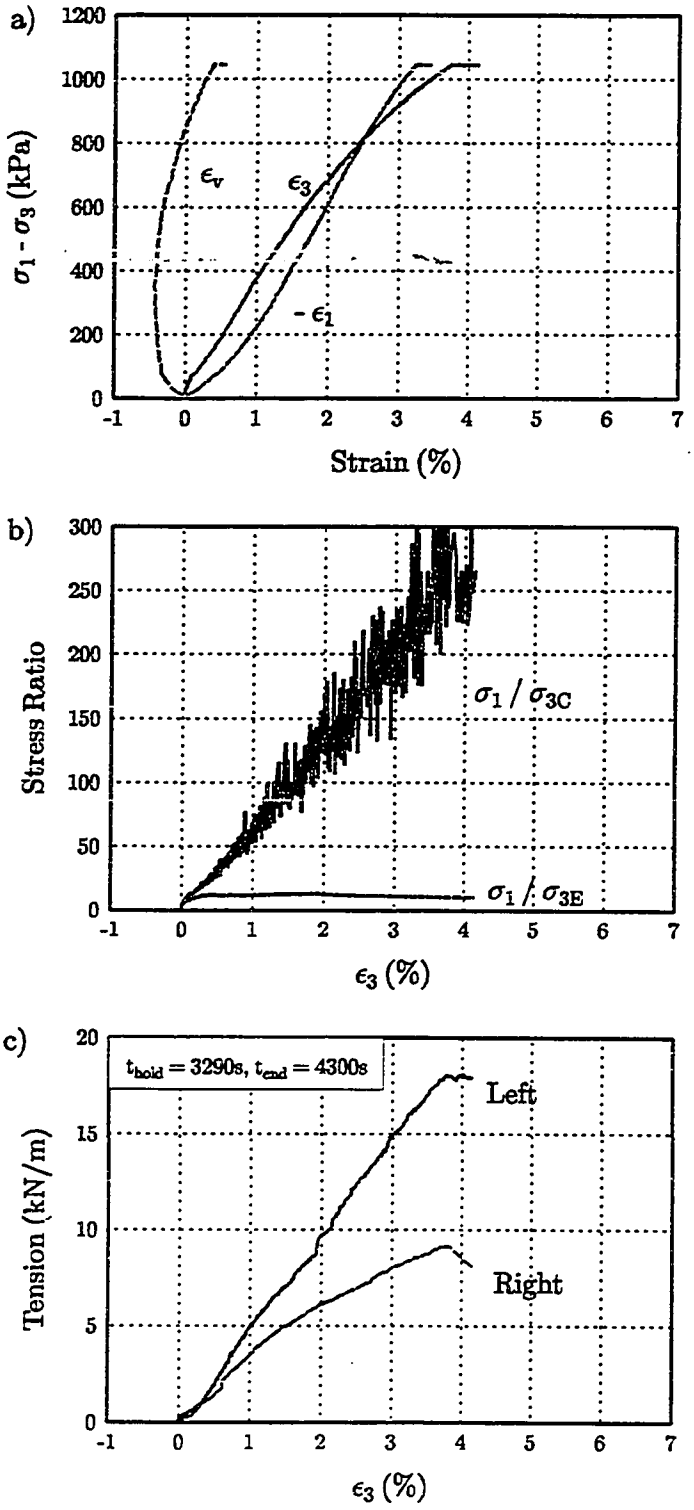

Figure C.37: Soil R, Reinforcing PP3. σ_{3C} = 12.5 kPa, Test 76.

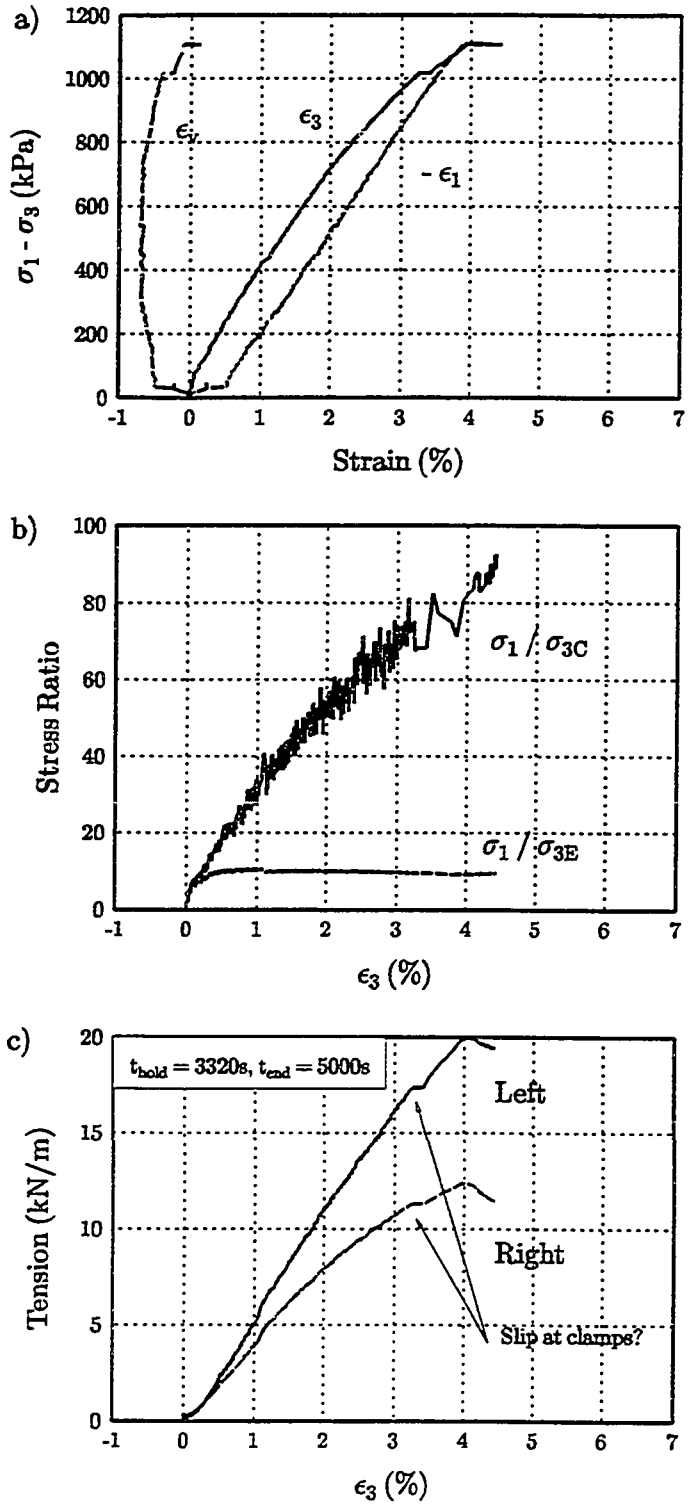

Figure C.38: Soil R, Reinforcing PP3, σ_{3C} = 12.5 kPa, Test 125.

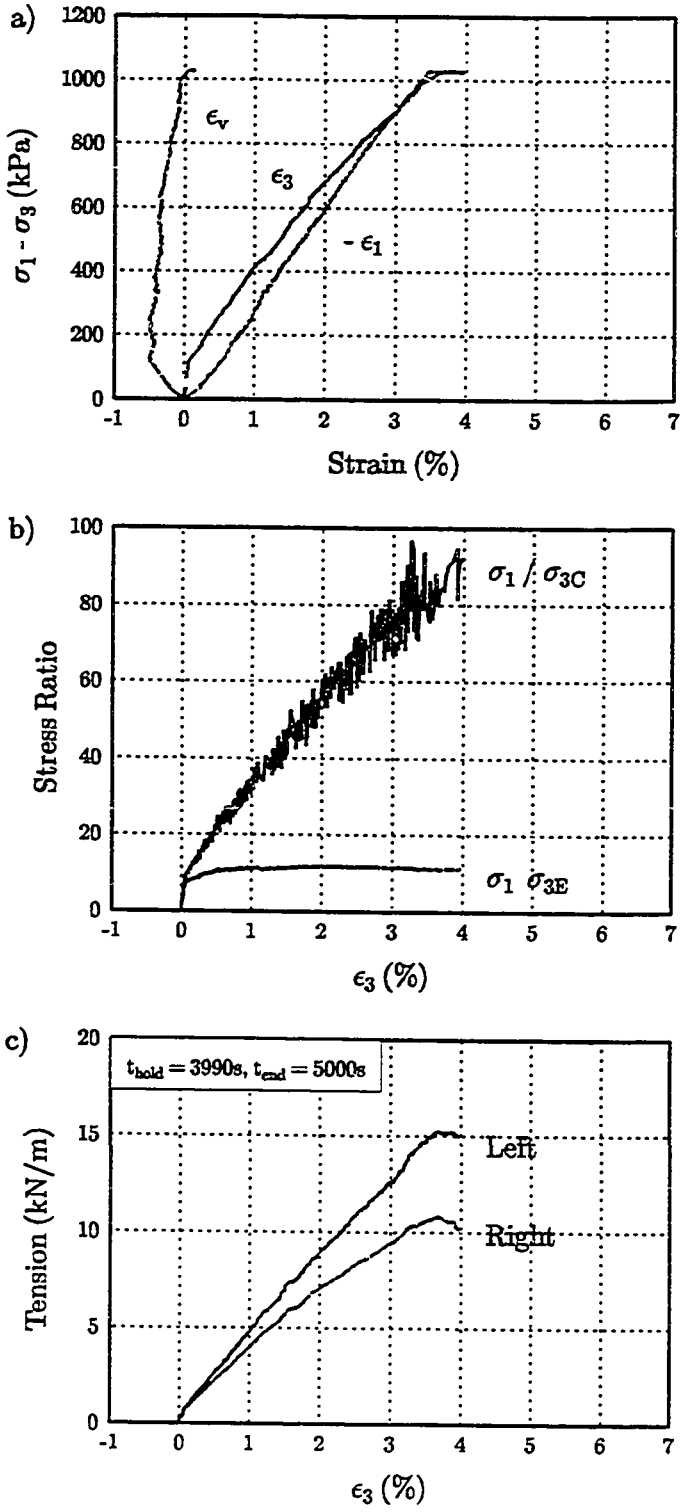

Figure C.39: Soil R, Reinforcing PP3, σ_{3C} = 12.5 kPa, Test 126.

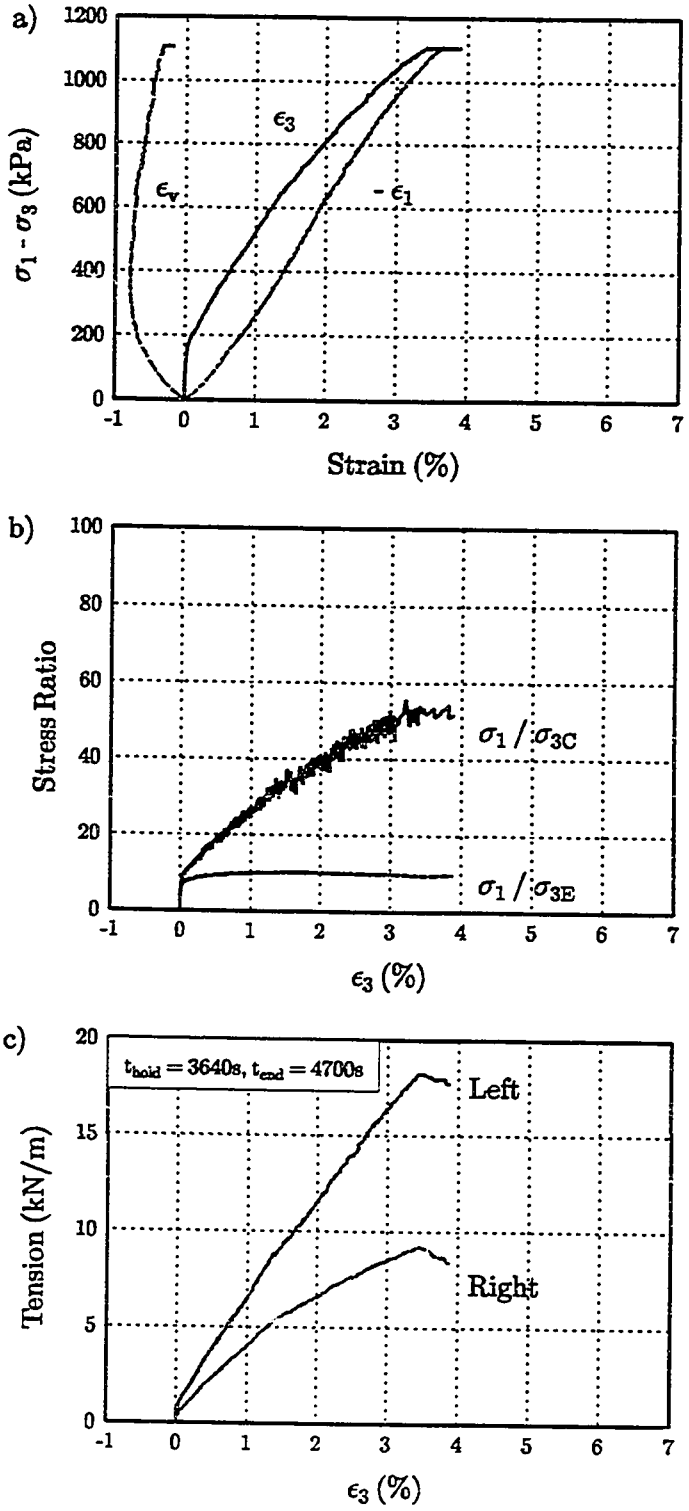

Figure C.40: Soil R, Reinforcing PP3, $\sigma_{3C} = 20$ kPa, Test 130.

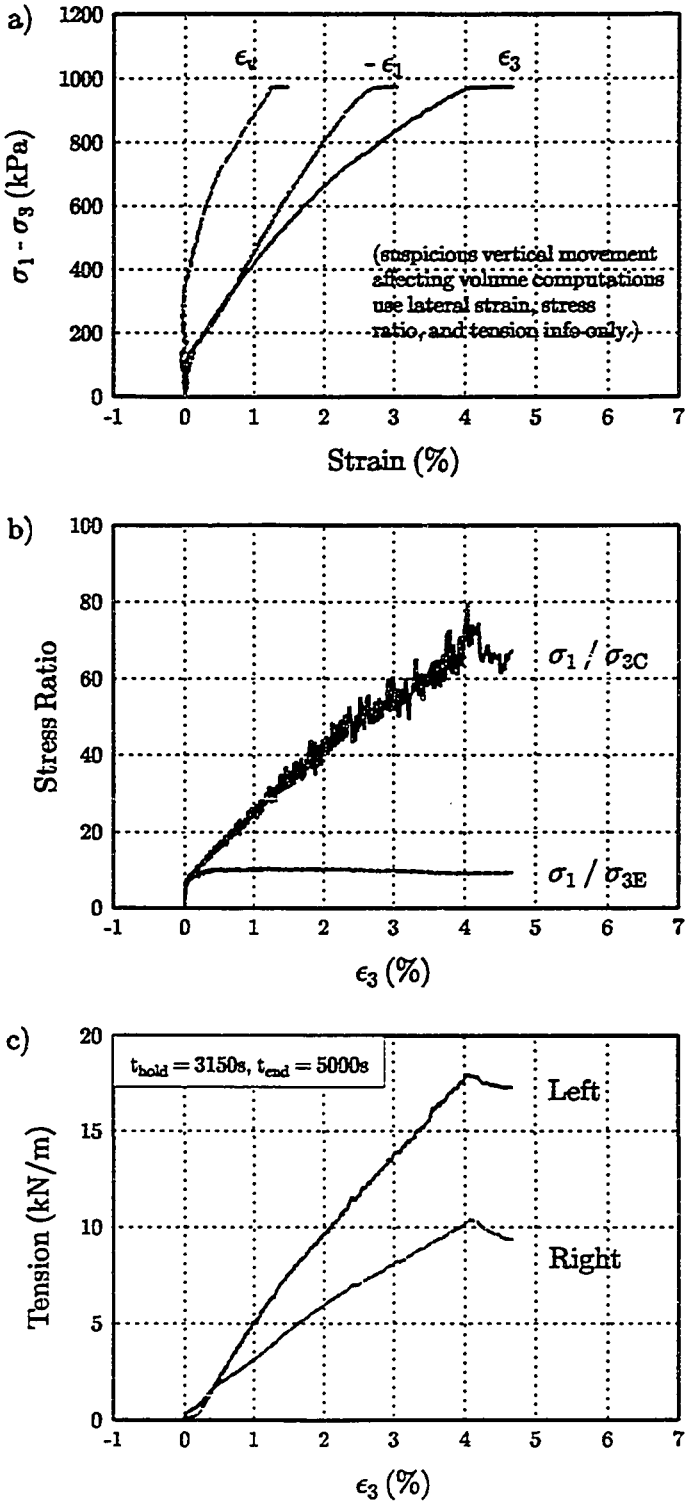

Figure C.41: Soil R, Reinforcing PP3, $\sigma_{3C} = 25$ kPa, Test 68.

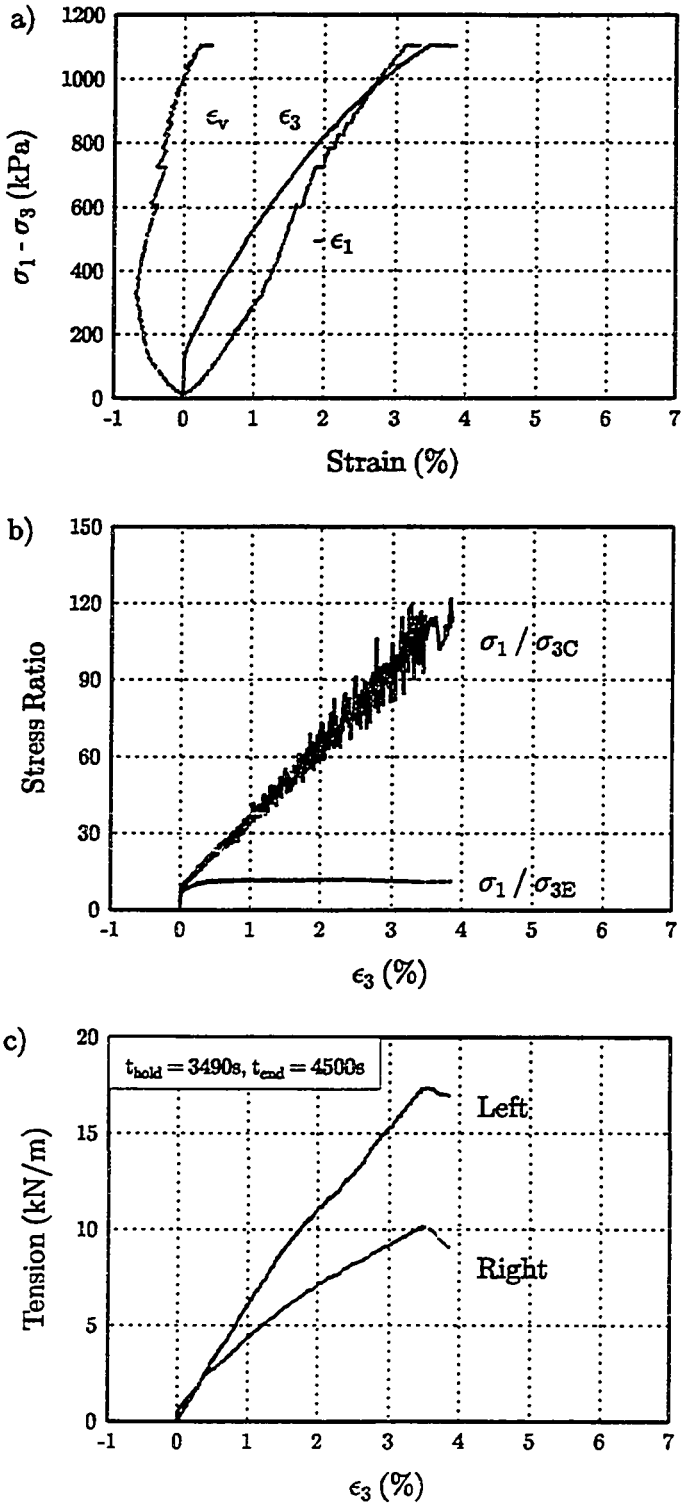

Figure C.42: Soil R, Reinforcing PP3, $\sigma_{3C} = 25$ kPa, Test 71.

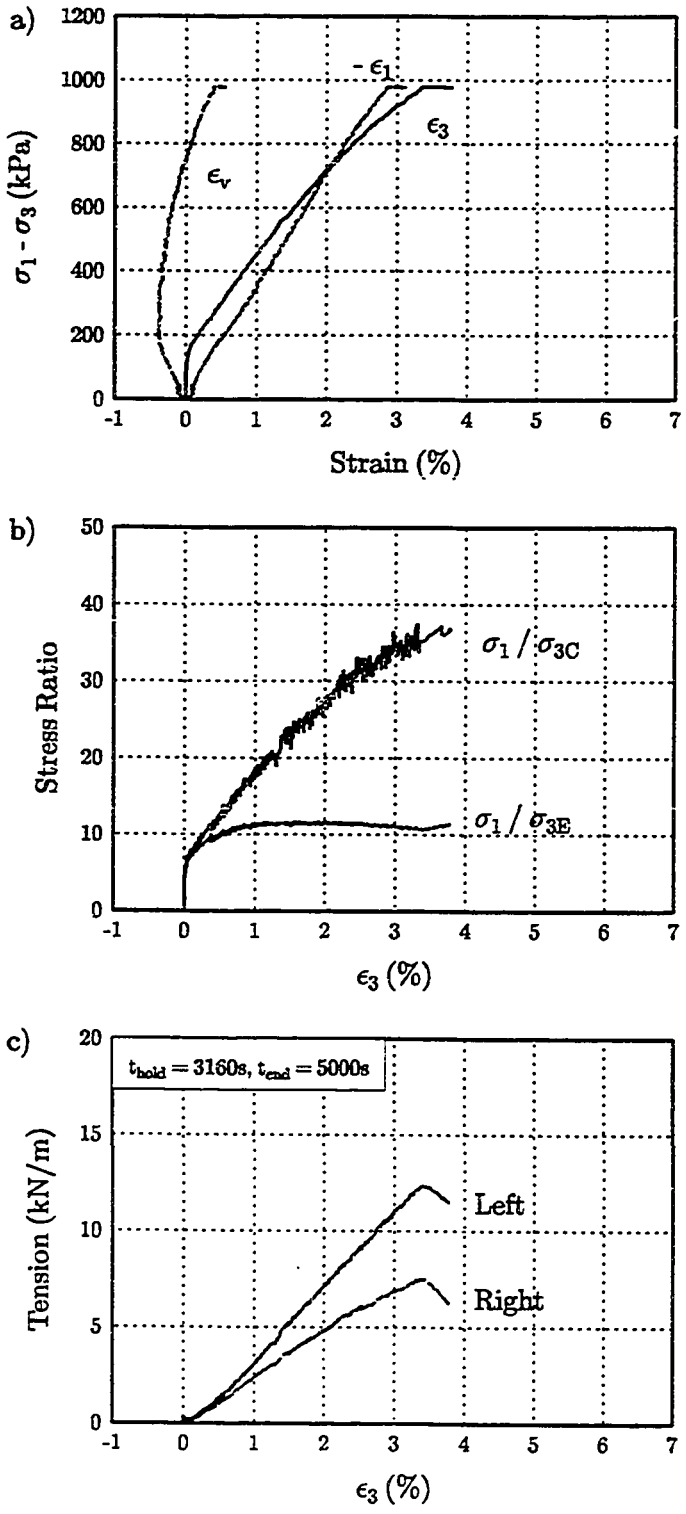

Figure C.43: Soil R, Reinforcing PP3, $\sigma_{3C} = 25$ kPa, Test 122.

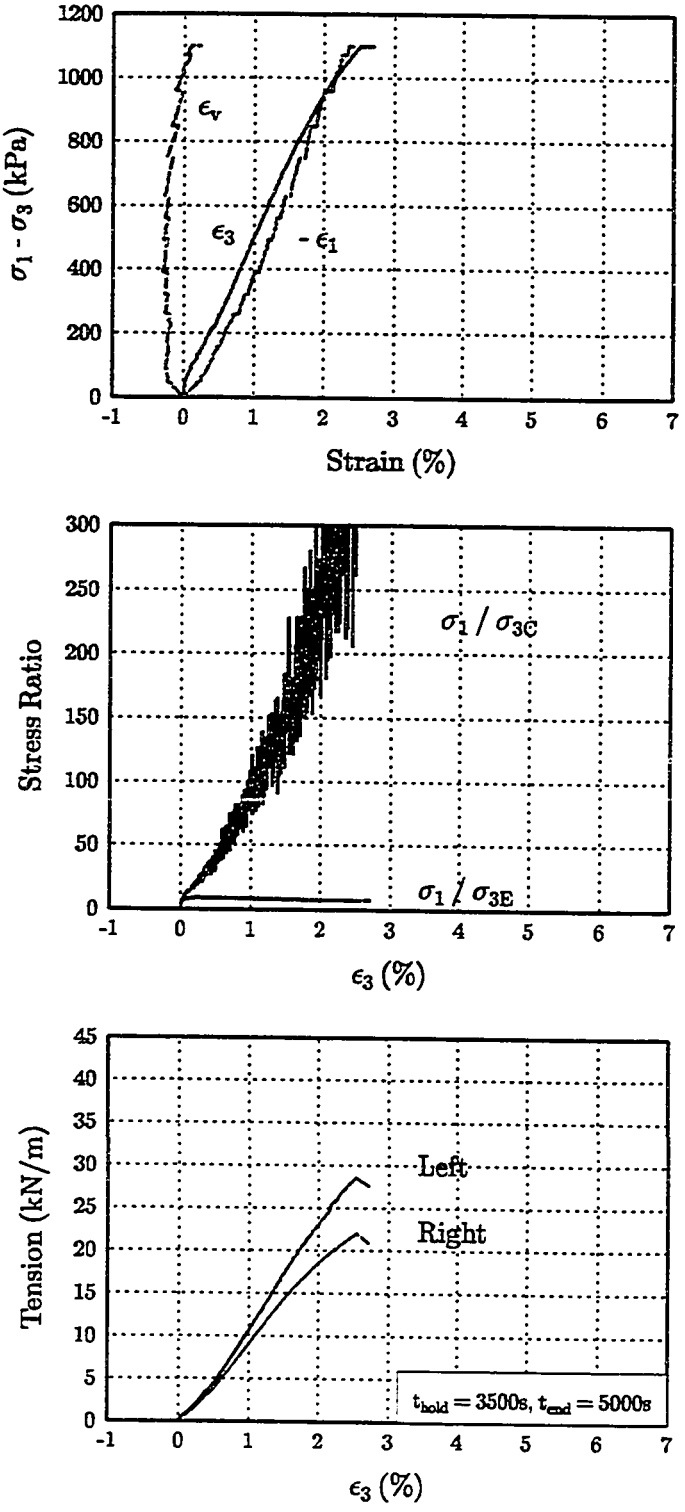

Figure C.44: Soil R, Reinforcing PET1, σ_{3C} = 12.5 kPa, Test 98.

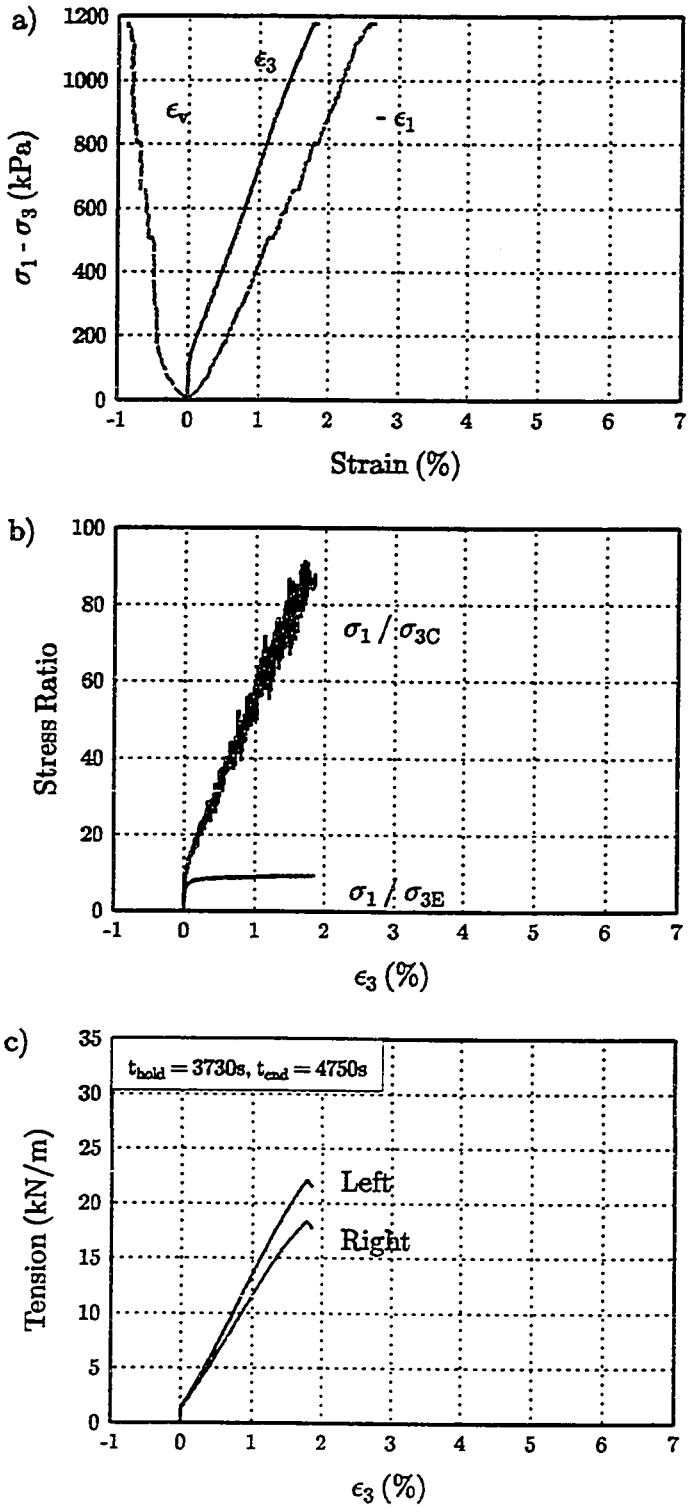

Figure C.45: Soil R, Reinforcing PET1, σ_{3C} = 12.5 kPa, Test 134.

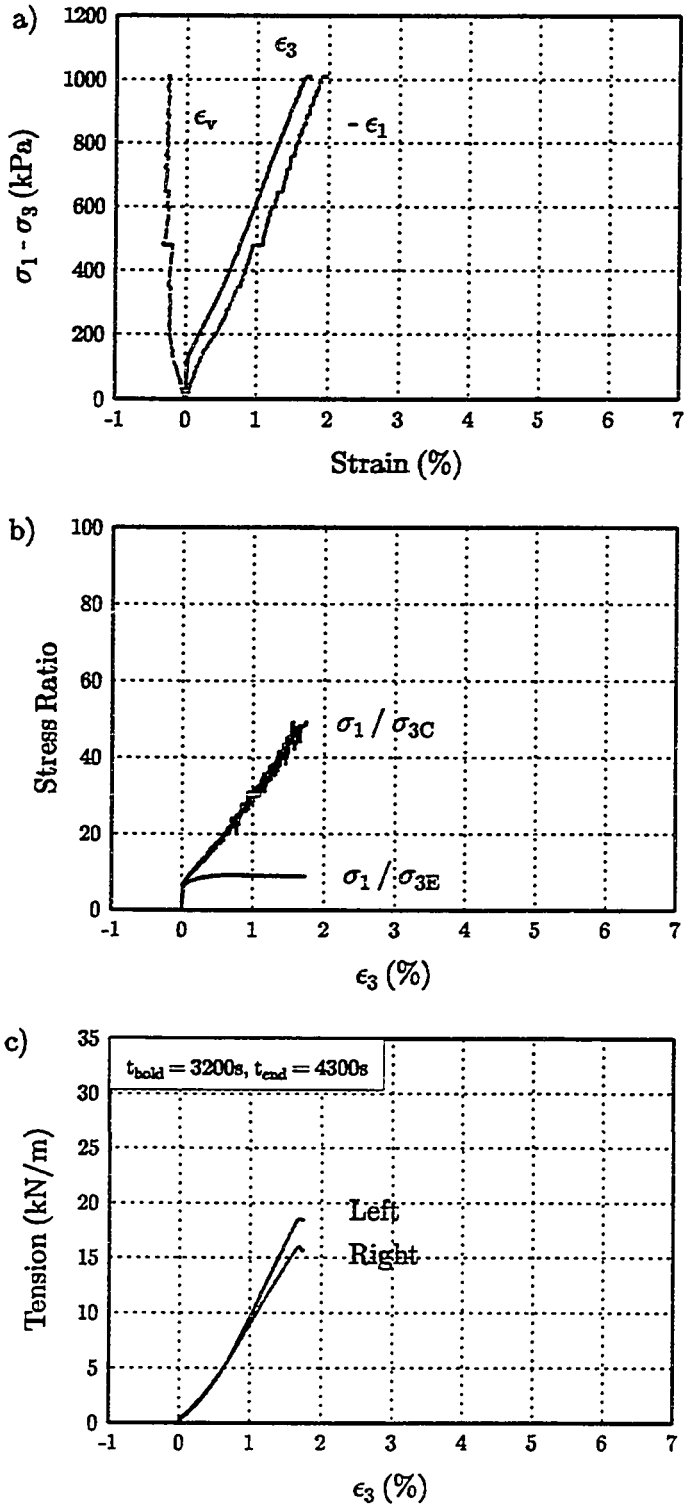

Figure C.46: Soil R, Reinforcing PET1, $\sigma_{3C} = 20$ kPa, Test 133.

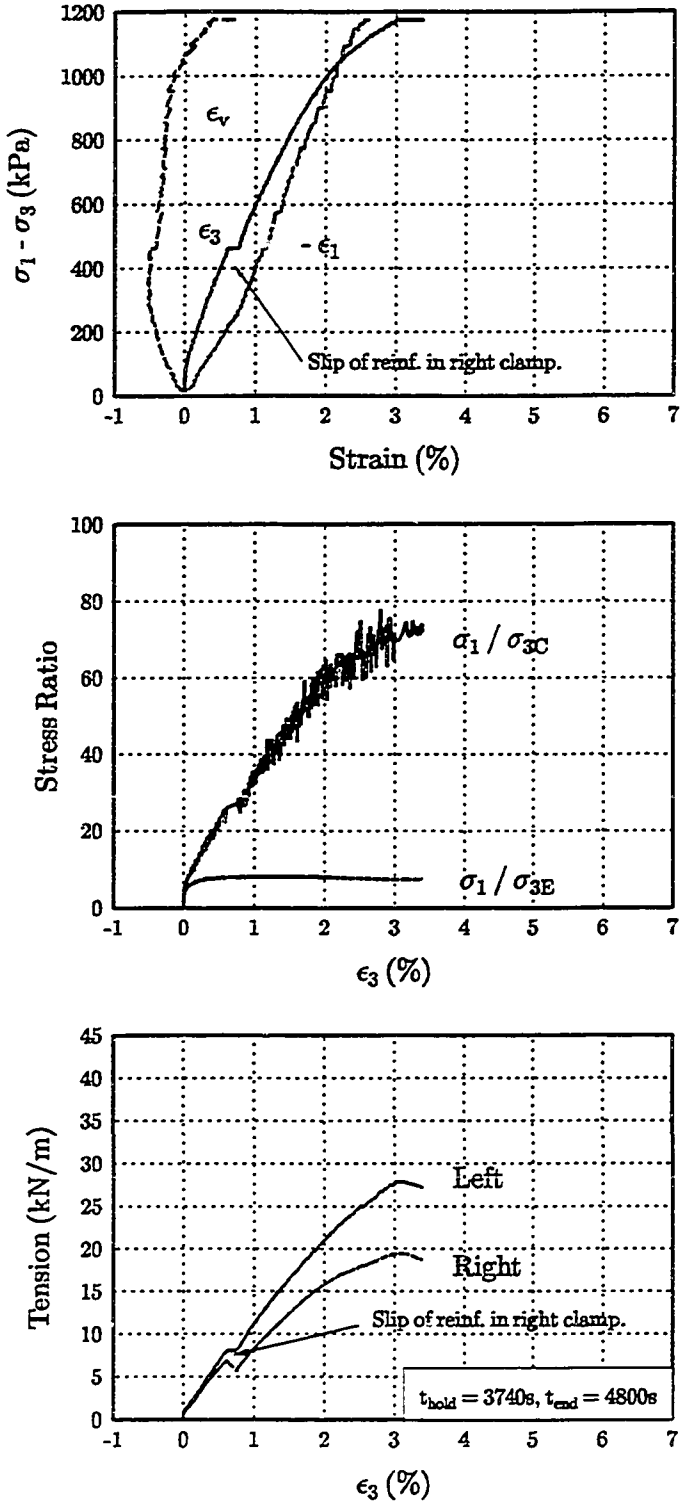

Figure C.47: Soil R, Reinforcing PET1, $\sigma_{3C} = 25$ kPa, Test 99.

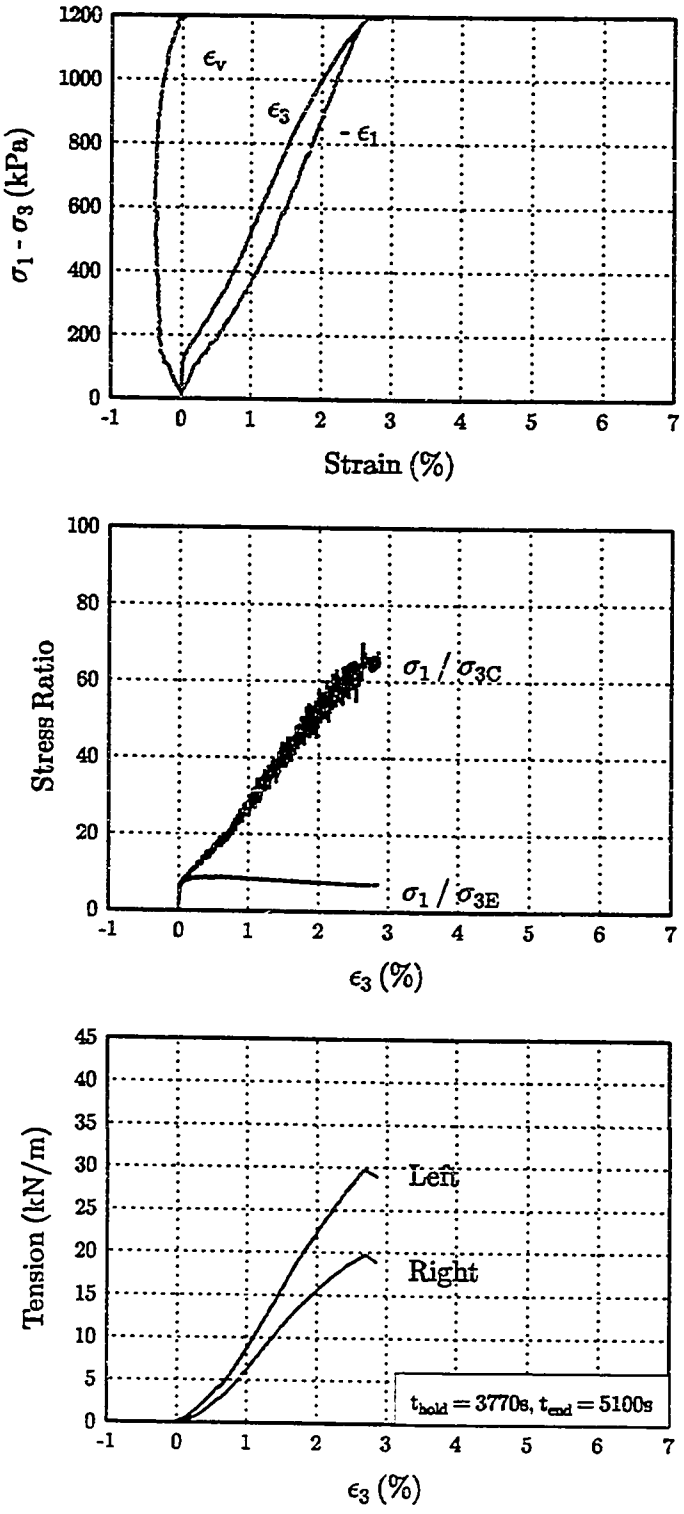

Figure C.48: Soil R, Reinforcing PET1, $\sigma_{3C} = 25$ kPa, Test 100.

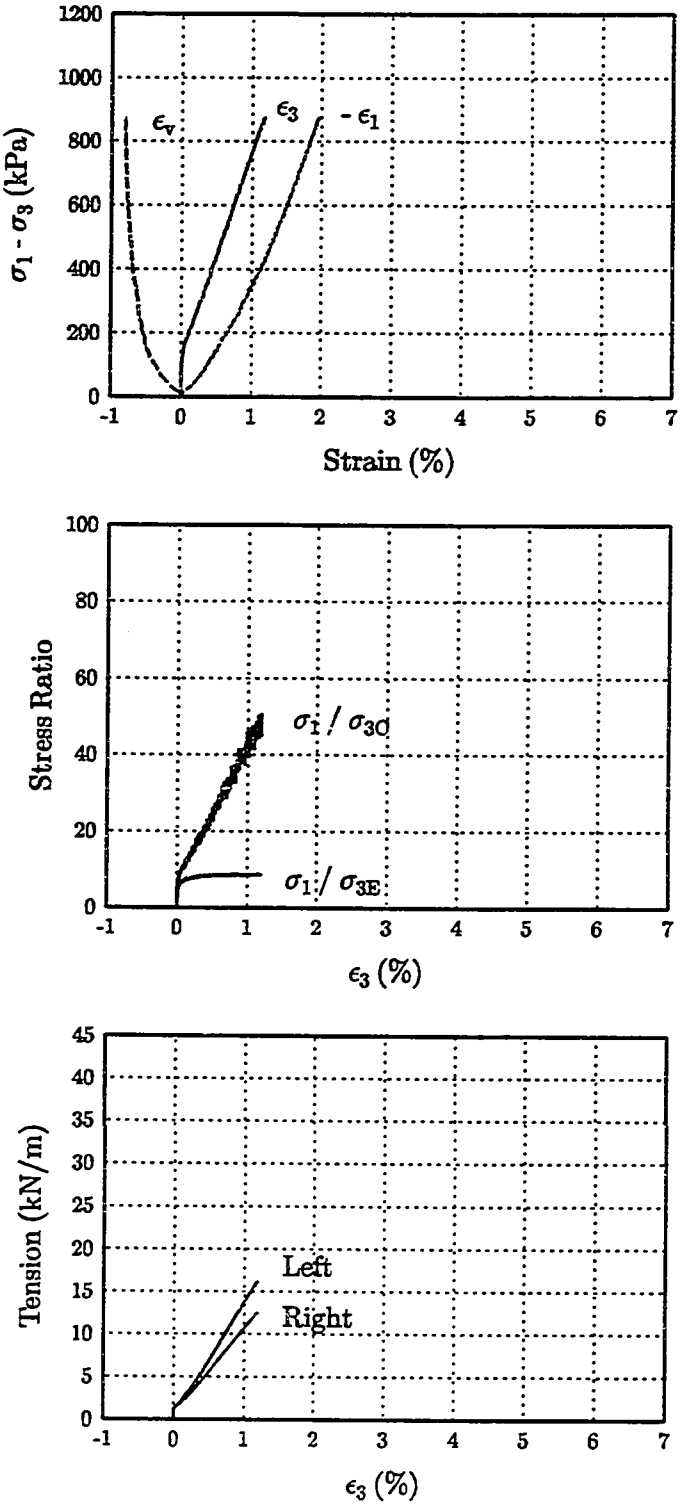

Figure C.49: Soil R, Reinforcing PET1, σ_{3C} = 25 kPa, Test 111.

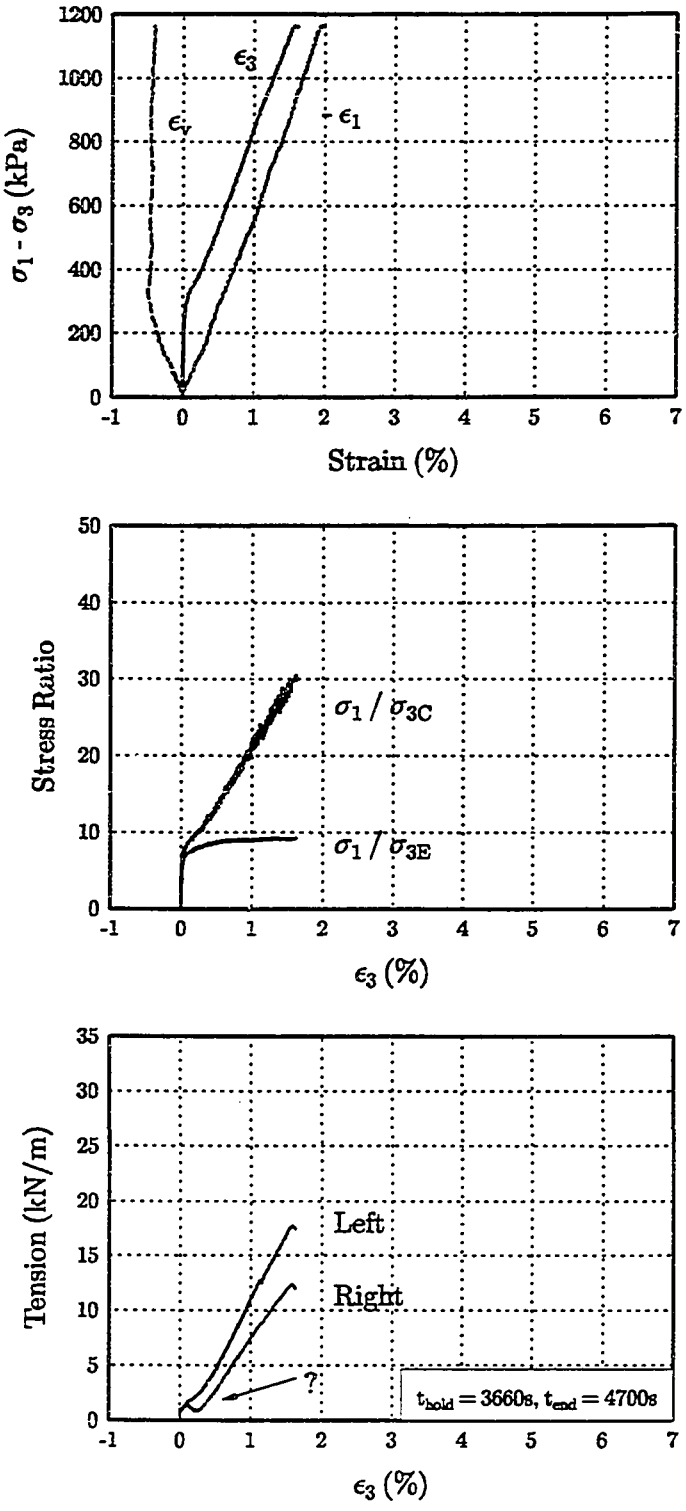

Figure C.50: Soil R, Reinforcing PET1, $\sigma_{3C} = 50$ kPa, Test 106.

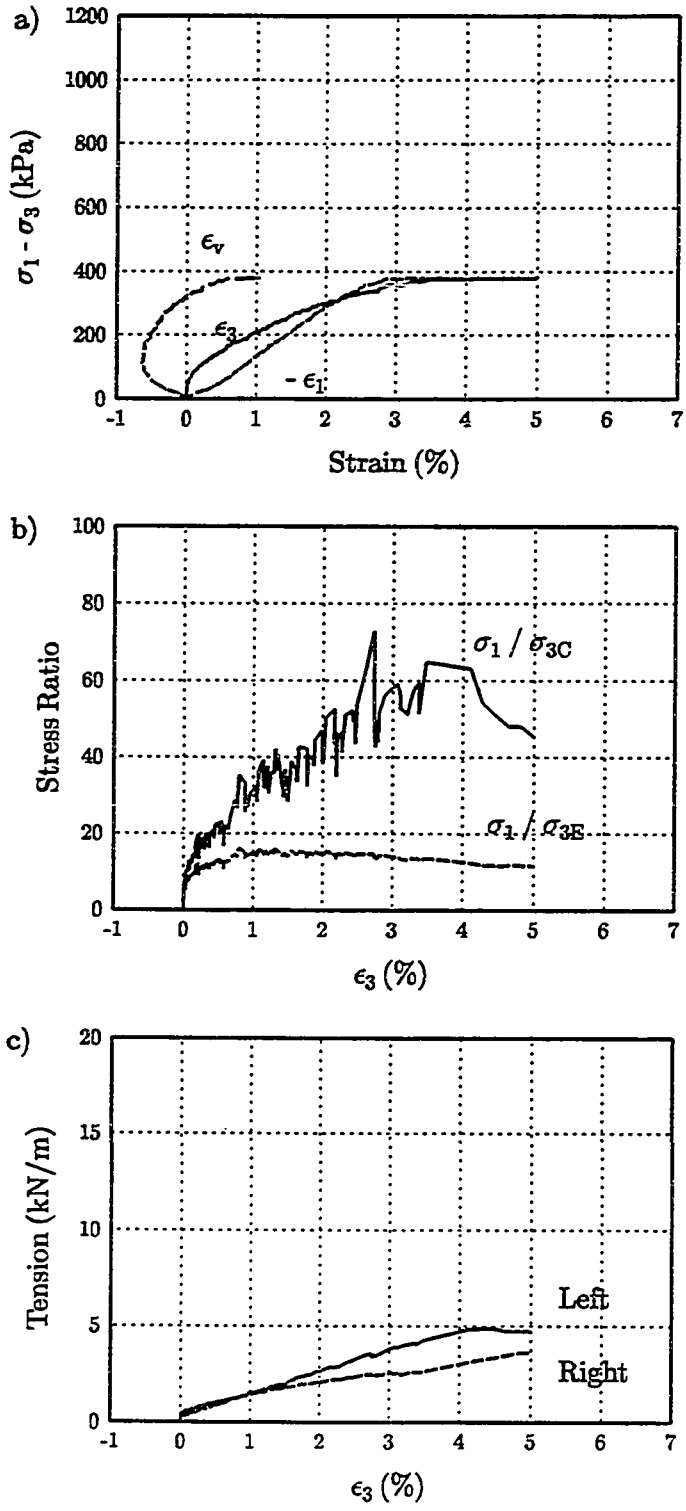

Figure C.51: Soil R, Reinforcing NW1, σ_{3C} = 12.5 kPa, Test 84.

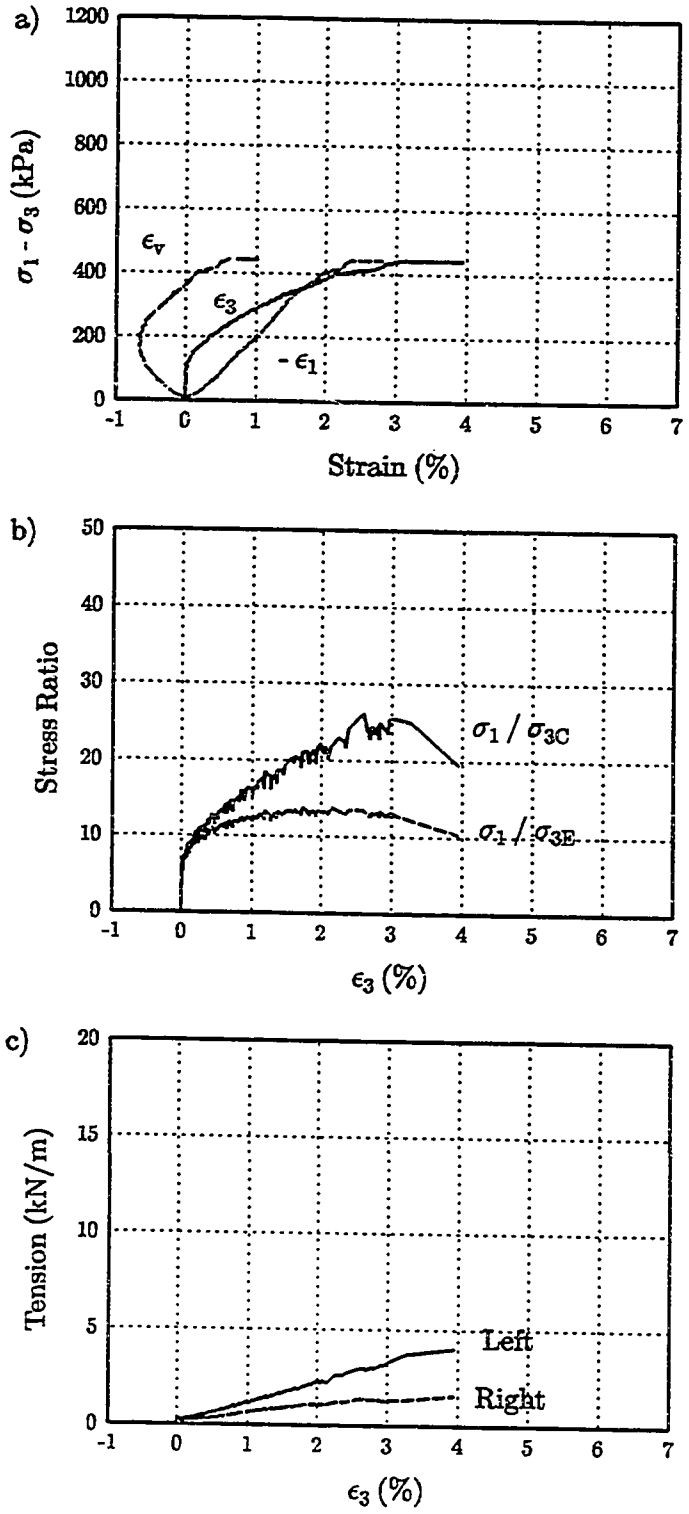

Figure C.52: Soil R, Reinforcing NW1, σ_{3C} = 25 kPa, Test 85.

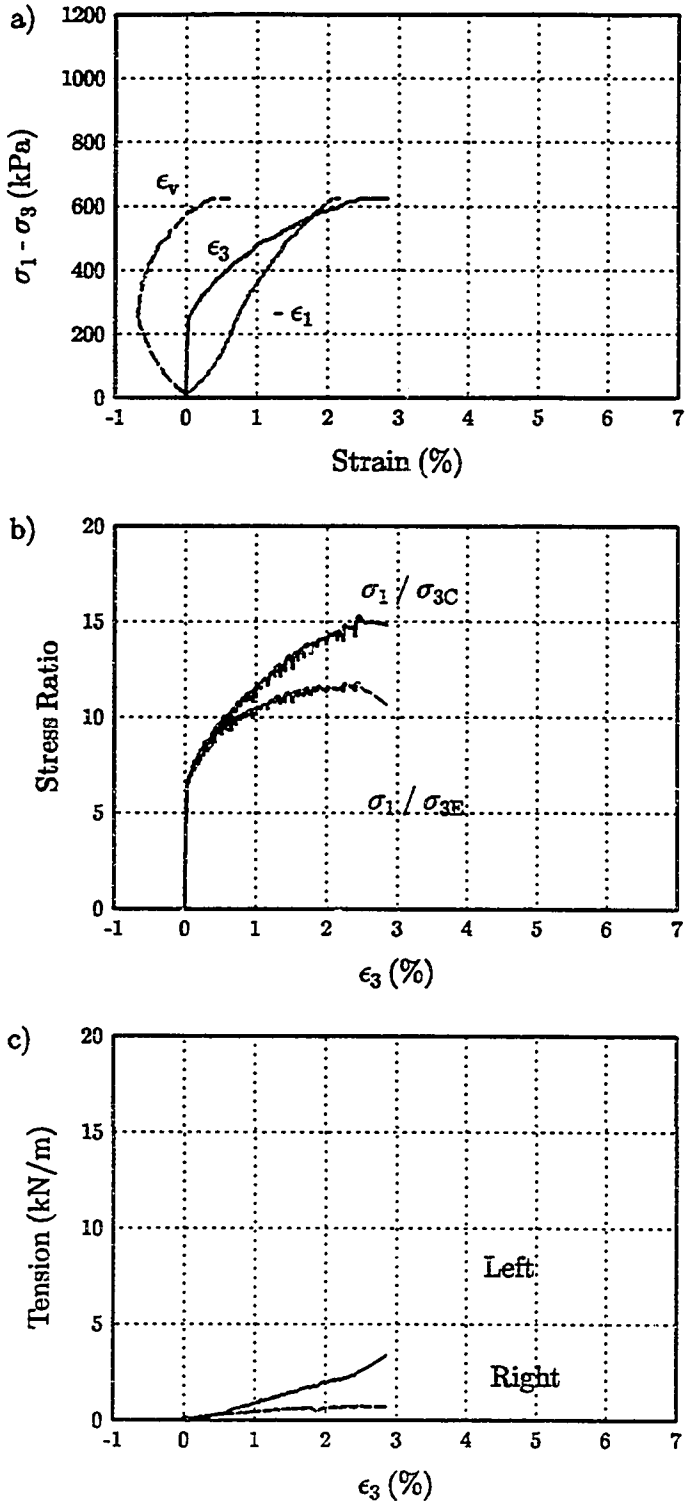

Figure C.53: Soil R, Reinforcing NW1, σ_{3C} = 12.5 kPa, Test 87.

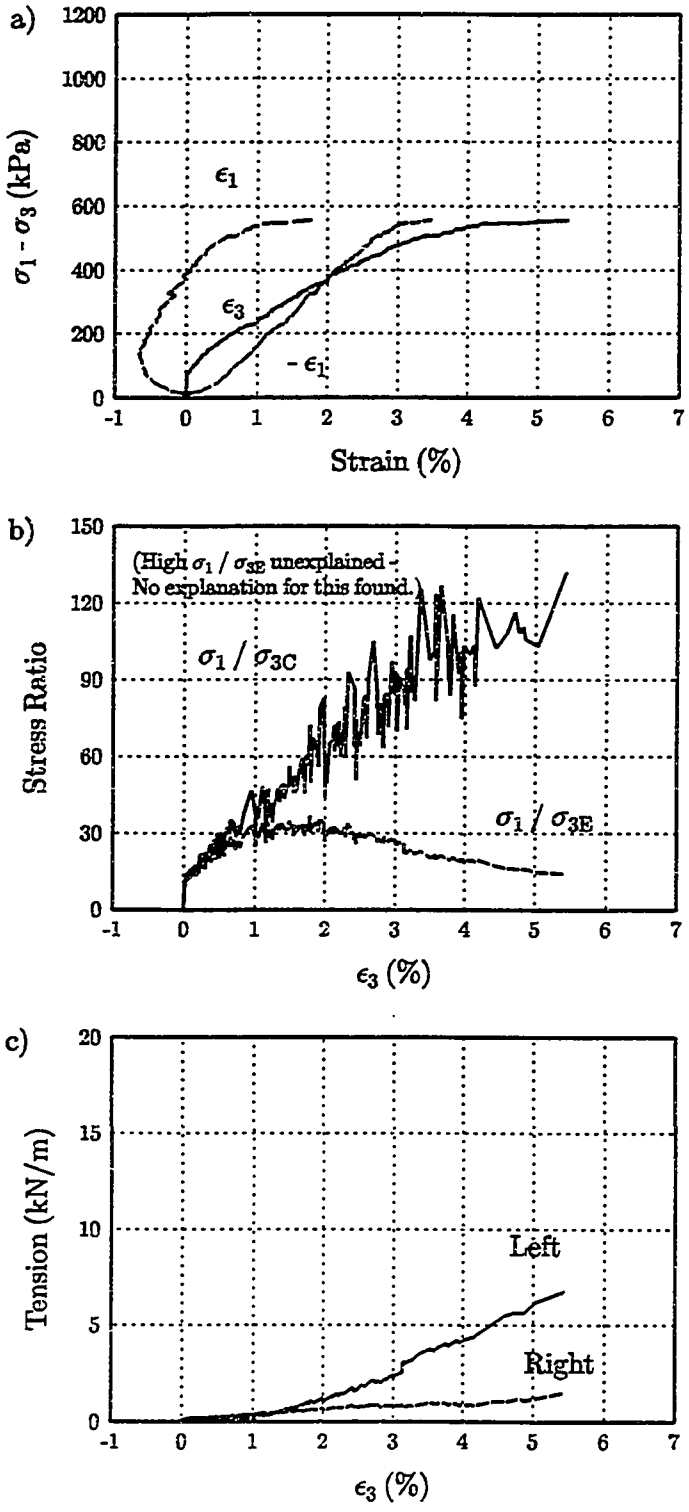

Figure C.54: Soil R, Reinforcing NW2, σ_{3C} = 12.5 kPa, Test 82.

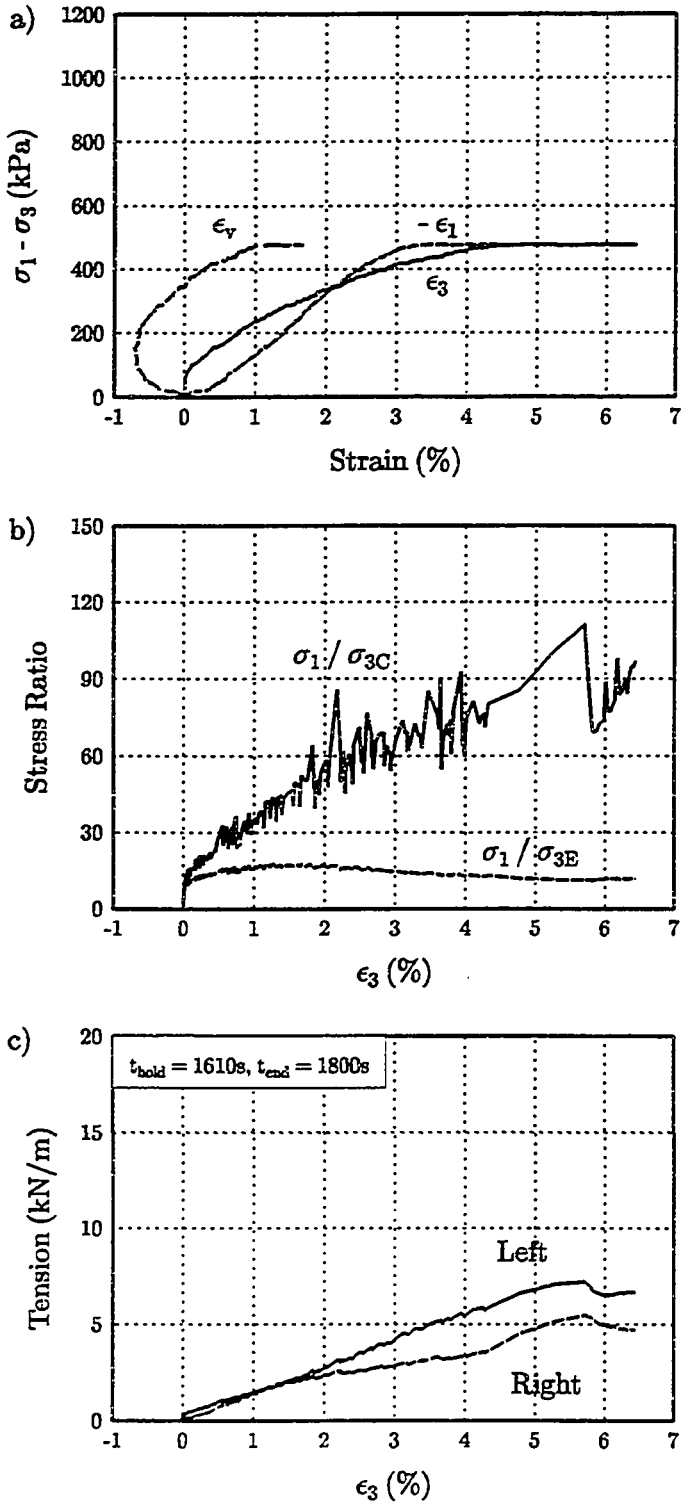

Figure C.55: Soil R, Reinforcing NW2, σ_{3C} = 12.5 kPa, Test 83.

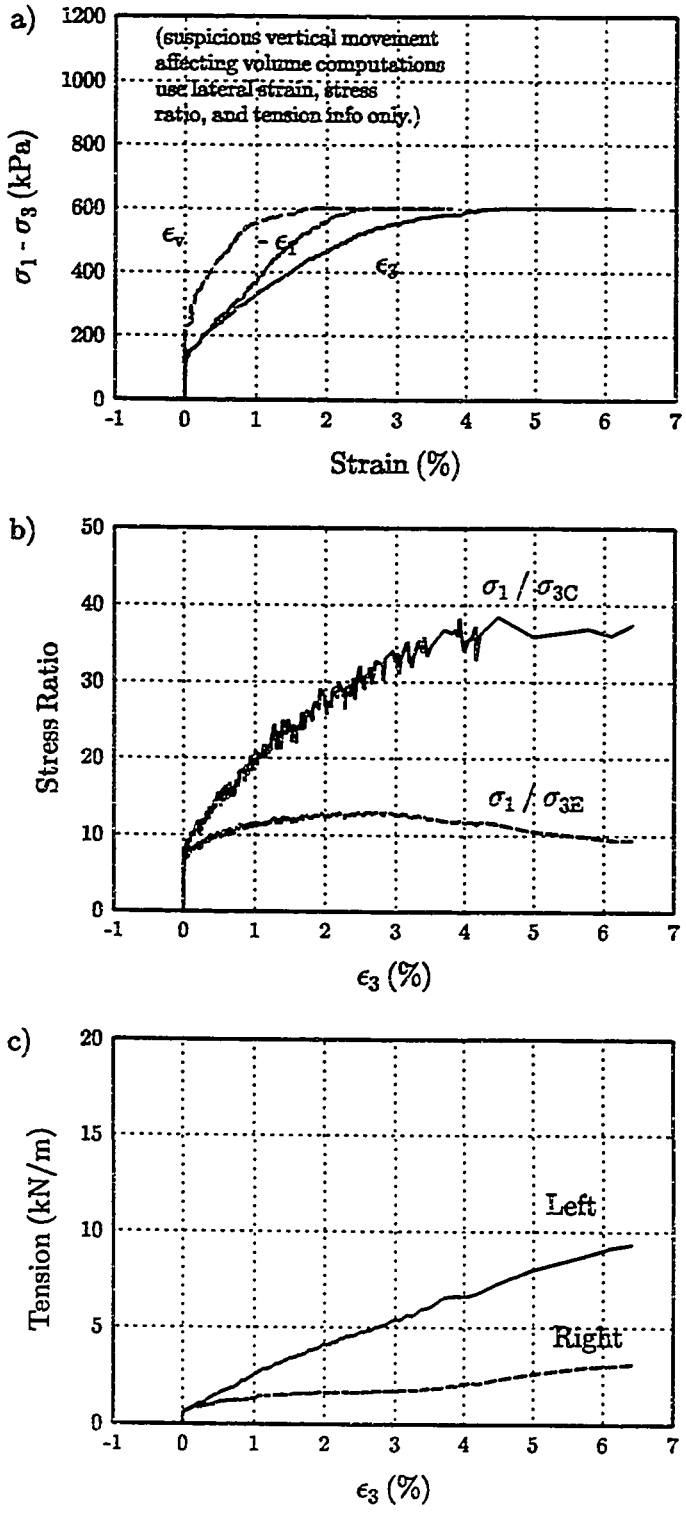

Figure C.56: Soil R, Reinforcing NW2, $\sigma_{3C} = 25$ kPa, Test 72.

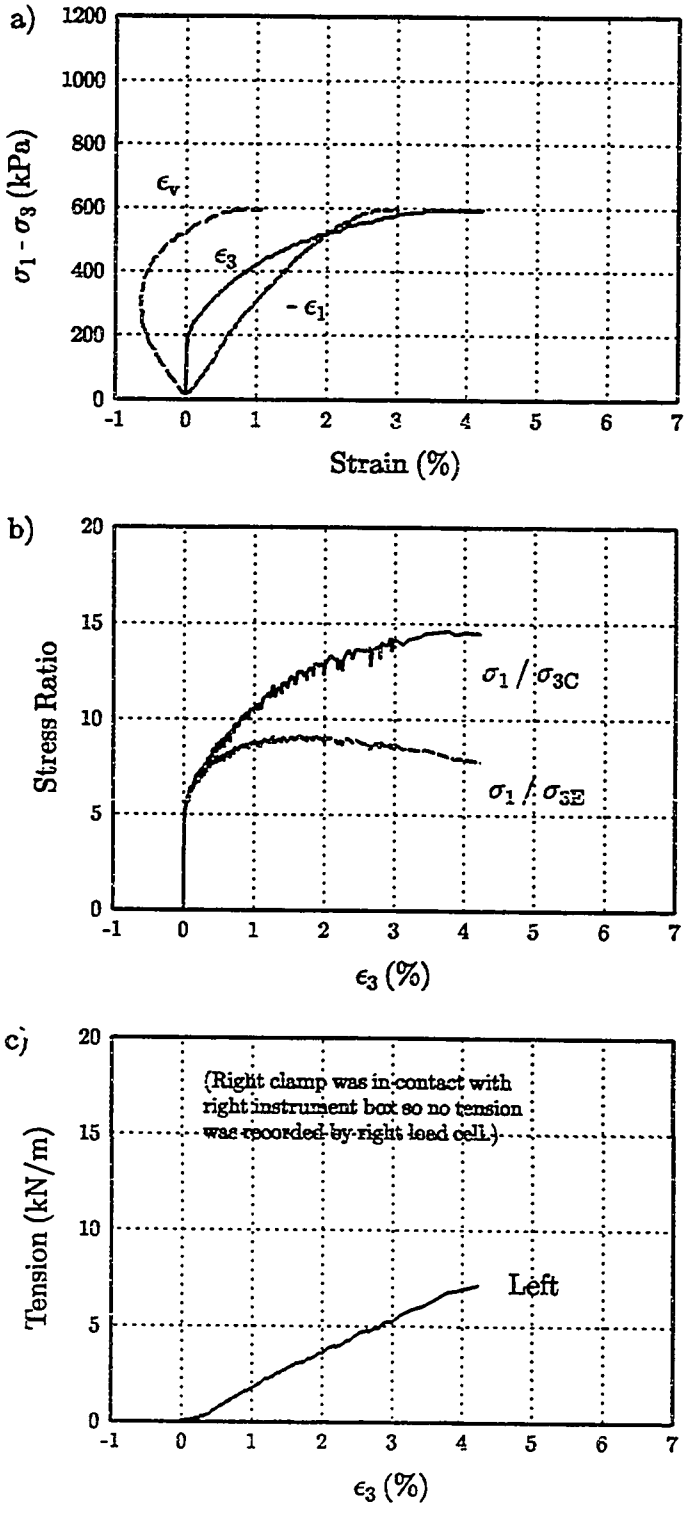

Figure C.57: Soil R, Reinforcing NW2, $\sigma_{3C} = 50$ kPa, Test 86.

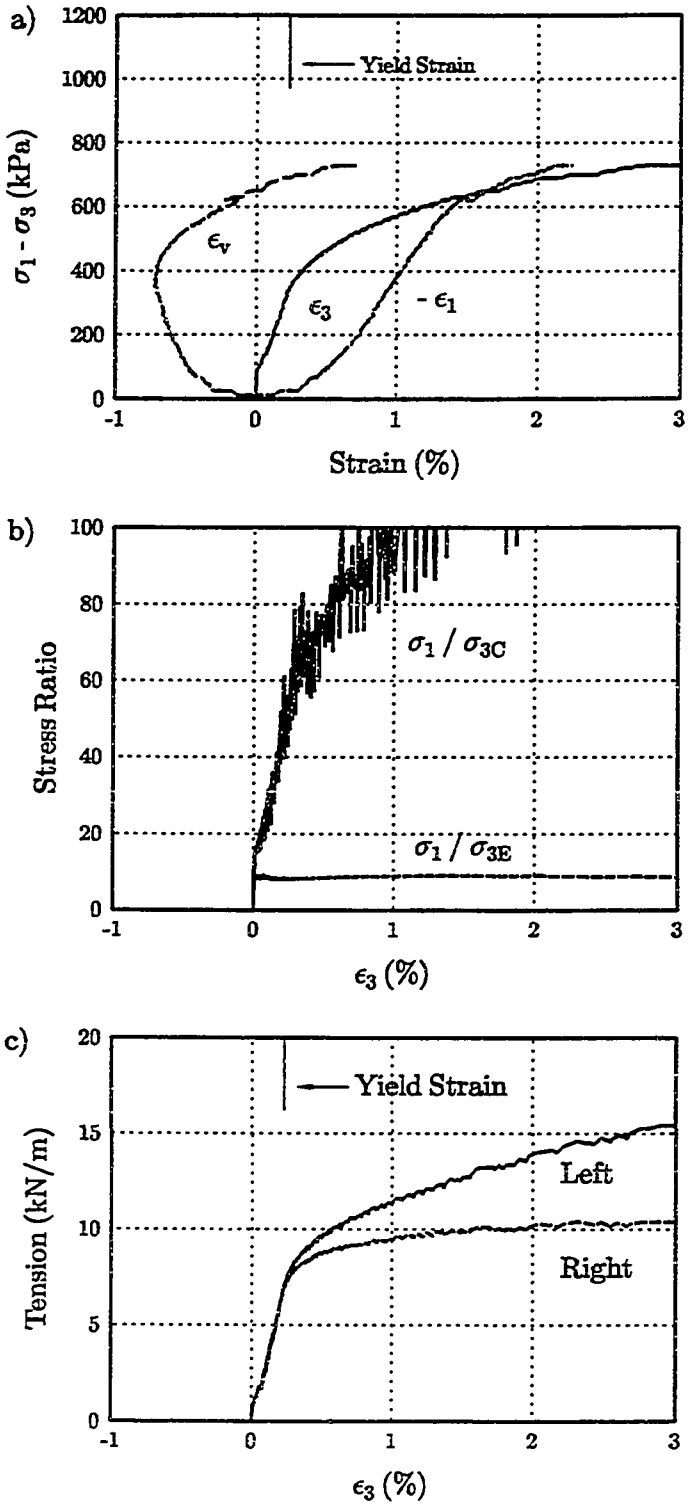

Figure C.58: Soil R, Reinforcing SS, σ_{3C} = 12.5 kPa, Test 101.

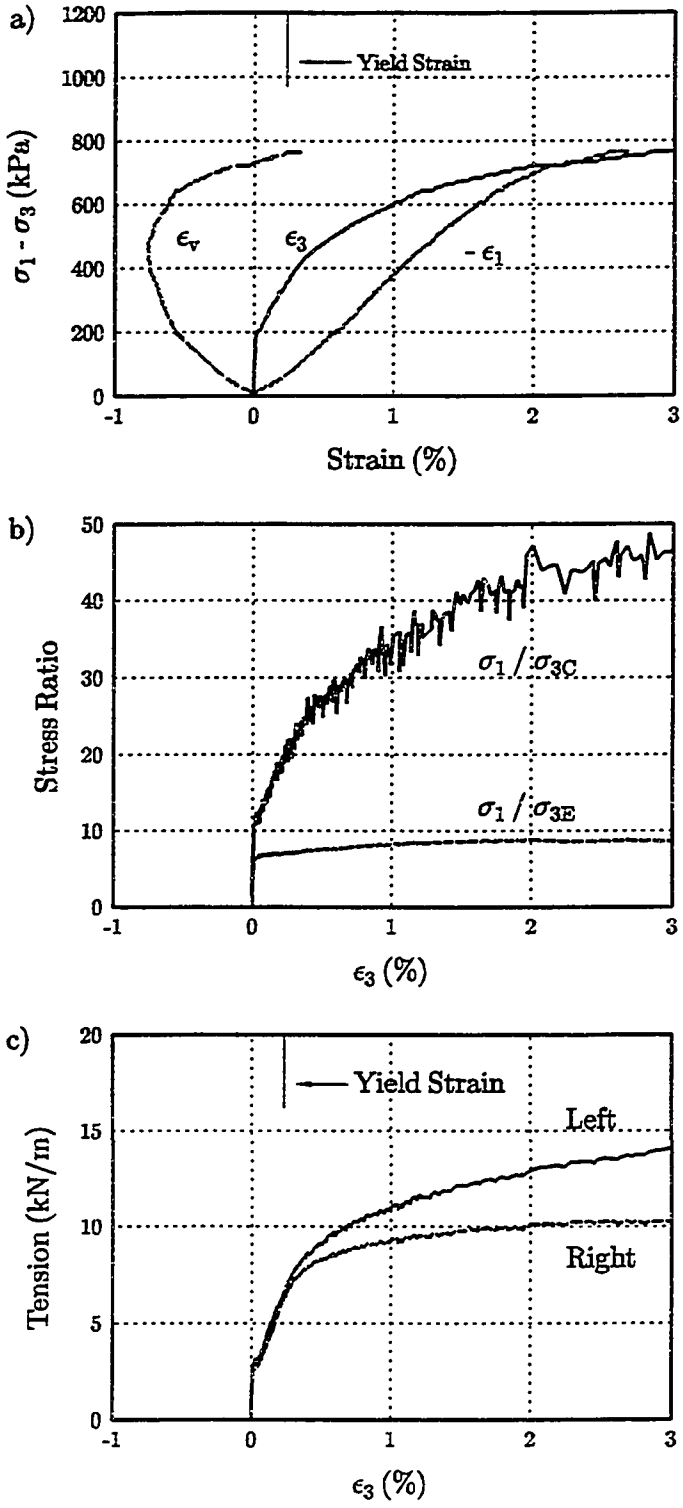

Figure C.59: Soil R, Reinforcing SS, σ_{3C} = 25 kPa, Test 102.

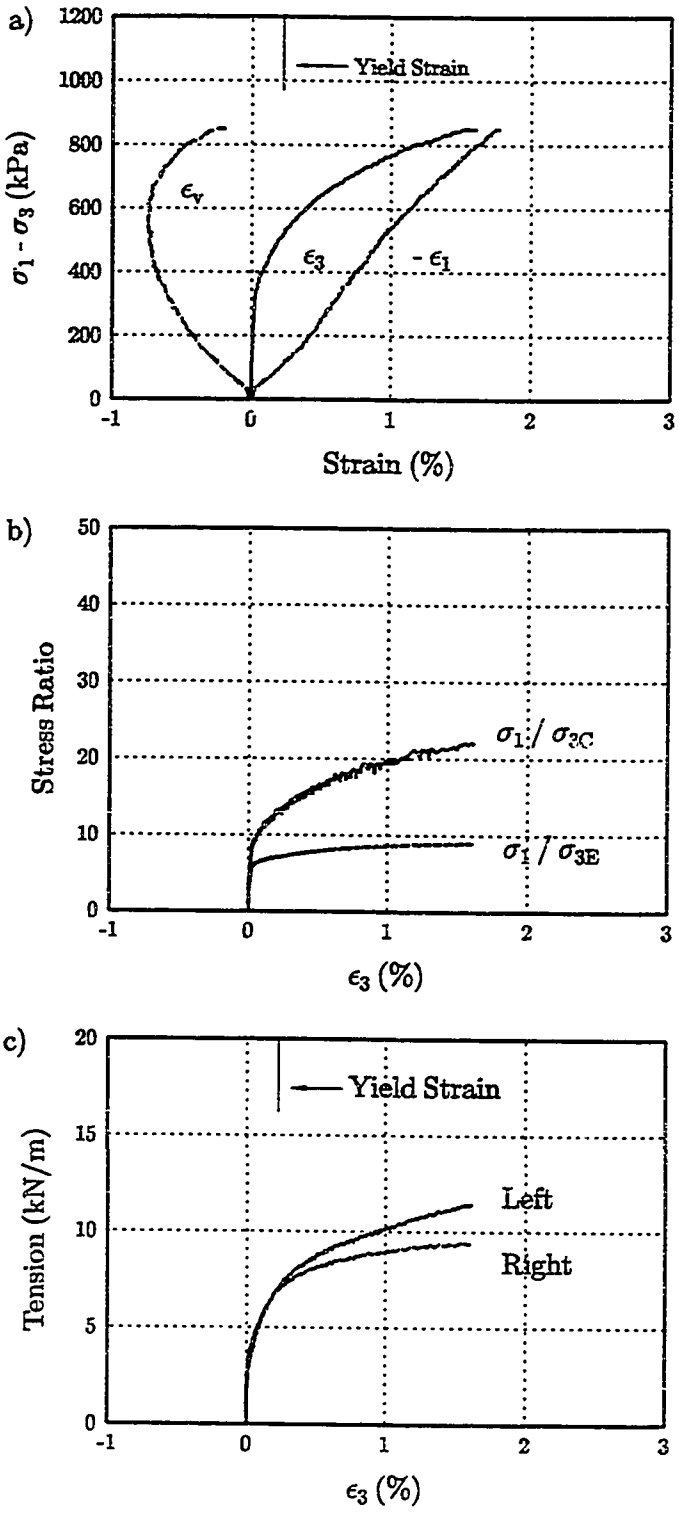

Figure C.60: Soil R, Reinforcing SS, σ_{3C} = 50 kPa, Test 104.

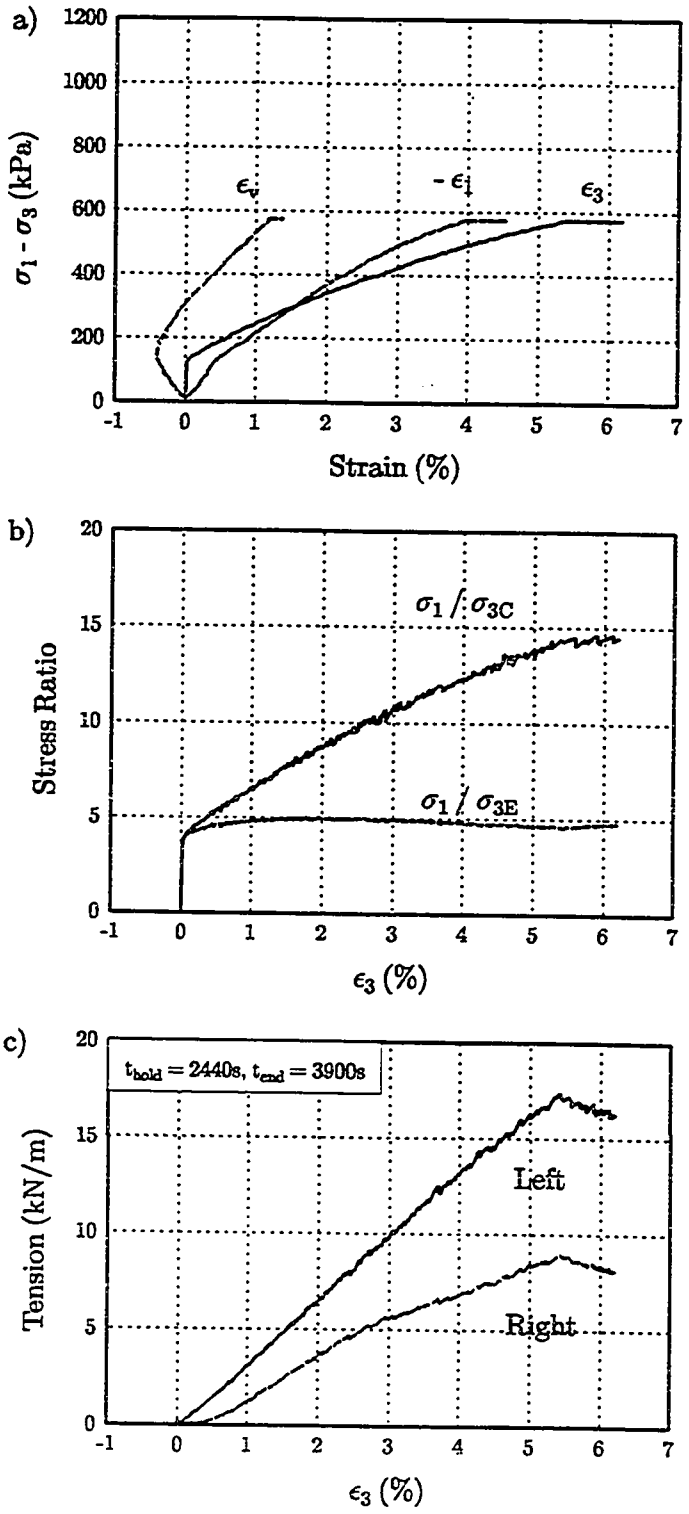

Figure C.61: Soil R, Reinforcing PP2, $\sigma_{3C} = 50$ kPa, Test 94.

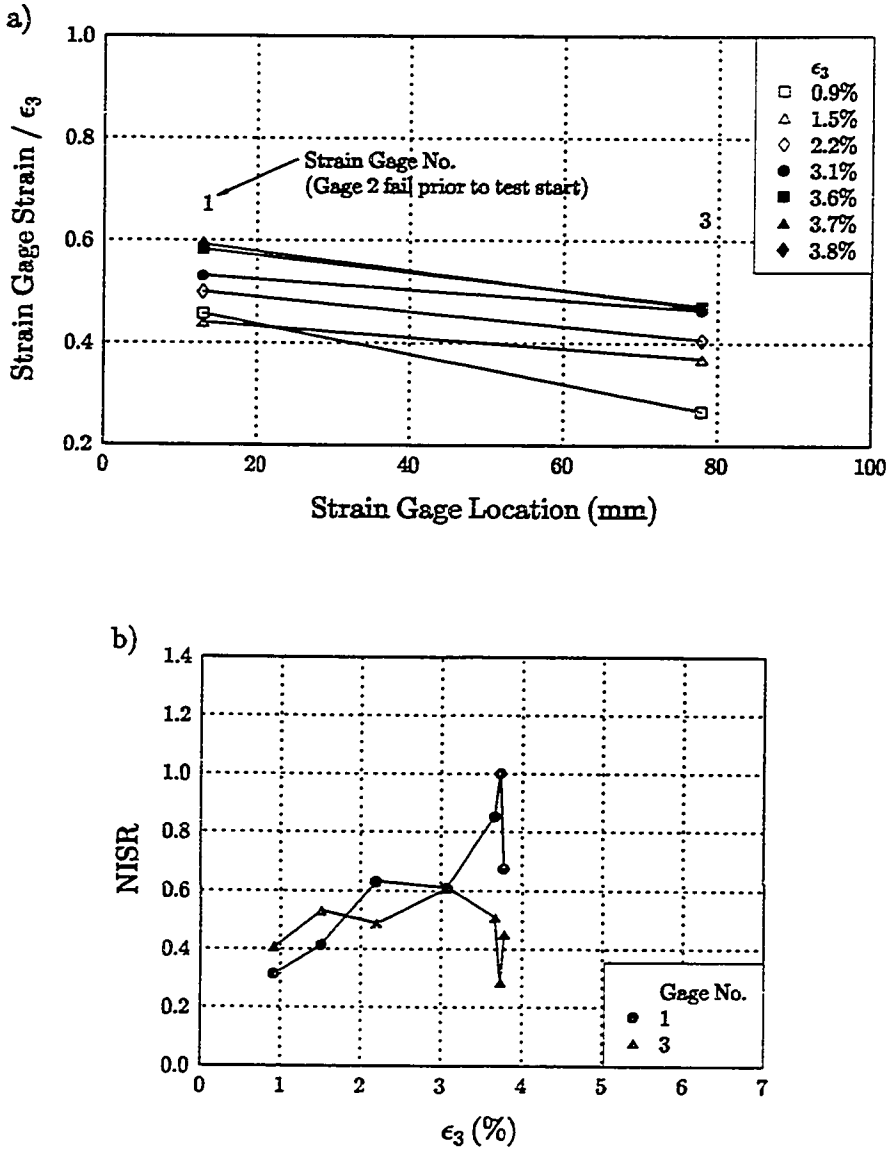

Figure C.62: Test 122, Strain Gage YL-2, Soil R, Reinforcing PP3, σ_{3C} = 25 kPa.

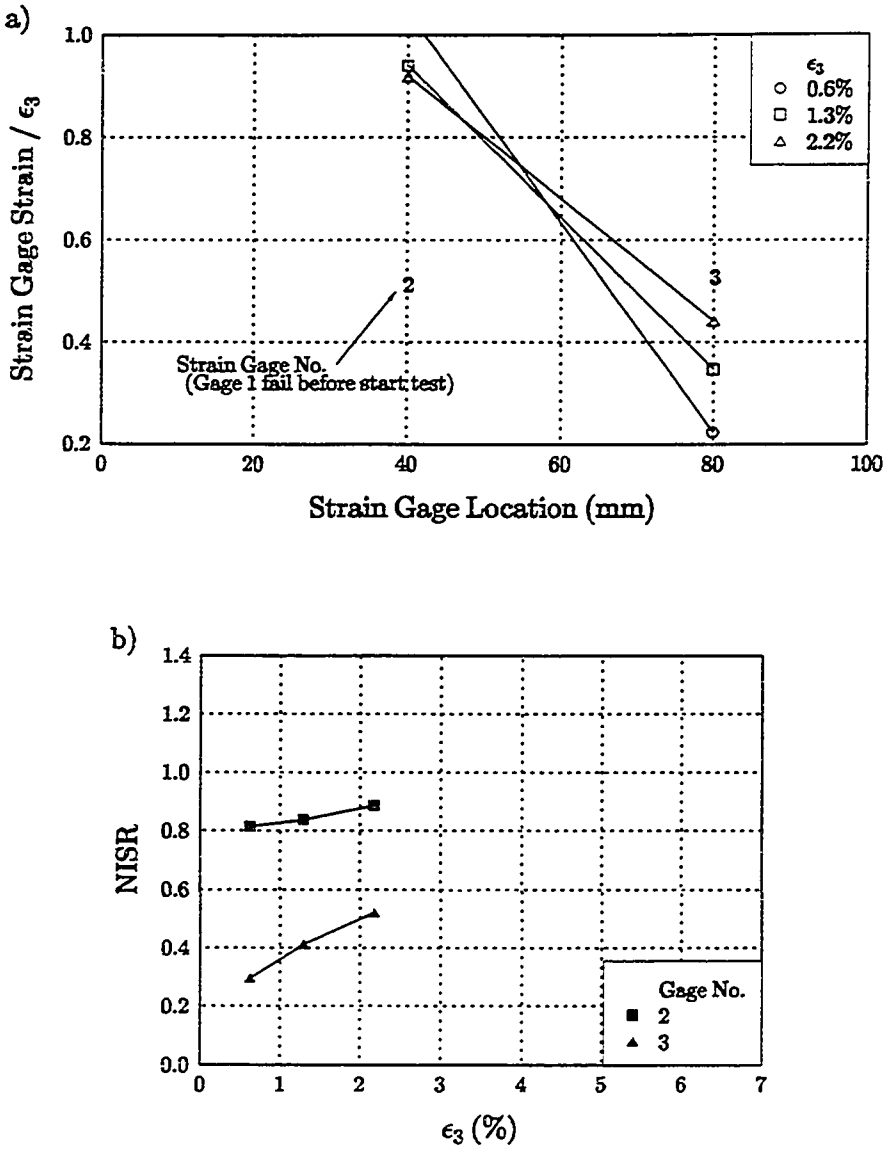

Figure C.63: Test 123, Strain Gage YL-2, Soil R, Reinforcing PP2, σ_{3C} = 25 kPa.

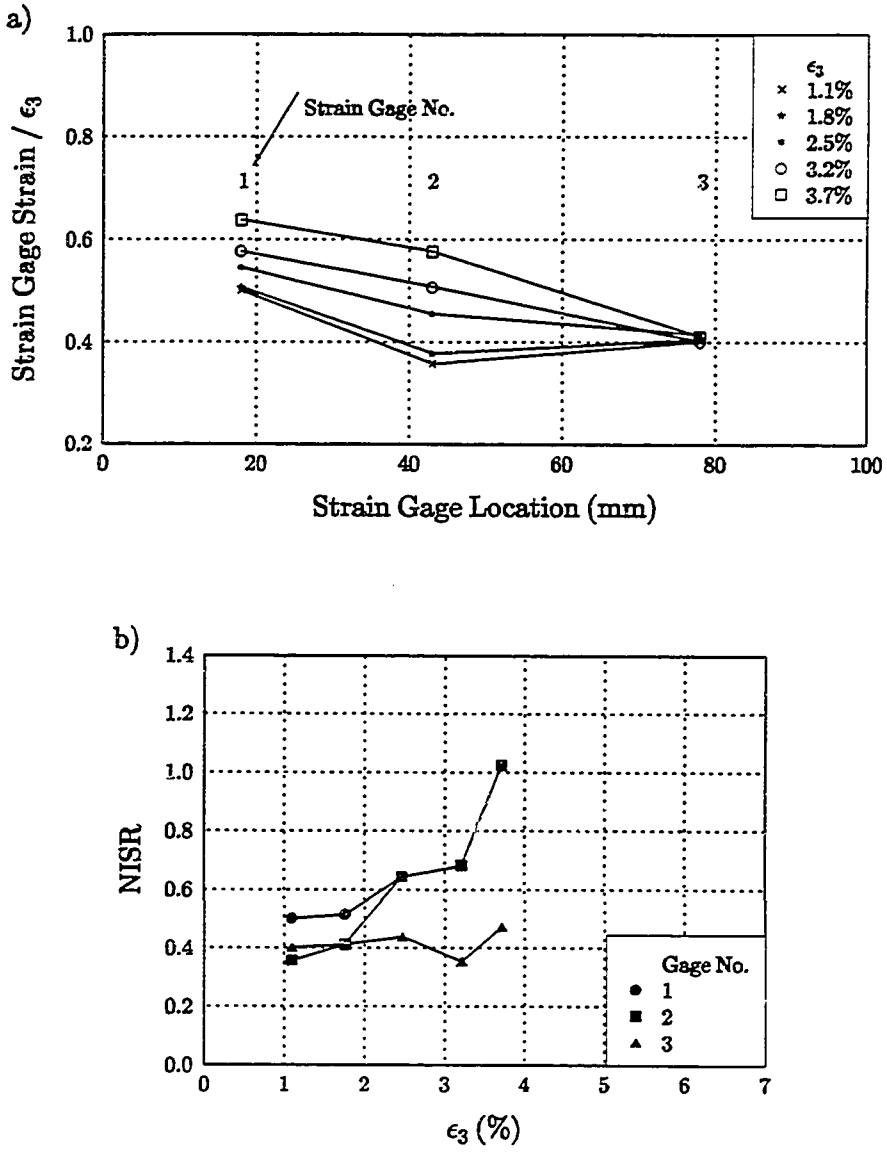

Figure C.64: Test 124, Strain Gage YL-2, Soil R, Reinforcing PP2, $\sigma_{3C} = 25$ kPa.

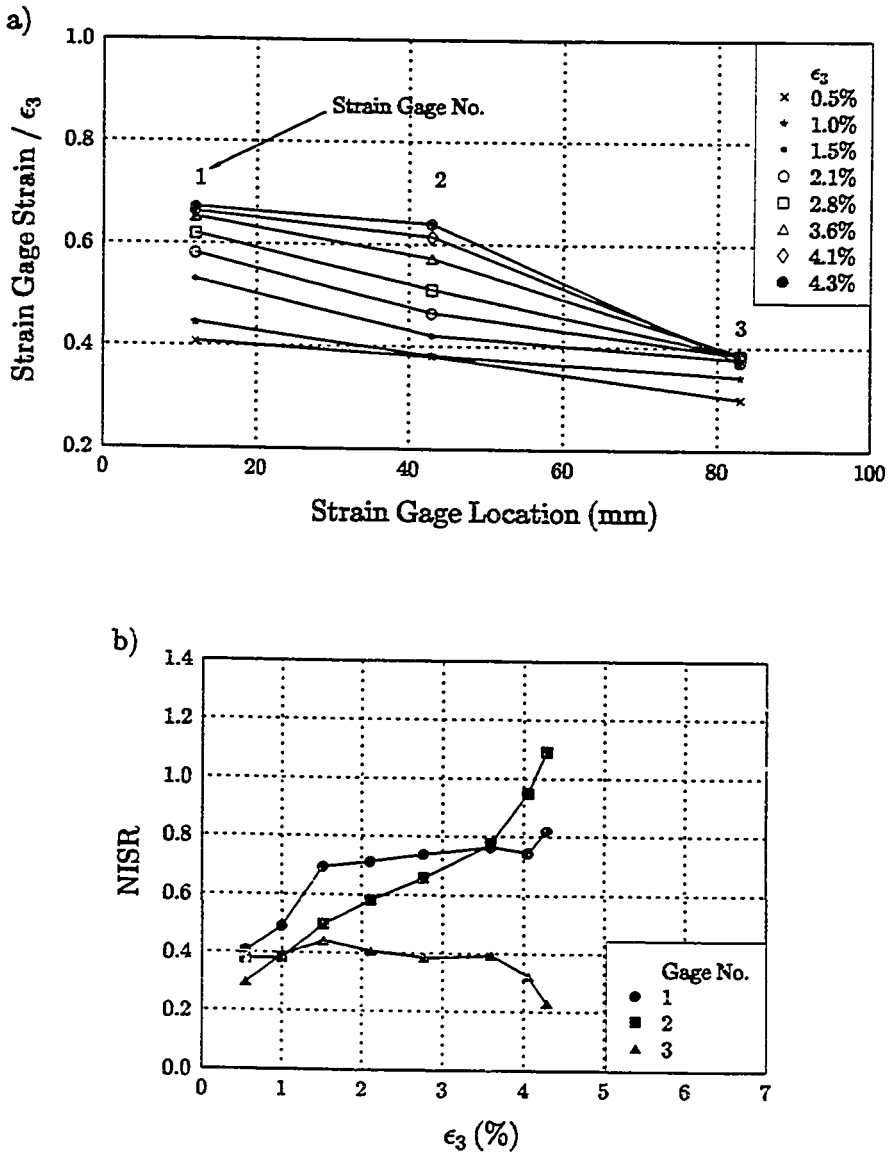

Figure C.65: Test 125, Strain Gage YL-2, Soil R, Reinforcing PP3, σ_{3C} = 12.5 kPa.

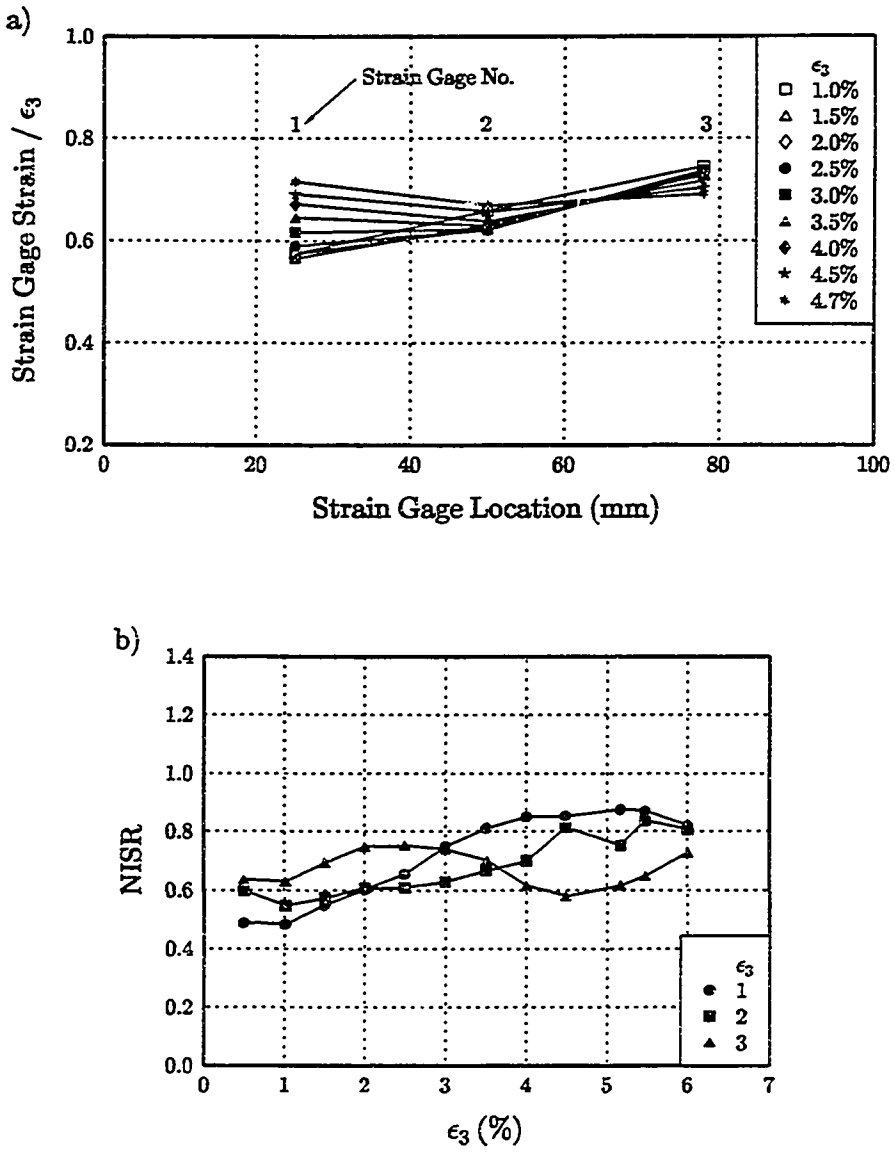

Figure C.66: Test 129, Strain Gage YL-10, Soil R, Reinforcing PP1, σ_{3C} = 25 kPa.

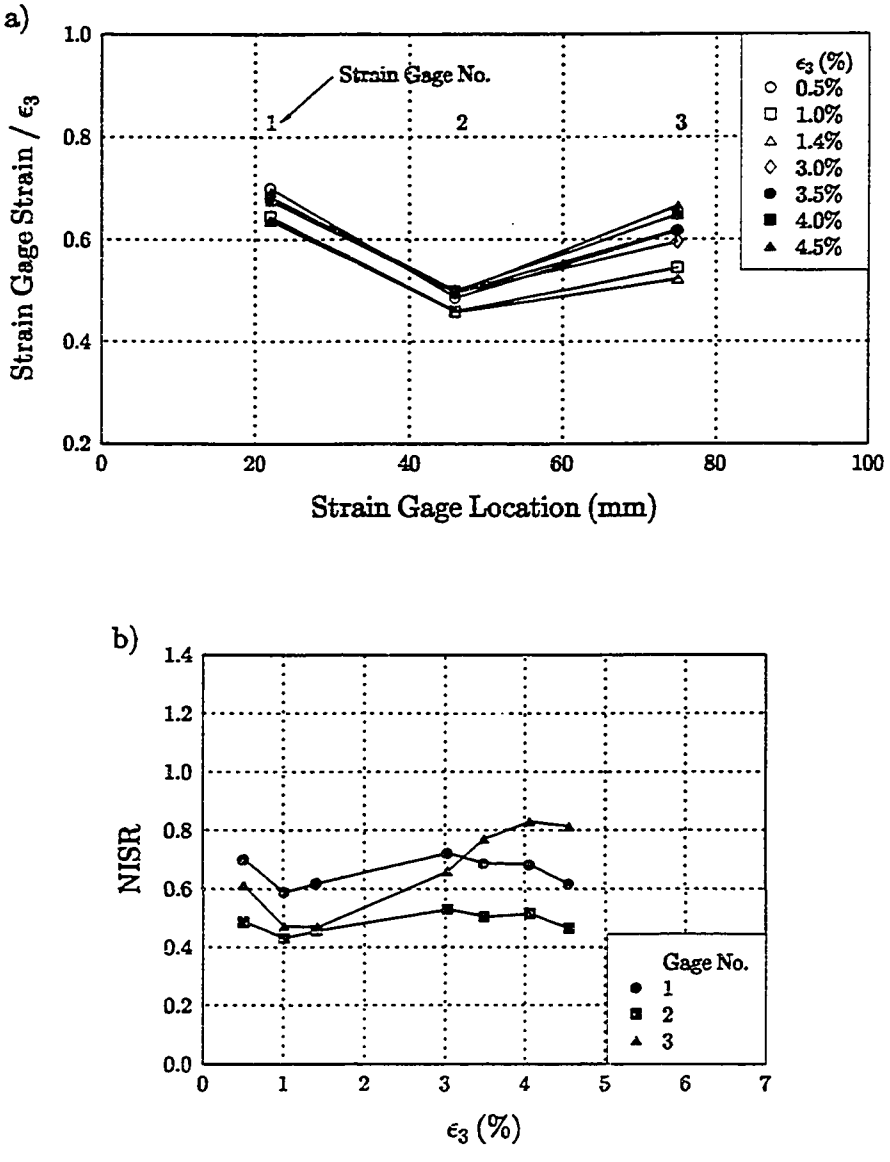

Figure C.67: Test 131, Strain Gage YL-10, Soil R, Reinforcing PP1, σ_{3C} = 12.5 kPa.

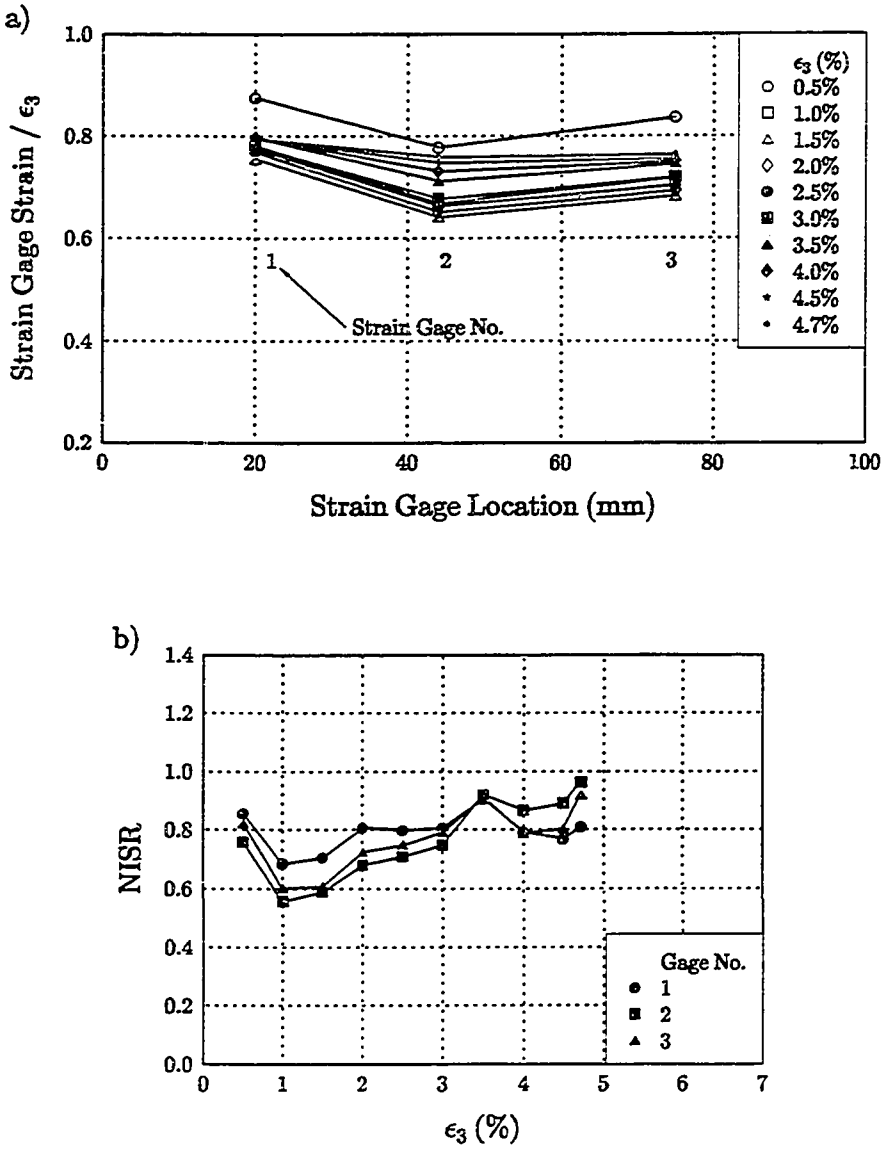

Figure C.68: Test 132, Strain Gage YL-10, Soil R, Reinforcing PP2, σ_{3C} = 20 kPa.

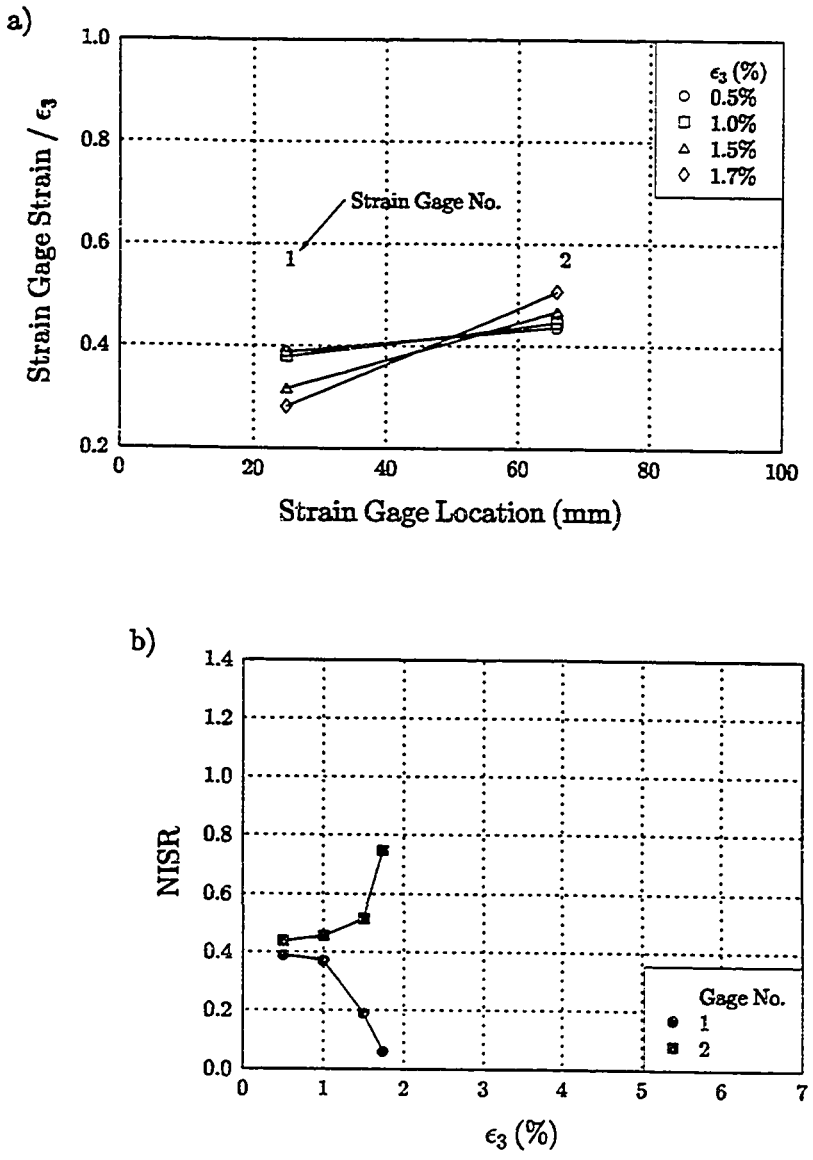

Figure C.69: Test 133, Strain Gage PA-7, Soil R, Reinforcing PET1, $\sigma_{3C} = 20$ kPa.

APPENDIX D

DERIVATIONS OF EQUATIONS FOR ELASTIC BODY DEFORMATION

D.1 Deflection due to Pure Bending of Cantilever Beam Subject to Triangular Loading

The deflection of a cantilever "beam" subjected to triangular loading, Figure D.1, assuming conditions of pure bending is derived in this section.

The general differential equation defining the curvature of the beam at any point is (Beer and Johnston, 1981):

$$EI \frac{d^2 \mu_{xb}}{dz^2} = M(z) \qquad \textbf{(D.1)}$$

Where the moment acting at any point on the beam is defined by:

$$M(z) = \frac{P}{6H} z^2 \qquad \textbf{(D.2)}$$

The slope of the beam at any point is obtained by substituting equation D.2 into D.1 and integrating with respect to z :

$$\frac{d\mu_{xb}}{dz} = \frac{1}{EI}\frac{P}{6H}\left(\frac{z^4}{4} + C_1\right) \qquad \textbf{(D.3)}$$

The equation for deflection of the beam is obtained by integrating once more:

$$\mu_{xb}(z) = \frac{1}{EI}\frac{P}{6H}\left(\frac{z^2}{20} + C_1 z + C_2\right) \qquad \textbf{(D.4)}$$

By applying the boundary conditions; x (z = H) = dx/dz (z = H) = 0, to equations D.3 and D.4 the two constants of integration are found to be:

$$C_1 = -\frac{H^4}{4} \qquad C_2 = \frac{4H^5}{20}$$

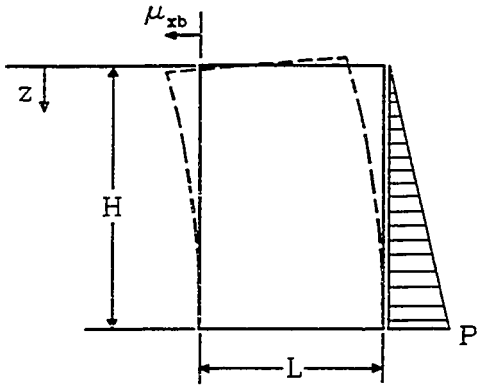

Figure D.1: Cantilever beam with triangular loading in pure bending.

Substituting these constants into equation D.4 defines the equation for deflection of the beam as:

$$\mu_{xb}(z) = \frac{1}{EI}\frac{P}{120H}\left(z^5 - 5H^4z + 4H^5\right) \qquad \textbf{(D.5)}$$

If it is assumed that the Poisson's ratio, ν, equals 0.5, G is the shear modulus, and the depth of the beam equals L, the elastic modulus and moment of inertia are defined by:

$$E = 2(1+\nu)G = 3G$$

$$I = \frac{L^3(1)}{12}$$

Defining the maximum load acting on the beam, P, as equal to $K_r\gamma H$ (where K_r is a lateral earth pressure coefficient and γ is a material unit weight), substituting for E, I, and P, and expressing the deflection as a function of the L/H ratio, Equation D.5, deflection of the beam due to pure bending, becomes:

$$\mu_{xb}(z) = \frac{K\gamma H^2}{30G}\left(\frac{H}{L}\right)^3\left\{\left(\frac{z}{H}\right)^5 - \frac{5z}{H} + 4\right\} \qquad \textbf{(D.6), (7.1)}$$

D.2 Deflection due to Pure Shear of Cantilever Beam Subject to Triangular Loading

The deflection of a cantilever "beam" subjected to triangular loading, Figure D.2, assuming conditions of pure shear is derived in this section.

The load acting on the body at any depth, z, is defined by:

$$p(z) = \frac{P}{H} z \qquad \textbf{(D.7)}$$

If it is assumed that the block may be divided into an infinite number of individual layers subjected to pure shear, Figure D.3, then equilibrium of each block is defined by:

$$\left(\tau + \left(\frac{\partial \tau}{\partial z}\right) dz\right) L - \tau(z) - 0.5\left(p(z) + p(z+dz)\right) dz = 0 \qquad \textbf{(D.8)}$$

which may be simplified to:

$$\left(\frac{\partial \tau}{\partial z}\right) dz = \left(\frac{1}{2L}\right)\left(\frac{P}{H} z + \frac{P}{H}(z+dz)\right) dz \qquad \textbf{(D.9)}$$

Taking the limit as $dz \rightarrow 0$, the equation for change in shear across each element with each increment in depth becomes:

$$\frac{\partial \tau}{\partial z} = \frac{P}{LH} z \qquad \textbf{(D.10)}$$

Defining G as the shear modulus, γ as the shear strain, and μ_{xs} as displacement then, by definition, the relationship between applied shear stresses and displacement is:

$$\tau = G\gamma = G \frac{d\mu_{xs}}{dz} \qquad \textbf{(D.11)}$$

Differentiating D.11 with respect to z:

$$\frac{\partial \tau}{\partial z} = G \frac{\partial^2 \mu_{xs}}{\partial z^2} \qquad \textbf{(D.12)}$$

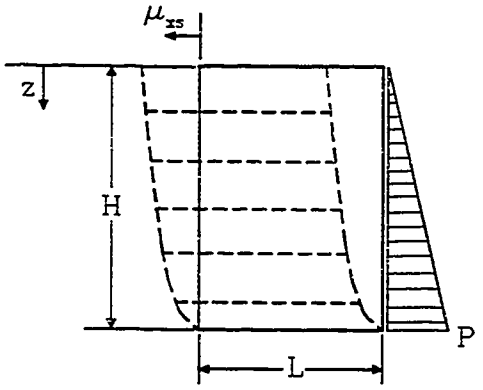

Figure D.2: Cantilever beam with triangular loading in pure shear.

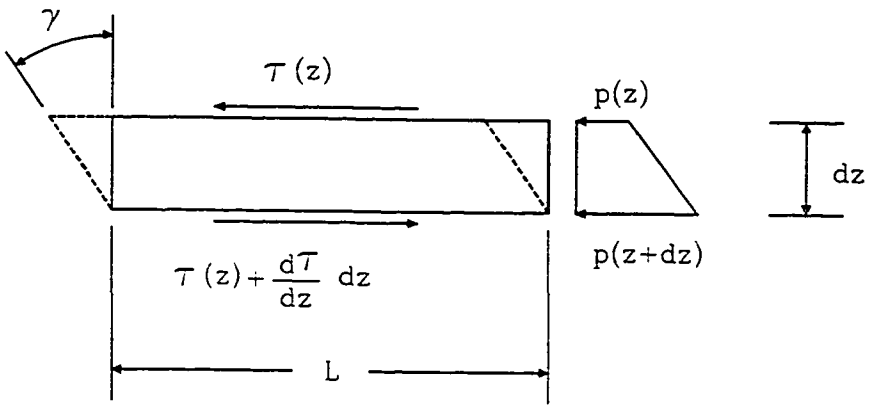

Figure D.3: Deformation of an element in shear.

The governing equation for deflection due to shear may be obtained by equating equations D.12 and D.10:

$$\frac{d^2\mu_{xs}}{dz^2} = \frac{P}{LHG} z \qquad \textbf{(D.13)}$$

The slope of the deformed beam and the displacement may be obtained by integrating Eq. D.13 with respect to z, once and twice, respectively.

$$\frac{d\mu_{xs}}{dz} = \frac{P}{2LHG} z^2 + C \qquad \textbf{(D.14)}$$

$$\mu_{xs}(z) = \frac{P}{6LHG} z^3 + C_1 z + C_2 \qquad \textbf{(D.15)}$$

Applying the boundary conditions, μ_{xs} (z = H) = 0, and τ (z = H) = PH/2L, the constants of integration are found to be:

$$C_1 = 0 \qquad C_2 = -\frac{PH^2}{6LG}$$

Substituting these constants into equation D.15, letting $P = K_r \gamma H$ (where K_r is a lateral earth pressure coefficient and γ has been redefined as a material unit weight), and expressing in terms of the L/H ratio, the equation for deflection of the beam due to pure shear becomes:

$$\mu_{xs}(z) = \frac{-K_r \gamma H^2}{6G}\left(\frac{H}{L}\right)\left(\left(\frac{z}{H}\right)^3 - 1\right) \qquad \textbf{(D.16), (7.2)}$$

D.3 Non-Dimensional Factors for an Elastic Body Subjected to Self Weight

Goodman and Brown (1963) derived the equations for stresses and displacements of an infinite embankment constructed incrementally with horizontal layers of a material

with unit weight, γ, Figure D.4. When a vertical face is considered, a = 0, $\alpha = \pi/2$, the stresses degenerate to

$$\sigma_{xx} = \sigma_{xz} = 0, \ \sigma_{zz} = -\gamma z \tag{D.17}$$

These are the same stresses as would occur in a single-stage analysis for this case, since in a vertical wedge there is no change of boundary conditions with each additional layer. For the a = 0 case, the equation for horizontal displacement degenerates to

$$\mu_x = \frac{\gamma \lambda}{2G(3\gamma + 2G)} \cdot z^2 \frac{x}{z} \tag{D.18}$$

where G is the shear modulus and λ is Lame's constant.

The horizontal strain component can be derived using the formula

$$\varepsilon_x = \frac{u_{x1} - u_{x2}}{x_1 - x_2} \tag{D.19}$$

Which upon substitution of Eq. D.18 becomes

$$\varepsilon_x = \frac{\gamma \lambda}{2G(3\lambda + 2G)} \cdot z \tag{D.20}$$

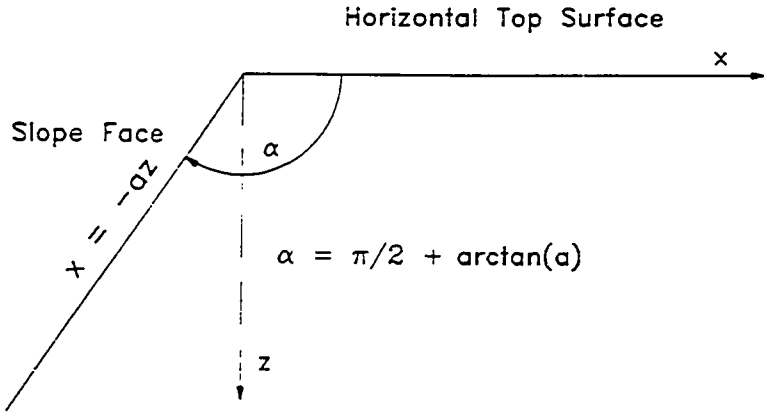

Figure D.4: Geometry of infinite embankment (after Goodman and Brown, 1963).

Equations D.18 and D.20 show, for an infinite quarterspace, the horizontal displacements and strains depend upon the elastic properties and material density and are constant for any given z. For the case where, $\nu = 0.5$, then $\lambda = \infty$ and the equations for displacement and strain become:

$$u_x = \frac{\gamma \lambda}{6G} \cdot z^2 \frac{x}{z} \tag{D.21}$$

$$\varepsilon_x = \frac{\gamma}{6G} \cdot z \tag{D.22}$$

Goodman and Brown (1963) non-dimensionalized vertical, horizontal, and shear stresses in terms of z for the general embankment, $\pi/2 \leq \alpha \leq \pi$, by dividing stresses by the term γz. Displacements and strains can be similarly non-dimensionalized using the terms from equations D.21 and D.22. For an infinite quarterspace the non-dimensional stress, strain, and displacement are, respectively:

$$\frac{\sigma}{\gamma z}; \quad \frac{\varepsilon G}{\gamma z}; \quad \frac{uG}{\gamma z^2}; \tag{D.23}$$

These same factors may be used for a finite body. Consider a finite elastic body with a given length to height ratio, L/H, and known distribution of stresses, strains, and displacements due to deformation under self weight. The non-dimensionalized stresses, strains, and displacements may be presented as a function of height, H, of the body by multiplying 1/z by z/H and $(1/z)^2$ by $(z/H)^2$ in Eq. D.23 to obtain:

$$\frac{\sigma}{\gamma H}; \quad \frac{\varepsilon G}{\gamma H}; \quad \frac{uG}{\gamma H^2}; \tag{D.24}$$

The non-dimensionalizing factors presented in Eq. D.24 have been applied in Chapter 7 of this dissertation.

VITA

Mr. Stanley R. Boyle received a B.S. in Civil Engineering from the University of Vermont (1983), a M.S. in Civil Engineering (Structural) from Carnegie-Mellon University (1984), and a Ph.D. in Civil Engineering (Geotechnical) from the University of Washington (1995). Mr. Boyle is a registered Professional Engineer in the state of Colorado and is active in the American Society of Civil Engineers.

While at Carnegie-Mellon University Mr. Boyle worked on various issues concerning the use of robots in construction and helped to develop a remotely operated vehicle for the investigation and cleanup of the Three Mile Island Nuclear Power Plant. At the University of Washington he investigated the behavior of geosynthetic reinforced soils and geosynthetic reinforced soil retaining walls. Some of the results from his work at the University of Washington were presented at the Fifth International Conference on Geotextiles, Geomembranes and Related Products in a paper entitled "Deformation Characteristics of Geosynthetic-Reinforced Soil" co-authored by Mr. Boyle and Dr. R.D. Holtz. Additional results were presented at Geosynthetics '95 where Mr. Boyle was awarded first place in a student paper competition at for his paper entitled "Unit Cell Tests on Reinforced Cohesionless Soils".

Mr. Boyle has over eight years of construction experience as a civil engineer. He has worked on site during the construction of two zoned earth dams, soil cement retaining structures, clay and concrete lined irrigation canals, large and small diameter pipelines, and a sewage treatment facility. Activities on these projects included dam foundation excavation, preparation and grouting; miscellaneous other excavations, some requiring ripping and blasting; installation of rock anchors; excavation dewatering; embankment material moisture conditioning, blending, and placement; rock crushing and screening; and the construction of concrete structures. He has also worked as a software engineer for the development of computer-aided design programs for civil engineering applications.